

**New Reactions and Reagents for Phosphorus-Carbon
Bond-Formation**

by

Michael B. Geeson

M. Chem, University of Oxford (2014)

Submitted to the Department of Chemistry
in partial fulfillment of the requirements for the degree of

Doctor of Philosophy in Chemistry

at the

MASSACHUSETTS INSTITUTE OF TECHNOLOGY

May 2020

© Massachusetts Institute of Technology 2020. All rights reserved.

Author.....
Department of Chemistry
May 8, 2020

Certified by.....
Christopher C. Cummins
Henry Dreyfus Professor of Chemistry
Thesis Supervisor

Accepted by.....
Robert W. Field
Haslam and Dewey Professor of Chemistry
Chairman, Department Committee on Graduate Theses

This Doctoral Thesis has been examined by a Committee of the Department of Chemistry as follows:

Professor Alexander T. Radosevich.....
Associate Professor of Chemistry
Chairman

Professor Christopher C. Cummins.....
Henry Dreyfus Professor of Chemistry
Thesis Supervisor

Professor Yogesh Surendranath.....
Paul M. Cook Career Development Assistant Professor
Committee Member

New Reactions and Reagents for Phosphorus-Carbon Bond-Formation

by
Michael B. Geeson

Submitted to the Department of Chemistry
on May 8, 2020, in partial fulfillment of the
requirements for the degree of
Doctor of Philosophy in Chemistry

Abstract

Chapter 1 takes the format of an “Outlook”, and sets forth the case for developing sustainable methods in the synthesis of phosphorus-containing compounds. Methods used by nature for phosphorus-carbon bond-formation, or in the chemistry of other elements such as silicon, are discussed as model processes for the future of phosphorus in chemical synthesis.

Chapter 2 describes the discovery of $[\text{TBA}][\text{P}(\text{SiCl}_3)_2]$, prepared from $[\text{TBA}]_3[\text{P}_3\text{O}_9] \cdot 2\text{H}_2\text{O}$ and trichlorosilane. The bis(trichlorosilyl)phosphide anion is used to prepare compounds that contain P–C, P–O, P–F, and P–H bonds in a method that bypasses white phosphorus (P_4), the traditional route to organophosphorus compounds.

Chapter 3 extends the phosphate precursors to $[\text{TBA}][\text{P}(\text{SiCl}_3)_2]$ from trimetaphosphate to crystalline phosphoric acid. Balanced equations are developed for the formation of $[\text{TBA}][\text{P}(\text{SiCl}_3)_2]$ from phosphate sources and the byproducts are identified as hexachlorodisiloxane and hydrogen gas. Extension of trichlorosilane reduction to bisulfate provides improved access to the known trichlorosilylsulfide anion, $[\text{TBA}][\text{SSiCl}_3]$. This anion was used as a thionation reagent to prepare thiobenzophenone and benzyl mercaptan from benzophenone and benzyl bromide, respectively.

Chapter 4 describes the synthesis of neutral phosphine, $\text{HP}(\text{SiCl}_3)_2$, obtained by protonation of $[\text{TBA}]\mathbf{1}$ with triflic acid. $\text{HP}(\text{SiCl}_3)_2$ is a highly efficient reagent for photochemical hydrophosphination of terminal alkenes. The phosphorus-silicon bonds in the hydrophosphination products can be functionalized to provide compounds of the general formulae: RPH_2 , $[\text{RP}(\text{R}')_3]\text{Cl}$, $\text{RP}(\text{O})(\text{H})(\text{OH})$, and $\text{RP}(\text{O})(\text{OH})_2$.

Chapter 5 describes a method to prepare phosphiranes (three-membered rings that contain a phosphorus atom) from anthracene-based phosphinidene precursors and styrenic olefins. The phosphinidene transfer reaction requires an organoiron and fluoride catalyst. The resulting phosphirane is prepared in good yield (73%) with high stereoselectivity (>99%). Experimental investigations into the mechanism point toward the intermediacy of an iron-coordinated fluorophosphide species.

Thesis Supervisor: Christopher C. Cummins
Title: Henry Dreyfus Professor of Chemistry

Acknowledgments

Looking back, my overwhelming feeling is that time has gone too quickly. That's not something I would have thought possible five years ago in June 2015, walking down Memorial Drive on my way to lab for the first time—coincidentally on the same day as Commencement. Although I am looking forward to moving home to the UK, a great part of me is not ready to leave my friends, ongoing chemistry projects, the crisp winter months and the colorful summers of Boston.

I must start by thanking Kit. I remember calling him up while still in London about coming over as a visiting student, and getting updates on the latest developments on the "anthracene project." I came to Boston before the formal start of my PhD in order to secure a place in his group, hoping to get a head start on any potential competition! I don't know if that strategy helped at all, but I was fortunate enough to join his group and haven't looked back since. First and foremost, I think he derives his joy in chemistry from perfecting the synthesis of a new molecule, perhaps one that others might consider "non-existent" or too challenging to prepare. This fundamental approach to science, increasingly rare these days, has certainly had an influence on me and I count myself lucky to have spent many hours discussing chemistry with him right here in my office. He has also taught me to never talk myself out of running an experiment: even if you don't get the result you were expecting, something else more interesting might happen. Though enthusiastic, he also maintains a healthy dispassion: ask nature the questions, feelings don't come into it. An unexpected benefit of my PhD is that my grasp of the English language has improved as a result our back-and-forth drafting process. I would like to thank him for the many opportunities he has afforded me, including the freedom to pursue a number of different projects over the years.

To me, the lab environment has felt like a tale of two eras. When I first arrived, Julia, Matt, Ioana, and Wes were the omnipotent senior graduate students. I sat next to Julia for several years and enjoyed talking to her about science and general departmental gossip. Looking back now, she also patiently tolerated me in our shared lab space despite me not cleaning my fair share of NMR tubes in those early days. Matt was a fountain of knowledge, always willing to share his time and experience. I also enjoyed going to my first football game at BC with him. Ioana was a positive and fun person to have around, and probably the most principled lab member I encountered. Wes, two years my senior, spanned both the early and latter periods of my time in the group. He was a great person to interact with daily: always ready to talk about our projects and the recent literature, and full of ideas for new reactions to try out. I'm glad to have spent a lot of time collaborating with him on the phosphirane project, although I wish we had shared the final success of the project together while he was still around!

Wes also formed part of the group of graduate students that made up the second period of my time in the group, along with Scott, Martin, Will and Tristan. We frequented the Muddy Charles pub religiously after group meeting on Thursday evenings and I have

enjoyed many memories there as a result. I'm sitting writing this on a Friday afternoon, before our weekly group lunch, which has always been a nice way to end the formal working week. Scott always has a good story to tell and has done a great job of developing trimetaphosphate, a seemingly inert substance, into a useful chemical reagent. Martin, my ultra-relaxed and long-term office mate, has been a great colleague and friend. We have spent many hours discussing our phosphorus chemistry and generating ideas. Critiquing the proposed mechanisms on the flurry of JACS, Science, and Nature papers on photoredox catalysis has also been a fun. Will made some nice contributions to the chemistry of the metaphosphates and I wish him luck in Toronto. Tristan, the newest graduate student, seems to have a lot of exciting ideas and I hope that among exploring them, he can find some time to finish off any loose ends I may have been forced to leave unfinished!

From the earlier days, I remember sharing many fun evenings with Shiyu, Max and Marc, all post-docs. With Marc in particular, I had a lot of fun hanging out and going skiing with. In the second half of my time here, both Pablo and Kevin became collaborators and good friends. Not only did they make social life in the group a lot of fun, but both hit the ground running with their projects which I was lucky enough to help out along the way. Over the years, many more students have come and gone. Each have made the lab a memorable place to be a part of, so thank-you to Tobi, Kirril, Can, Esau, Jeniffer, Kevin, Wendy, Jan, Paul, June, Miller, Molly, Rebecca, Marie, Matt B., Anna, Andre, Qing Xin, Yingying, Liz, Keita and anyone else I might have inadvertently omitted.

There have been many others who propelled me to the point of starting a PhD. I think Mr. Davidson, my high school chemistry teacher, had a larger effect on my degree choice than I realized at the time. My tutors at Oxford—Tim, Veronique, and Allison—were all accomplished researchers. Looking back now with a few years of research experience under my belt, the amount of time and dedication they put into teaching us mere undergraduates is humbling and sincerely appreciated. Later on, John and Jose let me join their labs as a joint student and gave me the opportunity to rediscover my love of chemistry after three years of fairly dry lectures and lab modules. It was with Jose in particular, along with my grad student mentor Andy, that I got the "research bug". My Thesis Committee, Alex and Yogi, have also been a great source for personal development. Yogi's insights into a career in academia were very helpful and his enviably broad knowledge of chemistry leaves no topic off-limits for discussion. Alex is located nearby and I have enjoyed the times we have started a conversation in the hallway and ended up on the whiteboard in his office discussing phosphorus chemistry. I'm glad he got a good laugh when I lost my passport and missed a trip to Amsterdam, because I certainly didn't find it funny at the time.

I have made a great group of friends here that have given me a life in Boston independent of my PhD. Alex and Joey were great room mates for two years and we had a lot of fun together. In later years, Alex, Jesus, Aaron, and Matt were always ready to hit the Muddy on a Friday evening. Our trips to clubs, bars, breweries, casinos and sports games have made for a surprisingly youthful late-twenties experience. Grilling on a rooftop overlooking the Charles River and St. Paddy's Day in 2019 were two highlights. Despite four out of

five of us being chemists, conversation never strayed too close to our work and that has probably been a healthy experience for us all.

My family have been incredibly loving and supportive. Mum and Dad were always ready to pick me up from the airport and make me laugh whenever I returned home. Walking down to the pub in Redbourn with them and our dog, Lucky, during the summer always made it difficult to leave. Like Mum and Dad, Alex and Ben have both been out to visit me here in Boston. Alex ruled the beer pong table and helped me eat seventy chicken wings during a marathon of Sunday football. Ben managed to cause carnage at an Independence Day party at the MIT sailing pavilion. All four are fundamentally good people and have had more positive influence on me than they know. They have never been far from my mind and I'm looking forward to spending more time with all of them when I return home. We all descend from Nan, Grandad, Baba and Deda; all four are so unique and have shaped us into the people we are today.

Finally, I would like to thank Lucia. When we met during my second year, I was unaware of how the course of my life would change for the better. With her inability to sit still and love for adventure I'm surprised I got any work done. We have exhaustively explored New England on skiing trips in Vermont, hiking trips in New Hampshire, weekends all over Maine, and days spent at Singing Beach in Manchester. We have ventured to the UK, Spain, Cuba, and Costa Rica on many unforgettable trips. In Boston, she fearlessly brought me into her circle of Spanish-speaking friends despite my ineptitude (or lack of effort) for learning the language. She has navigated the US schooling system and a variety of eclectic jobs in order to keep enjoying our life here in Boston, and is the most deserving person I know of for her new role at BCG. Her lack of chemistry-specific knowledge is far surpassed by her enthusiasm for the subject. She tells anyone who will listen about the bis(trichlorosilyl)phosphide anion, phosphiranes, or the dreaded ruthenium catalyst. I hope I can begin to match the many hours of effort, time, and love she has poured into our relationship over the years. Side by side, I look forward to whatever comes next.

Contents

Chapters

1	Let's Make White Phosphorus Obsolete	13
2	Phosphoric acid as a precursor to chemicals traditionally synthesized from white phosphorus	37
3	Orthophosphate and Sulfate Utilization for C–E (E = P, S) Bond Formation via Trichlorosilyl Phosphide and Sulfide Anions	81
4	Photochemical Alkene Hydrophosphination with Bis(Trichlorosilyl)Phosphine	147
5	Organoiron- and Fluoride-Catalyzed Phosphinidene Transfer to Styrenic Olefins in a Stereoselective Synthesis of Unprotected Phosphiranes	225

Appendices

A	Coordination Chemistry of RPA Compounds	287
B	Silicon-Chlorine Bond-Functionalization of the Bis(trichlorosilyl)-phosphide and Trichlorosilylsulfide Anions	323
C	Redox-Neutral Reactions of Phosphoric Acid	347

	Index of Unpublished Compounds and Reactions	369
--	--	-----

Chapters

Chapter 1

Let's Make White Phosphorus Obsolete

Contents

1.1	Introduction: The Phosphorus Industry	14
1.2	Fine chemical synthesis from phosphorus(V) precursors	15
1.3	Phosphorus sustainability and stewardship	19
1.4	P(III) compounds as the bottleneck	22
1.5	How does biology make phosphorus-carbon bonds?	25
1.6	Lessons from Group 14	26
1.7	Outlook: challenges and opportunities	29
	References	29

Abstract

Industrial and laboratory methods for incorporating phosphorus atoms into molecules within the framework of Green Chemistry are in their infancy. Current practice requires large inputs of energy, involves toxic intermediates, and generates substantial waste. Furthermore, a negligible fraction of phosphorus-containing waste is recycled which in turn contributes to negative environmental impacts such as eutrophication. Methods that begin to address some of these drawbacks are reviewed and some key opportunities to be realized by pursuing organophosphorus chemistry under the principles of Green Chemistry are highlighted. Methods used by nature, or in the chemistry of other elements such as silicon, are discussed as model processes for the future of phosphorus in chemical synthesis.

Reproduced in part with permission from: Geeson, M. B.; Cummins, C. C. *ACS Central Sci.* **2020**, in press (doi 10.1021/acscentsci.0c00332). Copyright © 2020 American Chemical Society.

1.1 Introduction: The Phosphorus Industry

The colors often associated with phosphorus are red and white, these being representative of the two most common allotropes of the element.¹ Green is uncommon,^{2,3} although with global issues surrounding waste, environmental pollution, sustainability, and climate change perhaps the concept of “green phosphorus” warrants serious consideration. The twelve principles of Green Chemistry are a blueprint for performing chemistry with high efficiency, while minimizing energy inputs, waste outputs, and potential for harm to the environment or indeed personal safety.⁴ In the case of synthesis surrounding the element phosphorus, these criteria are met infrequently.

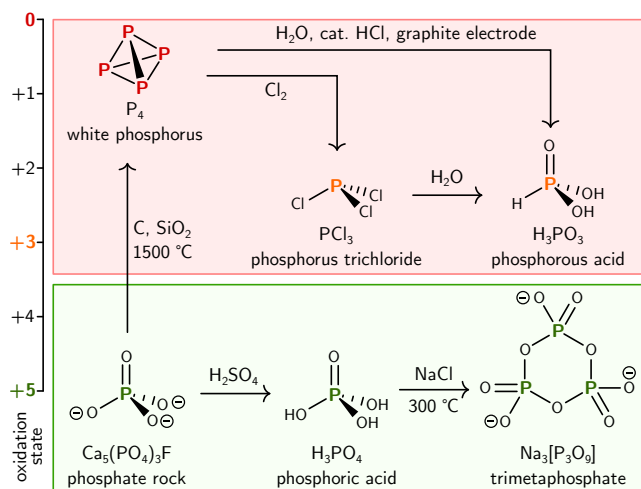


Figure 1.1 Summary of the synthesis of some key phosphorus-containing compounds and their formal oxidation states. Compounds in the green box are “redox-neutral” products derived from phosphate rock. Compounds in the red box are derived from P_4 . Orange phosphorus atoms are in the +3 oxidation state and are useful intermediates in chemical synthesis.

Phosphorus atoms that exist in man-made chemicals and materials began their life cycles, almost exclusively, in phosphate ores such as fluorapatite, $Ca_5(PO_4)_3F$. This is a relatively modern phenomenon: up until the end of the 19th century much of the world’s phosphorus came from guano, the excrement of birds and bats. Prior to guano, farmers relied on the scrupulous reuse of phosphate-containing materials, including mud from rivers where phosphorus from agriculture and sewage accumulates. The discovery of the “wet process” for producing phosphoric acid from phosphate rock and sulfuric acid (Figure 1.1) has led to an “anthropogenically broken natural-phosphorus cycle”,⁵ where phosphorus atoms now run from deposits of high concentrations on land to high dilution in the seas and soils.⁶

Approximately 95% of mined phosphate rock is destined for the wet process, and the resulting phosphoric acid is used to produce phosphate fertilizers.⁷ Sulfuric acid, required

stoichiometrically to operate the wet process, is produced from combustion of elemental sulfur which is in turn obtained from fossil fuel refining (or historically, from volcanic deposits).⁸ The wet process is the principal reason for sulfuric acid production, and in this scheme the industrial chemistry of phosphorus, sulfur, and fossil fuels are intertwined.⁹ As refinement of fossil fuels declines, future methods for obtaining useful products directly from phosphate rock or the use of acids other than sulfuric would therefore be desirable.

The remaining 5% of phosphate rock is converted to white phosphorus in what is known as the “thermal process”. This involves reduction with carbon in an electric arc furnace, in the presence of silica as an oxide acceptor (Figure 1.1). The thermal process predates the wet process, tracing its routes back to 1669 when Hennig Brand obtained white phosphorus by heating deposits of urine to high temperatures in a blast furnace.¹⁰ In this early setup, organic matter present in the urine, such as creatine, played the role of reducing agent for phosphate which is present in relatively high concentrations in urine. This abundant natural source of phosphorus is once again being exploited today by those interested in phosphorus sustainability (Section 1.3). The modern thermal process requires large inputs of energy for continuous electric arc furnace operation¹¹ and so production facilities are often centralized and close to cheap sources of power such as hydrothermal or nuclear.

At present, white phosphorus is the only industrially practicable way to obtain phosphorus-containing fine chemicals. This is achieved through intermediates such as PCl_3 which have phosphorus-chlorine bonds that can be functionalized readily by reduction or salt metathesis. Both white phosphorus and PCl_3 (made from the reaction of P_4 and Cl_2) have limitations as reagents within the framework of Green Chemistry. White phosphorus is a high-energy and toxic substance. For its military applications (smokescreens, incendiary bombs) white phosphorus goes by the nickname “Willie Pete”.¹⁰ The use of chlorine to make PCl_3 requires special measures to mitigate the hazards and reactivity of Cl_2 toward personnel and reactor construction materials. Neither P_4 nor PCl_3 have any significant direct applications and so they could in principle be omitted in the preparation of phosphorus-containing chemicals if alternative routes are discovered.

1.2 Fine chemical synthesis from phosphorus(V) precursors

Phosphate esters from phosphoric acid

Advantages of beginning the synthesis of phosphorus-containing chemicals with phosphoric acid include its widespread availability, omitted energy inputs required for the thermal process, and the absence of chlorine-containing byproducts generated when using PCl_3 . Furthermore, phosphoric acid can be produced from recycled sources of phosphorus (Section 1.3). Procedures for incorporating phosphoric acid-derived phosphorus atoms directly into molecules are scarce, though emerged as early as the 1950’s¹² including the pioneering work on nucleoside polyphosphate synthesis by Khorana.¹³

One recent procedure involves treating an alcohol with 1.1 equivalents of phosphoric

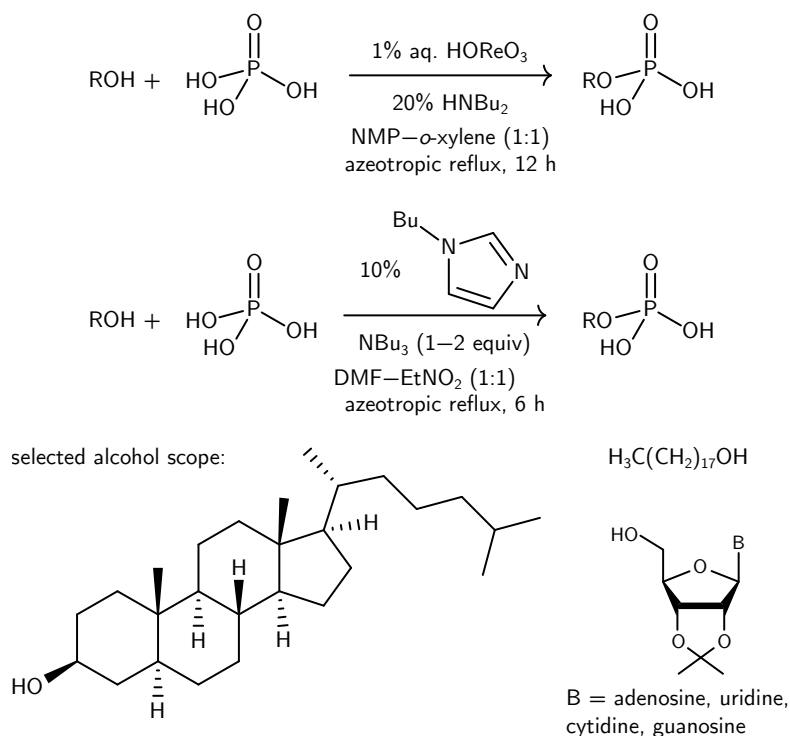


Figure 1.2 Procedures for converting alcohols into mono phosphate esters using phosphoric acid. NMP: N-methyl-2-pyrrolidone; DMF: N,N-dimethylformamide.

acid in the presence of a catalyst under azeotropic reflux in order to remove water (Figure 1.2).¹⁴ This allows for the phosphorylation of simple alcohols such as stearyl alcohol in high yields. One drawback of the procedure is the use of long-chain substrates, presumably imposed by the high reaction temperatures that would remove low-boiling alcohol substrates by distillation. Nevertheless, use of nearly equimolar amounts of alcohol and phosphoric acid, increasingly complex substrates such as 2',3'-*O*-isopropylidene ribonucleosides, and production of water as the only stoichiometric byproduct is impressive.^{15,16}

These reactions involve loss of water and so, naturally, reagents used to induce dehydration reactions have been investigated for their ability to promote phosphorylation of alcohols. The use of acetic anhydride¹⁷ or trichloroacetonitrile¹⁸ to activate phosphoric acid toward attack by a nucleophile allow for milder temperatures and the use of lower molecular weight alcohols such as allyl alcohol. However, from an atom-efficiency standpoint, the formation of water as the sole byproduct is the most attractive method for preparing organophosphate monoesters. The use of solid-state catalysts is also being investigated, potentially leading to improved separation procedures.¹⁹

Another strategy for preparing esters of phosphoric acid is the use of polyphosphoric acid which, as a dehydrated form of phosphoric acid, already includes the anhydride func-

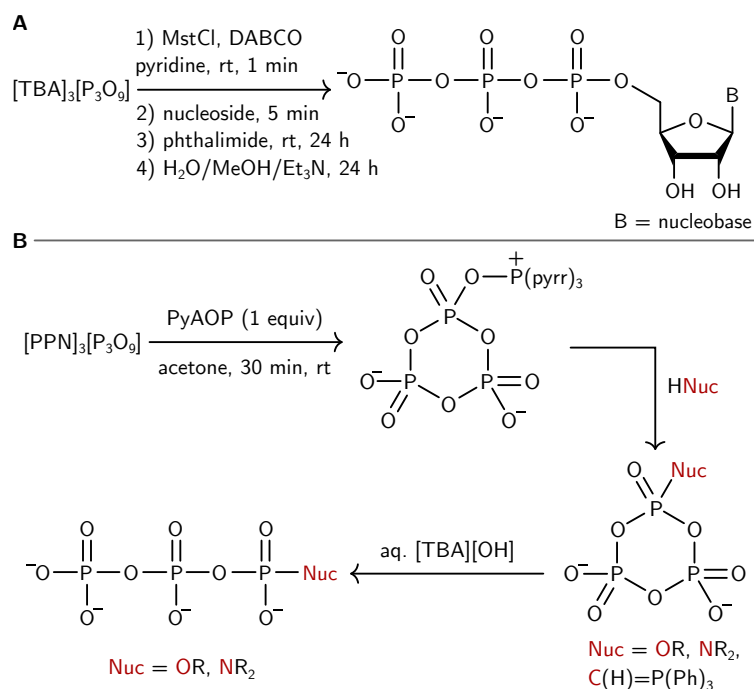


Figure 1.3 A: Procedure for triphosphorylation of nucleoside bases using [TBA]₃[P₃O₉].2H₂O. TBA: tetra-*n*-butylammonium; MstCl: 2-mesitylenesulfonyl chloride; DABCO: 1,4-diazabicyclo[2.2.2]octane; PyAOP: see text. **B:** Isolation of a triphosphorylating reagent and subsequent reaction with C, N, and O-based nucleophiles.

tionality necessary for phosphorylation of nucleophiles. A variety of methods exists for obtaining polyphosphoric acid and these can be broadly divided according to their reliance on either P₄ or H₃PO₄ for the input of phosphorus,²⁰ although a third method involves the action of microbes on waste water (Section 1.3). Methods that utilize H₃PO₄ require dehydration which is accomplished by heating, using either combustion of natural gas, electrothermal, or microwave irradiation as the input of thermal energy.²⁰ Polyphosphoric acid is used a catalyst or reagent in organic synthesis, for example in cyclization or dehydration reactions.²¹ Treatment of polyphosphoric acid with alcohols leads to the formation of a mixture of mono- and diesters of phosphoric acid which find applications in cleaning agents, cosmetics, and in the paper and textile industries.²²

Phosphorylation reactions using oligophosphates, the conjugate bases of polyphosphoric acids, to produce phosphoester linkages^{12,23} have been extended in recent years, with particular focus on the trimetaphosphate trianion or its derivatives which incorporate some P(V) centers derived from phosphoric acid.²⁴ The sodium salt of trimetaphosphate is produced by dehydration of phosphoric acid in the presence of sodium chloride at 300 °C and is therefore a useful starting material for synthesis of phosphorus-containing compounds in a

manner that bypasses P₄.²⁵ The sodium cations can be exchanged for organic alternatives such as bis(triphenylphosphine)iminium ([PPN]⁺) or tetra-*n*-butylammonium ([TBA]⁺) which endow favorable solubility properties to the resulting salts in organic solvents. Taylor has disclosed the synthesis of nucleotide triphosphates using [TBA]₃[P₃O₉].2H₂O,²⁶ while our group has isolated a triphosphorylating agent from the reaction of [PPN]₃[P₃O₉] with the peptide coupling reagent PyAOP ([pyrr]₃PON₄C₅H₃][PF₆], pyrr = pyrrolidino, NC₄H₈, Figure 1.3), and used it to prepare trimetaphosphate derivatives of carbon, nitrogen, and oxygen-based nucleophiles.²⁷

Using the bis(trichlorosilyl)phosphide anion

In an effort to bypass white phosphorus and phosphorus(III) chloride in the synthesis of phosphorus-containing fine chemicals, we recently reported a method for preparing the bis(trichlorosilyl)phosphide anion directly from trimetaphosphate and trichlorosilane (Figure 1.4).^{28–32} The new compound was converted to other products such as phosphonium salts, primary phosphines, alkyl phosphinic acids, and phosphine (PH₃). One attractive aspect of the reducing agent, trichlorosilane, is that it is a high production volume chemical used to produce high purity silicon metal for use in photovoltaics. However, silicon (from which HSiCl₃ is commonly derived) is prepared by the reduction of silica in a process resembling the thermal process for phosphorus. Fortunately, exciting progress is being made toward the production of SiCl₄ and HSiCl₃ using redox-neutral or sustainable processes, respectively (Section 1.6).

In addition to trimetaphosphate, we also showed it is possible to prepare *n*-octylphosphine from *n*-octylchloride and crystalline phosphoric acid, via the same phosphide anion which is generated in situ by trichlorosilane (Figure 1.4).³³ Mass balance studies showed that the main byproducts of the reduction of phosphate sources with trichlorosilane were H₂ gas and chlorosiloxanes, such as O(SiCl₃)₂.³³

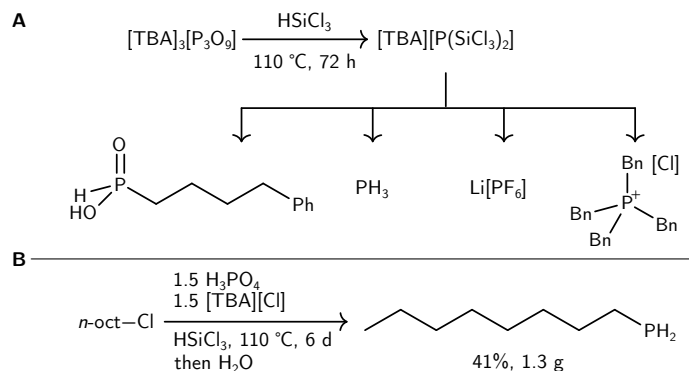


Figure 1.4 A: Preparation of [TBA]**1** from [TBA]₃[P₃O₉].2H₂O and trichlorosilane and subsequent conversion to phosphorus-containing products. **B:** One-pot synthesis of *n*-octylphosphine from *n*-octylchloride and phosphoric acid.

1.3 Phosphorus sustainability and stewardship

Methods for recovering phosphorus from waste

The phosphorus industry presents many opportunities for optimization under the guiding principles of Green Chemistry, particularly with regard to minimizing energy inputs and avoiding the use of toxic or hazardous intermediates. However, most of the opportunities for minimizing harm to the environment lie with phosphate pollution. As can be seen from the Sankey diagram (Figure 1.5), phosphorus is approximately evenly distributed between the natural and anthropogenic phosphorus cycles.³⁴ The latter has been described as a “broken cycle” because phosphate mining occurs on the order of Mt/y while the formation of new reserves occurs over thousands of millennia.⁵ Prior to large quantities of phosphate available from the wet process, phosphorus atoms would be cycled from the soil, to plants and animals, to manure, and back to the soil with high efficiency before substantial losses to surface body waters.³⁵ Nowadays, excessive application of phosphate fertilizers leads to substantial run-off into surface body waters and contributes to eutrophication.³⁶

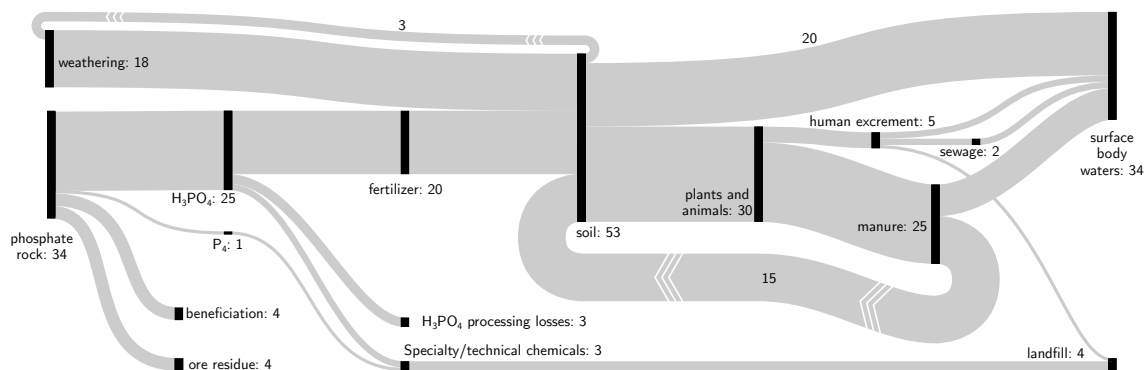


Figure 1.5 Sankey diagram depicting the global flows of phosphorus in 2011. Numbers refer to phosphorus flows in Mt/y. The values shown are adapted from the work of Scholz³⁴ which should be consulted for a detailed discussion of assumptions and errors. The numbers have uncertainties of approximately a factor of 2, and up to 5. Thus the diagram should be treated semi-qualitatively.

Another source of phosphate that contributes to eutrophication is sewage arising from human and animal excrement.³⁶ Not all sewage is processed and in some regions it proceeds directly to surface body waters without treatment. In places where waste-water treatment is practiced, there are obvious opportunities for recovering and recycling phosphorus. In several countries, legal limits on the concentration of phosphate in waste water have led to the adoption of processes for recovering phosphate. In Germany, a recent amendment requires recovery of 50% of the phosphorus from major sewage treatment plants.³⁷

A leading method for phosphate recovery is precipitation by the addition of magnesium salts to give struvite (magnesium ammonium phosphate, $\text{Mg}(\text{NH}_4)\text{PO}_4 \cdot 6\text{H}_2\text{O}$) which can be used as a slow release fertilizer. Struvite precipitation is practiced by at least forty

full-scale installations world-wide.³⁸ Two potential drawbacks of using struvite are (i) its direct contact with wastewater, raising concerns about the accumulation of pharmaceuticals and (ii) the accumulation of magnesium ions in soil where struvite is used extensively which could lead to fixation of subsequently dosed phosphate. At least with the former concern, Slootweg and coworkers have shown that bioaccumulation of micro-pollutants such as Ibuprofen in tomato crop fruit is of no significance toward human health concerns,³⁹ although investigations into other micro-pollutants and crops are necessary given the debate in the literature.⁴⁰ In part due to the low values for total phosphorus recovery by struvite precipitation (25–45%), other methods for removing phosphate from sewage sludge are under active investigation and involve extraction using carbon dioxide, mineral acids, or alkaline conditions.³⁸

A second method of phosphorus recovery involves incineration of sewage to produce sewage sludge ash (SSA). This produces a product with high phosphorus content and destroys organic pollutants, such as bacteria and drug residues.³⁸ Another advantage of the process is that the product is a dry powder, suitable for industrial recycling to phosphoric acid. Beginning in 2013, a variation on the wet process was adopted in Japan that uses phosphate rock blended with 2.5% SSA. This ratio is needed to guarantee the quality of both the phosphoric acid and the phosphogypsum products. The two main drivers for incorporating SSA into the process were cited as (i) minimizing risks associated with the volatility of phosphate rock price and (ii) recycling phosphate available from waste water treatment plants.⁴¹ In the Netherlands, a process for producing triple superphosphate fertilizer ($\text{Ca}(\text{H}_2\text{PO}_4)_2 \cdot \text{H}_2\text{O}$) allowed the ratio of SSA to phosphate rock to be pushed to 10%.³⁸ Extending the idea of using recycled phosphorus in known industrial processes, pilot studies are underway to produce white phosphorus from SSA in a process known as RecoPhos.⁴²

Biological processes for removing phosphate from sewage sludge are also under development. In a process known as Heatphos,⁴³ microorganisms capture phosphate and accumulate it in the form of polyphosphate (polyP), featuring phosphoanhydride bonds and chain lengths of up to 1000 residues.⁴⁴ In laboratory experiments, polyP is released from cells by heating to 70 °C for 1 h, and under these conditions shorter chains of polyP and species such as trimetaphosphate are detected.⁴⁵ Approximately 65% of the total phosphorus can be precipitated by the addition of CaCl_2 without adjusting the pH.⁴⁶ Interestingly, trimetaphosphate is not precipitated under these conditions, and remains soluble even up to a pH of 10. If trimetaphosphate could be separated from the mixture, it could have potential commercial value or be employed in chemical synthesis using known methods (Section 1.2). A pilot-scale plant study showed good assimilation (90–95%) of total phosphate intake by microorganisms, however the precipitation step using CaCl_2 led to recovery of only about 3% of P input,⁴⁷ although this could be improved to 40% by adjusting the pH.⁴⁸

Although recycling phosphorus from sewage presents a low barrier to entry, Scholz and Wellmer have identified significant waste of phosphorus before it enters either the

wet or thermal processes (Figure 1.5).⁴⁹ The two main mechanisms for these losses arise during mining and beneficiation. The former involves selecting rock of sufficient phosphorus content while the latter concerns upgrading of phosphate rock prior to processing in order to increase its economic value, principally via flotation. Scholz and Wellmer note these can be classed as *possible* or *delayed losses*, in theory recoverable if ore of lower phosphorus content becomes economically viable to extract in a future where highly concentrated reserves are exhausted.

Are phosphorus reserves running out?

The term “peak phosphorus” has been used to describe the phenomenon of phosphate rock production volumes reaching a maximum, resulting from exhaustion of high quality reserves.⁵⁰ Recent analysis suggests there are sufficient reserves for the next few centuries, although quality or accessibility will diminish (for example, low phosphorus content or located on the sea floor). On land, phosphate reserves are not geographically evenly distributed, with the majority of reserves concentrated in a handful of countries. As a result, 90% of countries are phosphate importers, and thus are not self sufficient for this resource.⁵ Recycling and re-use provides a domestic supply chain for phosphorus, desirable for food security. Therefore, the question of long term phosphate supply is perhaps of little consequence to the future of the phosphorus industry; moving to a circular phosphorus economy⁵¹ through decreased usage, increased recycling, and engaging in less energy-intensive processing methods all provide significant benefits independent of global supply.³⁷

A transition to phosphite?

A recent breakthrough in biotechnology has afforded GMO crops (soybeans, corn, cotton) to be developed that are capable of growth using phosphite, a phosphorus(III) compound, as fertilizer rather than the traditional phosphates.⁵²⁻⁵⁶ This has major implications for both controlling weeds and eliminating the water pollution that leads to eutrophication. Because only the GMO crops can grow on phosphite fertilizer, weed killers such as glyphosate are not needed to control weeds. Additionally, if there is rain and run-off, the non-GMO marine algae also cannot grow on the phosphite such that the marine ecosystems are protected from the harmful effects of algae blooms.

One potential drawback of this method is that under earth’s oxygen-rich atmosphere, phosphate is preferred thermodynamically over phosphite, and it is known that phosphite is oxidized naturally to phosphate either under atmospheric conditions or under the catalysis of microorganisms. Despite this, the method could still present an advantage because phosphite has the potential to be more easily sensed using devices due to its electrochemical response.⁵⁷ Thus, even if phosphite is eventually oxidized to phosphate, it would provide a source of fertilizer that could be accurately monitored in the short term and applied more strategically than is currently the case for phosphate fertilizers.

An issue hindering the implementation of such a process is the relatively high cost of phosphorous acid (H_3PO_3) and its derivatives, which are at present produced from P_4 (Figure 1.1). The development of scalable and efficient methods for producing phosphite from phosphate would therefore be desirable. Another strategy would be to recover phosphite from waste streams, such as those from electroless nickel plating.⁵⁸ At present, the P(III) waste from this process is chemically oxidized to phosphate and is not utilized further, although research is being conducted into the utilization of this phosphite waste in a biological setting.⁵⁹ Another source of phosphite waste is from PH_3 production from the reaction of P_4 with sodium hydroxide; the major byproduct of the reaction is hypophosphite ($[\text{H}_2\text{PO}_2]^-$), although some phosphite also forms (Scheme 1.1) and can be precipitated as the calcium salt.⁶⁰

1.4 P(III) compounds as the bottleneck

Phosphorus(III) chloride

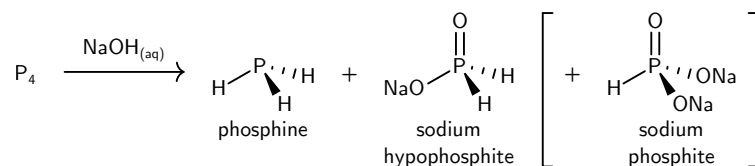
Phosphorus(III) chloride (PCl_3) is produced by the strongly exothermic reaction of P_4 with Cl_2 . The heat generated is sufficient to vaporize the PCl_3 which leads to its distillation and purification. Clearly, chemical energy is stored in the P–P and Cl–Cl bonds of the starting materials, energy that ultimately comes from the large scale industrial processes used for their production; the thermal process and the chloralkali processes, respectively. The oxidation states of phosphorus and chlorine in the starting materials are both zero, while in the product they are +3 and –1, respectively. Chloride exemplifies the only naturally occurring oxidation state of chlorine, while P(+3) is only two formal oxidation states away from naturally occurring phosphate (+5). With these considerations in mind, is it possible to design a process that minimizes redox reactions of the substituent atoms? If minimization of oxidation state change is considered a proxy for the energy requirements to produce a chemical, then such a process would be highly desirable.

This idea was investigated by Nordschild and Auner, who investigated the carbochlorination of calcium phosphate, $\text{Ca}_3(\text{PO}_4)_2$, with hydrogen chloride and carbon under microwave conditions. Phosphorus(III) chloride was collected in a cold trap and identified by its ^{31}P NMR chemical shift. The authors observed “white flashes”, attributed to electrical discharges or arcs, and assumed to be the reaction zones in which carbochlorination occurs. Further experiments for this interesting reaction are required analyze the efficiency of the inputs of microwave energy and the nature of reaction intermediates: do phosphorus-containing species in an oxidation state lower than +3 form? How much of the carbon reductant is converted to CO or CO_2 ?

Besides this report, processes that lead from a phosphate source to PCl_3 omitting the intermediacy of white phosphorus are scarce. However, clues as to how such a transformation could be achieved may lie in chemistry that is being actively developed for upgrading silicates and silica to silicon-containing chemicals of industrial importance (Section 1.6).

Phosphine (PH₃)

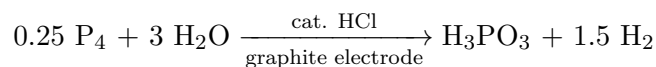
Phosphine is used for the synthesis of alkyl phosphines by the atom-efficient hydrophosphination of olefins. Phosphine itself is produced by oxidation of P₄ using sodium hydroxide, a process that also results in the formation of hypophosphite ([H₂PO₂]⁻) and phosphite (HPO₃²⁻) as byproducts (Scheme 1.1).⁶¹ The use of phosphine as opposed to PCl₃ for the synthesis of organophosphorus compounds is beneficial from a waste perspective because it does not result in stoichiometric halogen-containing byproducts. However, PH₃ does not offer access to product classes such as arylphosphines.²² Additionally, the control of product distribution between mono-, di-, and trialkylphosphines represents a difficulty as a result of the presence of three P–H bonds in PH₃.²² The major other phosphorus-containing product, hypophosphite, has been pioneered by Montchamp as an alternative reagent in synthesis that ordinarily requires PCl₃.^{62,63}



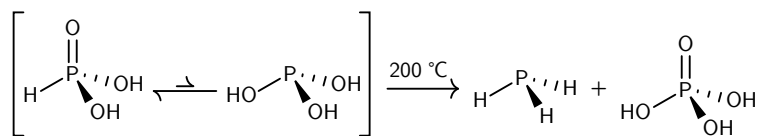
Scheme 1.1 Preparation of PH₃, NaH₂PO₂, and Na₂HPO₃ (minor byproduct).

Phosphorous acid (H₃PO₃) and its derivatives

Phosphorous acid (H₃PO₃), its conjugate base phosphite ([HPO₃]²⁻), and their many organic derivatives are typical phosphorus compounds in the +3 oxidation state (Scheme 1.2 shows the tautomerization between pentavalent and trivalent isomers). Although phosphite bears a simple relationship to phosphate by the subtraction of a single oxygen atom, production of phosphorous acid passes through the intermediacy of white phosphorus. The original industrial synthesis involved the hydrolysis of PCl₃, producing large quantities of HCl as a waste byproduct that presents disposal issues. In 1977, Monsanto disclosed a synthesis in which white phosphorus is subjected to electrolytic oxidation in the presence of an aqueous acid such as hydrogen chloride.⁶⁴ Concomitant H₂ gas formation leads to a net chemical reaction that does not produce hydrogen chloride waste:



The inorganic species phosphorous acid and phosphite find some direct applications, for example in the form of lead phosphite as a stabilizer for polyvinyl chloride. However, it is their organic derivatives, organophosphites, that are of notable use in chemical synthesis. Triorganophosphites (P(OR)₃) are the key reagents in the robust Arbuzov reaction⁶⁵ while diorganophosphites (HP(O)(OR)₂) are used to produce phosphonates by hydrophos-



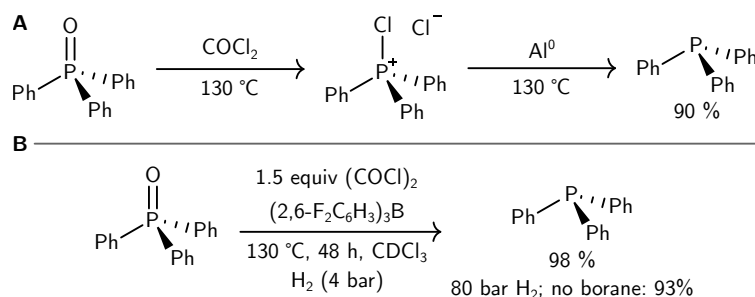
Scheme 1.2 Thermal decomposition of phosphorous acid to phosphine and phosphoric acid. In brackets: tautomerization of phosphorous acid between the pentavalent and trivalent isomers.

phonylation.⁶⁶ Organophosphites are derived from PCl_3 , and so their syntheses entail the stoichiometric formation of HCl . Methods to prepare organophosphites directly from P(V) precursors or at least from phosphorus acid (thereby bypassing PCl_3) would represent an advance by phosphorus sustainability standards, and would furnish products for which the chemistry for further functionalization has already been well established. Furthermore, procedures are known for the disproportionation of phosphorous acid to phosphine (PH_3) and phosphoric acid (Scheme 1.2) by heating to $200\text{ }^\circ\text{C}$.⁶⁷

P(V) to P(III) recycling in chemical synthesis

The case made thus far entails elimination of P_4 and PCl_3 in the synthesis of phosphorus-containing chemicals. However, another aspect of phosphorus sustainability that offers an opportunity for improvement is recycling chemicals that already contain phosphorus. Organophosphorus compounds such as triphenylphosphine are used in chemical synthesis as stoichiometric reagents, for example in the Wittig or Mitsunobu reactions, where a common theme is the formation of a strong $\text{P}=\text{O}$ double bond as a thermodynamic driving force. Therefore, an economically feasible method for the reduction of triphenylphosphine oxide back to triphenylphosphine has the potential to minimize waste. BASF achieved this by chlorination of Ph_3PO with phosgene to Ph_3PCl_2 , followed by reduction using aluminum metal at $130\text{ }^\circ\text{C}$ (Scheme 1.3).⁶⁸ In an effort to avoid the use of high temperatures and phosgene (which is toxic and gives CO_2 as a byproduct of the chlorination reaction), electrochemical methods for the reduction of triphenylphosphine oxide to triphenylphosphine are under active investigation.⁶⁹ Interested in utilizing H_2 as the reducing agent, Frustrated Lewis Pair (FLP) catalysis enabled the reduction of triphenylphosphine oxide to triphenylphosphine in the presence of H_2 (4 bar) and oxalyl chloride (Scheme 1.3).⁷⁰ Remarkably, increasing the pressure of H_2 (80 bar) led to a variant of the reaction in which the borane component was not required and triphenylphosphine could be obtained in 93% yield.

In addition to stoichiometric recycling, a complementary approach is the use of organophosphorus catalysts, in conjunction with sustainable stoichiometric reducing agents.⁷¹ Such efforts have been disclosed for several classes of organic reactions that typically generate stoichiometric quantities of phosphine oxides, such as the Wittig,⁷² Aza-Wittig,⁷³ Mitsunobu,⁷⁴ Appel,⁷⁵ and Staudinger⁷⁶ reactions, as well as several others.⁷⁷



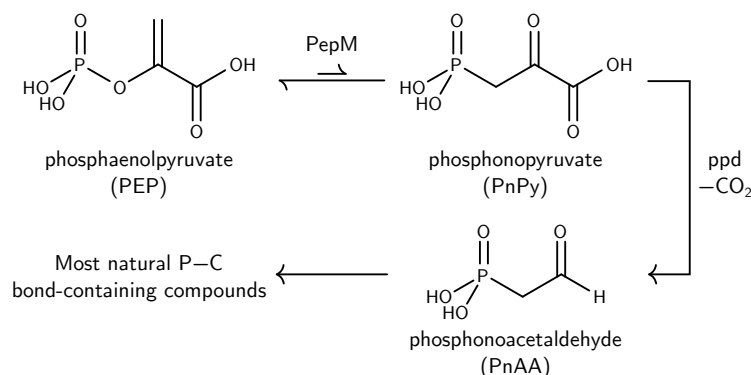
Scheme 1.3 Stoichiometric reductions of triphenylphosphine oxide to triphenylphosphine.

1.5 How does biology make phosphorus-carbon bonds?

Assimilation of inorganic phosphate

The wet process strategy of lowering pH to access otherwise insoluble phosphate is, of course, predated by nature. Phosphate solubilizing bacteria (PSB) achieve uptake of phosphate by the release of small molecular weight organic acids, such as citric or lactic acid.⁷⁸ These acids improve phosphate solubility by lowering the pH of the soil and by chelation of metal cations such as Ca^{2+} or Mg^{2+} . In addition to providing inspiration for our own methods of processing phosphate, PSB are also being investigated as biofertilizers that could lead to decreased application of synthetic fertilizers.⁷⁹

Phosphoenolpyruvate as the entryway



Scheme 1.4 Biosynthesis of phosphorus-carbon bonds. See text for abbreviations.

Natural product biosynthesis is a proven source of inspiration for reaction discovery. So how do P–C bonds form in nature? The key phosphorus-carbon bond-containing compounds in biology are phosphonates (RPO_3H_2), typically used by nature as antibacterial

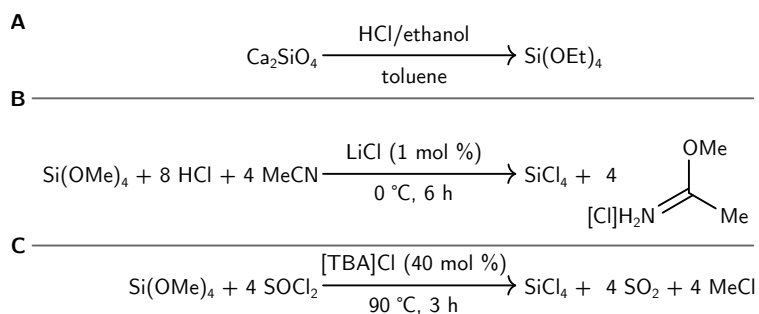
agents. The starting point for biological P–C bond-formation (Scheme 1.4) is phosphoenolpyruvate (PEP), widely available in cells as a key biological intermediate in the glycolysis metabolic pathway for adenosine triphosphate (ATP) biosynthesis. PEP is reversibly converted to phosphonopyruvate (PnPy) by the enzyme PEP mutase (PepM), which features a magnesium(II) ion in the active site and is thought to operate through a metaphosphate reactive intermediate.⁸⁰ Although the thermodynamic equilibrium between PEP and PnPy lies far toward PEP, probably a result of the strong P–O bond, nature overcomes this thermodynamic issue by linking P–C bond formation to a second, irreversible, decarboxylation event in which PnPy is converted by phosphonopyruvate decarboxylase (ppd) to phosphonoacetaldehyde (PnAA) which serves as a key intermediate to numerous P–C bond-containing compounds via subsequent functionalization.⁸¹

Linking biological intermediates to chemical synthesis, a recent study employed the potassium salt of PEP in conjunction with [TBA]HSO₄ as a catalyst for the phosphorylation of alcohols to give phosphate esters.⁸² Currently, commercially available PEP is accessed using chemistry derived from P₄. If obtained instead using enzymatic methods⁸³ or via reactions starting from wet-process P(V) precursors, this would constitute a method for the synthesis of phosphate esters in a manner that avoids reduction of phosphorus from its preferred oxidation state of +5.

1.6 Lessons from Group 14

Redox-neutral processing of silicate minerals to silicon(IV) chloride

Silicon also enters commercial products through the intermediacy of the elemental form, the production of which is analogous to the thermal process for obtaining white phosphorus. Industrially important silicon-containing polymers can be produced from chlorosilanes such as SiCl₄ and so the same arguments around redox-neutral processing can be made for both silicon and phosphorus.⁸⁴



Scheme 1.5 Examples of redox-neutral reactions using silicon(IV) compounds.

With these goals in mind, Goodman and Kenney showed in 1988 that tetraethoxysilane

(Si(OEt)₄, TEOS) could be obtained by treating silicate-containing minerals with ethanolic hydrogen chloride (Scheme 1.5).^{85,86} More recently, Choi described the preparation of TEOS from silica and ethanol, using molecular sieves to drive the dehydration reaction to completion.⁸⁷ The molecular sieves could be reactivated by heating (300 °C, 15 h), allowing the reaction to be cycled six times with no loss to the TEOS yield. Furthermore, rice hull ash (RHA), a product of agricultural rice production, could also be used as the source of silica to give TEOS in 60% yield. Further improvements to the procedure involve use of calcium oxide instead of molecular sieves as the desiccant, resulting in the formation of Ca(OH)₂.⁸⁸ A full technoeconomic and environmental assessment suggest the new procedure could result in a reduction of 7% to production costs and 34% to green house gas (GHG) emissions if the new process were implemented.⁸⁸

Tetraalkylsilanes such as TEOS are important chemical feedstocks for a variety of zeolites, ceramics, and silica based organic-inorganic hybrid materials. Industrially, they are produced from SiCl₄ and an alcohol, with the liberation of HCl. Researchers at Dow have taken steps toward producing SiCl₄ in a redox-neutral process by using tetraalkoxysilanes as their starting point. A first report dealt with the production of SiCl₄ from tetramethoxysilane (Si(OMe)₄, TMOS) and HCl, in the presence of lithium chloride as a catalyst.⁸⁹ Acetonitrile and additional equivalents of HCl were required in order to trap the methanol byproduct as an imidate salt and prevent its back reaction with SiCl₄ (Scheme 1.5). Using this procedure, the reported yield of SiCl₄ was 99%, as determined by ²⁹Si NMR spectroscopy.

In a second report, the chlorination reagent was changed from hydrogen chloride to thionyl chloride.⁹⁰ Thionyl chloride has several advantages over HCl; it can be used in smaller excess, it is easier to handle, and the absence of protons reduces the likelihood of condensing orthosilicates. A catalytic amount of a chloride salt such as tetra-*n*-butylammonium chloride was required for the success of the reaction, intended to activate the tetraalkoxysilane toward reaction with SOCl₂ by forming a hypervalent anionic silicon species. The main byproducts of the reaction are SO₂ and chloromethane, the latter being potentially recyclable to produce other useful silicone products via the Direct Process.⁹¹

Diverging requirements for elemental P vs. Si

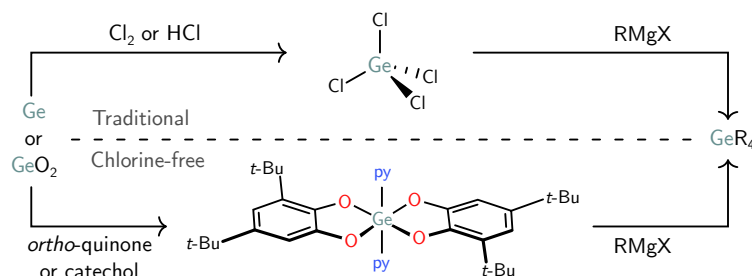
Despite the similarities between the industrial processes for obtaining elemental silicon and phosphorus, a key difference is the subsequent applications of the two products. Elemental silicon has large scale applications in the photovoltaics and electronics industries. Elemental phosphorus, on the other hand, has no major direct applications and is instead converted to compounds such as PCl₃ or H₃PO₃. Thus, elemental silicon can be regarded as an industrial product whereas elemental phosphorus is an intermediate. As such, there is no non-military requirement for P₄ production, should alternative methods utilizing phosphate become available. Elemental silicon, however, will continue to be required in a future that is increasingly reliant on solar electricity. This has spurred research into the production of

elemental silicon using green methods, such as electrochemical reduction of silica,⁹² or by the reduction of recycled SiCl₄ with sustainably generated H₂, through the intermediacy of HSiCl₃.^{93,94}

Towards chlorine-free processing of elements

A chlorine-free protocol for processing germanium was reported in 2017.⁹⁵ Treatment of germanium dioxide or germanium metal with either a catechol or ortho-quinone, respectively, led to the formation of germanium(IV) bis(catecholates), supported by two pyridine ligands (Scheme 1.6). The catecholate groups could be replaced with carbon-based nucleophiles to prepare tetraorganogermanes (GeR₄) in good yields (>91%). The argument made for processing germanium in a chlorine-free manner can also be applied to phosphorus or indeed any element chloride: Cl₂ is a highly toxic substance, is corrosive toward many materials, and is derived from an energy-intensive process. Additionally, the germanium(IV) bis(catecholates) are bench stable solids, while germanium tetrachloride is a moisture and air-sensitive liquid that produces HCl upon hydrolysis. Thus, the use of comparatively stable germanium catecholates represents an advance in terms of toxicity and potential for harm to the environment. Another benefit of the reported procedure was the use of mechanochemistry to perform the reactions, a methodology of growing interest due to low solvent usage, scalability, and fast reaction times.⁹⁶

One challenge posed by the objective of replacing chloride for organooxy groups in element processing is the relatively low cost of the halides. In this regard, future success on a large scale is likely to be met where the organic group is cheap and abundant, for example methyl, ethyl, or phenyl.



Scheme 1.6 A chlorine-free protocol for processing germanium.

Developing chlorine-free protocols for processing white phosphorus has been an active area of research for decades,^{97–101} and exciting new reactions are still emerging.^{102–104} The recent stabilization of white phosphorus in activated carbon¹⁰⁵ raises the possibility of decreasing the hazards associated with this pyrophoric intermediate, which is likely to feature in chemical synthesis for some time to come.

1.7 Outlook: challenges and opportunities

Clearly, there are many aspects of phosphorus chemistry that could be improved, as judged from the perspective of green chemistry. Here, we lay out some of the key challenges and opportunities for synthetic chemists.

1. **Develop selective reductions from P(V) to P(III).** While these are known for the reduction of organic molecules (e.g. OPPh_3 to PPh_3), selective reductions of inorganic P(V) to P(III) compounds are scarce. A selective reduction of phosphate to phosphite has the potential to make white phosphorus obsolete and minimize halogen-containing waste in the production of phosphorus-containing chemicals.
2. **Use of electrochemical methods for phosphate reduction.** Ideally, reduction of phosphate would be performed electrochemically where electricity can be supplied sustainably and the half reaction corresponding to phosphate reduction is balanced by the formation of O_2 from water oxidation.
3. **Use of renewable sources of phosphorus in chemical synthesis.** Such products include struvite, sewage sludge ash, or materials obtained from biological extraction processes such as polyphosphates.

If met, overcoming these challenges would provide the following opportunities:

1. **Decreased energy consumption and CO_2 emissions.** The thermal process requires large inputs of costly electricity. The chemistry of the thermal process requires the oxidation of carbon, eventually to CO_2 , a greenhouse gas.
2. **Extraction of phosphate rock is minimized.** Phosphate rock is considered a non-renewable resource over very long timescales. Over short timescales, recycling of phosphorus materials minimizes supply risks.
3. **Transition to a “circular” or “conical” phosphorus economy.** Waste products such as phosphogypsum are minimized, leading to reduced processing costs and potential for harm to the environment. The term “conical economy” refers to a circular economy that emphasizes reducing the consumptive footprint of the value chain, i.e. a circle with a smaller diameter.¹⁰⁶
4. **Discovery of new methods in organophosphorus chemistry.** Reaction discovery has the potential to increase “chemical space” among phosphorus compounds, which are important herbicides and pharmaceutical agents.
5. **Application of discoveries to other elements.** In the same way that the chemistry of silicon can shape a greener phosphorus industry, findings made as a result of research into phosphorus chemistry may have the ability to symbiotically improve the processing of other element oxides, such as those of silicon, boron, and germanium.

References

- [1] Greenwood, N. N.; Earnshaw, A. *Chemistry of the elements*, 2nd ed.; Butterworth-Heinemann,: Boston, Mass., 1997.
- [2] Jones, J. L.; Yingling, Y. G.; Reaney, I. M.; Westerhoff, P. *MRS Bulletin* **2020**, *45*, 7–10.
- [3] Withers, P. J. A.; Elser, J. J.; Hilton, J.; Ohtake, H.; Schipper, W. J.; Dijk, K. C. v. *Green Chem.* **2015**, *17*, 2087–2099.
- [4] Anastas, P. T.; Warner, J. C. *Green chemistry: theory and practice*, 1st ed.; Oxford Univ. Press: Oxford, 2000.
- [5] Ohtake, H., Tsuneda, S., Eds. “Foreword” by Scholz, R. in *Phosphorus Recovery and Recycling*; Springer: Singapore, 2019.
- [6] Cummins, C. C. *Daedalus* **2014**, *143*, 9–20.
- [7] Schipper, W. *Eur. J. Inorg. Chem.* **2014**, *2014*, 1567–1571.
- [8] Nehb, W.; Vydra, K. “Sulfur” in *Ullmann’s Encyclopedia of Industrial Chemistry*; Wiley, 2006.
- [9] Müller, H. “Sulfuric Acid and Sulfur Trioxide” in *Ullmann’s Encyclopedia of Industrial Chemistry*; Wiley, 2000.
- [10] Emsley, J. *The 13th element: the sordid tale of murder, fire and phosphorus*; Wiley: New York, 2000.
- [11] Diskowski, H.; Hofmann, T. “Phosphorus” in *Ullmann’s Encyclopedia of Industrial Chemistry*; Wiley, 2000.
- [12] (a) Cherbuliez, E.; Leber, J.-P. *Helv. Chim. Acta* **1952**, *35*, 644–664; (b) Cherbuliez, E.; Rabinowitz, J. *Helv. Chim. Acta* **1956**, *39*, 1455–1461; (c) Cherbuliez, E.; Rabinowitz, J. *Helv. Chim. Acta* **1958**, *41*, 1168–1175; (d) Long, R. F.; Morrison, A. L. *J. Chem. Soc.* **1954**, 3854–3856.
- [13] (a) Hall, R. H.; Khorana, H. G. *J. Am. Chem. Soc.* **1954**, *76*, 5056–5060; (b) Smith, M.; Khorana, H. G. *J. Am. Chem. Soc.* **1958**, *80*, 1141–1145.
- [14] Sakakura, A.; Katsukawa, M.; Ishihara, K. *Angew. Chem., Int. Ed.* **2007**, *46*, 1423–1426.
- [15] Sakakura, A.; Katsukawa, M.; Ishihara, K. *Org. Lett.* **2005**, *7*, 1999–2002.
- [16] Sakakura, A.; Katsukawa, M.; Hayashi, T.; Ishihara, K. *Green Chem.* **2007**, *9*, 1166–1169.
- [17] Dueymes, C.; Pirat, C.; Pascal, R. *Tetrahedron Lett.* **2008**, *49*, 5300–5301.
- [18] Lira, L. M.; Vasilev, D.; Pilli, R. A.; Wessjohann, L. A. *Tetrahedron Lett.* **2013**, *54*, 1690–1692.
- [19] (a) Shen, L.; Leng, Y.; Wang, J.; Ren, X.; Wu, Y.; Zhang, M.; Xu, Y. *Chin. J. Catal.* **2010**, *31*, 156–162; (b) Miao, H.; Xu, X.; Ju, W.-W.; Wan, H.-X.; Zhang, Y.; Zhu, D.-R.; Xu, Y. *Inorg. Chem.* **2014**, *53*, 2757–2759; (c) Liang, J.; Hu, X.; Wang, J.; Ren, X.; Yang, X.; Zhu, J. *Catal. Commun.* **2015**, *69*, 174–178; (d) Miao, H.; Hu, G.; Guo, J.; Wan, H.; Mei, H.; Zhang, Y.; Xu, Y. *Dalton Trans.* **2015**, *44*, 694–700.

- [20] Gilmour, R. *“Polyphosphoric Acid” in Phosphoric acid: purification, uses, technology, and economics*; CRC Press/Taylor & Francis: Boca Raton, FL, 2014.
- [21] (a) Popp, F. D.; McEwen, W. E. *Chem. Rev.* **1958**, *58*, 321–401; (b) Popp, F. D.; McEwen, W. E. *Trans. Kans. Acad. Sci.* **1960**, *63*, 169–193.
- [22] Svara, J.; Weferling, N.; Hofmann, T. *“Phosphorus Compounds, Organic” in Ullmann’s Encyclopedia of Industrial Chemistry*; Wiley: Weinheim, Germany, 2006.
- [23] Azevedo, C.; Singh, J.; Steck, N.; Hofer, A.; Ruiz, F. A.; Singh, T.; Jessen, H. J.; Saiardi, A. *ACS Chem. Biol.* **2018**, *13*, 1958–1963.
- [24] (a) Singh, J.; Steck, N.; De, D.; Hofer, A.; Ripp, A.; Captain, I.; Keller, M.; Wender, P. A.; Bhandari, R.; Jessen, H. J. *Angew. Chem., Int. Ed.* **2019**, *58*, 3928–3933; (b) Singh, J.; Ripp, A.; Haas, T. M.; Qiu, D.; Keller, M.; Wender, P. A.; Siegel, J. S.; Baldrige, K. K.; Jessen, H. J. *J. Am. Chem. Soc.* **2019**, *141*, 15013–15017; (c) Bezdold, D.; Dürr, T.; Singh, J.; Jessen, H. J. *Chem. - Eur. J.* **2019**, *26*, 2298–2308.
- [25] Pham Minh, D.; Ramarosan, J.; Nzihou, A.; Sharrock, P. *Ind. Eng. Chem. Res.* **2012**, *51*, 3851–3854.
- [26] (a) Mohamady, S.; Taylor, S. D. *Org. Lett.* **2016**, *18*, 580–583; (b) Mohamady, S.; Taylor, S. D. *Tetrahedron Lett.* **2016**, *57*, 5457–5459.
- [27] Shepard, S. M.; Cummins, C. C. *J. Am. Chem. Soc.* **2019**, *141*, 1852–1856.
- [28] Geeson, M. B.; Cummins, C. C. *Science* **2018**, *359*, 1383–1385.
- [29] Protasiewicz, J. D. *Science* **2018**, *359*, 1333–1333.
- [30] Slootweg, J. C. *Angew. Chem.* **2018**, *130*, 6494–6496.
- [31] Slootweg, J. C. *Angew. Chem., Int. Ed.* **2018**, *57*, 6386–6388.
- [32] Swager, T. M.; Peeks, M. D. *Synfacts* **2018**, *14*, 592.
- [33] Geeson, M. B.; Ríos, P.; Transue, W. J.; Cummins, C. C. *J. Am. Chem. Soc.* **2019**, *141*, 6375–6384.
- [34] Scholz, R. W.; Roy, A. H.; Hellums, D. T. In *Sustainable Phosphorus Management: A Global Transdisciplinary Roadmap*; Scholz, R. W., Roy, A. H., Brand, F. S., Hellums, D. T., Ulrich, A. E., Eds.; Springer Netherlands: Dordrecht, 2014; pp 1–128.
- [35] King, F. H. *Farmers of forty centuries: organic farming in China, Korea, and Japan*; Dover Publications: Mineola, N.Y, 2004.
- [36] Filippelli, G. M. *Elements* **2008**, *4*, 89–95.
- [37] Scholz, R. W.; Wellmer, F. *J. Ind. Ecol.* **2019**, *23*, 313–318.
- [38] Schipper, W. In *“Success Factors for Implementing Phosphorus Recycling Technologies” in Phosphorus Recovery and Recycling*; Ohtake, H., Tsuneda, S., Eds.; Springer: Singapore, 2019; pp 101–130.
- [39] de Boer, M. A.; Hammerton, M.; Slootweg, J. C. *Water Res.* **2018**, *133*, 19–26.
- [40] (a) Chen, Q.-L.; An, X.-L.; Zhu, Y.-G.; Su, J.-Q.; Gillings, M. R.; Ye, Z.-L.; Cui, L. *Environ. Sci. Technol.* **2017**, *51*, 8149–8157; (b) de Boer, M. A.; Kabbe, C.; Slootweg, J. C. *Environ. Sci. Technol.* **2018**, *52*, 14564–14565.

- [41] Mochiyama, T. In “*Industrial-Scale Manufacturing of Phosphoric Acid Using Sewage Sludge Ash*” in *Phosphorus Recovery and Recycling*; Ohtake, H., Tsuneda, S., Eds.; Springer: Singapore, 2019; pp 133–142.
- [42] Langeveld, K. In “*Phosphorus Recovery into Fertilizers and Industrial Products by ICL in Europe*” in *Phosphorus Recovery and Recycling*; Ohtake, H., Tsuneda, S., Eds.; Springer: Singapore, 2019; pp 235–252.
- [43] Takiguchi, N.; Kuroda, A.; Ohtake, H.; Tsuneda, S. In “*Heatphos Process for Recovering Phosphorus from Bio-P Sludge Before Anaerobic Digestion*” in *Phosphorus Recovery and Recycling*; Ohtake, H., Tsuneda, S., Eds.; Springer: Singapore, 2019; pp 515–526.
- [44] (a) Kulaev, I. S.; Vagabov, V. M. *Adv. Microb. Physiol.* **1983**, *24*, 83–171; (b) Kornberg, A. *J. Bacteriol.* **1995**, *177*, 491–496.
- [45] (a) Kuroda, A.; Takiguchi, N.; Gotanda, T.; Nomura, K.; Kato, J.; Ikeda, T.; Ohtake, H. *Biotechnol. Bioeng.* **2002**, *78*, 333–338; (b) Kashihara, H.; Kang, B. M.; Omasa, T.; Honda, K.; Sameshima, Y.; Kuroda, A.; Ohtake, H. *Biosci., Biotechnol., Biochem.* **2010**, *74*, 865–868.
- [46] Takiguchi, N.; Kishino, M.; Kuroda, A.; Kato, J.; Ohtake, H. *J. Biosci. Bioeng.* **2004**, *97*, 365–368.
- [47] Takiguchi, N.; Kuroda, A.; Kato, J.; Nukanobu, K.; Ohtake, H. *J. Chem. Eng. Jpn.* **2003**, *36*, 1143–1146.
- [48] Hirota, R.; Kuroda, A.; Kato, J.; Ohtake, H. *J. Biosci. Bioeng.* **2010**, *109*, 423–432.
- [49] Scholz, R. W.; Wellmer, F.-W. *Resour., Conserv. Recycl.* **2015**, *105*, 216–234.
- [50] (a) Cordell, D.; Drangert, J.-O.; White, S. *Glob. Environ. Change* **2009**, *19*, 292–305; (b) Cordell, D.; White, S. *Sustainability* **2011**, *3*, 2027–2049.
- [51] Keijer, T.; Bakker, V.; Slootweg, J. C. *Nat. Chem.* **2019**, *11*, 190–195.
- [52] López-Arredondo, D. L.; Herrera-Estrella, L. *Nat. Biotechnol.* **2012**, *30*, 889–893.
- [53] Pandeya, D.; López-Arredondo, D. L.; Janga, M. R.; Campbell, L. M.; Estrella-Hernández, P.; Bagavathiannan, M. V.; Herrera-Estrella, L.; Rathore, K. S. *Proc. Natl. Acad. Sci. U. S. A.* **2018**, *115*, E6946–E6955.
- [54] Catalá, R.; Salinas, J. *Proc. Natl. Acad. Sci. U. S. A.* **2018**, *115*, 7456–7458.
- [55] Achary, V. M. M.; Ram, B.; Manna, M.; Datta, D.; Bhatt, A.; Reddy, M. K.; Agrawal, P. K. *Plant Biotechnol. J.* **2017**, *15*, 1493–1508.
- [56] Loera-Quezada, M. M.; Leyva-González, M. A.; López-Arredondo, D.; Herrera-Estrella, L. *Plant Sci.* **2015**, *231*, 124–130.
- [57] Franzini, V.; Fugivara, C.; Benedetti, A.; Ribeiro, C.; Cavalheiro, E.; Neto, J. *Electroanalysis* **2007**, *19*, 1794–1798.
- [58] (a) Kuroda, A.; Hirota, R. *Global Environ. Res.* **2019**, *19*, 77–82; (b) Morton, S. C.; Edwards, M. *Crit. Rev. Environ. Sci. Technol.* **2005**, *35*, 333–364.
- [59] Hirota, R.; Motomura, K.; Kuroda, A. In “*Biological Phosphite Oxidation and Its Application to Phosphorus Recycling*” in *Phosphorus Recovery and Recycling*; Ohtake, H., Tsuneda, S., Eds.; Springer: Singapore, 2019; pp 499–513.

- [60] Estes, W. E. Method to improve yields of sodium hypophosphite. 1985; US4552737A.
- [61] Bettermann, G.; Krause, W.; Riess, G.; Hofmann, T. "Phosphorus Compounds, Inorganic" in *Ullmann's Encyclopedia of Industrial Chemistry*; Wiley: Weinheim, Germany, 2000.
- [62] Depréle, S.; Montchamp, J.-L. *Org. Lett.* **2004**, *6*, 3805–3808.
- [63] (a) Dumond, Y. R.; Baker, R. L.; Montchamp, J.-L. *Org. Lett.* **2000**, *2*, 3341–3344; (b) Montchamp, J.-L.; Dumond, Y. R. *J. Am. Chem. Soc.* **2001**, *123*, 510–511; (c) Depréle, S.; Montchamp, J.-L. *J. Org. Chem.* **2001**, *66*, 6745–6755; (d) Depréle, S.; Montchamp, J.-L. *J. Am. Chem. Soc.* **2002**, *124*, 9386–9387; (e) Depréle, S.; Montchamp, J.-L. *J. Organomet. Chem.* **2002**, *643-644*, 154–163; (f) Ribiére, P.; Bravo-Altamirano, K.; Antczak, M. I.; Hawkins, J. D.; Montchamp, J.-L. *J. Org. Chem.* **2005**, *70*, 4064–4072; (g) Gouault-Bironneau, S.; Depréle, S.; Sutor, A.; Montchamp, J.-L. *Org. Lett.* **2005**, *7*, 5909–5912; (h) Bravo-Altamirano, K.; Montchamp, J.-L. *Org. Lett.* **2006**, *8*, 4169–4171; (i) Bravo-Altamirano, K.; Montchamp, J.-L. *Tetrahedron Lett.* **2007**, *48*, 5755–5759; (j) Coudray, L.; Abrunhosa-Thomas, I.; Montchamp, J.-L. *Tetrahedron Lett.* **2007**, *48*, 6505–6508; (k) Bravo-Altamirano, K.; Abrunhosa-Thomas, I.; Montchamp, J.-L. *J. Org. Chem.* **2008**, *73*, 2292–2301; (l) Bravo-Altamirano, K.; Coudray, L.; Deal, E. L.; Montchamp, J.-L. *Org. Biomol. Chem.* **2010**, *8*, 5541–5551; (m) Petit, C.; Fécourt, F.; Montchamp, J.-L. *Adv. Synth. Catal.* **2011**, *353*, 1883–1888; (n) Fisher, H. C.; Prost, L.; Montchamp, J.-L. *Eur. J. Org. Chem.* **2013**, *2013*, 7973–7978; (o) Coudray, L.; Montchamp, J.-L. *Eur. J. Org. Chem.* **2008**, *2008*, 4101–4103; (p) Montchamp, J.-L. *Phosphorus, Sulfur Silicon Relat. Elem.* **2013**, *188*, 66–75; (q) Montchamp, J.-L. *Acc. Chem. Res.* **2014**, *47*, 77–87; (r) Berger, O.; Montchamp, J.-L. *Org. Biomol. Chem.* **2016**, *14*, 7552–7562; (s) Berger, O.; Winters, K.; Sabourin, A.; V. Dzyuba, S.; Montchamp, J.-L. *Org. Chem. Front.* **2019**, *6*, 2095–2108; (t) Montchamp, J.-L. *Pure Appl. Chem.* **2019**, *91*, 113–120.
- [64] Dolan, M. J. Electrolytic preparation of phosphorus acid from elemental phosphorus. 1977.
- [65] Bhattacharya, A. K.; Thyagarajan, G. *Chem. Rev.* **1981**, *81*, 415–430.
- [66] Han, L.-B.; Tanaka, M. *J. Am. Chem. Soc.* **1996**, *118*, 1571–1572.
- [67] Gokhale, S. D.; Jolly, W. L.; Thomas, S.; Britton, D. "Phosphine" in *Inorganic Syntheses*; Wiley, 1967; pp 56–58.
- [68] Hermeling, D.; Bassler, P.; Hammes, P.; Hugo, R.; Lechtken, P.; Siegel, H. Preparation of triphenylphosphine. 1996; US5527966A.
- [69] (a) Yanilkin, V. V.; Gromakov, Y. S.; Nigmatzyanov, F. F. *Russ. Chem. Bull.* **1996**, *45*, 1257–1258; (b) Elias, J. S.; Costentin, C.; Nocera, D. G. *J. Am. Chem. Soc.* **2018**, *140*, 13711–13718; (c) Manabe, S.; Wong, C. M.; Sevov, C. S. *J. Am. Chem. Soc.* **2020**, *142*, 3024–3031.
- [70] (a) Stepen, A. J.; Bursch, M.; Grimme, S.; Stephan, D. W.; Paradies, J. *Angew. Chem.*

- Int. Ed.* **2018**, *57*, 15253–15256; (b) Zhu, H.; Qu, Z.; Grimme, S. *Chem. Eur. J.* **2019**, *25*, 4670–4672.
- [71] (a) Voituriez, A.; Saleh, N. *Tetrahedron Lett.* **2016**, *57*, 4443–4451; (b) Guo, H.; Fan, Y. C.; Sun, Z.; Wu, Y.; Kwon, O. *Chem. Rev.* **2018**, *118*, 10049–10293.
- [72] (a) O'Brien, C. J.; Tellez, J. L.; Nixon, Z. S.; Kang, L. J.; Carter, A. L.; Kunkel, S. R.; Przeworski, K. C.; Chass, G. A. *Angew. Chem., Int. Ed.* **2009**, *48*, 6836–6839; (b) O'Brien, C. J. Catalytic Wittig and Mitsunobu Reactions. 2010; WO2010118042A2; (c) Fairlamb, I. J. S. *ChemSusChem* **2009**, *2*, 1021–1024; (d) Marsden, S. P. *Nature Chem* **2009**, *1*, 685–687; (e) O'Brien, C. J.; Lavigne, F.; Coyle, E. E.; Holohan, A. J.; Doonan, B. J. *Chem. - Eur. J.* **2013**, *19*, 5854–5858; (f) O'Brien, C. J.; Nixon, Z. S.; Holohan, A. J.; Kunkel, S. R.; Tellez, J. L.; Doonan, B. J.; Coyle, E. E.; Lavigne, F.; Kang, L. J.; Przeworski, K. C. *Chem. - Eur. J.* **2013**, *19*, 15281–15289; (g) Coyle, E. E.; Doonan, B. J.; Holohan, A. J.; Walsh, K. A.; Lavigne, F.; Krenske, E. H.; O'Brien, C. J. *Angew. Chem., Int. Ed.* **2014**, *53*, 12907–12911; (h) Werner, T.; Hoffmann, M.; Deshmukh, S. *Eur. J. Org. Chem.* **2014**, *2014*, 6630–6633; (i) Werner, T.; Hoffmann, M.; Deshmukh, S. *Eur. J. Org. Chem.* **2014**, *2014*, 6873–6876; (j) Hoffmann, M.; Deshmukh, S.; Werner, T. *Eur. J. Org. Chem.* **2015**, *2015*, 4532–4543; (k) Werner, T.; Hoffmann, M.; Deshmukh, S. *Eur. J. Org. Chem.* **2015**, *2015*, 3286–3295; (l) Rommel, S.; Belger, C.; Begouin, J.-M.; Plietker, B. *ChemCatChem* **2015**, *7*, 1292–1301; (m) Schirmer, M.-L.; Adomeit, S.; Werner, T. *Org. Lett.* **2015**, *17*, 3078–3081; (n) Tsai, Y.-L.; Lin, W. *Asian J. Org. Chem.* **2015**, *4*, 1040–1043; (o) Schirmer, M.-L.; Adomeit, S.; Spannenberg, A.; Werner, T. *Chem. - Eur. J.* **2016**, *22*, 2458–2465; (p) Lee, C.-J.; Chang, T.-H.; Yu, J.-K.; Madhusudhan Reddy, G.; Hsiao, M.-Y.; Lin, W. *Org. Lett.* **2016**, *18*, 3758–3761; (q) Saleh, N.; Voituriez, A. *J. Org. Chem.* **2016**, *81*, 4371–4377; (r) Saleh, N.; Blanchard, F.; Voituriez, A. *Adv. Synth. Catal.* **2017**, *359*, 2304–2315; (s) Wang, L.; Sun, M.; Ding, M.-W. *Eur. J. Org. Chem.* **2017**, *2017*, 2568–2578; (t) Zhang, K.; Cai, L.; Yang, Z.; Houk, K. N.; Kwon, O. *Chem. Sci.* **2018**, *9*, 1867–1872; (u) Lorton, C.; Castanheiro, T.; Voituriez, A. *J. Am. Chem. Soc.* **2019**, *141*, 10142–10147.
- [73] (a) van Kalker, H. A.; Grotenhuis, C. t.; Haasjes, F. S.; Hommersom, C. R. A.; Rutjes, F. P. J. T.; Delft, F. L. v. *Eur. J. Org. Chem.* **2013**, *2013*, 7059–7066; (b) Wang, L.; Wang, Y.; Chen, M.; Ding, M.-W. *Adv. Synth. Catal.* **2014**, *356*, 1098–1104; (c) Abed, H. B.; Mammoliti, O.; Bande, O.; Lommen, G. V.; Herdewijn, P. *Org. Biomol. Chem.* **2014**, *12*, 7159–7166; (d) Wang, L.; Xie, Y.-B.; Huang, N.-Y.; Yan, J.-Y.; Hu, W.-M.; Liu, M.-G.; Ding, M.-W. *ACS Catal.* **2016**, *6*, 4010–4016.
- [74] (a) Buonomo, J. A.; Aldrich, C. C. *Angew. Chem., Int. Ed.* **2015**, *54*, 13041–13044; (b) Hirose, D.; Gazvoda, M.; Košmrlj, J.; Taniguchi, T. *Org. Lett.* **2016**, *18*, 4036–4039; (c) Beddoe, R. H.; Andrews, K. G.; Magné, V.; Cuthbertson, J. D.; Saska, J.; Shannon-Little, A. L.; Shanahan, S. E.; Sneddon, H. F.; Denton, R. M. *Science* **2019**, *365*, 910–914.
- [75] (a) van Kalker, H. A.; Leenders, S. H. A. M.; Hommersom, C. R. A.; Rutjes, F. P.

- J. T.; van Delft, F. L. *Chem. - Eur. J.* **2011**, *17*, 11290–11295; (b) van Kalkerren, H. A.; van Delft, F. L.; Rutjes, F. P. J. T. *Pure Appl. Chem.* **2012**, *85*, 817–828.
- [76] (a) van Kalkerren, H. A. v.; Bruins, J. J.; Rutjes, F. P. J. T.; Delft, F. L. v. *Adv. Synth. Catal.* **2012**, *354*, 1417–1421; (b) Lenstra, D. C.; Wolf, J. J.; Mecinović, J. *J. Org. Chem.* **2019**, *84*, 6536–6545.
- [77] (a) Harris, J. R.; Haynes, M. T.; Thomas, A. M.; Woerpel, K. A. *J. Org. Chem.* **2010**, *75*, 5083–5091; (b) Kosal, A. D.; Wilson, E. E.; Ashfeld, B. L. *Angew. Chem., Int. Ed.* **2012**, *51*, 12036–12040; (c) Li, Y.; Lu, L.-Q.; Das, S.; Pisiewicz, S.; Junge, K.; Beller, M. *J. Am. Chem. Soc.* **2012**, *134*, 18325–18329; (d) Lenstra, D. C.; Rutjes, F. P. J. T.; Mecinović, J. *Chem. Commun.* **2014**, *50*, 5763; (e) Reichl, K. D.; Dunn, N. L.; Fastuca, N. J.; Radosevich, A. T. *J. Am. Chem. Soc.* **2015**, *137*, 5292–5295; (f) Zhao, W.; Yan, P. K.; Radosevich, A. T. *J. Am. Chem. Soc.* **2015**, *137*, 616–619; (g) Fourmy, K.; Voituriez, A. *Org. Lett.* **2015**, *17*, 1537–1540; (h) Nykaza, T. V.; Harrison, T. S.; Ghosh, A.; Putnik, R. A.; Radosevich, A. T. *J. Am. Chem. Soc.* **2017**, *139*, 6839–6842; (i) Nykaza, T. V.; Cooper, J. C.; Li, G.; Mahieu, N.; Ramirez, A.; Luzung, M. R.; Radosevich, A. T. *J. Am. Chem. Soc.* **2018**, *140*, 15200–15205; (j) Nykaza, T. V.; Ramirez, A.; Harrison, T. S.; Luzung, M. R.; Radosevich, A. T. *J. Am. Chem. Soc.* **2018**, *140*, 3103–3113; (k) Lecomte, M.; Lipshultz, J. M.; Kim-Lee, S.-H.; Li, G.; Radosevich, A. T. *J. Am. Chem. Soc.* **2019**, *141*, 12507–12512; (l) Ghosh, A.; Lecomte, M.; Kim-Lee, S.-H.; Radosevich, A. T. *Angew. Chem., Int. Ed.* **2019**, *58*, 2864–2869; (m) Nykaza, T. V.; Li, G.; Yang, J.; Luzung, M. R.; Radosevich, A. T. *Angew. Chem., Int. Ed.* **2020**, *59*, 4505–4510; (n) Longwitz, L.; Werner, T. *Angew. Chem., Int. Ed.* **2020**, *59*, 2760–2763.
- [78] Chen, Y. P.; Rekha, P. D.; Arun, A. B.; Shen, F. T.; Lai, W. A.; Young, C. C. *Applied Soil Ecology* **2006**, *34*, 33–41.
- [79] Rodríguez, H.; Fraga, R. *Biotechnol. Adv.* **1999**, *17*, 319–339.
- [80] (a) Liu, S.; Lu, Z.; Jia, Y.; Dunaway-Mariano, D.; Herzberg, O. *Biochemistry* **2002**, *41*, 10270–10276; (b) Xu, D.; Guo, H. *J. Phys. Chem. B* **2008**, *112*, 4102–4108.
- [81] Peck, S. C.; van der Donk, W. A. *Curr. Opin. Chem. Biol.* **2013**, *17*, 580–588.
- [82] Domon, K.; Puripat, M.; Fujiyoshi, K.; Hatanaka, M.; Kawashima, S. A.; Yamatsugu, K.; Kanai, M. *ACS Cent. Sci.* **2020**, *6*, 283–292.
- [83] Mattoo, R. L.; Waygood, E. B. *Anal. Biochem.* **1983**, *128*, 245–249.
- [84] Furgal, J. C.; Lenora, C. U. *Physical Sciences Reviews* **2020**, *5*.
- [85] Kenney, M. E.; Goodwin, G. B. Silicate esters and organosilicon compounds. 1988; US4717773A.
- [86] Goodwin, G. B.; Kenney, M. E. *Inorg. Chem.* **1990**, *29*, 1216–1220.
- [87] Fukaya, N.; Jib Choi, S.; Horikoshi, T.; Kataoka, S.; Endo, A.; Kumai, H.; Hasegawa, M.; Sato, K.; Choi, J.-C. *New J. Chem.* **2017**, *41*, 2224–2226.
- [88] Nguyen, T. T. H.; Fukaya, N.; Sato, K.; Choi, J.-C.; Kataoka, S. *Ind. Eng. Chem. Res.* **2018**, *57*, 2192–2199.

- [89] Roberts, J. M.; Eldred, D. V.; Katsoulis, D. E. *Ind. Eng. Chem. Res.* **2016**, *55*, 1813–1818.
- [90] Roberts, J. M.; Placke, J. L.; Eldred, D. V.; Katsoulis, D. E. *Ind. Eng. Chem. Res.* **2017**, *56*, 11652–11655.
- [91] Rösch, L.; John, P.; Reitmeier, R. “*Silicon Compounds, Organic*” in *Ullmann’s Encyclopedia of Industrial Chemistry*; Wiley, 2000.
- [92] Dong, Y.; Slade, T.; Stolt, M. J.; Li, L.; Girard, S. N.; Mai, L.; Jin, S. *Angew. Chem., Int. Ed.* **2017**, *56*, 14453–14457.
- [93] Ding, W.-J.; Yan, J.-M.; Xiao, W.-D. *Ind. Eng. Chem. Res.* **2014**, *53*, 10943–10953.
- [94] Knoth, J. F.; Eberle, H.-J.; Ruedinger, C. Process for converting silicon tetrachloride to trichlorosilane. 2017; US9776878B2.
- [95] Glavinović, M.; Krause, M.; Yang, L.; McLeod, J. A.; Liu, L.; Baines, K. M.; Frišćić, T.; Lumb, J.-P. *Sci. Adv.* **2017**, *3*, e1700149.
- [96] (a) Do, J.-L.; Frišćić, T. *ACS Cent. Sci.* **2017**, *3*, 13–19; (b) Tan, D.; García, F. *Chem. Soc. Rev.* **2019**, *48*, 2274–2292.
- [97] Cossairt, B. M.; Piro, N. A.; Cummins, C. C. *Chem. Rev.* **2010**, *110*, 4164–4177.
- [98] Caporali, M.; Gonsalvi, L.; Rossin, A.; Peruzzini, M. *Chem. Rev.* **2010**, *110*, 4178–4235.
- [99] Scheer, M.; Balázs, G.; Seitz, A. *Chem. Rev.* **2010**, *110*, 4236–4256.
- [100] Giffin, N. A.; Masuda, J. D. *Coord. Chem. Rev.* **2011**, *255*, 1342–1359.
- [101] Borger, J. E.; Ehlers, A. W.; Sloatweg, J. C.; Lammertsma, K. *Chem. - Eur. J.* **2017**,
- [102] K. Ghosh, S.; C. Cummins, C.; A. Gladysz, J. *Org. Chem. Front.* **2018**, *5*, 3421–3429.
- [103] Du, S.; Yang, J.; Hu, J.; Chai, Z.; Luo, G.; Luo, Y.; Zhang, W.-X.; Xi, Z. *J. Am. Chem. Soc.* **2019**, *141*, 6843–6847.
- [104] Lennert, U.; Arockiam, P. B.; Streitferdt, V.; Scott, D. J.; Rödl, C.; Gschwind, R. M.; Wolf, R. *Nat. Catal.* **2019**, *2*, 1101–1106.
- [105] Seitz, A. E.; Hippauf, F.; Kremer, W.; Kaskel, S.; Scheer, M. *Nat. Commun.* **2018**, *9*, 1–6.
- [106] The term “conical economy” was coined by Matt Scholz, and is a goal of the Phosphorus Sustainability Challenge (<https://psustainabilitychallenge.org/>). A video describing the concept of a conical economy can be viewed here: <https://youtu.be/MSeGOawrkds>, accessed March 2020.

Chapter 2

Phosphoric acid as a precursor to chemicals traditionally synthesized from white phosphorus

Contents

2.1	Introduction	38
2.2	Results and discussion	39
2.3	Conclusions	43
2.4	Experimental methods	44
2.5	Computational details	73
2.6	Fabrication of steel pressure reactor	75
	References	78

Abstract

White phosphorus, generated in the legacy thermal process for phosphate rock upgrading, has long been the key industrial intermediate for the synthesis of phosphorus-containing chemicals including herbicides, flame-retardants, catalyst ligands, battery electrolyte materials, pharmaceuticals, detergents, etc. On the other hand, phosphate fertilizers are made on a much larger scale from phosphoric acid, obtained by treating phosphate rock with sulfuric acid in what is known as the wet process. If non-fertilizer phosphorus

Reproduced in part with permission from: Geeson, M. B.; Cummins, C. C. *Science* **2018**, *359*, 1383–1385 (doi 10.1126/science.aar6620). Copyright © 2018 AAAS.

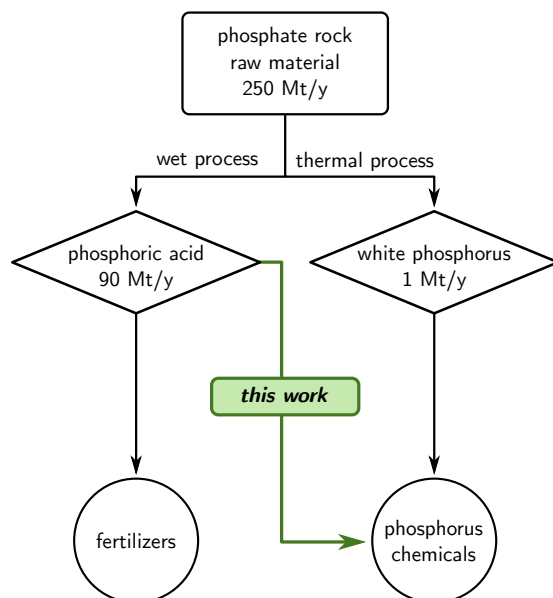
chemicals could be obtained from phosphoric acid, then their production would benefit from the economics of scale of the wet process. Dehydration of phosphoric acid using salt gives trimetaphosphate, and herein we report that trichlorosilane, primarily used for the production of high purity silicon, reduces trimetaphosphate to the previously unknown bis(trichlorosilyl)phosphide anion. This anion offers an entry point to value-added organophosphorus chemicals such as primary and secondary alkyl phosphines, and thus to organophosphinates, and can also be used to prepare phosphine gas and the hexafluorophosphate anion, all previously available only downstream from white phosphorus.

2.1 Introduction

Present industrial practice for production of most phosphorus-containing chemicals is by the energy intensive reduction of phosphate to white phosphorus (thermal process), followed by oxidation with environmentally hazardous chlorine to give phosphorus trichloride.¹ This is the case even for important compounds such as the herbicide glyphosate, and the battery electrolyte lithium hexafluorophosphate, that in the end contain no chlorine.^{2,3} For this reason, chemists have been seeking routes to connect the dots between elemental phosphorus and valuable chemicals featuring phosphorus-carbon bonds, thereby omitting chlorine from the sequence.^{4,5} A paradigm shift would be to obtain value-added phosphorus chemicals in a manner that bypasses *both* elemental phosphorus and chlorine with the potential to substantially reduce energy inputs, waste, and harm to the environment. Herein we describe such a process that borrows from the semiconductor industry for its energy inputs in the form of trichlorosilane, a high-production volume chemical that is the precursor to elemental silicon for the manufacture of solar panels.⁶

Global production of white phosphorus (P_4) is near 1 Mt/y, with most production taking place in China, and production to a much lesser degree taking place in Vietnam and Kazakhstan; production in the USA is limited to one plant, and the EU has no capacity for production, relying entirely on imports.⁷ In 2017, the EU added P_4 to its list of critical materials.⁸ Worldwide, a shift has taken place to manufacturing high purity phosphoric acid from wet process phosphate due to lower production costs and the appealing fact that this method does not incur the hazardous waste disposal issues that are connected with P_4 production.⁹ Like elemental chlorine, P_4 has been used for chemical warfare, and it is also toxic and pyrophoric.¹⁰ Since the wet process accounts for ca. 95% of all phosphate rock processed,¹ a shift to wet process phosphate as the starting point for phosphorus chemicals production would benefit from the economics of scale (Scheme 2.1). The foregoing considerations give substantial impetus for finding synthetic routes that utilize wet process phosphate, instead of P_4 , as the starting point for making value-added phosphorus chemicals.

Phosphate rock used for fertilizer production, underpinning global agriculture, is initially converted into phosphoric acid by the wet process that involves treatment with

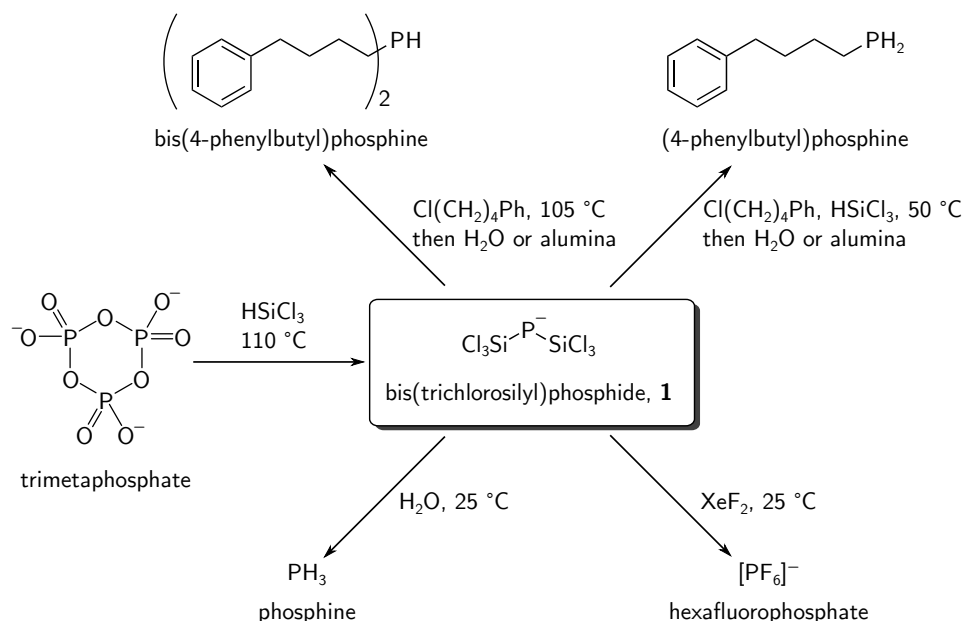


Scheme 2.1 Illustration of pathways taken by phosphorus atoms starting from the raw material, phosphate rock, via the legacy thermal process or via the wet process en route to phosphorus chemicals and fertilizers, respectively, as well as the new connection (green arrow) developed in this work.

sulfuric acid and is the major driver of that commodity chemical's production.⁹ It was shown recently that phosphoric acid can be dehydrated conveniently by reaction with sodium chloride at elevated temperatures to provide sodium trimetaphosphate.¹¹ We targeted trimetaphosphate, $[\text{P}_3\text{O}_9]^{3-}$, for direct conversion to value-added chemicals upon recognizing an analogy between the monomeric unit, metaphosphate ion (PO_3^-), and carbon dioxide: both are Lewis acidic species that may act as oxide ion acceptors to provide phosphate and carbonate, respectively.¹² We hypothesized that the Lewis acid character of metaphosphate vis-à-vis phosphate would make this form of the raw material more prone to favorable kinetics for a reductive process.

2.2 Results and discussion

We began our investigations by converting the sodium salt of trimetaphosphate to the tetrabutylammonium (TBA) salt, $[\text{TBA}]_3[\text{P}_3\text{O}_9]\cdot 2\text{H}_2\text{O}$,¹³ to allow our studies to proceed under homogeneous reaction conditions in organic solvent and to facilitate analysis of products by common laboratory characterization techniques such as nuclear magnetic resonance (NMR) spectroscopy. Upon heating $[\text{TBA}]_3[\text{P}_3\text{O}_9]\cdot 2\text{H}_2\text{O}$ in neat trichlorosilane, $^{31}\text{P}\{^1\text{H}\}$ NMR spectroscopy indicated clean conversion to one new phosphorus-containing product that was identified as the bis(trichlorosilyl)phosphide anion (**1**, Scheme 2.2). Anion



Scheme 2.2 Conversion of trimetaphosphate to bis(trichlorosilyl)phosphide (**1**), and subsequent reactions of this central anion illustrating formation of bonds between phosphorus and carbon, hydrogen, and fluorine.

1 gives rise to a diagnostic ^{31}P NMR singlet at -171.7 ppm, displaying $^{29}\text{Si}\{^1\text{H}\}$ satellites ($^1J_{\text{P-Si}} = 150$ Hz, Fig. 2.1A). Optimization of the reaction conditions by using a steel pressure reactor heated to 110°C for 72 h provided $[\text{TBA}][\mathbf{1}]$ in 65% yield on a gram scale. The identity of $[\text{TBA}][\mathbf{1}]$ was confirmed by multinuclear NMR spectroscopy, X-ray crystallography (Fig. 2.1B) and elemental analysis. Anion **1** is also unambiguously observable by negative-mode electrospray ionization mass spectrometry and has a characteristic isotope pattern with an average mass of 299.86 m/z (Fig. S10).

To the best of our knowledge, anion **1** has not been described previously, and is remarkable as a product resulting from complete deoxygenation of wet process phosphate in a reaction taking place under relatively mild conditions. Recently, the carbon¹⁴ and silicon¹⁵ analogues of anion **1** were successfully synthesized, suggesting a general stability of trichlorosilyl stabilized p-block anions. As the only phosphorus-containing species observable by ^{31}P NMR spectroscopy in the crude reaction mixture, **1** appears to be a stable thermodynamic sink for phosphorus under these reaction conditions. The stability of **1** is presumably a result of the electron-withdrawing trichlorosilyl groups. The phosphorus-silicon bonds are notably short at $2.128(5)$ Å (the sum of the single bond covalent radii is 2.27 Å),¹⁶ a distance contraction indicative of delocalization of phosphorus electron-density into the six $\sigma^*(\text{Si}-\text{Cl})$ bonds. This is supported by natural bond orbital (NBO) and natural resonance theory (NRT) calculations¹⁷ revealing that multiple resonance structures

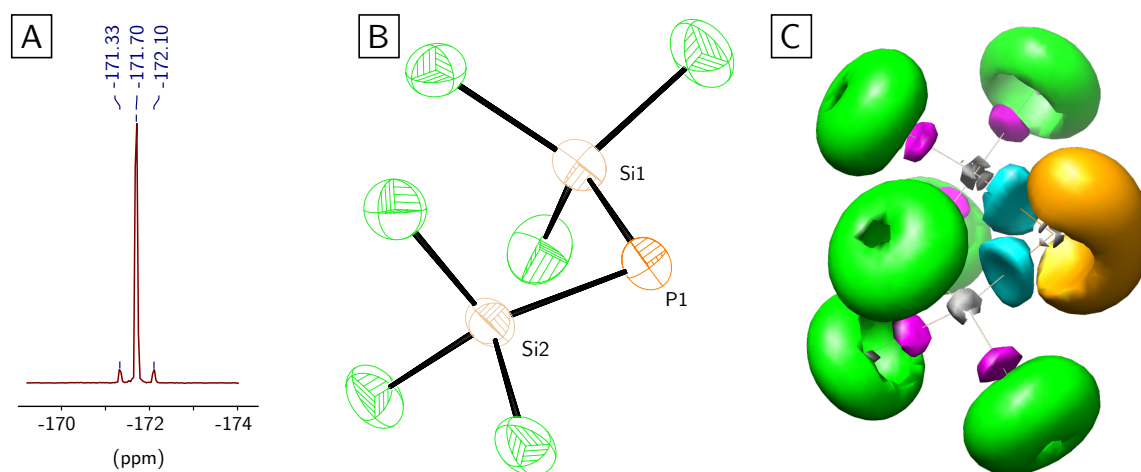
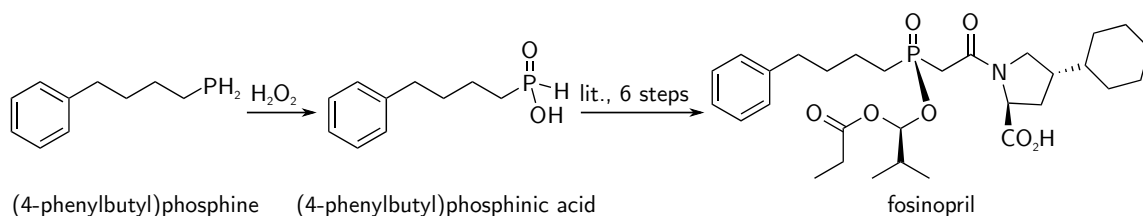


Figure 2.1 **A:** ^{31}P NMR spectrum of [TBA][**1**] displaying $^{29}\text{Si}\{^1\text{H}\}$ satellites. **B:** Molecular structure of **1** with thermal ellipsoids shown at the 50% probability level and the TBA cation omitted for clarity. Selected bond and angle metrics: P1–Si1: 2.141(2) Å, P1–Si2: 2.1439(19) Å, Si1–P1–Si2: 97.86(8) $^\circ$. **C:** Plot of the 0.83 ELF isosurface. Color key: orange, P lone pair basin; cyan, P–Si bond basins; magenta, Si–Cl bond basins; and green, Cl lone pair basins.

are needed to describe the total electron density of **1** (Table S5). The chemical bonding in anion **1** is visually summarized by an electron localization function (ELF)¹⁸ isosurface plot (Fig. 2.1C), where elongations of ELF P–Si bonding basins above and below the Si–P–Si plane are indicative of phosphorus-silicon multiple bonding. The packing of [TBA][**1**] in the solid state, as determined by an X-ray diffraction study, show that the shortest contacts between the bis(trichlorosilyl)phosphide anion and the TBA cation are between the chlorine and hydrogen centers respectively (2.78–2.94 Å). The phosphorus center, though it carries the formal negative charge, has significantly longer contact distances to the TBA cation (≥ 3.07 Å).

With [TBA][**1**] in hand, we were eager to see if this salt could be used to make phosphorus-carbon bonds. An alkyl halide, (4-chlorobutyl)benzene ($\text{Ph}(\text{CH}_2)_4\text{Cl}$), was selected as the reaction partner to target organophosphorus products of low volatility and of relevance to the pharmaceutical industry.¹⁹ Treatment of [TBA][**1**] with $\text{Ph}(\text{CH}_2)_4\text{Cl}$ (5 equiv.) in toluene gave the corresponding dialkylsilylphosphine ($\text{Ph}(\text{CH}_2)_4)_2\text{PSiCl}_3$ which was not isolated but rather converted during workup to the borane-protected secondary phosphine ($\text{Ph}(\text{CH}_2)_4)_2\text{P}(\text{BH}_3)\text{H}$ by using a solution of $\text{THF}\cdot\text{BH}_3$ followed by treatment with a solution of aqueous sodium hydroxide. Before the work-up procedure, silicon tetrachloride was detected as a byproduct in the crude reaction mixture using $^{29}\text{Si}\{^1\text{H}\}$ NMR spectroscopy. Air-stable phosphine-borane adduct ($\text{Ph}(\text{CH}_2)_4)_2\text{P}(\text{BH}_3)\text{H}$ could be purified by column chromatography and isolated in 19% yield (unoptimized).

Conditions selective for *mono*alkylation of anion **1** were discovered when a preparation



Scheme 2.3 Conversion of (4-phenylbutyl)phosphine to (4-phenylbutyl)phosphinic acid, an intermediate in the literature synthesis of fosinopril.

of the same secondary phosphine was attempted in a one-pot procedure. Accordingly, heating a mixture of $[\text{TBA}]_3[\text{P}_3\text{O}_9]\cdot 2\text{H}_2\text{O}$, $\text{Ph}(\text{CH}_2)_4\text{Cl}$ and trichlorosilane was found to yield clean alkylsilylphosphine $\text{Ph}(\text{CH}_2)_4\text{P}(\text{SiCl}_3)\text{H}$, which was identified by ^{31}P NMR spectroscopy. Cleavage of the phosphorus-silicon bond using either water or basic alumina gave the corresponding primary phosphine, $\text{Ph}(\text{CH}_2)_4\text{PH}_2$, which was purified by distillation and isolated in 64% yield. Anion **1** was implicated as a likely intermediate in this one-pot procedure, since the same primary phosphine was also obtained when pure $[\text{TBA}][\mathbf{1}]$ was used as the phosphorus-containing starting material under otherwise identical conditions. The presence or absence of trichlorosilane in alkylation reactions of **1** therefore provides tunably selective conditions for the preparation of primary and secondary phosphines, respectively. Existing routes from primary and secondary phosphines to several important classes of phosphorus-containing compounds such as phosphonates²⁰ and trialkylphosphines²¹ are already well established. Secondary phosphines in particular are valuable starting materials for hydrophosphination reactions.^{22,23}

With (4-phenylbutyl)phosphine in hand as the product of a one-pot procedure from trimetaphosphate, it was of interest to complete a formal synthesis of fosinopril, an angiotensin converting enzyme inhibitor used against hypertension and chronic heart failure, by oxidizing the primary phosphine to (4-phenylbutyl)phosphinic acid. This was accomplished with excellent selectivity upon treatment with hydrogen peroxide along the lines of a literature procedure (Scheme 2.3).²⁴ The resulting (4-phenylbutyl)phosphinic acid may be converted to the target prodrug fosinopril as reported by a group at Bristol-Meyers Squibb.¹⁹ Using their synthetic scheme, the key phosphorus-carbon bond-forming step involving radical addition of hypophosphorous acid was not entirely selective for addition to the terminal, olefinic carbon of 3-buten-1-yl-benzene. Chromatographic purification was necessitated in order to assess the impact of regioisomeric impurities on the quality of intermediates downstream. In the case of the new phosphorus-carbon bond forming methodology reported herein (Scheme 2.2), in which an alkyl chloride is used as the source of the 4-phenylbutyl group in the (4-phenylbutyl)phosphinic acid synthesized, no such regioisomeric impurities are produced as side products. This example illustrates how the new P-C bond-forming methodology, proceeding by way of in situ generated bis(trichlorosilyl)phosphide, can be plugged into existing synthetic pathways to value-added phosphorus chemicals.

After observing hydrolytic cleavage of phosphorus-silicon bonds, we wondered whether anion **1** might react in a similar fashion to produce phosphine (PH_3 , Scheme 2.2), which is primarily used in the fumigation industry and is typically produced by hydrolysis of metal phosphides.²⁵ Treatment of a dichloromethane solution of [TBA][**1**] with water (15 equiv.) gave clean formation of PH_3 in at least 65% yield, as determined by quantitative ^{31}P NMR spectroscopy. This reactivity is reminiscent of that reported for trisilylphosphines, such as $\text{P}(\text{SiMe}_3)_3$, which also react with water to give phosphine, indicative of a highly reduced phosphorus center.²⁶ Accordingly, such compounds, traditionally synthesized from white phosphorus, are used as versatile reagents for the synthesis of metal phosphides²⁷ and quantum dots.²⁸

Having established the reduced nature of the phosphorus atom in **1**, it was of interest to determine whether oxidation of the phosphorus-silicon bonds with a source of fluorine might give the hexafluorophosphate anion, which is extensively employed as an electrolyte component in lithium ion batteries.² Treatment of [TBA][**1**] with xenon difluoride, a convenient laboratory source of elemental fluorine,²⁹ gave clean conversion to the hexafluorophosphate anion as assayed by its characteristic ^{19}F and ^{31}P NMR multiplets; the hexafluorophosphate could be isolated as its lithium salt after precipitation with lithium tetrakis(pentafluorophenyl)borate ethyl etherate (Scheme 2.2) in 70% yield.

2.3 Conclusions

In the past, when high purity phosphoric acid for the detergent industry was manufactured from white phosphorus, the latter was a linchpin synthetic intermediate for phosphorus fine chemicals,³⁰ and it is still essential for those derived today from phosphorus trichloride. With the present work we illustrate an alternative pathway to phosphorus chemicals originating with wet process phosphate. It is clear that several classes of phosphorus chemicals will be accessible using the chemistry described herein, passing through the key molecular intermediate bis(trichlorosilyl)phosphide anion, a new simple inorganic anion produced in a reaction employing trichlorosilane, a high-production-volume chemical. In a possible future in which white phosphorus production were to cease, the new methodology could be adopted as a replacement keeping supply chains open for critical chemicals that currently rely on the manufacture of P_4 .

2.4 Experimental methods

2.4.1 General methods

All manipulations were performed in a Vacuum Atmospheres model MO-40M glovebox under an inert atmosphere of purified N₂ or using standard Schlenk techniques. When reagents were removed from a stock bottle containing a Sure/Seal, the equivalent volume of dry nitrogen was injected into the bottle prior to removing the desired volume of solution with a syringe. All solvents were obtained anhydrous and oxygen-free by bubble degassing (argon) and purification by passing through columns of alumina and Q5.³¹ Once collected, solvents were stored over activated 4 Å molecular sieves (20 wt%) inside the glovebox.³² All glassware was oven-dried for at least 6 h prior to use, at temperatures greater than 150 °C.

Tetrabutylammonium hydroxide (40 wt% in water, Millipore-Sigma), trisodium trimetaphosphate (Millipore-Sigma), xenon difluoride (Alfa Aesar), and trichlorosilane (Millipore-Sigma) were used as received. (4-chlorobutyl)benzene (TCI) was degassed three times by the freeze-pump-thaw method and stored over activated 4 Å molecular sieves for 48 h prior to use. Borane (1.0 M in THF, Millipore-Sigma) was stored in a fridge at -10 °C. Hydrogen peroxide (30% (w/w) in H₂O, Alfa Aesar) was stored in a fridge at 5 °C. Dichloromethane-*d*₂, benzene-*d*₆, acetonitrile-*d*₃ and chloroform-*d* were purchased from Cambridge Isotope Labs and were degassed three times by the freeze-pump-thaw method and stored over activated 4 Å molecular sieves for 48 h in the glovebox prior to use. Diatomaceous earth (Celite 435, EM Science), 4 Å molecular sieves (Millipore-Sigma) and basic alumina (Millipore-Sigma) were dried by heating to 200 °C under dynamic vacuum for at least 48 h prior to use. Silica gel 60 was purchased from EMD. The temperature of the aluminum shot used to heat reagents or reaction mixtures was measured using a Hanna Instruments K-type Thermocouple Thermometer (model HI935005).

NMR spectra were obtained on Varian Inova 300 and 500 instruments equipped with Oxford Instruments superconducting magnets, on a Jeol ECZ-500 instrument equipped with an Oxford Instruments superconducting magnet, or on a Bruker Avance 400 instrument equipped with a Magnex Scientific or with a SpectroSpin superconducting magnet. ¹H and ¹³C NMR spectra were referenced to residual dichloromethane-*d*₂ (¹H = 5.32 ppm, ¹³C = 54.0 ppm), benzene-*d*₆ (¹H = 7.16 ppm, ¹³C = 128.06 ppm), acetonitrile-*d*₃ (¹H = 1.94 ppm, ¹³C = 118.26 ppm) or chloroform-*d* (¹H = 7.26 ppm, ¹³C = 77.16 ppm). ³¹P NMR spectra were referenced externally to 85% H₃PO₄ (0 ppm). ¹⁹F NMR spectra were referenced externally to hexafluorobenzene in benzene-*d*₆ (0.2 M, -164.9 ppm). ¹¹B NMR spectra were referenced externally to 15% (w/w) BF₃·OEt₂ in CDCl₃ (0 ppm). ⁷Li NMR spectra were referenced externally to 1.0 M LiCl in D₂O (0 ppm).

Electrospray ionization mass spectrometry (ESI-MS) was performed using a Micromass Q-TOF ESI spectrometer (see section 2.4.10 for details).

Raman spectra were collected using a Renishaw Invia Reflex Micro Raman (see section

2.4.11 for details).

Elemental combustion analyses were performed by Robertson Microлит Laboratories (Ledgewood, NJ, USA).

2.4.2 Synthesis of $[\text{TBA}]_3[\text{P}_3\text{O}_9]\cdot 2\text{H}_2\text{O}$

$[\text{TBA}]_3[\text{P}_3\text{O}_9]\cdot 2\text{H}_2\text{O}$ was prepared using a modified literature procedure.¹³ Dowex 50WX8 Hydrogen form (1.7 meq/mL) was added to a 200 mL beaker containing deionized water (50 mL) until a wetted bed volume of 96 mL (163 meq) was achieved. The slurry was transferred to a 1000 mL Erlenmeyer flask, and the volume of the solution increased to 500 mL. $[\text{TBA}][\text{OH}]$ (40 wt% in water, 105 mL, 162 mmol) was measured into a beaker, then transferred to the flask containing the Dowex ion exchange resin. The final volume was increased to 1000 mL using deionized water, and left to stir at 23 °C for 24 h. The slurry was loaded into a column (60 cm \times 2 cm) which was washed with additional deionized water (160 mL), using a positive pressure of air to increase the flow rate. Sodium trimetaphosphate (10.0 g, 32.7 mmol) was dissolved in deionized water (500 mL) and the solution was added to the ion exchange column, and allowed to flow through at a rate of 2 mL/min. The first 100 mL of eluent was discarded, and the rest collected in a 1000 mL Erlenmeyer flask. The column was rinsed with additional deionized water (100 mL), maintaining a flow rate of 2 mL/min. Water was removed from the solution using a rotary evaporator, to give a clear viscous oil, which became a waxy solid after an additional hour on the rotary evaporator. The solids were washed with diethyl ether (3 \times 90 mL) by adding ether, breaking up the solids with a spatula, then decanting off the clear diethyl ether solution. The solids obtained were dried for 18 h on a vacuum line at 45 °C. The material so obtained was dissolved in 1,2-dichloroethane (125 mL) and the solution was passed through a frit (fine porosity, 30 mL) to remove any undissolved material. Diethyl ether (700 mL) was added to the clear solution to give a fine precipitate, which was washed with diethyl ether (3 \times 90 mL) by stirring for 5 minutes then decanting off the clear diethyl ether. The obtained solids were transferred to a Schlenk flask, where they were dried at 45 °C for 24 h before being isolated in the glovebox as a free-flowing white powder (24.9 g, 24.9 mmol, 76% yield). ^1H NMR (300 MHz, CD_2Cl_2 , δ) 4.30 (s), 3.41 – 3.23 (m, 2H), 1.64 (m, 2H), 1.45 (m, 2H), 0.99 (t, 7 Hz, 3H). $^{31}\text{P}\{^1\text{H}\}$ NMR (121 MHz, CD_2Cl_2 , δ) –19.77 (s).

2.4.3 Synthesis of $[\text{TBA}][\text{P}(\text{SiCl}_3)_2]$

Caution: $[\text{TBA}][\text{P}(\text{SiCl}_3)_2]$ releases toxic phosphine gas (PH_3) upon exposure to water (Section 2.4.4). The preparation of this compound generates volatile dichlorosilane, chlorosilane and hydrogen, as determined by ^1H NMR spectroscopy.³³ The preparation should be carried out behind a blast shield. Reactor size is important to allow enough head space for volatile products and to avoid excessive pressure build-up.

2.4.3.1 In a thick-walled glass reactor

In the glovebox, $[\text{TBA}]_3[\text{P}_3\text{O}_9]\cdot 2\text{H}_2\text{O}$ (1.0 g, 1.0 mmol) was transferred to a thick-walled 100 mL glass reactor equipped with a gas-tight valve and a Teflon-coated magnetic stir bar (10 mm). The flask was removed from the glovebox and connected to a Schlenk line in the fume hood. The nitrogen manifold of the Schlenk line was equipped with an oil bubbler, followed by a water bubbler in series; the function of the water bubbler was to scrub any moisture-reactive gases released from the flask. Under a flow of nitrogen, trichlorosilane (10.0 mL, 99.2 mmol) was added to the flask using a syringe, directly from the stock bottle which was equipped with a Sure/Seal. The addition of trichlorosilane caused an exothermic reaction with bubbling, so the flask was left open to the nitrogen manifold for 20 min after the initial addition. The flask was sealed then heated with stirring in a preheated oil bath behind a blast shield at 65 °C for 3 h. (*Note: When reaching around the blast shield to move the flask or to adjust a valve, a thick leather glove was worn to protect against the risk of explosion.*) The flask was removed from the oil bath and cooled to 23 °C before being opened to the nitrogen manifold of the Schlenk line to equalize the pressure inside the reaction flask. The flask was sealed and placed back in the oil bath at 65 °C for 240 h. Every 24 h, the pressure inside the flask was equalized as described above. After 240 h, the flask was removed from the oil bath, and allowed to cool to 23 °C. Volatile materials were removed in vacuo for 2 h. The flask was brought inside the glovebox, and the material was dissolved in THF (20 mL) to give a cloudy solution. The solution was passed through diatomaceous earth (3 cm bed) in a frit (fine porosity, 15 mL). The diatomaceous earth was washed with THF (2×10 mL) and volatile material was removed from the filtrate in vacuo over the course of 8 h to give a tacky white oil. The oil was triturated with diethyl ether (3×5 mL) to give a white paste. The paste was dissolved in DCM (4 mL) and the solution was passed through a piece of filter paper inside a pipette into a scintillation vial (20 mL). Diethyl ether (16 mL) was added, causing a white precipitate to form immediately. The vial was capped and taped shut using electrical tape and placed in a freezer at -35 °C overnight. The solids that formed were broken up with a spatula and collected on a frit (fine porosity, 15 mL), and were washed with pentane (3×10 mL, -35 °C) before being dried to constant mass to give a free-flowing white powder (1.150 g, 2.1 mmol, 70.7% yield). Elem. Anal. Calcd(found) for $\text{C}_{16}\text{H}_{36}\text{Cl}_6\text{N}_1\text{P}_1\text{Si}_2$: C 35.44(36.03), H 6.69(6.70), N 2.58(2.83). ^1H NMR (500 MHz, CD_2Cl_2 , δ) 3.24 – 3.17 (m, 2H), 1.68 – 1.58 (m, 2H), 1.42 (m, $J = 7.3$ Hz, 2H), 1.00 (t, $J = 7.3$ Hz, 3H). $^{13}\text{C}\{^1\text{H}\}$ NMR (126 MHz, CD_2Cl_2 , δ) 59.45, 24.47, 20.21, 13.91. ^{31}P NMR (203 MHz, CD_2Cl_2 , δ) -171.7 (s, $J_{\text{P-Si}} = 156$ Hz). $^{29}\text{Si}\{^1\text{H}\}$ NMR (99 MHz, CD_2Cl_2 , δ) 11.8 (d, $J_{\text{P-Si}} = 156$ Hz).

2.4.3.2 In a steel pressure reactor

Note: This method is preferred for the preparation of [TBA]/[1] due to the shorter reaction time and decreased risk of explosion due to the use of a steel pressure reactor instead of a glass pressure vessel. In the glovebox, $[\text{TBA}]_3[\text{P}_3\text{O}_9]\cdot 2\text{H}_2\text{O}$ (1.0 g, 1.0 mmol) was

transferred to a 25 mL steel pressure reactor, equipped with a Teflon-coated magnetic stir bar (20 mm), a needle valve and a relief valve (see section 2.6 and Fig. 2.2 for details). The reactor was sealed using Teflon tape on the threading, removed from the glovebox and connected to a Schlenk line in the fume hood. Under a positive flow of nitrogen, trichlorosilane (10.0 mL, 99.2 mmol) was added to the flask using a syringe, directly from the stock bottle which was equipped with a Sure/Seal. The reactor was heated to 110 °C in a heating mantle filled with aluminum shot for 72 h behind a blast shield. (*Note: It was found that the heating mantle had a thermal gradient of typically 20 °C from top to bottom; the temperature of the reaction flask was determined by taking the average of the temperature at the bottom (temperature probe placed at the very base of the heating mantle, 120 °C) and top (temperature probe placed 2 cm beneath the top of the aluminum shot, 100 °C) of the heating mantle.*) The reactor was then allowed to cool to 23 °C over the course of 2 h. The needle valve was opened to an oil bubbler, followed by a water bubbler in series to equalize the pressure inside the reactor. (*Note: When reaching around the blast shield to move the flask or to adjust a valve, a thick leather glove was worn to protect against the risk of explosion.*) The reactor was removed from behind the blast shield and volatile material was removed on a Schlenk line for 2 h. The reactor was pumped into the glovebox, and the crude material subjected to the same work up as detailed in section 2.4.3.1 to give [TBA][1] as a free-flowing white powder (1.60 g, 1.96 mmol, 65.2% yield). The material obtained by this method was spectroscopically identical to the material obtained in section 2.4.3.1.

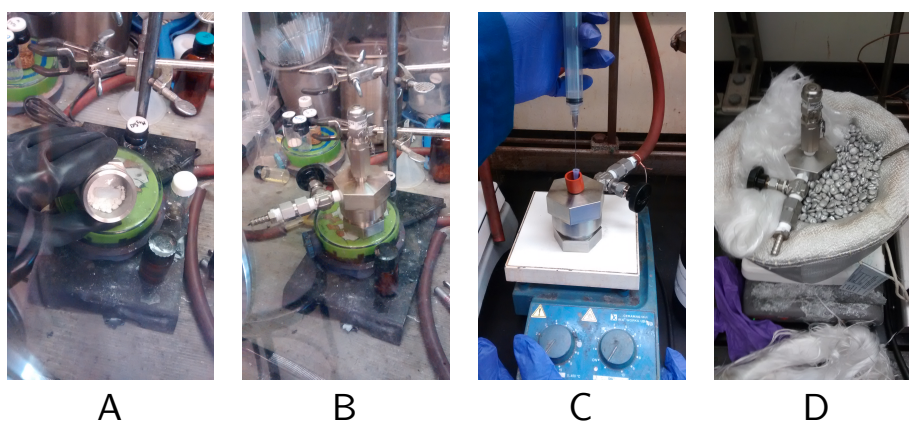


Figure 2.2 **A:** $[\text{TBA}]_3[\text{P}_3\text{O}_9]\cdot 2\text{H}_2\text{O}$ being loaded into the steel reactor inside the glovebox. **B:** The steel pressure reactor sealed inside glovebox. **C:** Process of adding trichlorosilane to the steel reactor under a flow of nitrogen on the Schlenk line. **D:** The steel reactor in a heating mantle filled with aluminum shot.

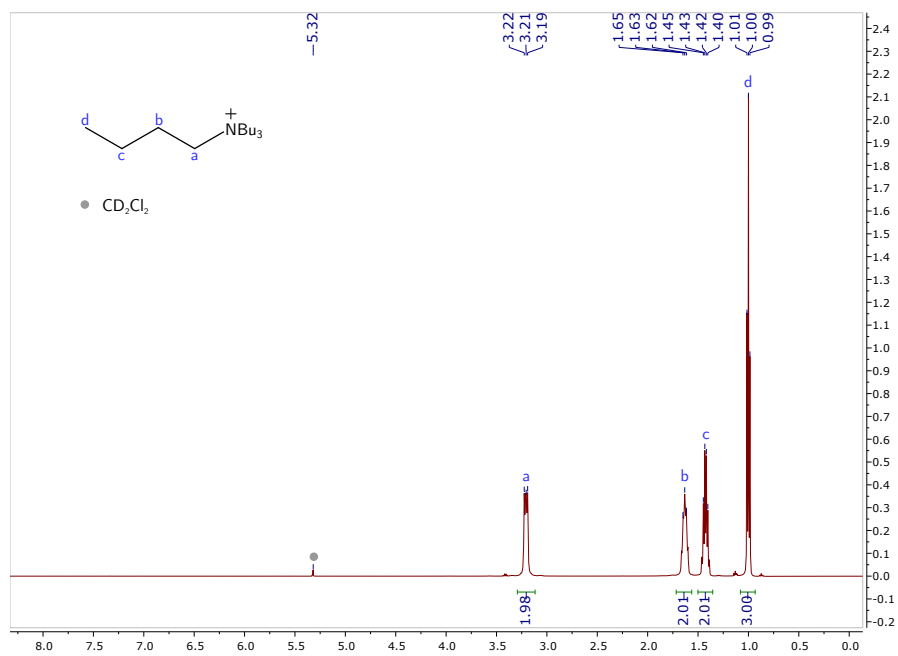


Figure 2.3 ^1H NMR spectrum of [TBA][1] in CD_2Cl_2 at 25 °C, recorded at 500 MHz.

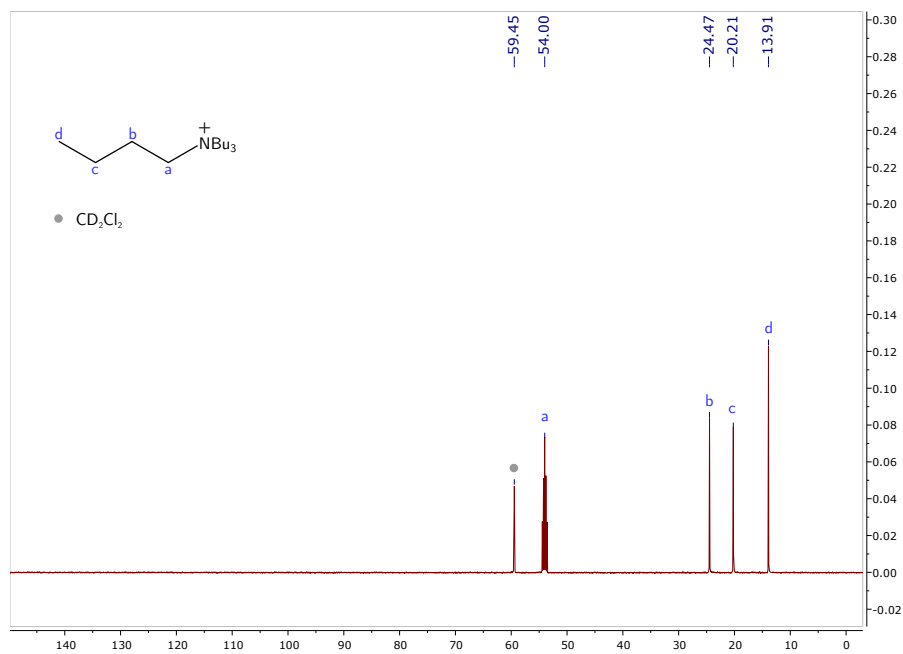


Figure 2.4 $^{13}\text{C}\{^1\text{H}\}$ NMR spectrum of [TBA][1] in CD_2Cl_2 at 25 °C, recorded at 126 MHz.

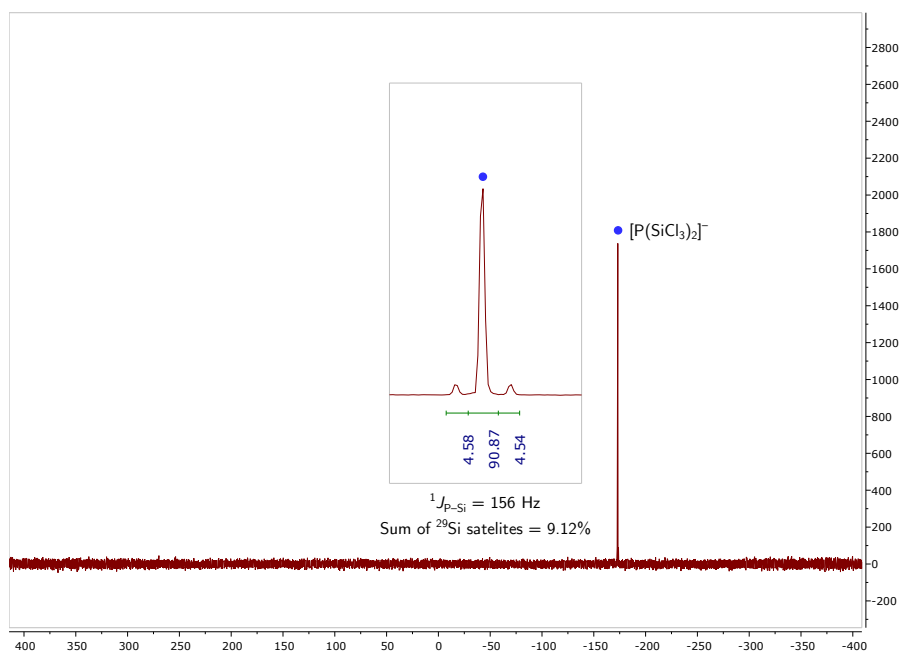


Figure 2.5 ^{31}P NMR spectrum of [TBA][1] in CD_2Cl_2 at 25°C , recorded at 203 MHz.

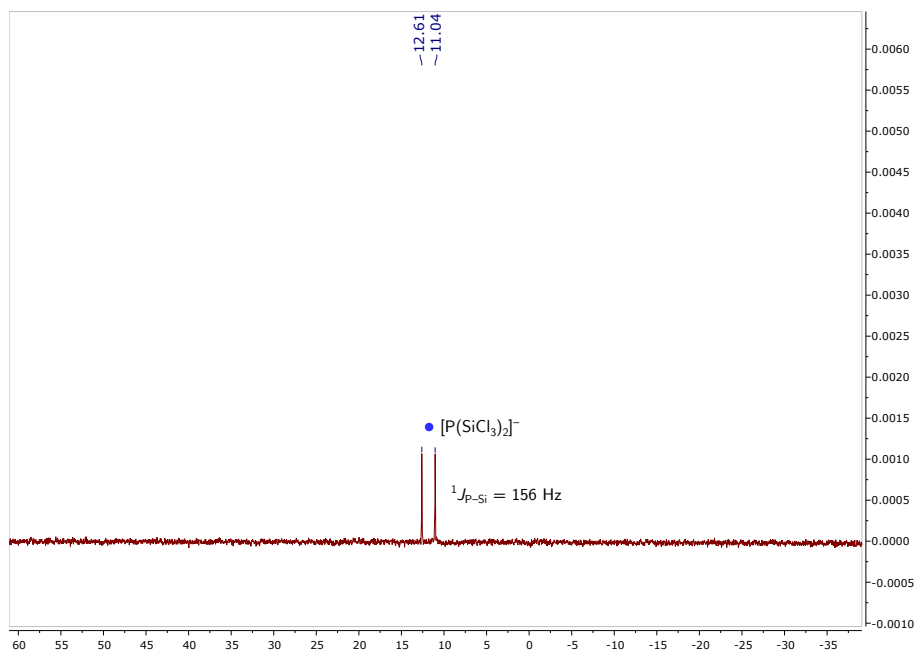


Figure 2.6 $^{29}\text{Si}\{^1\text{H}\}$ NMR spectrum of [TBA][1] in CD_2Cl_2 at 25°C , recorded at 99 MHz.

2.4.4 Synthesis and quantification of PH₃ from [TBA][P(SiCl₃)₂]

This experiment was carried out in quadruplicate. Capillaries for quantitative ³¹P NMR spectroscopy were prepared by dissolving chromium(III) acetylacetonate (10.0 mg, 0.03 mmol) and triphenylphosphine (270 mg, 1.03 mmol) in C₆D₆ (2.0 mL). The purpose of the chromium(III) acetylacetonate was to act as a paramagnetic relaxation agent.³⁴ This stock solution (70 μL) was transferred to a capillary which was then flame sealed. In the glovebox, [TBA][1] (100 mg, 0.18 mmol) was weighed into a vial and dissolved in DCM (0.5 mL). The solution was transferred to an NMR tube equipped with a J. Young valve and the capillary was inserted. The *T*₁ for triphenylphosphine and [TBA][1] were measured (Bruker 400) to be 4.35 s and 6.07 s respectively using the inversion recovery experiment (Fig. 2.7). Quantitative ³¹P NMR spectra (Fig. 2.8) were acquired (8 transients) using a d1 of ≥5**T*₁, which was chosen to guarantee integration accuracy of 1%.³⁵ The solutions were frozen inside the NMR tubes using liquid nitrogen, then degassed water (50 μL) was added using a microsyringe against a positive flow of nitrogen. The tubes were sealed then removed from the liquid nitrogen and allowed to warm to 23 °C. The *T*₁ of the phosphine produced by the reaction was measured using the inversion recovery method (Fig. 2.7). Quantitative ³¹P NMR spectra (Fig. 2.9) were acquired (8 transients) using a d1 of ≥5**T*₁. Integration of resonances relative to triphenylphosphine were used to calculate the yield (≥ 63%, Table 2.1). ³¹P{¹H} NMR (162 MHz, DCM, δ) -241.1 (s). ³¹P NMR (162 MHz, DCM, δ) -241.1 (q, *J*_{P-H} = 188 Hz).

Run	Phosphide (% ²⁹ Si)	PH ₃	Yield
1	4.34 (8%)	2.90	67%
2	3.24 (8%)	2.06	63%
3	4.11 (8%)	3.49	85%
4	4.35 (9%)	2.79	64%

Table 2.1 Integration of species relative to PPh₃ for each of the four experimental runs

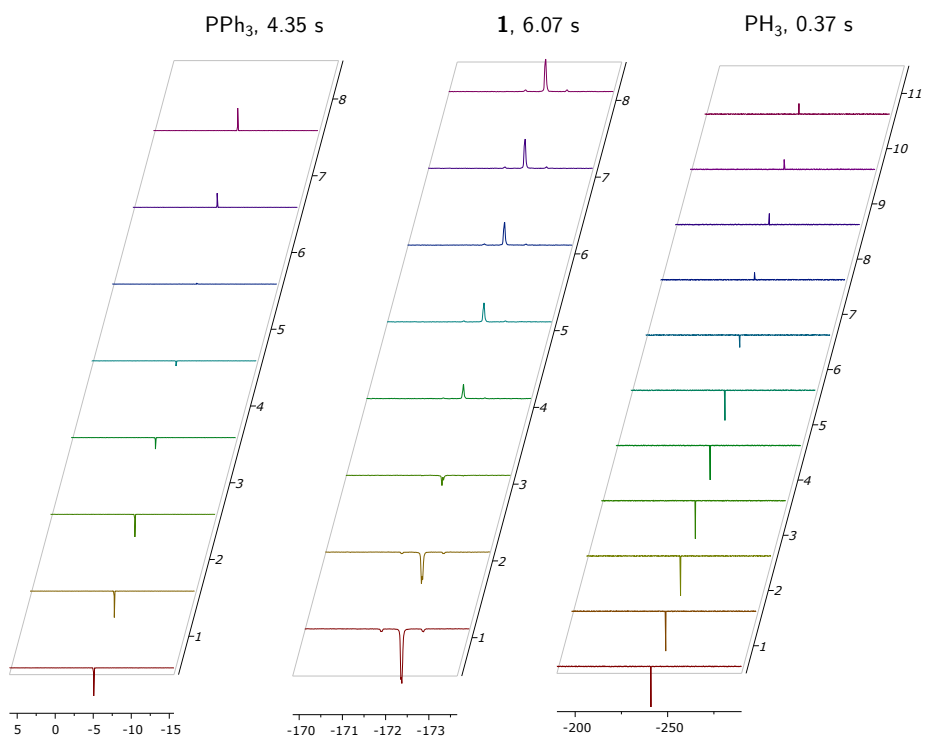


Figure 2.7 Array of ^{31}P NMR spectra of the species studied by the inversion recovery experiment. The times at the top of the figure correspond to the T_1 time for each of the species.

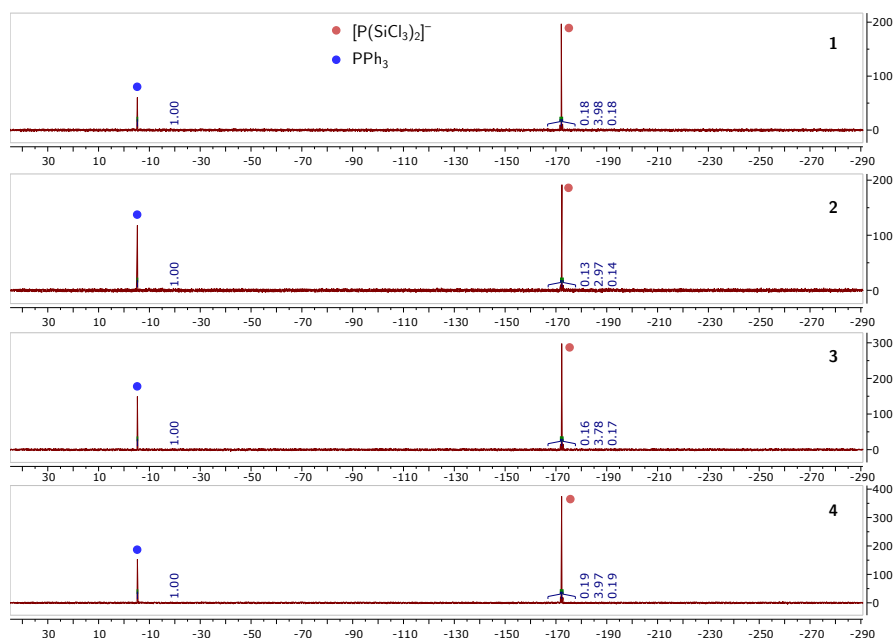


Figure 2.8 Quantitative ^{31}P NMR spectra of the four reaction mixtures at 25 °C before the addition of water to a DCM solution of [TBA][1]. Integrations are shown above the baseline for clarity.

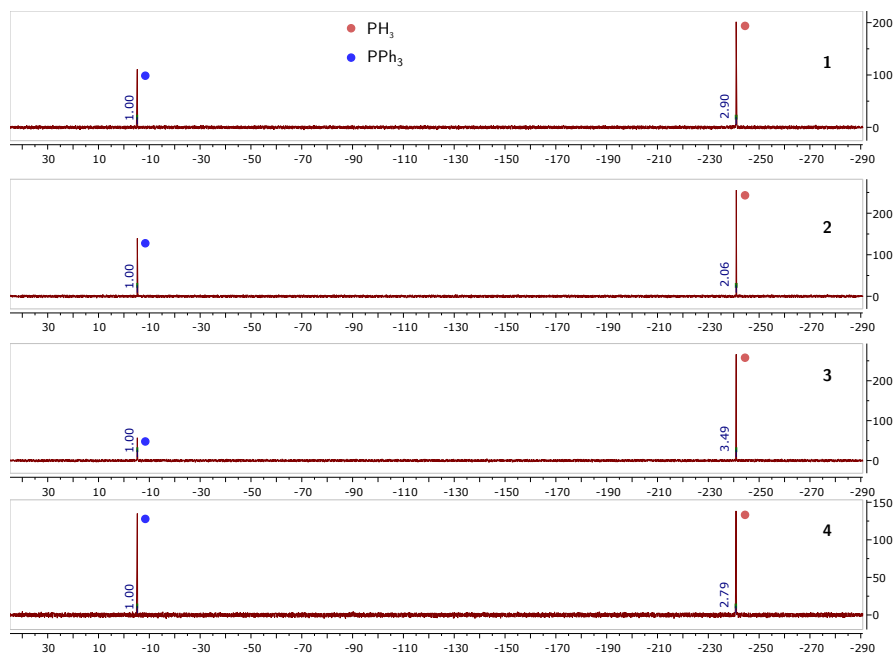


Figure 2.9 Quantitative ^{31}P NMR spectra at 25 °C of the four reaction mixtures after the addition of water to a DCM solution of [TBA][1].

2.4.5 Synthesis of LiPF₆ from [TBA][P(SiCl₃)₂]

In the glovebox, [TBA][1] (108 mg, 0.2 mmol) was weighed into a vial containing a Teflon-coated magnetic stir bar (10 mm) and dissolved in DCM (4 mL). Xenon difluoride (270 mg, 1.6 mmol) was weighed into a separate vial (20 mL) and dissolved in DCM (4 mL). Both solutions were placed in the glovebox coldwell, which was cooled with liquid nitrogen, until frozen. Once removed and upon thawing, the solution of xenon difluoride was added dropwise to the stirring solution of [TBA][1]. After stirring for one hour, the solution was filtered into a fresh vial (20 mL) through a piece of filter paper inside a pipette. Lithium tetrakis(pentafluorophenyl)borate ethyl etherate (174 mg, 0.2 mmol) in DCM (2 mL) was added to the reaction mixture, causing a white precipitate to form immediately. The precipitate was collected on a piece of filter paper inside a pipette, then washed with DCM (2 × 2 mL). The collected material was washed from the filter paper into a preweighed vial using acetonitrile (4 × 3 mL). Volatile material was removed in vacuo to give LiPF₆ as a white solid (21 mg 0.14 mmol, 70% yield). ¹⁹F NMR (376 MHz, CD₃CN, δ) -73.0 (d, *J*_{P-F} = 706 Hz). ³¹P NMR (162 MHz, CD₃CN, δ) -144.6 (sept., *J*_{P-F} = 706 Hz). ⁷Li NMR (155 MHz, CD₃CN, δ) -1.9 (s). Elemental analysis was not performed due to minor observable impurities by ³¹P and ¹⁹F NMR spectroscopy; one of these impurities was identified as the bifluoride anion, by comparison of its ¹⁹F NMR chemical shift with values from the literature.³⁶

A crude yield was also obtained by quantitative ³¹P NMR spectroscopy. In the glovebox, [TBA][1] (30 mg, 0.056 mmol) was weighed into an NMR tube equipped with a J. Young valve and dissolved in DCM (0.5 mL). Capillaries for quantitative ³¹P NMR spectroscopy were prepared as described in Section 2.4.4. A capillary was inserted into each NMR tube and the resonance of [TBA][1] was integrated relative to the resonance of triphenylphosphine. The NMR tubes were brought into the glovebox and xenon difluoride (75 mg, 0.44 mmol) was slowly added to the tube (*caution: gas evolution!*). The tubes were left open to the glovebox atmosphere for thirty minutes to allow any gases produced to escape before being sealed. The *T*₁ of the [PF₆]⁻ anion was measured using the inversion recovery method, and was found to be 5.12 s (Fig. 2.10). Quantitative spectra were acquired using a d1 of ≥5**T*₁ and 8 transients. Signals were integrated relative to the triphenylphosphine resonance (Fig. 2.11). The average yield was found to be 68% by this method (Table 2.2).

Run	Phosphide (% ²⁹ Si)	[PF ₆] ⁻	Yield
1	1.75 (9%)	1.18	68%
2	1.85 (8%)	1.21	66%
3	1.95 (8%)	1.34	69%

Table 2.2 Integration of species relative to PPh₃ for each of the four experimental runs.

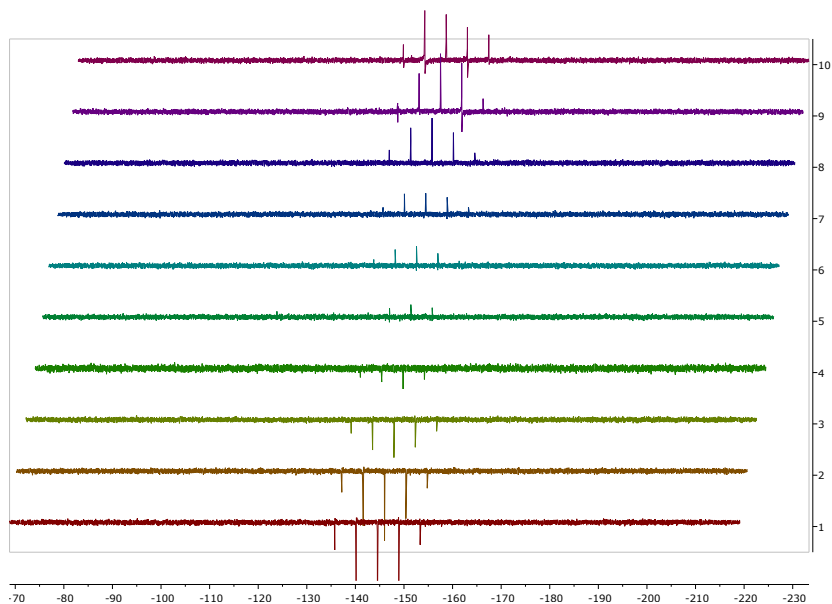


Figure 2.10 Array of ^{31}P NMR spectra from the measurement of the T_1 of $[\text{PF}_6]^-$ by the inversion recovery method.

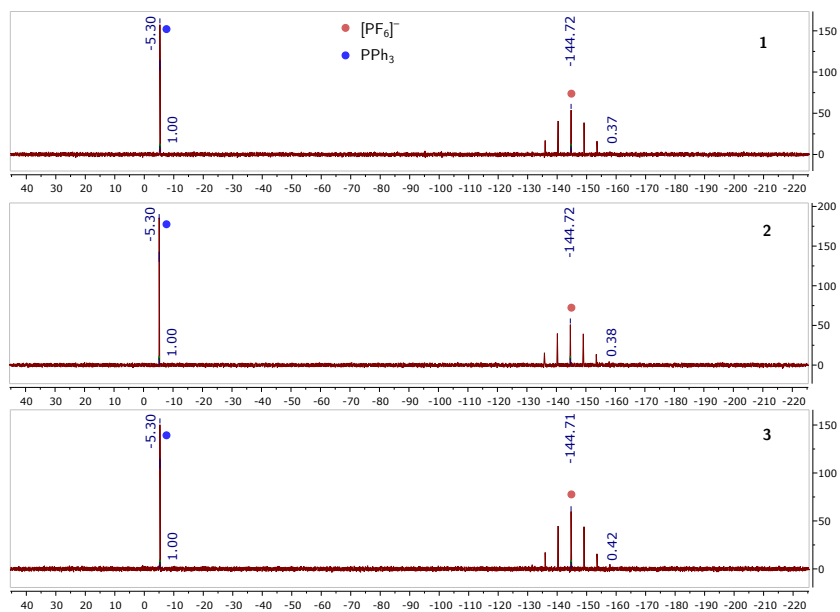


Figure 2.11 Quantitative ^{31}P NMR spectra at 25 °C of the solutions after the addition of xenon difluoride to $[\text{TBA}][\mathbf{1}]$. The integration of the resonance of the $[\text{PF}_6]^-$ corresponds to the central line of the septet.

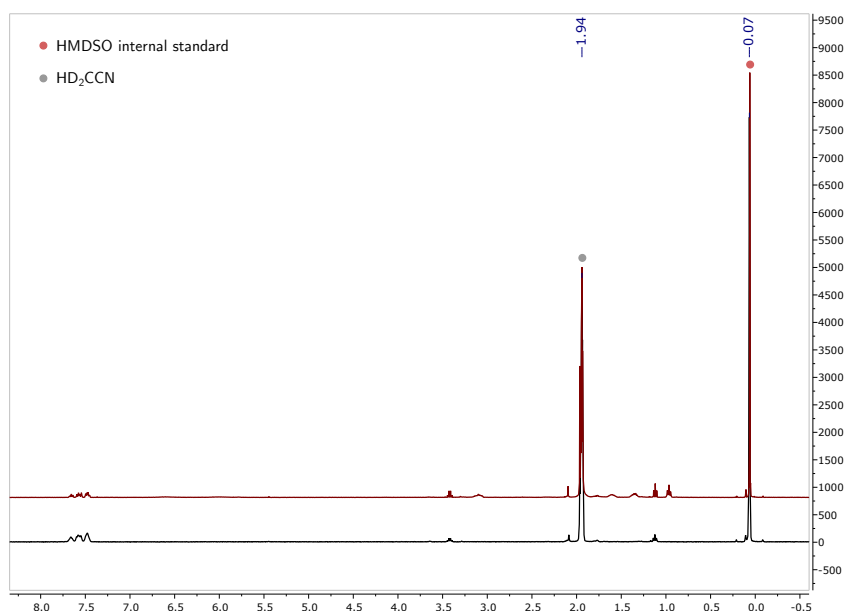


Figure 2.12 400 MHz ^1H NMR spectrum of LiPF_6 prepared as described in section 2.4.5 in CD_3CN at 25°C . The black spectrum shows a blank of the NMR solvent before the product was dissolved in it (red). The intensity of the spectra have been normalized to the most intense peak, and offset from one another. These spectra were acquired to check for the absence of the tetrabutylammonium cation.

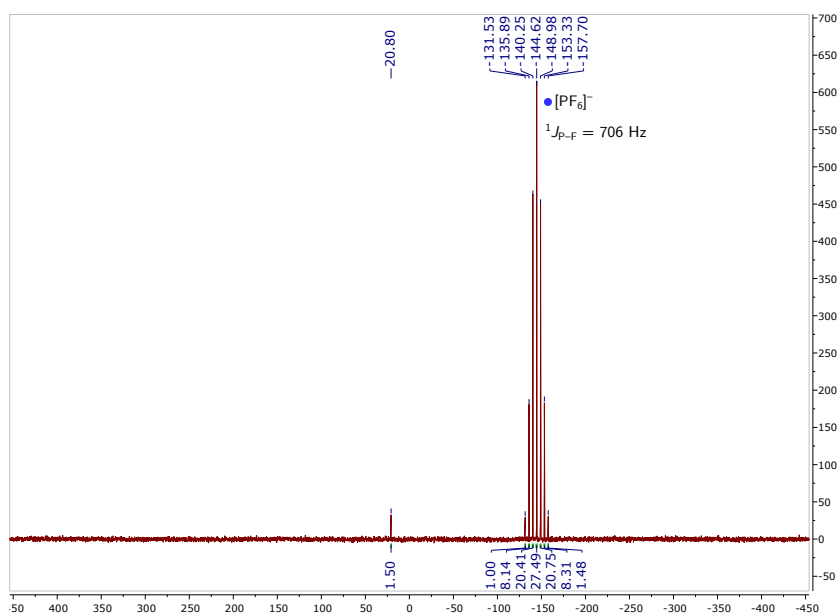


Figure 2.13 162 MHz ^{31}P NMR spectrum of LiPF_6 prepared as described in section 2.4.5 in CD_3CN at 25°C .

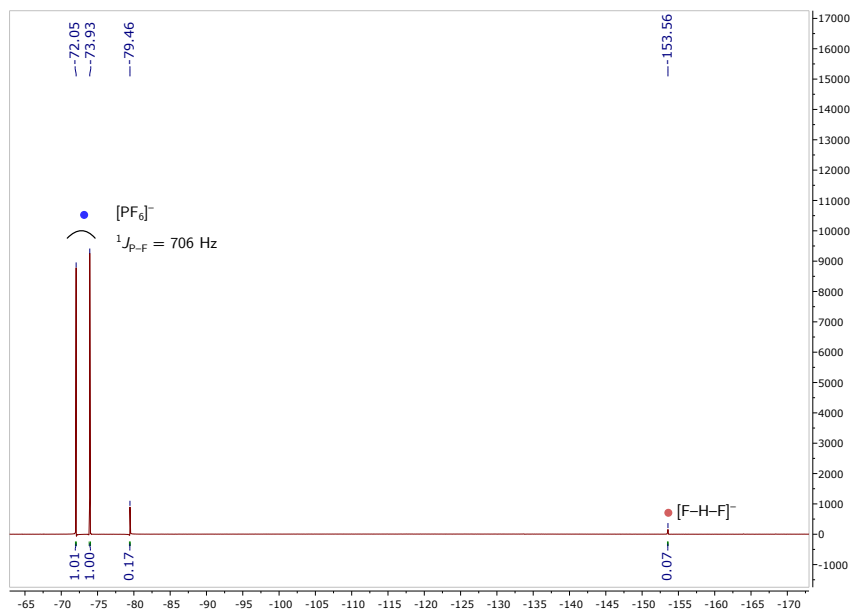


Figure 2.14 376 MHz ^{19}F NMR spectrum of LiPF_6 prepared as described in section 2.4.5 in CD_3CN at 25 °C.

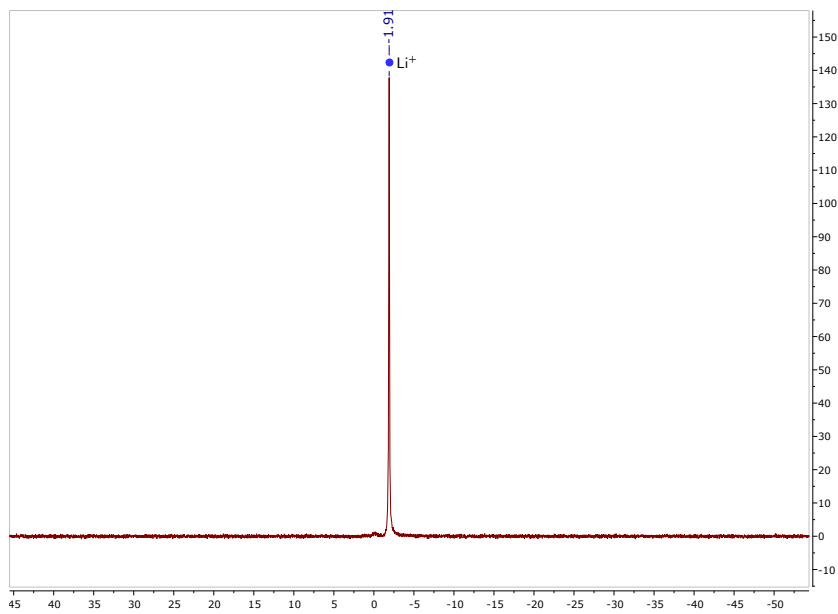


Figure 2.15 155 MHz ^7Li NMR spectrum of LiPF_6 prepared as described in section 2.4.5 in CD_3CN at 25 °C.

2.4.6 Synthesis of $\text{Ph}(\text{CH}_2)_4\text{PH}_2$

2.4.6.1 From $[\text{TBA}][\text{P}(\text{SiCl}_3)_2]$

In the glovebox, $[\text{TBA}][\text{P}(\text{SiCl}_3)_2]$ (50 mg, 0.09 mmol) was weighed into an NMR tube equipped with a J. Young valve. (4-chlorobutyl)benzene (309 mg, 1.83 mmol) was added by pipette. The tube was sealed and removed from the glovebox. On the Schlenk line, trichlorosilane (0.3 mL, 2.97 mmol) was added, directly from the stock bottle which was equipped with a Sure/Seal, using a syringe against a positive flow of nitrogen. The tube was sealed and heated to 50 °C behind a blast shield for 144 h. ^{31}P NMR spectroscopy showed alkylsilylphosphine $\text{Ph}(\text{CH}_2)_4\text{P}(\text{SiCl}_3)\text{H}$ as the major product, as well as some $[\text{TBA}][\mathbf{1}]$ and primary phosphine $\text{Ph}(\text{CH}_2)_4\text{PH}_2$. Volatile material was removed in vacuo and the residue obtained was taken up in DCM (5 mL). The resulting solution was passed through a short column of basic alumina, which converts the $\text{P}-\text{SiCl}_3$ to a $\text{P}-\text{H}$ bond, to give the desired primary phosphine as a colorless oil (3 mg, 0.018 mmol, 20% yield). Alkylsilylphosphine, $\text{Ph}(\text{CH}_2)_4\text{P}(\text{SiCl}_3)\text{H}$: $^{31}\text{P}\{^1\text{H}\}$ NMR (203 MHz, HSiCl_3 , δ) -130.25 (s, $J_{\text{P-Si}} = 68$ Hz). ^{31}P NMR (203 MHz, HSiCl_3 , δ) -130.25 (dm, $J_{\text{P-H}} = 202$ Hz). Alkylphosphine, $\text{Ph}(\text{CH}_2)_4\text{PH}_2$: $^{31}\text{P}\{^1\text{H}\}$ NMR (203 MHz, HSiCl_3 , δ) -140.44 (s). ^{31}P NMR (203 MHz, HSiCl_3 , δ) -140.44 (dm, $J_{\text{P-H}} = 187$ Hz).

2.4.6.2 From $[\text{TBA}]_3[\text{P}_3\text{O}_9]\cdot 2\text{H}_2\text{O}$

Note: This method is preferred to the procedure described in section 2.4.6.1 for the preparation of $\text{Ph}(\text{CH}_2)_4\text{PH}_2$ because it does not require isolation of $[\text{TBA}][\mathbf{1}]$. Instead, $[\text{TBA}][\mathbf{1}]$ is formed in situ. In the glovebox, $[\text{TBA}]_3[\text{P}_3\text{O}_9]\cdot 2\text{H}_2\text{O}$ (1.0 g, 1.0 mmol) was weighed into a 25 mL steel pressure reactor containing a Teflon-coated magnetic stir bar (20 mm), a needle valve and a relief valve (see section 2.6 for details). (4-chlorobutyl)benzene (338 mg, 2.0 mmol) was weighed into the reactor, which was then sealed using Teflon tape on the threading, and brought outside the glovebox. The reactor was connected to a Schlenk line and trichlorosilane (10.0 mL, 99.2 mmol) was added directly from the stock bottle, which was equipped with a Sure/Seal, against a positive flow of nitrogen. The reactor was heated to 130 °C with stirring behind a blast shield for 96 h, before being allowed to cool to 23 °C over the course of 2 h. Volatile material was removed in vacuo for 2 h and the reactor was brought into the glovebox. Analysis of the crude material by ^{31}P NMR spectroscopy showed alkylsilylphosphine $\text{Ph}(\text{CH}_2)_4\text{PH}(\text{SiCl}_3)$ and $[\text{TBA}][\mathbf{1}]$ as the major species in solution. The material was dissolved in DCM (15 mL) and transferred to a vial (20 mL). Basic alumina (8.0 g) was added to form a slurry, which was stirred for 2 h, then filtered through basic alumina (2 cm bed) in a frit (fine porosity, 15 mL). The frit was washed with DCM (3×10 mL) and the combined washings were dried in vacuo to give white oily solids and a clear oil. The material obtained was slurried in pentane (10 mL) and the solution passed through basic alumina (2 cm) in a pipette plug. Volatile material was removed from filtrate in vacuo to give a cloudy colorless oil. The oil

was purified by trap-to-trap distillation under static vacuum (60 mTorr, measured using a Duniway thermocouple vacuum gauge, model DST-531). An oil bath at 60 °C was used to heat the crude material side and dry ice/acetone bath at -78 °C was used to condense product on the collection side. The product was washed from the distillation apparatus using pentane (10 mL) and dried to constant mass in vacuo to give a colorless oil (214 mg, 1.28 mmol, 64% yield). ^1H NMR (400 MHz, CDCl_3 , δ) 7.37 – 7.10 (m, 5H), 2.69 (dt, $J_{\text{P-H}} = 195$ Hz, $J = 7$ Hz, 2H), 2.62 (t, $J = 7$ Hz, 2H), 1.77–1.63 (m, 2H), 1.63 - 1.42 (m, 4H). $^{13}\text{C}\{^1\text{H}\}$ NMR (101 MHz, CDCl_3 , δ) 142.38, 128.39, 128.30, 125.72, 35.55, 32.48 ($J_{\text{P-C}} = 3$ Hz), 32,34 ($J_{\text{P-C}} = 6$ Hz), 13.65 ($J_{\text{P-C}} = 8$ Hz). $^{31}\text{P}\{^1\text{H}\}$ NMR (162 MHz, CDCl_3 , δ) -136.22 (s). ^{31}P NMR (162 MHz, CDCl_3 , δ) -136.22 (tm, $J_{\text{P-H}} = 195$ Hz). This material failed elemental analysis. A minor impurity was identified as 4-chlorobutylbenzene ($\leq 3\%$ as determined by ^1H NMR spectroscopy). The material was judged to be sufficiently pure for further synthetic applications.

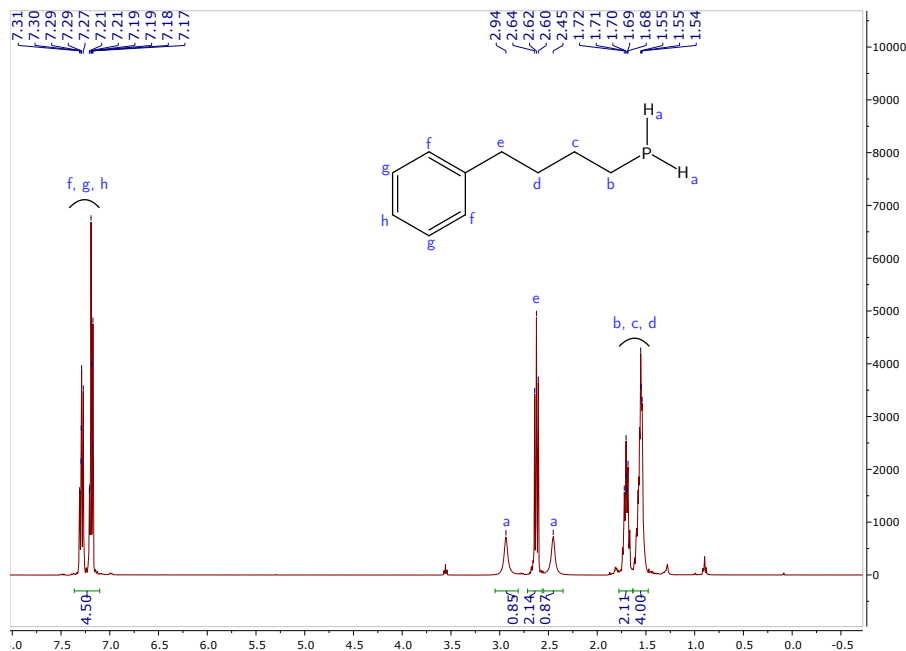


Figure 2.16 ^1H NMR spectrum of $\text{Ph}(\text{CH}_2)_4\text{PH}_2$ in CDCl_3 at 25 °C, recorded at 400 MHz.

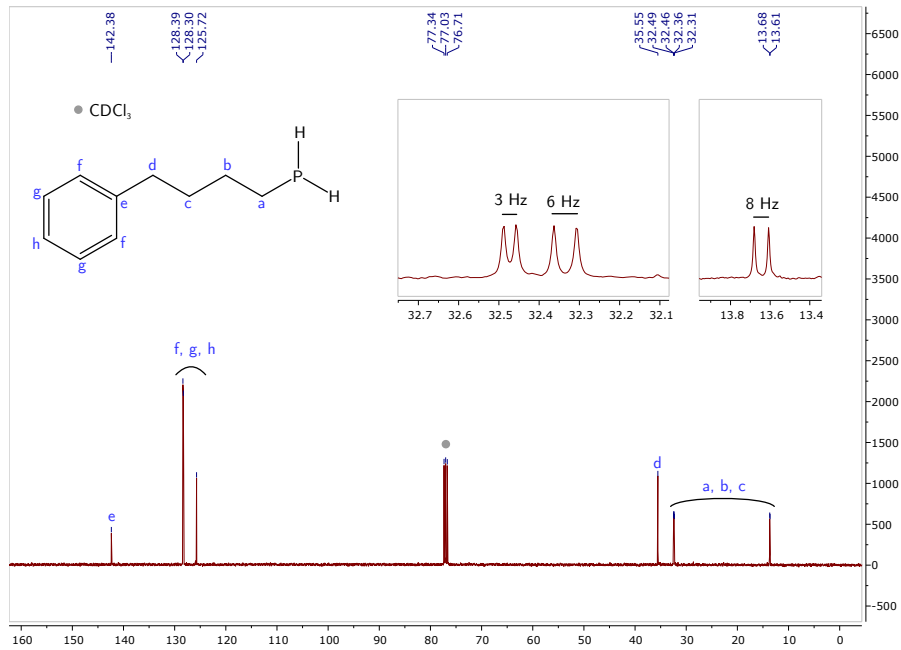


Figure 2.17 $^{13}\text{C}\{^1\text{H}\}$ NMR spectrum of $\text{Ph}(\text{CH}_2)_4\text{PH}_2$ in CDCl_3 at 25°C , recorded at 101 MHz.

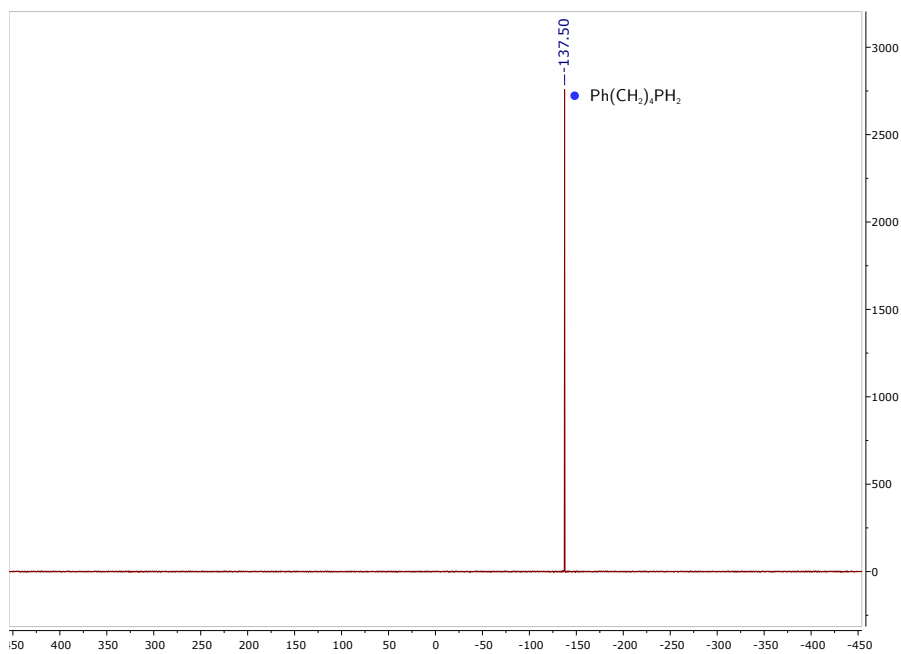


Figure 2.18 $^{31}\text{P}\{^1\text{H}\}$ NMR spectrum of $\text{Ph}(\text{CH}_2)_4\text{PH}_2$ in CDCl_3 at 25°C , recorded at 162 MHz.

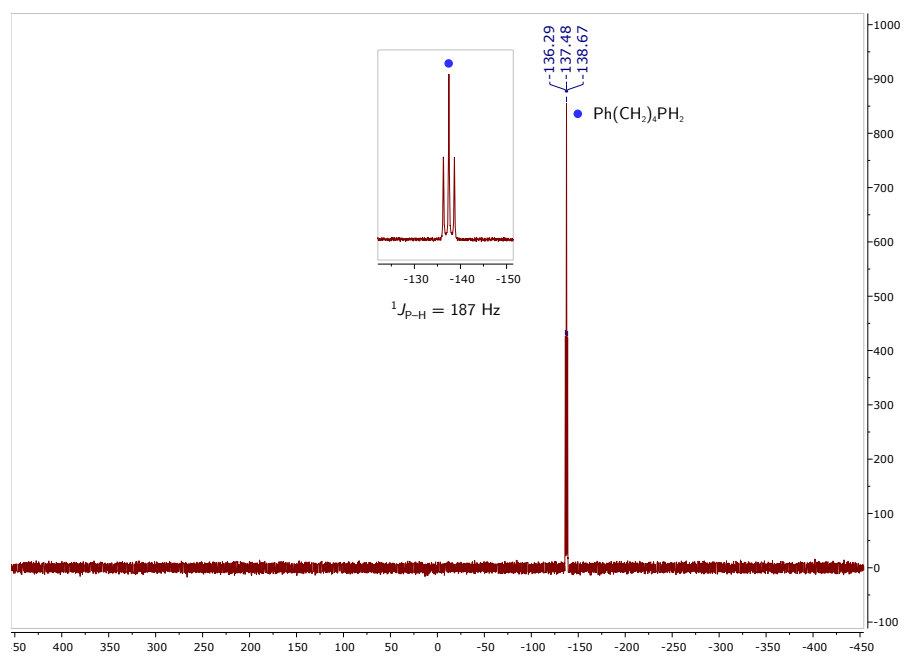


Figure 2.19 ^{31}P NMR spectrum of $\text{Ph}(\text{CH}_2)_4\text{PH}_2$ in CDCl_3 at 25°C , recorded at 162 MHz .

2.4.7 Synthesis of $(\text{Ph}(\text{CH}_2)_4)_2\text{PH}$

2.4.7.1 Method 1: Isolation as borane adduct

In the glovebox, solid [TBA][1] (1.084 g, 2.0 mmol) was weighed into a 100 mL Schlenk flask equipped with a Teflon-coated magnetic stir bar (10 mm). (4-chlorobutyl)benzene (1.69 g, 10.0 mmol) was weighed into a vial (20 mL), and added to the Schlenk flask using a pipette. The vial used to weigh (4-chlorobutyl)benzene was washed with toluene (2×4 mL) which was subsequently added to the Schlenk flask. The flask was sealed and placed in a preheated oil bath at 105 °C for 108 h. After this time, it was connected to a Schlenk line and placed in an ice bath. After cooling to 0 °C, a THF solution of BH_3 (1.0 M, 7.0 mL, 7.0 mmol) was added to the flask using a syringe against a positive pressure of nitrogen. The solution was stirred for one hour at 0 °C followed by one hour at 23 °C. The product was worked up using a modified literature procedure for the isolation of other secondary alkylphosphine-borane compounds.³⁷ The solution was carefully added to an aqueous solution of sodium hydroxide (1.0 M, 80 mL, *caution: exothermic!*) and once the addition was complete the mixture was stirred for 2 h. DCM (30 mL) was added to the mixture which was then stirred for an additional twenty minutes. The organic layer was separated using a separatory funnel and the aqueous portion extracted with DCM (3×30 mL). The organic layers were combined and dried over anhydrous magnesium sulfate, then filtered through a frit (fine porosity, 15 mL) into a round bottom flask (200 mL). Volatile material was removed in vacuo on the Schlenk line to give a colorless oil. The crude material was purified on silica gel using hexane/EtOAc (95:5) as the eluent to give $(\text{Ph}(\text{CH}_2)_4)_2\text{P}(\text{BH}_3)\text{H}$ as a colorless oil (120 mg, 0.38 mmol, 19% yield). The major phosphorus-containing product of this reaction was identified as the primary phosphine $\text{Ph}(\text{CH}_2)_4\text{PH}_2$, as determined by further experiments (section 2.4.7.3). ^1H NMR (500 MHz, CDCl_3 , δ) 7.52 – 6.96 (m, 10H), 4.54 (dm, $J_{\text{P-H}} = 355.9$ Hz, 1H), 2.81 – 2.47 (m, 4H), 1.90 – 1.41 (m, 12H), 0.43 (m, 3H). $^{13}\text{C}\{^1\text{H}\}$ NMR (126 MHz, CDCl_3 , δ) 141.77, 128.50, 128.44, 126.03, 35.42, 32.50 (d, $J_{\text{P-C}} = 11.2$ Hz), 24.11, 20.40 (d, $J_{\text{P-C}} = 34.8$ Hz). $^{31}\text{P}\{^1\text{H}\}$ NMR (203 MHz, CDCl_3 , δ) –8.13 (d, $J_{\text{P-B}} = 70.0$ Hz). ^{31}P NMR (203 MHz, CDCl_3 , δ) –8.13 (d, $^{31}\text{P}\{^1\text{H}\} = 355.9$ Hz). ^{11}B NMR (161 MHz, CDCl_3 , δ) –42.41 (d, $J = 52.5$ Hz). Elemental analysis was not performed due to observable impurities by ^1H and ^{31}P NMR spectroscopy.

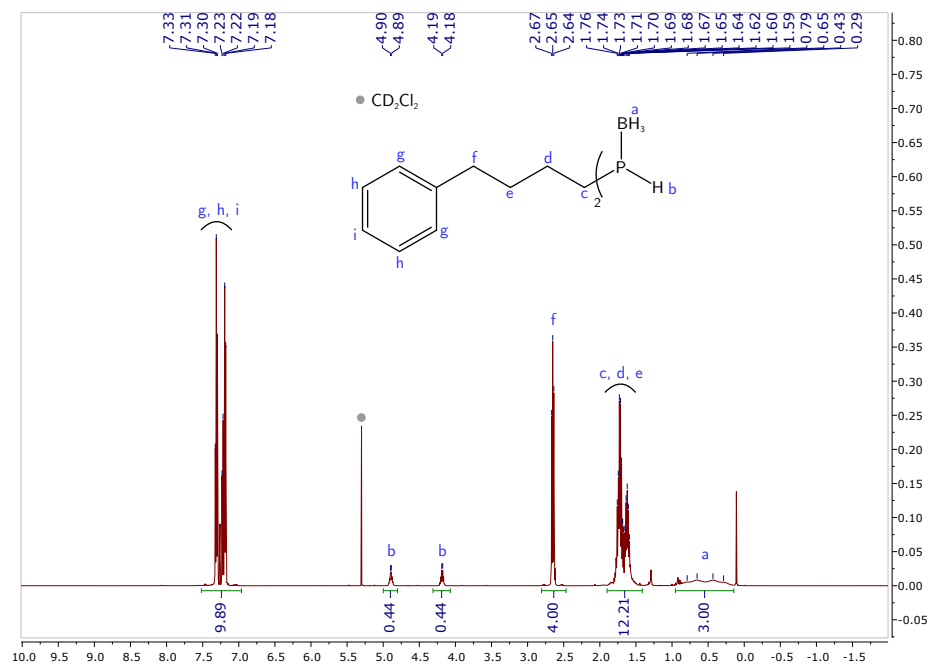


Figure 2.20 ^1H NMR spectrum of $(\text{Ph}(\text{CH}_2)_4)_2\text{P}(\text{BH}_3)\text{H}$ in CDCl_3 at 25°C , recorded at 500 MHz.

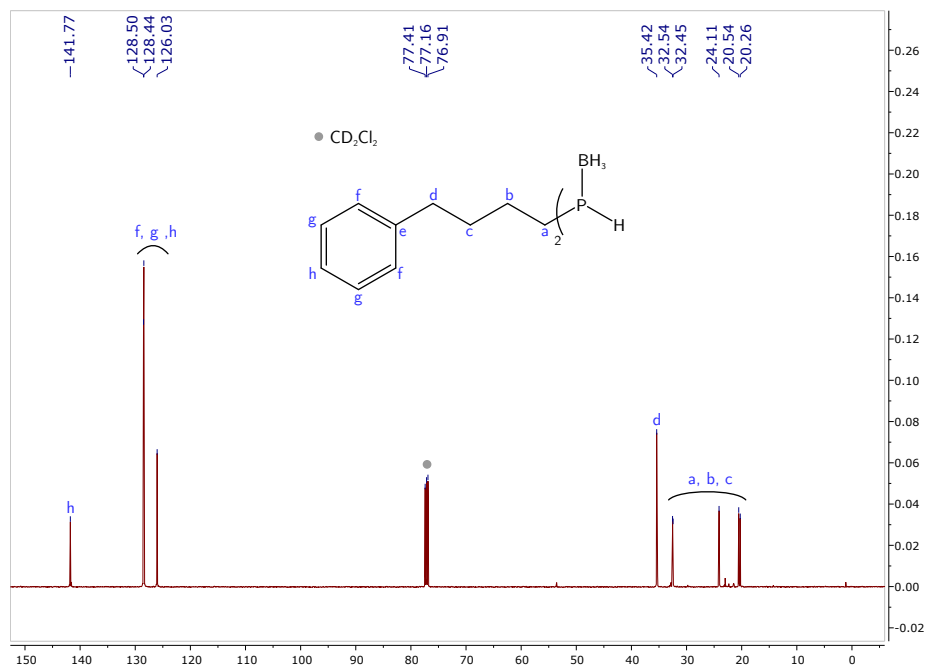


Figure 2.21 $^{13}\text{C}\{^1\text{H}\}$ NMR spectrum of $(\text{Ph}(\text{CH}_2)_4)_2\text{P}(\text{BH}_3)\text{H}$ in CDCl_3 at 25°C , recorded at 126 MHz.

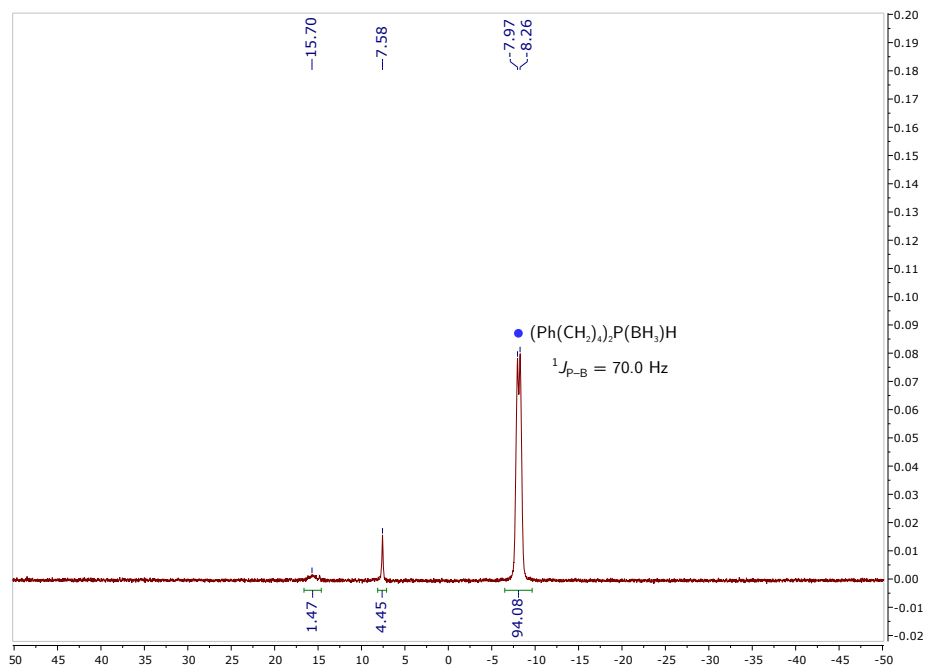


Figure 2.22 $^{31}\text{P}\{^1\text{H}\}$ NMR spectrum of $(\text{Ph}(\text{CH}_2)_4)_2\text{P}(\text{BH}_3)\text{H}$ in CDCl_3 at 25°C , recorded at 203 MHz.

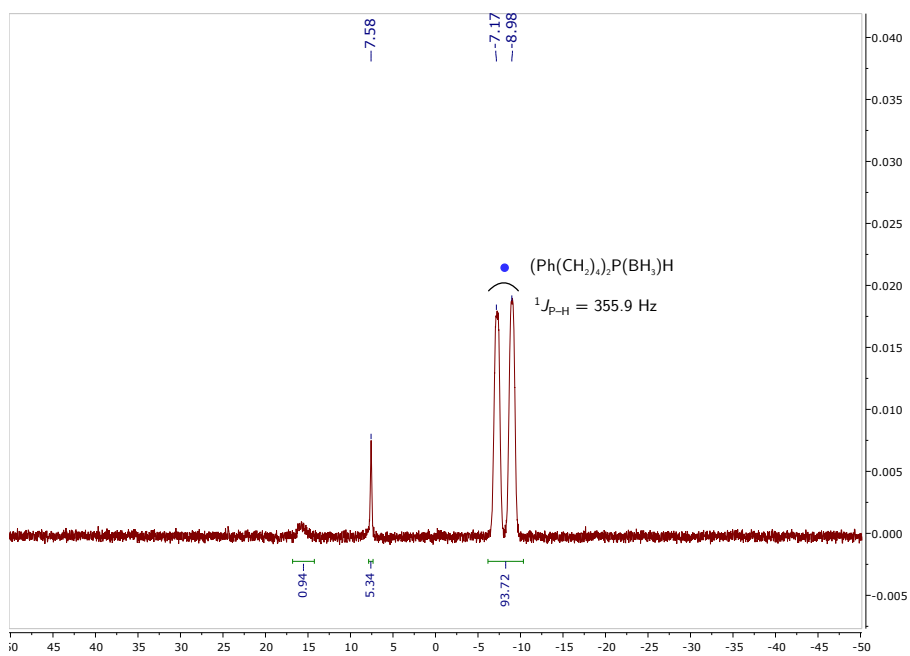


Figure 2.23 ^{31}P NMR spectrum of $(\text{Ph}(\text{CH}_2)_4)_2\text{P}(\text{BH}_3)\text{H}$ in CDCl_3 at 25°C , recorded at 203 MHz.

2.4.7.2 Method 2: Isolation as unprotected phosphine

In the glovebox, [TBA][1] (1.084 g, 2.0 mmol) was weighed into a 100 mL thick-walled Schlenk flask equipped with a Teflon-coated magnetic stir bar (10 mm). (4-chlorobutyl)benzene (1.690 g, 10.0 mmol) was weighed into a vial (20 mL) and transferred to the Schlenk flask using toluene (4 mL, 2 × 2 mL; 8 mL total). The flask was sealed and removed from the glovebox, then placed in a preheated oil bath at 110 °C for 108 h. After this time, it was allowed to cool to 25 °C. On the Schlenk line, volatile material was briefly removed in vacuo for 5 minutes to remove any volatile silicon containing species. The flask was then brought into the glovebox and the solution transferred to a vial (20 mL); pentane (10 mL) was used to aid transfer of the material. Activated basic alumina (8.0 g) was added to the vial, and the solution was stirred for 20 minutes. The solution was poured into a frit (60 mL, fine porosity) that had been filled with activated basic alumina (45 mL). The alumina bed was washed with pentane (100 mL) and the filtrate was discarded (¹H NMR spectroscopy showed it contained (4-chlorobutyl)benzene. The alumina bed was washed with additional pentane (100 mL) followed by DCM (100 mL). Volatile material was removed in vacuo, to give a clear colorless oil, which was purified by column chromatography inside the glovebox. The stationary phase was activated basic alumina (50 mL dry volume), and the eluent was pentane/DCM (5:1 v/v) which also contained triethylamine (0.1% v/v). Before the crude material was loaded onto the column, the stationary phase was treated with pentane:DCM:triethylamine (49.5:49.5:1 v/v/v, 100 mL). Fractions (12 mL) were analyzed by TLC and ³¹P NMR spectroscopy, with the desired compound eluting between fractions 4–10. The sixth fraction was used to collect the NMR data shown in Figs. 2.24–2.27, so as to unambiguously assign the product by its NMR data. The fractions containing the desired product were combined and dried to constant mass to give bis(4-phenylbutyl)phosphine as a clear colorless oil (143 mg, 0.480 mmol, 24% yield). The purity of the product was assessed by use of an internal standard and ¹H NMR spectroscopy, and the final yield adjusted to 20%. The major phosphorus-containing product of this reaction was identified as the primary phosphine Ph(CH₂)₄PH₂, as determined by further experiments (section 2.4.7.3). ¹H NMR (500 MHz, CDCl₃, δ) 7.35 – 7.16 (m, 10H), 3.11 (dm, *J*_{P-H} = 199.5 Hz, 1H), 2.70 – 2.60 (m, 4H), 1.77–1.45 (m, 12H). ¹³C{¹H} NMR (126 MHz, CDCl₃, δ) 142.57, 128.53, 128.42, 125.82, 35.76, 32.90 (d, *J*_{P-C} = 8.7 Hz), 28.09 (d, *J*_{P-C} = 10.0 Hz), 20.32 (d, *J*_{P-C} = 9.2 Hz). ³¹P{¹H} NMR (203 MHz, CDCl₃, δ) –69.16. ³¹P NMR (203 MHz, CDCl₃, δ) –69.16 (d, *J*_{P-H} = 199.5 Hz). Elemental analysis was not performed due to observable minor impurities by ¹H and ³¹P NMR spectroscopy.

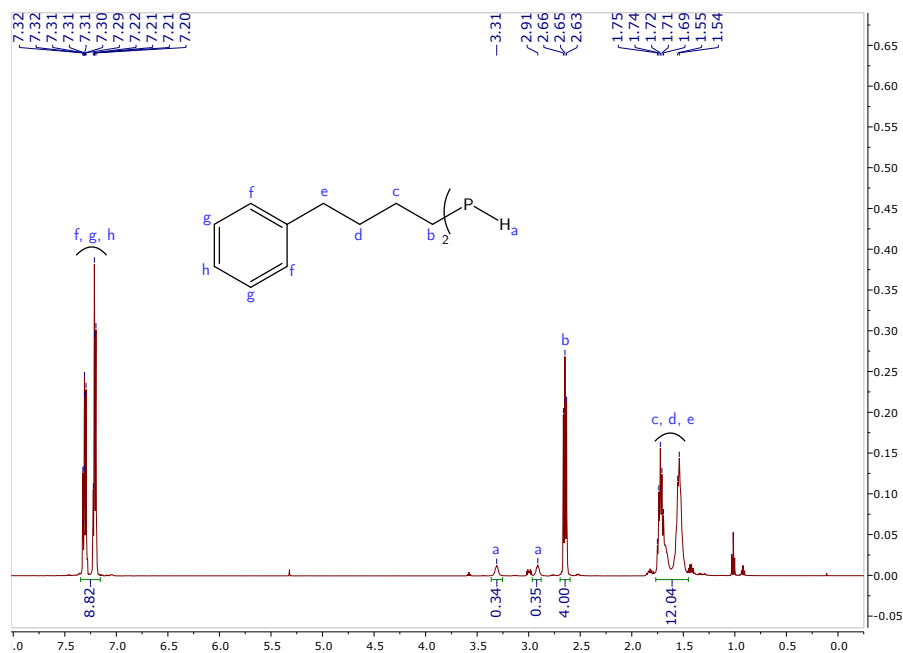


Figure 2.24 ^1H NMR spectrum of $(\text{Ph}(\text{CH}_2)_4)_2\text{PH}$ in CDCl_3 at $25\text{ }^\circ\text{C}$, recorded at 500 MHz.

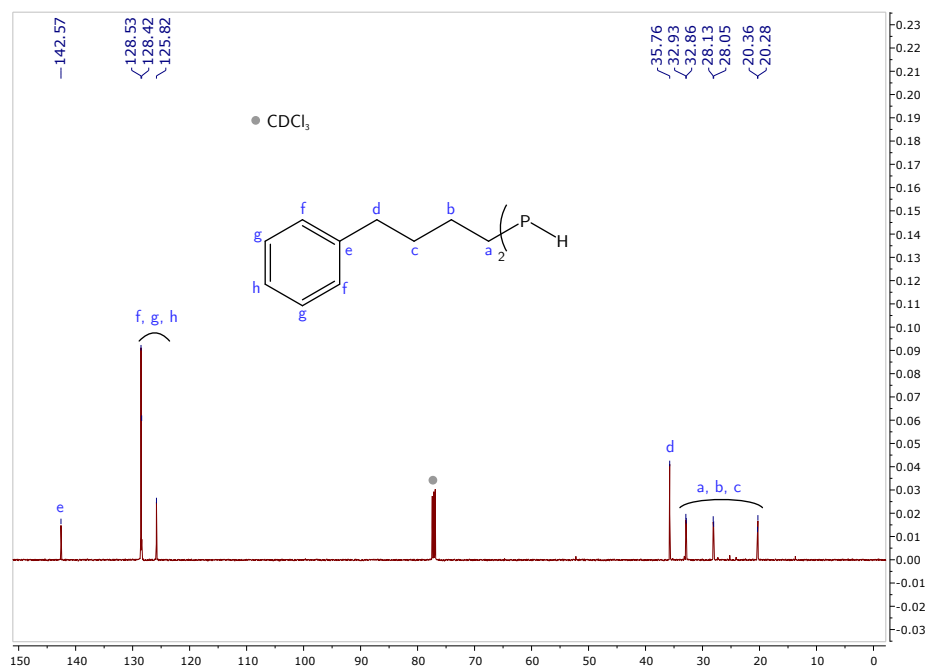


Figure 2.25 $^{13}\text{C}\{^1\text{H}\}$ NMR spectrum of $(\text{Ph}(\text{CH}_2)_4)_2\text{PH}$ in CDCl_3 at $25\text{ }^\circ\text{C}$, recorded at 126 MHz.

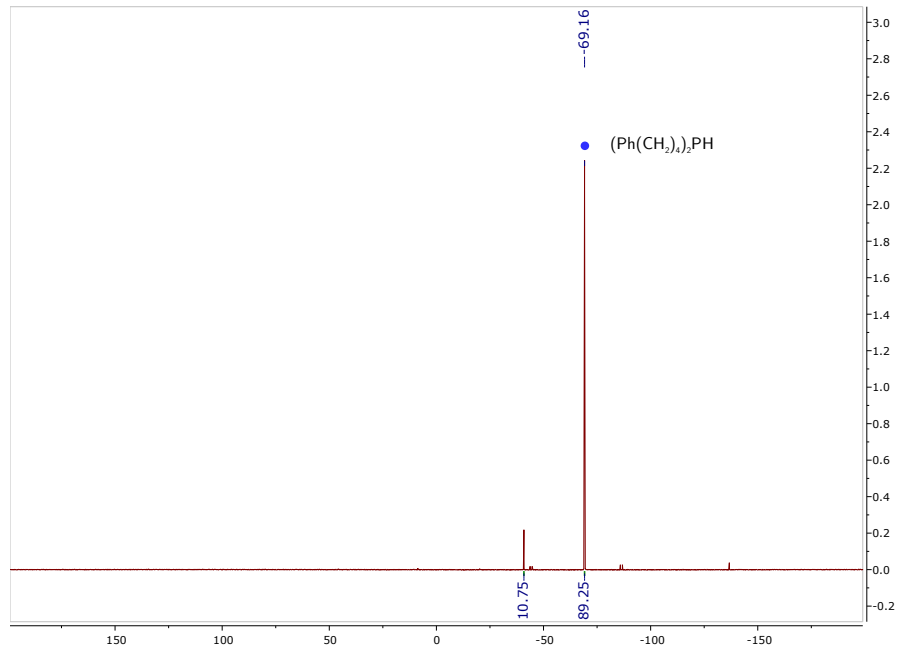


Figure 2.26 $^{31}\text{P}\{^1\text{H}\}$ NMR spectrum of $(\text{Ph}(\text{CH}_2)_4)_2\text{PH}$ in CDCl_3 at 25°C , recorded at 203 MHz.

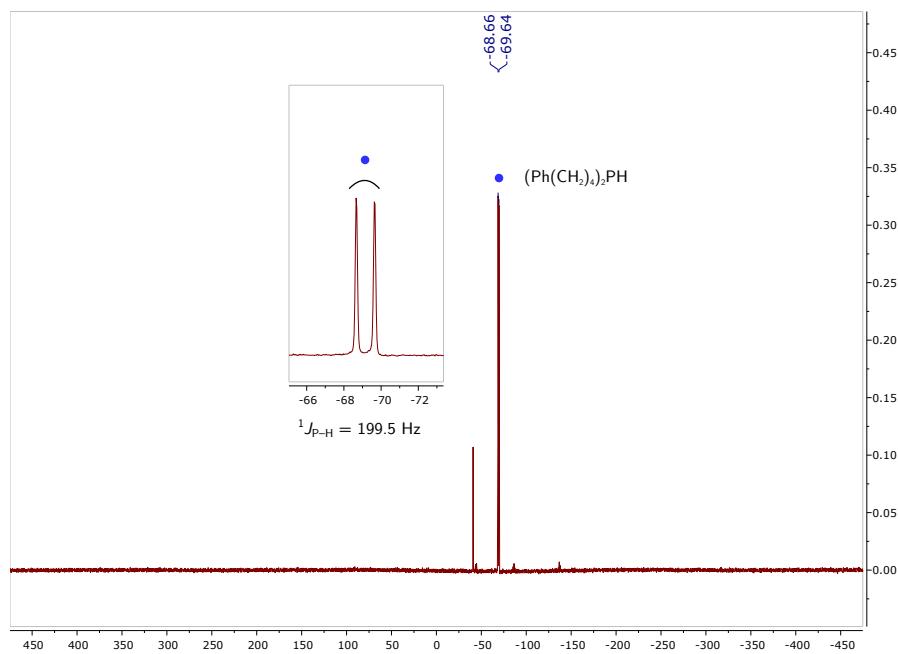


Figure 2.27 ^{31}P NMR spectrum of $(\text{Ph}(\text{CH}_2)_4)_2\text{PH}$ in CDCl_3 at 25°C , recorded at 203 MHz.

2.4.7.3 In situ yield of $(\text{Ph}(\text{CH}_2)_4)_2\text{PH}$

In the glovebox, $[\text{TBA}][\mathbf{1}]$ (21 mg, 0.04 mmol) was weighed into an NMR tube equipped with a J. Young valve. (4-chlorobutyl)benzene (33 mg, 0.2 mmol) was weighed into a vial (20 mL) and transferred to the NMR tube using toluene- d_8 (0.6 mL total, in three washes). A capillary, prepared as described in section 2.4.4, was inserted into the NMR tube. The tube was sealed and the T_1 of the ^{31}P nucleus of $[\text{TBA}][\mathbf{1}]$ was measured and found to be 2.94 s. The NMR tube was placed in a preheated oil bath at 105 °C for 120 h. The T_1 of the ^{31}P nucleus of the $(\text{Ph}(\text{CH}_2)_4)_2\text{PSiCl}_3$ that formed was measured by the inversion recovery method and found to be 0.67 s. A quantitative ^{31}P NMR spectrum was acquired (8 transients) with a d_1 of $\geq 5 \cdot T_1$ (Fig. 2.28). Water (70 μL , 3.8 mmol), bubble degassed with nitrogen for 20 minutes, was added using a micro syringe to the NMR tube against a flow of nitrogen. The solution was heated to 70 °C for 2 h. The T_1 of the ^{31}P nucleus of the $(\text{Ph}(\text{CH}_2)_4)_2\text{PH}$ that formed was measured and found to be 4.83 s. A quantitative ^{31}P NMR spectrum was acquired (8 transients) with a d_1 of $\geq 5 \cdot T_1$. The in situ yield of $(\text{Ph}(\text{CH}_2)_4)_2\text{PH}$ was found to be 38%.

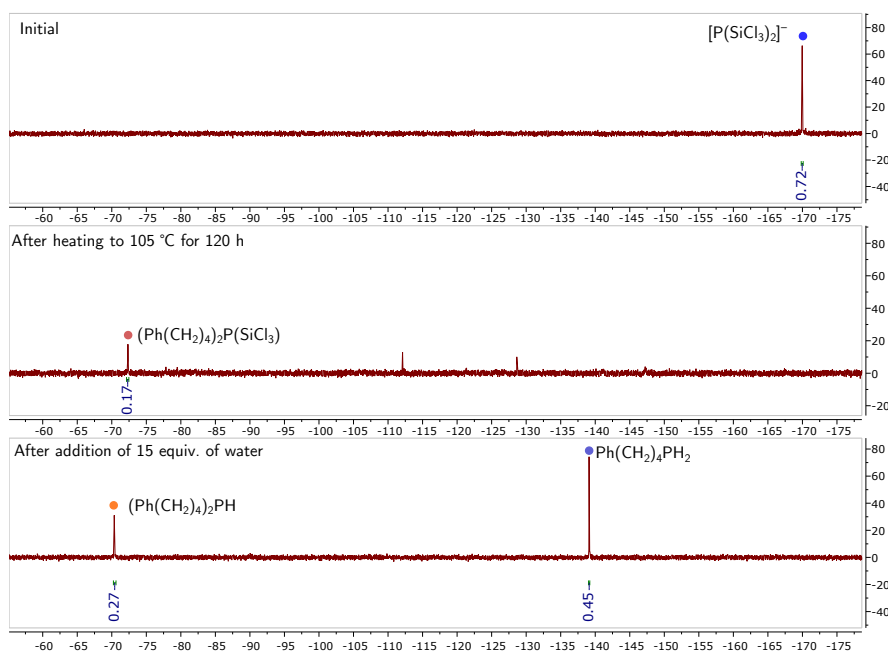


Figure 2.28 Quantitative ^{31}P NMR spectra of the reaction mixture at three different time points in toluene- d_8 at 25 °C. Top: spectrum immediately after dissolving $[\text{TBA}][\mathbf{1}]$ and (4-chlorobutyl)benzene in toluene- d_8 . Middle: spectrum after heating the reaction mixture at 105 °C for 120 h. Bottom: spectrum after addition of water (15 equiv.) to the reaction mixture, followed by heating to 70 °C for 2h. Integrations are given relative to the integration of the PPh_3 resonance which was set to 1.00 and omitted for clarity.

2.4.8 Synthesis of Ph(CH₂)₄P(O)(OH)H

In the glovebox, (4-phenylbutyl)phosphine (30 mg, 0.18 mmol) was weighed into a vial (20 mL) containing a Teflon-coated magnetic stir bar (10 mm) and dissolved in acetonitrile (2 mL). The vial was brought outside the glovebox and an aqueous solution of H₂O₂ (30% (w/w) in H₂O, 40 μL, 0.40 mmol) was added using a micro syringe. The solution was stirred for two hours with the vial cap on, before volatile material was removed in vacuo to give a sticky colorless residue. The residue was partitioned between brine (4 mL) and ethyl acetate (4 mL), and the organic phase separated. The brine was washed with additional ethyl acetate (4 mL), and the organic phases were combined and dried over magnesium sulfate. The solids were removed by filtration and volatile material was removed in vacuo. The oil obtained was triturated once with chloroform (2 mL) to give the product as a clear colorless viscous oil (32 mg, 0.16 mmol, 90% yield). ¹H NMR (500 MHz, CDCl₃, δ) 10.40 (s, 1H), 7.31 – 7.15 (m, 5H), 7.08 (d, *J*_{P-H} = 542 Hz, 1H), 2.64 (t, *J* = 7 Hz, 2H), 1.92 – 1.48 (m, 6H). ¹³C{¹H} NMR (126 MHz, CDCl₃, δ) 141.82, 128.50, 128.45, 126.03, 35.55, 32.27 (d, *J*_{P-C} = 15.9 Hz), 29.19 (d, *J*_{P-C} = 94.1 Hz), 20.42. ³¹P{¹H} NMR (203 MHz, CDCl₃, δ) 38.77 (s). ³¹P NMR (203 MHz, CDCl₃, δ) 38.77 (d, *J*_{P-H} = 542 Hz). These spectral data match reported values from the literature.^{19,38}

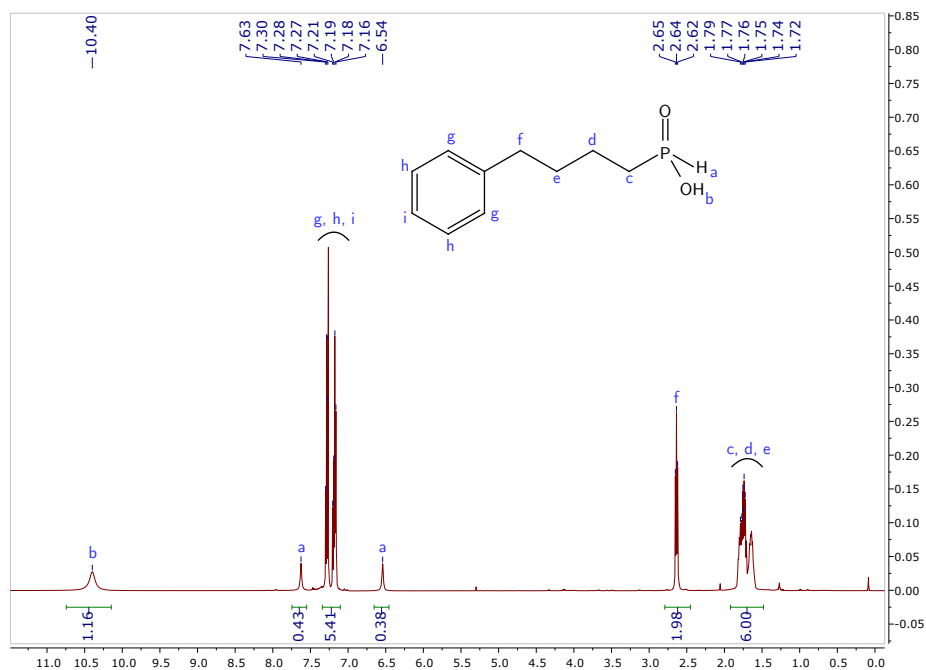


Figure 2.29 ¹H NMR spectrum of Ph(CH₂)₄P(O)(OH)H in CDCl₃ at 25 °C, recorded at 500 MHz.

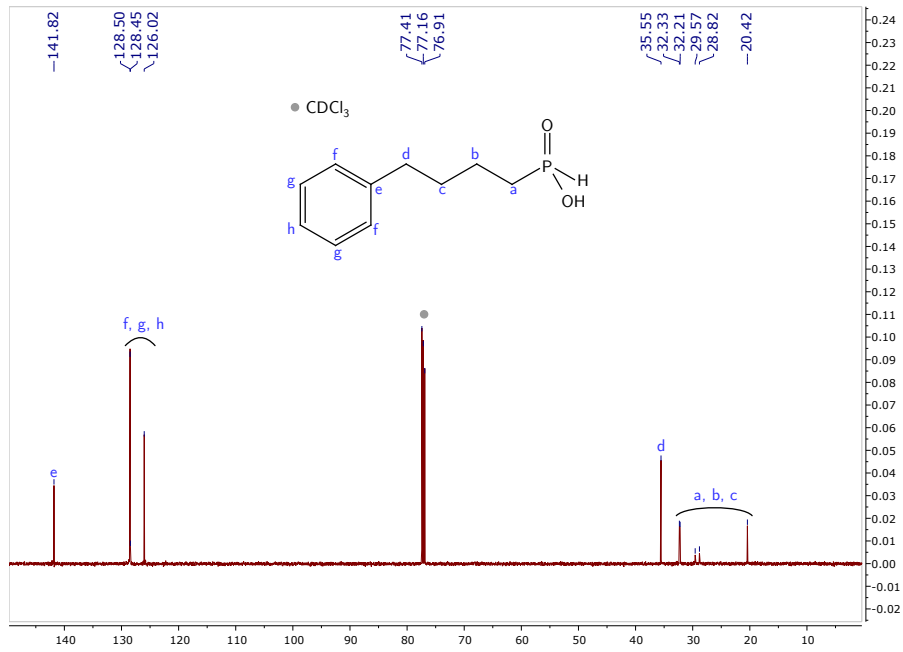


Figure 2.30 $^{13}\text{C}\{^1\text{H}\}$ NMR spectrum of $\text{Ph}(\text{CH}_2)_4\text{P}(\text{O})(\text{OH})\text{H}$ in CDCl_3 at 25°C , recorded at 126 MHz.

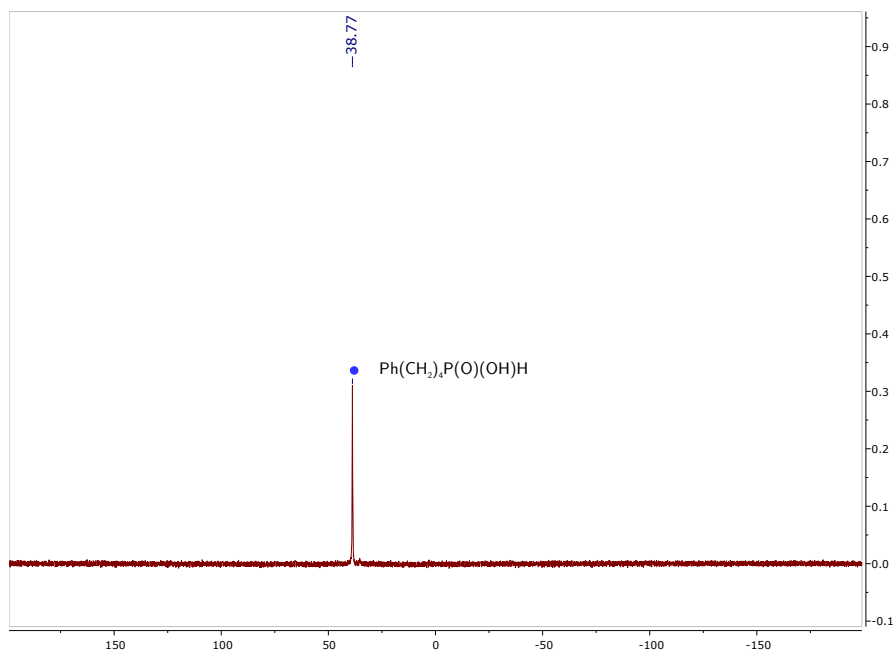


Figure 2.31 $^{31}\text{P}\{^1\text{H}\}$ NMR spectrum of $\text{Ph}(\text{CH}_2)_4\text{P}(\text{O})(\text{OH})\text{H}$ in CDCl_3 at 25°C , recorded at 203 MHz.

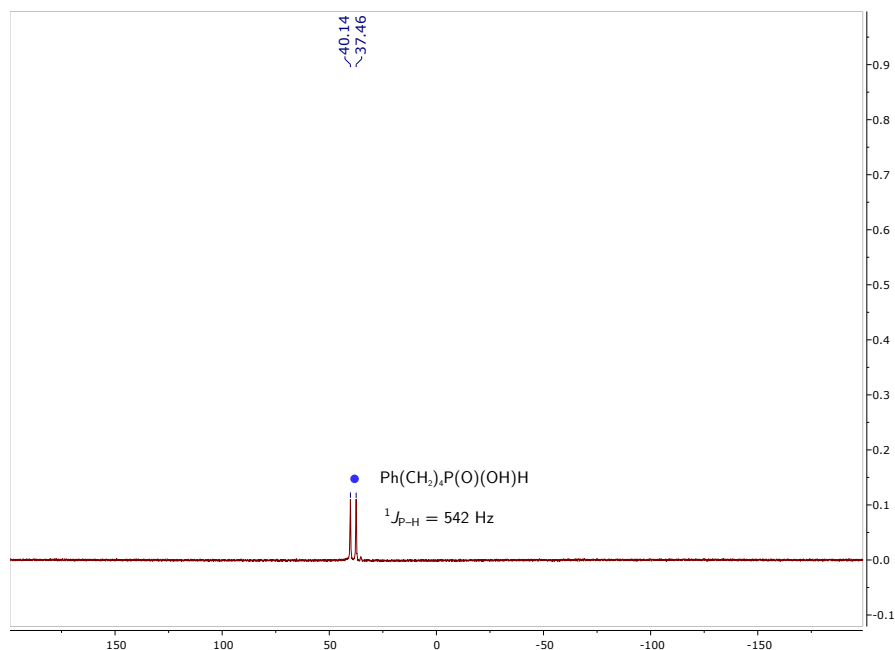


Figure 2.32 ^{31}P NMR spectrum of $\text{Ph}(\text{CH}_2)_4\text{P}(\text{O})(\text{OH})\text{H}$ in CDCl_3 at $25\text{ }^\circ\text{C}$, recorded at 203 MHz.

2.4.9 X-ray Diffraction Studies of [TBA][1]

Diffraction-quality, colorless crystals were grown by dissolving [TBA][1] (300 mg, 0.55 mmol) in DCM (1 mL), followed by addition of diethyl ether (2 mL) to produce a white precipitate. The mixture was stored in the freezer (with no filtration step) at $-35\text{ }^\circ\text{C}$ for 48 h. A single crystal was selected under a microscope and mounted in hydrocarbon oil on a nylon loop. Low-temperature (100 K) data were collected on a Bruker-AXS X8 Kappa Duo diffractometer coupled to a Smart Apex2 CCD detector with Mo $\text{K}\alpha$ radiation ($\lambda = 0.71073\text{ \AA}$) with ϕ - and ω -scans. A semi-empirical absorption correction was applied to the diffraction data using SADABS.^{39,40} The structure was solved by direct methods using SHELXT^{41,42} and refined against F^2 on all data by full-matrix least squares with ShelXle.⁴³ All non-hydrogen atoms were refined anisotropically. All hydrogen atoms were included in the model at geometrically calculated positions and refined using a riding model. The isotropic displacement parameters of all hydrogen atoms were fixed to 1.2 times the U_{eq} value of the atoms they are linked to (1.5 times for methyl groups).

[TBA][1] crystallizes with two anions and two cations in the asymmetric unit. One of the tetrabutylammonium cations was disordered; the disorder was treated with a simple model to restrain chemically equivalent methylene and methyl groups to be the same (SAME command). One of the bis(trichlorosilylphosphide) anions was disordered over two sites; this disorder was modeled as a major and minor component. During the refinement, the two disordered anions were restrained to be the same. However, these restraints could

be lifted at the end of the refinement procedure to provide a stable solution. The other bis(trichlorosilyl)phosphide anion was not disordered and was refined without restraints. Similar-ADP and rigid bond restraints (SIMU and RIGU commands, respectively) were applied to the entire structure.

CSD identification code	1815508
Reciprocal net code	X8_17117
Empirical formula	C ₁₆ H ₃₆ Cl ₆ NPSi ₂
Formula weight	542.31 g/mol
Color / morphology	colorless / needle
Temperature	100(2) K
Wavelength	0.71073 Å
Crystal system	Orthorhombic
Space group	<i>P</i> 2 ₁ 2 ₁ 2 ₁
Unit cell dimensions	<i>a</i> = 15.511(3) Å <i>α</i> = 90° <i>b</i> = 17.665(3) Å <i>β</i> = 90° <i>c</i> = 20.303(3) Å <i>γ</i> = 90°
Volume	5562.9(15) Å ³
<i>Z</i>	8
Density (calculated)	1.295 g/cm ³
Absorption coefficient	0.766 mm ⁻¹
<i>F</i> (000)	2272
Crystal size	0.138 × 0.090 × 0.090 mm ³
Theta ranges for data collection	1.528 to 27.877°
Index ranges	-20 ≤ <i>h</i> ≤ 20, -23 ≤ <i>k</i> ≤ 23, -26 ≤ <i>l</i> ≤ 26
Reflections collected	83971
Independent reflections	13268 [<i>R</i> _{int} = 0.0727]
Completeness to <i>θ</i> = 25.242°	100.0%
Absorption correction	Semi-empirical from equivalents
Refinement method	Full-matrix least-squares on <i>F</i> ²
Data \restraints \parameters	13268 \1406 \708
Goodness-of-fit on <i>F</i> ²	1.037
Final <i>R</i> indices [<i>I</i> > 2σ(<i>I</i>)]	<i>R</i> ₁ = 0.0507, <i>wR</i> ₂ = 0.1079
<i>R</i> indices (all data)	<i>R</i> ₁ = 0.0730, <i>wR</i> ₂ = 0.1174
Absolute structure parameter	-0.02(3)
Extinction coefficient	n/a
Largest diff. peak and hole	0.728 and -0.391 e·Å ⁻³

Table 2.3 X-ray crystallographic information for [TBA][1]

2.4.10 Mass spectral studies of [TBA][1]

[TBA][1] (5 mg, 0.01 mmol) was dissolved in DCM (5 mL). This stock solution (1 mL) was transferred to a GC vial (2 mL) equipped with a septum. The GC vial was placed inside a scintillation vial (20 mL) which was capped and sealed with electrical tape to minimize air exposure prior to data acquisition. The capillary of the instrument was washed with dry DCM (3 mL) before the data were collected in negative ion mode, using a source temperature of 100 °C and a desolvation temperature of 150 °C. Anion **1** was identified as a species with low signal intensity (Fig. 2.33). Decreasing the capillary voltage from 3400 to 2800 V gave a concomitant increase in the signal of **1** relative to the most intense fragment. Other fragments were identified as $[\text{Cl}_6\text{OPSi}_2]^-$ ($m/z = 315.86$) and $[\text{Cl}_6\text{O}_2\text{PSi}_2]^-$ ($m/z = 331.86$).

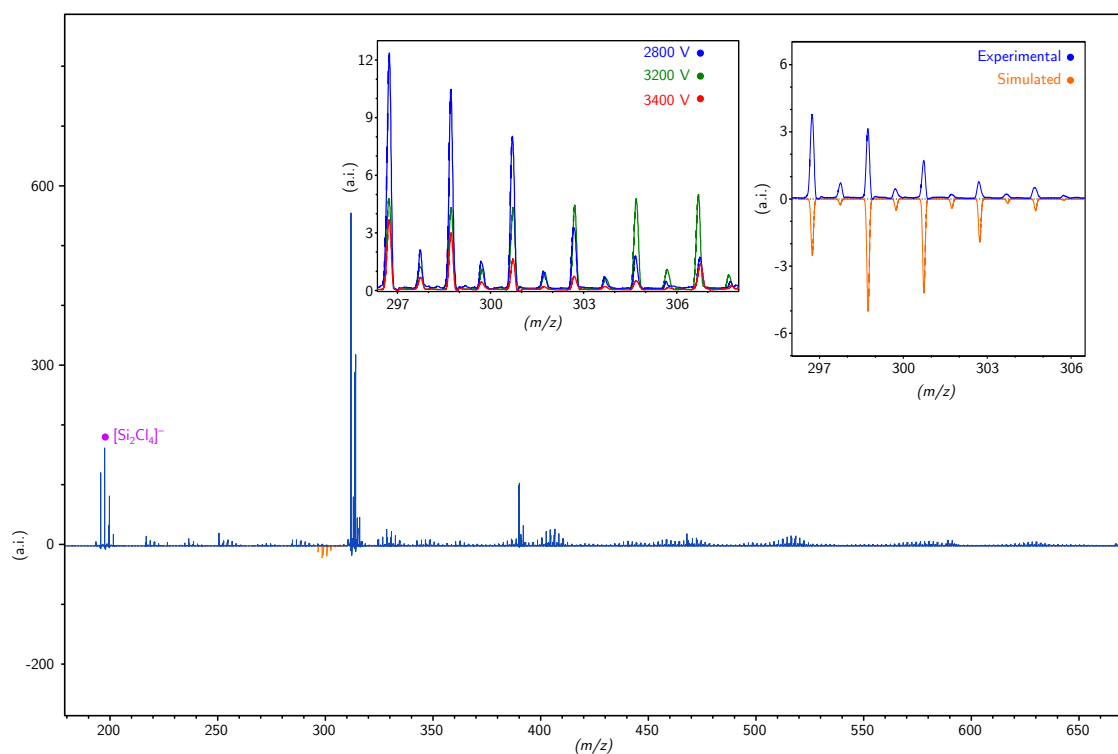


Figure 2.33 ESI-MS(-) of a DCM solution containing [TBA][1]. Inset: (left) Relative intensity of **1** as a function of capillary voltage, (right) comparison of the experimental (2800 V) and simulated mass spectrum of **1**.

2.4.11 Raman spectrum of [TBA][1]

In the glovebox, [TBA][1] (3 mg, 0.006 mmol) was loaded into a quartz capillary, and the opening was sealed with vacuum grease. The capillary was placed in the instrument, and analyzed using 785 nm wavelength irradiation. Density functional theory (DFT) calculations were performed as described in section 2.5.3. An intense band was observed in the experimental spectrum at 378 cm^{-1} (Fig. 2.34), corresponding to the A_1 stretching mode (according to idealized C_{2v} symmetry).

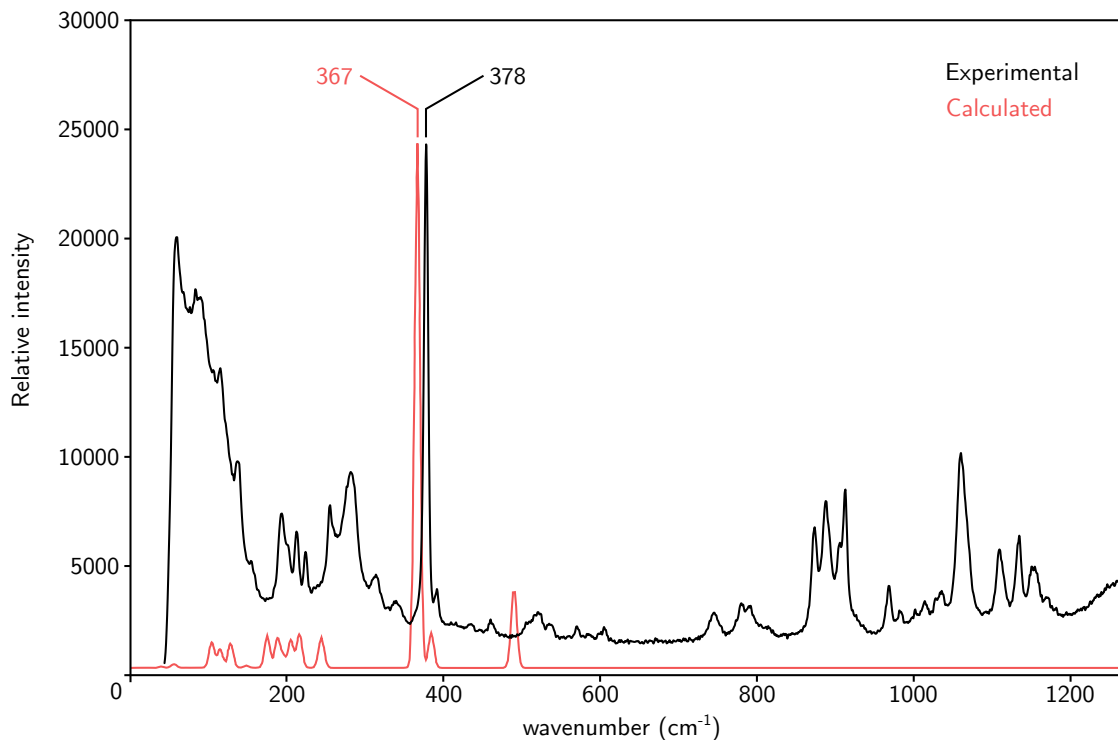


Figure 2.34 Experimental (black) and calculated (red) Raman spectra of [TBA][1] and **1**, respectively.

2.5 Computational details

Calculations were performed using Orca 4.0.0.⁴⁴ The geometries of stationary points were found to have zero imaginary frequencies, as determined by vibrational frequencies calculations.

2.5.1 Natural bond order (NBO) analysis of **1**

The geometry of **1** was optimized at the M062X/ma-def2-TZVPP level of theory. Solvation effects were modeled using COSMO, and the solvent was selected as DMSO. The optimized structure (Table 2.4) was analyzed by the NBO method.¹⁷ The results (Table 2.5) were obtained with the NRT keyword.

Element	X	Y	Z
P	-0.0185850000	0.0179640000	-0.9657100000
Si	-0.6907010000	-1.8507850000	-0.1421610000
Si	1.9583370000	0.2180480000	-0.1423770000
Cl	0.5478510000	-3.5185880000	-0.2487080000
Cl	-2.4040430000	-2.3670430000	-1.2159580000
Cl	-1.3142460000	-1.8569380000	1.8516590000
Cl	2.4869410000	2.2226580000	-0.3543400000
Cl	3.5108540000	-0.7890080000	-1.1089960000
Cl	2.2577170000	-0.2272220000	1.8641680000

Table 2.4 Optimized cartesian coordinates of **1** at the M062X/ma-def2-TZVPP level of theory.

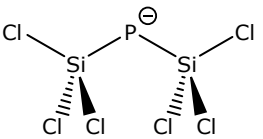
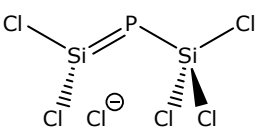
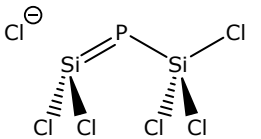
Resonance structure			
Weight	22%	8%	2%
Degeneracy	1	4	2
Total	22%	32%	4%
Net total		58%	

Table 2.5 Leading resonance structures for **1**

2.5.2 Electron localization function (ELF) analysis of **1**

The geometry of **1** was optimized at the ω B97X-D3/def2-TZVPP level of theory. The program Multiwfn⁴⁵ was used to generate the ELF cube file. Chimera⁴⁶ was used to make the figure shown in the manuscript.

2.5.3 Calculated Raman spectrum of **1**

The geometry of **1** was the same as obtained in section 2.5.1. Vibrational frequencies and Raman activities and polarizations were calculated at the M062X/ma-def2-TZVPP level of theory (Table 2.6). The calculated spectrum was plotted using Avogadro;⁴⁷ no scaling factor was employed.

Frequency / cm^{-1}	Activity	Depolarization
40.54	0.299195	0.685709
56.87	0.857369	0.404067
105.31	6.113329	0.710889
116.06	4.379565	0.746071
129.33	5.889518	0.518846
149.31	0.554515	0.736762
176.11	7.707499	0.525424
189.05	6.872388	0.733365
196.32	2.558793	0.723032
206.17	6.604676	0.749695
217.10	8.008290	0.726101
244.96	7.453775	0.124526
367.04	125.835812	0.004776
384.81	8.519372	0.741051
489.19	10.063755	0.748864
491.64	10.363886	0.721530
497.58	12.445801	0.746545
508.32	8.318944	0.658862
558.45	3.982386	0.744372
585.06	15.754700	0.091124

Table 2.6 Calculated vibrational frequencies and corresponding Raman activity and depolarization.

2.6 Fabrication of steel pressure reactor

Caution: The integrity of this pressure reactor was not tested. Reactions should be carried out behind a blast shield. The steel pressure reactor was fabricated at the MIT central machine shop. Drawings of the nut and bolt are shown in Fig. 2.35 and Fig. 2.36, respectively. The parts ordered from Swagelok to assemble the relief valve (top of nut part) and needle valve (side of nut part) are given in Table 2.7. A Teflon ring was cut to fit inside the nut part of the reactor, which formed a gas-tight seal by tightening the nut and bolt assembly.

Part description	Swagelok part number
Spring for relief valve	177-R3A-K1-F
Proportional Relief Valve, 1/4 in. MNPT x 1/4 in. FNPT	SS-4R3A5
Needle Valve, 1/8 in. MNPT	SS-1RM2
Pipe Plug, 1/4 in. Male NPT	SS-4-P
Hex Coupling, 1/8 in. Female NPT	SS-2-HCG
Hose Connector, 1/8 in. Male NPT, 1/4 in. Hose ID	SS-4-HC-1-2

Table 2.7 Parts ordered from Swagelok for the steel pressure reactor.

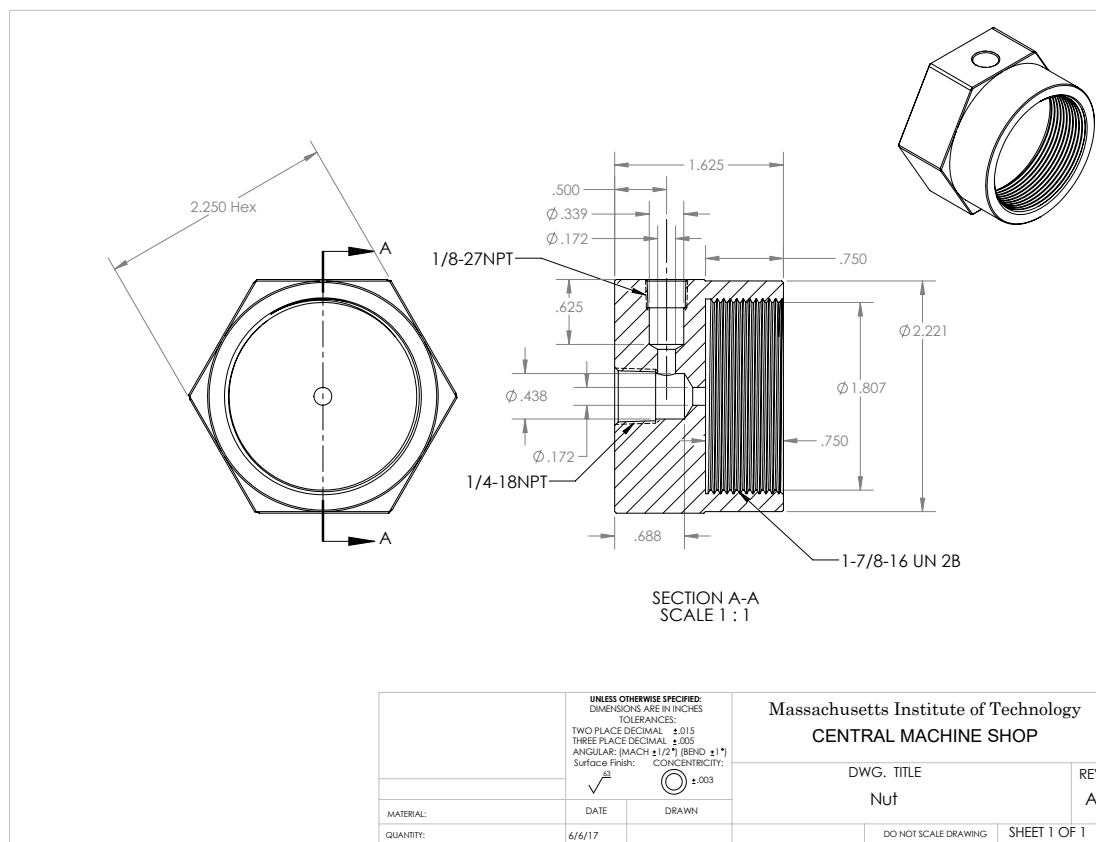


Figure 2.35 Schematic drawing of the nut part of the steel pressure reactor.

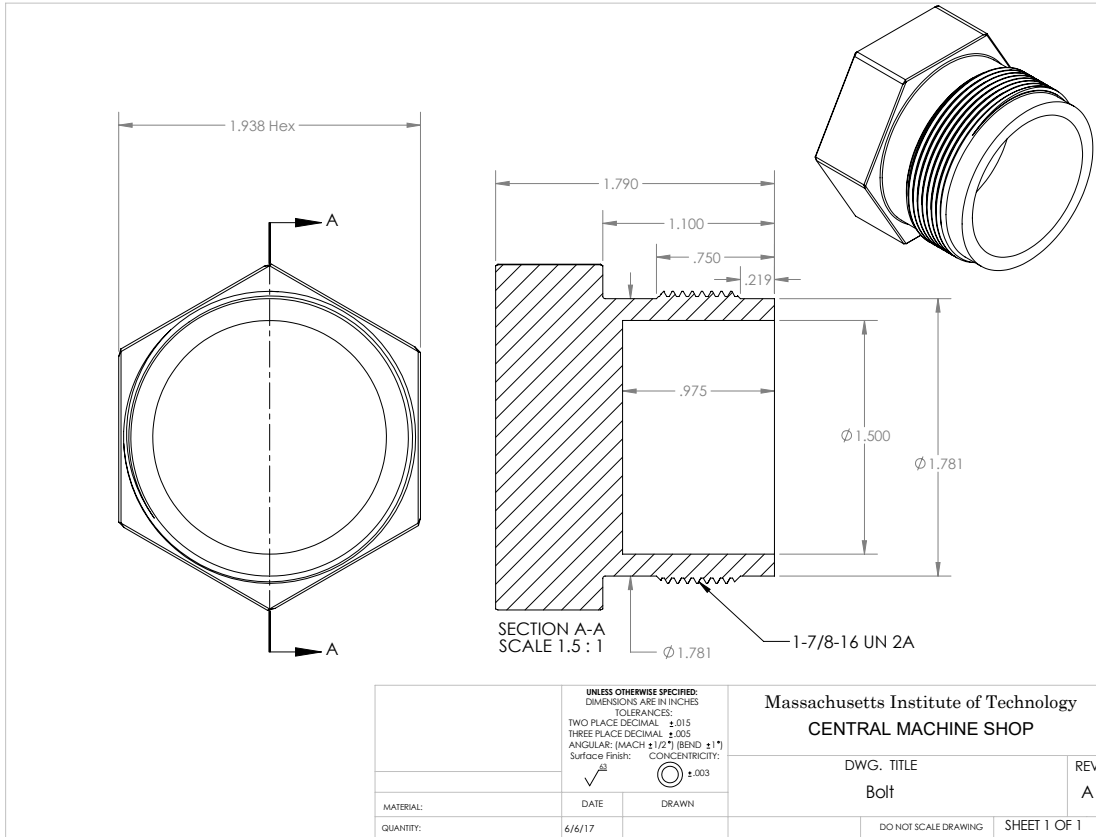


Figure 2.36 Schematic drawing of the bolt part of the steel pressure reactor.

References

- [1] Diskowski, H.; Hofmann, T. “Phosphorus”, *Ullmann’s Encyclopedia of Industrial Chemistry*; Wiley, 2000.
- [2] Younesi, R.; Veith, G. M.; Johansson, P.; Edström, K.; Vegge, T. *Energy Environ. Sci.* **2015**, *8*, 1905–1922.
- [3] Franz, J. E.; Sikorski, J. A.; Mao, M. K. *Glyphosate: A unique global herbicide*; American Chemical Society: Washington DC, 1997.
- [4] Peruzzini, M.; Gonsalvi, L.; Romerosa, A. *Chem. Soc. Rev.* **2005**, *34*, 1038.
- [5] Borger, J. E.; Ehlers, A. W.; Slootweg, J. C.; Lammertsma, K. *Chem. - Eur. J.* **2017**, *23*, 11738–11746.
- [6] Simmler, W. “Silicon Compounds, Inorganic”, *Ullmann’s Encyclopedia of Industrial Chemistry*; Wiley: Weinheim, Germany, 2000.
- [7] Deloitte Sustainability, British Geological Survey, Bureau de Recherches Géologiques et Minières, Netherlands Organisation for Applied Scientific Research, *Study on the review of the list of critical raw materials*; 2017; <https://doi.org/10.2873/398823>.
- [8] European Commission, 2017 list of Critical Raw Materials for the EU. 2017.
- [9] Schrödter, K.; Bettermann, G.; Staffel, T.; Wahl, F.; Klein, T.; Hofmann, T. “Phosphoric Acid and Phosphates”, *Ullmann’s Encyclopedia of Industrial Chemistry*; Wiley: Weinheim, Germany, 2008.
- [10] Emsley, J. *The 13th element: the sordid tale of murder, fire and phosphorus*; Wiley: New York, 2000.
- [11] Pham Minh, D.; Ramarosan, J.; Nzihou, A.; Sharrock, P. *Ind. Eng. Chem. Res.* **2012**, *51*, 3851–3854.
- [12] Rebek observed a similar analogy stating “The phosphorus analogs to the ketenes are the metaphosphates” in: J. Rebek, *Tetrahedron* **35**, 723 (1979).
- [13] Besecker, C. J.; Day, V. W.; Klemperer, W. G. *Organometallics* **1985**, *4*, 564–570.
- [14] Böhme, U.; Gerwig, M.; Gründler, F.; Brendler, E.; Kroke, E. *Eur. J. Inorg. Chem.* **2016**, *2016*, 5028–5035.
- [15] Olaru, M.; Hesse, M. F.; Rychagova, E.; Ketkov, S.; Mebs, S.; Beckmann, J. *Angew. Chem. Int. Ed.* **2017**,
- [16] Pyykkö, P.; Atsumi, M. *Chem. Eur. J.* **2009**, *15*, 12770–12779.
- [17] Weinhold, F.; Landis, C. R. *Valency and bonding: a natural bond orbital donor-acceptor perspective*; Cambridge University Press: Cambridge, UK; New York, 2005.
- [18] Becke, A. D.; Edgecombe, K. E. *J. Chem. Phys.* **1990**, *92*, 5397–5403.
- [19] Anderson, N. G.; Coradetti, M. L.; Cronin, J. A.; Davies, M. L.; Gardineer, M. B.; Kotnis, A. S.; Lust, D. A.; Palaniswamy, V. A. *Org. Process Res. Dev.* **1997**, *1*, 315–319.
- [20] Quin, L. D. “The Common 3-Coordinate Functions (σ^3 , λ^3)” in *A Guide to Organophosphorus Chemistry*; Wiley, 2000; pp. 82-83.
- [21] Werner, H.; Canepa, G.; Ilg, K.; Wolf, J. *Organometallics* **2000**, *19*, 4756–4766.

- [22] Chan, V. S.; Stewart, I. C.; Bergman, R. G.; Toste, F. D. *J. Am. Chem. Soc.* **2006**, *128*, 2786–2787.
- [23] Wicht, D. K.; Glueck, D. S. In *“Hydrophosphination and Related Reactions” in Catalytic Heterofunctionalization*; Togni, A., Grützmacher, H., Eds.; Wiley, 2001; pp 143–170.
- [24] Buckler, S.; Epstein, M. *Tetrahedron* **1962**, *18*, 1221–1230.
- [25] Bettermann, G.; Krause, W.; Riess, G.; Hofmann, T. *“Phosphorus Compounds, Inorganic”*, *Ullmann’s Encyclopedia of Industrial Chemistry*; Wiley: Weinheim, Germany, 2000.
- [26] Gary, D. C.; Cossairt, B. M. *Chem. Mater.* **2013**, *25*, 2463–2469.
- [27] Healy, M. D.; Laibinis, P. E.; Stupik, P. D.; Barron, A. R. *J. Chem. Soc., Chem. Commun.* **1989**, *0*, 359–360.
- [28] Tamang, S.; Lincheneau, C.; Hermans, Y.; Jeong, S.; Reiss, P. *Chem. Mater.* **2016**, *28*, 2491–2506.
- [29] Bartlett, N.; Sladky, F. O. *Chem. Commun. (London)* **1968**, *0*, 1046–1047.
- [30] Gilmour, R. *Phosphoric acid: purification, uses, technology, and economics*; CRC Press/Taylor & Francis: Boca Raton, FL, 2014; pp. 15–19.
- [31] Pangborn, A. B.; Giardello, M. A.; Grubbs, R. H.; Rosen, R. K.; Timmers, F. J. *Organometallics* **1996**, *15*, 1518–1520.
- [32] Williams, D. B. G.; Lawton, M. *J. Org. Chem.* **2010**, *75*, 8351–8354.
- [33] Thorshaug, K.; Swang, O.; Dahl, I. M.; Olafsen, A. *J. Phys. Chem. A* **2006**, *110*, 9801–9804.
- [34] Levy, G. C.; Komoroski, R. A. *J. Am. Chem. Soc.* **1974**, *96*, 678–681.
- [35] Saito, T.; Nakaie, S.; Kinoshita, M.; Ihara, T.; Kinugasa, S.; Nomura, A.; Maeda, T. *Metrologia* **2004**, *41*, 213–218.
- [36] Landini, D.; Molinari, H.; Pensa, M.; Rampoldi, A. *Synthesis* **1988**, *1988*, 953–955.
- [37] Baccolini, G.; Boga, C.; Mazzacurati, M.; Sangirardi, F. *Org. Lett.* **2006**, *8*, 1677–1680.
- [38] Deprèle, S.; Montchamp, J.-L. *Organic Letters* **2004**, *6*, 3805–3808.
- [39] Bruker, SADABS. 2008.
- [40] Krause, L.; Herbst-Irmer, R.; Sheldrick, G. M.; Stalke, D. *J. Appl. Crystallogr.* **2015**, *48*, 3–10.
- [41] Sheldrick, G. M. *Acta Crystallogr., Sect. A: Found. Adv.* **2015**, *71*, 3–8.
- [42] Sheldrick, G. M. *Acta Crystallogr., Sect. A: Found. Crystallogr.* **2008**, *64*, 112–122.
- [43] Hübschle, C. B.; Sheldrick, G. M.; Dittrich, B. *J. Appl. Crystallogr.* **2011**, *44*, 1281–1284.
- [44] Neese, F. *Wiley Interdiscip. Rev.: Comput. Mol. Sci.* **2012**, *2*, 73–78.
- [45] Lu, T.; Chen, F. *J. Comput. Chem.* **2012**, *33*, 580–592.
- [46] Pettersen, E. F.; Goddard, T. D.; Huang, C. C.; Couch, G. S.; Greenblatt, D. M.; Meng, E. C.; Ferrin, T. E. *J. Comput. Chem.* **2004**, *25*, 1605–1612.
- [47] Hanwell, M. D.; Curtis, D. E.; Lonie, D. C.; Vandermeersch, T.; Zurek, E.; Hutchison, G. R. *J. Cheminf.* **2012**, *4*, 17.

Chapter 3

Orthophosphate and Sulfate Utilization for C–E (E = P, S) Bond Formation via Trichlorosilyl Phosphide and Sulfide Anions

Contents

3.1	Introduction	82
3.2	Results and discussion	84
3.3	Conclusions	96
3.4	Experimental methods	97
3.5	Computational methods	136
	References	141

Abstract

Reduction of phosphoric acid (H_3PO_4) or tetra-*n*-butylammonium bisulfate ($[\text{TBA}][\text{HSO}_4]$) with trichlorosilane leads to the formation of the bis(trichlorosilyl)phosphide ($[\text{P}(\text{SiCl}_3)_2]^-$, **1**) and trichlorosilylsulfide ($[\text{Cl}_3\text{SiS}]^-$, **2**) anions, respectively. Balanced equations for the formation of the TBA salts of anions **1** and **2** were formulated based on the identification of hexachlorodisiloxane and hydrogen gas as byproducts arising from these reductive

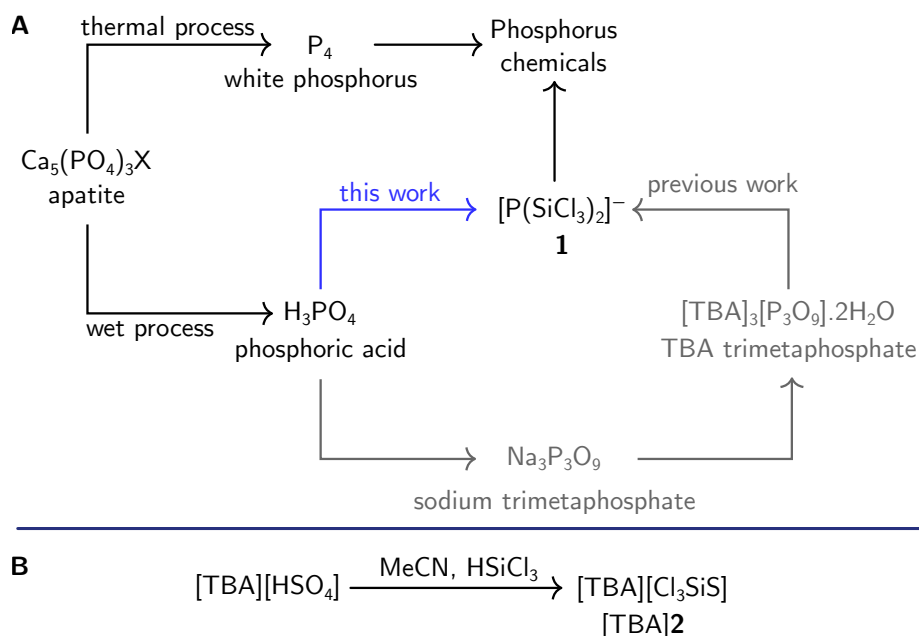
Reproduced in part with permission from: Geeson, M. B.; Rios, P.; Transue, W. J.; Cummins, C. C. *J. Am. Chem. Soc.* **2019**, *141*, 6375–6384 (doi 10.1021/jacs.9b01475). Copyright © 2018 American Chemical Society.

processes: *i*) $[\text{H}_2\text{PO}_4]^- + 10 \text{HSiCl}_3 \rightarrow \mathbf{1} + 4 \text{O}(\text{SiCl}_3)_2 + 6 \text{H}_2$ for P and *ii*) $[\text{HSO}_4]^- + 9 \text{HSiCl}_3 \rightarrow \mathbf{2} + 4 \text{O}(\text{SiCl}_3)_2 + 5 \text{H}_2$ for S. Hexachlorodisiloxane was identified by ^{29}Si NMR spectroscopy and hydrogen gas was identified by its subsequent use to hydrogenate an alkene ((-)-terpinen-4-ol) using Crabtree’s catalyst ($[(\text{COD})\text{Ir}(\text{py})(\text{PCy}_3)][\text{PF}_6]$, COD = 1,5-cyclooctadiene, py = pyridine, Cy = cyclohexyl). Phosphide **1** was generated in situ by the reaction of phosphoric acid and trichlorosilane, and used to convert an alkyl chloride (*n*-chlorooctane) to the corresponding primary phosphine, which was isolated in 41% yield. Anion **1** was also prepared from $[\text{TBA}][\text{H}_2\text{PO}_4]$ and isolated in 62% yield on a gram scale. Treatment of $[\text{TBA}]\mathbf{1}$ with an excess of benzyl chloride leads to the formation of tetrabenzylphosphonium chloride, which was isolated in 61% yield. Sulfide **2** was used as a thionation reagent, converting benzophenone to thiobenzophenone in 62% yield. It also converted benzyl bromide to benzyl mercaptan in 55% yield. The TBA salt of trimetaphosphate ($[\text{TBA}]_3[\text{P}_3\text{O}_9]\cdot 2\text{H}_2\text{O}$), also a precursor to anion **1**, was found to react with either trichlorosilane or silicon(IV) chloride to provide bis(trimetaphosphate)silicate, $[\text{TBA}]_2[\text{Si}(\text{P}_3\text{O}_9)_2]$, which was isolated in 27% yield and characterized by NMR spectroscopy, X-ray crystallography and elemental analysis. Trichlorosilane reduction of $[\text{TBA}]_2[\text{Si}(\text{P}_3\text{O}_9)_2]$ also provided anion **1**. The electronic structures of **1** and **2** were investigated using second order Møller-Plesset (MP2), Natural Bond Orbital (NBO) and Generalized Valance Bond (GVB) theories; the computational studies suggest that the trichlorosilyl ligand is a good π -acceptor and forms σ -bonds with a high degree of *s* character. One-bond ^{31}P - ^{29}Si coupling constants obtained computationally compared well with those determined by experiment for a series of phosphorus-silicon bond-containing species.

3.1 Introduction

White phosphorus has long been the critical intermediate for the synthesis of nearly all phosphorus-containing non-fertilizer chemicals.¹⁻³ The production of white phosphorus, in what is known as the “thermal process”, requires the energy-intensive reduction of phosphate rock and is conducted in an electric arc furnace at 1500 °C.³ White phosphorus is a toxic and pyrophoric substance that has been used as a chemical warfare agent and its transport has led to high-profile catastrophes.⁴ The legacy thermal process for the production of P_4 has served a secondary role as a method of purification; the phosphorus volatilized from the electric arc furnace allows for it to be separated from chiefly sulfur- and silicon-containing impurities.⁵ However, it struggles to separate arsenic, which is toxic to humans,⁶ because As replaces P in the P_4 lattice.^{3,7}

In contrast, phosphoric acid, H_3PO_4 , is produced by the “wet process”, which involves treating phosphate rock with sulfuric acid.⁵ In this scheme, the industrial chemistry of sulfur and phosphorus are intimately intertwined; sulfur is a secondary product from the petrochemical industry, and the vast majority of it is used to make sulfuric acid, allowing



Scheme 3.1 A: Synthetic routes to phosphorus-containing chemicals from phosphate rock. TBA = tetra-*n*-butylammonium. Most commonly, phosphate rock has the formula $\text{Ca}_5(\text{PO}_4)_3\text{X}$, where X is typically F, Cl or OH, collectively referred to as apatite. **B:** Application of trichlorosilane reduction to the chemistry of sulfur by preparation of [TBA]2 from [TBA][HSO₄].

the wet process to operate.⁸ The scale of the latter is much larger than that of the thermal process, accounting for the fate of 95% of the phosphate rock mined annually.³ Improvements in the methods for purifying phosphoric acid have been such that, nowadays, the purity of H_3PO_4 produced by the wet process rivals that produced by the thermal process, allowing wet process phosphoric acid to be used in food-grade applications.⁹ The higher energy requirements of the thermal process, in addition to the toxicity and pyrophoric properties of P_4 , provide motivation for eliminating P_4 in favor of phosphoric acid as the key starting material for the production of P-containing chemicals.^{10–14} Along these lines, a microwave-assisted preparation of PCl_3 from calcium phosphate in a scheme that is thought to bypass elemental P has also been reported.¹⁵

We recently reported the synthesis and characterization of the bis(trichlorosilyl)phosphide anion **1**, as its TBA salt, by reduction of trimetaphosphate with trichlorosilane (Scheme 3.1A).¹⁰ [TBA]1 was shown to be a versatile reagent for the preparation of several phosphorus-containing products previously only available downstream of white phosphorus, such as $\text{Li}[\text{PF}_6]$, RPH_2 and PH_3 . We also demonstrated that [TBA]1 does not need to be isolated and purified, and can instead be generated in situ for the conversion of a primary alkyl chloride to a corresponding alkyl phosphine.

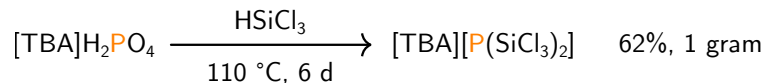
Trichlorosilane, the reducing agent used to prepare anion **1**, is manufactured on an

industrial scale for the production of high-purity elemental silicon, which is in turn used to produce photovoltaic (PV) cells.¹⁶ It is listed as a high production volume (HPV)¹⁷ chemical, produced in the US in the range of 1–5 billion pounds (2016).¹⁸ The majority of trichlorosilane is produced by the reaction of hydrogen chloride gas and elemental silicon, the latter being derived from a similarly high energy process to thermal P₄ production.¹⁶ More recently however, sustainable and less energy-intensive approaches for preparing trichlorosilane have been explored. One example, already practiced industrially, is the reaction of silicon(IV) chloride with hydrogen.^{19,20} Silicon(IV) chloride is a waste product of the PV industry,¹⁹ or can alternatively be prepared in a redox-neutral process that involves converting silicate-containing minerals to a tetraalkyl orthosilicate²¹ and subsequent chlorination to silicon(IV) chloride.^{22,23} A method for producing silicon(IV) chloride from silica in a process that avoids elemental silicon entirely was described and patented in 2012.^{15,24} Finally, new methods for preparing silicon from silica using electrochemical techniques are areas of active investigation.²⁵ These recent developments in the field of sustainable silicon chemistry hold promise for the use of trichlorosilane as a reducing agent for other element oxides.

3.2 Results and discussion

3.2.1 Reduction of orthophosphate with trichlorosilane

Trimetaphosphate, the precursor to [TBA]**1**, is produced by the dehydration of monosodium dihydrogenphosphate at 300–500 °C,⁵ or more recently by a similarly high-temperature dehydration of H₃PO₄ in the presence of sodium chloride.²⁶ We wondered whether it might be possible to obviate this dehydration step, and instead prepare anion **1** more directly from a source of orthophosphate. Despite the well-documented reactivity of water and alcohols with Si–Cl bonds to give silanols,²⁷ our initial system tolerated the two equivalents of water present in the [TBA]₃[P₃O₉]·2H₂O starting material.²⁸ We therefore considered sources of orthophosphate containing acidic protons as potentially viable substrates for the preparation of [TBA]**1**.

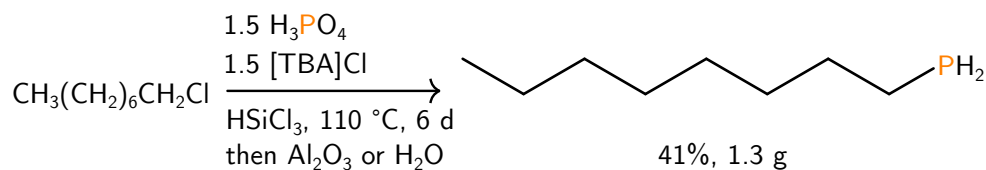


Scheme 3.2 Preparation of [TBA]**1** starting from [TBA][H₂PO₄].

Crystalline phosphoric acid,^{29,30} typically obtained from an aqueous 85% solution of H₃PO₄, accordingly was tested for its ability to serve as a precursor to anion **1**. In order to target the stable TBA salt of **1**, crystalline phosphoric acid was heated with [TBA]Cl in neat trichlorosilane. After heating at 110 °C for 86 h an aliquot was analyzed by ³¹P NMR spectroscopy; the characteristic signal for anion **1** was observed at –171.7 ppm. Despite several attempts, we were unable to obtain [TBA]**1** as a pure compound using this

preparative method due to the formation of byproducts, including $[\text{TBA}]_2[\text{Si}_6\text{Cl}_{14}]$,^{31–33} which was identified by ²⁹Si NMR spectroscopy (3.4.3.2). Instead, we used phosphoric acid to generate anion **1** in situ. In the presence of *n*-octylchloride, anion **1** undergoes a key carbon-phosphorus bond forming reaction and, after workup, *n*-octylphosphine could be isolated in 41% yield based on *n*-octylchloride as the limiting reactant (Scheme 3.3).

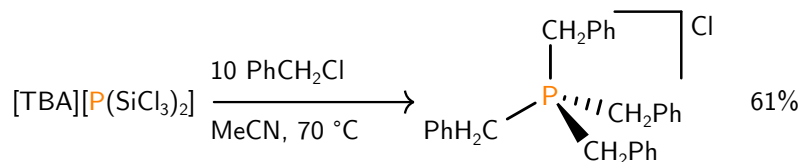
Although unactivated alkyl halides can be reduced with trichlorosilane in the presence of a halide catalyst to give trichlorosilyl-functionalized alkanes, such reactions typically require even more forcing conditions than we have employed here for P–C bond formation.³⁴ In support of a mechanism in which a primary alkyl chloride undergoes nucleophilic attack by anion **1**, we have previously shown that cleanly isolated $[\text{TBA}]\mathbf{1}$ reacts with an alkyl chloride to give P–C bond-containing products in the absence of additional trichlorosilane.¹⁰ This method for the preparation of primary alkyl phosphines is attractive because it constitutes a one-step procedure from commercially available starting materials (Scheme 3.1A) and gives a primary alkyl phosphine in two steps from phosphate rock, the raw material that is mined from the ground. *n*-Octylphosphine is a useful precursor to stannylphosphines,^{35,36} as well as phosphacyclohexanes.³⁷ Octylphosphine can also be oxidized to octylphosphonic acid,³⁸ which finds applications as a ligand for nanoparticles^{39,40} and for heavy metal extraction processes.^{41,42}



Scheme 3.3 Synthesis of *n*-octylphosphine from *n*-octylchloride and phosphoric acid.

Interested in having a reliable preparation of pure samples of $[\text{TBA}]\mathbf{1}$ from a source of orthophosphate, we considered the possibility that tetra-*n*-butylammonium dihydrogenphosphate, $[\text{TBA}][\text{H}_2\text{PO}_4]$,⁴³ might be a more suitable phosphate-containing starting material. By avoiding the introduction of additional chloride to the reaction, as was the case for the initial $\text{H}_3\text{PO}_4/[\text{TBA}]\text{Cl}$ conditions, we sought to minimize the formation of byproducts such as $[\text{TBA}]_2[\text{Si}_6\text{Cl}_{14}]$ which had impeded isolation of pure $[\text{TBA}]\mathbf{1}$. Gratifyingly, $[\text{TBA}]\mathbf{1}$ could be isolated pure and in a moderate yield (62%) when $[\text{TBA}][\text{H}_2\text{PO}_4]$ was subjected to the standard conditions for preparing anion **1** (Scheme 3.2). Importantly, we encountered no difficulties in the typical workup and purification procedure. Over the prolonged reaction times employed, decomposition of TBA to give tri-*n*-butylammonium ($[\text{Bu}_3\text{NH}]^+$) was observed, although based on the moderate yield of $[\text{TBA}]\mathbf{1}$ from $[\text{TBA}][\text{H}_2\text{PO}_4]$ (62%, Scheme 3.2) this process appears to be slow. $[\text{TBA}]\mathbf{1}$ melts with slight decomposition at 105–108 °C; analysis of a sample of $[\text{TBA}]\mathbf{1}$ that was maintained at 110 °C for 20 minutes partially redissolved in DCM to show the presence of anion **1** by ³¹P NMR spectroscopy (3.4.3.3). Nonetheless, future work will seek to determine which cations that can be paired

with anion **1** to provide salts with superior thermal stabilities.



Scheme 3.4 Synthesis of tetrabenzyl phosphonium chloride from [TBA]**1** and benzyl chloride.

With a method in hand for preparing [TBA]**1** directly from a source of orthophosphate, we set out to further explore the reactivity of **1** with carbon-based electrophiles. Heating [TBA]**1** with an excess (10 equiv.) of benzyl chloride led to the formation of tetrabenzylphosphonium, identified by its ^{31}P NMR spectrum (δ 24.5 ppm, displaying coupling to 8 equivalent protons to give a binomial nonet with $^2J_{\text{P-H}} = 14$ Hz), in line with previous literature reports.⁴⁴ The phosphonium salt was separated from any TBA salts using water; while both the TBA and phosphonium salts were soluble in boiling water, only the TBA salts were soluble at 23 °C. Accordingly, recrystallization of the crude product from boiling water provided tetrabenzylphosphonium chloride in 61% yield (Scheme 3.4). Tetrabenzylphosphonium can be converted to the corresponding Wittig reagent and subsequently used to make carbon-carbon double bonds.⁴⁵

3.2.2 Intermediates in the HSiCl_3 reduction of phosphate sources

3.2.2.1 With trimetaphosphate as the P source

Reduced P-containing species other than anion **1** were not observed upon trichlorosilane treatment of phosphate sources. However, a small but significant shift (10 ppm) of the trimetaphosphate resonance in the ^{31}P NMR spectrum was observed when the initial reaction of $[\text{TBA}]_3[\text{P}_3\text{O}_9]\cdot 2\text{H}_2\text{O}$ with trichlorosilane was monitored at 23 °C. Such changes in chemical shift are diagnostic of trimetaphosphate coordinating as a ligand.^{46,47} Diluting the reaction mixture in dichloromethane, thereby lowering the concentration of trichlorosilane and slowing the rate of reaction, led to the observation of an additional species (**3**, Fig. 3.1), which by ^{31}P NMR spectroscopy was indicative of two trimetaphosphate units coordinated to two separate silicon centers. The connectivity of intermediate **3** was assigned based on the integration ratios and chemical shifts of the κ^3 coordinated⁴⁶ (P_a), ultraphosphate⁴⁷ (P_b) and branched⁴⁸ (P_c) polyphosphate regions, as well as the coupling pattern (AB_2 , $^2J_{\text{P-P}} = 27$ Hz) of P_b and P_c . After 48 h, this intermediate had converted to one having a single ^{31}P NMR resonance at δ 29.4 ppm, which is formulated as $[\text{TBA}]_2[\text{Si}(\text{P}_3\text{O}_9)_2]$.

This compound could be prepared independently by reaction of SiCl_4 with $[\text{TBA}]_3[\text{P}_3\text{O}_9]\cdot 2\text{H}_2\text{O}$, allowing for its isolation in 27% yield. An X-ray diffraction study confirmed the connectivity of $[\text{TBA}]_2[\text{Si}(\text{P}_3\text{O}_9)_2]$, featuring a six-coordinate central silicate moiety sandwiched between two trimetaphosphate ligands. Anion $[\text{Si}(\text{P}_3\text{O}_9)_2]^{2-}$ is a rare

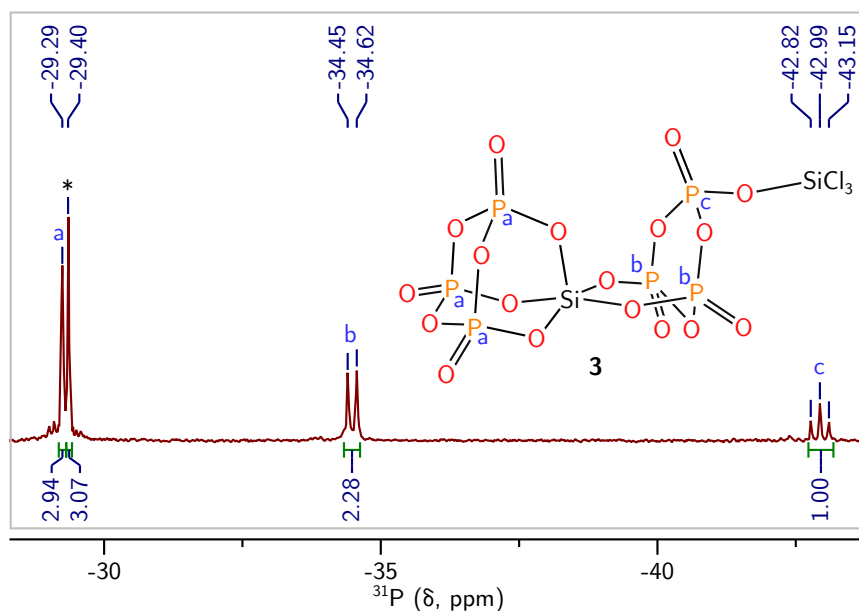


Figure 3.1 $^{31}\text{P}\{^1\text{H}\}$ NMR spectrum of the reaction mixture obtained when $[\text{TBA}]_3[\text{P}_3\text{O}_9]\cdot 2\text{H}_2\text{O}$ and SiCl_4 are mixed for 30 minutes in DCM at 23°C . The resonances correspond to intermediate **3** (inset) in the synthesis of $[\text{TBA}]_2[\text{Si}(\text{P}_3\text{O}_9)_2]$. The asterisk (*) denotes $[\text{TBA}]_2[\text{Si}(\text{P}_3\text{O}_9)_2]$.

example of an entirely inorganic molecular silicophosphate; the majority of structurally characterized molecular silicophosphates contain organic substituents at silicon.⁴⁹ Like $[\text{TBA}]_2[\text{Si}(\text{P}_3\text{O}_9)_2]$, silicophosphate materials generally feature silicon in an all-oxygen six-coordinate environment.⁵⁰ However, their syntheses generally proceed at higher temperatures⁵¹ than we have found to be the case for $[\text{TBA}]_2[\text{Si}(\text{P}_3\text{O}_9)_2]$.

Silicophosphate $[\text{TBA}]_2[\text{Si}(\text{P}_3\text{O}_9)_2]$ forms quickly and quantitatively (≥ 20 min) when a DCM solution of **1** is treated with a large excess of trichlorosilane (23 equiv.) at room temperature. It was confirmed that the $[\text{Si}(\text{P}_3\text{O}_9)]^{2-}$ anion can serve as a P-source in the generation of **1**, by subjecting an independently prepared sample of $[\text{TBA}]_2[\text{Si}(\text{P}_3\text{O}_9)_2]$ to the standard synthesis conditions (neat HSiCl_3 , 110°C). Although no other intermediates were observed by ^{31}P NMR spectroscopy, the reduction of $[\text{TBA}]_2[\text{Si}(\text{P}_3\text{O}_9)_2]$ by trichlorosilane might proceed through mechanisms similar to those which have been proposed for related organic phosphine oxide reductions.⁵² These have been postulated to proceed through either attack of the trichlorosilyl anion, $[\text{SiCl}_3]^-$,⁵³⁻⁵⁶ at the phosphorus center or via a λ^5 phosphorane intermediate.⁵⁷ Disproportionation and redistribution reactions of chlorosilanes by either a nucleophile or a base are well known,³¹⁻³³ and so a potentially large number of silicon-containing species could be responsible for reduction of the phosphate sources we have identified as precursors to **1**. Given that we do not observe additional intermediates by ^{31}P NMR spectroscopy, the first reduction event at

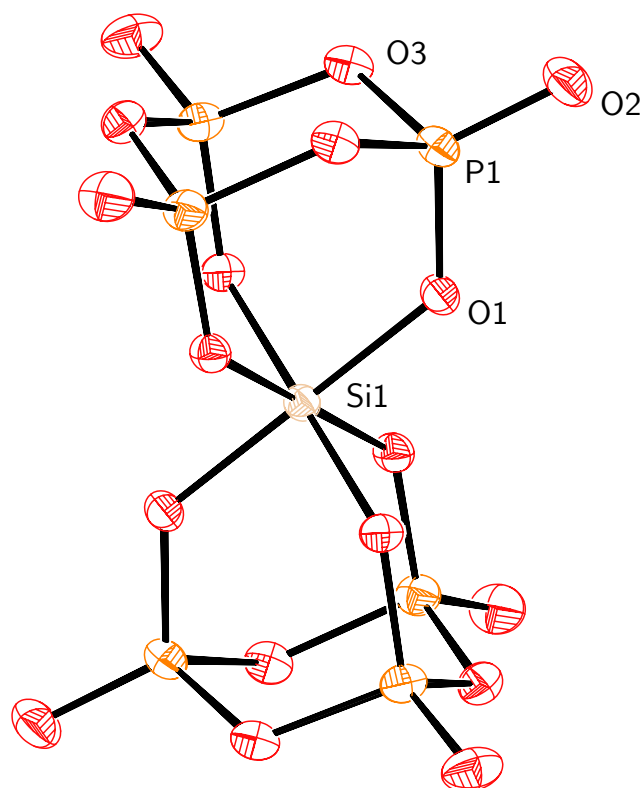


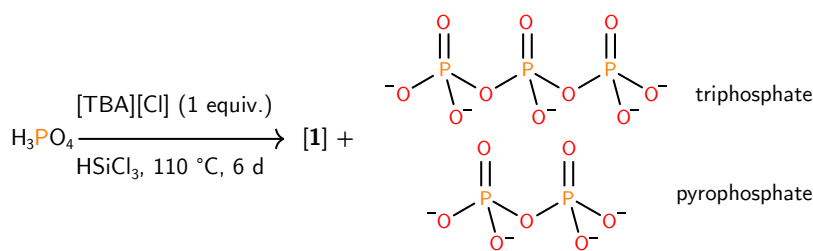
Figure 3.2 Molecular structure of $[\text{TBA}]_2[\text{Si}(\text{P}_3\text{O}_9)_2]$ with the ellipsoids at the 50% probability level and the two TBA cations omitted for clarity. Color coding: phosphorus (orange), oxygen (red) and silicon (tan). Selected bond distances (given as the average of chemically equivalent bonds) (Å): Si1–O1: 1.7717(21), O1–P1: 1.5254(23), P1–O2: 1.4448(25), P1–O3: 1.6121(34).

phosphate is likely rate-determining. Remarkably, anion **1** forms selectively under the reaction conditions; analogs in which a Cl is replaced by a hydrogen atom, a trichlorosilyl group, or a trichlorosiloxy group ($-\text{OSiCl}_3$) were not observed by ^{31}P NMR. Each of these three scenarios seems reasonable, given the facile redistribution of H for Cl in chlorosilanes,⁵⁸ the ease at which chlorosilane oligomers are formed^{31,59} and the existence of a related anion in which a phosphide features two dichloroaryloxysilyl functional groups ($[\text{P}(\text{SiCl}_2\text{OR})_2]^-$ (R = 2,4,6-*t*-Bu)₃C₆H₂)).⁶⁰

3.2.2.2 With phosphoric acid as the P source

Condensed phosphates are observed (^{31}P NMR) to form under the reduction conditions for the preparation of **1** from phosphoric acid, demonstrating trichlorosilane must serve the role of dehydrating agent in addition to its role as the reducing agent. At the end of the

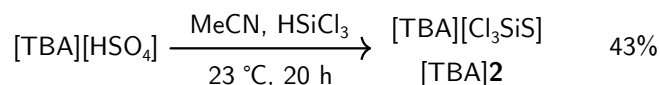
reaction used to prepare anion **1** in situ from H_3PO_4 , a white precipitate was seen to have formed that was insoluble in common organic solvents. The material dissolved completely in water and analysis of this aqueous solution by ^{31}P NMR spectroscopy revealed the presence of pyrophosphate and linear triphosphate (Scheme 3.5). Trichlorosilane is clearly capable of condensing orthophosphate into longer chain polyphosphates, and this may play a role in the mechanism governing the formation of $[\text{TBA}]\mathbf{1}$. Presumably, condensed phosphates formed under the dehydrative conditions employed are capable of acting as ligands towards silicate centers, in a manner similar to the formation of $[\text{TBA}]_2[\text{Si}(\text{P}_3\text{O}_9)_2]$ from trimetaphosphate and trichlorosilane. The longer reaction times required for orthophosphate to be converted to anion **1**, versus trimetaphosphate, are in line with our previous arguments that metaphosphates are kinetically more prone to reductive processes.¹⁰



Scheme 3.5 Under the conditions used to prepare anion **1** in situ, pyrophosphate and linear triphosphate were observed by ^{31}P NMR spectroscopy. Line drawings of the polyphosphate products are shown in their fully deprotonated states for clarity.

3.2.3 Sulfate reduction by trichlorosilane

The ability of trichlorosilane to effect the dehydration and complete deoxygenation of phosphate suggests a likely strategy for the reduction of other p-block oxoanions to give products containing the E– SiCl_3 group. Such compounds (E = C, Si, Ge) have received interest in recent years due to their potential applications in deposition processes⁶¹ and chemical synthesis.⁶² A survey of the literature returned the trichlorosilylsulfide anion ($[\text{Cl}_3\text{SiS}]^-$, **2**), which was prepared previously from tetraethylammonium hydrogen sulfide upon treatment with silicon tetrachloride in liquid hydrogen sulfide.⁶³ Given the above results for generation of **1** from dihydrogen phosphate and phosphoric acid, it follows that **2** might be accessed by reduction of bisulfate with trichlorosilane: a procedure that would avoid the use of liquefied H_2S , which is both extremely toxic and dangerous.⁶⁴ Accordingly, $[\text{TBA}]\mathbf{2}$ was prepared in moderate yield (43%) by stirring $[\text{TBA}][\text{HSO}_4]$ in an acetonitrile/trichlorosilane mixture at 23 °C for 20 h (Scheme 3.6). Conditions leading to the formation of $[\text{TBA}]\mathbf{2}$ are notably milder than the conditions required for the corresponding preparation of $[\text{TBA}]\mathbf{1}$ (3.4.3.6). We also found that reduction of $[\text{TBA}][\text{HSO}_4]$ with trichlorosilane leads to the formation of some elemental sulfur. A single crystal obtained from the crude reaction mixture in the



Scheme 3.6 Preparation of [TBA]2 from [TBA][HSO4].

preparation of [TBA]2 was unambiguously identified as S₈ by comparison of its unit cell with previous literature reports.⁶⁵

[TBA]2 was characterized by multinuclear NMR, IR, and Raman spectroscopies in addition to elemental analysis and X-ray crystallography (Fig. 3.3). The IR and Raman data are consistent with those provided in the single previous report of anion 2, which had been isolated as the tetraethylammonium (TEA) salt.⁶³ The previous report also described the solid-state structure of [TEA][2] but the data were of insufficient quality to permit a detailed discussion of the bond metrics of the anion. Fortunately, our crystallographic study of [TBA]2 permitted unambiguous assignment of the sulfur and chlorine atoms of anion 2. The assignment of the sulfur and chlorine atoms is also supported by the different Si–S and Si–Cl lengths, which match well with those we calculated at the ωB97X-D3/ma-Def2-QZVPP level of theory.^{66,67} Anion 2 displays a Si–S bond of 1.9756(14) Å, significantly shorter than the sum of the covalent single bond radii, 2.19 Å.⁶⁸ This bond length contraction is indicative of multiple bonding between silicon and sulfur, a phenomenon we have analyzed using a suite of theoretical methods (see Electronic Structure and Bonding section).

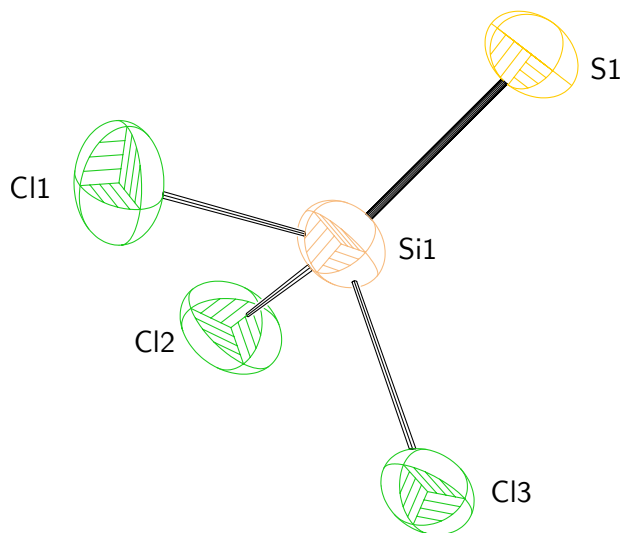
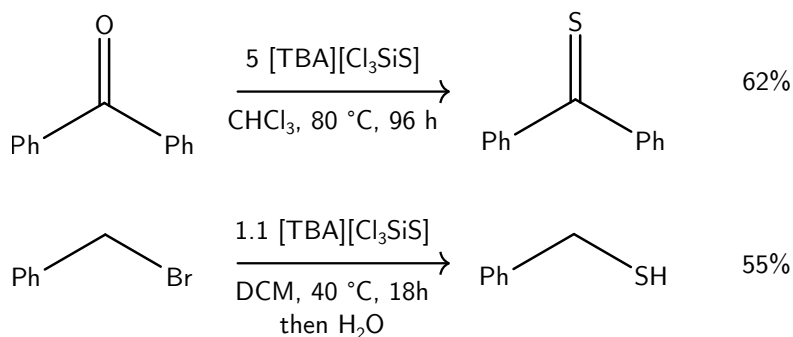


Figure 3.3 Molecular structure of [TBA]2, with ellipsoids at the 50% probability level and the TBA cation omitted for clarity. Selected bond lengths (Å) and angles (°): Si1–S1: 1.9756(14), Si1–Cl_{av.}: 2.073(7), S1–Si1–Cl_{av.}: 115.59(25), Cl–Si1–Cl_{av.}: 102.69(30).



Scheme 3.7 Use of [TBA]**2** as a thionation reagent to give benzyl mercaptan and thiobenzophenone from benzyl bromide and benzophenone respectively.

3.2.4 Carbon-sulfur bond-forming reactions

With [TBA]**2** in hand, we set out to test the value of this reagent for the preparation of organosulfur compounds (Scheme 3.7). Although the conjugate acid of **2**, Cl_3SiSH , has been known for half a century,⁶⁹ the use of this species in chemical synthesis seems to be largely unexplored. It seems reasonable to expect that formation of Si-X bonds (X = O, Cl, Br) from the reaction of anion **2** with C-X bond-containing substrates would provide a thermodynamic driving force for such reactions. Such is the case for an organic analog of **2**, $[\text{S}-\text{SiMe}_3]^-$, recently prepared by desilylation of $\text{S}(\text{SiMe}_3)_2$ by ionic liquids⁷⁰ and thought to be an intermediate for thionation reactions employing $\text{S}(\text{SiMe}_3)_2$.⁷¹ Treatment of benzyl bromide with [TBA]**2** gave rise to a major new species in solution, identified as benzyl trichlorosilylsulfide by its NMR data (3.4.9.1). A hydrolytic workup and purification by vacuum transfer allowed for the isolation of benzyl mercaptan in 55% yield. We also found that [TBA]**2** showed comparable reactivity to other thionating compounds, such as Lawesson's reagent, which can be used for the conversion of carbonyl to thiocarbonyl functional groups.⁷² Accordingly, thiobenzophenone could be prepared from benzophenone using [TBA]**2** (5 equiv.) in chloroform. An excess of [TBA]**2** was required in order to achieve a reasonable reaction time. Thiobenzophenone was extracted from the TBA-containing byproducts using hexanes and isolated in 62% yield.

3.2.5 Electronic structure and bonding

Electronic structure calculations on sulfide **2** at the MP2/aug-cc-pVTZ level of theory (C_{3v} -optimized metrical parameters (Å, °): Si-S, 1.984; Si-Cl, 2.103; S-Si-Cl, 116.8) are indicative of multiple bonding between sulfur and silicon. Analysis of this wavefunction using GAMESS^{73,74} gave a Mayer bond order of 1.784 for the S-Si linkage.⁷⁵ Submitting the same wavefunction for natural bond orbital (NBO) analysis^{76,77} provided via the natural resonance theory (NRT) routine an even larger estimate of this bond order, at 2.037, while

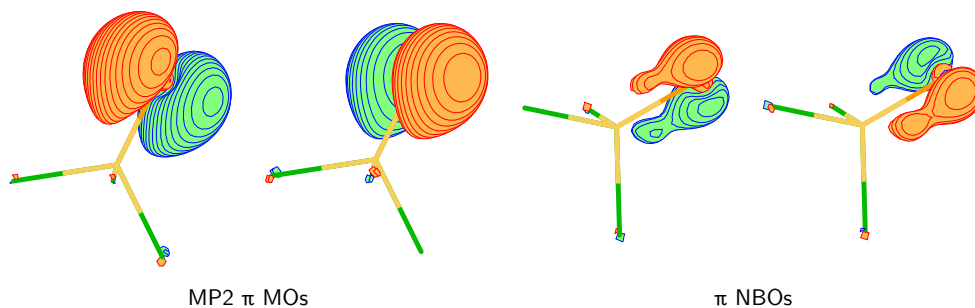


Figure 3.4 Comparison of the π interaction between silicon and sulfur in anion **2**. The MP2 π MOs resemble p-orbital lone pairs on sulfur, whereas the corresponding π NBOs suggest the presence of polar π bonds. Green: chlorine, tan: silicon, orange: sulfur.

indicating the presence of multiple resonance structures contributing greater than 10% to the overall electron density. The leading resonance structure, at ca. 22%, is the one corresponding to the NBOs and having a triple bond between sulfur and silicon together with three Si–Cl single bonds. The π bonds for this resonance structure are highly polar with 6% Si dp character and 94% S p character; thus, these π bonds are close to the NBO bonding/nonbonding cutoff. The S–Si σ bond is much more covalent with 35% Si $sp^{1.52}$ character and 64% S $sp^{3.1}$ character. The short nature of the Si–S bond is likely due to the large amount of s character used by silicon to form the σ interaction. This is in line with Bent’s rule considerations that a central atom (here, Si) will accumulate s -orbital character in forming bonds to less electronegative elements. Accordingly, silicon uses majority p -orbital character, $sp^{2.5}d^{1.4}$, in forming the polar (19% Si, 81% Cl) Si–Cl bonds. In terms of their appearance (Fig. 3.4) the MP2 π molecular orbitals (left) look like p -orbital lone pairs polarized in the direction of silicon, while the corresponding S–Si π NBOs (right) do a better job of suggesting the presence of polar π bonds. Finally, analysis of the generalized valance bond (GVB) wavefunction (Fig. 3.5) using the VB2000 program⁷⁸ as implemented in GAMESS,^{73,74} treating the Si–S bond at the CASVB(6,6)/6-31++G** level of theory, gave a Si–S bond order of 1.84.

Analyzed similarly, there is some evidence of multiple bond character between phosphorus and silicon in phosphide **1**; the anion was geometry optimized with C_2 point group symmetry (key metrical parameters (Å, °): P–Si, 2.145; Si–P–Si, 95.4). Analysis of the MP2/aug-cc-pVTZ wavefunction using GAMESS^{73,74} gives a P–Si Mayer bond order of 1.318. In this case, NBO analysis indicates the presence of two lone pairs at the phosphorus atom, the first of which points along the C_2 rotational axis of symmetry and accumulates two-thirds s -orbital character ($sp^{0.5}$ hybridization). The second P lone pair is contained in a pure p -orbital for which the PSi_2 plane is a nodal plane. The P–Si σ bonds are formed from overlap of sp^5 and $sp^{1.44}$ hybrids at P and Si, respectively, such that once again, silicon reserves much of its p -orbital percentage for bonding to the chlorine substituents, with s -orbital character being strong in silicon’s contributions to the P–Si σ bonds.

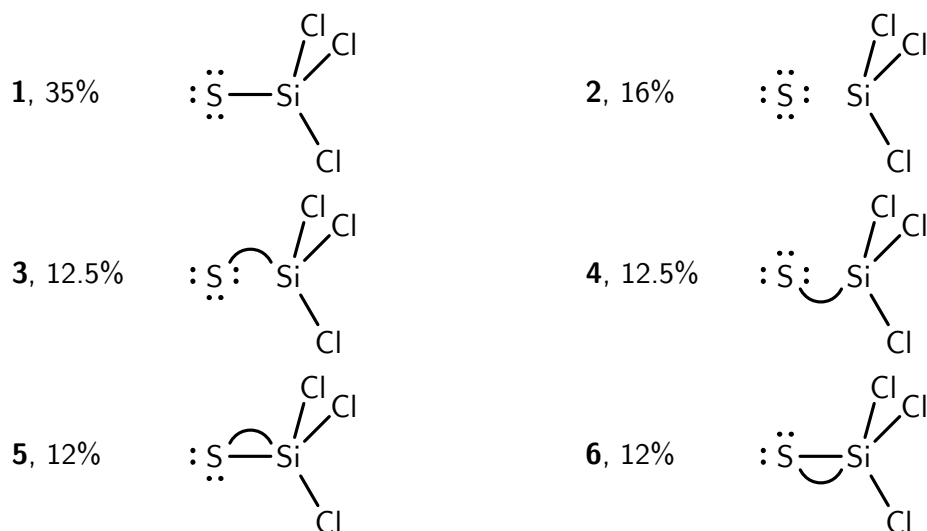


Figure 3.5 Summary of the generalized valence bond (GVB) wavefunction for anion **2** treating the Si-S bond at the CASVB(6,6)/6-31++G** level of theory. Analysis of the GVB wavefunction gives a Si-S bond order of 1.84.

In anion **1**, the σ bonds are quite covalent (55% P, 45% Si). From inspection of the NBO second order perturbation theory analysis of the Fock matrix, the strongest delocalizations come from the π lone pair into the Si-Cl σ^* orbitals. The NRT analysis gives a natural bond order of 1.340 in this case, close to the value obtained from the GAMESS analysis of the MP2 wavefunction. Once again, due to the importance of multiple ionic resonance structures in which P-Si π bonds are formed at the expense of Si-Cl σ bonds, the leading resonance structure has a weight of only 22%.

3.2.6 Calculation of $^1J_{\text{P-Si}}$ coupling constants

Theoretical analysis of the electronic structure of anions **1** and **2** predicted the s character of the Si-E (E= P, S) bonds to be high, principally due to the electronegative chloride substituents on silicon. In the case of anion **1**, we sought to experimentally validate this analysis by interpretation of the $^1J_{\text{P-Si}}$ coupling constant, as measured by NMR spectroscopy. The magnitude of the $^1J_{\text{P-X}}$ coupling constant is dominated by the Fermi-contact interaction, proportional to the bond s character.⁷⁹ Comparison to a series of related $^1J_{\text{P-Si}}$ values was approached with quantum chemical calculations (Table 3.1). These provided both the signs and magnitudes of the scalar couplings, as these can be difficult to determine in the presence of second-order coupling patterns.⁸⁰ The geometry of each species was optimized at a low level of theory (B3LYP/6-31G(d,p)) then the total nuclear spin-spin coupling constants (J) were calculated at the PBE/aug-cc-pVQZ level of theory.^{81,82} Linear regression between experimental and calculated scalar coupling constants⁸¹ provided

Table 3.1 Comparison of the experimental and predicted values for the $^1J_{\text{P-Si}}$ coupling constants and the % *s*-orbital character in the P–Si bonds for a series of compounds

Species	$^1J_{\text{P-Si}} / \text{Hz}$		% <i>s</i> character ^a	
	Exp. ^b	Pred. ^c	$\sigma(\text{P-Si})^d$	Si ^e
Me ₃ SiPPh ₂ ·BH ₃	−44 ⁸³	−42	20	8
F ₃ SiPH ₂	15 ⁸⁴	22	21	15
HP(SiH ₃) ₂	35 ⁸⁵	20	17	9
Cl ₃ SiPH ₂	52 ⁸⁶	54	21	15
(<i>i</i> -Pr)P(SiCl ₃) ₂	73 ⁸⁷	85	21	15
[P(SiH ₃) ₂] [−]	77 ⁸⁰	76	22	14
(<i>i</i> -Pr)P(NPh ₂)(SiCl ₃)	125 ⁸⁸	115	23	18
[P(SiCl ₃) ₂] [−] , 1	158 ¹⁰	159	26	20

^a Determined by NBO analysis

^b Experimental value determined by ³¹P NMR spectroscopy

^c Predicted value determined by evaluation of the calculated $^1J_{\text{P-Si}}$ value in Eqn. 3.1

^d Sum of the P and S *s*-orbital character in the P–Si bond

^e S *s*-orbital character in the P–Si bond

an excellent correlation ($R^2 = 0.98$, Eqn. 3.1):

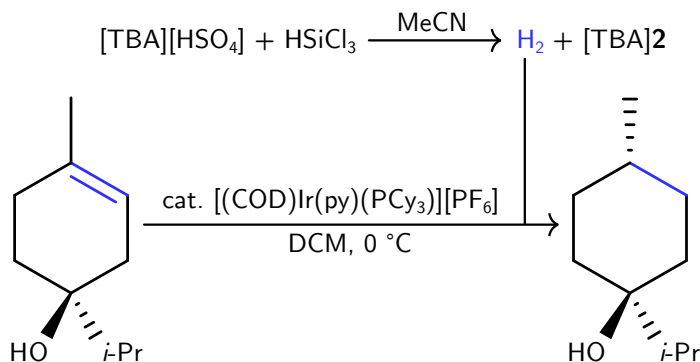
$$^1J_{\text{P-Si}}(\text{calc.}) = 0.77 \times ^1J_{\text{P-Si}}(\text{exp.}) - 38.57 \quad (3.1)$$

The species included in our study contained a range of different substituents on both phosphorus and silicon, as well as two-, three-, and four-coordinate phosphorus compounds (Table 3.1). Anion **1** exhibits the largest positive $^1J_{\text{P-Si}}$ value among all the species studied, consistent with a large amount of *s* character in its P–Si bonds, imparted by the trichlorosilyl groups. Trichlorosilyl groups consistently enhance P–Si scalar coupling, giving rise to four of the five largest constants in Table 3.1. The anionic charge of **1** may also increase $^1J_{\text{P-Si}}$ as suggested by the large value for [P(SiH₃)₂][−]. In order to determine the amount of *s* character of the phosphorus-silicon bonds, natural bond order (NBO) calculations were carried out. The *s* character of the $\sigma(\text{P-Si})$ bonds, and in particular the *s* character arising from silicon, correlated moderately well with the experimental $^1J_{\text{P-Si}}$ constants, ($R^2 = 0.54$ and 0.76, respectively).

3.2.7 Balancing the equations for the formation of anions **1** and **2**

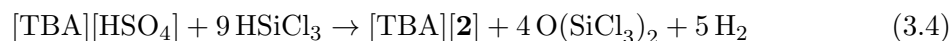
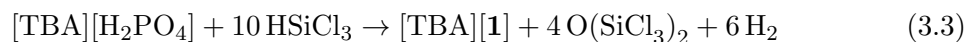
An important question we wished to address in these two reductive processes was the fate of the hydrogen atoms, originating from trichlorosilane and the protic substrates H₃PO₄ and [TBA][HSO₄]. H₂ or HCl would be the most likely gaseous hydrogen-containing byproducts with the former considered the more likely candidate given that P–Si and S–Si bonds of **1**

or **2**, respectively, would be cleaved by HCl. Under the assumption of H₂ as the gaseous byproduct, we carried out a two-compartment experiment where the hydrogen generated from the reduction of bisulfate could be used to hydrogenate an alkene. We selected Crabtree's catalyst for the hydrogenation of (–)-terpinen-4-ol (Scheme 3.8) due to the high efficiency of this reaction at mild pressures and temperatures.⁸⁹ Using a two-flask setup, we were able to confirm the formation of the hydrogenated product, *trans*-4-methyl-1-isopropylcyclohexan-1-ol, by ¹H NMR spectroscopy.



Scheme 3.8 Identification of the hydrogen produced from the reduction of [TBA][HSO₄] to [TBA]**2** using trichlorosilane; the hydrogen generated from the reduction was used to hydrogenate (–)-terpinen-4-ol using Crabtree's catalyst.

Control experiments showed that this method was unsuitable for the quantification of hydrogen (3.4.11.3), so instead we turned to a simple gas collection experiment.⁹⁰ The evolved hydrogen gas was collected by the displacement of water (3.4.13), and this method indicated production of 4.45 equivalents of hydrogen gas per mole of added [TBA][HSO₄], compared to the theoretical maximum of 5.0 (Eqn. 3.4). An analogous study to quantify the H₂ produced by the formation of [TBA]**1** from H₃PO₄ gave 5.0 equivalents of H₂, representing 71% of the theoretical maximum of 7 equivalents (Eqn. 3.2). Although not experimentally verified, the corresponding balanced equation leading to the formation of [TBA]**1** from [TBA][H₂PO₄] is shown in Eqn. 3.3.



Analysis of the volatile liquid products at the end of the reaction was carried out

to determine the fate of the oxygen atoms. Following the synthesis of [TBA]**1**, volatile material was removed under reduced pressure from the reaction vessel and collected in a liquid nitrogen cooled trap. Analysis of this material by ^{29}Si NMR spectroscopy confirmed the presence of hexachlorodisiloxane ($\text{Cl}_3\text{Si-O-SiCl}_3$) and pentachlorodisiloxane ($\text{Cl}_3\text{Si-O-SiCl}_2\text{H}$) (3.4.3.8). Also observed was the formation of a white precipitate that was insoluble in common organic solvents, but which dissolved in aqueous sodium hydroxide solution to yield orthosilicate, as determined by ^{29}Si NMR spectroscopy.⁹¹ These observations are consistent with the formation of some amount of silica, which is known to form when silicon tetrachloride is exposed to even substoichiometric quantities of water.⁹²

3.3 Conclusions

The scope of P(V) reagents that can be used to prepare anion **1** has been extended to [TBA][H_2PO_4] and H_3PO_4 . Both present a significant advance over the use of trimetaphosphate, obtained by dehydration at elevated temperatures. Instead, trichlorosilane is employed to carry out both the dehydration and reduction of phosphate at 110 °C.

The present work opens the door for further reduction of p-block oxoanions using trichlorosilane as a viable strategy for the preparation of trichlorosilyl stabilized anions, which are known for the elements C,^{33,62} Si,⁹³ Ge,⁶¹ N,⁹⁴ P¹⁰ and S.⁶³ [TBA]**1** and [TBA]**2** are useful reagents for the preparation of phosphorus-carbon and sulfur-carbon bonds respectively, with concomitant formation of Si-X (X = Cl, Br, O) bonds as a thermodynamic driving force for such reactions, demonstrating the utility of such trichlorosilyl substituted anions in chemical synthesis.

3.4 Experimental methods

3.4.1 General methods

All manipulations were performed in a Vacuum Atmospheres model MO-40M glovebox under an inert atmosphere of purified N₂ or using standard Schlenk techniques. When reagents were removed from a stock bottle containing a Sure/Seal, the equivalent volume of dry nitrogen was injected into the bottle prior to removing the desired volume of solution with a syringe. All solvents were obtained anhydrous and oxygen-free by bubble degassing (argon) and purification by passing through columns of alumina and Q5.⁹⁵ Once collected, solvents were stored over activated 4 Å molecular sieves (20 wt%) inside the glovebox.⁹⁶ All glassware was oven-dried for at least 6 h prior to use, at temperatures greater than 150 °C.

Trichlorosilane (Millipore-Sigma) was used as received. Tetrabutylammonium dihydrogen phosphate (Alfa Aesar), tetrabutylammonium chloride (Millipore-Sigma), tetrabutylammonium hydrogen sulfate (Acros) and phosphoric acid (crystalline, Millipore-Sigma) were dried at 23 °C in vacuo for 12 hours prior to use. Benzyl bromide (Alfa) and 1-chlorooctane (Millipore-Sigma) were degassed three times by the freeze-pump-thaw method and stored over activated 4 Å molecular sieves for 48 h prior to use. Dichloromethane-*d*₂, C₆D₆, CD₃CN and CDCl₃ were purchased from Cambridge Isotope Labs and were degassed three times by the freeze-pump-thaw method and stored over activated 4 Å molecular sieves for 48 h in the glovebox prior to use. Diatomaceous earth (Celite 435, EM Science), 4 Å molecular sieves (Millipore-Sigma) and basic alumina (Millipore-Sigma) were dried by heating to 200 °C under dynamic vacuum for at least 48 h prior to use. The temperature of the aluminum shot used to heat reagents or reaction mixtures was measured using a Hanna Instruments K-type Thermocouple Thermometer (model HI935005).

NMR spectra were obtained on Varian Inova 300 and 500 instruments equipped with Oxford Instruments superconducting magnets, on a Jeol ECZ-500 instrument equipped with an Oxford Instruments superconducting magnet, or on a Bruker Avance 400 instrument equipped with a Magnex Scientific or with a SpectroSpin superconducting magnet. ¹H and ¹³C NMR spectra were referenced to residual CD₂Cl₂ (¹H = 5.32 ppm, ¹³C = 54.0 ppm), C₆D₆ (¹H = 7.16 ppm, ¹³C = 128.06 ppm), CD₃CN (¹H = 1.94 ppm, ¹³C = 118.26 ppm) or chloroform-*d* (¹H = 7.26 ppm, ¹³C = 77.16 ppm). ³¹P NMR spectra were referenced externally to 85% H₃PO₄ (0 ppm). ²⁹Si NMR spectra were externally referenced to TMS in CDCl₃.

Raman spectra were collected using a Renishaw Invia Reflex Micro Raman.

Infrared spectra were collected using a Bruker ATR-IR Tensor 37. Samples were removed from the glovebox in sealed vials and briefly handled in air prior to data collection.

High resolution mass spectral (HRMS) data were collected using a Jeol AccuTOF 4G LC-Plus mass spectrometer equipped with an Ion-Sense DART source. Data were calibrated to a sample of PEG-600 and were collected in positive-ion mode. Samples were

prepared in DCM (10 μ M concentration) and were briefly exposed to air (<5 s) before being placed in front of the DART source.

Electrospray ionization mass spectrometry (ESI-MS) was performed using a Micromass Q-TOF ESI spectrometer.

Elemental combustion analyses were performed by Midwest Micro Laboratories (Indianapolis, IN, USA).

3.4.2 Safety and hygiene considerations

3.4.2.1 Procedures and notes pertaining to [TBA]1

[TBA]1 has been shown to release toxic phosphine (PH_3) gas upon exposure to water.¹⁰ Although the hydrolysis of [TBA]2 was not investigated, highly toxic H_2S is a plausible product of such a reaction.⁶⁹ Glassware that was contaminated with [TBA]1 or [TBA]2 was quickly quenched with household bleach in a well ventilated fume hood upon initial exposure to the atmosphere. Glassware decontaminated in this manner was left in contact with bleach for 24 hours, after which time the glassware was rinsed clean with water.

When removing contaminated glassware from the glovebox and transporting it to the fume hood, a secondary container with a good seal was used to avoid exposing the lab environment to malodorous and potentially toxic vapors. A squirt bottle of bleach was readily available to rinse the downspout of the liquid nitrogen-cooled trap that was connected to the glovebox, as this was frequently a source of malodorous vapors. For larger scale reactions, volatile material is preferably removed on a Schlenk line in a fume hood, so as to avoid contaminating the lab environment when taking down a liquid nitrogen-cooled trap located outside of a fume hood.

Inside the glovebox, glassware contaminated with [TBA]1 and [TBA]2 was immediately stored in a secondary container. It was found that if contaminated glassware was left in the glovebox for prolonged periods, a fine white powder was produced. This white powder was also found to coat clean, nearby objects too.

3.4.2.2 Procedure for quenching trichlorosilane

In a fume hood, trichlorosilane (100 mL) was added dropwise to isopropyl alcohol (1 L) in a two-necked round bottom flask (2000 mL) with vigorous stirring. The isopropyl alcohol was pre-chilled in a water/ice bath for 20 minutes before the addition of trichlorosilane began. The temperature of the mixture was monitored using a thermometer, and did not exceed 40 °C. Once the addition of trichlorosilane was complete the resulting solution was stirred overnight. The solution was added portionwise to aqueous sodium hydroxide solution (1.5 M, 3000 mL) in a Erlenmeyer flask (4 L). The addition is exothermic and produces gas, and so was performed slowly with the temperature not exceeding 40 °C. Once the addition was complete, the mixture was stirred overnight and then discarded.

Any residue contaminating the glassware was removed using aqueous sodium hydroxide solution (1.0 M).

3.4.3 Preparation of [TBA][P(SiCl₃)₂]

3.4.3.1 General notes and procedure for the purification of [TBA]1

[TBA]1 is water- and air-sensitive; rigorously dry solvents and glassware should be used throughout the preparative procedures. Recrystallization of impure material can be accomplished using DCM and pentane at $-35\text{ }^{\circ}\text{C}$. A typical procedure for purification is provided below.

[TBA]1 (ca. 1.0 g, 1.8 mmol), was dissolved in DCM (20 mL) and filtered through a pipette plug containing diatomaceous earth (1 cm bed). (Note: if the pipette filter becomes blocked, additional pipette filters can be used. Alternatively, a frit (fine porosity, 15 mL) containing diatomaceous earth (1 cm bed) can be used.) The filtrate was concentrated to 4 mL. (Note: if precipitate is observed after concentration then the solution is filtered through a filter pipette containing diatomaceous earth (1 cm)). Addition of pentane (16 mL, 4:1 v:v) to the filtrate produced a cloudy solution. (Note: addition of the pentane with agitation is preferred to careful layering; the latter sometimes does not result in formation of solid material and instead produces an oil.) The resulting mixture was placed in the glovebox freezer overnight ($-35\text{ }^{\circ}\text{C}$), after which time a white precipitate developed. (Note: occasionally, the precipitate develops only after shaking the vial, or scratching with a metal spatula.) The solids were collected on a frit (15 mL, fine porosity) while the mixture was still cold, then quickly washed with pentane ($3 \times 7\text{ mL}$, $-35\text{ }^{\circ}\text{C}$). Solvent was removed from the collected material under vacuum (rough pump) for an hour to give spectroscopically pure [TBA]1.

3.4.3.2 Attempt from phosphoric acid

In the glovebox, a steel Parr reactor (300 mL) containing a glass liner and a dumbbell shaped stir bar (4 cm length) was charged with tetrabutylammonium chloride (9.17 g, 33.0 mmol, 1 equiv) and crystalline phosphoric acid (3.26 g, 33.0 mmol, 1 equiv). The reactor was sealed and removed from the glovebox and connected to the Schlenk line. Trichlorosilane (100 mL, 1.0 mol, 30 equiv) was added directly from the stock bottle using a cannula. The volume was estimated using the diameter of the stock bottle; 2.5 cm of vertical height of trichlorosilane was added from the bottle (500 mL, Millipore-Sigma). Once addition of trichlorosilane was complete, the reactor was sealed and heated in an aluminum heating block at $110\text{ }^{\circ}\text{C}$ for 86 hours. The reactor was allowed to cool to ambient temperature overnight, then vented to an oil bubbler followed by a water bubbler in series, to scrub any moisture reactive gases. Once vented, the reactor was connected to the Schlenk line and volatile material was removed under reduced pressure over the course of 4 hours. DCM ($3 \times 100\text{ mL}$) was used to wash the contents of the reactor into a

Schlenk flask (1000 mL). The slurry was allowed to settle overnight, then the supernatant was transferred to a fresh Schlenk flask (1000 mL) to separate it from solid material. The DCM was removed under reduced pressure and the resulting material was dissolved in THF (200 mL). The mixture was allowed to settle overnight, then the supernatant was passed through a Schlenk frit (fine porosity, 100 mL) into a Schlenk flask (500 mL). The Schlenk flask that had contained the material before the filtration was rinsed with THF (70 mL), and the resulting slurry was also passed through the Schlenk frit. Volatile material was removed from the combined filtrate under reduced pressure to give a yellow oil. The oil was triturated with ether (3×100 mL); however the obtained material remained an oil.

The material was brought into the glovebox. Benzene (100 mL) was added and the slurry was stirred for a week. This procedure was followed based on the ability of benzene to separate $[\text{TBA}]_2[\text{Si}_6\text{Cl}_{14}]$ from $[\text{TBA}][\text{C}(\text{SiCl}_3)_3]$.³³ After allowing the mixture to settle, two phases separated out. The lower phase was opaque and white, while the upper phase was clear and yellow. Both phases were analyzed by ^{29}Si NMR spectroscopy (Fig. 3.6). The upper phase contained $[\text{TBA}]\mathbf{1}$ and no $[\text{TBA}]_2[\text{Si}_6\text{Cl}_{14}]$ whilst the lower phase contained both. The clear yellow phase was removed from the lower opaque white phase using a pipette and passed through a frit (fine porosity, 30 mL) containing diatomaceous earth (2 cm bed). The white phase was washed with additional benzene (50 mL), and the benzene washings were passed through the same frit. The diatomaceous earth was washed with additional benzene (20 mL), then volatile material was removed from the combined filtrate to give a thick yellow oil. The oil was dissolved in DCM (30 mL), to which pentane (400 mL) was added. The solution was placed in the freezer (-35 °C) overnight to give a solid compound.

The solids were broken up with a spatula and collected on a frit (30 mL, fine porosity). The solids were washed with pentane (3×30 mL, -35 °C). As the solids slowly warmed to room temperature, they formed a thick gel. The material was redissolved in DCM (30 mL) and the resulting solution was passed through a fine porosity frit (30 mL), where the frit surface had been covered in a layer of microfibre filter paper. On top of the filter paper was placed diatomaceous earth (2 cm bed). The oil was filtered through the frit and the frit was washed with DCM (20 mL). The resulting solution was filtered through a Pasteur pipette containing microfibre filter paper into a 400 mL flask. Pentane (400 mL) was added and the mixture was placed in the freezer (-35 °C). The solids that formed overnight were collected on a frit (fine porosity, 30 mL), but became an oil after warming to ambient temperature. The material was discarded.

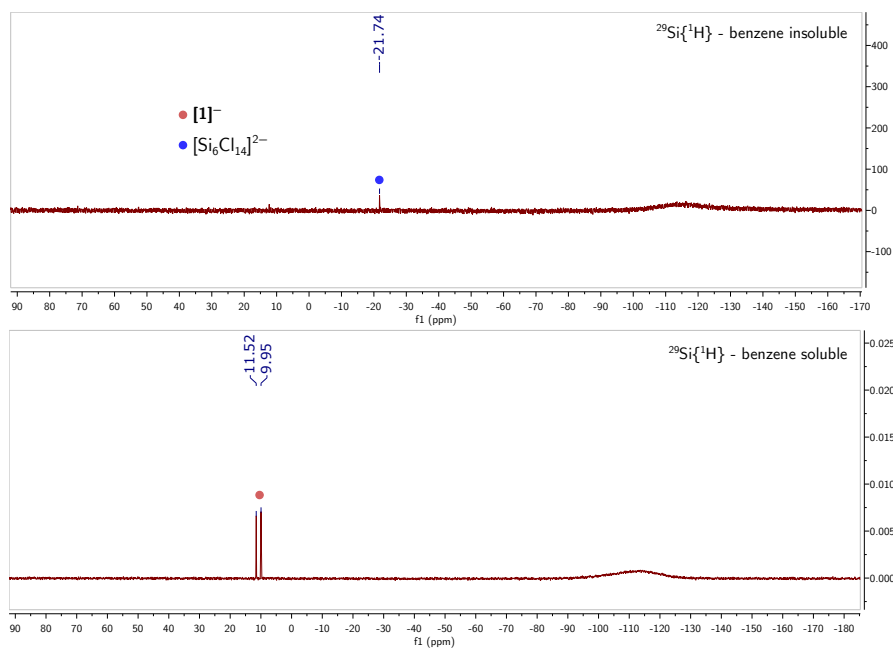


Figure 3.6 $^{29}\text{Si}\{^1\text{H}\}$ NMR spectrum of benzene insoluble (top) and benzene soluble (bottom) material during the workup described in section 3.4.3.2, at 25 °C, recorded at 99 MHz. The top spectrum was recorded in DCM and the bottom spectrum in benzene.

3.4.3.3 From [TBA][H₂PO₄]

In the glovebox, [TBA][H₂PO₄] (1017 mg, 3.0 mmol, 1 equiv) was weighed into a steel pressure reactor (25 mL)¹⁰ equipped with a stir bar (2 cm length). The reactor was sealed using Teflon tape and removed from the glovebox. On the Schlenk line, trichlorosilane (10.0 mL, 13.4 g, 99.2 mmol, 33 equiv) was added against a positive pressure of nitrogen using a needle and syringe. The reactor was sealed and placed in a heating mantle filled with aluminum shot, then heated to 110 °C. This temperature was determined by taking the average temperature at the bottom (120 °C) and surface (100 °C) of the aluminum shot in the heating mantle. The reaction vessel was heated for 6 days, then vented to an oil bubbler followed by a water bubbler in series, to scrub any moisture reactive gases. Volatile material was removed in vacuo on the Schlenk line over the course of 2 h, then the reactor was brought into the glovebox. The solid white material was dissolved in THF (20 mL) and the resulting solution was passed through a frit (fine porosity, 30 mL) containing diatomaceous earth (1 cm bed). The frit was washed with additional THF (2 × 10 mL). Volatile material was removed from the filtrate to give a white solid that was triturated with ether (3 × 5 mL). The solids so obtained were dissolved in DCM (20 mL) then passed through a frit (fine porosity, 15 mL) containing diatomaceous earth (1 cm bed). The diatomaceous earth was washed with DCM (2 × 2 mL), then volatile material was removed from the filtrate in vacuo. The resulting oil was redissolved in DCM (4 mL) then filtered into a fresh vial through a pipette filter. Ether (16 mL) was added to the vial which was taped shut with electrical tape and placed in the freezer overnight (−35 °C). The solids obtained were collected on a frit (fine porosity, 15 mL) and washed with pentane (−35 °C, 3 × 7 mL). The material was brought to constant mass under vacuum (1.016 g, 1.874 mmol, 62% yield). The ¹H and ³¹P NMR spectra of the obtained material are in agreement with the published data.¹⁰

3.4.3.4 From [TBA]₃[P₃O₉].2H₂O

Note: This procedure is analogous to our previous report,¹⁰ but is on a larger scale and can be carried out using Schlenk techniques, as opposed to inside a glovebox. A glovebox is only required for the isolation of the final product. In the glovebox, [TBA]₃[P₃O₉].2H₂O (9.9 g, 9.9 mmol, 1.0 equiv) was weighed into a 300 mL Parr reactor containing a glass liner and a dumbbell shaped stir bar (4 cm length). The reactor was sealed then removed from the glovebox. Against a positive flow of nitrogen on the Schlenk line, trichlorosilane (ca. 100 mL, 992 mmol, 100 equiv) was added from the stock bottle by cannula transfer. The volume was estimated using the diameter of the stock bottle; 2.5 cm of vertical height of trichlorosilane was added from the bottle (500 mL, Millipore-Sigma). The reactor was sealed and heated to 110 °C in an aluminum heating block for 72 h, then allowed to cool to room temperature overnight. The reactor was vented to an oil bubbler followed by a water bubbler in series, to scrub any moisture reactive gases. Volatile material was removed under reduced pressure on a Schlenk line over the course of 4 h. The material in

the reactor was extracted using DCM (3×100 mL) by transferring DCM to the reactor, stirring the contents for five minutes, then transferring the solution to a Schlenk flask (500 mL). The resulting mixture was allowed to settle overnight then the clear supernatant was transferred by filter cannula (prepared by folding a piece of filter paper around the end of a steel cannula and securing it with Teflon tape) to a fresh Schlenk flask (500 mL). *Note: This filtration step can take several hours, and may require refreshing of the filter cannula.* Volatile material was removed from the filtrate to give a sticky yellow oil which was kept under vacuum for an additional 2 h. THF (200 mL) was added to the residue, resulting in most of the material dissolving. The mixture was allowed to settle overnight. The supernatant was transferred by filter cannula into a Schlenk flask (1000 mL). Volatile material was removed from the filtrate to give a sticky yellow oil. Addition of diethyl ether (50 mL) caused a fine white precipitate to form. The flask was brought into the glovebox and the solids collected on a frit (fine porosity, 30 mL), then washed with additional diethyl ether (4×50 mL). Volatile material was removed from the product under vacuum bringing it to constant mass (10.065 g, 18.5 mmol, 63%). The NMR data are consistent with the previously published data.¹⁰ [TBA]**1** has a melting point of 105–108 °C; upon melting there is a slight discoloration from white to yellow. Analysis (³¹P NMR) of [TBA]**1** (20 mg) after being melted in an NMR tube in an oil bath at 110 °C for 20 minutes showed the presence of [TBA]**1**, however not all of the material dissolved in DCM after melting.

3.4.3.5 From [TBA]₂[Si(P₃O₉)₂]

[TBA]₂[Si(P₃O₉)₂] was prepared according to section 3.4.4. In the glovebox, [TBA]₂[Si(P₃O₉)₂] (99 mg, 0.1 mmol, 1 equiv) and tetra-*n*-butylammonium chloride (111 mg, 0.4 mmol, 4 equiv) were weighed into a steel pressure reactor (25 mL).¹⁰ The reactor was sealed using Teflon tape then removed from the glovebox. Trichlorosilane (5 mL, 27.6 mmol, 276 equiv) was added against a positive flow of nitrogen on the Schlenk line. The reactor was sealed and placed in a heating mantle filled with aluminum shot. The reactor was heated to 110 °C for 72 h. The temperature of the reactor was determined to be halfway between the temperature at the bottom of the heating mantle (120 °C) and the top (100 °C), as measured by a thermocouple thermometer. The reactor was allowed to cool to 23 °C then volatile material was removed under reduced pressure on the Schlenk line. The reactor was brought into the glovebox and the residue dissolved in DCM (10 mL). An aliquot was analyzed by ³¹P NMR spectroscopy, which showed a single resonance corresponding to [TBA]**1** (Fig. 3.7). The material was not subjected to further work up and so a yield was not recorded. ³¹P{¹H} NMR (203 MHz, CH₂Cl₂, δ) –172.8.

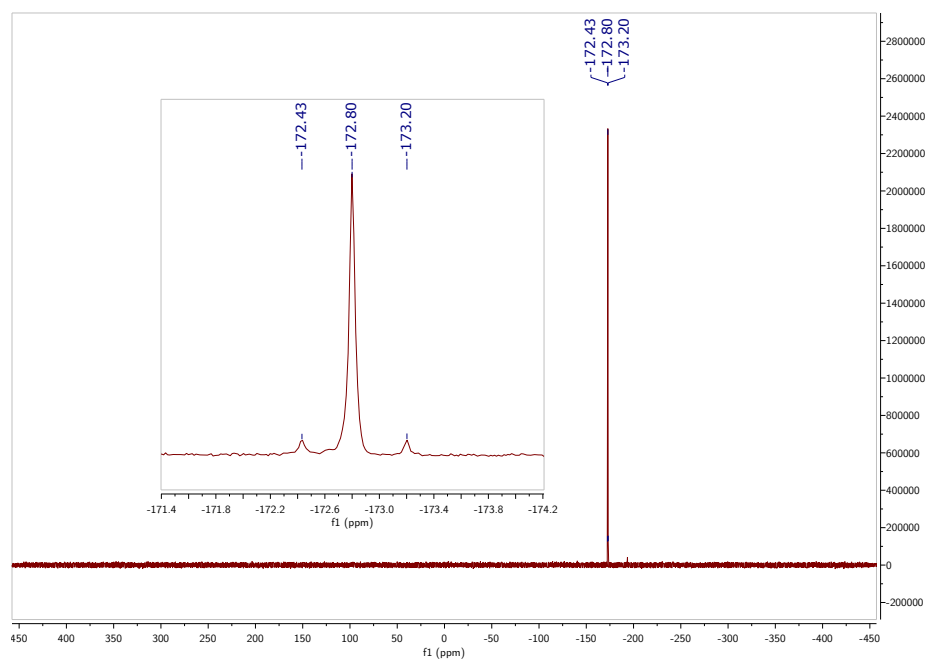


Figure 3.7 $^{31}\text{P}\{^1\text{H}\}$ NMR spectrum of the crude product obtained as described in section 3.4.3.5, in DCM at 25 °C, recorded at 203 MHz.

3.4.3.6 Attempt using the conditions used for the preparation of [TBA]2

In the glovebox, [TBA][H₂PO₄] (50 mg, 0.147 mmol, 1 equiv) was weighed into a vial. Acetonitrile (0.4 mL) was added to the vial, and the resulting solution transferred to an NMR tube equipped with a J. Young Valve. The NMR tube was sealed and removed from the glovebox. On the Schlenk line, trichlorosilane (0.3 mL, 2.98 mmol, 20 equiv) was added to the NMR tube using a syringe against a positive flow of N₂. The tube was then sealed and allowed to stand at 23 °C for 48 h. Analysis of the solution by ³¹P NMR spectroscopy did not show formation of anion **1**. The only phosphorus-containing product was observed at 34.04 ppm; this peak was also observed in the commercially obtained starting material, which was used as received with no purification besides drying at 23 °C under vacuum for 12 h prior to use.

3.4.3.7 Observation of condensed polyphosphates under the conditions used to prepare [TBA]1

A small portion (ca. 50 mg) of the crude white material obtained after removing volatile material from the reaction vessel, as described in Section 3.4.3.2, was placed in a pipette filter and washed with THF (5 mL) then DCM (10 mL). The white material was dissolved in water (0.7 mL), then transferred to an NMR tube and analyzed by ³¹P NMR spectroscopy. The observed species were assigned as orthophosphate, pyrophosphate, end-chain and mid-chain phosphates based on their chemical shifts (Fig 3.8).

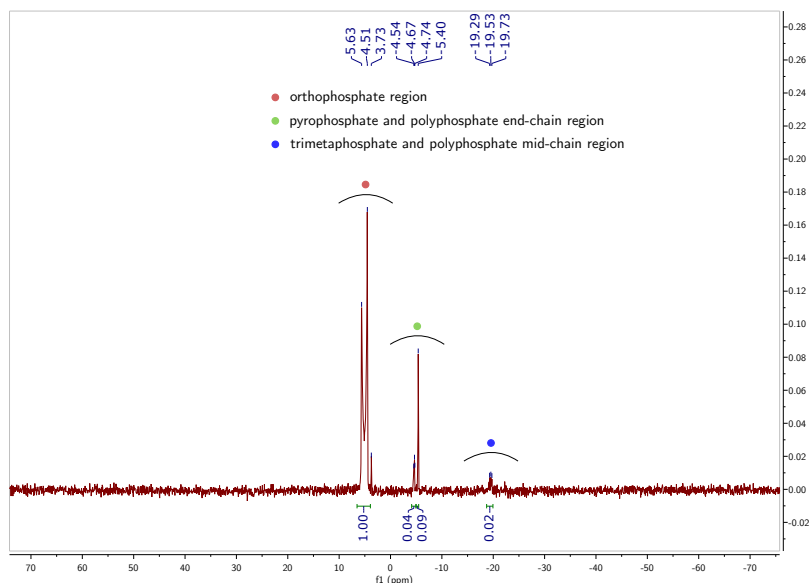


Figure 3.8 ³¹P{¹H} NMR spectrum of the white material obtained as described in section 3.4.3.7, in H₂O at 25 °C, recorded at 203 MHz.

3.4.3.8 Characterization of the volatile silicon-containing byproducts from the synthesis of [TBA]1

Following a synthesis of [TBA]1 as described in Section 3.4.3.4, volatile material that was removed in vacuo from the crude reaction mixture was collected in a liquid-nitrogen cooled Schlenk flask (250 mL). The flask was allowed to warm to ambient temperature under an atmosphere of nitrogen then an aliquot (0.7 mL) was transferred by cannula into a NMR tube equipped with a J. Young valve. The NMR tube was sealed and the sample was analyzed by ^{29}Si NMR spectroscopy. Two of the products could be assigned as hexachlorodisiloxane and pentachlorodisiloxane based previous reports in the literature.^{97,98} Hexachlorodisiloxane ($\text{Cl}_3\text{Si-O-SiCl}_3$): $^{29}\text{Si}\{^1\text{H}\}$ NMR (99 MHz, HSiCl_3 , δ) -46.38 . Pentachlorodisiloxane ($\text{Cl}_3\text{Si-O-SiHCl}_2$): $^{29}\text{Si}\{^1\text{H}\}$ NMR (99 MHz, HSiCl_3 , δ) -46.07 , -36.13 . ^{29}Si NMR (99 MHz, HSiCl_3 , δ) -46.07 , -36.13 (d, $^1J_{\text{Si-H}} = 362$ Hz).

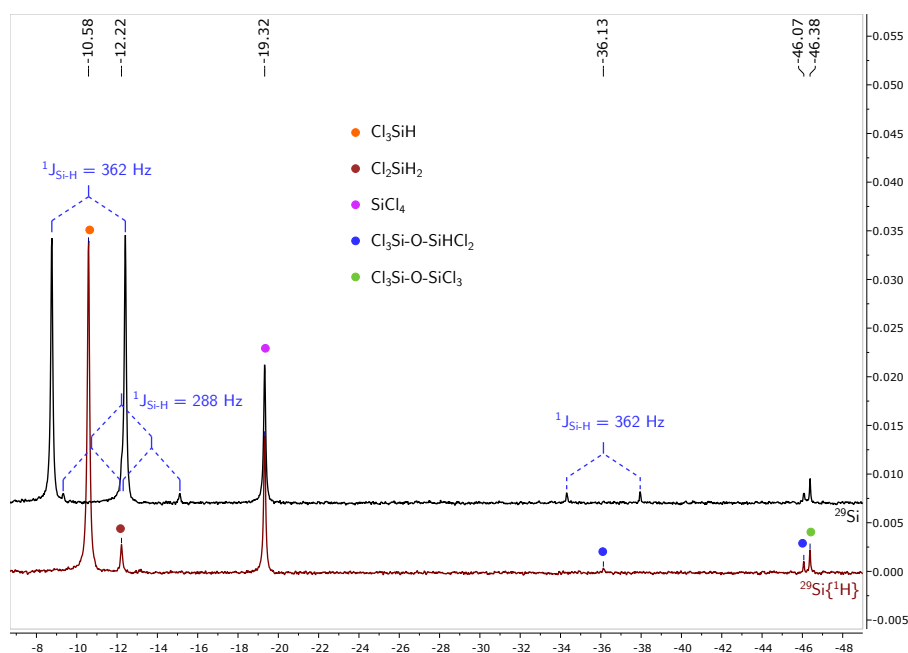


Figure 3.9 Overlay of $^{29}\text{Si}\{^1\text{H}\}$ and ^{29}Si NMR spectra of the distillate obtained in section 3.4.3.8 at 25 °C, recorded at 99 MHz.

3.4.3.9 Characterization of non-volatile silicon-containing byproducts from the synthesis of [TBA]1

Following an attempted synthesis of [TBA]1 as described in section 3.4.3.2, the insoluble material that had settled from the DCM extraction was collected on a frit (fine porosity, 30 mL). A portion of this material (40 mg) was dissolved in water (0.7 mL) and filtered through a piece of microfiber filter paper in a pipette into an NMR tube. A single resonance was observed, attributable to orthosilicate dissolved in basic aqueous solution.⁹¹

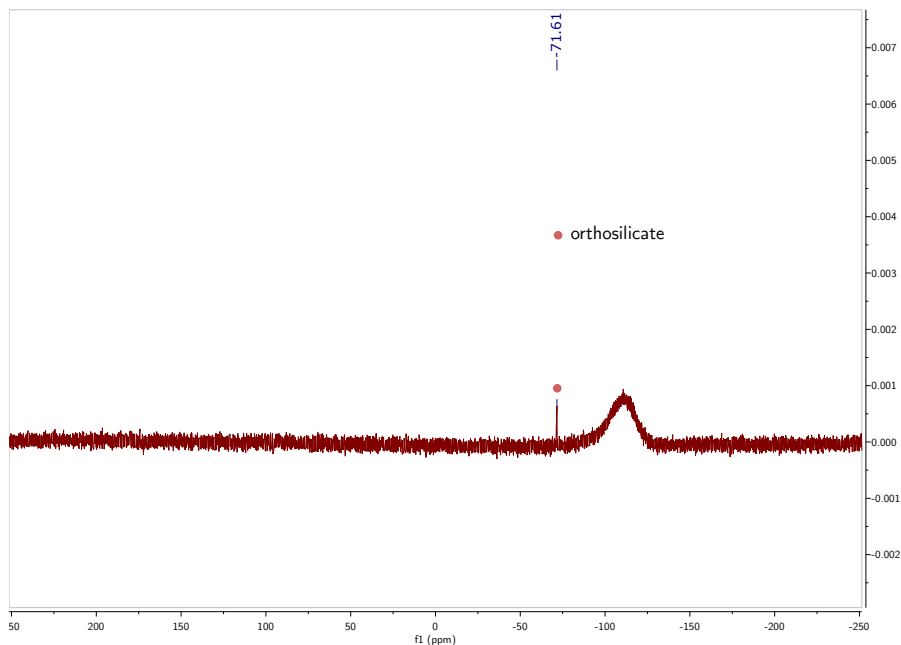


Figure 3.10 $^{29}\text{Si}\{^1\text{H}\}$ NMR spectrum of the residue dissolved in aqueous sodium hydroxide (1.0 M) (section 3.4.3.9) at 25 °C, recorded at 203 MHz.

3.4.4 Preparation of [TBA]₂[Si(P₃O₉)₂]

In the glovebox, [TBA]₃[P₃O₉].2H₂O (2.0 g, 2.0 mmol, 1.0 equiv) was weighed into a Schlenk flask (25 mL) equipped with a Teflon screw cap. DCM (15 mL) was added to the flask, which was then sealed and removed from the glovebox. On the Schlenk line, silicon(IV) chloride (1.36 mL, 12.0 mmol, 6 equiv) was added against a flow of nitrogen using a syringe. The flask was sealed and stirred at ca. 23 °C for 24 h. Volatile material was removed under reduced pressure to give a sticky white oil. The flask was brought into the glovebox and the residue slurried in THF (8 mL). The mixture was passed through a frit (medium porosity, 30 mL). The white solid that collected on the frit was recrystallized by dissolving the material in DCM (8 mL) then filtering the resulting mixture through a piece of microfibre filter paper in a pipette to give a clear colorless solution. Diethyl ether (12 mL) was added to the solution and the resulting slurry was placed in the freezer. The solids that formed were collected on a frit (15 mL, fine porosity) and the material was subjected to the same DCM/diethyl ether recrystallization procedure as described in the preceding two sentences. The solid material that formed was collected on a frit (15 mL, fine porosity) and washed with diethyl ether (3 × 5 mL). Volatile material was removed from the product under vacuum bringing it to constant mass to give [TBA]₂[Si(P₃O₉)₂] as a crystalline white powder (253 mg, 0.266 mmol, 27%). ¹H NMR (500 MHz, CH₂Cl₂, δ) 3.23–3.02 (m), 1.62 (p, *J* = 8.1, 7.7 Hz), 1.42 (h, *J* = 7.0 Hz), 1.01 (t, *J* = 7.8 Hz). ³¹P{¹H} NMR (203 MHz, CH₂Cl₂, δ) –30.0. A ²⁹Si NMR signal was not observed, despite collecting 2000 scans with a saturated sample of [TBA]₂[Si(P₃O₉)₂] in DCM on a 500 MHz instrument. This was attributed to the low signal/noise that would be expected from the binomial septet coupling pattern arising from 6 magnetically equivalent phosphorus nuclei. Elem. Anal. Calcd(found) for C₃₂H₇₂N₂O₁₈P₆Si₁: C 38.95(38.71), H 7.35(7.01), N 2.84(2.51). Signals corresponding to [O₁₈P₆Si]²⁻ and [C₁₆H₃₆NO₁₈P₆Si]⁻ were observed in the negative mode ESI mass spectrum (Fig.3.13)

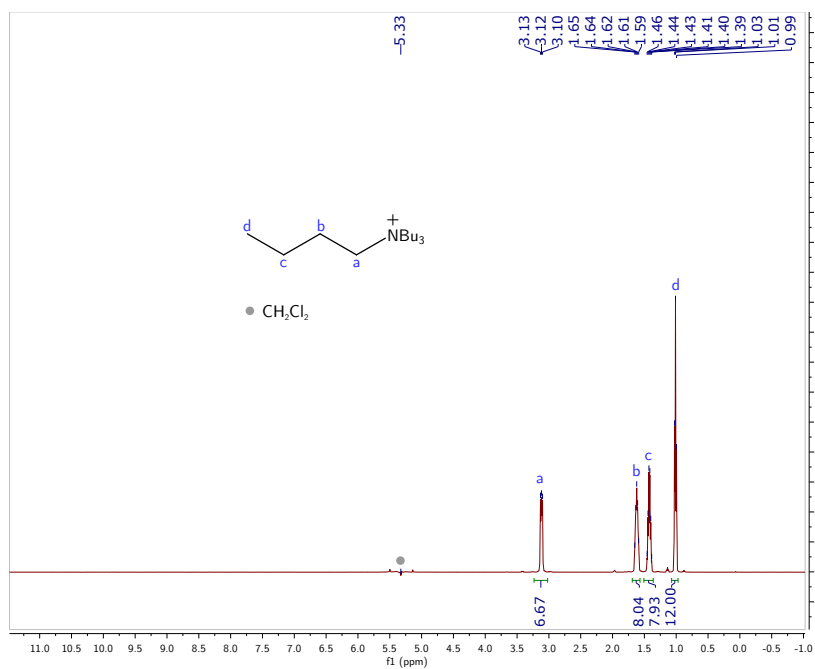


Figure 3.11 1H NMR spectrum of $[TBA]_2[Si(P_3O_9)_2]$ in DCM at 25 °C, recorded at 500 MHz.

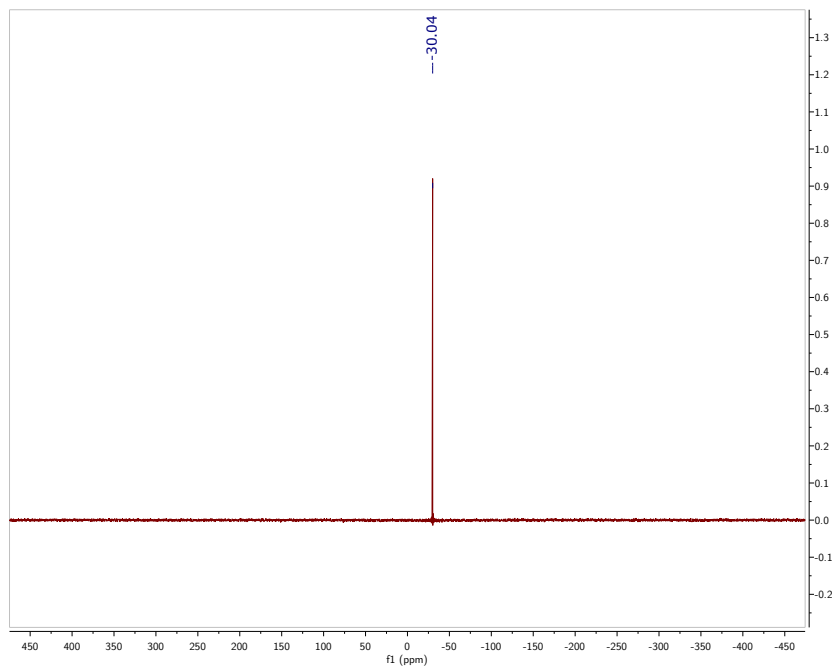


Figure 3.12 $^{31}P\{^1H\}$ NMR spectrum of $[TBA]_2[Si(P_3O_9)_2]$ in DCM at 25 °C, recorded at 203 MHz.

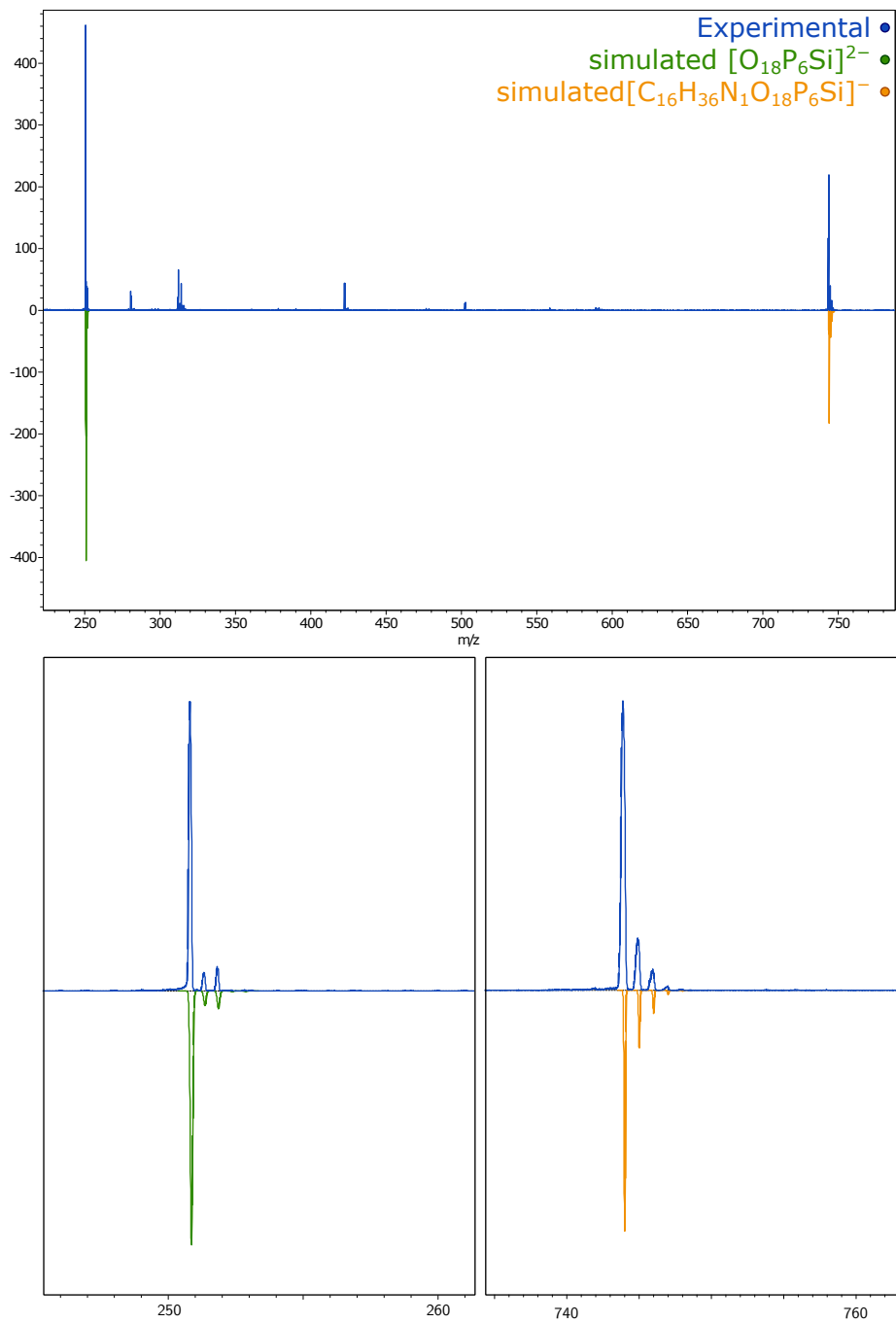


Figure 3.13 Negative mode ESI mass spectrum of a solution of $[TBA]_2[Si(P_3O_9)_2]$ in acetonitrile.

3.4.5 Monitoring the formation of $[\text{TBA}]_2[\text{Si}(\text{P}_3\text{O}_9)_2]$

3.4.5.1 From SiCl_4

In the glovebox, $[\text{TBA}]_3[\text{P}_3\text{O}_9] \cdot 2\text{H}_2\text{O}$ (30 mg, 0.031 mmol, 1 equiv) was weighed into an NMR tube and dissolved in DCM (0.6 mL). The tube was sealed and removed from the glovebox. On the Schlenk line, SiCl_4 (50 μL , 0.439 mmol, 14 equiv) was added using a microsyringe against a positive flow of nitrogen. The reaction mixture was analyzed by ^{31}P NMR spectroscopy after 30 minutes and 48 hours. After 30 minutes, the solution contained a mixture of $[\text{TBA}]_2[\text{Si}(\text{P}_3\text{O}_9)_2]$ and an intermediate species. After 48 h, all signals had converged to one assigned to $[\text{TBA}]_2[\text{Si}(\text{P}_3\text{O}_9)_2]$ (Fig. 3.14).

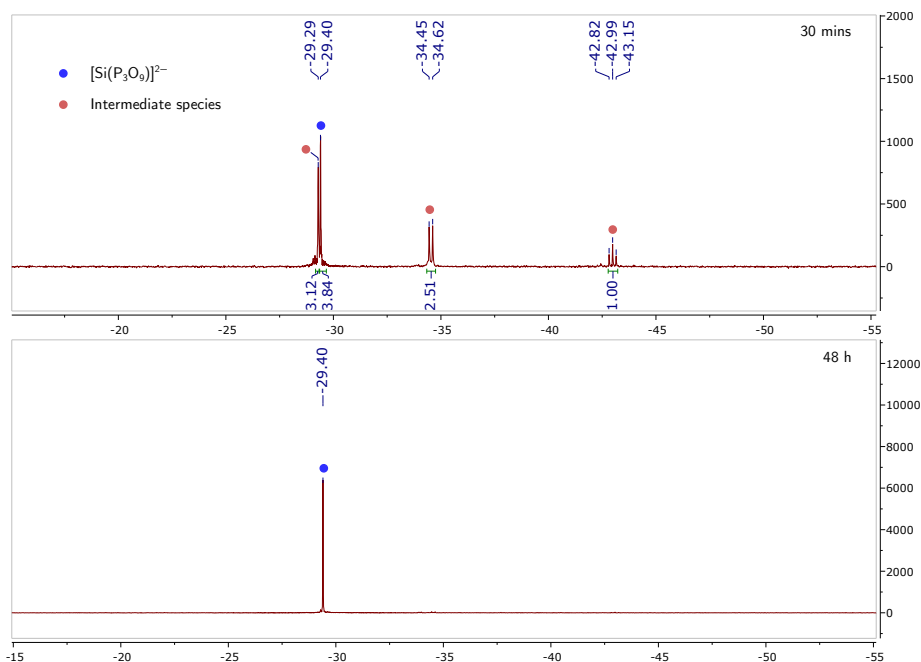


Figure 3.14 $^{31}\text{P}\{^1\text{H}\}$ NMR spectra of the reaction mixture obtained upon mixing $[\text{TBA}]_3[\text{P}_3\text{O}_9] \cdot 2\text{H}_2\text{O}$ and SiCl_4 in DCM (as described in section 3.4.5.1) at 25 °C, recorded at 162 MHz.

3.4.5.2 From HSiCl_3

In the glovebox, $[\text{TBA}]_3[\text{P}_3\text{O}_9] \cdot 2\text{H}_2\text{O}$ (43 mg, 0.043 mmol, 1 equiv) was dissolved in CD_2Cl_2 (0.6 mL). The sample was analyzed by ^{31}P NMR spectroscopy. On the Schlenk line, trichlorosilane (0.1 mL, 0.99 mmol, 23 equiv) was added by syringe against a flow of nitrogen. Immediate bubbling was observed. Once the bubbling stopped, the NMR tube was sealed and analyzed by ^{31}P NMR spectroscopy after 20 min and 3 h. Upon addition of trichlorosilane, a shift of 8 ppm of the ^{31}P NMR resonance of the trimetaphosphate signal

was observed, consistent with the formation of $[\text{TBA}]_2[\text{Si}(\text{P}_3\text{O}_9)_2]$ (Fig. 3.15). A species of low intensity was also observed, with chemical shifts in line with the intermediate observed between SiCl_4 and $[\text{TBA}]_3[\text{P}_3\text{O}_9]\cdot 2\text{H}_2\text{O}$ (Section 3.4.5.1).

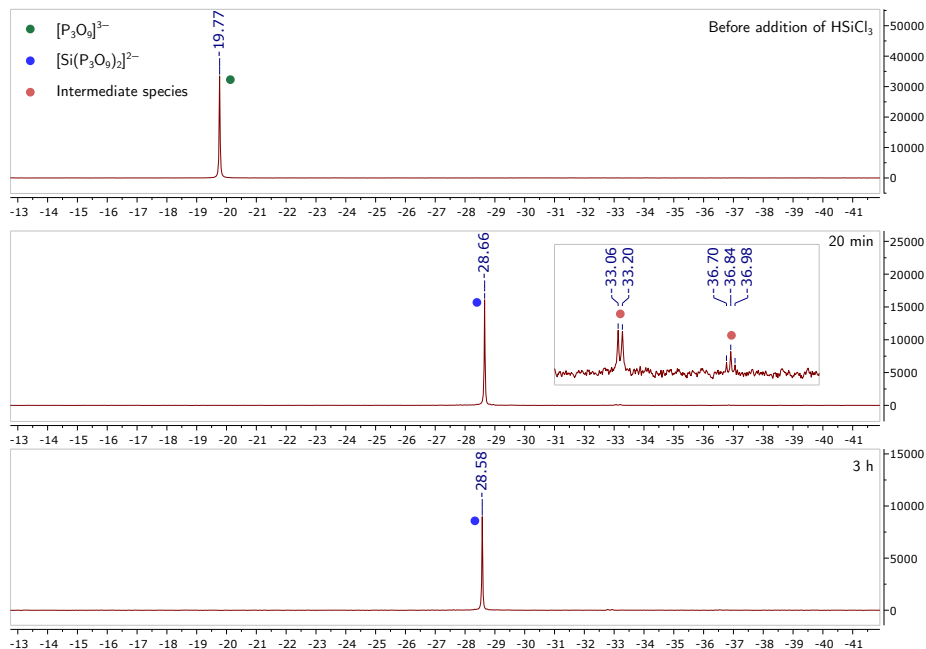


Figure 3.15 $^{31}\text{P}\{^1\text{H}\}$ NMR spectra of the reaction mixture obtained upon mixing $[\text{TBA}]_3[\text{P}_3\text{O}_9]\cdot 2\text{H}_2\text{O}$ and HSiCl_3 in DCM (as described in section 3.4.5.2) at 25°C , recorded at 121 MHz.

3.4.6 Preparation of *n*-octylphosphine

In the glovebox, a steel Parr reactor (300 mL) equipped with a glass liner and a dumbbell-shaped stir bar (4 cm length) was charged with tetrabutylammonium chloride (9.17 g, 33 mmol, 1.5 equiv), crystalline H_3PO_4 (3.23 g, 33 mmol, 1.5 equiv) and 1-chlorooctane (3.27 g, 22 mmol, 1 equiv). The reactor was sealed and removed from the glovebox. On the Schlenk line, against a positive flow of nitrogen, trichlorosilane (100 mL, 1 mol, 45 equiv) was added to the reactor using a syringe and needle. The reactor was sealed and placed in an aluminum block and heated to 120°C for 144 h. After this time, the reactor was cooled to 23°C using a water bath. The reactor was vented to an oil bubbler, then volatile material was removed under reduced pressure and collected in a liquid nitrogen-cooled trap. The material inside the reactor was heated at 60°C for 6 h under dynamic vacuum to remove any unreacted 1-chlorooctane. A Schlenk flask (1000 mL) that contained basic alumina (100 g), both of which had been stored in an oven overnight, were cooled to 23°C on the Schlenk line under dynamic vacuum. Once cool, the flask was carefully cycled

between nitrogen and dynamic vacuum, taking care not to pull the fine alumina into the vacuum manifold. The material in the reactor was transferred to the Schlenk flask that contained the alumina using DCM (3×100 mL). *Caution: evolution of PH_3 !* The gases that formed were exhausted to the back of a well-ventilated fume hood using an exit needle in the septum of the Schlenk flask followed by an oil-bubbler. The resulting slurry was stirred vigorously overnight. A Schlenk frit (1000 mL) that contained diatomaceous earth (2 cm bed) was dried in the oven overnight prior to use. It was allowed to cool under dynamic vacuum on the Schlenk line, then carefully cycled between nitrogen and dynamic vacuum three times, taking care not to pull diatomaceous earth into the vacuum manifold. The DCM/alumina slurry was transferred to the Schlenk frit, then filtered into a receiving Schlenk flask (1000 mL). The solid material that collected on the frit was washed with further DCM (3×100 mL). Volatile material was removed from the combined filtrate at 0°C to give a sticky white residue. The residue was slurried in pentane (100 mL). Deionized water (20 mL) was sparged with nitrogen for an hour to deoxygenate it. Water (0.4 mL) deoxygenated by this method was added to the pentane slurry, and the resulting mixture was stirred vigorously for an hour to give a fine white precipitate. A Schlenk frit (300 mL) containing basic alumina (3 cm bed) was dried in the oven overnight prior to use. It was allowed to cool to 23°C under dynamic vacuum on the Schlenk line before being cycled between nitrogen and dynamic vacuum three times, taking care not to pull alumina into the vacuum manifold. The pentane was transferred by cannula to the Schlenk frit, and filtered into a receiving Schlenk flask (500 mL). The alumina was rinsed with further pentane (2×100 mL). Volatile material was removed from the combined pentane filtrate at -40°C to give a colorless oil (ca. 10 mL). The oil was brought into the glovebox and transferred to an H-cell apparatus for carrying out vacuum-transfer operations. The Schlenk flask was rinsed with additional pentane (3×3 mL) and the washings were transferred to the H-cell. The H-cell was removed from the glovebox, and the excess pentane was removed at -40°C . The resulting oil was transferred under static vacuum to the receiving side of the H-cell; the receiving side was cooled to -78°C with a dry ice/acetone bath while the crude material was heated to 50°C using an oil bath. A heat gun was used to aid the transfer of any oil that was observed on the sides of the flask. The material obtained was brought into the glovebox and transferred to a pre-weighed vial to give *n*-octylphosphine as a colorless oil (1.32 g, 9.02 mmol, 41%). ^1H NMR (500 MHz, CDCl_3 , δ) 2.68 (dt, $^1J_{\text{P-H}} = 194.9$ Hz, 7.2 Hz, 2H), 1.61–1.18 (m, 14H), 0.88 (t, $J = 7.0$ Hz, 3H). ^{13}C NMR (126 MHz, CDCl_3 , δ) 33.06 (d, $J = 2.0$ Hz), 32.01, 30.73 (d, $J = 5.7$ Hz), 29.37, 29.34, 22.82, 14.27, 13.90 ($J = 6.9$ Hz). $^{31}\text{P}\{^1\text{H}\}$ NMR (203 MHz, CDCl_3 , δ) -136.50 . ^{31}P NMR (162 MHz, CDCl_3 , δ) -136.50 (t, $^1J_{\text{P-H}} = 194.9$ Hz). These NMR data are consistent with those reported in the literature.³⁵ HRMS: $[\text{M}+\text{H}]^+$; observed(calc.) m/z : 147.128174 (147.130264).

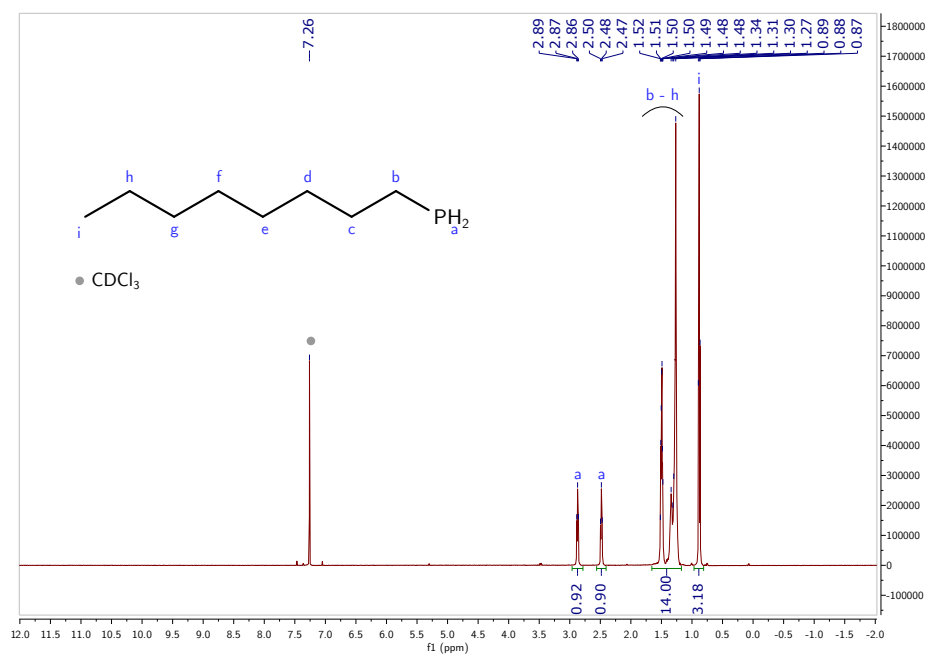


Figure 3.16 ^1H NMR spectrum of *n*-octylphosphine in CDCl_3 at 25 °C, recorded at 500 MHz.

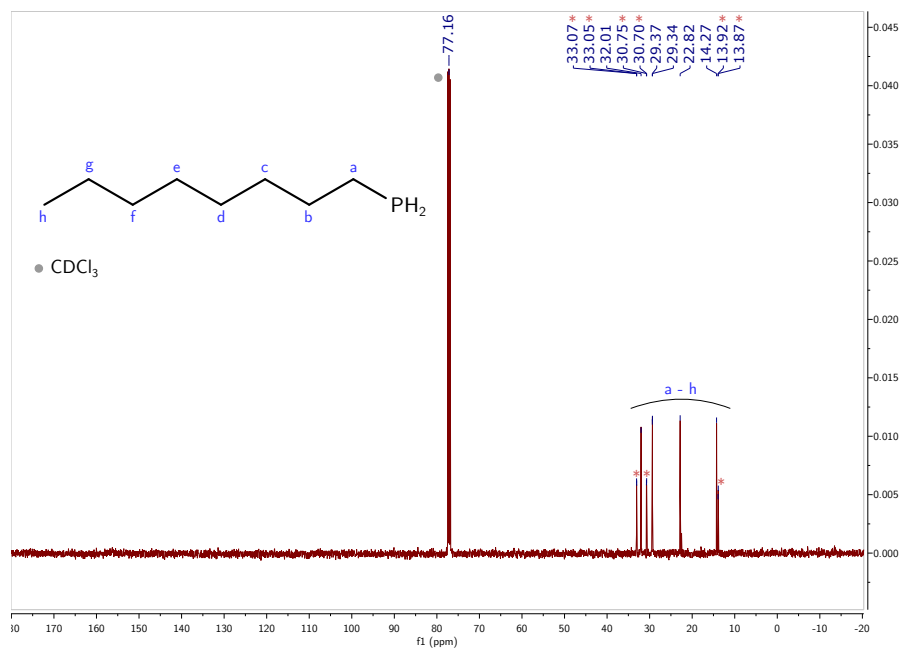


Figure 3.17 ^{13}C NMR spectrum of *n*-octylphosphine in CDCl_3 at 25 °C, recorded at 126 MHz. Resonances marked with a red asterisk correspond to doublets arising from $^1J_{\text{P-C}}$ coupling.

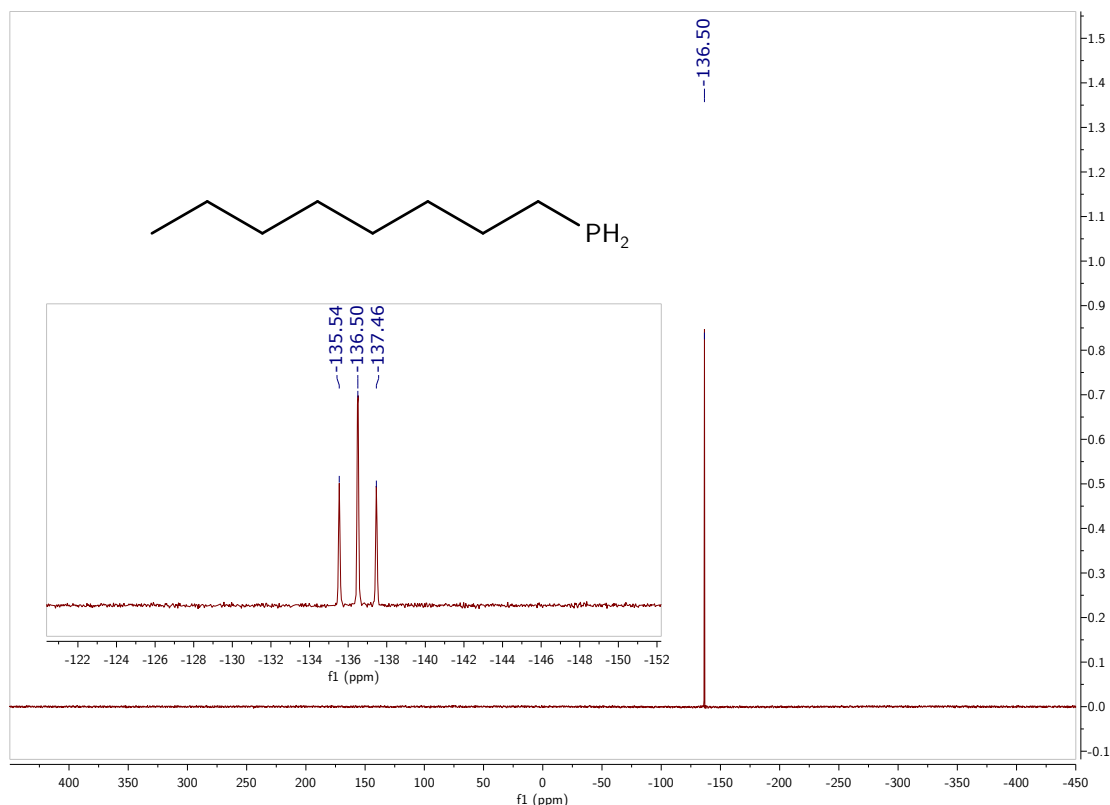


Figure 3.18 $^{31}\text{P}\{^1\text{H}\}$ NMR spectrum and ^{31}P NMR spectrum (inset) of *n*-octylphosphine in CDCl_3 at 25°C , recorded at 203 MHz.

3.4.7 Preparation of tetrabenzylphosphonium chloride

In the glovebox, [TBA]1 (1.50 g, 2.77 mmol, 1.0 equiv) was weighed into a Schlenk flask (100 mL). To the same flask was added benzyl chloride (3.51 g, 27.7 mmol, 10 equiv) followed by acetonitrile (10 mL). The flask was sealed and the reaction mixture was heated at 70°C for 36 h. The reaction mixture was allowed to cool to 23°C , before being added dropwise to water (40 mL) in an Erlenmeyer flask. Acetonitrile (2×4 mL) was used to rinse the reaction flask, and these washings were transferred to the Erlenmeyer flask. The solution was stirred for 5 minutes, then extracted with DCM (100 mL, then 4×50 mL). To the combined organic filtrate, which was slightly cloudy, was added a scoop of anhydrous magnesium sulfate, resulting in a clear colorless solution. The clear solution was decanted away from the white solids into a round bottom flask (500 mL). The white solids were washed with DCM (2×10 mL), and the washings were transferred to the round bottom flask. The flask was placed in an oil bath and the DCM distilled off until the volume of the solution was around 40 mL. Deionized water (200 mL) was added to

the round bottom flask, and the resulting mixture was boiled at 100 °C for 2 h, resulting in a clear colorless solution and a small amount of yellow oil depositing on the sides of the flask. The flask was removed from the oil bath and allowed to cool to 23 °C overnight, during which time feathery white needles formed. The needles were collected on a frit (fine porosity, 30 mL) and washed with water (4 × 20 mL) then diethyl ether (4 × 20 mL). The solids were collected in a pre-weighed vial and the material brought to constant mass under vacuum at 60 °C to give tetrabenzylphosphonium chloride as a white crystalline solid (0.728 g, 1.69 mmol, 61%). ¹H NMR (500 MHz, CDCl₃, δ) 7.34–7.05 (m, 20H), 4.01 (d, *J* = 14.7 Hz, 8H). ¹³C NMR (101 MHz, CDCl₃, δ) 130.72 (d, *J* = 5.2 Hz), 129.64 (d, *J* = 2.9 Hz), 128.68 (d, *J* = 3.5 Hz), 127.83 (d, *J* = 8.2 Hz), 26.97 (d, *J* = 42.9 Hz). ³¹P{¹H} NMR (162 MHz, CDCl₃, δ) 24.49. ³¹P NMR (162 MHz, CDCl₃, δ) 24.49 (m). These NMR data are consistent with those in the literature.⁴⁴ HRMS: [M]⁺; observed(calc.) *m/z*: 395.192413 (395.192864).

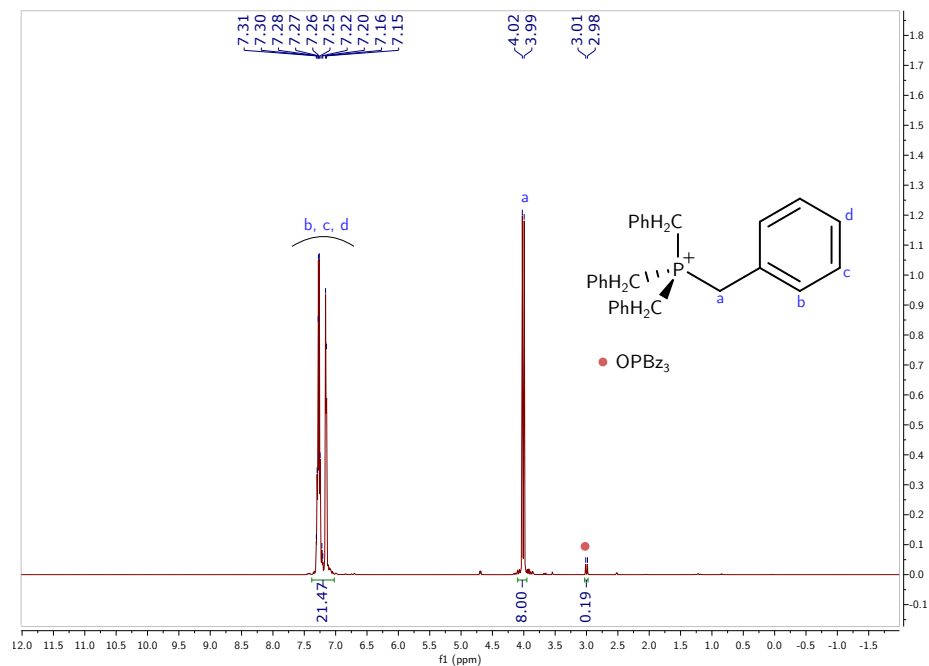


Figure 3.19 ¹H NMR spectrum of tetrabenzylphosphonium chloride in CDCl₃ at 25 °C, recorded at 500 MHz.

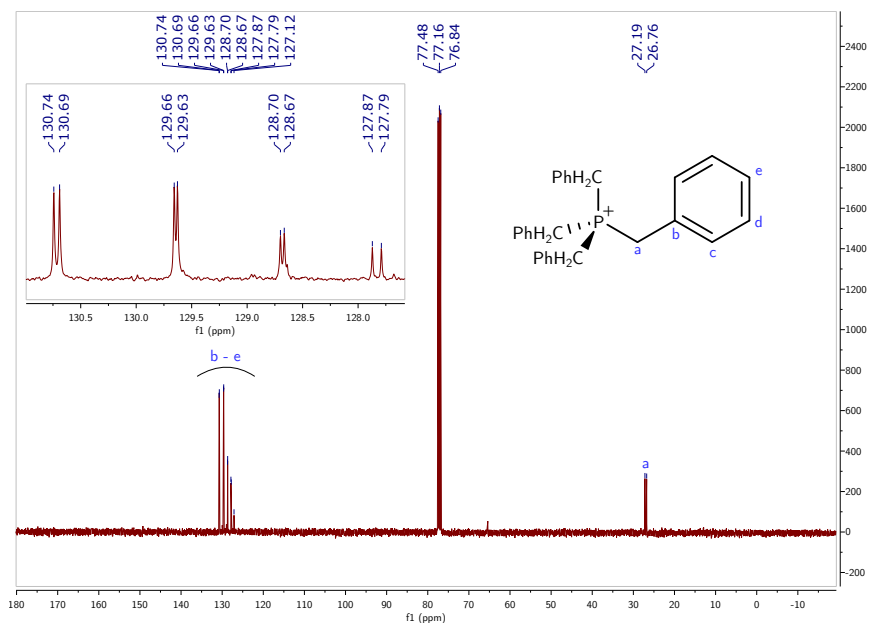


Figure 3.20 ^{13}C NMR spectrum of tetrabenzylphosphonium chloride in CDCl_3 at 25°C , recorded at 101 MHz.

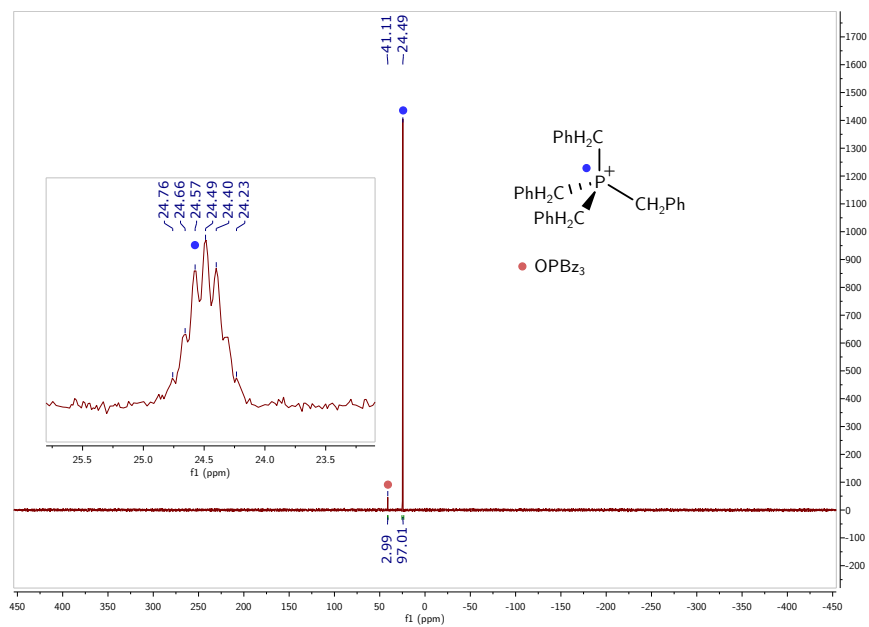


Figure 3.21 $^{31}\text{P}\{^1\text{H}\}$ NMR spectrum and ^{31}P NMR spectrum (inset) of tetrabenzylphosphonium chloride in CDCl_3 at 25°C , recorded at 162 MHz.

3.4.8 Preparation of [TBA]2

In a glovebox, [TBA][HSO₄] (1.0 g, 2.94 mmol) was weighed into a thick-walled 100 mL Schlenk flask. The material was dissolved in acetonitrile (5 mL). The flask was sealed and connected to a Schlenk line. Against a positive pressure of nitrogen, trichlorosilane (6 mL, 59.5 mmol) was added using a syringe. The solution was stirred vigorously at 23 °C for 20 h, at which time volatile material was removed in vacuo for a total of 2 h. The flask was brought into the glovebox and the material slurried in THF (20 mL) then stirred for five minutes. The mixture was passed through a frit (15 mL, fine porosity) containing diatomaceous earth (2 cm bed). The diatomaceous earth was washed with THF (3 × 7 mL). Volatile material was removed from the filtrate in vacuo to give a sticky white oil. The oil was triturated with diethyl ether (3 × 7 mL) to give a yellow solid. The material was dissolved in DCM (3 mL), then passed through a piece of filter paper in a pipette into a vial (20 mL). The flask was washed with DCM (1 mL) and the washings passed through the filter paper into the vial. Diethyl ether was added to the vial to produce a white precipitate and the resulting solution was stored in the freezer (−35 °C) overnight. The solids were collected on a frit (fine porosity, 15 mL) and washed with diethyl ether (−35 °C, 3 × 7 mL). The material obtained was dissolved in 10 mL DCM, and the undissolved material was removed by passing through a piece of filter paper in a pipette, that contained approximately 1 cm of diatomaceous earth. If the filter got clogged, a new pipette with filter paper and 1 cm of diatomaceous earth was used. The solution was concentrated to 3 mL and diethyl ether (17 mL) was added to produce a white precipitate. The mixture was stored in the glovebox freezer overnight. The solids were collected on a frit (fine porosity, 15 mL) and washed with diethyl ether (−35 °C, 3 × 7 mL) then transferred to a vial and brought to constant mass under vacuum (520 mg, 1.27 mmol, 43% yield). This material was judged to be of sufficient purity for further reactions described in the following sections. However, this material was recrystallized for elemental analysis by subjecting it to an additional round of recrystallization as described above. Elem. Anal. Calcd(found) for C₁₆H₃₆Cl₃N₁S₁Si₁: C 46.99(47.08), H 8.87(9.02), N 3.42(3.44). ¹H NMR (500 MHz, CDCl₃, δ) 3.27–3.11 (m, 8H), 1.64 (p, *J* = 7.9 Hz, 8H), 1.44 (h, *J* = 7.3 Hz, 8H), 1.02 (t, *J* = 7.3 Hz, 12H). ¹³C NMR (126 MHz, CDCl₃, δ) 59.57, 24.52, 20.25, 13.94. ²⁹Si NMR (99 MHz, CDCl₃, δ) −21.50.

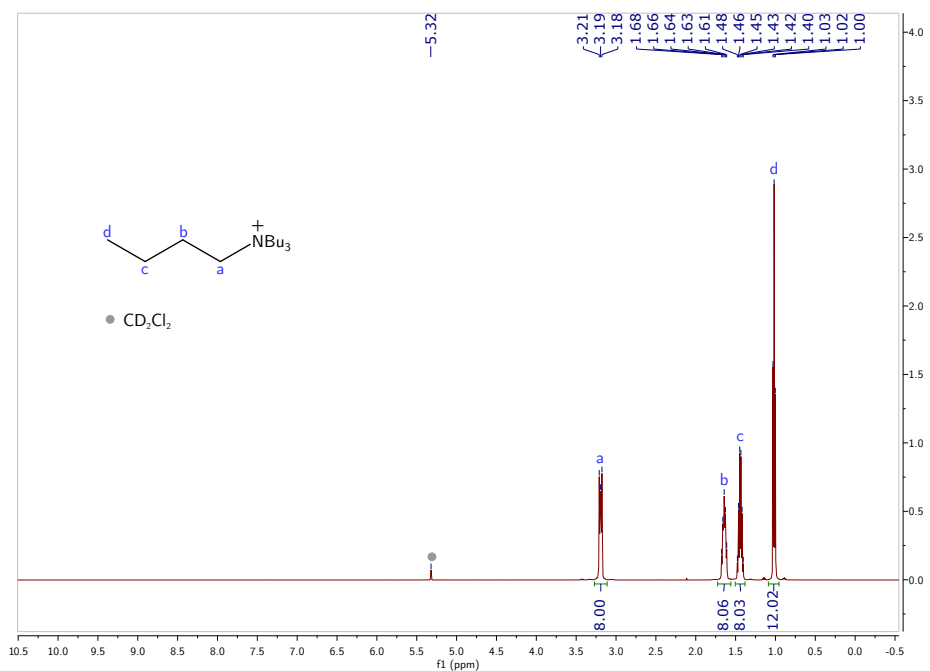


Figure 3.22 ¹H NMR spectrum of [TBA][SSiCl₃] in CD₂Cl₂ at 25 °C, recorded at 500 MHz.

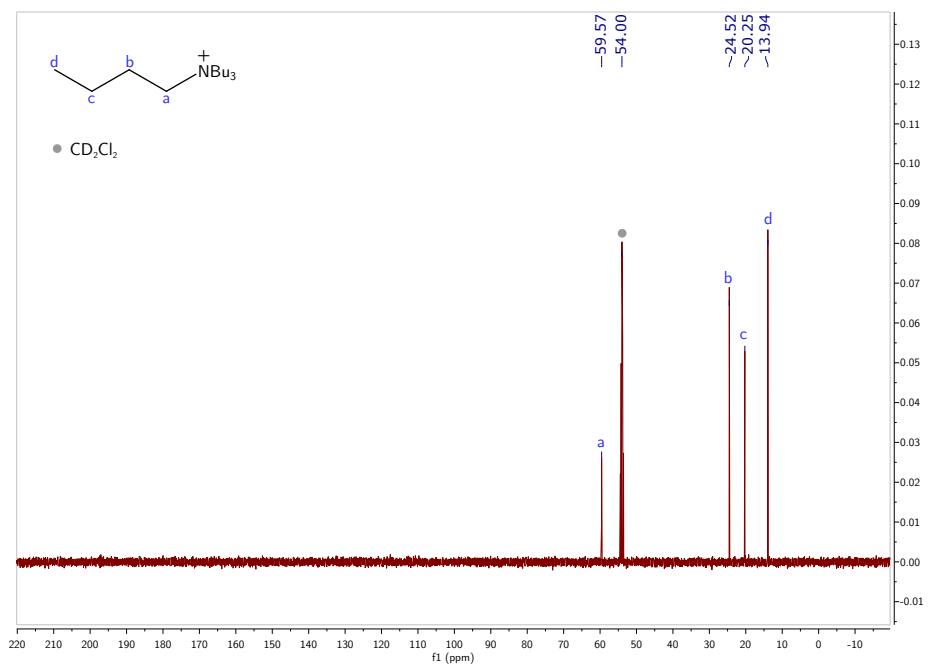


Figure 3.23 ¹³C NMR spectrum of [TBA][SSiCl₃] in CD₂Cl₂ at 25 °C, recorded at 126 MHz.

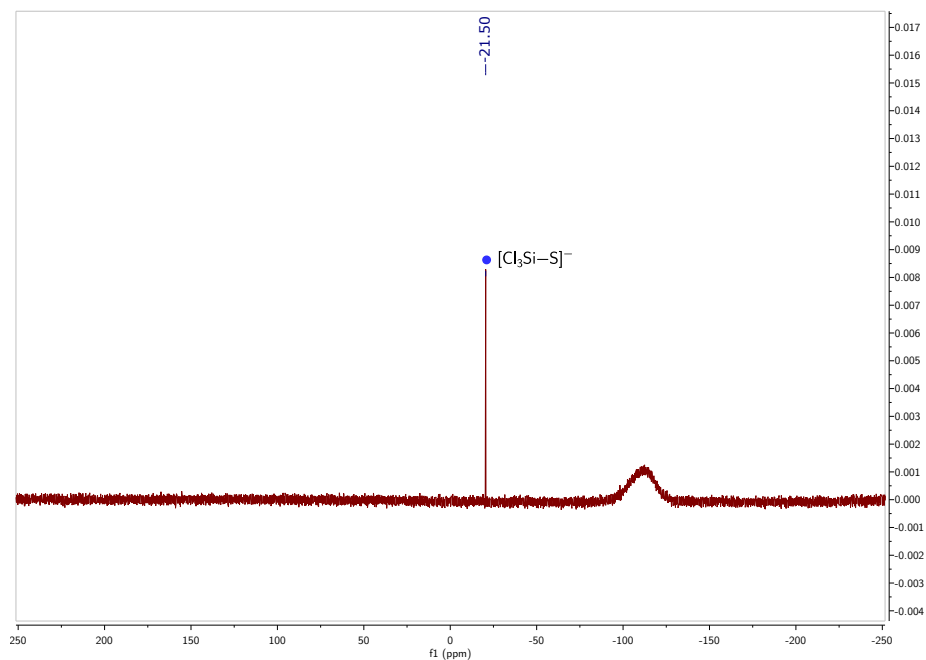


Figure 3.24 ^{29}Si NMR spectrum of $[\text{TBA}][\text{SSiCl}_3]$ in CD_2Cl_2 at $25\text{ }^\circ\text{C}$, recorded at 99 MHz.

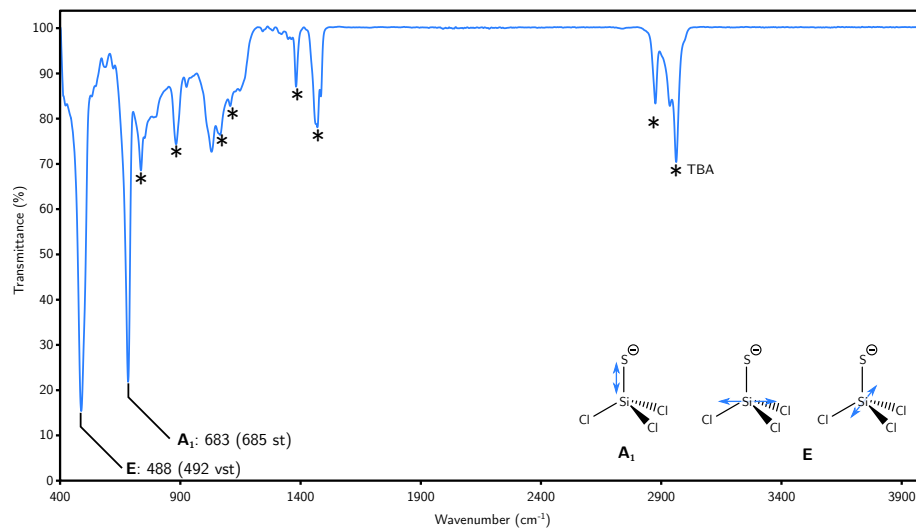


Figure 3.25 IR spectrum of $[\text{TBA}]_2$, recorded on a Bruker ATR (Tensor 37) infrared spectrometer. The numbers in parentheses are of previously reported values.⁶³ st= strong, vst = very strong.

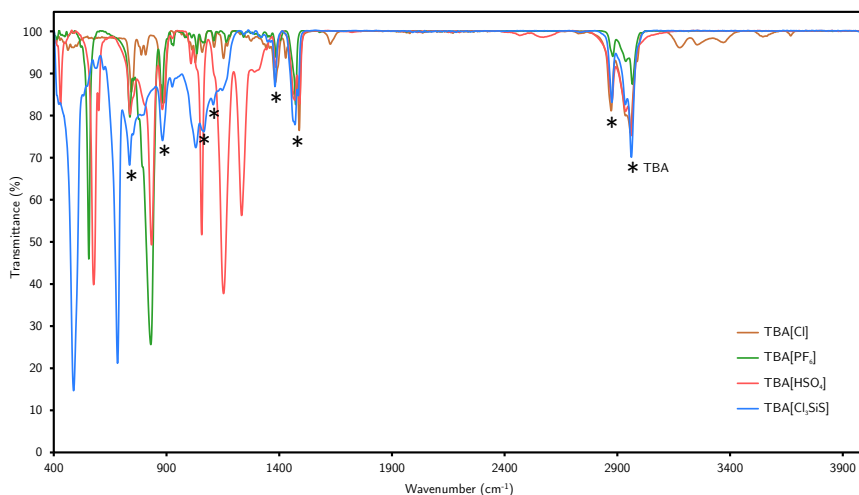


Figure 3.26 Overlay of the IR spectra of [TBA]2, [TBA][HSO₄], [TBA][Cl], and [TBA][PF₆]. This shows there is no remaining bisulfate in [TBA]2 as prepared in section 3.4.8. The spectra of [TBA][Cl] and [TBA][PF₆] were collected in order to assign the peaks arising from the tetrabutylammonium cation.

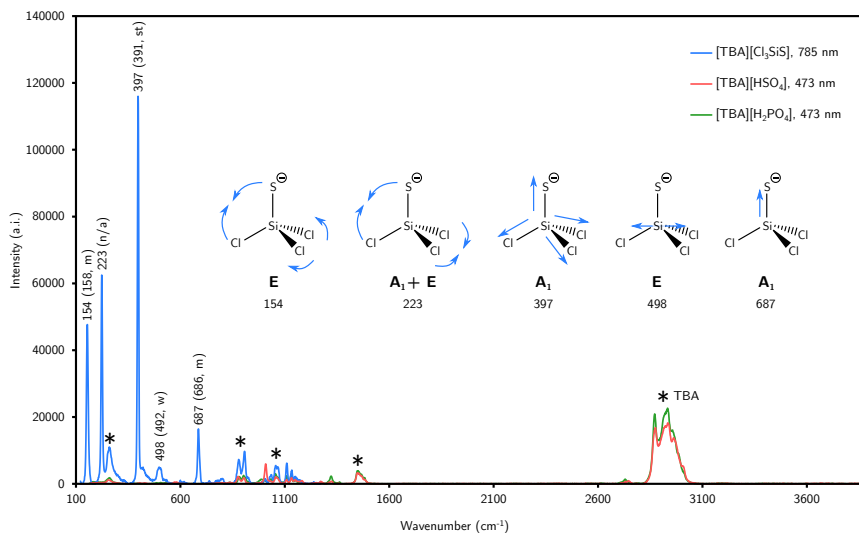


Figure 3.27 Overlay of the Raman spectra of [TBA]2, [TBA][HSO₄], and [TBA][H₂PO₄]. The spectra of [TBA][HSO₄] and [TBA][H₂PO₄] were collected in order to assign the peaks arising from the tetrabutylammonium cation. The numbers provided in nanometers (top right) correspond to the excitation wavelength used to record the spectrum. The numbers in parentheses are of the previously reported values.⁶³ w=weak, m=medium, st=strong, vst = very strong.

3.4.9 Preparation of benzyl mercaptan

In the glovebox, [TBA]**2** (658 mg, 1.61 mmol) was weighed into a 25 mL Schlenk flask. Benzyl bromide (180 mg, 1.05 mmol) was weighed into a vial (20 mL) and transferred to the Schlenk flask using DCM (3 mL, then 2 × 1 mL). The flask was sealed and heated to 40 °C for 18 h. After this time, deionized water (150 μL, deoxygenated by sparging with N₂ for 20 minutes) was added to the reaction mixture which was then stirred for 20 minutes. The resulting mixture was passed through a silica plug in a frit (fine porosity, 15 mL, 2/3 full of silica) in the fume hood. DCM (100 mL) was used to wash the plug into an Erlenmeyer flask. The filtrate was concentrated to ca. 5 mL and transferred to an H-cell. The Erlenmeyer flask was rinsed with additional DCM (2 × 3 mL), which was transferred to the H-cell. DCM was removed from the solution and the resulting oil was purified by trap-to-trap distillation. The side of the cell containing the crude oil was heated to 70 °C in an oil bath while the collection side was cooled with a liquid N₂ bath. The cell walls were heated with a heat gun for approximately 20 minutes once transfer was observed to be complete. The cell was allowed to come to ambient temperature, then the distillate was washed out into a pre-weighed vial using DCM (5 × 3 mL). The material was brought to constant mass under vacuum, giving benzyl mercaptan as a yellow oil (72 mg, 0.58 mmol, 55% yield). ¹H NMR (500 MHz, CDCl₃, δ) 7.37-7.28 (m, 5H), 3.75 (d, *J* = 7.6 Hz, 2H), 1.76 (t, *J* = 7.5 Hz, 1H). ¹³C NMR (126 MHz, CDCl₃, δ) 141.28, 128.82, 128.15, 127.18, 29.13. These NMR data are consistent with those in the literature.⁹⁹ HRMS: [M-H]⁺; observed(calc.) *m/z*: 123.02246 (123.026847).

3.4.9.1 In situ characterization of benzyl trichlorosilylsulfide

In the glovebox, [TBA][**2**] (40 mg, 0.097 mmol, 1.1 equiv) was weighed directly into an NMR tube equipped with a J. Young valve. CD₂Cl₂ (0.5 mL) was added to produce a clear colorless homogeneous solution. Benzyl bromide (10.6 μL, 0.089 mmol, 1 equiv) was added using a micro syringe (50 μL). The NMR tube was sealed and monitored by ¹H NMR spectroscopy at three time points; 20 minutes, 1 hour, and two hours (Fig. 3.28). After 18 hours, ¹H-¹³C HSQC (Fig. 3.29) and ¹H-²⁹Si HMBC (Fig. 3.30) spectra were collected to aid characterization of the observed intermediates. One major new signal was assigned as benzyl trichlorosilylsulfide based on its NMR data. An additional minor species that also displayed a cross-peak in the ¹H-²⁹Si HMBC was assigned as an unknown intermediate or side-product. Benzyl trichlorosilylsulfide (PhCH₂SSiCl₃): ¹H NMR (500 MHz, CD₂Cl₂, δ) 4.10 (PhCH₂SSiCl₃). ¹³C NMR (126 MHz, CD₂Cl₂, δ) 33.52 (PhCH₂SSiCl₃). ²⁹Si{¹H} NMR (99 MHz, CD₂Cl₂, δ) -1.67.

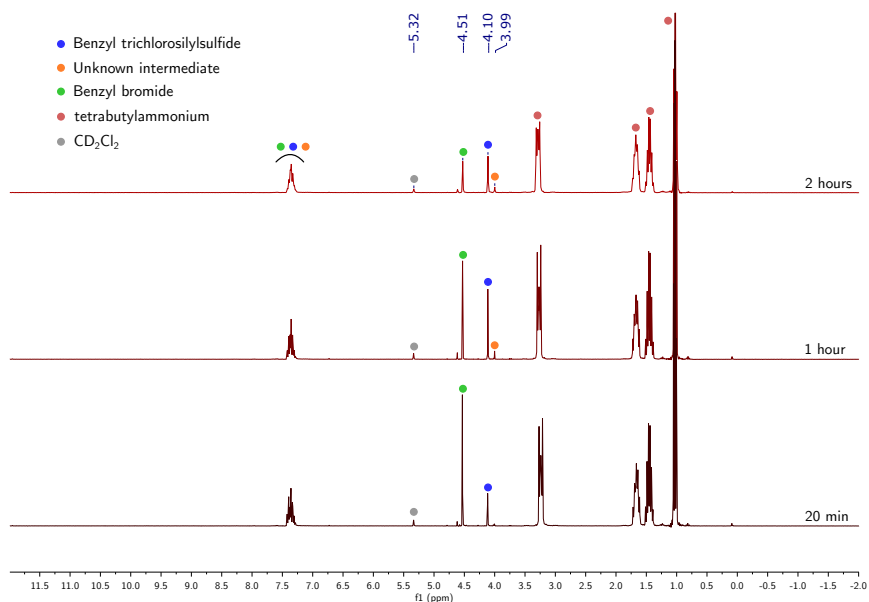


Figure 3.28 ^1H NMR spectra of the reaction of benzyl bromide with [TBA][2] at three time points in CD_2Cl_2 at 25 °C, recorded at 300 MHz.

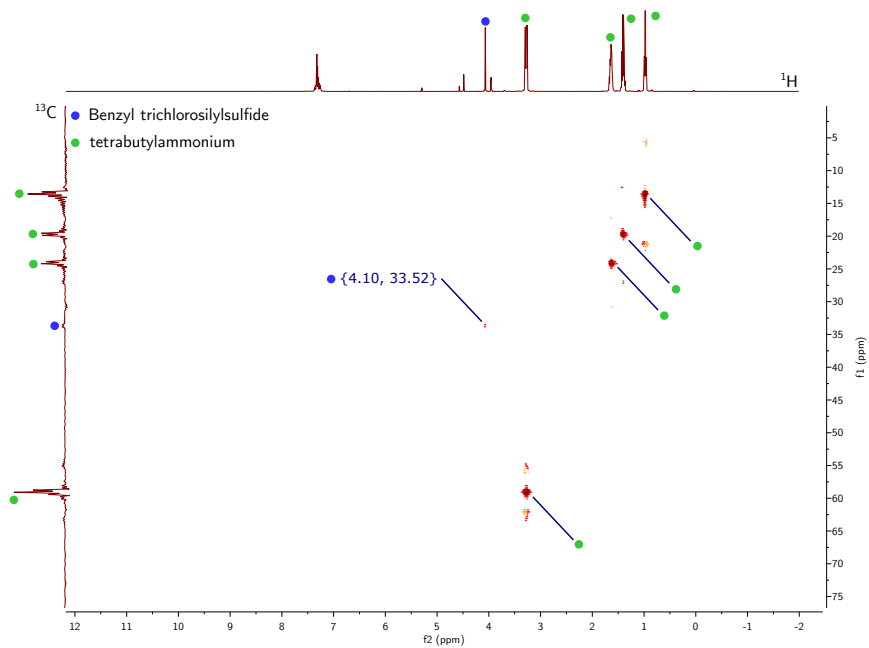


Figure 3.29 ^1H - ^{13}C HSQC spectrum of the reaction of benzyl bromide with [TBA][2] after 18 h in CD_2Cl_2 at 25 °C, recorded on a 500 MHz instrument.

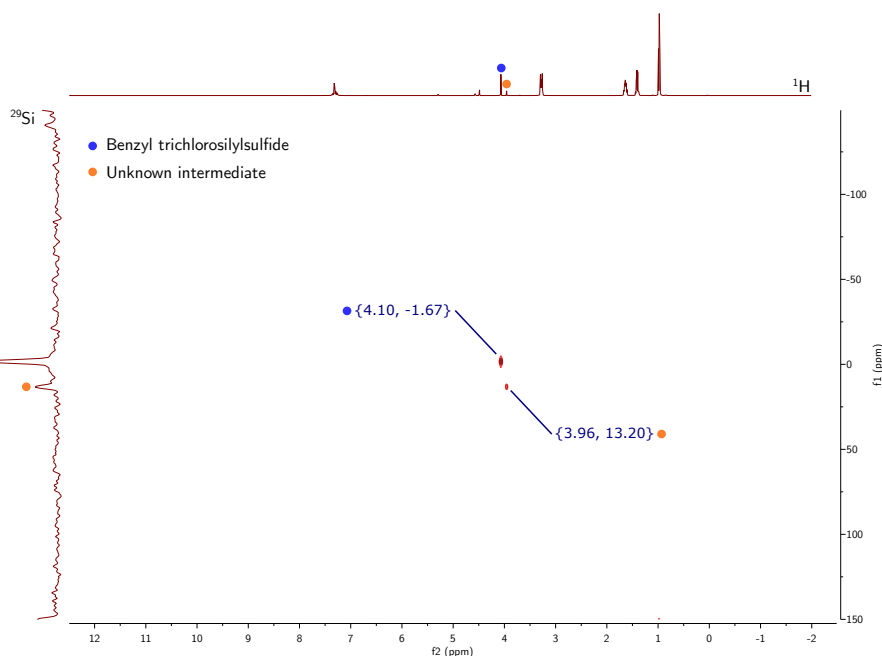


Figure 3.30 ^1H - ^{29}Si HMBC spectrum of the reaction of benzyl bromide with [TBA][2] after 18 h in CD_2Cl_2 at 25 °C, recorded on a 500 MHz instrument.

3.4.10 Preparation of thiobenzophenone

In a glovebox, benzophenone (61 mg, 0.335 mmol, 1 equiv) was weighed directly into a Schlenk flask (20 mL) equipped with a J. Young valve. [TBA]2 (700 mg, 1.711 mmol, 5.1 equiv) was weighed directly into the Schlenk flask. Chloroform (5 mL) was added to the flask, giving a clear colorless solution. The flask was sealed and removed from the glovebox, then heated to 80 °C for 96 h, to give a deep blue solution. The flask was brought into the glovebox and the solution was transferred to a vial (20 mL); DCM (2 × 2 mL) was used to rinse the flask and the resulting washings were transferred to the vial. Volatile material was removed in vacuo to give a sticky blue oil. The oil was triturated with pentane (3 × 6 mL). The resulting oil was extracted with pentane and broken up using a spatula until the blue color did not persist, and the solids in the vial became a fine white powder (4 × 8 mL). The resulting blue solution was filtered through a piece of filter paper in a Pasteur pipette into a fresh vial and the solution evaporated to constant mass to give thiobenzophenone as a crystalline blue solid (41 mg, 0.207 mmol, 62% yield). ^1H NMR (500 MHz, CDCl_3 , δ) 7.72 (d, $J=7.5$ Hz, 2H), 7.57 (d, $J = 7.5$ Hz, 1H), 7.39 (t, $J = 7.7$ Hz, 2H). ^{13}C NMR (126 MHz, CDCl_3 , δ) 238.69, 147.47, 132.17, 129.79, 128.13. These NMR data are consistent with those in the literature.¹⁰⁰ HRMS: $[\text{M}+\text{H}]^+$; observed(calc.) m/z : 199.057857/(199.058147).

3.4.11 Identification of hydrogen gas formed in the synthesis of [TBA]2

3.4.11.1 Hydrogenation of (–)-terpinen-4-ol

Note: The hydrogenation of (–)terpinen-4-ol was carried out using a tank of commercial hydrogen gas and Crabtree’s catalyst in order to obtain full ^1H NMR characterization of the hydrogenated cyclohexane product. A modified literature procedure was followed.⁸⁹ In the glovebox, (–)-terpinen-4-ol and $[\text{Ir}(\text{PCy}_3)_3(\text{py})(\text{COD})][\text{PF}_6]$ were weighed into separate vials. DCM (2.0 g) was weighed into a third vial. Approximately 75% of the DCM was used to transfer the catalyst to a Schlenk flask (50 mL) equipped with a 14/20 ground glass joint. The cyclohexene substrate was added to the same Schlenk flask, then the remaining 25% of the DCM was used to rinse the two vials and the washings transferred to the Schlenk flask. The flask was sealed with a glass stopper, removed from the glovebox, and connected to the Schlenk line. The flask was chilled to 0 °C using an ice bath, and allowed to equilibrate temperature for 5 minutes. Against a positive flow of nitrogen, the glass stopper was switched for a rubber septum, which was secured using copper wire. The flask was purged with dihydrogen, using a balloon of volume ca. 500 mL. The balloon was then refilled with dihydrogen and left open to the Schlenk flask. The solution was stirred for 90 minutes at 0 °C, then passed through a silica plug (2 cm) in a glass pipette. The plug was washed with additional DCM (6 mL), and volatile material was removed in vacuo to give a white powder. ^1H NMR (500 MHz, CDCl_3 , δ) 1.88 (sept., $J=6.9$ Hz, 1H), 1.83 (m, 2H), 1.66 (m, 2H), 1.55 (m, 1H), 1.30 (m, 2H), 1.16 (s, 1H), 1.13–1.04 (m, 2H), 0.90 (d, $J = 6.7$ Hz, 3H), 0.89 (d, $J = 6.9$ Hz, 6H).

3.4.11.2 Hydrogenation of (–)-terpinen-4-ol with hydrogen produced from the preparation of [TBA]2

In the glovebox, [TBA][HSO_4] (200 mg, 0.589 mmol, 1 equiv) was weighed into a vial. Acetonitrile (1.0 g) was weighed into a separate vial and used to transfer the [TBA][HSO_4] to a Schlenk flask (20 mL) in three washes. The flask was sealed, removed from the glovebox, and connected to a Schlenk line in the fume hood. The solution was frozen in a dry ice/acetone bath at –78 °C, and trichlorosilane (1.8 mL, 17.8 mmol, 30 equiv) was added to the flask against a positive flow of nitrogen. The flask was quickly sealed, and allowed to stir at 23 °C for 24 h.

In the glovebox, Crabtree’s catalyst (82 mg, 0.101 mmol, 0.171 equiv) and (–)-terpinen-4-ol (681 mg, 4.41 mmol, 7.58 equiv) were weighed into separate vials. Crabtree’s catalyst was dissolved in DCM (2 mL) and transferred to a Schlenk flask (100 mL). The vial was washed with additional DCM (2×2 mL) which was transferred to the Schlenk flask. (–)-Terpinen-4-ol was transferred to the Schlenk flask, and the vial that had contained it was washed with DCM (2×2 mL) which was transferred to the Schlenk flasks. The total volume of DCM was 10 mL. The flask was removed from the glovebox and connected to the Schlenk line (Fig. 3.31). Both the flask containing the hydrogenation reaction mixture

and flask used to prepare [TBA]2 were frozen in liquid nitrogen for ten minutes. The two flasks were connected using rubber hosing via a two-way glass valve. One of the two-way outlets was connected directly to the vacuum manifold of the Schlenk line. The other was connected to the gas manifold of the Schlenk line via an oil bubbler. The tap to the hydrogenation flask was opened, and the system evacuated for five minutes. The two way glass valve was closed, and the tap to the Schlenk containing [TBA]2 was opened, connecting the head space between the two Schlenk flasks. The tap to the flask containing [TBA]2 reaction was closed, and the system equilibrated with nitrogen delivered via the oil bubbler. The hydrogenation flask was placed in an ice bath. The flask containing the [TBA]2 was removed from the liquid nitrogen and allowed to thaw, releasing dissolved gases into the partial vacuum above. The solution was refrozen in liquid nitrogen and the tap opened to connect the head space of the two Schlenk flasks. This procedure was repeated twice more. The hydrogenation reaction mixture was then allowed to stir for 90 minutes. Volatile material was removed in vacuo, and a small portion of the residue analyzed in chloroform-*d*. The ¹H NMR spectrum was collected using a d1 of 90 s to ensure accurate integrations. Integration of the starting material relative to product gave an NMR yield of 0.735 mmol of hydrogenated product. This corresponds to 0.735 mmol of H₂ being consumed. The theoretical maximum of H₂ evolved by the preparation of [TBA]2 is 2.95 mmol, based on 5 equivalents per added [TBA][HSO₄]. This gives a yield of H₂ based on the following idealized balanced equation of 25%.

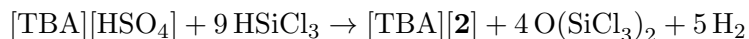


Figure 3.31 Photo of the experimental setup used to hydrogenate (–)-terpinen-4-ol with the hydrogen generated from the preparation of [TBA]2.

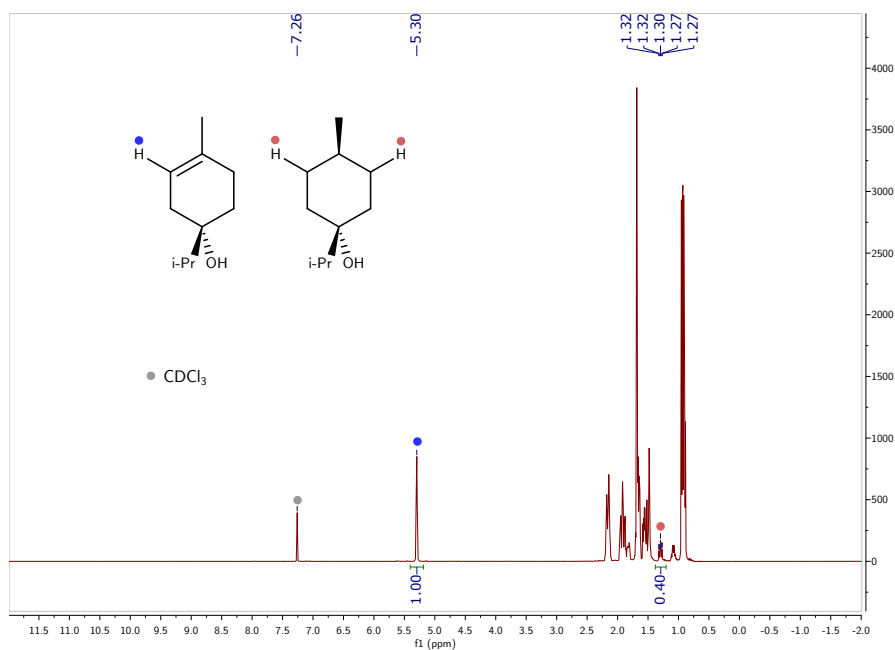


Figure 3.32 Quantitative ^1H NMR spectrum of the crude material obtained after hydrogenation in CDCl_3 at $25\text{ }^\circ\text{C}$, recorded at 500 MHz.

3.4.11.3 Hydrogenation of (–)-terpinen-4-ol with substoichiometric hydrogen to determine the efficiency of the reaction

Note: This experiment was carried out to determine whether this method was suitable to quantify the amount of H_2 from the reduction of phosphate or sulfate by trichlorosilane. In the glovebox, DCM (4.46 g), (–)-terpinen-4-ol (223 mg, 1.44 mmol, 1 equiv) and Crabtree's catalyst (26 mg, 0.032 mmol, 0.022 equiv) were weighed into three separate vials. The DCM was used to transfer the two reagents to a 50 mL Schlenk flask equipped with a stir bar, using multiple washes. The flask was sealed, removed from the glovebox and placed in an ice bath at $0\text{ }^\circ\text{C}$. The flask was attached to the setup described in section 3.4.11.2 (Fig. 3.31). A Schlenk flask with a total volume of 16.6 mL (measured by filling the flask with water and pouring the contents into a measuring cylinder) was filled with hydrogen. The pressure of the flask was measured to be 118 kPa using a pressure transducer. The hydrogen was allowed to mix with the reaction vessel by opening the two taps, and a backing pressure of N_2 was provided through the oil bubbler. The reaction mixture was stirred at $0\text{ }^\circ\text{C}$ for 10 hours (the ice bath was periodically replenished with ice) and then for 18 h at $23\text{ }^\circ\text{C}$ as the ice bath warmed overnight. An aliquot of the resulting solution (0.3 mL) was transferred to a vial and volatile material was removed in vacuo. The resulting oil was dissolved in chloroform-*d* and the sample analyzed by ^1H NMR spectroscopy (400 MHz, 8 scans, $d_1 = 90\text{ s}$). The molar ratio of hydrogenated product to starting material

was 30%. The theoretical maximum would have been 55%, based on the amount of H₂ introduced to the system (0.790 mmol). The yield of H₂ incorporated into the product based on the added volume was calculated to be 54%. In view of this result, this method was not deemed suitable for quantifying the H₂ that had formed in the experiments where sulfate or phosphate were reduced by trichlorosilane.

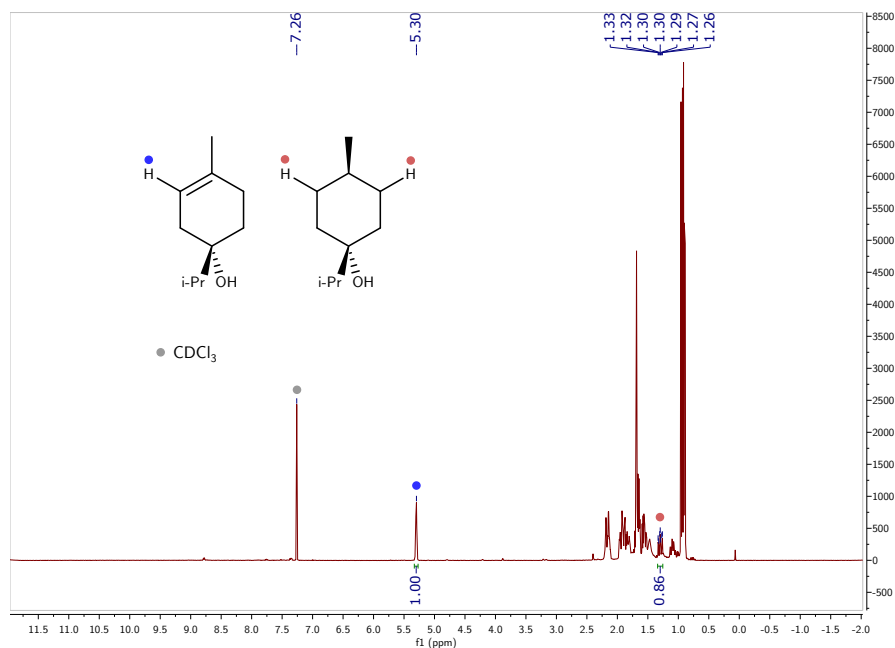


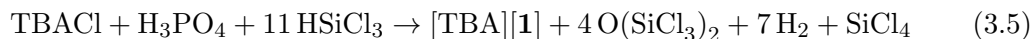
Figure 3.33 Quantitative ¹H NMR spectrum of the crude material obtained after hydrogenation in CDCl₃ at 25 °C, recorded at 400 MHz.

3.4.12 Volumetric quantification of H₂ formed in the synthesis of [TBA]1

3.4.12.1 From H₃PO₄

Salt [TBA]1 was prepared in situ as according to Section 3.4.3.2. At the end of the reaction time of 72 h, the Parr reactor was allowed to cool to 23 °C over the course of 2 h. The reactor was placed in a dry ice/acetone slush bath (−78 °C) for 1.5 h to condense volatile silicon-containing species. Separately, a 4 L plastic solvent bottle was filled with water, and sealed with a rubber septum. The actual volume of the 4 L solvent flask was measured by filling it with water, then pouring the water into a measuring cylinder. The rubber septum was pierced with two holes, through which 10 mm tubing was threaded. One of these tubes was connected to the Parr reactor. The solvent bottle was inverted and placed in a trough of water. The valve to the Parr reactor was slowly opened, and the gas allowed to collect in the inverted solvent bottle. Once the gas had finished collecting in the solvent

bottle, it was sealed while still under water. The water remaining in the solvent bottle was measured using a measuring cylinder (1000 mL) to determine the amount of gas that had been collected (3.70 L, 0.165 mol, 71%). The idealized balanced equation used to calculate the theoretical maximum yield of H₂ is given in Eqn. 3.5.



3.4.12.2 From [TBA]₃[P₃O₉].2H₂O

[TBA][**1**] was prepared as described in section 3.4.3.4. At the end of the reaction time of 72 h, the volume of gas that had been produced was determined as according to the experimental procedure described above in section 3.4.12.1 (2.83 L, 0.126 mol, 74%). The balanced equation used to calculate the theoretical maximum yield of H₂ is given in Eqn. 3.6.



3.4.13 Volumetric quantification of H₂ formed in the synthesis of [TBA]**2**

The volume of a Schlenk flask was measured by filling it with water, then decanting the water into a measuring cylinder. The volume of the Schlenk flask used for these experiments was found to be 16.6 mL. In the glovebox, [TBA][HSO₄] (200 mg, 0.589 mmol) was weighed into a scintillation vial (20 mL). Acetonitrile (1.00 g) was weighed into a separate vial. Approximately half of the acetonitrile was used to dissolve the [TBA][HSO₄], and the resulting solution was transferred to the Schlenk flask. The remainder of the acetonitrile was used to rinse the vial that had contained the solution of [TBA][HSO₄], and the washings added to the Schlenk flask. The Schlenk flask was removed from the glovebox and connected to the Schlenk line. The solution was frozen in a dry ice/acetone cold bath at −78 °C. This was done to prevent any reaction with trichlorosilane before the flask could be sealed. Against a positive flow of nitrogen, trichlorosilane (1.2 mL, 11.87 mmol) was added to the flask. The cap was replaced, but the flask not fully sealed. The nitrogen manifold was allowed to equilibrate with the flask for a minute, then the pressure of the manifold measured with a pressure transducer (*p*_{N₂}, Table 3.2). The flask was then sealed and allowed to warm to 23 °C. Stirring was maintained for 18 hours behind a blast shield.

The side-arm of the flask was connected to 3 mm Teflon tubing, that led to an inverted measuring cylinder (100 mL) that had been filled with water and had been placed in a water bath (Fig. 3.34A). The Teflon tube had been secured to the inverted measuring cylinder using a pierced 24/40 septum, which had been perforated in two additional locations to allow the passage of water between the inverted cylinder and water bath (Fig. 3.34C). These perforations were kept open by using 4 mm diameter pieces of plastic tubing.

The reaction mixture was cooled to −45 °C to condense non-hydrogen and non-nitrogen gases. The cap was slowly opened, and the gases displaced the water from the inverted

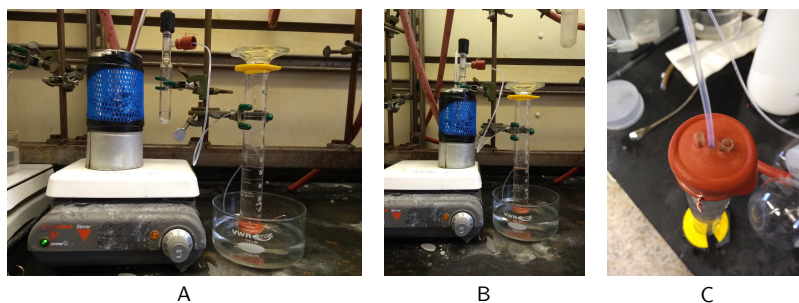


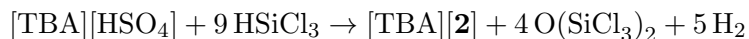
Figure 3.34 **A:** Photo of the experimental setup before venting the gases. **B:** Photo of the experimental setup after cooling the solution and venting the gases. **C:** Photo of the perforated septum used to cap the measuring cylinder.

Run	$V_{\text{N}_2 + \text{H}_2}$	$p_{\text{N}_2}/\text{kPa}$	$V_{\text{N}_2(\text{calc})}/\text{mL}$	$V_{\text{H}_2(\text{calc})}/\text{mL}$	Yield of $\text{H}_2/\%$
1	83	123	19	64	89
2	81	138	21	60	83
3	88	136	21	67	93
Av.				64(4)	88(5)

Table 3.2 Volume of gases collected

measuring cylinder (Fig. 3.34B). The volume of gas was recorded ($V_{\text{N}_2 + \text{H}_2}$), and the results tabulated in Table 3.2.

The volume of nitrogen gas at atmospheric pressure was calculated using the ideal gas law, $pV = nRT$. In the equation, pressure was recorded as the pressure of the nitrogen manifold of the Schlenk line (p_{N_2}). The volume of nitrogen ($V_{\text{N}_2(\text{calc})}$) was calculated by subtracting the volume of trichlorosilane and acetonitrile from the volume of the Schlenk flask. $V_{\text{N}_2(\text{calc})}$ was subtracted from $V_{\text{N}_2 + \text{H}_2}$ to give the volume of hydrogen gas collected ($V_{\text{H}_2(\text{calc})}$). The average yield of H_2 over three runs was calculated to be 64(4) mL, 2.6 mmol, 88%. The idealized balanced equation used to calculate the theoretical yield of H_2 is given below:



3.4.14 X-ray crystallographic studies

3.4.14.1 General methods

Single crystals were selected under a microscope and mounted in hydrocarbon oil on a nylon loop. Low-temperature (100 K) data were collected on a Bruker-AXS X8 Kappa Duo diffractometer coupled to a Smart Apex2 CCD detector with Mo K α radiation ($\lambda = 0.71073$ Å) with ϕ - and ω -scans. A semi-empirical absorption correction was applied to the diffraction data using SADABS.^{101,102} The structure was solved by direct methods using SHELXT^{103,104} and refined against F^2 on all data by full-matrix least squares with ShelXle.¹⁰⁵ All non-hydrogen atoms were refined anisotropically. All hydrogen atoms were included in the model at geometrically calculated positions and refined using a riding model. The isotropic displacement parameters of all hydrogen atoms were fixed to 1.2 times the U_{eq} value of the atoms they are linked to (1.5 times for methyl groups).

3.4.14.2 [TBA]2

Diffraction-quality, colorless crystals were grown by dissolving [TBA]2 (100 mg, 0.24 mmol) in DCM (7 mL), followed by careful layering of diethyl ether (7 mL) to produce a clear solution. The mixture was stored in the freezer at -35 °C for 168 h, producing no crystals. Pentane (3 mL) was layered carefully on top of the solution while it was still cold to produce a white precipitate. The vial was taped with electrical tape and placed back in the freezer. Overnight, large colorless blocks grew on the bottom of the vial. These blocks were transferred to hydrocarbon oil on a microscope slide inside the glovebox.

[TBA]2 crystallizes with two anions and two cations in the asymmetric unit. One of the tetrabutylammonium cations was entirely disordered; the disorder was treated with a simple model to restrain chemically equivalent methylene and methyl groups to be the same (SAME command). The other tetrabutylammonium cation showed some disorder in the penultimate methylene and methyl group of two of the *n*-butyl groups; these were modeled as minor components and restrained to be the same as other *n*-butyl chains in the other TBA cations (SAME command). One of the trichlorosilylsulfide anions was disordered by a simple rotation along the Si–S axis; this disorder was modeled as a major and minor component. The other trichlorosilylsulfide anion showed some spurious electron density around the sulfur and chlorine atoms, but a suitable model to describe the presumed disorder could not be found. It was left as a single anion because the nearby electron density was still low ($\leq 1.03 e\cdot\text{Å}^{-3}$). Similar-ADP and rigid bond restraints (SIMU and RIGU commands, respectively) were applied to the entire structure.

CSD identification code	1841573
Reciprocal net code	X8_18045
Empirical formula	C ₁₆ H ₃₆ Cl ₃ NSiS
Formula weight	408.96 g/mol
Color / morphology	colorless / plate
Temperature	100(2) K
Wavelength	0.71073 Å
Crystal system	Monoclinic
Space group	<i>P</i> 2 ₁ / <i>c</i>
Unit cell dimensions	<i>a</i> = 17.253(12) Å α = 90° <i>b</i> = 15.242(11) Å β = 103.363(12)° <i>c</i> = 18.394(13) Å γ = 90°
Volume	4706(6) Å ³
<i>Z</i>	8
Density (calculated)	1.154 g/cm ³
Absorption coefficient	0.527 mm ⁻¹
<i>F</i> (000)	1760
Crystal size	0.428 × 0.344 × 0.156 mm ³
Theta ranges for data collection	1.755 to 27.877°
Index ranges	-22 ≤ <i>h</i> ≤ 22, -20 ≤ <i>k</i> ≤ 20, -24 ≤ <i>l</i> ≤ 24
Reflections collected	134795
Independent reflections	11224 [<i>R</i> _{int} = 0.0705]
Completeness to $\theta = 25.242^\circ$	100.0%
Absorption correction	Semi-empirical from equivalents
Refinement method	Full-matrix least-squares on <i>F</i> ²
Data \restraints \parameters	11224 \1420 \622
Goodness-of-fit on <i>F</i> ²	1.032
Final <i>R</i> indices [<i>I</i> > 2σ(<i>I</i>)]	<i>R</i> ₁ = 0.0582, <i>wR</i> ₂ = 0.1436
<i>R</i> indices (all data)	<i>R</i> ₁ = 0.0778, <i>wR</i> ₂ = 0.1580
Extinction coefficient	n/a
Largest diff. peak and hole	1.025 and -0.754 e·Å ⁻³

Table 3.3 X-ray crystallographic information for [TBA]2

During the initial phase of the refinement, all of the atoms bonded to silicon were refined as chlorine atoms. Once the tetrabutylammonium cation disorder and rotation disorder in one of the anions was suitably modeled, the atom with the closest contact to silicon and the least electron density was refined to be the sulfur atom. To further support the assignment of the chlorine and sulfur atoms in the two anions, the model was sequentially modified to switch a sulfur and chlorine atom in the same anion. The weighting scheme

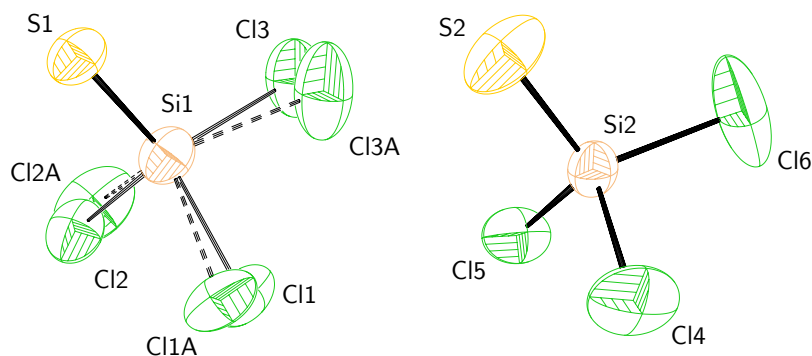


Figure 3.35 Molecular structure of the two anions in the asymmetric unit of [TBA]**2**. The thermal ellipsoids are shown at the 50% probability level.

Atoms interchanged	R_1	wR_2
None	0.0582	0.1580
S1↔C11	0.0605	0.1720
S1↔C12	0.0606	0.1700
S1↔C13	0.0603	0.1683
S2↔C14	0.0597	0.1670
S2↔C15	0.0593	0.1655
S2↔C16	0.0595	0.1643

Table 3.4 Values of R_1 and wR_2 for various refinement models of [TBA]**2**.

was adjusted to convergence, and the R_1 and wR_2 values were tabulated (Table 3.4). The original refinement gave the best fit with experiment.

The thermal ellipsoid plot shown in Fig. 3.35 was generated from the molecule that showed the smallest amounts of disorder. This comprised Si1, S1, C11, C12 and C13. The error for the average of the bond metrics was calculated by taking the square root of the sum of the squares of the individual errors.¹⁰⁶

3.4.14.3 [TBA]₂[Si(P₃O₉)₂]

Diffraction quality crystals were grown from a DCM/diethylether solution at -35 °C inside the glovebox freezer. The model was refined isotropically, then anisotropically. The positions of the hydrogen atoms were calculated using HFIX commands. The weighting scheme was adjusted and the model considered complete.

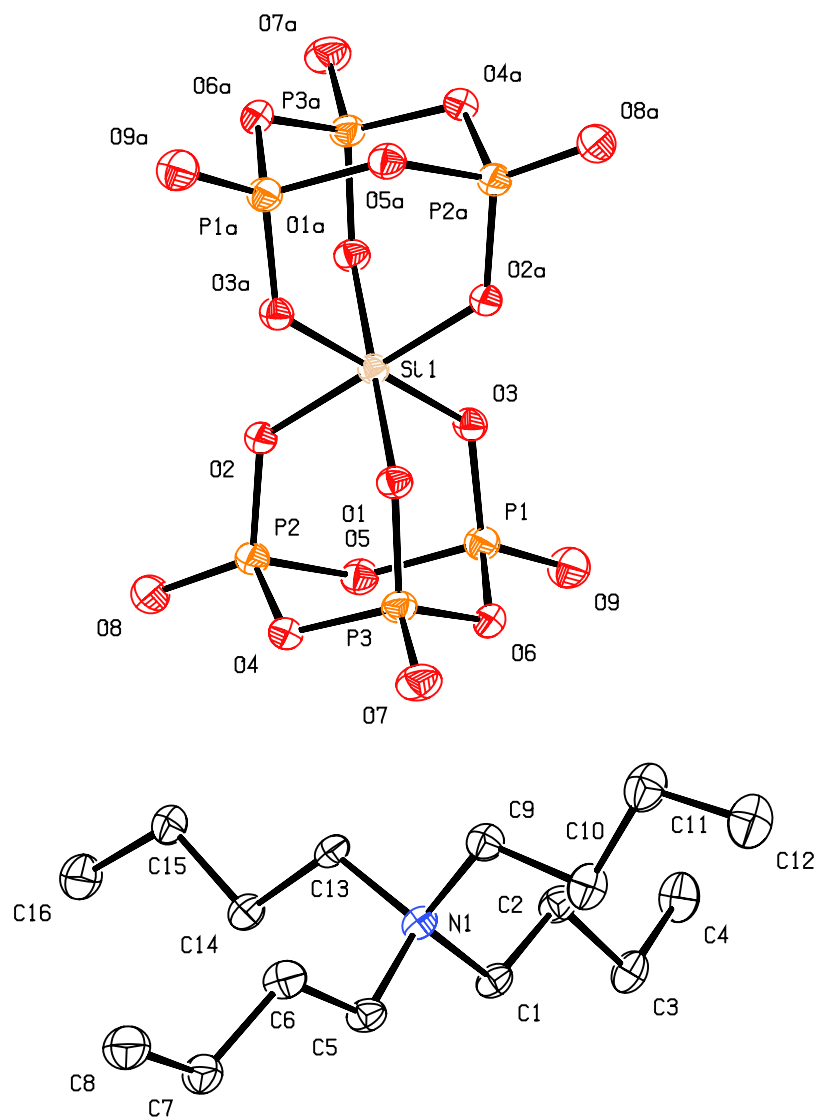


Figure 3.36 Molecular structure of $[TBA]_2[Si(P_3O_9)_2]$ with the thermal ellipsoids are shown at the 50% probability level and hydrogen atoms omitted for clarity.

CSD identification code	1888218
Reciprocal net code	X8_17115
Empirical formula	C ₁₆ H ₃₆ NO ₉ P ₃ Si _{0.5}
Formula weight	493.41 g/mol
Color / morphology	colorless / block
Temperature	100(2) K
Wavelength	0.71073 Å
Crystal system	Orthorhombic
Space group	<i>Pccn</i>
Unit cell dimensions	$a = 13.1805(17) \text{ \AA}$ $\alpha = 90^\circ$ $b = 18.929(2) \text{ \AA}$ $\beta = 90^\circ$ $c = 19.042(2) \text{ \AA}$ $\gamma = 90^\circ$
Volume	4751.1(10) Å ³
<i>Z</i>	8
Density (calculated)	1.380 g/cm ³
Absorption coefficient	0.321 mm ⁻¹
<i>F</i> (000)	2104
Crystal size	0.152 × 0.081 × 0.059 mm ³
Theta ranges for data collection	1.883 to 30.018°
Index ranges	-18 ≤ <i>h</i> ≤ 18, -25 ≤ <i>k</i> ≤ 25, -26 ≤ <i>l</i> ≤ 26
Reflections collected	69898
Independent reflections	6953 [<i>R</i> _{int} = 0.0853]
Completeness to $\theta = 25.242^\circ$	100.0%
Absorption correction	Semi-empirical from equivalents
Refinement method	Full-matrix least-squares on <i>F</i> ²
Data \restraints \parameters	6953 \0 \272
Goodness-of-fit on <i>F</i> ²	1.021
Final <i>R</i> indices [<i>I</i> > 2σ(<i>I</i>)]	<i>R</i> ₁ = 0.0430, <i>wR</i> ₂ = 0.0890
<i>R</i> indices (all data)	<i>R</i> ₁ = 0.0801, <i>wR</i> ₂ = 0.1027
Extinction coefficient	n/a
Largest diff. peak and hole	0.380 and -0.395 e·Å ⁻³

Table 3.5 X-ray crystallographic information for [TBA]₂[Si(P₃O₉)₂]

3.5 Computational methods

3.5.1 Geometry optimization of anion 2

The geometry of **2** was optimized using ORCA 4.0.1¹⁰⁷ at the ω B97X-D3/ma-Def2-QZVPP level of theory using the following input file. The coordinates obtained from this calculation are shown in Table 3.6.

```
! PAL8 RIJCOSX wB97X-D3 ma-Def2-QZVPP Def2/J TightSCF
! Grid6 NoFinalGrid GridX6 NoFinalGridX
! Opt TightOpt NumFreq
* xyzfile -1 1 geom.xyz
```

Atom	x	y	z
Si	-0.00552263	-0.00189007	0.18115999
S	0.00634629	-0.00153759	2.16621009
Cl	1.88125725	0.03441738	-0.76028989
Cl	-0.91919139	-1.65379669	-0.76523322
Cl	-0.96288952	1.62280698	-0.76915698

Table 3.6 Optimized coordinates of $[\text{Cl}_3\text{SiS}]^-$.

3.5.2 GVB calculations on anion 2

Generalized Valance Bond (GVB) calculations were performed using VB2000 integrated with GAMESS.⁷⁴ The Si-S bond was treated at the CASVB(6,6)/6-31++G** level of theory.

3.5.3 Natural Bond Order (NBO) calculations on anion 2

Natural bond order calculations (NBO and NRT) were performed using NBO6,⁷⁷ implemented within GAMESS.^{73,74} The wavefunction was calculated at the MP2/aug-cc-pVTZ level of theory. The results of NRT analysis are shown in Fig. 3.37.

3.5.4 Electron Localization Function (ELF) analysis of anion 2

A .wfn file was generated using ORCA 4.0.1. The .wfn file was used to perform the ELF analysis using Multiwfn.¹⁰⁸ The images were created using Chimera.¹⁰⁹

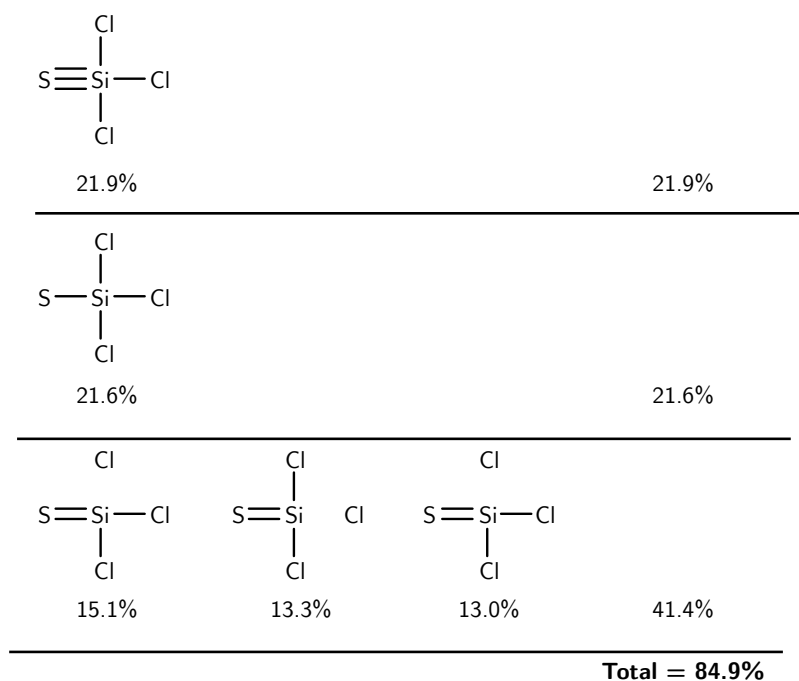


Figure 3.37 Primary resonance structures of anion **2** obtained from the NRT analysis.

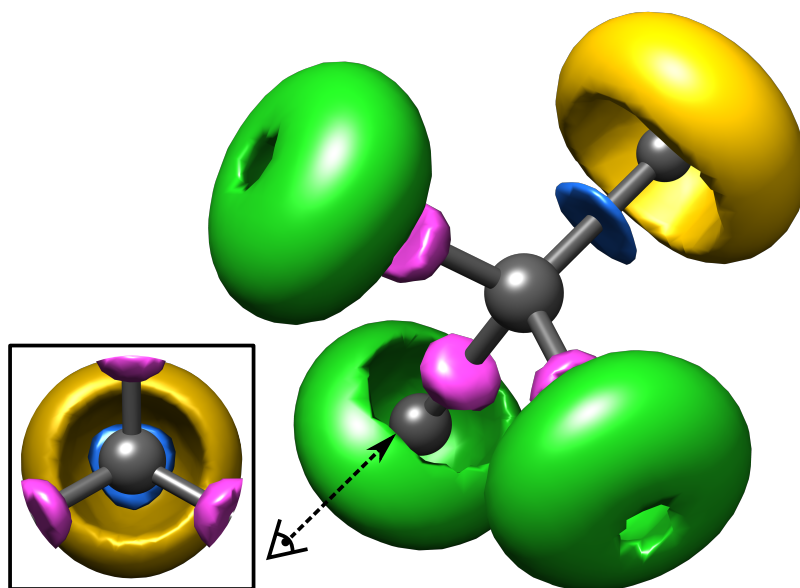


Figure 3.38 Plot of the 0.83 ELF isosurface of **2**. Yellow: sulfur lone pair basins; green: chlorine lone pair basins; blue: silicon-sulfur bonding basin; magenta: silicon-chlorine bonding basins. **B** (inset): view of the ELF isosurface down the C_3 axis of **2**, showing the shape of the Si-S bonding basin (blue).

3.5.5 Wavefunction analysis using GAMESS

Electronic structure calculations were carried out using GAMESS^{73,74} (VERSION = 14 FEB 2018) at the MP2/aug-cc-pVTZ level of theory. Coordinates of the optimized structures are given in Section 3.5.8. The Mayer bond order provided in the manuscript was obtained directly from the output file.

3.5.6 Calculation of $^1J_{\text{P-Si}}$ coupling constants

Coupling constants were calculated using Gaussian09. Models were built using Avogadro, then the geometries were optimized at the B3LYP/6-31G(d,p) level of theory. All species were subjected to a frequencies calculation, with the result that none possessed imaginary frequencies. Coupling constants were calculated using the PBE functional and the NMR=(spinspin) keyword. The aug-cc-pVQZ basis set was used on phosphorus and silicon, and the 6-311G(2df,p) basis set was used for all other atoms. An example input file is shown below. The total nuclear spin-spin coupling J (Hz) was plotted against the experimental $^1J_{\text{P-Si}}$ values and a linear regression analysis performed.

```
$RunGauss
# NMR=(spinspin) PBEPBE Gen

Comment

O 1
P      0.0248350000      1.0315500000      0.0000000000
Si     0.0248350000     -0.4368200000      1.7374590000
H     -1.3823860000      1.2529750000      0.0000000000
Si     0.0248350000     -0.4368200000     -1.7374590000
H      1.3846360000     -1.0280740000     -1.8289970000
H     -0.2598980000      0.3180230000     -2.9847700000
H     -0.9674870000     -1.5375850000     -1.6054380000
H     -0.2598980000      0.3180230000      2.9847700000
H      1.3846360000     -1.0280740000      1.8289970000
H     -0.9674870000     -1.5375850000      1.6054380000

H 0
6-311G(2df,p)
****
P Si 0
aug-cc-pVQZ
****
```

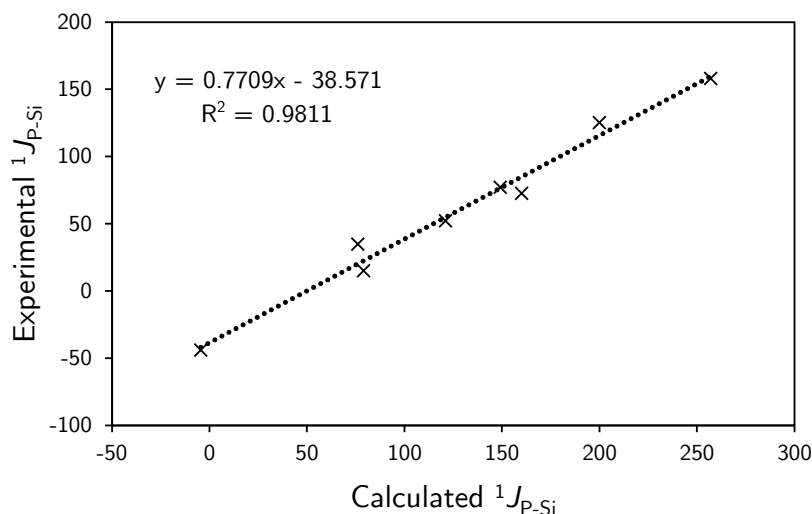


Figure 3.39 Plot of the calculated vs. experimental $^1J_{\text{P-Si}}$ values.

3.5.7 Determination of the s character in P–Si bond containing species using NBO analysis.

NBO analysis was carried out using ORCA 4.0.1.¹⁰⁷ The geometries used for each of the species were taken from section 3.5.6. The optimized geometries can be found in a multiple .xyz file (all.xyz). The aug-cc-pVQZ basis sets were used on phosphorus and silicon, and the 6-311G(2df,2pd) basis set was used for all other atoms. The s character in the phosphorus-silicon bonds was determined from the natural bond orbital output. The outputs are summarized in Table 3.7.

Species	Coefficient/%		%s hybrid		%s character		
	P	Si	P	Si	P	Si	$\sigma(\text{P-Si})$
$\text{Me}_3\text{SiPPH}_2 \cdot \text{BH}_3$	63	37	20	21	13	8	20
F_3SiPH_2	60	40	10	38	6	15	21
$\text{HP}(\text{SiH}_3)_2$	59	41	14	23	8	9	17
Cl_3SiPH_2	54	46	11	33	6	15	21
$(i\text{-Pr})\text{P}(\text{SiCl}_3)_2$	56	44	12	33	7	15	21
$[\text{P}(\text{SiH}_3)_2]^-$	54	45	14	31	8	14	22
$(i\text{-Pr})\text{P}(\text{NPh}_2)(\text{SiCl}_3)$	51	49	11	36	6	18	23
$[\text{P}(\text{SiCl}_3)_2]^-$, 1	52	48	12	41	6	20	26

Table 3.7 Tabulated coefficients, %s hybrid and %s character for the P–Si bonds as determined by NBO analysis.

3.5.8 Coordinates of optimized structures

Atom	X	Y	Z
Si	-0.0000000000	0.0000000000	0.0303192720
S	0.0000000000	0.0000000000	2.0143027936
Cl	-0.9381754075	1.6249674723	-0.9183973552
Cl	-0.9381754075	-1.6249674723	-0.9183973552
Cl	1.8763508151	0.0000000000	-0.9183973552

Table 3.8 Optimized coordinates of anion **2** using GAMESS at the MP2/aug-cc-pVTZ level of theory.

Atom	X	Y	Z
P	0.0000000000	-0.0000000000	1.6595755141
Si	1.5865943041	0.0239055617	0.2161811935
Si	-1.5865943041	-0.0239055617	0.2161811935
Cl	3.3420605654	0.5919499583	1.1868556679
Cl	-3.3420605654	-0.5919499583	1.1868556679
Cl	1.4683894149	1.3026215529	-1.4176884952
Cl	-1.4683894149	-1.3026215529	-1.4176884952
Cl	2.1235933066	-1.7857475582	-0.6673761233
Cl	-2.1235933066	1.7857475582	-0.6673761233

Table 3.9 Optimized coordinates of anion **1** using GAMESS at the MP2/aug-cc-pVTZ level of theory

References

- [1] Schipper, W. *Eur. J. Inorg. Chem.* **2014**, *2014*, 1567–1571.
- [2] Borger, J. E.; Ehlers, A. W.; Slootweg, J. C.; Lammertsma, K. *Chem. - Eur. J.* **2017**, *23*, 11738–11746.
- [3] Diskowski, H.; Hofmann, T. “Phosphorus” in *Ullmann’s Encyclopedia of Industrial Chemistry*; Wiley, 2000.
- [4] Emsley, J. *The 13th element: the sordid tale of murder, fire and phosphorus*; Wiley: New York, 2000.
- [5] Schrödter, K.; Bettermann, G.; Staffel, T.; Wahl, F.; Klein, T.; Hofmann, T. “Phosphoric Acid and Phosphates” in *Ullmann’s Encyclopedia of Industrial Chemistry*; Wiley: Weinheim, Germany, 2008.
- [6] Vahidnia, A.; van der Voet, G.; de Wolff, F. *Hum. Exp. Toxicol.* **2007**, *26*, 823–832.
- [7] Cossairt, B. M.; Diawara, M.-C.; Cummins, C. C. *Science* **2009**, *323*, 602–602.
- [8] Müller, H. “Sulfuric Acid and Sulfur Trioxide” in *Ullmann’s Encyclopedia of Industrial Chemistry*; Wiley: Weinheim, Germany, 2000.
- [9] Gilmour, R. *Phosphoric acid: purification, uses, technology, and economics*; CRC Press/Taylor & Francis: Boca Raton, FL, 2014.
- [10] Geeson, M. B.; Cummins, C. C. *Science* **2018**, *359*, 1383–1385.
- [11] Protasiewicz, J. D. *Science* **2018**, *359*, 1333–1333.
- [12] Slootweg, J. C. *Angew. Chem.* **2018**, *130*, 6494–6496.
- [13] Slootweg, J. C. *Angew. Chem., Int. Ed.* **2018**, *57*, 6386–6388.
- [14] Swager, T. M.; Peeks, M. D. *Synfacts* **2018**, *14*, 592.
- [15] Nordschild, S.; Auner, N. *Chem. - Eur. J.* **2008**, *14*, 3694–3702.
- [16] Simmler, W. “Silicon Compounds, Inorganic” in *Ullmann’s Encyclopedia of Industrial Chemistry*; Wiley: Weinheim, Germany, 2000.
- [17] A chemical is categorized as HPV if it is manufactured in, or imported into, the United States in amounts equal to or exceeding 1 million pounds a year. Chemical Right to Know High Production Volume Chemicals Frequently Asked Questions, <https://nepis.epa.gov/Exe/ZyPURL.cgi?Dockey=7000052X.txt>, accessed January 2019.
- [18] This figure was obtained from the Chemical Data Reporting tool, <https://www.epa.gov/chemical-data-reporting>, accessed January 2019.
- [19] Ding, W.-J.; Yan, J.-M.; Xiao, W.-D. *Ind. Eng. Chem. Res.* **2014**, *53*, 10943–10953.
- [20] Knoth, J. F.; Eberle, H.-J.; Ruedinger, C. Process for converting silicon tetrachloride to trichlorosilane. 2017; US9776878B2.
- [21] Goodwin, G. B.; Kenney, M. E. *Inorg. Chem.* **1990**, *29*, 1216–1220.
- [22] Roberts, J. M.; Placke, J. L.; Eldred, D. V.; Katsoulis, D. E. *Ind. Eng. Chem. Res.* **2017**, *56*, 11652–11655.
- [23] Roberts, J. M.; Eldred, D. V.; Katsoulis, D. E. *Ind. Eng. Chem. Res.* **2016**, *55*, 1813–1818.

- [24] Auner, N.; Bauch, C.; Deltshew, R.; Holl, S.; Mohsseni, J. Method for the production of high-purity silicon. 2012; WO2012032129A1.
- [25] Dong, Y.; Slade, T.; Stolt, M. J.; Li, L.; Girard, S. N.; Mai, L.; Jin, S. *Angew. Chem., Int. Ed.* **2017**, *56*, 14453–14457.
- [26] Pham Minh, D.; Ramarason, J.; Nzihou, A.; Sharrock, P. *Ind. Eng. Chem. Res.* **2012**, *51*, 3851–3854.
- [27] (a) Cella, J. A.; Carpenter, J. C. *J. Organomet. Chem.* **1994**, *480*, 23–26; (b) Takiguchi, T. *J. Am. Chem. Soc.* **1959**, *81*, 2359–2361; (c) Kondo, S.-i.; Harada, T.; Tanaka, R.; Unno, M. *Org. Lett.* **2006**, *8*, 4621–4624.
- [28] Besecker, C. J.; Day, V. W.; Klemperer, W. G. *Organometallics* **1985**, *4*, 564–570.
- [29] Ross, W. H.; Jones, R. M. *J. Am. Chem. Soc.* **1925**, *47*, 2165–2170.
- [30] Smith, J. P.; Brown, W. E.; Lehr, J. R. *J. Am. Chem. Soc.* **1955**, *77*, 2728–2730.
- [31] Tillmann, J.; Meyer, L.; Schweizer, J. I.; Bolte, M.; Lerner, H.-W.; Wagner, M.; Holthausen, M. C. *Chem. - Eur. J.* **2014**, *20*, 9234–9239.
- [32] Choi, S.-B.; Kim, B.-K.; Boudjouk, P.; Grier, D. G. *J. Am. Chem. Soc.* **2001**, *123*, 8117–8118.
- [33] Böhme, U.; Gerwig, M.; Gründler, F.; Brendler, E.; Kroke, E. *Eur. J. Inorg. Chem.* **2016**, *2016*, 5028–5035.
- [34] (a) Benkeser, R. A. *Acc. Chem. Res.* **1971**, *4*, 94–100; (b) Kang, S.-H.; Han, J. S.; Lee, M. E.; Yoo, B. R.; Jung, I. N. *Organometallics* **2003**, *22*, 2551–2553; (c) Kang, S.-H.; Han, J. S.; Yoo, B. R.; Lee, M. E.; Jung, I. N. *Organometallics* **2003**, *22*, 529–534.
- [35] Greulich, T. W.; Suzuki, N.; Daniliuc, C. G.; Fukazawa, A.; Yamaguchi, E.; Studer, A.; Yamaguchi, S. *Chem. Commun.* **2016**, *52*, 2374–2377.
- [36] Li, Y.; Chakrabarty, S.; Mück-Lichtenfeld, C.; Studer, A. *Angew. Chem., Int. Ed.* **2016**, *55*, 802–806.
- [37] Mackewitz, T.; Ahlers, W.; Zeller, E.; Roper, M.; Paciello, R.; Papp, R.; Knoll, K.; Voss, H.; Roeper, M. Phosphacyclohexanes and the use thereof in the hydroformylation of olefins. 2004; US2004106512 (A1).
- [38] Buckler, S.; Epstein, M. *Tetrahedron* **1962**, *18*, 1221–1230.
- [39] Cozzoli, P. D.; Kornowski, A.; Weller, H. *J. Am. Chem. Soc.* **2003**, *125*, 14539–14548.
- [40] Langley, S.; Helliwell, M.; Sessoli, R.; Teat, S. J.; Winpenny, R. E. P. *Inorg. Chem.* **2008**, *47*, 497–507.
- [41] Lavaud, C.; Goettmann, F.; Causse, J.; Grandjean, A. Procédé sol-gel pour séparer des ions métalliques d’une solution aqueuse. 2014; FR3001961A1.
- [42] Svava, J.; Weferling, N.; Hofmann, T. “Phosphorus Compounds, Organic” in *Ullmann’s Encyclopedia of Industrial Chemistry*; WileyVCH, 2006.
- [43] Julia, M.; Mestdag, H.; Rolando, C. *Tetrahedron* **1986**, *42*, 3841–3849.
- [44] Verstuyft, A. W.; Redfield, D. A.; Cary, L. W.; Nelson, J. H. *Inorg. Chem.* **1977**, *16*, 2776–2786.
- [45] McKenna, E. G.; Walker, B. J. *Tetrahedron Lett.* **1988**, *29*, 485–488.

- [46] Manna, C. M.; Nassar, M. Y.; Tofan, D.; Chakarawet, K.; Cummins, C. C. *Dalton Trans.* **2014**, *43*, 1509–1518.
- [47] Jiang, Y.; Chakarawet, K.; Kohout, A. L.; Nava, M.; Marino, N.; Cummins, C. C. *J. Am. Chem. Soc.* **2014**, *136*, 11894–11897.
- [48] Shepard, S. M.; Cummins, C. C. *J. Am. Chem. Soc.* **2019**, *141*, 1852–1856.
- [49] (a) Styskalik, A.; Babiak, M.; Machac, P.; Relichova, B.; Pinkas, J. *Inorg. Chem.* **2017**, *56*, 10699–10705; (b) Jähnigen, S.; Brendler, E.; Böhme, U.; Kroke, E. *Chem. Commun.* **2012**, *48*, 7675–7677; (c) Styskalik, A.; Skoda, D.; Moravec, Z.; Babiak, M.; Barnes, C. E.; Pinkas, J. *J. Mater. Chem. A* **2015**, *3*, 7477–7487.
- [50] (a) Hesse, K.-F. *Acta Crystallogr., Sect. B: Struct. Crystallogr. Cryst. Chem.* **1979**, *35*, 724–725; (b) Poojary, D. M.; Borade, R. B.; Campbell, F. L.; Clearfield, A. *J. Solid State Chem.* **1994**, *112*, 106–112; (c) Poojary, D. M.; Borade, R. B.; Clearfield, A. *Inorg. Chim. Acta* **1993**, *208*, 23–29.
- [51] Liebau, F.; Bissert, G.; Köppen, N. *Z. Anorg. Allg. Chem.* **1968**, *359*, 113–134.
- [52] Hérault, D.; Nguyen, D. H.; Nuel, D.; Buono, G. *Chem. Soc. Rev.* **2015**, *44*, 2508–2528.
- [53] Benkeser, R. A.; Voley, K. M.; Grutzner, J. B.; Smith, W. E. *J. Am. Chem. Soc.* **1970**, *92*, 697–698.
- [54] Oehme, H.; Weiss, H. *J. Organomet. Chem.* **1987**, *319*, C16–C18.
- [55] Teichmann, J.; Bursch, M.; Köstler, B.; Bolte, M.; Lerner, H.-W.; Grimme, S.; Wagner, M. *Inorg. Chem.* **2017**, *56*, 8683–8688.
- [56] Teichmann, J.; Wagner, M. *Chem. Commun.* **2018**, *54*, 1397–1412.
- [57] (a) Krenske, E. H. *J. Org. Chem.* **2012**, *77*, 3969–3977; (b) Krenske, E. H. *J. Org. Chem.* **2012**, *77*, 1–4; (c) Naumann, K.; Zon, G.; Mislow, K. *J. Am. Chem. Soc.* **1969**, *91*, 7012–7023.
- [58] Huang, X.; Ding, W.-J.; Yan, J.-M.; Xiao, W.-D. *Ind. Eng. Chem. Res.* **2013**, *52*, 6211–6220.
- [59] Neumeyer, F.; Schweizer, J. I.; Meyer, L.; Sturm, A. G.; Nadj, A.; Holthausen, M. C.; Auner, N. *Chem. - Eur. J.* **2017**, *23*, 12399–12405.
- [60] Although we were unable to find a literature report associated with this compound, it can be accessed in the Cambridge Structural Database as a private communication under the refcode CCDC 183389.
- [61] Teichmann, J.; Kunkel, C.; Georg, I.; Moxter, M.; Santowski, T.; Bolte, M.; Lerner, H.-W.; Bade, S.; Wagner, M. *Chem. - Eur. J.* **2019**, *25*, 2740–2744.
- [62] Georg, I.; Teichmann, J.; Bursch, M.; Tillmann, J.; Endeward, B.; Bolte, M.; Lerner, H.-W.; Grimme, S.; Wagner, M. *J. Am. Chem. Soc.* **2018**, *140*, 9696–9708.
- [63] Müller, U.; Krug, V. *Z. Naturforsch., B: J. Chem. Sci.* **1985**, *40*.
- [64] Greenwood, N. N.; Earnshaw, A. *Chemistry of the elements*, 2nd ed.; Butterworth-Heinemann: Boston, Mass., 1997.
- [65] Rettig, S. J.; Trotter, J. *Acta Crystallogr., Sect. C: Cryst. Struct. Commun.* **1987**, *43*, 2260–2262.

- [66] Weigend, F.; Ahlrichs, R. *Phys. Chem. Chem. Phys.* **2005**, *7*, 3297.
- [67] Chai, J.-D.; Head-Gordon, M. *J. Chem. Phys.* **2008**, *128*, 084106.
- [68] Pyykkö, P.; Atsumi, M. *Chem. - Eur. J.* **2009**, *15*, 186–197.
- [69] Panckhurst, D. J.; Wilkins, C. J.; Brault, A. T.; Angelici, R. J. In “*Trichlorosilane-thiol*” in *Inorg. Synth.*; Kleinberg, J., Ed.; John Wiley & Sons, Inc.: Hoboken, NJ, USA, 1963; Vol. 7; pp 28–30.
- [70] (a) Finger, L. H.; Scheibe, B.; Sundermeyer, J. *Inorg. Chem.* **2015**, *54*, 9568–9575; (b) Finger, L. H.; Guschlbauer, J.; Harms, K.; Sundermeyer, J. *Chem. - Eur. J.* **2016**, *22*, 16292–16303.
- [71] Degl’Innocenti, A.; Capperucci, A.; Castagnoli, G.; Malesci, I. *Synlett* **2005**, *13*, 1965–1983.
- [72] Pedersen, B. S.; Scheibye, S.; Nilsson, N. H.; Lawesson, S.-O. *Bull. Soc. Chim. Belg.* **1978**, *87*, 223–228.
- [73] Gordon, M. S.; Schmidt, M. W. In “*Advances in electronic structure theory: GAMESS a decade later*” in *Theory and Applications of Computational Chemistry: the first forty years*; Dykstra, C., Frenking, G., Kim, K., Scuseria, G., Eds.; Elsevier, 2005; pp 1167–1189.
- [74] Schmidt, M. W.; Baldrige, K. K.; Boatz, J. A.; Elbert, S. T.; Gordon, M. S.; Jensen, J. H.; Koseki, S.; Matsunaga, N.; Nguyen, K. A.; Su, S.; Windus, T. L.; Dupuis, M.; Montgomery, J. A. *J. Comput. Chem.* **1993**, *14*, 1347–1363.
- [75] Mayer, I. *Chem. Phys. Lett.* **1983**, *97*, 270–274.
- [76] Glendening, E. D.; Badenhoop, J. K.; Reed, A. E.; Carpenter, J. E.; Bohmann, J. A.; Morales, C. M.; Landis, C. R.; Weinhold, F. NBO 6.0. 2013.
- [77] Weinhold, F.; Landis, C. R. *Valency and bonding: a natural bond orbital donor-acceptor perspective*; Cambridge University Press: Cambridge, UK ; New York, 2005.
- [78] (a) Li, J.; McWeeny, R. *Int. J. Quantum Chem.* **2002**, *89*, 208–216; (b) Li, J.; McWeeny, R. VB2000 Version 2.7. 2013; <http://www.vb2000.net>.
- [79] Verkade, J. G., Quin, L. D., Eds. “*Theoretical Considerations: Spin-Spin Coupling*” in *Phosphorus-31 NMR spectroscopy in stereochemical analysis*; Methods in stereochemical analysis v. 8; VCH Publishers: Deerfield Beach, Fla, 1987; pp 211–217.
- [80] Becker, G.; Eschbach, B.; Käshammer, D.; Mundt, O. *Z. Anorg. Allg. Chem.* **1994**, *620*, 29–40.
- [81] Suardíaz, R.; Pérez, C.; Crespo-Otero, R.; García de la Vega, J. M.; Fabián, J. S. *J. Chem. Theory Comput.* **2008**, *4*, 448–456.
- [82] Helgaker, T.; Jaszuński, M.; Ruud, K. *Chem. Rev.* **1999**, *99*, 293–352.
- [83] Whittell, G. R.; Balmond, E. I.; Robertson, A. P. M.; Patra, S. K.; Haddow, M. F.; Manners, I. *Eur. J. Inorg. Chem.* **2010**, *2010*, 3967–3975.
- [84] Fritz, G.; Schäfer, H.; Demuth, R.; Grobe, J. *Z. Anorg. Allg. Chem.* **1974**, *407*, 287–294.
- [85] Fritz, G.; Schäfer, H.; Hölderich, W. *Z. Anorg. Allg. Chem.* **1974**, *407*, 266–286.
- [86] Driess, M.; Monsé, C.; Merz, K. *Z. Anorg. Allg. Chem.* **2001**, *627*, 1225–1230.

- [87] Müller, L.-P.; Zanin, A.; Jeske, J.; Jones, P. G.; du Mont, W.-W. In *“Trichlorosilane/Triethylamine An Alternative to Hexachlorodisilane in Reductive Trichlorosilylation Reactions?” in Organosilicon Chemistry Set*; Auner, N., Weis, J., Eds.; Wiley-VCH Verlag GmbH: Weinheim, Germany, 2005; pp 286–290.
- [88] Müller, L.-P.; Mont, W.-W. D.; Jeske, J.; Jones, P. G. *Chem. Ber.* **1995**, *128*, 615–619.
- [89] Crabtree, R. H.; Davis, M. W. *Organometallics* **1983**, *2*, 681–682.
- [90] L. Conley, B.; J. Williams, T. *Chem. Commun.* **2010**, *46*, 4815–4817.
- [91] Kinrade, S. D.; Swaddle, T. W. *Inorg. Chem.* **1988**, *27*, 4253–4259.
- [92] (a) Chambers, D. W. S.; Wilkins, C. J. *J. Chem. Soc.* **1960**, 5088; (b) Schumb, W. C.; Stevens, A. J. *J. Am. Chem. Soc.* **1950**, *72*, 3178–3182.
- [93] Olaru, M.; Hesse, M. F.; Rychagova, E.; Ketkov, S.; Mebs, S.; Beckmann, J. *Angew. Chem., Int. Ed.* **2017**, *56*, 16490–16494.
- [94] (a) Schwarze, B.; Milius, W.; Schnick, W. *Z. Naturforsch., B: J. Chem. Sci.* **1997**, *52*, 819–822; (b) Wannagat, U.; Schmidt, P.; Schulze, M. *Angew. Chem., Int. Ed.* **1967**, *6*, 447–448; (c) Moretto, H.-H.; Schmidt, P.; Wannagat, U. *Z. Anorg. Allg. Chem.* **1972**, *394*, 125–132.
- [95] Pangborn, A. B.; Giardello, M. A.; Grubbs, R. H.; Rosen, R. K.; Timmers, F. J. *Organometallics* **1996**, *15*, 1518–1520.
- [96] Williams, D. B. G.; Lawton, M. *J. Org. Chem.* **2010**, *75*, 8351–8354.
- [97] Horn, H.-G.; Marsmann, H. C. *Makromol. Chem.* **1972**, *162*, 255–267.
- [98] Chernyshev, E. A.; Krasnova, T. L.; Mudrova, N. A.; Bochkarev, V. N. **1992**, *62*, 1828–37.
- [99] Choi, J.; Yoon, N. M. *Synthesis* **1995**, *1995*, 373–375.
- [100] Pathak, U.; Pandey, L. K.; Tank, R. *J. Org. Chem.* **2008**, *73*, 2890–2893.
- [101] Bruker (2001). SADABS. Bruker AXS Inc., Madison, Wisconsin, USA.
- [102] Krause, L.; Herbst-Irmer, R.; Sheldrick, G. M.; Stalke, D. *J. Appl. Crystallogr.* **2015**, *48*, 3–10.
- [103] Sheldrick, G. M. *Acta Crystallogr., Sect. A: Found. Adv.* **2015**, *71*, 3–8.
- [104] Sheldrick, G. M. *Acta Crystallogr., Sect. A: Found. Crystallogr.* **2008**, *64*, 112–122.
- [105] Hübschle, C. B.; Sheldrick, G. M.; Dittrich, B. *J. Appl. Crystallogr.* **2011**, *44*, 1281–1284.
- [106] Propagation of Error. 2013; <https://chem.libretexts.org>.
- [107] Neese, F. *Wiley Interdiscip. Rev.: Comput. Mol. Sci.* **2012**, *2*, 73–78.
- [108] Lu, T.; Chen, F. *J. Comput. Chem.* **2012**, *33*, 580–592.
- [109] Pettersen, E. F.; Goddard, T. D.; Huang, C. C.; Couch, G. S.; Greenblatt, D. M.; Meng, E. C.; Ferrin, T. E. *J. Comput. Chem.* **2004**, *25*, 1605–1612.

Chapter 4

Photochemical Alkene Hydrophosphination with Bis(Trichlorosilyl)Phosphine

Contents

4.1	Introduction	148
4.2	Results and Discussion	148
4.3	Conclusions	155
4.4	Future work	155
4.5	Experimental methods	157
	References	220

Abstract

Bis(trichlorosilyl)phosphine ($\text{HP}(\text{SiCl}_3)_2$, **1**) was prepared from $[\text{TBA}][\text{P}(\text{SiCl}_3)_2]$ ($[\text{TBA}]_2$, TBA = tetra-*n*-butylammonium) and triflic acid in 36% yield. The phosphine is an efficient reagent for hydrophosphination of unactivated terminal olefins under UV irradiation (15–60 min) and gives rise to bis(trichlorosilyl)alkylphosphines ($\text{RP}(\text{SiCl}_3)_2$, R = $(\text{CH}_2)_5\text{CH}_3$, 88%; $(\text{CH}_2)_2\text{C}(\text{CH}_3)_3$, 76%; CH_2Cy , 93%; $(\text{CH}_2)_2\text{Cy}$, 95%; $\text{CH}_2\text{CH}(\text{CH}_3)(\text{CH}_2)_2\text{CH}_3$, 82%; $(\text{CH}_2)_3\text{O}(\text{CH}_2)_3\text{CH}_3$, 95%; $(\text{CH}_2)_3\text{Cl}$, 83%; $(\text{CH}_2)_2\text{SiMe}_3$, 92%; $(\text{CH}_2)_5\text{C}(\text{H})\text{CH}_2$, 44%) in excellent yields. The products require no further purification beyond filtration and removal of volatile material under reduced pressure. The P–Si bonds of prototypical product $\text{H}_3\text{C}(\text{CH}_2)_5\text{P}(\text{SiCl}_3)_2$ are readily functionalized to give further phosphorus-containing products: $\text{H}_3\text{C}(\text{CH}_2)_5\text{PCl}_2$ (72%); $\text{H}_3\text{C}(\text{CH}_2)_5\text{PH}_2$ (88%), $[\text{H}_3\text{C}(\text{CH}_2)_5\text{P}(\text{CH}_2\text{Ph})_3]\text{Br}$ (77%),

$\text{H}_3\text{C}(\text{CH}_2)_5\text{P}(\text{O})(\text{H})(\text{OH})$ (93%), and $\text{H}_3\text{C}(\text{CH}_2)_5\text{P}(\text{O})(\text{OH})_2$ (73%). Experimental mechanistic investigations, accompanied by quantum chemical calculations, point toward a radical-chain mechanism. The method is a fast, high-yielding, and atom-efficient way to prepare compounds that contain phosphorus-carbon bonds.

4.1 Introduction

Hydrophosphination, the addition of a P–H bond to an unsaturated substrate such as an olefin, is an atom-efficient method for constructing new phosphorus-carbon bonds.¹ Recent progress has been achieved using transition-metal catalysis, with breakthroughs allowing for double hydrophosphination of alkynes to give diphosphine ligands,² enantioselective hydrophosphination procedures to give chiral phosphine products,³ and increasingly selective reactions when two or more P–H bonds are present in the phosphine.⁴ Another avenue of research is toward catalyst-free methods, eliminating the requirement for purification of reaction products from catalysts or initiators.^{5,6}

Despite these significant advances, there are three major obstacles facing hydrophosphination reactions:⁷ (i) limited scope of the phosphine substrate (Ph_2PH and PH_3 are used almost exclusively);⁸ (ii) limited scope of the olefinic substrate (activated olefins such as styrene and acrylonitrile are most commonly encountered);⁹ and (iii) low selectivity for single or multiply hydrophosphinated products where more than one P–H bond is present in the phosphine (i.e. PH_3 , RPH_2).¹⁰ Herein, we address these issues by preparing bis(trichlorosilyl)phosphine ($\text{HP}(\text{SiCl}_3)_2$, **1**), and using it to selectively hydrophosphinate unactivated, terminal olefins. Furthermore, the phosphorus-silicon bonds in the resulting products ($\text{RP}(\text{SiCl}_3)_2$) are readily converted to P–X ($\text{X} = \text{H}, \text{C}, \text{Cl}, \text{O}$) bonds to give a range of desirable phosphorus-containing products such as dichlorophosphines, primary phosphines, alkyl phosphinic acids, phosphonates, and phosphonium salts.

4.2 Results and Discussion

Our investigations began with treating the phosphide salt $[\text{TBA}]\mathbf{2}$ with an acid in order to prepare the neutral phosphine $\text{HP}(\text{SiCl}_3)_2$ (**1**). Our interest in $[\text{TBA}]\mathbf{2}$ is motivated by its ready availability (>10 g, 70%) from phosphate sources and because it can be used to prepare phosphorus-containing compounds in a manner that bypasses the intermediacy of white phosphorus, a high energy and toxic intermediate.^{11–16}

Treatment of a pentane slurry of $[\text{TBA}]\mathbf{2}$ with triflic acid (1 equiv) led to the formation of $\text{HP}(\text{SiCl}_3)_2$ (**1**) and TBA triflate (Figure 4.1). After filtration and a simple trap-to-trap vacuum transfer procedure (40 to -78°C), **1** was isolated as a colorless liquid in 36% yield (0.54 g). This low yield is attributed to the formation of H_2PSiCl_3 and PH_3 , the concentrations of which increase when acids other than triflic acid, such as trifluoroacetic acid, are used. The $^{31}\text{P}\{\text{^1H}\}$ NMR spectrum of **1** features a singlet resonance at -171.5 ppm,

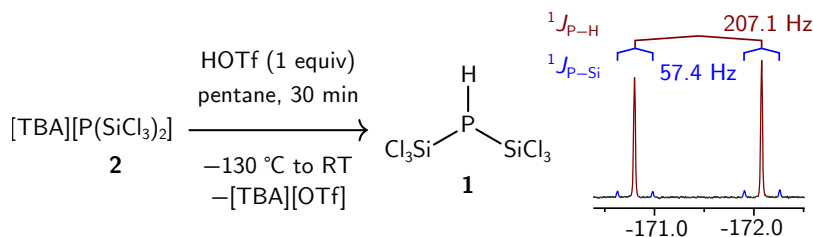


Figure 4.1 Preparation of phosphine **1** and region of the ^{31}P NMR spectrum highlighting the splitting pattern.

which chemical shift is remarkably similar to that of the anionic phosphide **2** (-172.8 ppm). However, the value of $^1J_{\text{P-Si}}$ drops markedly from 156.0 to 57.4 Hz upon protonation. In the ^{31}P and ^1H NMR spectra, the expected doublets are observed with a $^1J_{\text{P-H}}$ value of 207.1 Hz.

Several conditions are known for the initiation of hydrophosphination reactions, falling under the following broad themes: acid, base, thermal, light, and additives such as azobisisobutyronitrile (AIBN).¹⁷ Of particular relevance to the current study, Norman pioneered the use of trimethylsilylphosphine (Me_3SiPH_2) in hydrophosphination reactions, using AIBN as a radical initiator with mild heating (ca. 80 °C).^{18,19} We found hydrophosphination of the unactivated olefin 1-hexene (2 equiv) with $\text{HP}(\text{SiCl}_3)_2$ proceeded rapidly (<20 min) upon UV irradiation (254 nm) of a hexane solution of both compounds in a photoreactor (Figure 4.2). The product, obtained in 88% yield, was identified as $(\text{Cl}_3\text{Si})_2\text{P}(n\text{-hex})$ (**3a**), resulting from anti-Markovnikov addition and the formation of new P-C and C-H bonds as assayed by multinuclear NMR spectroscopy and high resolution mass spectrometry (HRMS).

The reaction tolerates a variety of substitution patterns on aliphatic α -olefin substrates, including *gem*-disubstitution (**3c**, **3e**). Functional groups compatible with the reaction conditions include alkyl chlorides (**3g**), ethers (**3f**), and silanes (**3h**). The $\text{RP}(\text{SiCl}_3)_2$ compounds were isolated by filtration (glass microfiber) followed by removal of volatile material (hexane solvent and excess olefin) to give spectroscopically pure products in the majority of cases (**3a-3h**). The selective hydrophosphination of one of the alkene groups in 1,6-heptadiene was achieved using stoichiometry control (5 equiv of diene) to give alkene-containing phosphine **3i** in moderate yield (44%, ^{31}P NMR). Compounds **3a-3i** have not been described previously, but their NMR data are in line with a handful of other reported bis(trichlorosilyl)alkylphosphines,²⁰⁻²³ with ^{31}P NMR chemical shifts in the range of -102.7 to -120.8 ppm and $^1J_{\text{P-Si}}$ values of 56.5 – 73.4 Hz.

The use of photochemistry and observed short reaction times is suggestive of a radical reaction mechanism. Therefore, radical clock substrates were subjected to the reaction conditions in order to probe this hypothesis. Use of 1,6-heptadiene as the substrate (Figure 4.3A) did not lead to the formation of the 5-*exo*-trig ring-closure product, a process

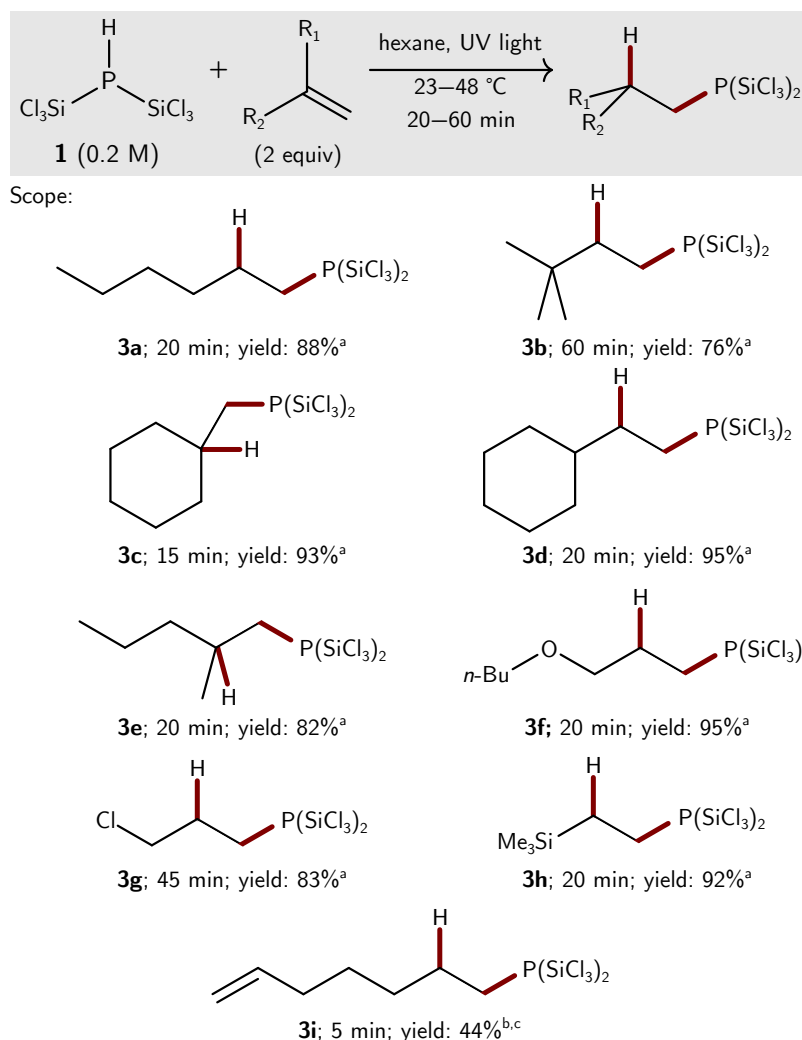


Figure 4.2 Scope of products available from the hydrophosphination procedure. ^aisolated yield. ^byield determined by ³¹P{¹H} NMR spectroscopy. ^c0.5 mmol (5 equiv) of substrate used.

that has a first order rate constant of ca. $1.3 \times 10^5 \text{ s}^{-1}$,²⁴ but instead gave linear **3i** as the product. Next, the radical clock 1,1-difluoro-vinylcyclopropane was tested because of its rapid ring opening ($k_r = 6 \times 10^{10} \text{ s}^{-1}$) when a radical forms on the carbon adjacent to the cyclopropane ring.²⁵ A control reaction confirmed that 1,1-difluoro-vinylcyclopropane is unchanged by UV irradiation in our photoreactor over the course of 10 min, but in the presence of **1** leads to the formation of ring-opened product **3j**, obtained as a mixture of the *E* and *Z* isomers (87:13), consistent with the intermediacy of radical species.

Further evidence of radical intermediates was provided by unsuccessful attempts to

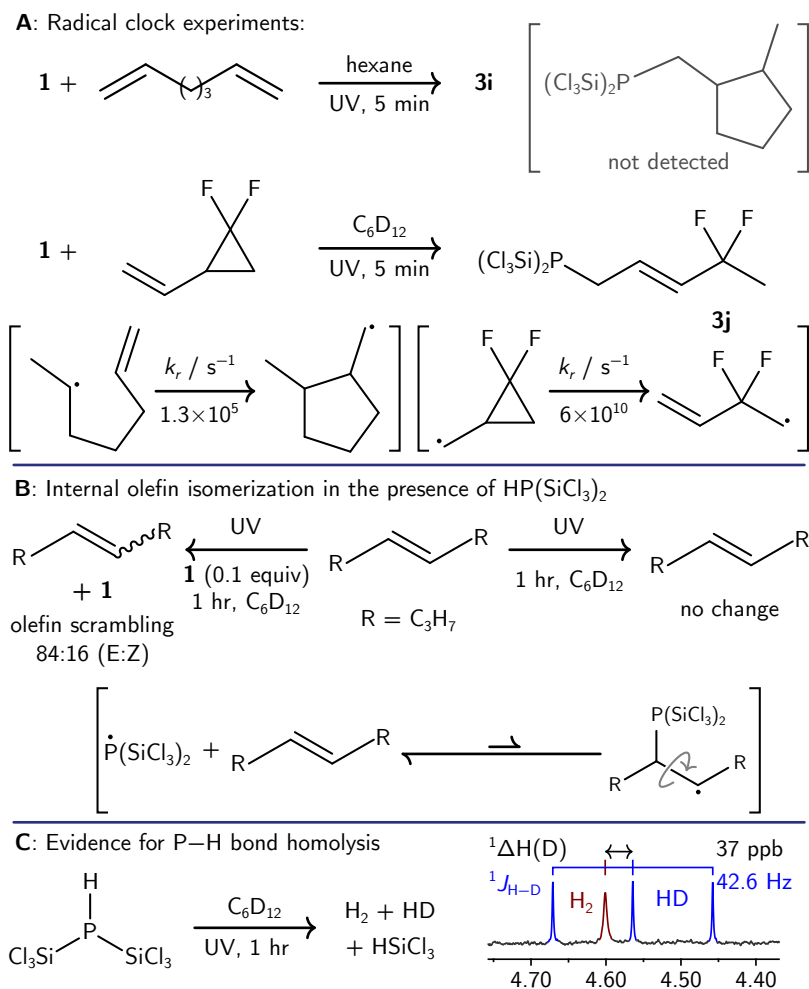


Figure 4.3 A: Testing radical clock 1,1-difluoro-vinylcyclopropane as a substrate leads to observation of the product derived from ring opening. **B:** Irradiation of *trans*-4-octene in the presence of $\text{HP}(\text{SiCl}_3)_2$ leads to internal olefin isomerization; without $\text{HP}(\text{SiCl}_3)_2$ no scrambling is observed. **C:** Irradiation of $\text{HP}(\text{SiCl}_3)_2$ in C_6D_{12} leads to the formation of H_2 and HD.

hydrophosphinate the internal olefin *trans*-4-octene with $\text{HP}(\text{SiCl}_3)_2$. A control experiment confirmed that irradiation of a C_6D_{12} solution of *trans*-4-octene (borosilicate NMR tube) in our photoreactor did not lead to *cis/trans* isomerization after 1 h. However, the addition of $\text{HP}(\text{SiCl}_3)_2$ (0.1 equiv) to the reaction mixture followed by irradiation (1 h) led to a mixture of *trans*- and *cis*-4-octene in a ratio of ca. 84:16. Thus, the addition of $\text{HP}(\text{SiCl}_3)_2$ to the reaction mixture catalyzes the isomerization. We interpret this observation as arising from addition of $\cdot\text{P}(\text{SiCl}_3)_2$ to the internal olefin, permitting C–C bond rotation about the former-alkene group, followed by reformation of the phosphorus radical and the isomerized internal olefin (Figure 4.3B).²⁶ The absence of hydrophosphination product with *trans*-4-octene is in accord with the well-documented sensitivity of radical additions to the olefin substitution pattern.²⁷

The unchanged ^1H NMR spectrum of *trans*-4-octene after UV irradiation (Figure 4.3B) suggests the olefin is not responsible for the generation of any radicals, and instead that $\text{HP}(\text{SiCl}_3)_2$ might be playing the role of initiator. To test this idea, $\text{HP}(\text{SiCl}_3)_2$ was irradiated with UV light in C_6D_{12} for 1 h and the resulting mixture was analyzed by NMR spectroscopy. By ^{31}P NMR spectroscopy, the major species was unchanged $\text{HP}(\text{SiCl}_3)_2$. However, in the ^1H NMR spectrum, the most notable products were HSiCl_3 and HD gas, which was recognizable by its 1:1:1 triplet resonance with a $^1J_{\text{H-D}}$ value of 42.6 Hz and an isotope shift of 37 ppb relative to H_2 (Figure 4.3C).²⁸ The presence of HD points towards the homolysis of the P–H bond of $\text{HP}(\text{SiCl}_3)_2$ as a plausible initiation step, with the generated hydrogen atom capable of abstracting a deuterium atom from the solvent.²⁹ The UV–vis spectrum of $\text{HP}(\text{SiCl}_3)_2$ features an absorbance at 206.0 nm, which according to DFT calculations (pred. 210 nm) corresponds to a HOMO-LUMO transition. These orbitals display phosphorus lone pair and P–H antibonding character, respectively (Fig 4.69). The use of wavelengths other than 254 nm resulted in lower conversion to product (300 nm) or no conversion at all (420 nm).

Based on these experimental observations we propose a simple radical-based reaction mechanism (Figure 4.4), which was investigated with quantum chemical calculations. Geometries and thermochemistry for the relevant species were calculated at the $\omega\text{B97X-D3/def2-TZVP}$ ³⁰ level of theory and SCF single point energies came from accurate DLPNO-CCSD(T)/cc-pVTZ calculations³¹ (as implemented in the ORCA^{32,33} software package) in order to provide a reasonable description of the proposed open-shell species. The neutral radical $\cdot\text{P}(\text{SiCl}_3)_2$, presumably generated upon photolysis of $\text{HP}(\text{SiCl}_3)_2$,³⁴ can add in an anti-Markovnikov manner (**TS1**) to an α -olefin; in the case of our calculations the substrate was 1-propene to save on computational cost. The resulting carbon-centered radical in **I1** abstracts a hydrogen atom from $\text{HP}(\text{SiCl}_3)_2$ via **TS2** to give the bis(silyl)-alkylphosphine product and regenerate another equivalent of $\cdot\text{P}(\text{SiCl}_3)_2$ in a radical-chain process. The relative energies obtained using this computational procedure for transition states **TS1** and **TS2** of +10.7 and +14.8 kcal/mol, respectively, are remarkably similar to those calculated for the corresponding mechanism for the thiol-ene reaction.³⁵

Next, we sought to investigate the nature of the P–H bond in $\text{HP}(\text{SiCl}_3)_2$ and compare

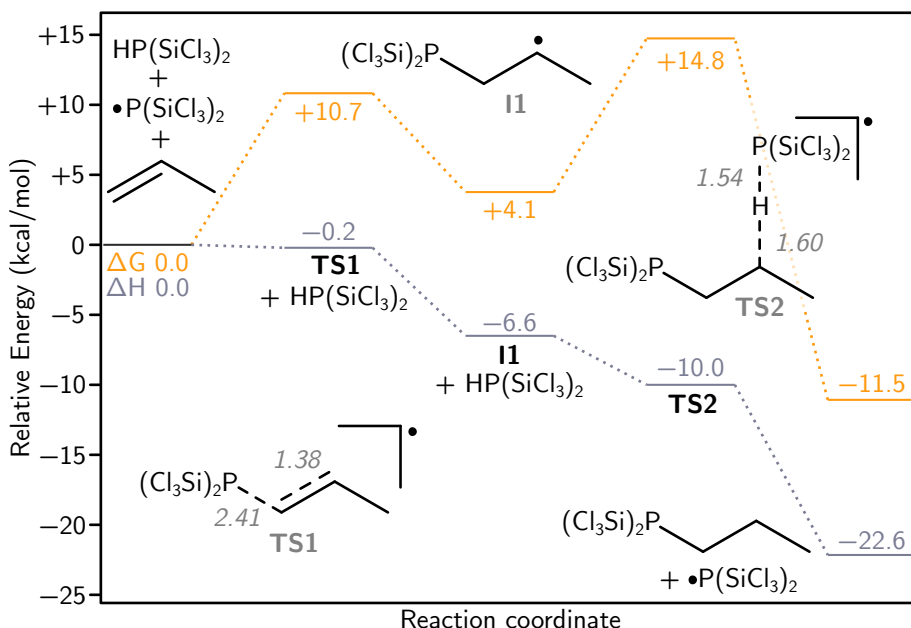


Figure 4.4 Calculated minimum energy pathway for a model reaction.

it to the corresponding bonds in PH_3 and Ph_2PH which are prototypical phosphines used in hydrophosphination procedures. Due to a lack of experimental data on the bond dissociation enthalpies (BDE) of P–H bonds,³⁶ they were calculated using the DLPNO-CCSD(T) method described above. The $\text{BDE}_g^{298\text{ K}}(\text{P-H})$ of **1** was found to be 82.2 kcal/mol, comparable to that of PH_3 (calcd: 82.1; expt: 82.5 kcal/mol³⁷). Both of these values are higher than for the P–H bond in Ph_2PH (calcd: 75.8 kcal/mol) presumably due to resonance delocalization in the radical derived from the latter. Thus, the trichlorosilyl groups do not seem to have any large stabilizing effect on the putative radical $\cdot\text{P}(\text{SiCl}_3)_2$ compared to the parent phosphine radical $\cdot\text{PH}_2$.

Attempts to determine the $\text{p}K_a$ of $\text{HP}(\text{SiCl}_3)_2$ in acetonitrile solution were hampered by rapid redistribution reactions of hydrogen and trichlorosilyl substituents at phosphorus in the presence of nitrogen-containing bases. Nonetheless, NMR studies point toward **1** having a $\text{p}K_a$ slightly higher than the pyridinium cation ($\text{p}K_a(\text{MeCN}) = 12.5$). Calculations predicted the $\text{p}K_a$ of $\text{HP}(\text{SiCl}_3)_2$ in acetonitrile to be 13.3, consistent with the NMR experiments. Applying the same method of calculating $\text{p}K_a$ to PH_3 and Ph_2PH indicates that **1** is significantly more acidic (ca. 15 $\text{p}K_a$ units) than either of these two phosphines, in line with the known stability of the conjugate anion of **1** as its TBA salt.^{11,12} In concert, these two properties (typical BDE; low $\text{p}K_a$) point toward the electrophilicity of radical intermediate $\cdot\text{P}(\text{SiCl}_3)_2$ as a key driver for the efficient hydrophosphination of unactivated terminal olefins using **1**. Indeed, calculations show that the lowest energy unoccupied

Table 4.1 Selected calculated properties for **1**, PH₃, and Ph₂PH.

Species	p <i>K</i> _a (MeCN) ^a	BDE _(P-H) ^{b,d}	SOMO _(·PR₂) ^{c,d}
1	13.3	82.2	-0.378
PH ₃	31.6	82.1	1.198
Ph ₂ PH	32.4	75.8	1.581

^a Determined by DFT calculation and regression against experimental p*K*_a values

^b Bond dissociation enthalpy (kcal/mol; gas phase, 298 K)

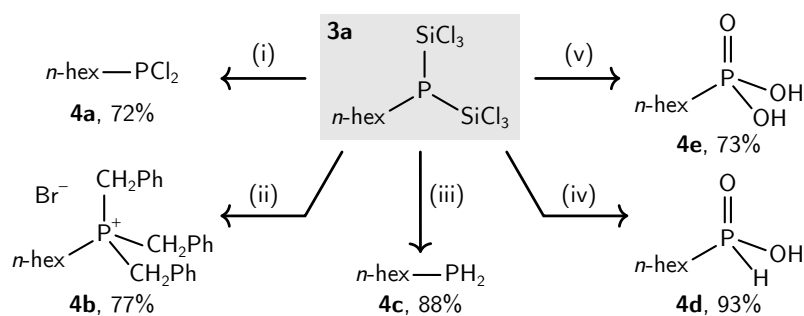
^c Singly Occupied Molecular Orbital (eV); energy corresponds to that of the unoccupied β-spin orbital

^d Determined at the DLPNO-CCSD(T)/cc-pVTZ level of theory

β-spin orbital is significantly lower for ·P(SiCl₃)₂ than those of ·PH₂ or ·PPh₂ (Table 4.1).

The electrochemistry of [TBA]**2** was investigated in order to triangulate the P–H bond dissociation free energy (BDFE) using a “square scheme” approach and in turn corroborate our *in silico* thermochemistry data. An acetonitrile (MeCN) solution of [TBA]**2** (0.01 M) with [TBA][PF₆] as the supporting electrolyte displayed an irreversible oxidation (*E*_{pa}) at +0.255 V versus the Fc/Fc⁺ couple, providing a BDFE_{MeCN}^{298 K}(P–H) of 80.1(±3³⁸) kcal/mol using theory refined by Mayer.³⁹ This value corresponds³⁹ to a BDE_g^{298 K}(P–H) for HP(SiCl₃)₂ of 83.2 kcal/mol, in good agreement with the calculated value (82.2) presented in Table 4.1.

In contrast to the majority of reported hydrophosphination reactions, the presence of two P–Si bonds in the reaction products provides a useful synthetic handle for further functionalization at phosphorus (Scheme 4.1). Treatment of bis(silyl)hexylphosphine **3a** with hexachloroethane led to the formation of hexyldichlorophosphine (**4a**). Aliphatic dichlorophosphines such as **4a** can be challenging to prepare⁴⁰ because treatment of PCl₃ with common organometallic compounds such as alkyllithium or Grignard reagents leads to intractable mixtures of products and thus transmetalation (to Cd, Hg, or Zn) has been necessary to achieve useful yields.⁴¹ Alternatively, chlorodiaminophosphines undergo selective alkylation at the P–Cl bond but the amino protecting groups must then be cleaved with hydrogen chloride.⁴² Hydrolysis of **3a** led to the primary phosphine **4c** while alkylation with benzyl bromide led to formation of the mixed phosphonium salt **4b**. Oxidation to the alkylphosphinic acid (**4d**) or the phosphonate (**4e**) was accomplished using aqueous hydrogen peroxide (30%), with the selectivity for the oxidation product being determined by the stoichiometry of oxidant (2.2 vs. 5 equiv) and the temperature at which the reaction was performed at (23 vs. 75 °C), respectively.



Scheme 4.1 Functionalization of bis(silyl)alkylphosphine **3a**. Conditions: (i): C_2Cl_6 (4 equiv), MeCN, 60 °C, 1 h; (ii): PhCH_2Br , MeCN, 80 °C, 2h; (iii): H_2O (32 equiv), CDCl_3 , 5 min; (iv): $\text{H}_2\text{O}_2(\text{aq})$ (2.2 equiv), MeCN, 23 °C, 5 min; (v): $\text{H}_2\text{O}_2(\text{aq})$ (5 equiv), MeCN, 60 °C, 12 h. Yields were determined spectroscopically (^{31}P NMR) by integration against an internal standard.

4.3 Conclusions

This work introduces $\text{HP}(\text{SiCl}_3)_2$, an efficient hydrophosphination reagent for preparing a number of bis(trichlorosilyl)alkylphosphines. The two P–Si bonds provide a platform for functionalization,⁴³ resulting in a modular synthesis of several classes of phosphorus compounds. The hydrophosphination reaction is selective for the anti-Markovnikov product and overcomes limitations germane to hydrophosphination using PH_3 by effectively masking two of the P–H bonds as trichlorosilyl substituents. This reagent and reaction methodology opens the door to a number of new phosphorus-containing compounds, which are themselves indispensable in chemical synthesis and catalysis.

4.4 Future work

There are a small number of experiments required in order to publish the work described in this chapter. The compounds obtained from P–Si bond functionalization require characterization by HRMS and NMR spectroscopy (^1H , ^{13}C), which will be aided by developing purification procedures that provide spectroscopically pure compounds. In the case of primary phosphine **4c**, filtration through an alumina plug is expected to provide material of sufficiently purity. Dichlorophosphine **4a** is expected to be purified by removing volatile material, followed by filtration (microfiber filter paper). With sufficient material, this compound may also be amenable to purification by distillation. Compounds **4d** and **4e**, obtained from the oxidation of **3a** with 2 and 5 equiv of aqueous hydrogen peroxide (30%), respectively, are expected to be purified by liquid/liquid extraction from ethyl acetate/brine, following a literature procedure for a related alkyl phosphinic acid.¹¹ Finally, phosphonium salt **4b** is expected to be obtained as a pure compound following recrystallization from boiling water, along the lines of the reported purification procedure for the

related phosphonium salt $[\text{P}(\text{CH}_2\text{Ph})_4]\text{Br}$.¹²

A second aspect that requires further experimentation is the isolation of a bis(silyl)alkylphosphine such as **3a** on a larger scale. An appropriate set-up for such an experiment could include the use of $\text{HP}(\text{SiCl}_3)_2$ (150 mg, 0.5 mmol) with 1-hexene (2 equiv) in hexane, using the same concentrations as reported on a 0.1 mmol scale. The glassware for this experiment would be a Schlenk flask, equipped with a J. Young valve and with a high surface to volume ratio, to mimic the properties of an NMR tube. Following photolysis, the product is expected to be amenable to the same workup as described for the reaction performed on a scale using 0.1 mmol of $\text{HP}(\text{SiCl}_3)_2$.

Other experiments that could form the basis of a future publication can also be envisioned. One compound of potential interest is diphosphine $(\text{Cl}_3\text{Si})_2\text{PP}(\text{SiCl}_3)_2$, which can be considered a dimer of the neutral bis(trichlorosilyl)phosphinyl radical. The diphosphine could plausibly be made from the one-electron oxidation of the phosphide anion as its TBA salt, $[\text{TBA}][\text{P}(\text{SiCl}_3)_2]$. Initial experiments to optimize such a procedure have so far led to the formation of a precipitate that has not yet undergone further characterization (Section 4.5.20). Initial experiments point to ferrocenium as the $[\text{BArF}_{24}]^-$ salt as a superior oxidant than the corresponding hexafluorophosphate salt. Additional characterization of the neutral phosphinyl radical could be achieved by oxidation of the phosphide anion using ferrocenium, followed by freezing the reaction mixture and analysis by low-temperature EPR spectroscopy.

Finally, generation of the bis(trichlorosilyl)phosphinyl radical is expected to have other applications for the formation of phosphorus-carbon bonds. Initial experiments (Section 4.5.19) show that irradiation of $\text{HP}(\text{SiCl}_3)_2$ in chlorobenzene (neat) leads to the formation of $\text{PhP}(\text{SiCl}_3)\text{H}$ and $\text{PhP}(\text{SiCl}_3)_2$, identified by ^{31}P NMR spectroscopy. Further experiments are required to improve the selectivity and yields of these two products, which could include testing other aryl(pseudo)halides as reaction partners (i.e. iodide, bromide, triflate). The use of the aryl(pseudo)halide in smaller excess than was used for the preliminary reaction (neat) would also be of interest. It is conceivable that the presence of aryl groups in the product could endow decreased photostability compared to the bis(silyl)alkylphosphines described in this chapter. Therefore, it would be beneficial to explore other initiation procedures for generating the bis(trichlorosilyl)phosphinyl radical, such as using thermal initiators such as AIBN or using photoinitiators that work with longer wave UV irradiation, such as BAPO. Such initiation procedures would also be of interest for the hydrophosphination of other substrates, for example styrenes, which were not found to react under the conditions reported in this chapter. Also of interest to the generation of the bis(trichlorosilyl)phosphinyl radical would be the determination of the quantum yield with which it forms from $\text{HP}(\text{SiCl}_3)_2$ under UV irradiation (254 nm), which could be determined by chemical actinometry.

4.5 Experimental methods

4.5.1 General methods

All manipulations were performed in a Vacuum Atmospheres model MO-40M glovebox under an inert atmosphere of purified N₂ or using standard Schlenk techniques. When reagents were removed from a stock bottle containing a Sure/Seal, the equivalent volume of dry nitrogen was injected into the bottle prior to removing the desired volume of solution with a syringe. All solvents were obtained anhydrous and oxygen-free by bubble degassing (argon) and purification by passing through columns of alumina and Q5.⁴⁴ Once collected, solvents were stored over activated 4 Å molecular sieves (20 wt%) inside the glovebox.⁴⁵ All glassware was oven-dried for at least 6 h prior to use, at temperatures greater than 150 °C.

Triflic acid (Strem) was used as received. Substrates 1,1-difluoro-2-vinylcyclopropane, vinylcyclohexane (Millipore-Sigma), 1-hexene, 3,3-dimethyl-1-butene, 2-methyl-1-pentene, methylenecyclohexane, cis-1,4-hex-diene, vinyltrimethylsilane, vinylcyclohexane, 1-hexyne, 1,6-heptadiene, trans-4-octene (all Sigma-Millipore) were degassed three times via the freeze-pump-thaw method then stored over activated 4 Å molecular sieves in the glovebox for 24 h prior to use.

[TBA]1 was prepared according to published methods.^{11,12}

Deuterated solvents were purchased from Cambridge Isotope Labs and were degassed three times by the freeze-pump-thaw method and stored over activated 4 Å molecular sieves for 48 h in the glovebox prior to use. Diatomaceous earth (Celite 435, EM Science), 4 Å molecular sieves (Millipore-Sigma) and basic alumina (Millipore-Sigma) were dried by heating to 200 °C under dynamic vacuum for at least 48 h prior to use. The temperature of the aluminum shot used to heat reagents or reaction mixtures was measured using a Hanna Instruments K-type Thermocouple Thermometer (model HI935005).

NMR spectra were obtained on Varian Inova 300 and 500 instruments equipped with Oxford Instruments superconducting magnets, on a Jeol ECZ-500 instrument equipped with an Oxford Instruments superconducting magnet, or on a Bruker Avance 400 instrument equipped with a Magnex Scientific or with a SpectroSpin superconducting magnet. ¹H and ¹³C NMR spectra were referenced to residual CD₂Cl₂ (¹H = 5.32 ppm, ¹³C = 54.0 ppm), C₆D₆ (¹H = 7.16 ppm, ¹³C = 128.06 ppm), CD₃CN (¹H = 1.94 ppm, ¹³C = 118.26 ppm) or CDCl₃ (¹H = 7.26 ppm, ¹³C = 77.16 ppm). ³¹P NMR spectra were referenced externally to 85% H₃PO₄ (0 ppm).

Infrared spectra were collected using a Bruker ATR-IR Tensor 37. Samples were removed from the glovebox in sealed vials and briefly handled in air prior to data collection.

High resolution mass spectral (HRMS) data were collected using a Jeol AccuTOF 4G LC-Plus mass spectrometer equipped with an Ion-Sense DART source. Data were calibrated to a sample of PEG-600 and were collected in positive-ion mode. Samples were prepared in DCM (10 μM concentration) and were briefly exposed to air (<5 s) before

being placed in front of the DART source.

Electrospray ionization mass spectrometry (ESI-MS) was performed using a Micromass Q-TOF ESI spectrometer.

Photochemistry was performed using a setup described previously.⁴⁶ Briefly, the apparatus comprises a Rayonet photochemical reactor (RPR200, Southern New England Ultra Violet Company) loaded with 16 RPR2537A lamps, each emitting ca. 35 W at 253.7 nm.

Electrochemistry was performed using a BioLogic Science Instruments SP-150 potentiostat using EC Lab V 10.44 software. Full details can be found in Section 4.5.7.

UV-vis spectroscopy was performed using an Agilent Technologies Cary 60 UV-vis spectrometer. Data was processed using the Cary WinUV software. Further details are provided in Section 4.5.6.

4.5.2 Preparation of $\text{HP}(\text{SiCl}_3)_2$ (**1**)

In the glovebox, [TBA]**1** (2.710 g, 5 mmol, 1 equiv) was weighed into a Schlenk flask (150 mL) containing a magnetic stir bar (2 cm), then slurried in pentane (100 mL). The resulting mixture was stirred vigorously for one hour resulting in a fine white powder. The reaction mixture was cooled in the glovebox coldwell until the solution began to freeze. Triflic acid (750 mg, 5.0 mmol, 1 equiv) was then added with rapid stirring. The slurry was stirred for 30 minutes then solids were allowed to settle over the course of five minutes. The solution was filtered through a frit (fine porosity, 15 mL). The solids were washed with pentane (2×10 mL) and the washings filtered through the same frit. The resulting solution was concentrated to ca. 30 mL and transferred to a H-cell used for trap-to-trap distillations. On the Schlenk line, pentane was removed under reduced pressure and the resulting oil was distilled (40 °C) and collected at -78 °C using a dry ice/acetone cooling bath. The distillate was transferred to a pre-weighed vial to give $\text{HP}(\text{SiCl}_3)_2$ as a clear colorless oil (550 mg, 1.87 mmol, 36%). ^1H NMR (500 MHz, C_6D_6 , δ) 2.21 (d, $J_{\text{P-H}} = 207$ Hz, $J_{\text{Si-H}} = 9$ Hz). ^{31}P NMR (162 MHz, C_6D_{12} , δ) -171.5 (d, $J_{\text{P-H}} = 207.1$ Hz, $J_{\text{P-Si}} = 57.4$ Hz).

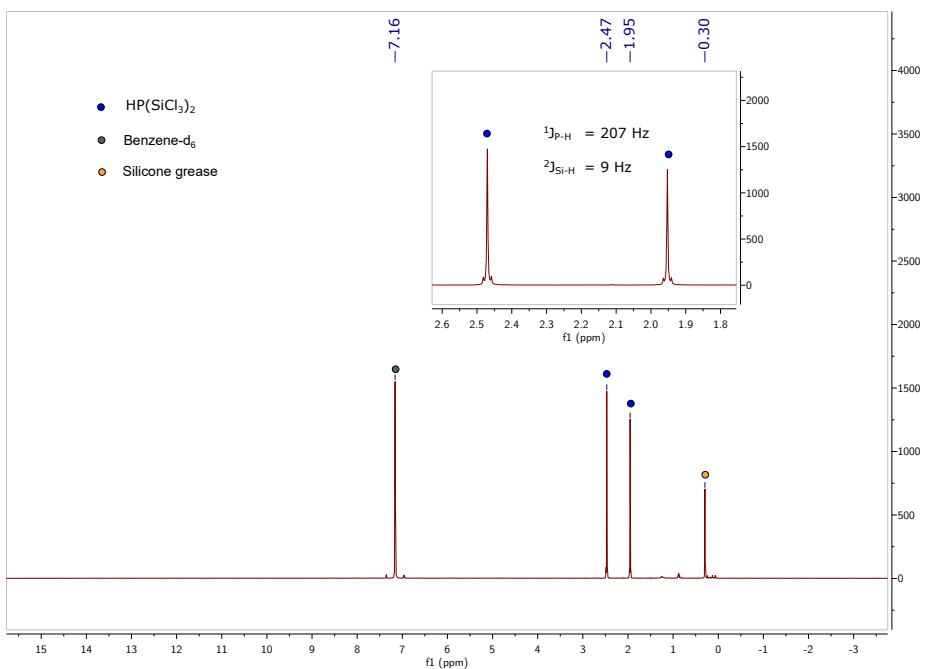


Figure 4.5 ^1H NMR spectra of $\text{HP}(\text{SiCl}_3)_2$ in C_6D_6 at 25°C , recorded at 500 MHz.

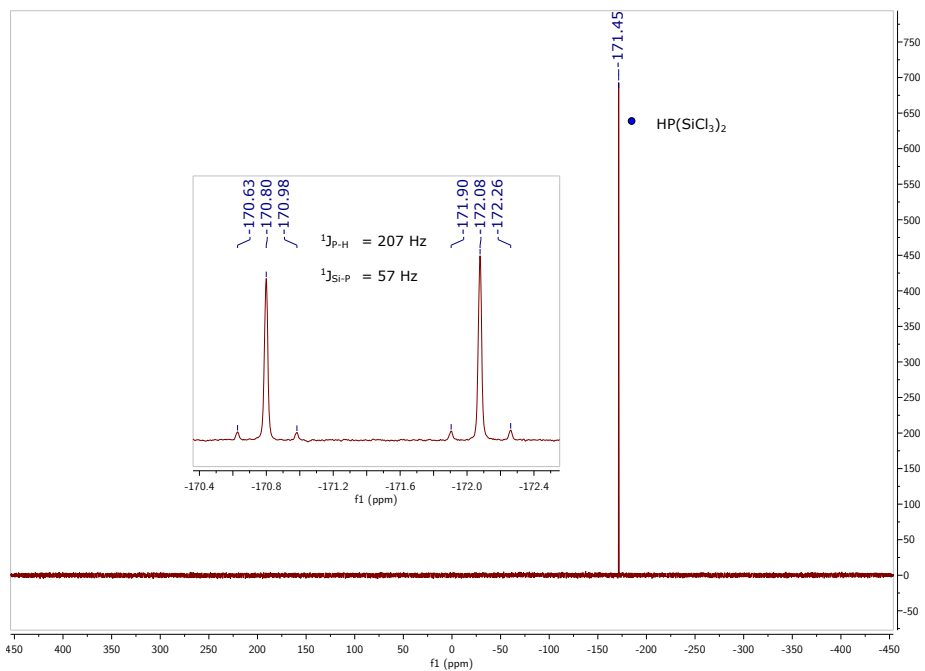
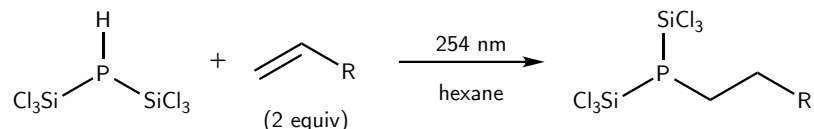


Figure 4.6 $^{31}\text{P}\{^1\text{H}\}$ and ^{31}P (inset) NMR spectra of $\text{HP}(\text{SiCl}_3)_2$ in C_6D_6 at 25°C , recorded at 162 MHz.

4.5.3 Preparation of bis(trichlorosilyl)alkylphosphines

4.5.3.1 General procedure



Scheme 4.2 General method for preparing bis(trichlorosilyl)alkylphosphines.

In the glovebox, $\text{HP}(\text{SiCl}_3)_2$ (30 mg, 0.1 mmol, 1 equiv) was weighed into a borosilicate NMR tube equipped with a J. Young valve. The phosphine was diluted in hexane (0.5 mL) then the substrate (0.2 mmol, 2 equiv) was added using a microsyringe (50 μL). An NMR spectrum of the material was acquired, then the reaction mixture was irradiated (254 nm) and progress was monitored by ^{31}P NMR spectroscopy. After all of the $\text{HP}(\text{SiCl}_3)_2$ had been consumed (times provided in the main text), the reaction mixture was filtered through glass microfiber in a pipette into a pre-weighed vial. The NMR tube was washed with hexane ($3 \times 1 \text{ mL}$) and the washings were filtered into the vial. Volatile material was removed under reduced pressure to give the corresponding bis(trichlorosilyl)alkylphosphine as a colorless oil.

In two cases (**3i** and **3k**) the obtained oils were judged to be of insufficient purity to record an isolated yield. In these cases, a yield was obtained spectroscopically. A capillary containing PPh_3 as an external standard (prepared as described in Section 4.5.4) was inserted into the NMR tube and a quantitative $^{31}\text{P}\{^1\text{H}\}$ spectrum was recorded before and after irradiation. The products were isolated as described above to obtain characterization data.

All products were characterized in CDCl_3 on a 500 MHz instrument at 25 $^\circ\text{C}$. ^1H , ^{31}P , $^{31}\text{P}\{^1\text{H}\}$, and $^{13}\text{C}\{^1\text{H}\}$ were collected for all products. HRMS was recorded according to the General Methods section 4.5.1.

4.5.3.2 From 1-hexene to give 3a

^1H NMR (500 MHz, CDCl_3 , δ) 2.17–2.07 (m, 2H), 1.70 (ddt, $J = 15.6, 11.5, 7.7$ Hz, 2H), 1.46 (p, $J = 7.2$ Hz, 2H), 1.32 (dq, $J = 7.5, 3.4$ Hz, 4H), 0.96–0.84 (m, 3H). ^{13}C NMR (126 MHz, CDCl_3 , δ) 31.06, 30.28 (d, $J = 13.5$ Hz), 29.05 (d, $J = 15.1$ Hz), 22.42, 18.04 (d, $J = 16.3$ Hz), 13.97. $^{31}\text{P}\{^1\text{H}\}$ NMR (203 MHz, CDCl_3 , δ) -111.09 ($J_{\text{P-Si}} = 68.2$ Hz). ^{31}P NMR (203 MHz, CDCl_3 , δ) -111.09 (t, $J_{\text{P-H}} = 11.3$ Hz $J_{\text{P-Si}} = 68.2$ Hz). $^{29}\text{Si}\{^1\text{H}\}$ (99 MHz, CDCl_3 , δ) HRMS (m/z , (%relative intensity)): $[\text{M} + \text{H} + 2(\text{H} \leftrightarrow \text{SiCl}_3)]^+$ calcd for $\text{C}_6\text{H}_{16}\text{P}_1$, 119.098964; found, 119.097130 (100%).

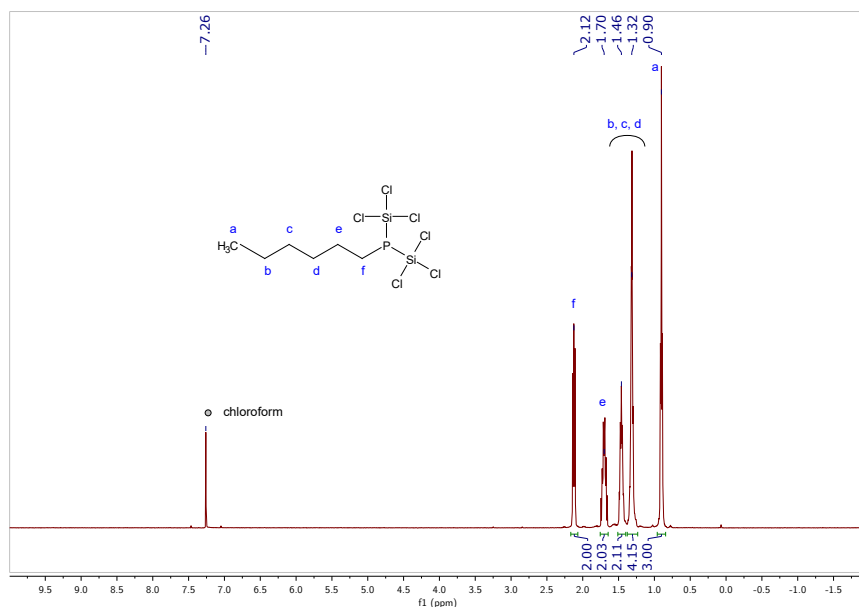


Figure 4.7 ^1H NMR spectra of **3a** in CDCl_3 at 25 °C, recorded at 500 MHz.

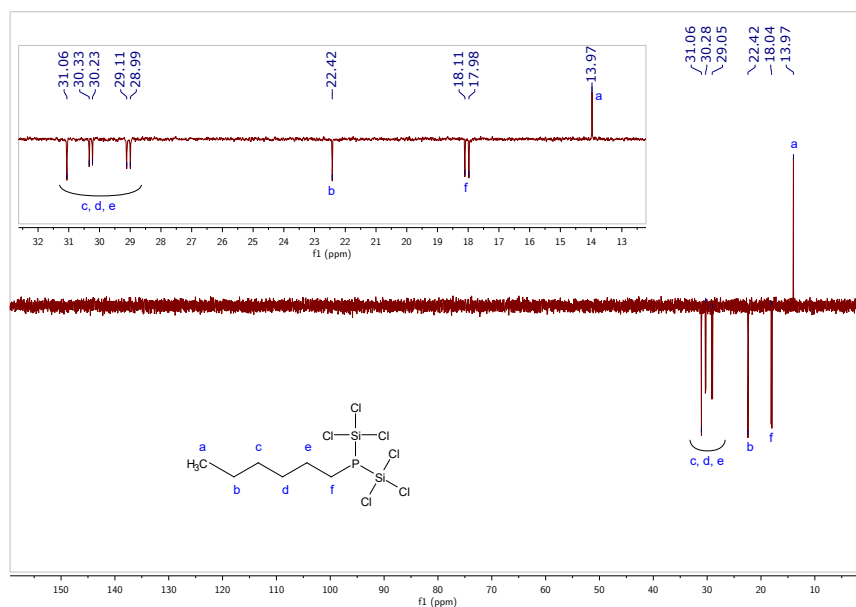


Figure 4.8 ¹³C{¹H} NMR spectrum of **3a** in CDCl₃ at 25 °C, recorded at 126 MHz.

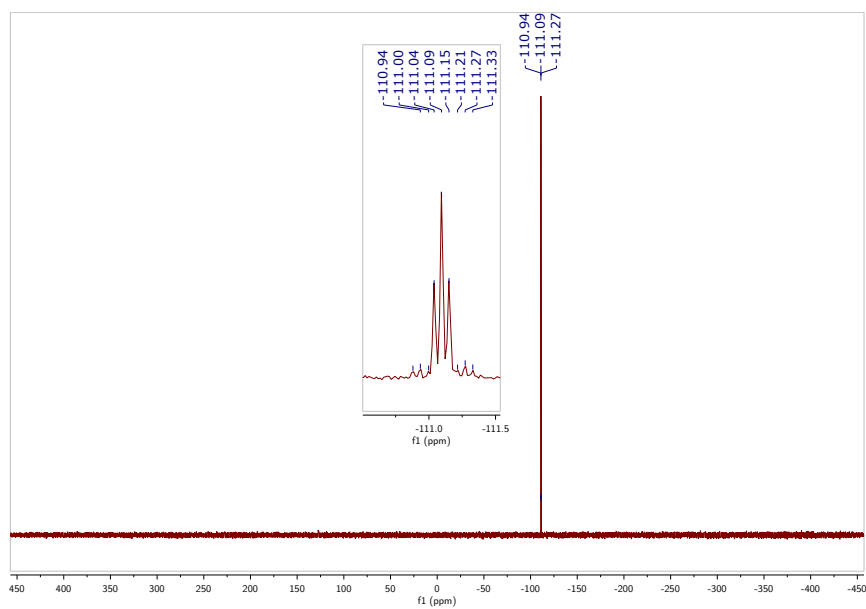


Figure 4.9 ³¹P{¹H} and ³¹P (inset) NMR spectra of **3a** in CDCl₃ at 25 °C, recorded at 203 MHz.

4.5.3.3 From 3,3-dimethyl-1-butene to give 3b

^1H NMR (500 MHz, CDCl_3 , δ) 2.10–2.04 (m, 2H), 1.62–1.55 (m, 2H), 0.94 (s, 9H). ^{13}C NMR (126 MHz, CDCl_3 , δ) 43.54 (d, $J = 15.1$ Hz), 31.89 (d, $J = 14.0$ Hz), 28.90, 13.73 (d, $J = 15.7$ Hz). $^{31}\text{P}\{^1\text{H}\}$ NMR (203 MHz, CDCl_3 , δ) -108.36 ($J_{\text{P-Si}} = 68.1$ Hz). ^{31}P NMR (203 MHz, CDCl_3 , δ) -108.36 (t, $J = 7.8$ Hz, $J_{\text{P-Si}} = 68.1$ Hz). HRMS (m/z , (%relative intensity)): $[\text{M} + \text{H} + 2(\text{H}\leftrightarrow\text{SiCl}_3)]^+$ calcd for $\text{C}_6\text{H}_{16}\text{P}_1$, 119.098964; found, 119.09172 (66.8%).

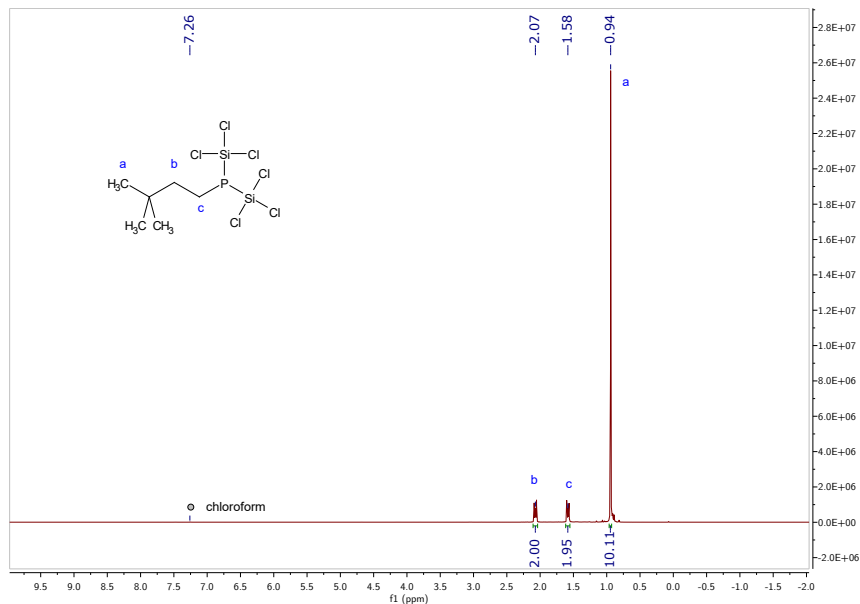


Figure 4.10 ^1H NMR spectra of **3b** in CDCl_3 at 25 °C, recorded at 500 MHz.

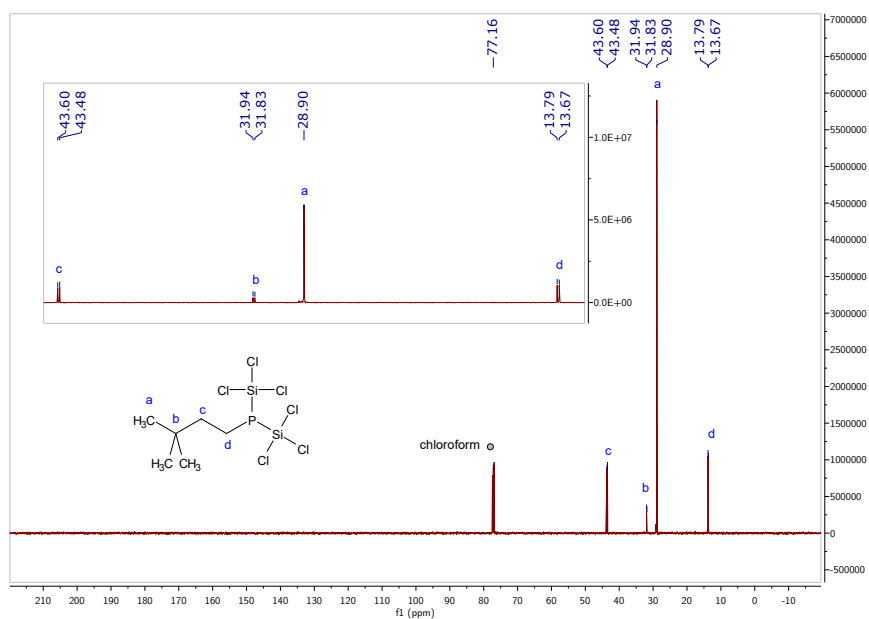


Figure 4.11 $^{13}\text{C}\{^1\text{H}\}$ NMR spectrum of **3b** in CDCl_3 at $25\text{ }^\circ\text{C}$, recorded at 126 MHz.

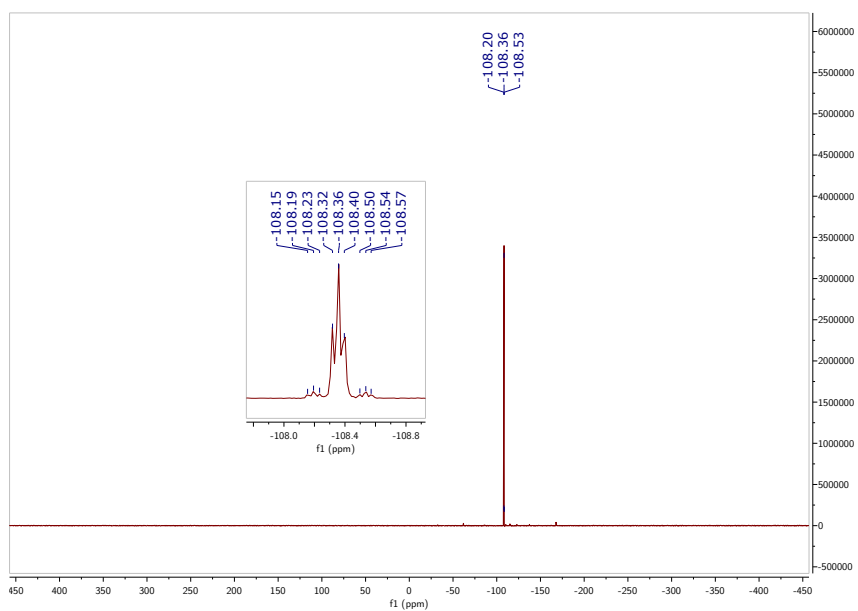


Figure 4.12 $^{31}\text{P}\{^1\text{H}\}$ and ^{31}P (inset) NMR spectra of **3b** in CDCl_3 at $25\text{ }^\circ\text{C}$, recorded at 203 MHz.

4.5.3.4 From methylenecyclohexane to give **3c**

^1H NMR (500 MHz, CDCl_3 , δ) 2.04 (dd, $J = 7.2, 2.3$ Hz, 2H), 1.97–1.89 (m, 2H), 1.76 (dt, $J = 12.7, 3.5$ Hz, 2H), 1.68 (dddd, $J = 12.2, 5.1, 3.2, 1.5$ Hz, 1H), 1.55 (ddtt, $J = 13.0, 10.9, 7.4, 3.7$ Hz, 1H), 1.29 (dt, $J = 12.4, 3.5$ Hz, 1H), 1.26–1.12 (m, 2H), 1.00 (qd, $J = 12.4, 3.5$ Hz, 2H). ^{13}C NMR (126 MHz, CDCl_3 , δ) 37.48 (d, $J = 14.1$ Hz), 34.00 (d, $J = 10.2$ Hz), 26.01 (d, $J = 1.1$ Hz), 25.99 (d, $J = 0.9$ Hz), 25.52 (d, $J = 16.2$ Hz). $^{31}\text{P}\{^1\text{H}\}$ NMR (203 MHz, CDCl_3 , δ) -117.04 ($J_{\text{P-Si}} = 67.2$ Hz). ^{31}P NMR (203 MHz, CDCl_3 , δ) -117.04 (d, $J = 8.5$ Hz, $J_{\text{P-Si}} = 67.2$ Hz). HRMS (m/z , (%relative intensity)): $[\text{M} + \text{H} + 2(\text{H} \leftrightarrow \text{SiCl}_3)]^+$ calcd for $\text{C}_7\text{H}_{16}\text{P}_1$, 131.098964; found, 131.09917 (100%).

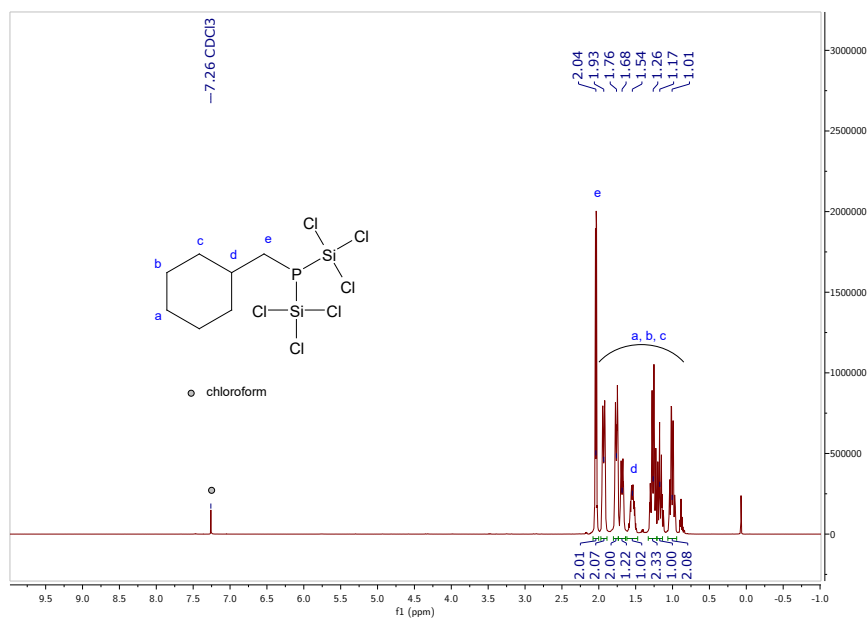


Figure 4.13 ^1H NMR spectra of **3c** in CDCl_3 at 25 °C, recorded at 500 MHz.

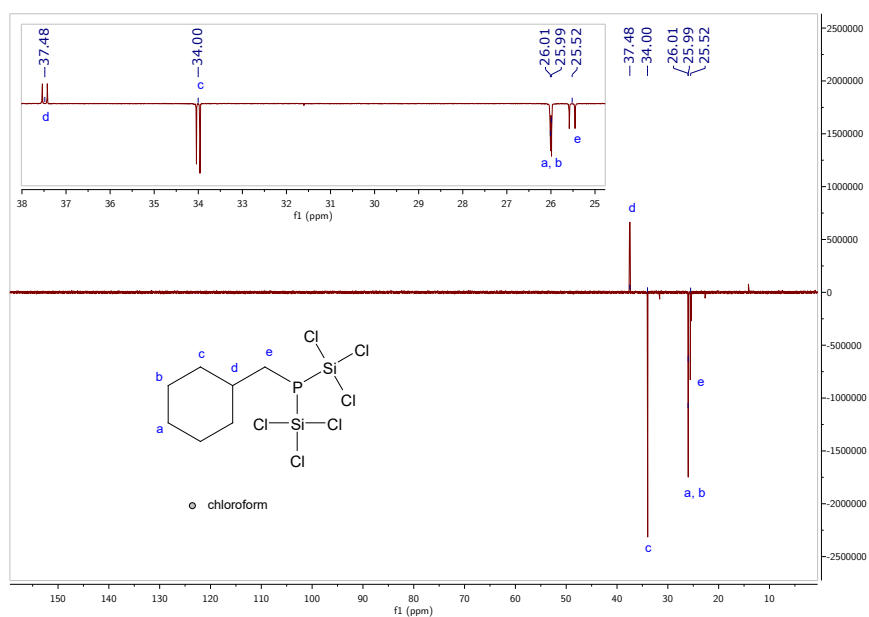


Figure 4.14 ¹³C (DEPT) NMR spectrum of **3c** in CDCl₃ at 25 °C, recorded at 126 MHz.

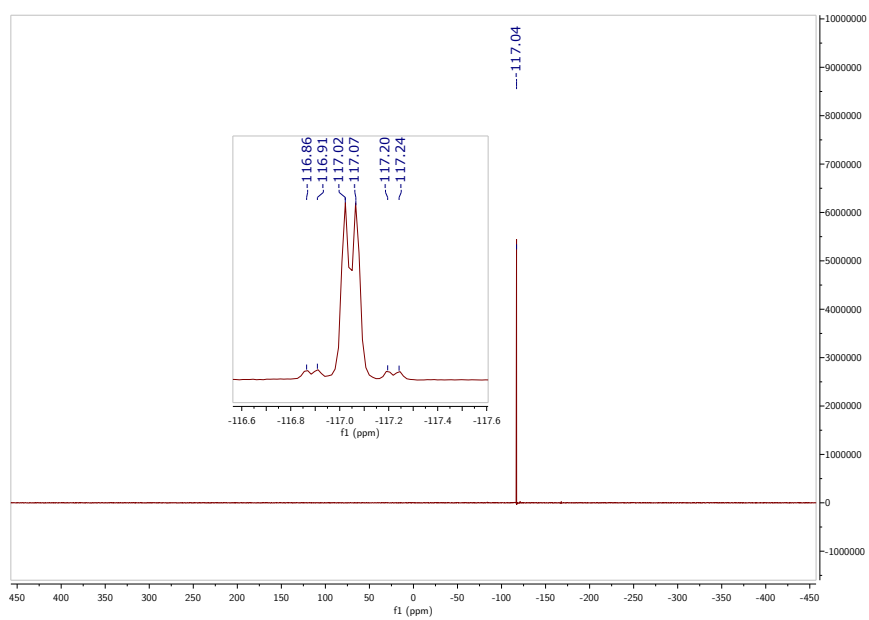


Figure 4.15 ³¹P{¹H} and ³¹P (inset) NMR spectra of **3c** in CDCl₃ at 25 °C, recorded at 203 MHz.

4.5.3.5 From vinylcyclohexane to give **3d**

^1H NMR (500 MHz, CDCl_3 , δ) 2.19–2.08 (m, 2H), 1.80–1.69 (m, 4H), 1.66 (dddt, $J = 12.1$, 5.2, 3.6, 1.8 Hz, 1H), 1.59 (tdd, $J = 10.9$, 8.3, 6.4 Hz, 2H), 1.38 (dddd, $J = 14.7$, 8.0, 6.6, 4.7, 2.4 Hz, 1H), 1.31–1.10 (m, 3H), 0.93 (qd, $J = 14.1$, 13.0, 4.2 Hz, 2H). ^{13}C NMR (126 MHz, CDCl_3 , δ) 38.48 (d, $J = 13.3$ Hz), 36.47 (d, $J = 14.7$ Hz), 32.64, 26.39, 26.06, 15.64 (d, $J = 16.1$ Hz). $^{31}\text{P}\{^1\text{H}\}$ NMR (203 MHz, CDCl_3 , δ) -110.52 ($J_{\text{P-Si}} = 69.1$ Hz). ^{31}P NMR (203 MHz, CDCl_3 , δ) -110.52 (d, $J = 10.6$ Hz, $J_{\text{P-Si}} = 69.1$ Hz). HRMS (m/z , (%relative intensity)): $[\text{M} + \text{H} + 2(\text{H} \leftrightarrow \text{SiCl}_3)]^+$ calcd for $\text{C}_8\text{H}_{18}\text{P}_1$, 145.114614; found, 145.11421 (100%).

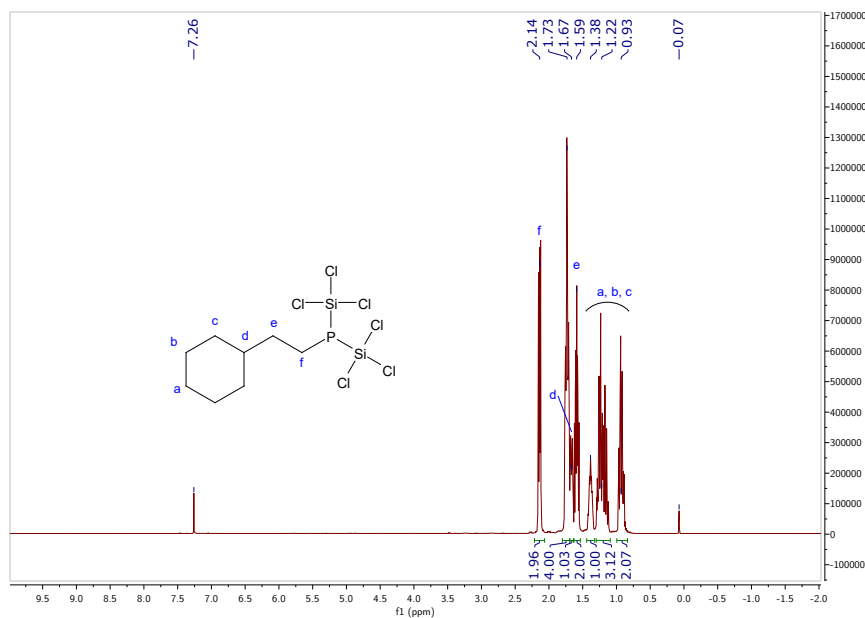


Figure 4.16 ^1H NMR spectra of **3d** in CDCl_3 at 25 °C, recorded at 500 MHz.

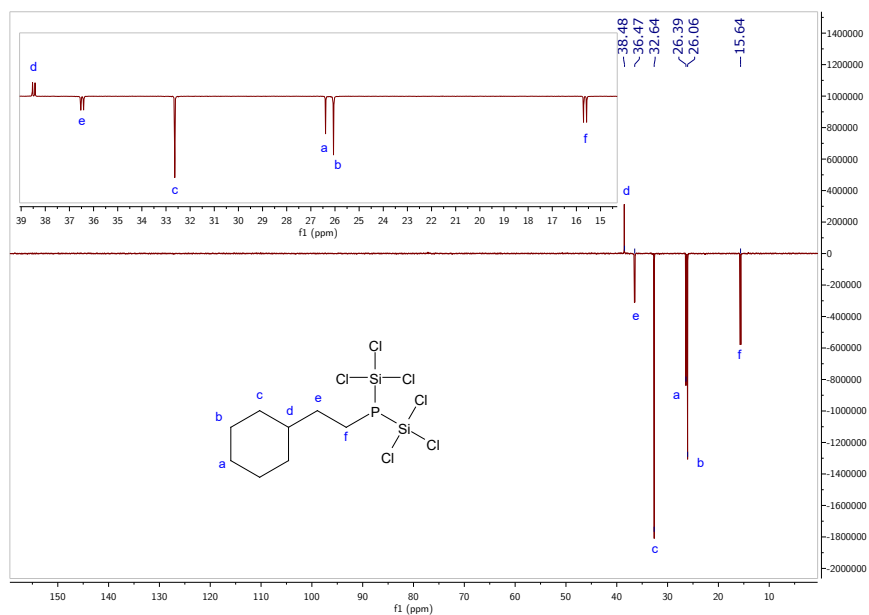


Figure 4.17 ^{13}C (DEPT) NMR spectrum of **3d** in CDCl_3 at 25°C , recorded at 126 MHz.

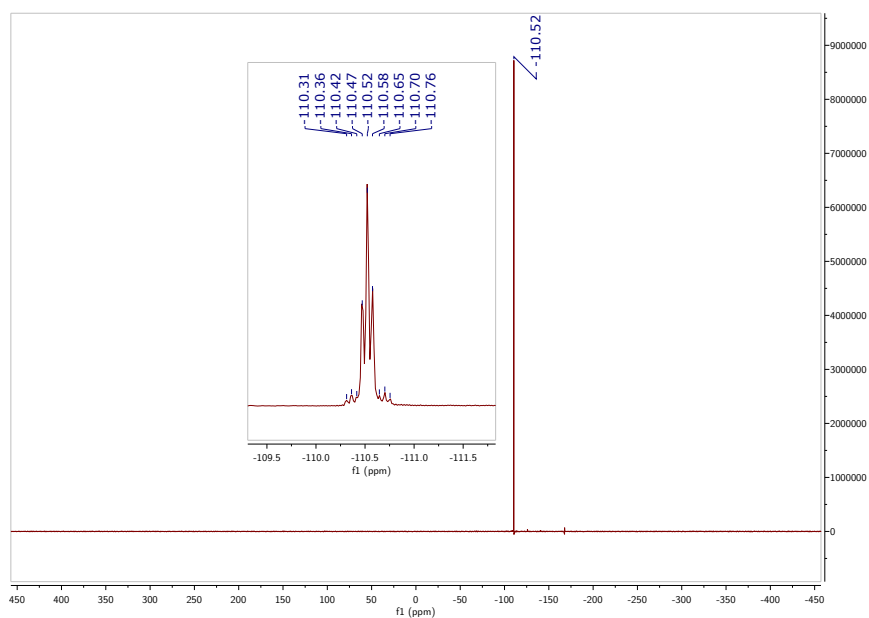


Figure 4.18 $^{31}\text{P}\{^1\text{H}\}$ and ^{31}P (inset) NMR spectra of **3d** in CDCl_3 at 25°C , recorded at 203 MHz.

4.5.3.6 From 2-methyl-1-pentene to give 3e

^1H NMR (500 MHz, CDCl_3 , δ) 2.20 (ddd, $J = 13.9, 5.9, 3.7$ Hz, 1H), 1.92 (ddd, $J = 13.9, 8.2, 1.0$ Hz, 1H), 1.83–1.71 (m, 1H), 1.51–1.22 (m, 4H), 1.07 (d, $J = 6.6$ Hz, 3H), 0.92 (t, $J = 7.1$ Hz, 3H). ^{13}C NMR (126 MHz, CDCl_3 , δ) 39.75 (d, $J = 9.7$ Hz), 32.79 (d, $J = 14.3$ Hz), 25.62 (d, $J = 15.7$ Hz), 20.41 (d, $J = 10.0$ Hz), 19.94, 14.05. $^{31}\text{P}\{^1\text{H}\}$ NMR (203 MHz, CDCl_3 , δ) -116.16 ($J_{\text{P-Si}} = 66.3$ Hz). ^{31}P NMR (203 MHz, CDCl_3 , δ) -116.16 (d, $J = 10.2$ Hz, $J_{\text{P-Si}} = 66.3$ Hz). HRMS (m/z , (%relative intensity)): $[\text{M} + \text{H} + 2(\text{H} \leftrightarrow \text{SiCl}_3)]^+$ calcd for $\text{C}_6\text{H}_{16}\text{P}_1$, 119.098964; found, 119.09773 (100%).

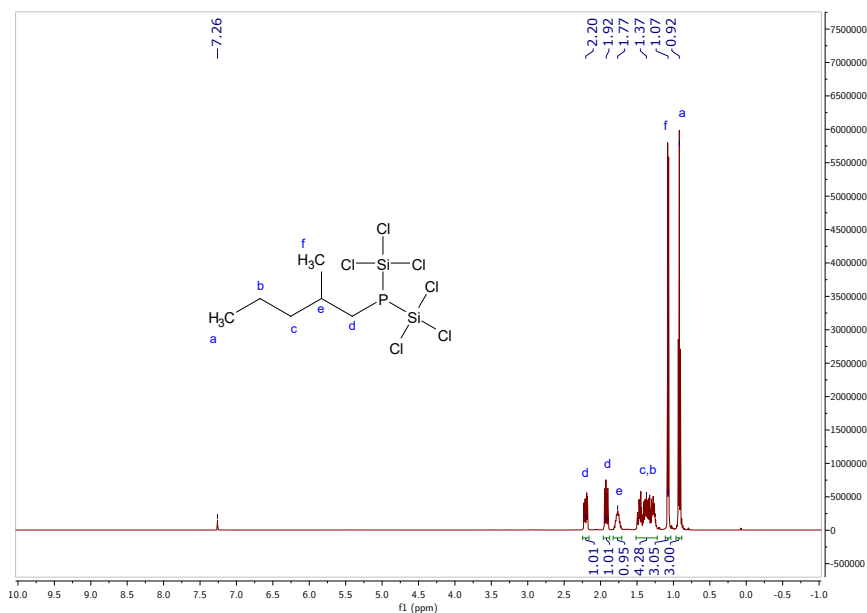


Figure 4.19 ^1H NMR spectra of **3e** in CDCl_3 at 25 °C, recorded at 500 MHz.

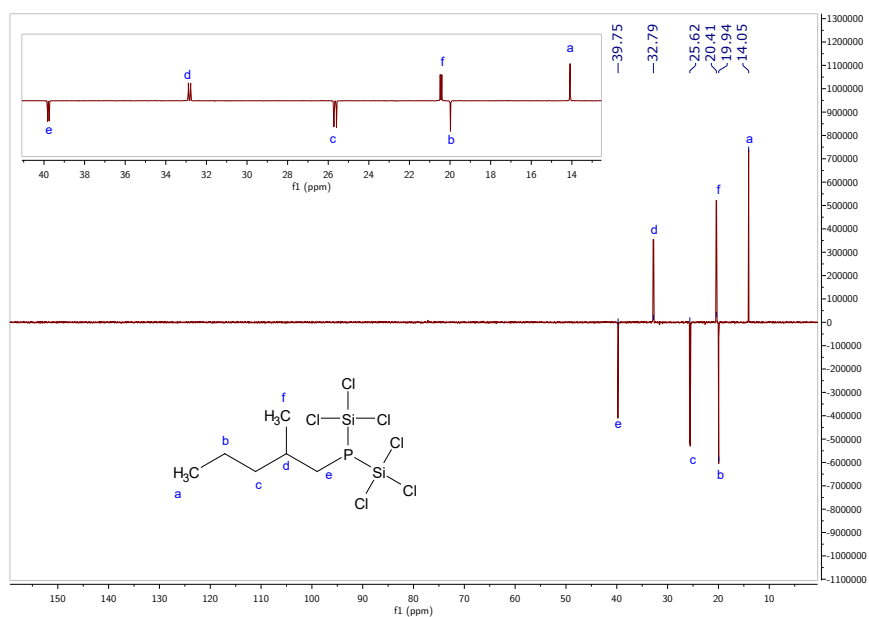


Figure 4.20 ^{13}C (DEPT) NMR spectrum of **3e** in CDCl_3 at 25°C , recorded at 126 MHz.

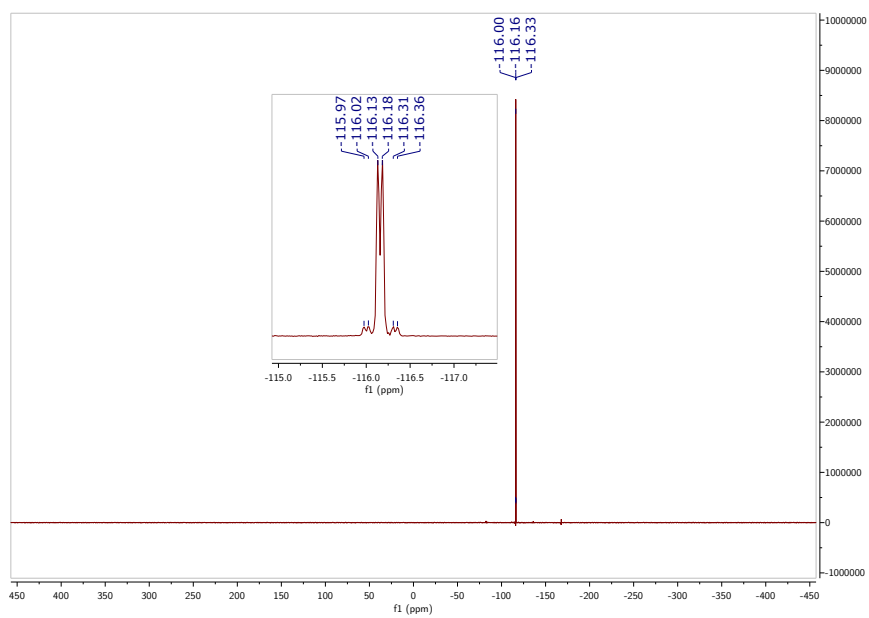


Figure 4.21 $^{31}\text{P}\{^1\text{H}\}$ and ^{31}P (inset) NMR spectra of **3e** in CDCl_3 at 25°C , recorded at 203 MHz.

4.5.3.7 From *n*-butyl allyl ether to give **3f**

^1H NMR (500 MHz, CDCl_3 , δ) 3.52 (t, $J = 5.9$ Hz, 2H), 3.42 (t, $J = 6.6$ Hz, 2H), 2.23 (ddd, $J = 9.4, 5.9, 1.3$ Hz, 2H), 1.96 (dddd, $J = 15.7, 12.0, 7.8, 5.9$ Hz, 2H), 1.61–1.51 (m, 2H), 1.43–1.33 (m, 2H), 0.92 (t, $J = 7.4$ Hz, 3H). ^{13}C NMR (126 MHz, CDCl_3 , δ) 70.76, 69.54 (d, $J = 14.0$ Hz), 31.71, 28.94 (d, $J = 15.7$ Hz), 19.32, 14.74 (d, $J = 15.8$ Hz), 13.88. $^{31}\text{P}\{^1\text{H}\}$ NMR (203 MHz, CDCl_3 , δ) -112.72 ($J_{\text{P-Si}} = 66.7$ Hz). ^{31}P NMR (203 MHz, CDCl_3 , δ) -112.72 (d, $J = 12.0$ Hz, $J_{\text{P-Si}} = 66.7$ Hz). HRMS (m/z , (%relative intensity)): $[\text{M} + \text{H} + 2(\text{H} \leftrightarrow \text{SiCl}_3)]^+$ calcd for $\text{C}_7\text{H}_{18}\text{O}_1\text{P}_1$, 149.109529; found, 149.10042 (100%).

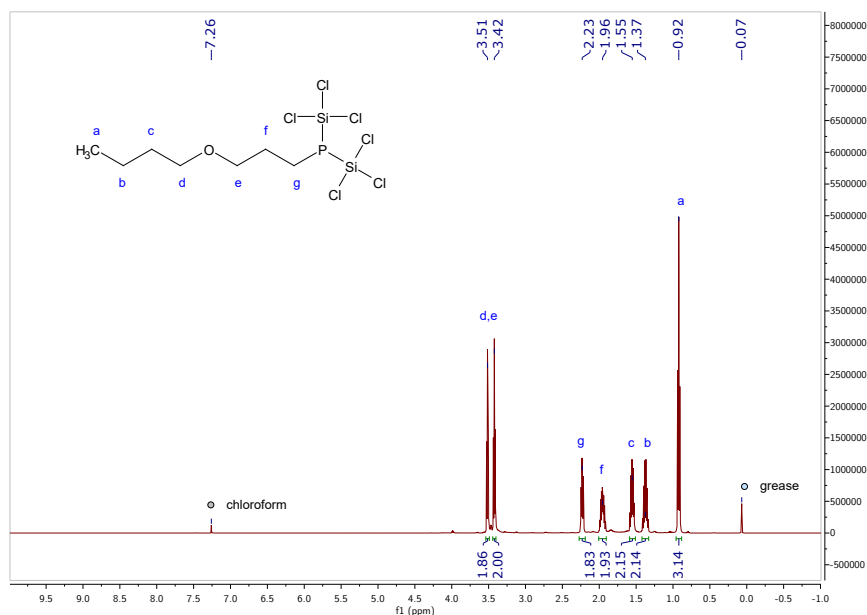


Figure 4.22 ^1H NMR spectra of **3f** in CDCl_3 at 25 °C, recorded at 500 MHz.

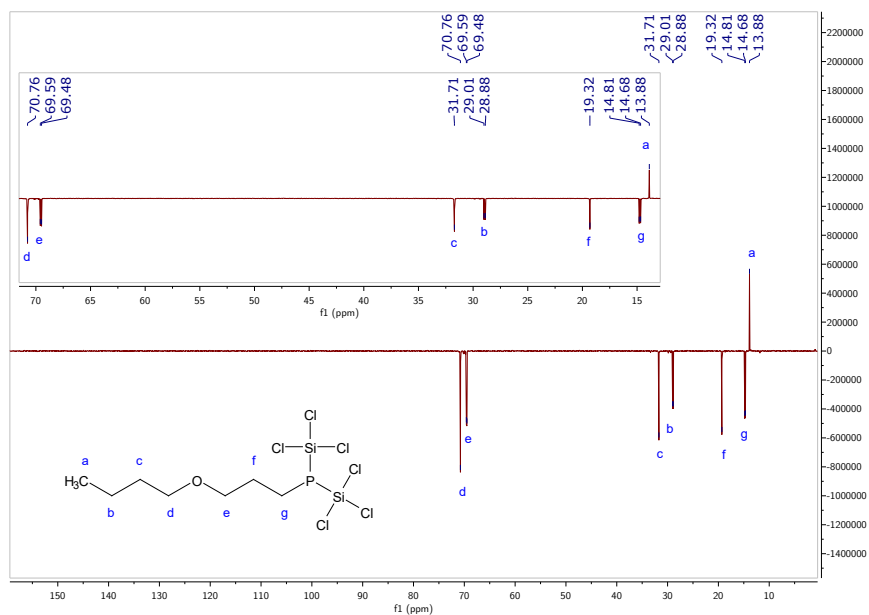


Figure 4.23 ^{13}C (DEPT) NMR spectrum of **3f** in CDCl_3 at 25°C , recorded at 126 MHz.

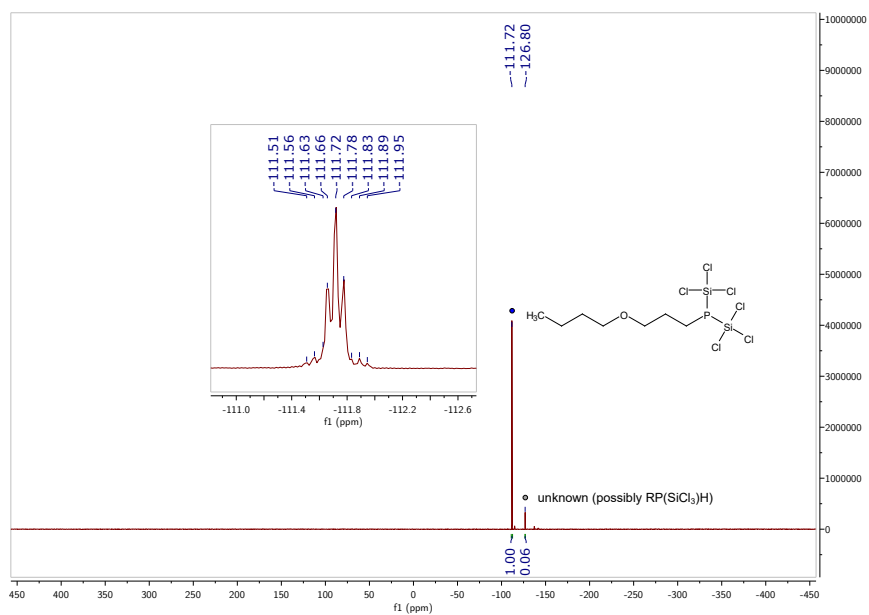


Figure 4.24 $^{31}\text{P}\{^1\text{H}\}$ and ^{31}P NMR spectra of **3f** in CDCl_3 at 25°C , recorded at 203 MHz.

4.5.3.8 From allylchloride to give 3g

^1H NMR (500 MHz, CDCl_3 , δ) 3.66 (t, $J = 6.1$ Hz, 2H), 2.33–2.27 (m, 2H), 2.21–2.12 (m, 2H). ^{13}C NMR (126 MHz, CDCl_3 , δ) 44.21 (d, $J = 16.0$ Hz), 31.45 (d, $J = 17.9$ Hz), 15.22 (d, $J = 16.1$ Hz). $^{31}\text{P}\{^1\text{H}\}$ NMR (203 MHz, CDCl_3 , δ) -112.68 ($J_{\text{P-Si}} = 63.2$ Hz). ^{31}P NMR (203 MHz, CDCl_3 , δ) -112.68 (d, $J = 1.3$ Hz, $J_{\text{P-Si}} = 63.2$ Hz). HRMS (m/z , (%relative intensity)): $[\text{M} + \text{H} + 2(\text{H} \leftrightarrow \text{SiCl}_3)]^+$ calcd for $\text{C}_3\text{H}_9\text{Cl}_1\text{P}_1$, 111.013041; found, 111.0081 (48%).

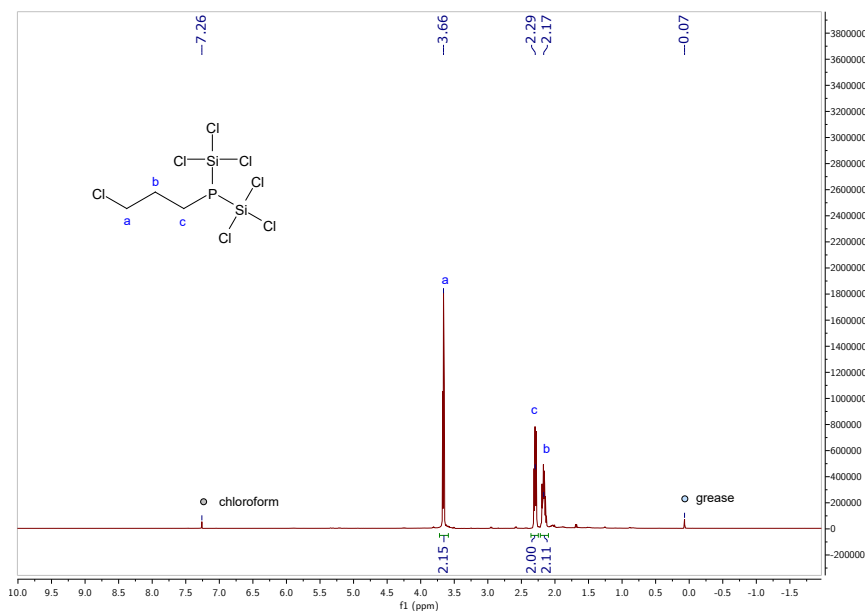


Figure 4.25 ^1H NMR spectra of **3g** in CDCl_3 at 25 °C, recorded at 500 MHz.

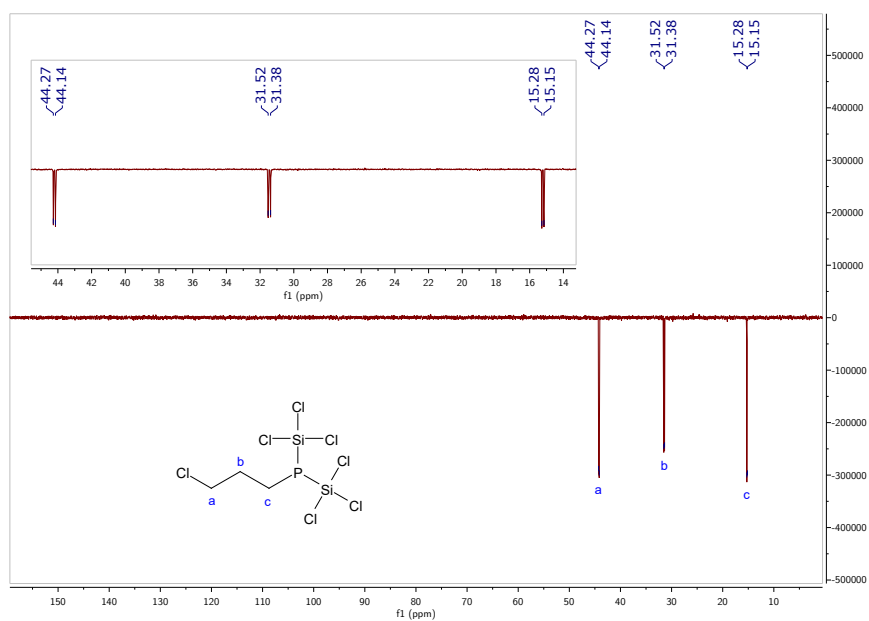


Figure 4.26 ^{13}C (DEPT) NMR spectrum of **3g** in CDCl_3 at 25 °C, recorded at 126 MHz.

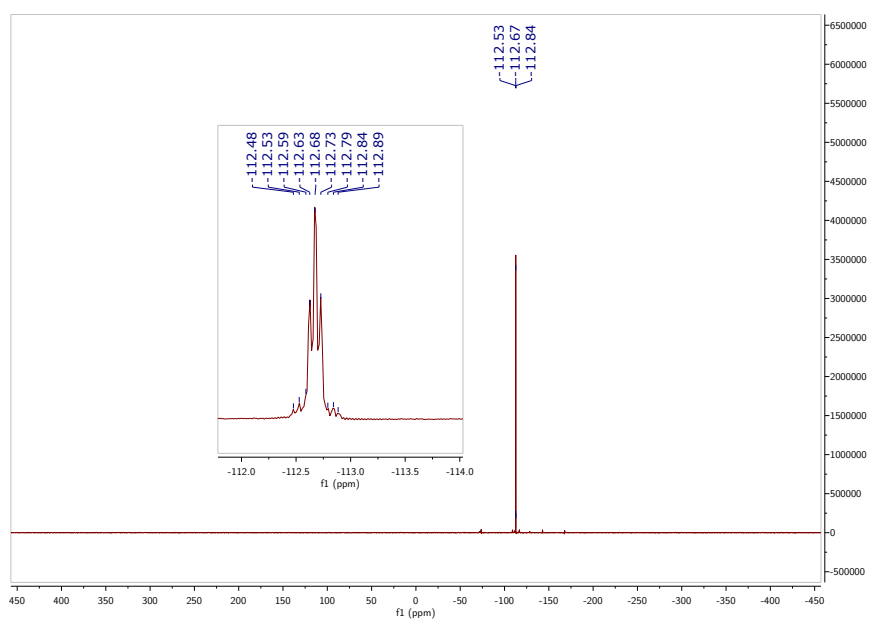


Figure 4.27 $^{31}\text{P}\{^1\text{H}\}$ and ^{31}P (inset) NMR spectra of **3g** in CDCl_3 at 25 °C, recorded at 203 MHz.

4.5.3.9 From vinyltrimethylsilane to give 3h

^1H NMR (500 MHz, CDCl_3 , δ) 2.19–2.09 (m, 2H), 0.99–0.91 (m, 2H), 0.07 (s, 9H). ^{13}C NMR (126 MHz, CDCl_3 , δ) 17.08 (d, $J = 8.6$ Hz), 13.43 (d, $J = 20.7$ Hz), -2.15 . $^{31}\text{P}\{^1\text{H}\}$ NMR (203 MHz, CDCl_3 , δ) -102.65 ($J_{\text{P-Si}} = 73.4$ Hz). ^{31}P NMR (203 MHz, CDCl_3 , δ) -102.65 (d, $J = 11.2$ Hz, $J_{\text{P-Si}} = 73.4$ Hz). HRMS (m/z , (%relative intensity)): $[\text{M} + \text{H} + 2(\text{H}\leftrightarrow\text{SiCl}_3)]^+$ calcd for $\text{C}_5\text{H}_{16}\text{P}_1\text{Si}_1$, 135.075891; found, 135.07529 (100%).

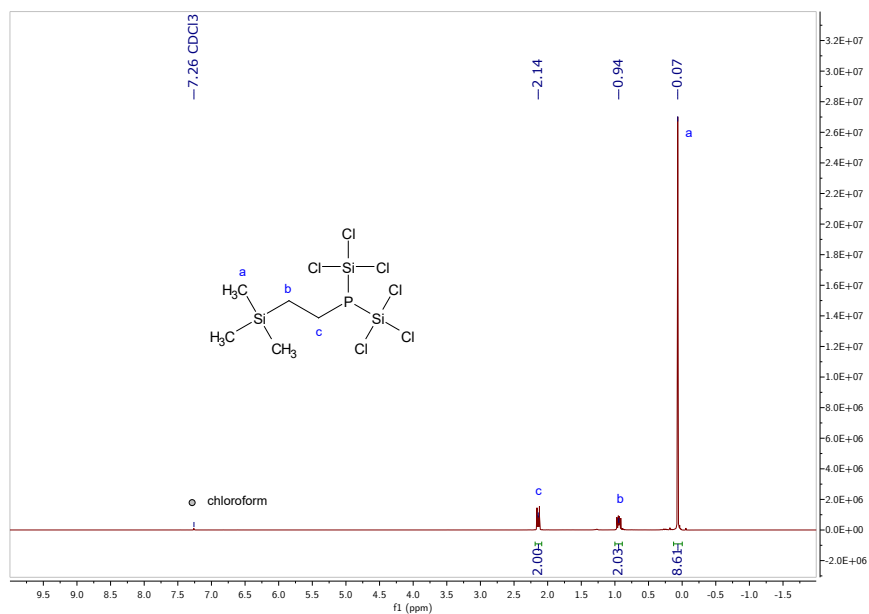


Figure 4.28 ^1H NMR spectra of **3h** in CDCl_3 at 25 °C, recorded at 500 MHz.

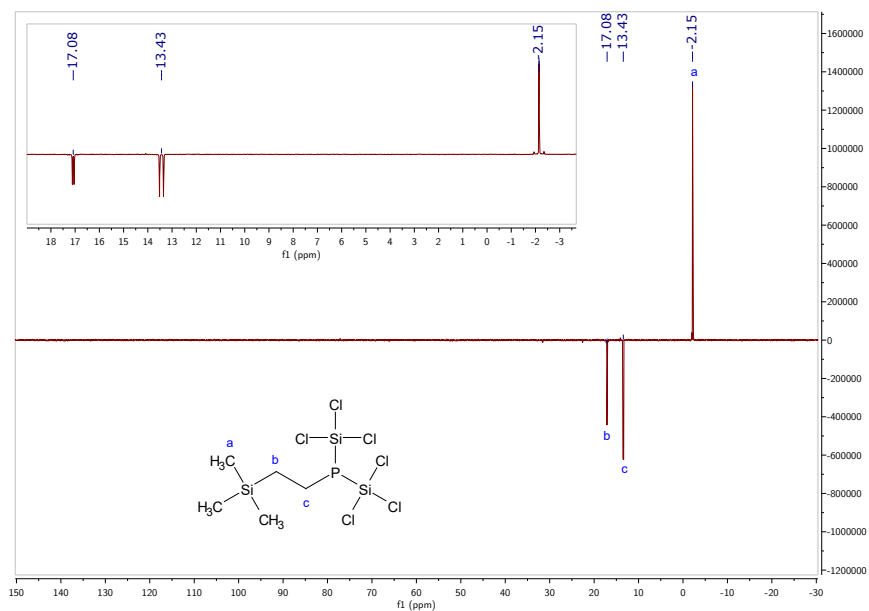


Figure 4.29 ^{13}C (DEPT) NMR spectrum of **3h** in CDCl_3 at 25°C , recorded at 126 MHz.

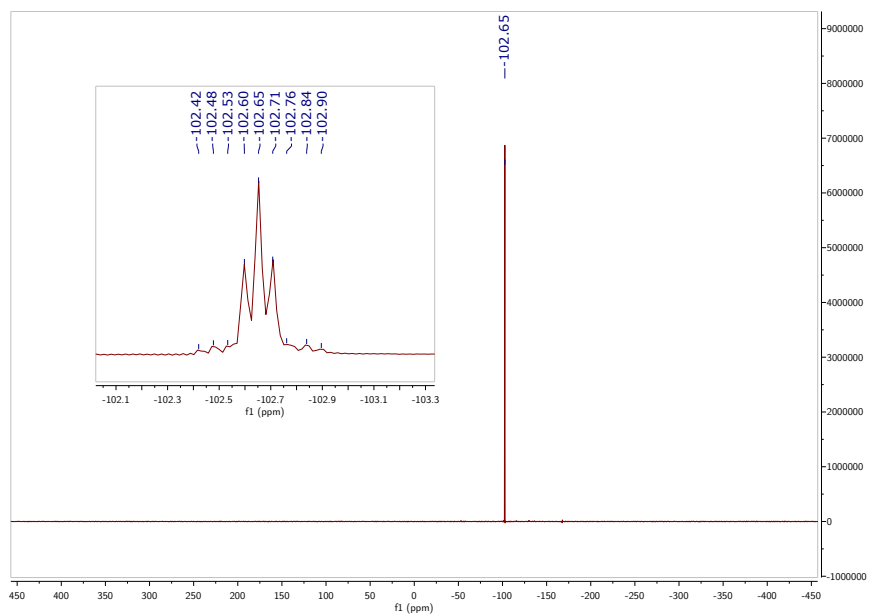


Figure 4.30 $^{31}\text{P}\{^1\text{H}\}$ and ^{31}P (inset) NMR spectra of **3h** in CDCl_3 at 25°C , recorded at 203 MHz.

4.5.3.10 From 1,6-heptadiene to give **3i**

Note: 0.5 mmol, 5 equiv, of substrate was used in this reaction instead of 0.2 mmol as described in the general procedure. ^1H NMR (500 MHz, CDCl_3 , δ) 5.82 (ddt, $J = 17.0$, 10.2, 6.7 Hz, 1H), 5.08–4.93 (m, 2H), 2.15 (dd, $J = 9.6$, 6.4 Hz, 2H), 2.09 (q, $J = 7.0$ Hz, 2H), 1.78–1.69 (m, 2H), 1.54–1.37 (m, 4H). ^{13}C NMR (126 MHz, CDCl_3 , δ) 138.45, 114.75, 33.45, 30.03 (d, $J = 13.6$ Hz), 28.95 (d, $J = 15.3$ Hz), 28.13, 17.99 (d, $J = 16.3$ Hz). $^{31}\text{P}\{^1\text{H}\}$ NMR (203 MHz, CDCl_3 , δ) -111.13 ($J_{\text{P-Si}} = 66.5$ Hz). ^{31}P NMR (203 MHz, CDCl_3 , δ) -111.13 (d, $J = 22.8$ Hz, $J_{\text{P-Si}} = 66.5$ Hz). HRMS (m/z , (%relative intensity)): $[\text{M} + \text{H} + 2(\text{H}\leftrightarrow\text{SiCl}_3)]^+$ calcd for $\text{C}_7\text{H}_{16}\text{P}_1$, 131.098964; found, 131.08459 (100%).

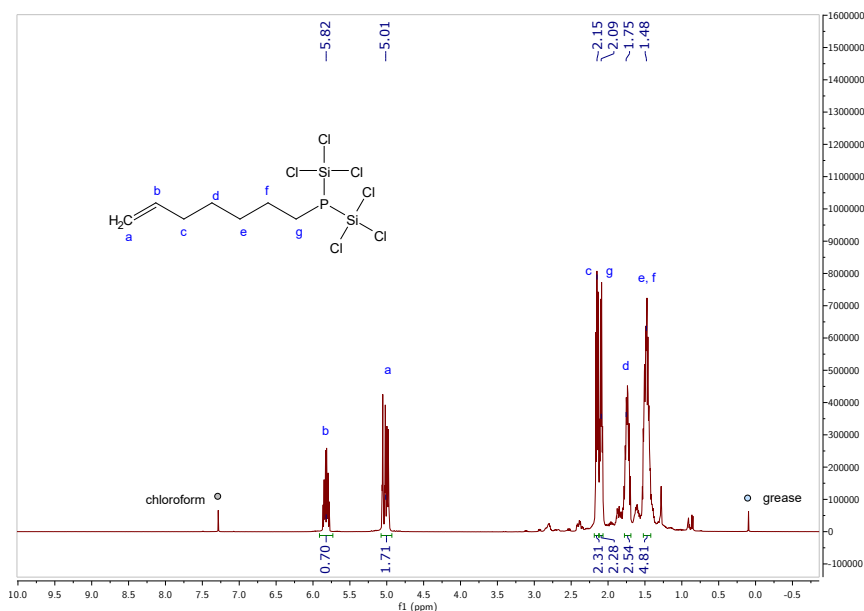


Figure 4.31 ^1H NMR spectra of **3i** in CDCl_3 at 25 °C, recorded at 500 MHz.

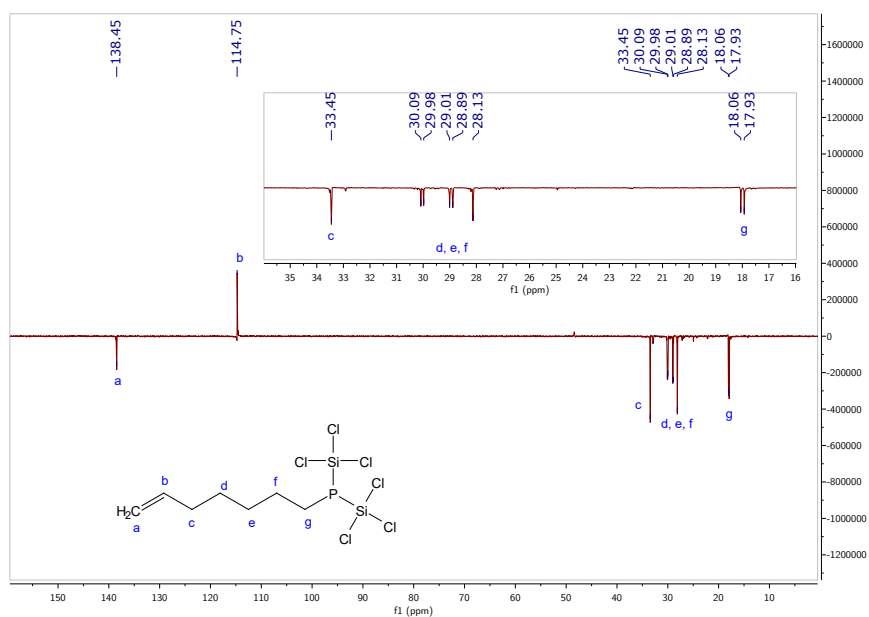


Figure 4.32 ^{13}C (DEPT) NMR spectrum of **3i** in CDCl_3 at 25°C , recorded at 126 MHz.

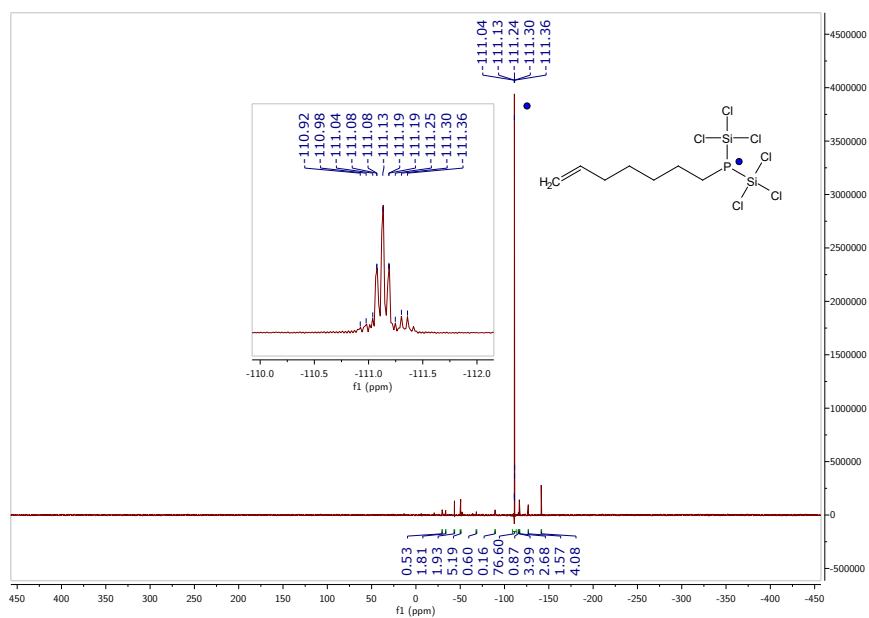


Figure 4.33 $^{31}\text{P}\{^1\text{H}\}$ and ^{31}P (inset) NMR spectra of **3i** in CDCl_3 at 25°C , recorded at 203 MHz.

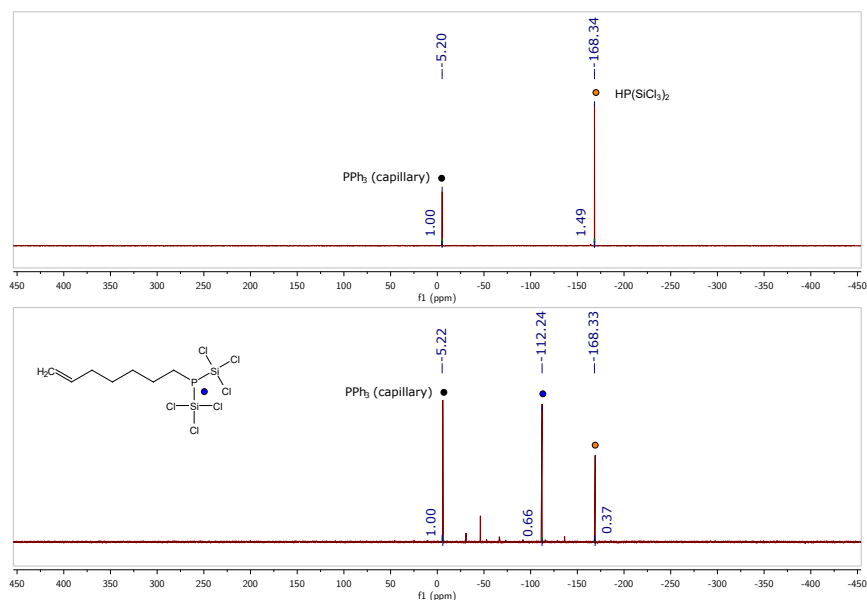


Figure 4.34 Comparison of $^{31}\text{P}\{^1\text{H}\}$ NMR spectra before and after irradiation to obtain a spectroscopic yield for **3i**. Spectra recorded in hexane at 25 °C, 203 MHz.

4.5.3.11 From 1-hexyne to give **3k**

^1H NMR (500 MHz, CDCl_3 , δ) 6.77 (ddt, $J = 28.8, 10.6, 7.4$ Hz, 1H), 5.89 (ddt, $J = 10.6, 3.0, 1.3$ Hz, 1H), 2.43 (qdd, $J = 7.4, 3.0, 1.4$ Hz, 2H), 1.59–1.28 (m, 4H), 0.93 (t, $J = 7.3$ Hz, 3H). ^{13}C NMR (126 MHz, CDCl_3 , δ) 156.66 (d, $J = 24.6$ Hz), 108.04 (d, $J = 11.3$ Hz), 31.40 (d, $J = 20.6$ Hz), 30.77, 22.21, 13.85. $^{31}\text{P}\{^1\text{H}\}$ NMR (203 MHz, CDCl_3 , δ) -120.82 ($J_{\text{P-Si}} = 56.5$ Hz). ^{31}P NMR (203 MHz, CDCl_3 , δ) -120.82 (d, $J = 28.8$ Hz, $J_{\text{P-Si}} = 56.5$ Hz). HRMS (m/z , (%relative intensity)): $[\text{M} + \text{H} + 2(\text{H} \leftrightarrow \text{SiCl}_3)]^+$ calcd for $\text{C}_6\text{H}_{14}\text{P}_1$, 117.083314; found, 117.08448 (29%).

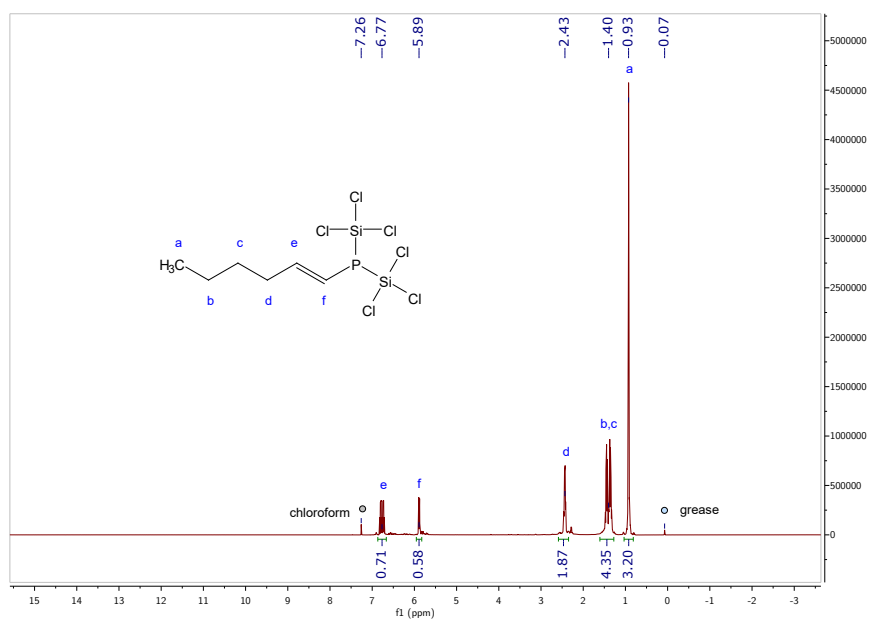


Figure 4.35 ¹H NMR spectra of **3k** in CDCl₃ at 25 °C, recorded at 500 MHz.

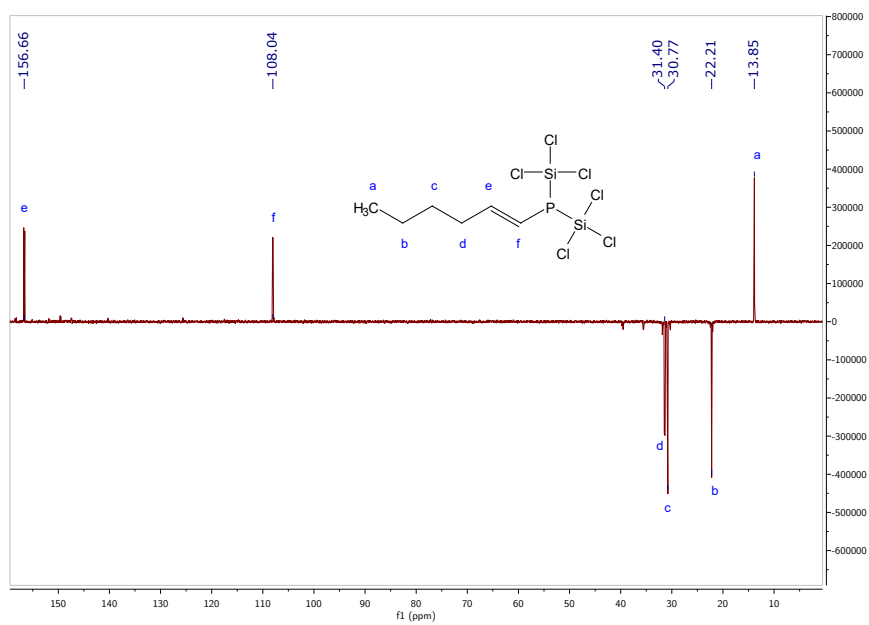


Figure 4.36 ¹³C (DEPT) NMR spectrum of **3k** in CDCl₃ at 25 °C, recorded at 126 MHz.

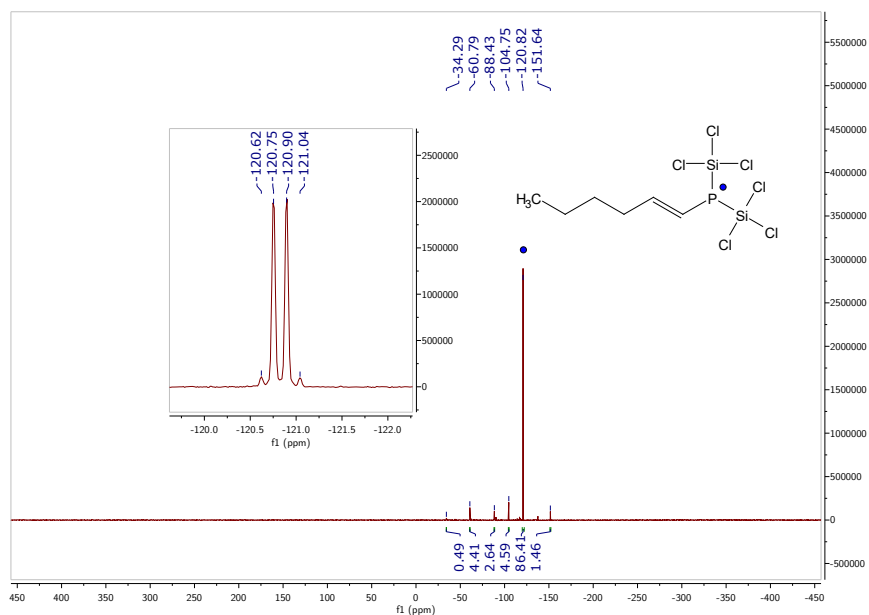


Figure 4.37 $^{31}\text{P}\{^1\text{H}\}$ and ^{31}P (inset) NMR spectra of **3k** in CDCl_3 at $25\text{ }^\circ\text{C}$, recorded at 203 MHz.

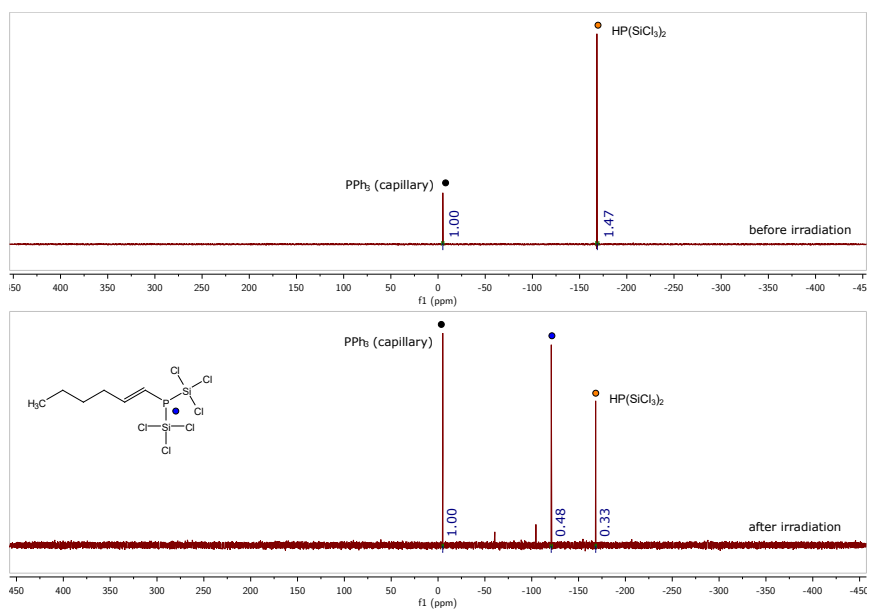


Figure 4.38 Comparison of $^{31}\text{P}\{^1\text{H}\}$ NMR spectra before and after irradiation to obtain a spectroscopic yield for **3k**. Spectra recorded in hexane at $25\text{ }^\circ\text{C}$, 203 MHz.

4.5.4 Functionalization reactions of bis(trichlorosilyl)hexylphosphine

4.5.4.1 General information

Compound **3a** was prepared according to Section 4.5.3. Capillaries for quantitative ^{31}P NMR spectroscopy were prepared by dissolving chromium(III) acetylacetonate (10.0 mg, 0.03 mmol) and triphenylphosphine (270 mg, 1.03 mmol) in C_6D_6 (2.0 mL). The purpose of the chromium(III) acetylacetonate was to act as a paramagnetic relaxation agent.⁴⁷ This stock solution (70 μL) was transferred to a capillary which was then flame sealed.

4.5.4.2 With C_2Cl_6 (4 equiv) to give *n*-hex- PCl_2 (**4a**)

In the glovebox, a solution of **3a** (10 mg, 0.0260, 1 equiv) was prepared in acetonitrile (0.5 mL) in an NMR tube equipped with a J. Young valve and containing a capillary (prepared as described in 4.5.1). A quantitative $^{31}\text{P}\{^1\text{H}\}$ NMR spectrum was collected. The tube was brought back into the glovebox and hexachloroethane (24 mg, 0.102 mmol, 4 equiv) was added. The reaction mixture was heated to 60 $^\circ\text{C}$ for 1 hr then analyzed by quantitative $^{31}\text{P}\{^1\text{H}\}$ spectroscopy. Yield (spectroscopic): 72%. $^{31}\text{P}\{^1\text{H}\}$ NMR (203 MHz, MeCN, δ) 200.2 (s). The above NMR data were consistent with previous reports of the compound.⁴⁰

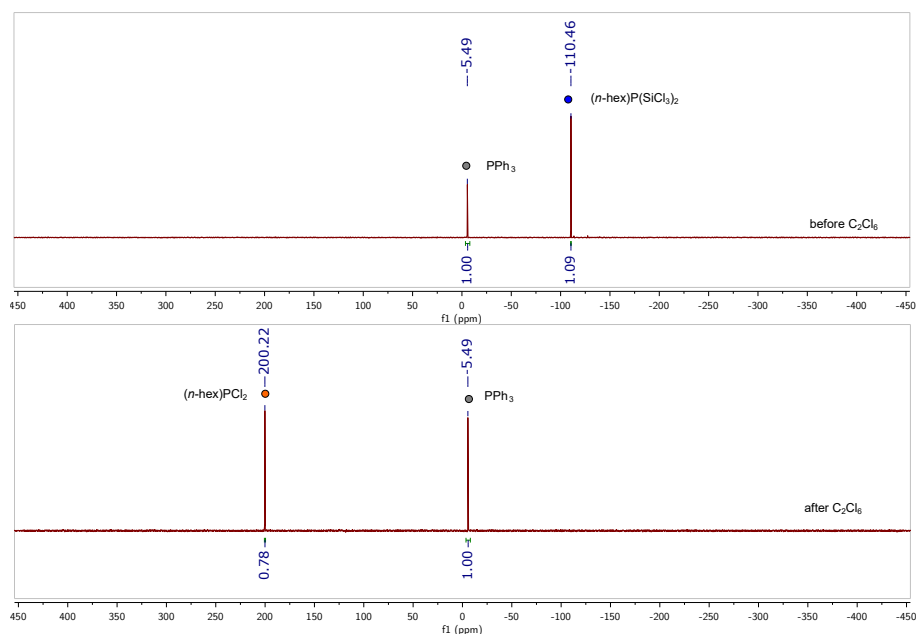


Figure 4.39 $^{31}\text{P}\{^1\text{H}\}$ NMR spectra of **3a** before and after treatment with C_2Cl_6 in acetonitrile at 25 $^\circ\text{C}$, recorded at 162 MHz.

4.5.4.3 With PhCH₂Br (5 equiv) to give [*n*-hex-P(CH₂Ph)₃][Br] (4b)

In the glovebox, a solution of **3a** (10 mg, 0.0260, 1 equiv) was prepared in acetonitrile (0.5 mL) in an NMR tube equipped with a J. Young valve and containing a capillary (prepared as described in 4.5.1). A quantitative ³¹P{¹H} NMR spectrum was collected. The tube was brought back into the glovebox and benzyl bromide (22 mg, 0.129 mmol, 5 equiv) was added. The reaction mixture was heated to 75 °C for 18 hr then analyzed by quantitative ³¹P{¹H} spectroscopy. Yield (spectroscopic): 77%. ³¹P{¹H} NMR (203 MHz, MeCN, δ) 28.06 (s). The NMR data are consistent with the phosphonium salt [P(CH₂Ph)₄][Cl].⁴⁸

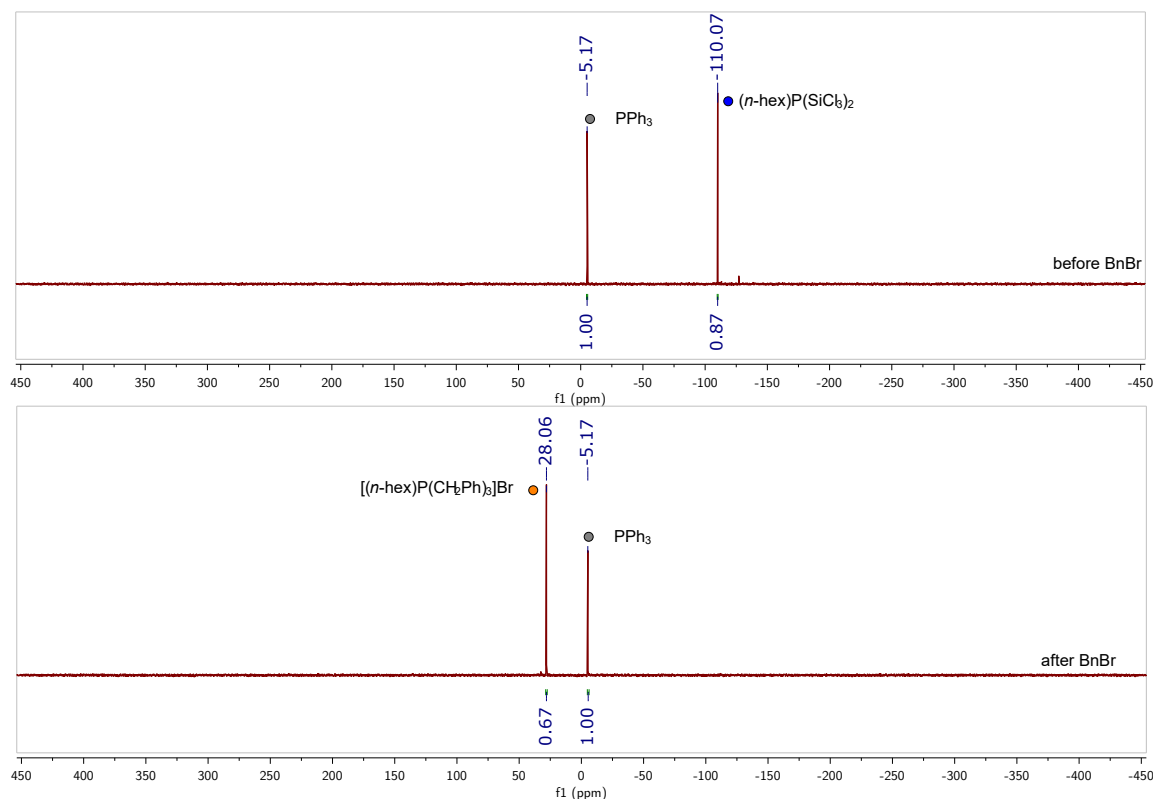


Figure 4.40 ³¹P{¹H} NMR spectra of **3a** before and after treatment with PhCH₂Br in acetonitrile at 25 °C, recorded at 162 MHz.

4.5.4.4 With H₂O (32 equiv) to give *n*-hex-PH₂ (4c)

In the glovebox, a solution of **3a** (10 mg, 0.0260, 1 equiv) was prepared in CDCl₃ (0.5 mL) in an NMR tube equipped with a J. Young valve and containing a capillary (prepared as described in 4.5.1). A quantitative ³¹P{¹H} NMR spectrum was collected. Against a flow of N₂, water (15 μL, 0.83 mmol, 32 equiv; degassed, 20 min N₂ sparge) was added to the NMR tube. The tube was sealed and a quantitative ³¹P{¹H} NMR spectrum was collected. Spectroscopic yield: 88%. ³¹P{¹H} NMR (162 MHz, CDCl₃, δ) -137.4 (s). The above NMR data were consistent with previous reports of the compound.¹⁹

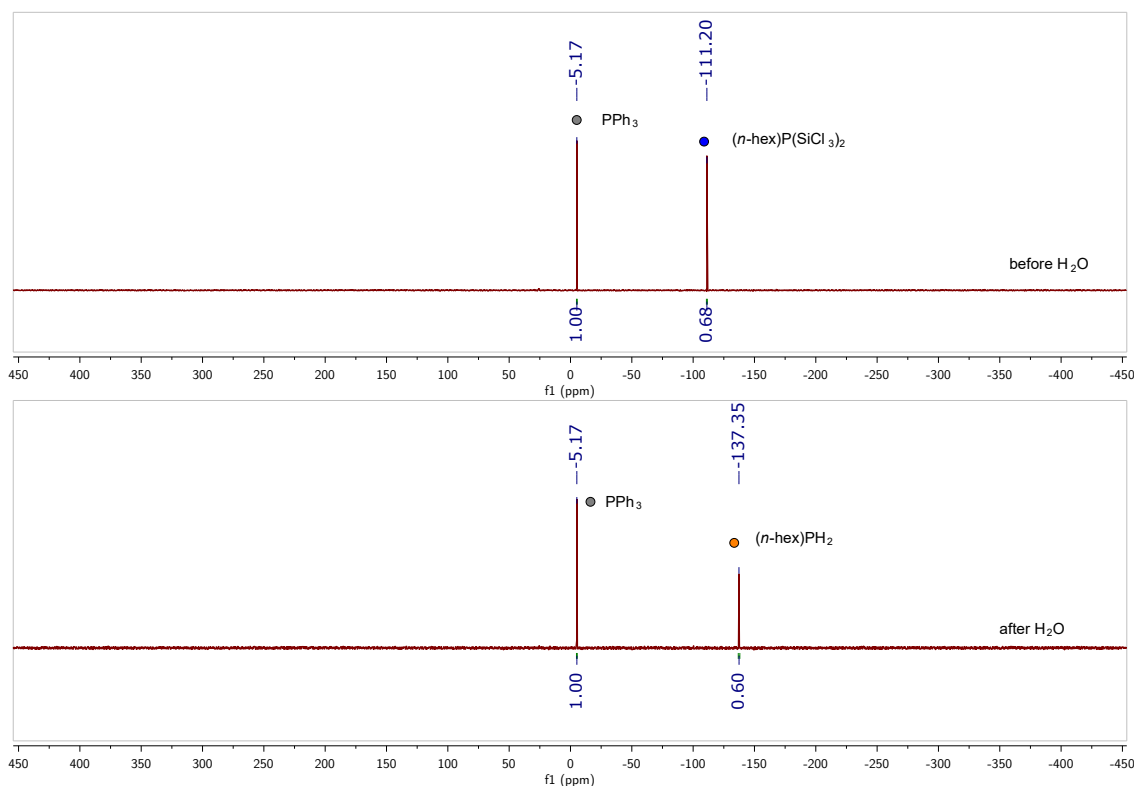


Figure 4.41 ³¹P{¹H} NMR spectra of **3a** before and after treatment with H₂O in acetonitrile at 25 °C, recorded at 162 MHz.

4.5.4.5 With H₂O₂ (2.2 equiv) to give *n*-hex-P(O)(OH)H (4d)

In the glovebox, a solution of **3a** (10 mg, 0.060 mmol, 1 equiv) was prepared in acetonitrile (0.5 mL) in an NMR tube equipped with a J. Young valve and containing a capillary (Section 4.5.3). An initial quantitative ³¹P{¹H} NMR spectrum was acquired. Against a flow of nitrogen, aqueous H₂O₂ (27% w/w; 7 μL, 0.0571 mmol, 2.2 equiv) was added using a microsyringe (10 μL). The NMR tube was sealed and analyzed immediately by quantitative ³¹P{¹H} spectroscopy. Yield (spectroscopic): 93%. ³¹P{¹H} NMR (203 MHz, MeCN, δ) 42.9 (s). ³¹P{¹H} NMR (203 MHz, MeCN, δ) 42.9 (dp, *J*_{P-H} = 566.3, 14.5 Hz). The above NMR data were consistent with previous reports of the compound.⁴⁹

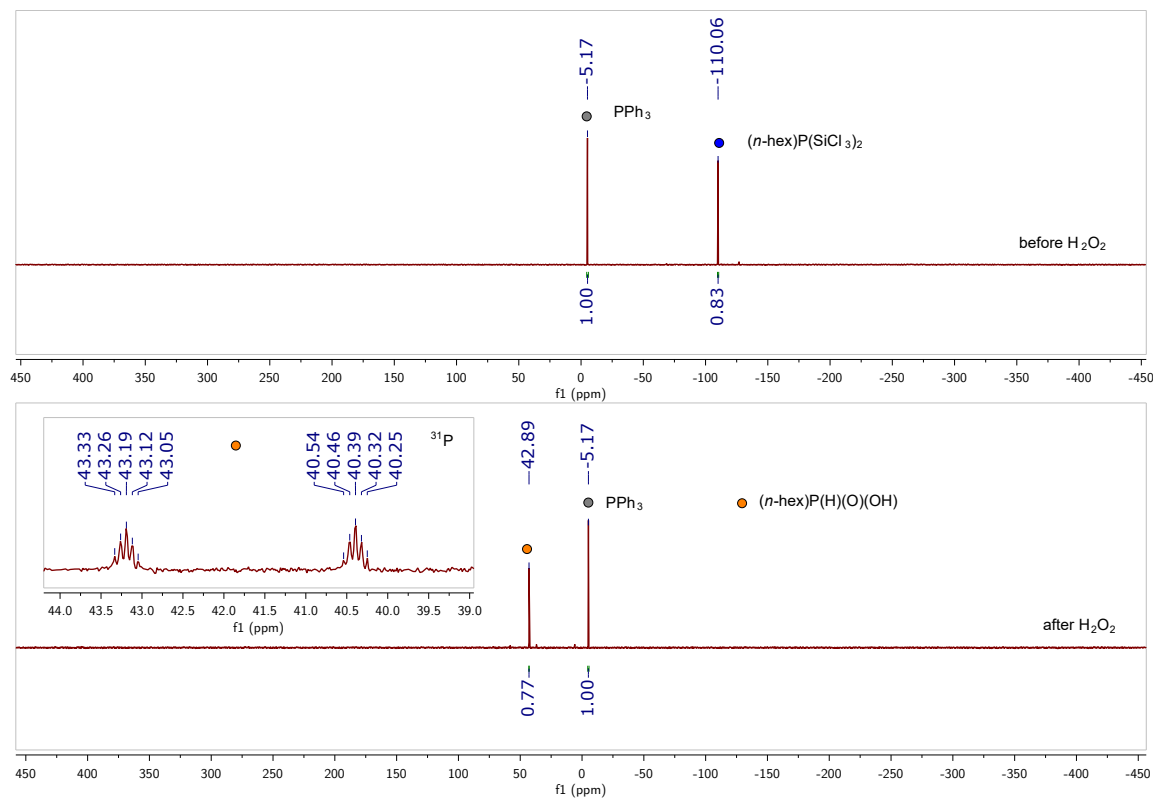


Figure 4.42 ³¹P{¹H} and ³¹P{¹H} (inset) NMR spectra of **3a** before and after treatment with aqueous H₂O₂ (2.2 equiv) in acetonitrile at 25 °C, recorded at 162 MHz.

4.5.4.6 With H₂O₂ (5 equiv) to give *n*-hex-P(O)(OH)₂ (4e)

In the glovebox, a solution of **3a** (10 mg, 0.060 mmol, 1 equiv) was prepared in acetonitrile (0.5 mL) in an NMR tube equipped with a J. Young valve and containing a capillary (Section 4.5.3). An initial quantitative ³¹P{¹H} NMR spectrum was acquired. Against a flow of nitrogen, aqueous H₂O₂ (27% w/w; 18 μL, 0.143 mmol, 5 equiv) was added using a microsyringe (50 μL). The NMR tube was heated to 60 °C for 12 h then analyzed by quantitative ³¹P{¹H} spectroscopy. Yield (spectroscopic): 73%. ³¹P{¹H} NMR (203 MHz, MeCN, δ) 33.3 (s). ³¹P NMR (203 MHz, MeCN, δ) 33.3 (m). The above NMR data were consistent with previous reports of the compound.⁵⁰

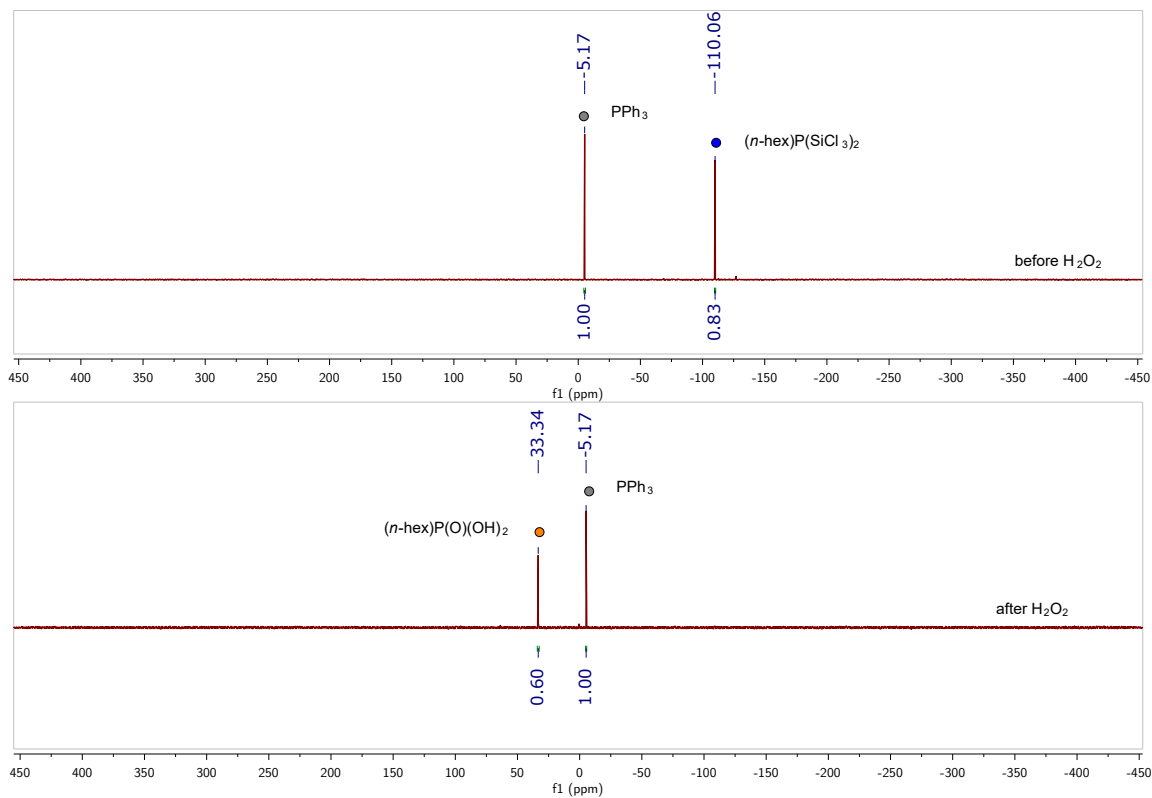


Figure 4.43 ³¹P{¹H} NMR spectra of **3a** before and after treatment with aqueous H₂O₂ (5 equiv) in acetonitrile at 25 °C, recorded at 162 MHz.

4.5.5 Bracketing of the pK_a of $\text{HP}(\text{SiCl}_3)_2$ (1)

Based on a calculated pK_a value of 13.3 in MeCN (Section 4.5.15), various nitrogen-containing bases with pK_a values (of their conjugate acids) in a similar range were exposed to acetonitrile solutions of $\text{HP}(\text{SiCl}_3)_2$. The solutions were generally unstable; in some cases formation of $\text{H}_2\text{P}(\text{SiCl}_3)$ and an insoluble yellow precipitate was observed within 5 minutes (Table 4.2). When large amounts of H_2PSiCl_3 were formed, the base was not assumed to be capable of deprotonation of $\text{HP}(\text{SiCl}_3)_2$ due to alternate possible pathways for decomposition to the observed species. Nevertheless, the qualitative results are shown in Table 4.2. In CDCl_3 , only small amounts of H_2PSiCl_3 formed with 1 equiv of pyridine, and the acidic proton appeared to be in equilibrium between the phosphine and pyridine, indicating similar pK_a values in this solvent (Fig. 4.44).

Table 4.2 Qualitative description of the reaction between $\text{HP}(\text{SiCl}_3)_2$ and various nitrogen-containing bases.

Base	pK_a (MeCN)	Deprotonates $\text{HP}(\text{SiCl}_3)_2$?	Decomp?
Pyridine	12.53	Yes	some H_2PSiCl_3
Pyridine ^a	–	Yes	minimal H_2PSiCl_3
2,6-di(<i>t</i> -Bu)pyridine	11.4	Yes	mostly H_2PSiCl_3
Diphenylamine	5.98	Yes	mostly H_2PSiCl_3
Triphenylamine	1.28	No	No

^a in CDCl_3

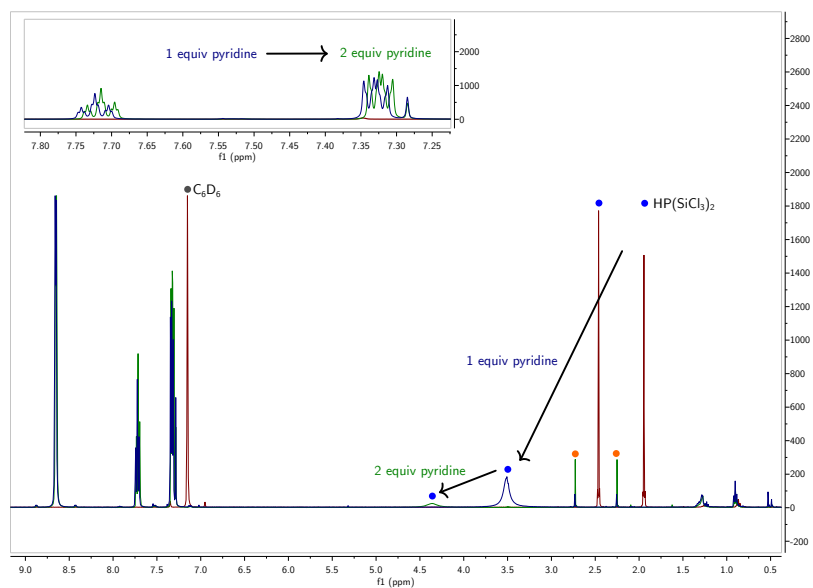


Figure 4.44 ^1H NMR spectra of $\text{HP}(\text{SiCl}_3)_2$ after dosing with 0, 1, and 2 equiv of pyridine. Spectrum recorded at 25 °C, 400 MHz.

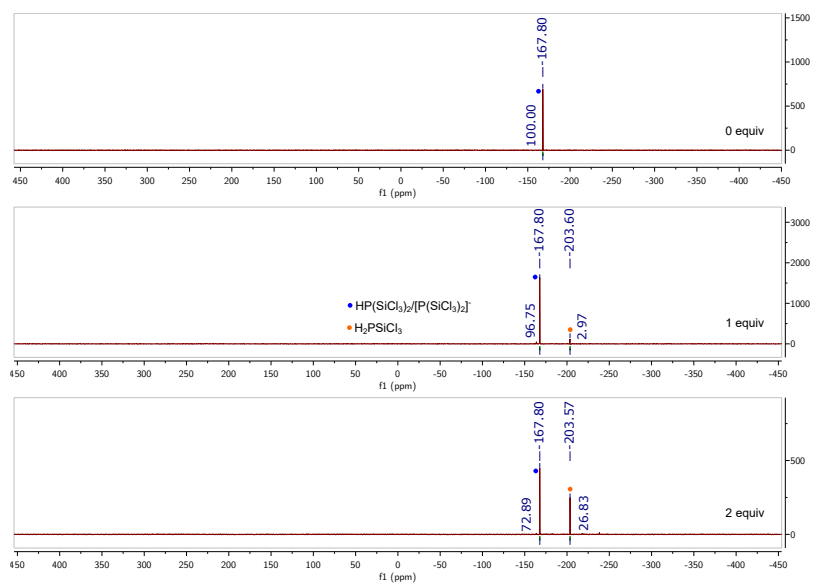


Figure 4.45 $^{31}\text{P}\{^1\text{H}\}$ NMR spectra of $\text{HP}(\text{SiCl}_3)_2$ after dosing with 0, 1, and 2 equiv of pyridine. Spectrum recorded at 25 °C, 162 MHz.

4.5.6 UV-vis spectrum of $\text{HP}(\text{SiCl}_3)_2$ (1)

A “blank” spectrum was first recorded. In the glovebox, hexane (4 mL) was added to a gas-tight UV-vis cuvette that was then sealed with Teflon tape. A UV-vis spectrum was recorded from 600–190 nm. The cuvette was brought into the glovebox. A solution of $\text{HP}(\text{SiCl}_3)_2$ (1.5 mg, 0.005 mmol) in hexane (10.00 g, 15.27 mL, 3.27 mM) was prepared and added to the cuvette, which was sealed in the same way and a UV-vis spectrum recorded. *Note: the small absorbance at ca. 252 nm was present in the hexane blank and despite multiple attempts could not be removed by background subtraction.*

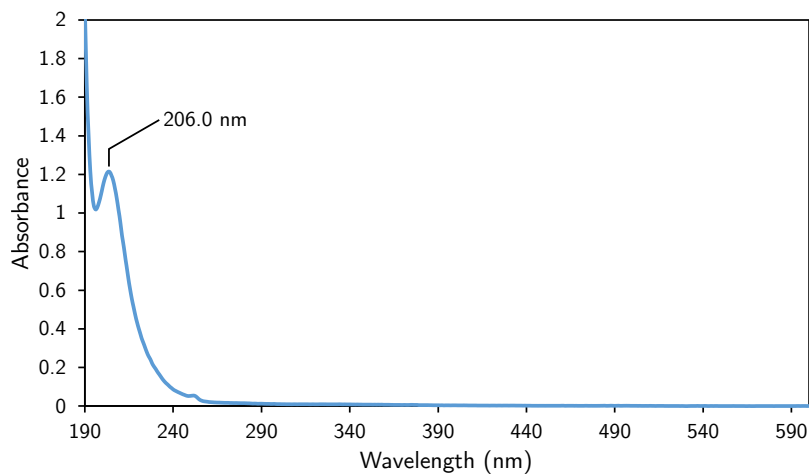


Figure 4.46 UV-Vis spectrum of $\text{HP}(\text{SiCl}_3)_2$ (3.27 mM in hexane).

4.5.7 Electrochemistry of [TBA]1 (5)

In the glovebox, a cyclic voltammogram was recorded by preparing a solution of [TBA]1 (22 mg, 0.04 mmol, 0.01 M) and [TBA][PF₆] (155 mg, 0.4 mmol, 0.1 M) in MeCN (4 mL). After a background CV was recorded (supporting electrolyte only) a CV was recorded at 400 mV/s, using a glassy carbon working electrode, a platinum counter electrode, and a silver reference electrode. The CV was referenced to the ferrocene/ferrocenium redox couple.

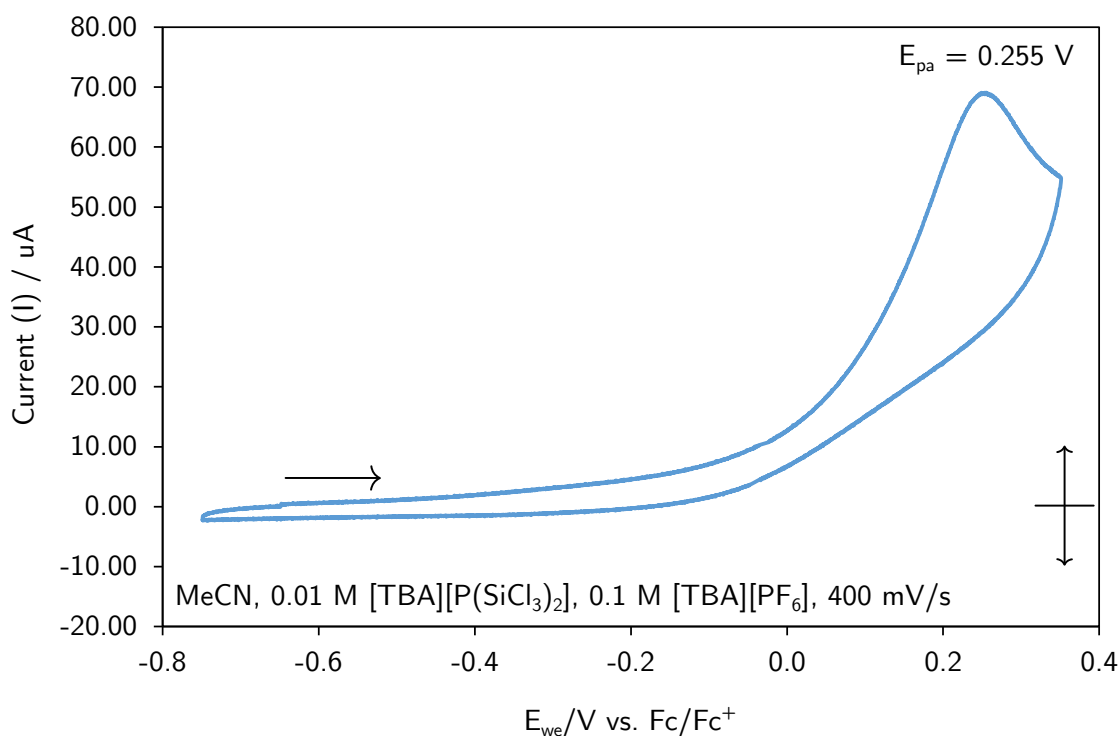


Figure 4.47 Cyclic voltammogram of [TBA]1.

4.5.8 Determination of $\text{BDFE}_{\text{MeCN}}^{298 \text{ K}}$ using a square scheme

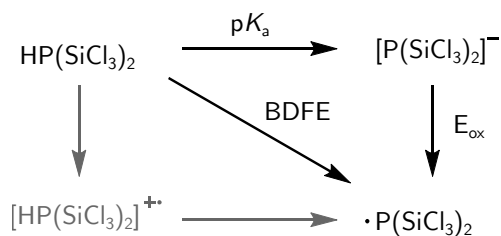


Figure 4.48 Square scheme used for calculation of the $\text{BDFE}_{\text{MeCN}}(\text{P-H})$ in $\text{HP}(\text{SiCl}_3)_2$.

The $\text{BDFE}_{\text{MeCN}}^{298 \text{ K}}$ of the P-H bond in $\text{HP}(\text{SiCl}_3)_2$ was determined using Eq 4.1.³⁹

$$\text{BDFE}_{\text{MeCN}}(\text{P-H}) = 1.37 \times \text{p}K_a + 23.06 \times E_{\text{ox}} + C_{\text{G,MeCN}} \quad (4.1)$$

where $\text{p}K_a$ was taken to be the calculated value of 14.1 and $C_{\text{G,MeCN}} = 54.9$. The value for E_{ox} was substituted for $E_{\text{pa}} = 0.255$ due to the irreversible nature of the oxidation. Thus,

the obtained value of $\text{BDFE}_{\text{MeCN}}(\text{P-H}) = 80.1$. Sources of error include the calculation of $\text{p}K_{\text{a}}$ (Section 4.5.15), substitution of E_{ox} for E_{pa} , and in the measurement of $C_{\text{G,MeCN}}$. Errors have been reported to be on the order of ± 3 kcal/mol by Bordwell³⁸ for irreversible oxidations such as those displayed by [TBA]**2**, and is the value used in the manuscript.

This value was converted to a gas-phase bond dissociation energy ($\text{BDE}_{\text{g}}^{298\text{ K}}$) using equations 10 and 11 in the review by Mayer,³⁹ reproduced here as Eqs 4.2 and 4.3, respectively.

$$\text{BDFE}_{\text{g}}(\text{XH}) = \text{BDE}_{\text{g}}(\text{XH}) - \text{TS}^{\ominus}(\text{H}\cdot) - \text{T}\{\text{S}^{\ominus}(\text{X}\cdot) - \text{S}^{\ominus}(\text{XH})\} \quad (4.2)$$

$$\text{BDFE}_{\text{MeCN}}(\text{XH}) = \text{BDFE}_{\text{g}}(\text{XH}) + \Delta G_{\text{solv}}^{\ominus}(\text{H}\cdot) + \Delta G_{\text{solv}}^{\ominus}(\text{X}\cdot) - \Delta G_{\text{solv}}^{\ominus}(\text{XH}) \quad (4.3)$$

The assumptions³⁹ (i) $\text{S}^{\ominus}(\text{X}\cdot) = \text{S}^{\ominus}(\text{XH})$ and (ii) $\Delta G_{\text{solv}}^{\ominus}(\text{X}\cdot) = \Delta G_{\text{solv}}^{\ominus}(\text{XH})$, used with values for $\text{S}^{\ominus}(\text{H}\cdot)$ and $\Delta G_{\text{solv}}^{\ominus}(\text{H}\cdot)$ of $27.42 \text{ cal K}^{-1} \text{ mol}^{-1}$ and $5.12 \text{ kcal mol}^{-1}$, respectively, lead to a value for $\text{BDE}_{\text{g}}^{298\text{ K}}(\text{P-H})$ of 83.2 kcal/mol .

4.5.9 Experiments related to mechanism

4.5.9.1 Analysis of compound **3i** to determine whether products arising from cyclization form

Compound **3i** was prepared according to Section 4.5.3.10. The crude product was dissolved in C_6D_6 (0.5 mL) and stirred with basic alumina (500 mg) for twenty minutes in order to form a primary phosphine. The mixture was filtered through microfibre filter paper in a pipette and analyzed by NMR spectroscopy. The reaction mixture was also analyzed by GCMS (Figure 4.52). No evidence for a primary phosphine other than hept-6-en-1-ylphosphine was observed. 5.75 (ddt, $J = 16.9, 10.2, 6.7 \text{ Hz}$, 1H), 5.08–4.94 (m, 2H), 2.91–2.80 (m, 1H), 2.43–2.33 (m, 1H), 1.98–1.85 (m, 3H), 1.41–1.07 (m, 13H).

^1H NMR (400 MHz, C_6D_6 , δ) 5.75 (ddt, $J = 16.9, 10.2, 6.7 \text{ Hz}$, 1H), 5.08–4.94 (m, 2H), 2.91–2.80 (m, 1H), 2.43–2.33 (m, 1H), 1.98–1.85 (m, 3H), 1.41–1.07 (m, 13H). $^{31}\text{P}\{^1\text{H}\}$ NMR (162 MHz, CDCl_3 , δ) -138.4 . ^{31}P NMR (162 MHz, CDCl_3 , δ) -138.4 (tm, $J_{\text{P-H}} = 190.1 \text{ Hz}$). GCMS (EI): retention time = 4.31 min; $[\text{M}]^+$ calcd for $\text{C}_6\text{H}_{16}\text{P}_1$, 130.09; found, 130 (100%).

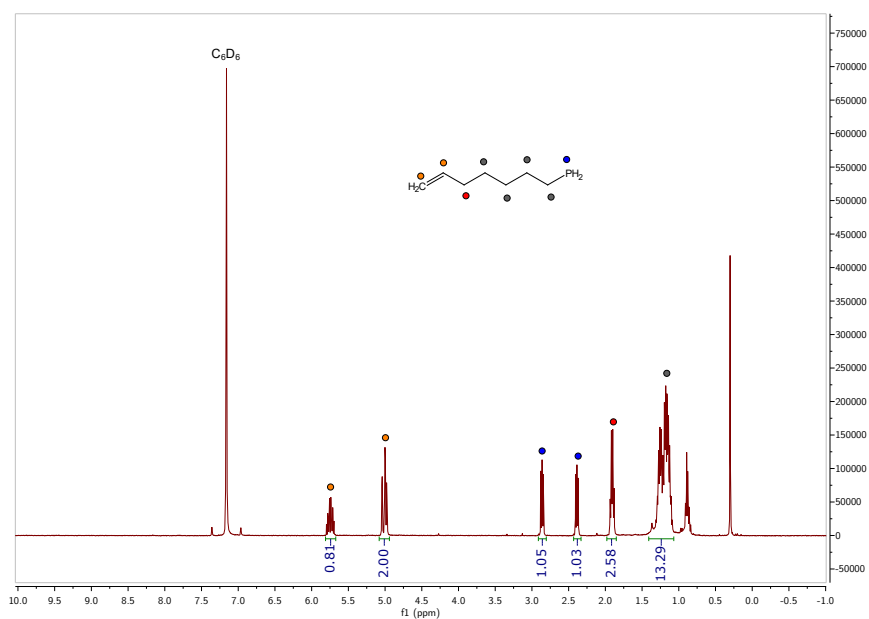


Figure 4.49 ^1H NMR spectrum of hept-6-en-1-ylphosphine in C_6D_6 at 25°C , recorded at 400 MHz.

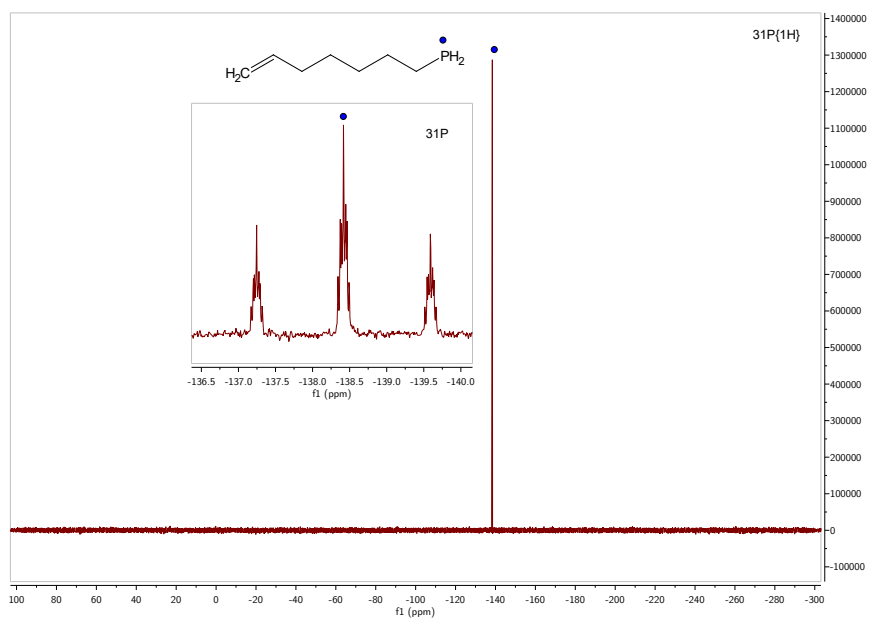


Figure 4.50 $^{31}\text{P}\{^1\text{H}\}$ NMR spectrum (inset: ^{31}P) of hept-6-en-1-ylphosphine in C_6D_6 at 25°C , recorded at 162 MHz.

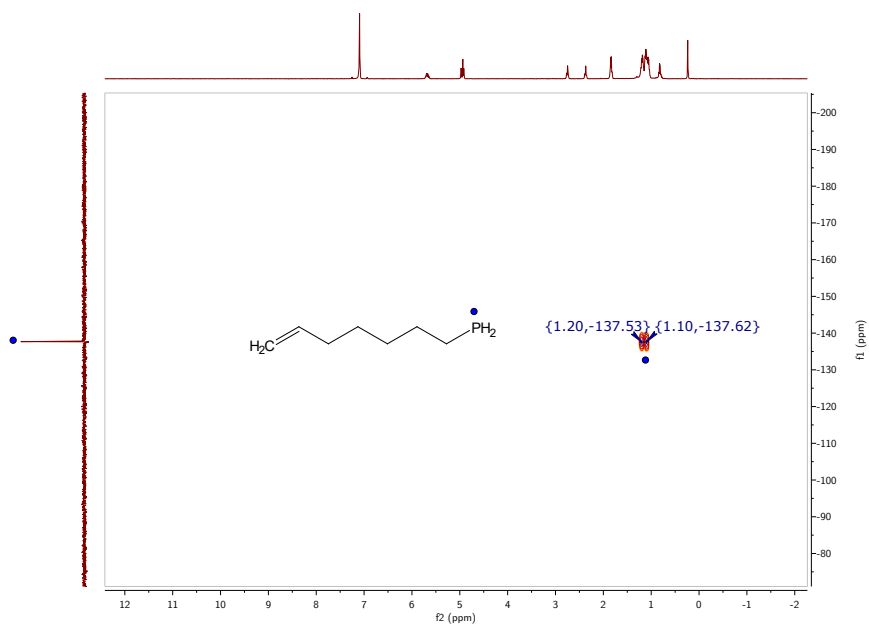


Figure 4.51 ^{31}P - ^1H HMBC NMR spectrum of hept-6-en-1-ylphosphine in C_6D_6 at 25 °C, recorded at 500 MHz.

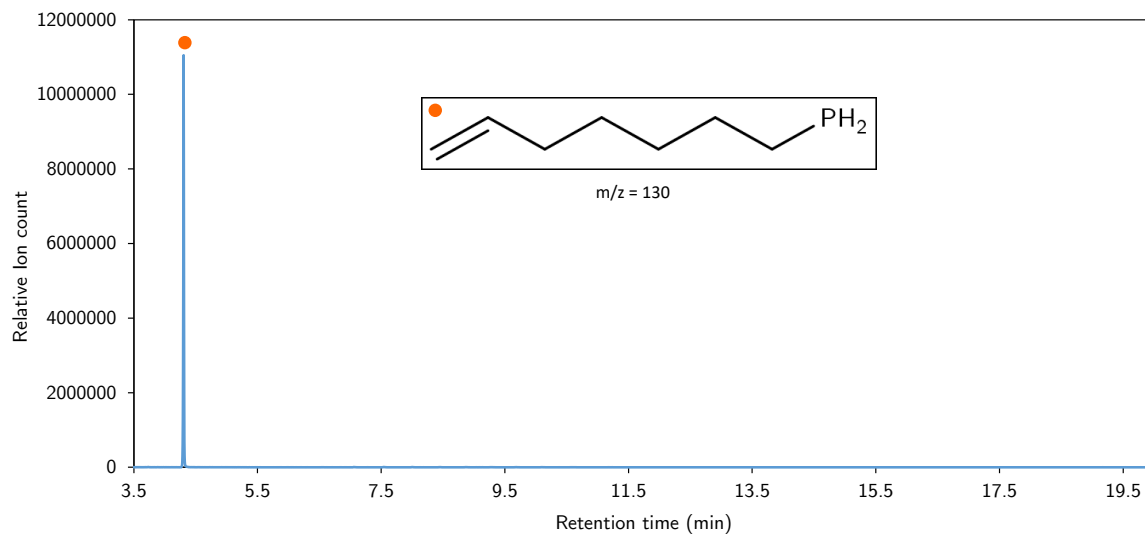


Figure 4.52 GCMS trace of product obtained in Section 4.5.9.1, corresponding to hept-6-en-1-ylphosphine.

4.5.9.2 Reaction of $\text{HP}(\text{SiCl}_3)_2$ (1) with 1,1-difluoro-2-vinylcyclopropane

A control reaction was performed in order to test the stability of 1,1-difluoro-2-vinylcyclopropane to UV light. In the glovebox, 1,1-difluoro-2-vinylcyclopropane (17 mg, 0.163 mmol) was weighed into an NMR tube and diluted with hexane (0.5 mL). An initial $^{19}\text{F}\{^1\text{H}\}$ NMR spectrum was recorded. The solution was irradiated with UV light for ten minutes then analyzed by $^{19}\text{F}\{^1\text{H}\}$. No change was observed between the spectra before and after irradiation.

In the glovebox, $\text{HP}(\text{SiCl}_3)_2$ (10 mg, 0.033 mmol, 1 equiv) was weighed out in the end of a pipette. 1,1-difluoro-2-vinylcyclopropane (10 mg, 10 μL , 0.1 mmol, 3 equiv) was measured out using a microsyringe (10 μL) and dispensed into an NMR tube equipped with a J. Young valve. The phosphine was washed into the NMR tube from the end of the pipette using C_6D_{12} (0.5 mL). The NMR tube was irradiated for five minutes then analyzed by NMR spectroscopy. The major product corresponded to that of the E-isomer of the ring opened product. A minor amount of a species tentatively assigned as the Z-isomer was also detected by NMR spectroscopy. **E-3j**: ^1H NMR (500 MHz, C_6D_{12} , δ) 6.15–6.03 (m, 1H), 5.86–5.73 (m, 1H), 2.94–2.85 (m, 2H), 1.58 (t, $J = 17.5$ Hz, 3H). ^{31}P NMR (203 MHz, C_6D_{12} , δ) –110.38 (p, $J_{\text{P-H}} = 5$ Hz, $J_{\text{P-F}} = 5$ Hz). ^{19}F NMR (471 MHz, C_6D_{12} , δ) –90.52 (m).

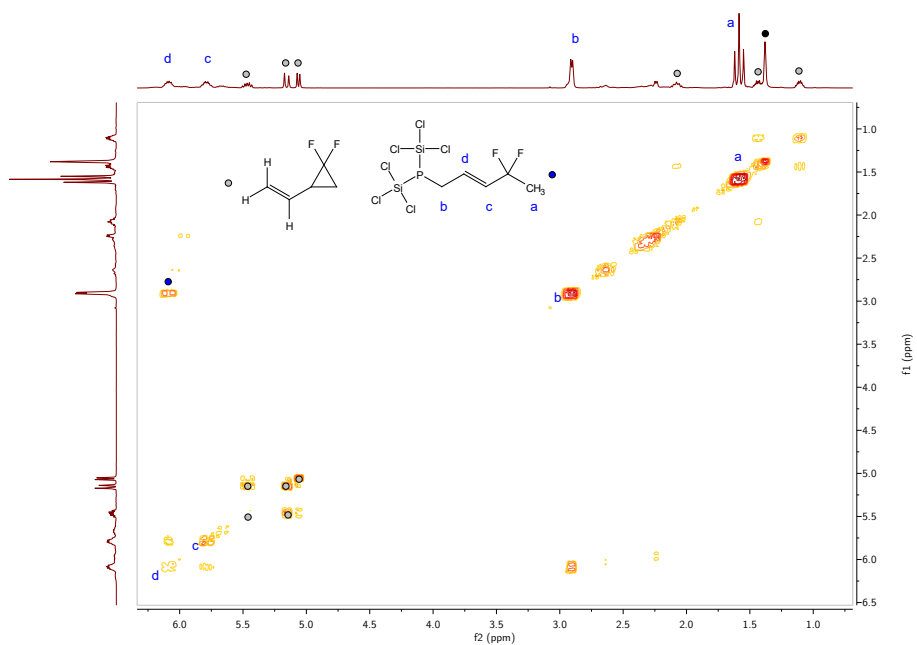


Figure 4.54 ^1H - ^1H COSY spectrum of E-3j in C_6D_{12} at 25 °C, recorded at 500 MHz.

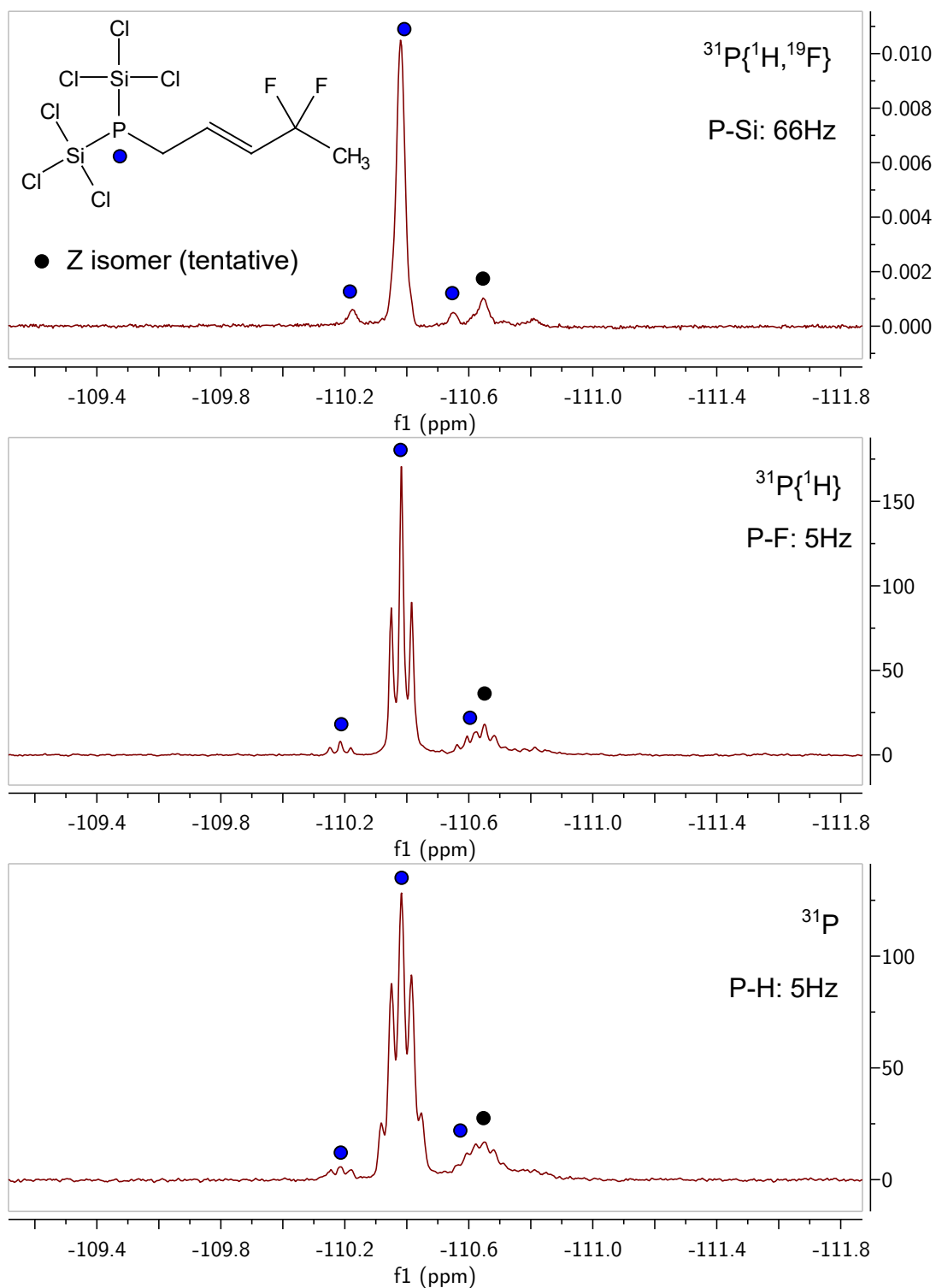


Figure 4.55 Stack of $^{31}\text{P}\{^1\text{H}, ^{19}\text{F}\}$ (top), $^{31}\text{P}\{^1\text{H}\}$ (middle), and ^{31}P NMR (bottom) spectra of E-3j in C_6D_{12} at 25 °C, recorded at 203 MHz.

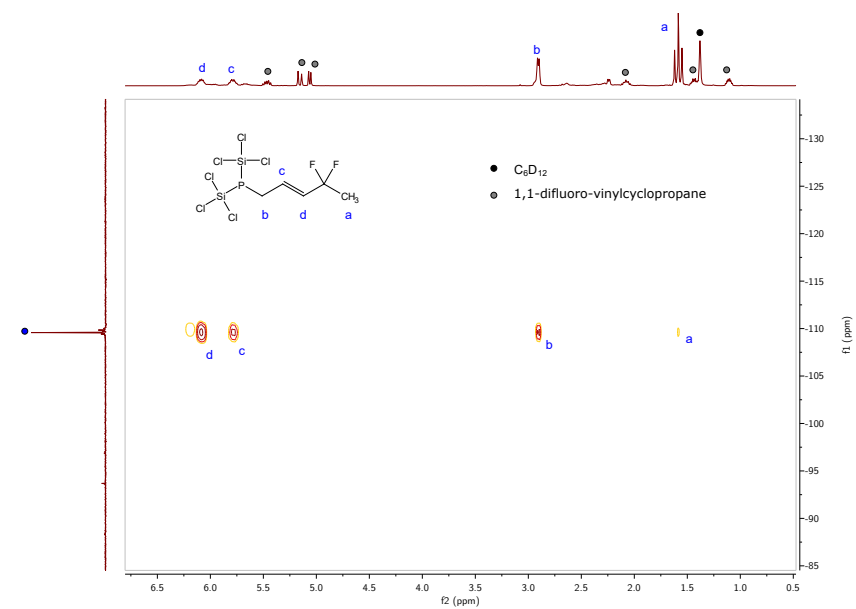


Figure 4.56 ^{31}P - ^1H -HMBC spectrum of E-3j in C_6D_{12} at 25°C , recorded at 500 MHz.

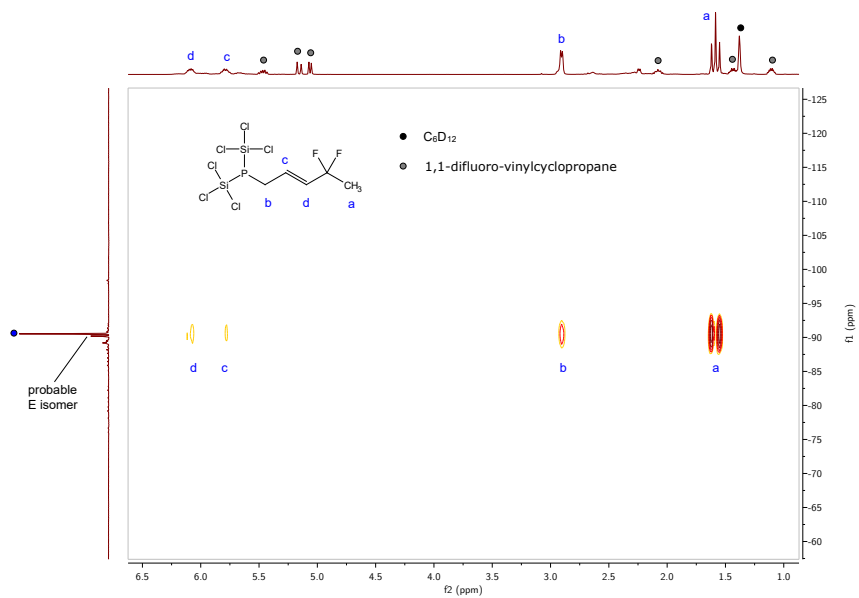


Figure 4.57 ^{19}F - ^1H -HMBC spectrum of E-3j in C_6D_{12} at 25°C , recorded at 500 MHz.

4.5.9.3 Reaction of $\text{HP}(\text{SiCl}_3)_2$ (1) with *trans*-4-octene

In the glovebox, *trans*-4-octene (22 mg, 0.2 mmol, 1 equiv) was weighed from a vial into an NMR tube equipped with a J. Young valve using a pipette. The material was diluted in C_6D_{12} . A ^1H NMR spectrum was recorded. The reaction mixture was irradiated with UV light for 1 h, then analyzed by ^1H NMR spectroscopy. No change to the spectrum was observed. $\text{HP}(\text{SiCl}_3)_2$ (6 mg, 0.02 mmol, 0.1 equiv) was weighed into the end of a pipette and added to the reaction mixture which was then irradiated with UV light for 1 hr. Analysis by ^1H NMR spectroscopy (Figure 4.58) showed the formation of *cis*-4-octene, with the ratio of *trans*- to *cis*-4-octene being ca. 84:16 (16% isomerization). The ratio was estimated by integration of the vinyl resonances. Analysis by $^{31}\text{P}\{^1\text{H}\}$ NMR spectroscopy (Figure 4.59) showed almost exclusively $\text{HP}(\text{SiCl}_3)_2$ and some H_2PSiCl_3 .

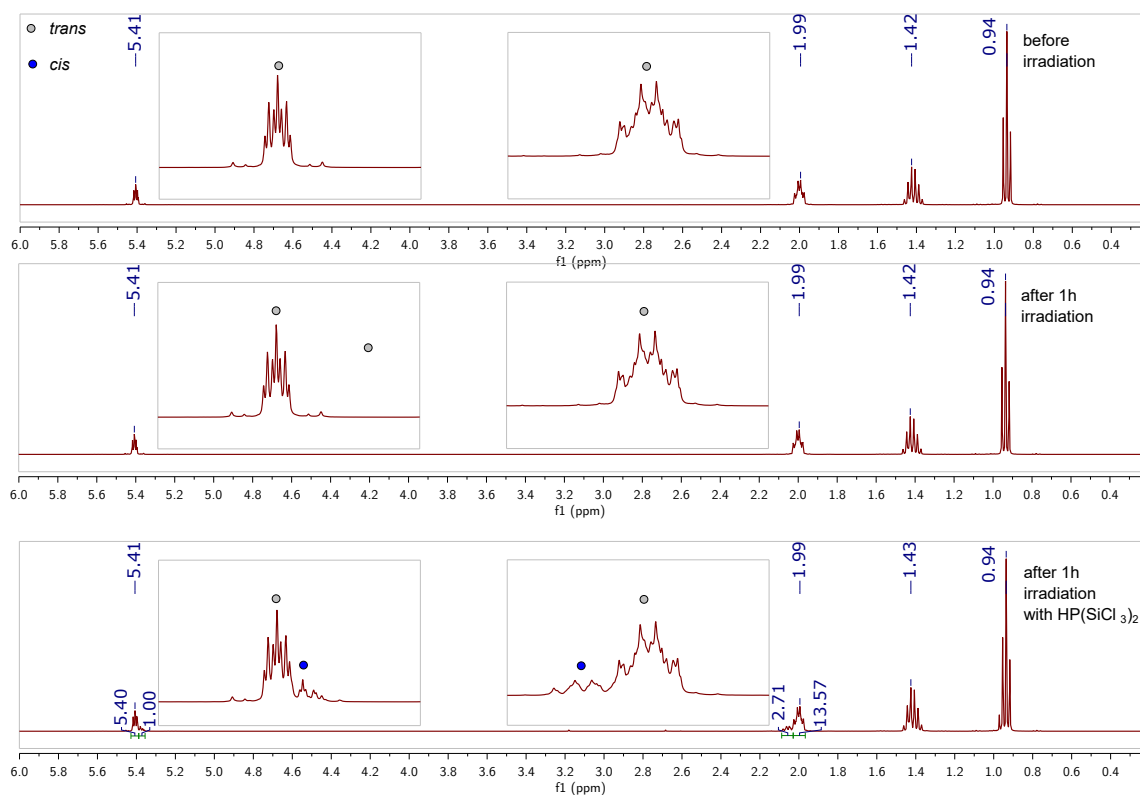


Figure 4.58 ^1H NMR spectra of: top: *trans*-4-octene in; middle: after UV irradiation for 1 hr; bottom: after irradiation with $\text{HP}(\text{SiCl}_3)_2$ for 1 hr in C_6D_{12} at 25 °C, recorded at 400 MHz.

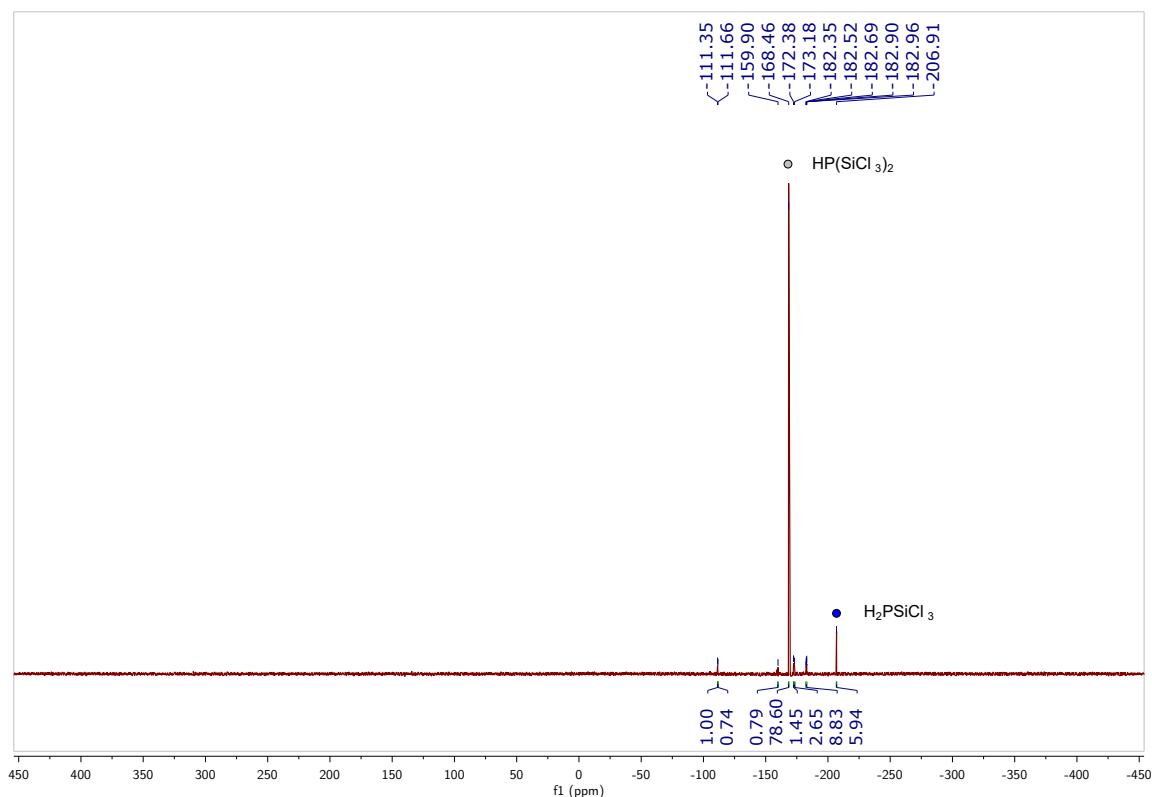


Figure 4.59 $^{31}\text{P}\{^1\text{H}\}$ NMR spectra of *trans*-4-octene after irradiation with $\text{HP}(\text{SiCl}_3)_2$ for 1 hr in C_6D_{12} at 25 °C, recorded at 162 MHz. Besides $\text{HP}(\text{SiCl}_3)_2$ and H_2PSiCl_3 , no other species were assigned.

4.5.9.4 UV Irradiation of $\text{HP}(\text{SiCl}_3)_2$ in C_6D_{12}

In the glovebox, $\text{HP}(\text{SiCl}_3)_2$ (10 mg, 0.033 mmol) was weighed into the end of a pipette. The material was washed into an NMR tube equipped with a J. Young valve using C_6D_{12} . An initial ^1H NMR spectrum was recorded to identify any impurities that were present at baseline concentrations. The sample was irradiated with UV light and analyzed by NMR spectroscopy after 1, 2, and 15 h. The formation of H_2 , HD ,²⁸ and HSiCl_3 ⁵¹ were observed at the 1 hr time point. After 15 h, starting material was still present. The spectrum shown in the manuscript was collected at the 15 h time point (64 scans). Figures 4.60 and 4.61 show the full spectra at the 0, 1, and 15 h time points.

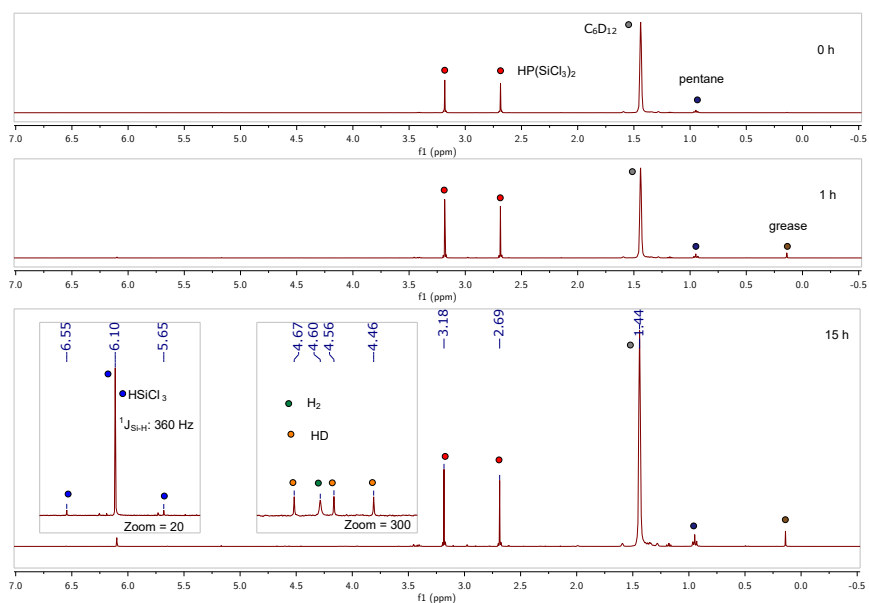


Figure 4.60 ^1H NMR spectra of $\text{HP}(\text{SiCl}_3)_2$ after UV (0 h, 1 h, 15 h) in C_6D_{12} at 25 °C, recorded at 400 MHz.

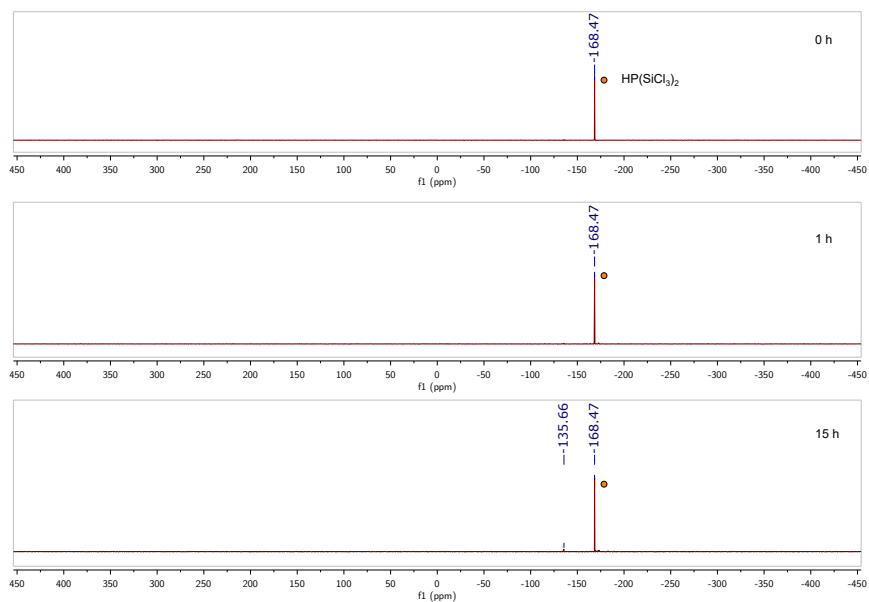


Figure 4.61 $^{31}\text{P}\{^1\text{H}\}$ NMR spectra of $\text{HP}(\text{SiCl}_3)_2$ after UV irradiation (0 h, 1 h, 15 h) in C_6D_{12} at 25 °C, recorded at 162 MHz.

4.5.10 Wavelength dependence of hydrophosphination

A Rayonet Photoreactor (RPR) was equipped with 8 bulbs of varying wavelengths; 254 nm, 300 nm, and 420 nm. In the glovebox, three samples were prepared containing $\text{HP}(\text{SiCl}_3)_2$ (10 mg, 0.033 mmol, 1 equiv) and 1-hexene (6 mg, 0.066 mmol, 2 equiv) in hexane (0.5 mL). Each of these samples was irradiated for 15 min at one of the wavelengths listed above. Each was analyzed by $^{31}\text{P}\{^1\text{H}\}$ NMR spectroscopy to determine approximate ratios of starting material to product. The ratios ($\text{HP}(\text{SiCl}_3)_2/\mathbf{3a}$) were found to be 52:48, 73:27, and 98:2 at 254, 300, and 420 nm, respectively.

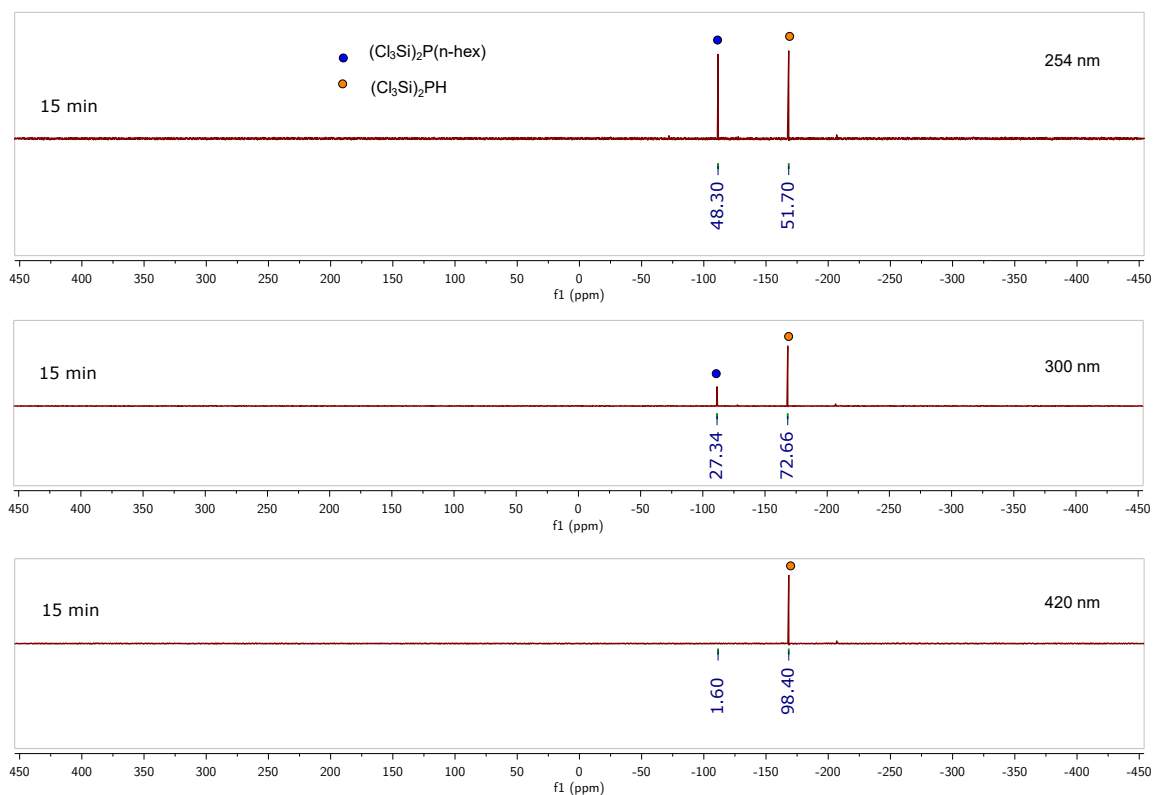


Figure 4.62 $^{31}\text{P}\{^1\text{H}\}$ NMR spectra of a hexane solution of $\text{HP}(\text{SiCl}_3)_2$ and 1-hexene after irradiation with varying wavelengths of light in a RPR, recorded at 25 °C, 162 MHz.

4.5.10.1 Attempt at hydrophosphination using either blue or ambient light as the method of photoactivation

In the glovebox, a hexane solution (0.5 mL) of $\text{HP}(\text{SiCl}_3)_2$ (10 mg, 0.033 mmol, 1 equiv) and 1-hexene (6 mg, 0.066 mmol, 2 equiv) was prepared in an NMR tube. The tube was sealed with electrical tape and a $^{31}\text{P}\{^1\text{H}\}$ NMR spectrum was recorded, showing formation of ca. 3% $(\text{Cl}_3\text{Si})_2\text{P}(n\text{-hex})$ (**3a**). The tube was placed in front of a blue Kessil lamp (5 cm, 32 W) for 15 minutes then reanalyzed by $^{31}\text{P}\{^1\text{H}\}$, with no discernible change to the spectrum observed. The NMR tube was brought into the glovebox and the solution was split equally between two NMR tubes. One tube was taped to the window for three hours (11–2 PM) and the other was wrapped in aluminum foil to exclude ambient light. The samples were analyzed in succession after 3 h by $^{31}\text{P}\{^1\text{H}\}$ spectroscopy. The tube that had been exposed to ambient light showed formation of **3a** in ca. 17% yield, while the tube kept protected from the light remained at 3%.

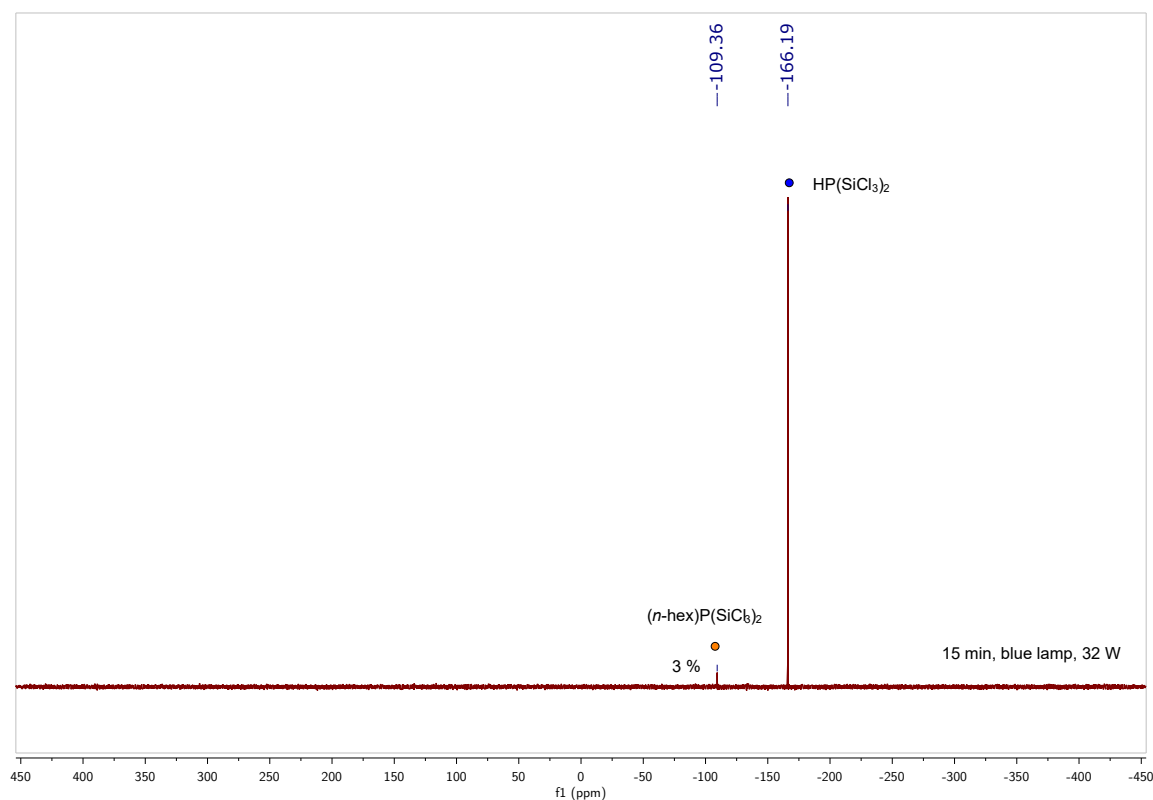


Figure 4.63 $^{31}\text{P}\{^1\text{H}\}$ NMR spectra of a hexane solution of $\text{HP}(\text{SiCl}_3)_2$ and 1-hexene after irradiation with a blue light source, recorded at 25 °C, 162 MHz.

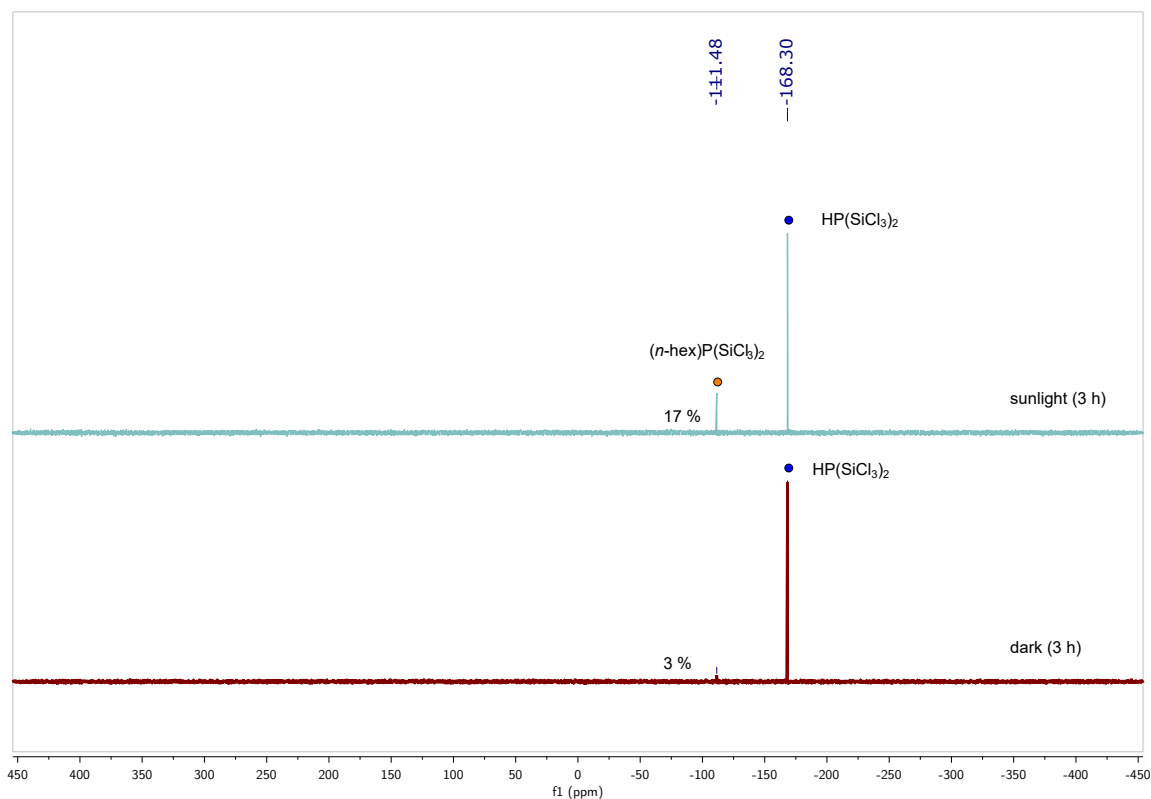


Figure 4.64 Comparison of the $^{31}\text{P}\{^1\text{H}\}$ NMR spectra of hexane solutions of $\text{HP}(\text{SiCl}_3)_2$ and 1-hexene after exposure to ambient light and being kept in the dark (3 h), recorded at 25 °C, 162 MHz.

4.5.11 Comparing $\text{HP}(\text{SiCl}_3)_2$ and Ph_2PH for the hydrophosphination of 1-hexene

In the glovebox, two samples were prepared containing either $\text{HP}(\text{SiCl}_3)_2$ (10 mg, 0.033 mmol, 1 equiv) or Ph_2PH (6 mg, 0.033 mmol, 1 equiv) and 1-hexene (6 mg, 0.066 mmol, 2 equiv) in hexane (0.5 mL). Each of these samples was irradiated for 15 min. Each was analyzed by $^{31}\text{P}\{^1\text{H}\}$ NMR spectroscopy to determine approximate ratios of starting material to product. The ratios (starting material:product) were found to be 50:50 and 99:1 for $\text{HP}(\text{SiCl}_3)_2$ and Ph_2PH , respectively.

4.5.12 General computational methods

Calculations were performed using ORCA 4.1.0 and 4.2.0.³³ Geometries were optimized at the specified level of theory and a frequencies calculation was performed, showing zero imaginary frequencies for intermediates and one imaginary frequency for transition states.

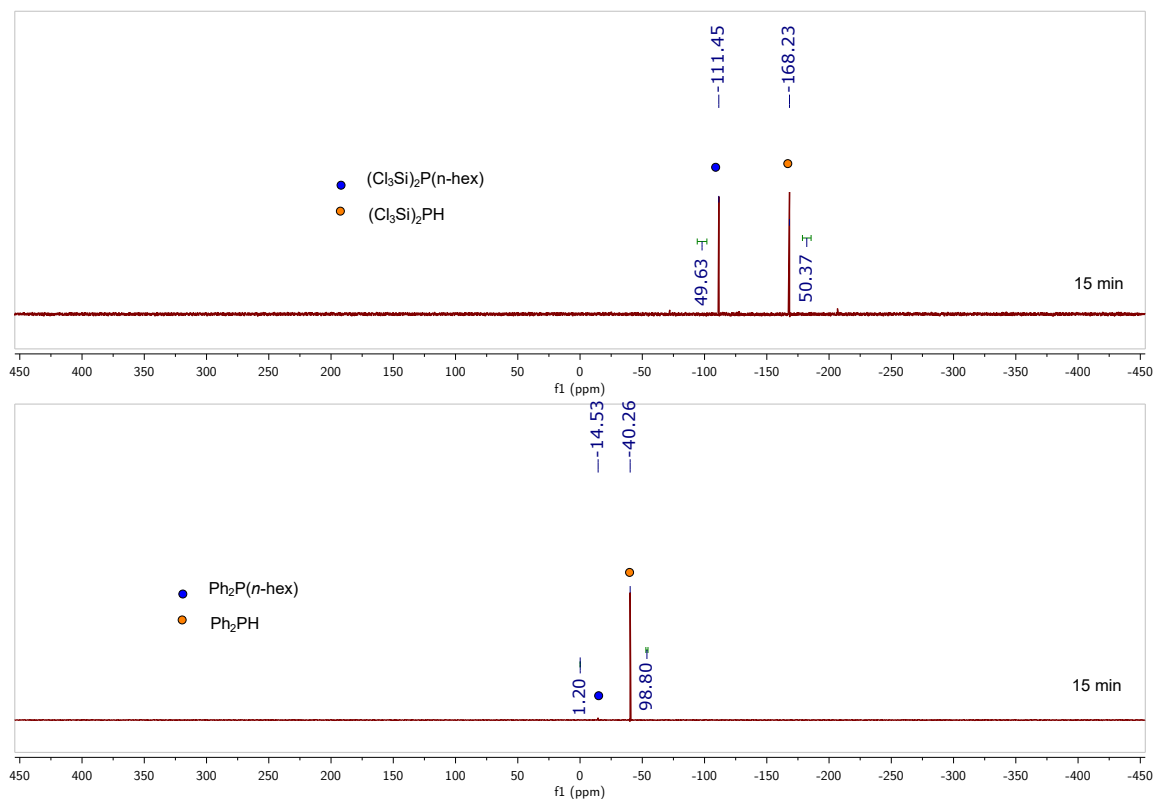


Figure 4.65 $^{31}\text{P}\{^1\text{H}\}$ NMR spectra of two reaction mixtures, prepared as described in section 4.5.11, recorded at 25 °C, 162 MHz.

Calculations were performed using the Massachusetts Green High-Performance Computing Center. Results were visualized using Avogadro.⁵²

4.5.13 Minimum energy pathway calculations

Calculations were performed at the $\omega\text{B97X-D3}/\text{def2-TZVP}/\text{CPCM}(\text{hexane})$ (Method A) level of theory. An example input is provided below:

```
%pal nprocs 16 end
% MaxCore 8000

! wB97X-D3 RIJCOSX def2-TZVP def2/J TightSCF Grid4 GridX4 FinalGrid5
Opt NumFreq CPCM(hexane)

* xyzfile 0 1 filename.xyz
```

Single point calculations were performed on the geometries obtained by Method A at the DLPNO-CCSD(T)/cc-pTVZ/CPCM(hexane) (Method B) level of theory. The RIJK approximation was used, in conjunction with the appropriate coulomb and exchange fitting basis sets. The TightPNO keyword was used. An example input is shown below:

```
%pal nprocs 16 end
% MaxCore 2000

! UHF DLPNO-CCSD(T) cc-pVTZ cc-pVTZ/C cc-pVTZ/JK TIGHTSCF RIJK TightPNO
Grid4 GridX4 FinalGrid5 CPCM(hexane)

* xyzfile 0 1 filename.xyz
```

Single point SCF energies obtained from Method B were combined with thermochemical quantities obtained from Method A (Tables 4.3 and 4.4). Free energies were corrected from gas phase to their standard state by -1.89 kcal/mol.⁵³ The values obtained were used to calculate relative energy differences (Table 4.5).

Table 4.3 Calculated energies (Method A) for species relevant to minimum energy pathway calculations

Compound	ImF/cm ⁻¹	ω -B97X-D3/def2-TZVP/CPCM(hexane)			
		E _{h, DFT} ^a	H _{sol, DFT}	G _{sol, DFT}	G _{sol, DFT} [⊖] ^b
HP(SiCl ₃) ₂	none	-3682.593 29	-3682.556 27	-3682.612 19	-3682.609 17
1-propene	none	-117.915 62	-117.830 65	-117.860 62	-117.857 61
•P(SiCl ₃) ₂	none	-3681.955 05	-3681.927 03	-3681.983 05	-3681.980 04
TS1	-288.2	-3799.873 68	-3799.760 10	-3799.825 73	-3799.822 72
I1	none	-3799.887 82	-3799.773 72	-3799.839 63	-3799.836 62
(<i>n</i> -Pr)P(SiCl ₃) ₂	none	-3800.552 90	-3800.424 39	-3800.489 55	-3800.486 54
TS2	-909.6	-7482.486 99	-7482.336 37	-7482.432 83	-7482.429 81
2-butene	none	-157.237 45	-157.122 70	-157.156 51	-157.153 50
I1-2-butene	none	-3839.203 53	-3839.059 84	-3839.128 76	-3839.125 75

^a All energies are in Hartrees^b Corrected for the standard state by -1.89 kcal/mol; 1 hartree = 627.509 kcal/mol**Table 4.4** Calculated energies (Method B) for species relevant to minimum energy pathway calculations

Compound	DLPNO-CCSD(T)/cc-pVTZ/CPCM(hexane)			
	E _{h, DLPNO} ^a	H _{sol, DLPNO} ^c	G _{sol, DLPNO} ^d	G _{sol, DLPNO} [⊖] ^{b,e}
HP(SiCl ₃) ₂	-3678.367 61	-3678.330 60	-3678.386 52	-3678.383 50
1-propene	-117.682 40	-117.597 42	-117.627 39	-117.624 38
•P(SiCl ₃) ₂	-3677.732 77	-3677.704 75	-3677.760 77	-3677.757 76
TS1	-3795.416 04	-3795.302 46	-3795.368 09	-3795.365 08
I1	-3795.426 82	-3795.312 73	-3795.378 64	-3795.375 63
(<i>n</i> -Pr)P(SiCl ₃) ₂	-3796.092 59	-3795.964 08	-3796.029 24	-3796.026 23
TS2	-7473.799 33	-7473.648 71	-7473.745 17	-7473.742 16
2-butene	-156.925 09	-156.810 34	-156.844 15	-156.841 14
I1-2-butene	-3834.664 92	-3834.521 22	-3834.590 15	-3834.587 14

^a All energies are in Hartrees^b Corrected for the standard state by -1.89 kcal/mol; 1 hartree = 627.509 kcal/mol^c (H_{sol, DFT}) - (E_{h, DFT}) + (E_{h, DLPNO})^d (G_{sol, DFT}) - (E_{h, DFT}) + (E_{h, DLPNO})^e (G_{sol, DFT}[⊖]) - (E_{h, DFT}) + (E_{h, DLPNO})

Table 4.5 Relative energies of calculated transition states and intermediates for the minimum energy pathway calculations

Species	ω -B97X-D3/def2-TZVP/CPCM(hexane)		DLPNO-CCSD(T)/cc-pVTZ/CPCM(hexane)	
	H _{rel, sol, DFT} ^b	G _{rel, sol, DFT} [⊖]	H _{rel, sol, DLPNO}	G _{rel, sol, DLPNO} [⊖]
1 + \cdot P(SiCl ₃) ₂ + 1-propene	0.0	0.0	0.0	0.0
1 + TS1	-1.5	9.4	-0.2	10.7
1 + I1	-10.1	0.6	-6.6	4.1
TS2	-14.1	10.7	-10.0	14.7
(<i>n</i> -Pr)P(SiCl ₃) ₂ + \cdot P(SiCl ₃) ₂	-23.5	-12.4	-22.6	-11.5
\cdot P(SiCl ₃) ₂ + 2-butene	0.0	0.0	0.0	0.0
I1 -2-butene	-6.3	4.9	-3.8	7.4

^a All energies in kcal/mol; 1 hartree = 627.509 kcal/mol^b $\sum E_{\text{products}} - \sum E_{\text{reactants}}$

4.5.14 Analysis of charge and spin densities for TS1

A relaxed surface scan was performed, stepping the P–C bond closer between $\cdot\text{P}(\text{SiCl}_3)_2$ and 1-propene, using the following input:

```
%pal nprocs 16 end
% MaxCore 8000

! wB97X-D3 RIJCOSX def2-TZVP def2/J Grid4 GridX4 FinalGrid5 Opt
CPCM(hexane)

%geom scan
B 0 9 = 3.614, 1.8, 30
end
end

* xyzfile 0 2 filename.xyz
```

At each step of the calculation, ORCA prints the Mulliken population analysis. The partial charges were summed over $\cdot\text{P}(\text{SiCl}_3)_2$ and 1-propene and tabulated using Excel. These results were used to generate the figure in the manuscript. NBO⁵⁴ and QTAIM⁵⁵ electron and spin densities were generated at selected points in the relaxed surface scan using the NBO keyword in ORCA or the multiWFN package,⁵⁶ respectively. The results of all three methods are shown in Fig. 4.66.

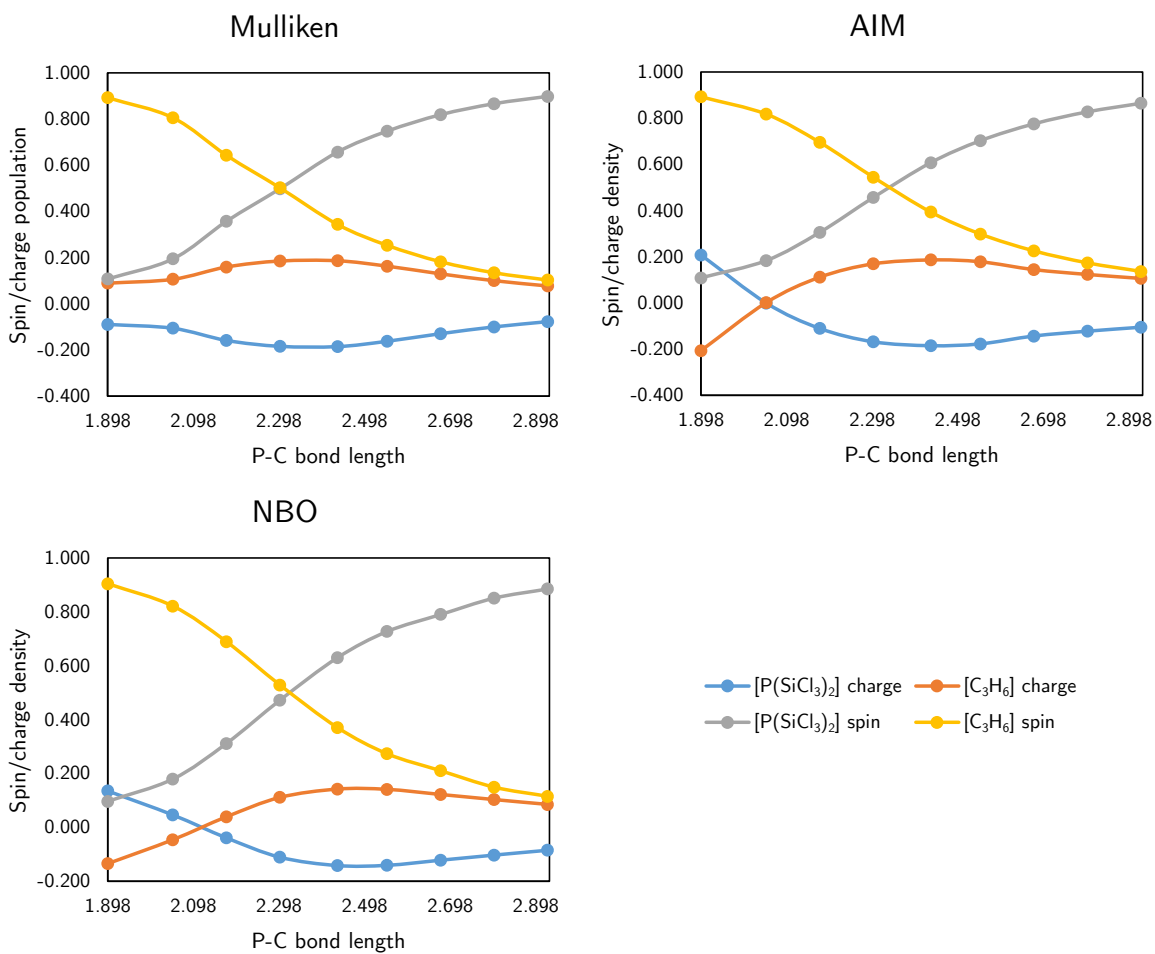


Figure 4.66 Comparison of the charge and spin on the $[P(SiCl_3)_2]$ and $[C_3H_6]$ fragments as assayed by Mulliken population, QTAIM density, and NBO density.

4.5.15 Calculation of pK_a values in acetonitrile

Thermochemistry for 11 known acids⁵⁷ were calculated at the ω B97X-D3/def2-TZVP/-CPCM(acetonitrile) level of theory. An example input is shown below:

```
%pal nprocs 16 end
% MaxCore 8000

! wB97X-D3 RIJCOSX def2-TZVPP def2/J TightSCF Grid4 GridX4 FinalGrid5
Opt NumFreq CPCM(acetonitrile)

* xyzfile 0 1 filename.xyz
```

The enthalpies of the acid and conjugate base are tabulated in Table 4.6. The difference in these two values was plotted against the experimental pK_a to give a line of best fit (Figure 4.67).

Table 4.6 Calculated and experimental parameters related to the pK_a 's of 11 acids.

Acid	$H_{\text{sol}}(\text{HX})^a$	$H_{\text{sol}}(\text{X}^-)$	$ H_{\text{sol}}(\text{HX}-\text{X}^-) $	Exp. pK_a	Pred. pK_a^b	Error ^c
HI	-298.363 63	-297.951 57	0.412 06	2.8	3.4	-0.6
Picric acid	-920.976 51	-920.541 09	0.435 42	11.0	12.0	-1.0
HCl	-460.813 56	-460.385 92	0.427 64	10.3	9.2	1.1
HBr	-2574.815 03	-2574.398 32	0.416 71	5.5	5.1	0.4
HClO ₄	-761.443 67	-761.043 14	0.400 53	1.83	-0.8	2.6
Acetic acid	-229.068 78	-228.610 18	0.458 61	23.51	20.5	3.0
Ph ₃ NH ⁺	-749.461 48	-749.874 74	0.413 26	1.28	3.9	-2.6
pyridinium	-248.211 93	-248.655 09	0.443 16	12.53	14.8	-2.3
PhNH ₃ ⁺	-287.515 42	-287.947 85	0.432 43	10.62	10.9	-0.3
Ph ₂ NH ₂ ⁺	-518.488 77	-518.912 82	0.424 06	5.98	7.8	-1.9
(CN) ₂ C=C(CN)(OH)	-430.507 71	-430.096 55	0.411 16	4.69	3.1	1.6
Ph ₂ PH	-805.087 34	-804.596 36	0.490 98		32.4	
HP(SiCl ₃) ₂	-3682.559 61	-3682.120 76	0.438 85		13.3	
PH ₃	-343.123 91	-342.635 22	0.488 69		31.6	
Standard deviation						1.9

^a All energies Hartrees

^b Predicted pK_a determined by evaluation of $|H_{\text{sol}}(\text{HX}-\text{X}^-)|$ against a line of best fit; Pred. $pK_a = 367.04 \times |H_{\text{sol}}(\text{HX}-\text{X}^-)| - 147.81$

^c Exp. $pK_a - \text{Calc. } pK_a$

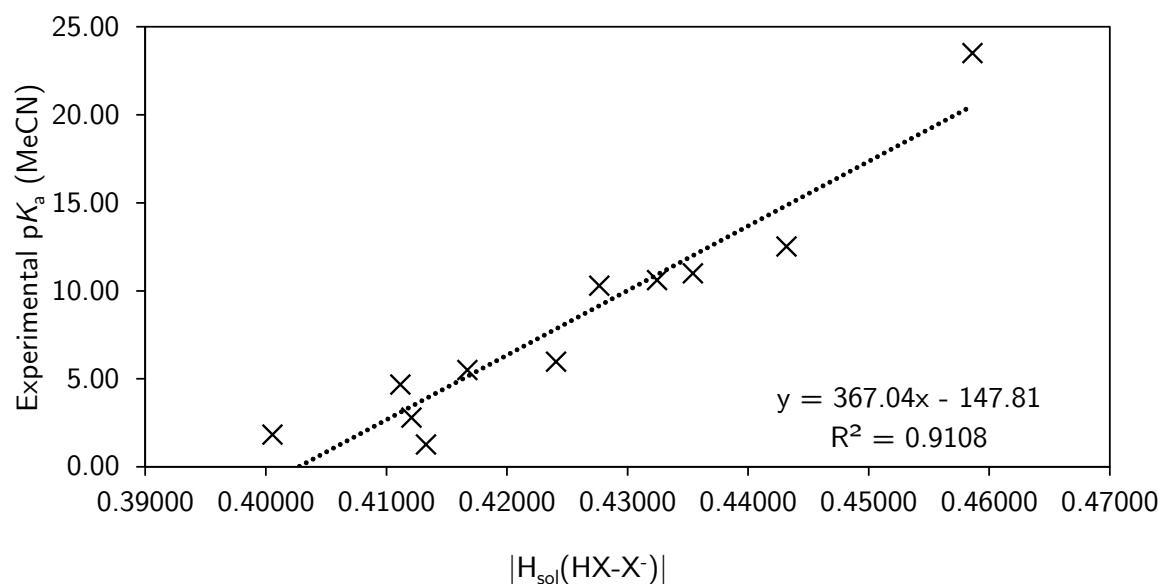


Figure 4.67 Regression of experimental pK_a against $|H_{sol}(HX-X^-)|$ to generate a line of best fit.

4.5.16 Calculated UV-vis spectrum of $\text{HP}(\text{SiCl}_3)_2$

The UV-vis spectrum of $\text{HP}(\text{SiCl}_3)_2$ was calculated using the TDDFT functionality within ORCA. The input is provided below:

```
! wB97X-D3 RIJCOSX def2-TZVP def2/J TightSCF Grid4 GridX4 FinalGrid5

%moinp "old.gbw"

%tddft
maxdim 5
nroots 50
end

* xyzfile 0 1 filename.xyz
```

The spectrum was plotted in Excel and is shown in Fig. 4.68.

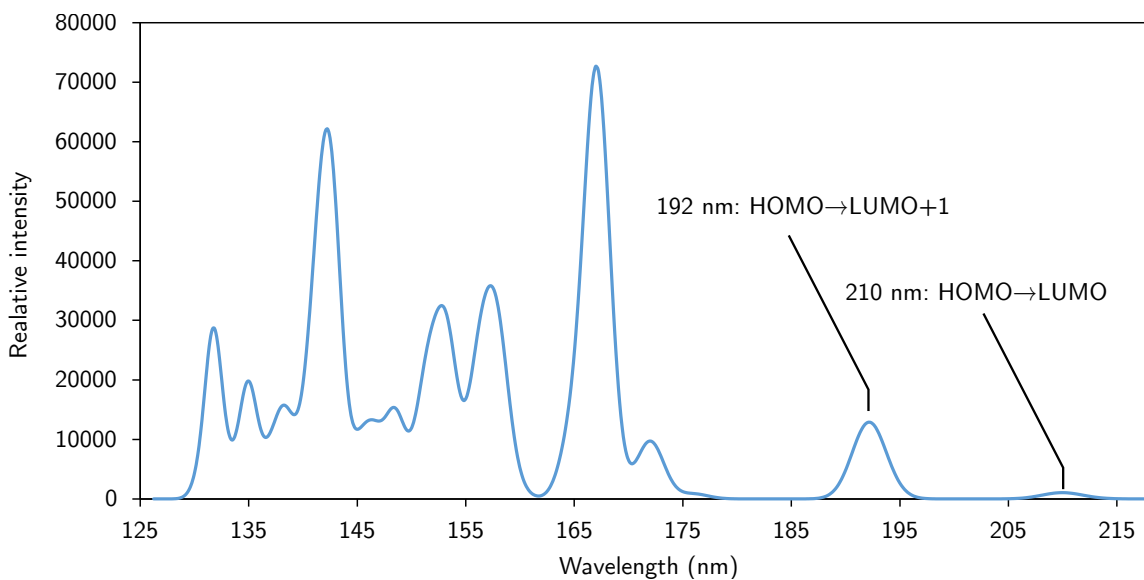


Figure 4.68 Calculated UV-vis spectrum of $\text{HP}(\text{SiCl}_3)_2$.

The Kohn–Sham orbitals corresponding to the HOMO, LUMO, and LUMO+1 are displayed in Figure 4.69.

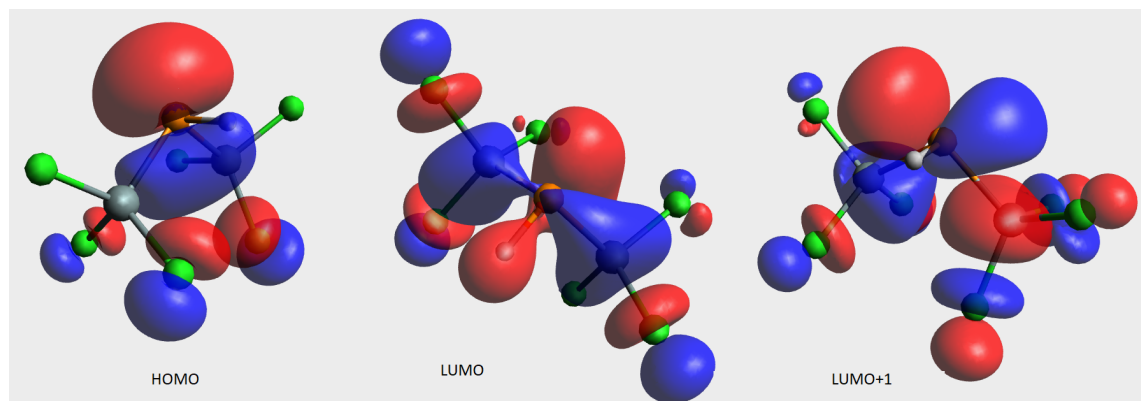


Figure 4.69 Kohn–Sham molecular orbitals for HP(SiCl₃)₂; HOMO (left), LUMO (middle), LUMO+1 (right).

4.5.17 Calculation of bond dissociation enthalpy (BDE)

Bond dissociation energies were calculated at the same level of theory as described in Section 4.5.13. The electronic energy of the hydrogen atom was taken as the exact value, $-0.5 E_h$. A summary of the energies are provided in Tables 4.7 and 4.8. The use of a solvation model (CPCM(hexane)) was found to have a negligible effect on the value of the BDE for $\text{HP}(\text{SiCl}_3)_2$, thus solvation *was* included for the other species to facilitate comparison of energies obtained from these calculations with those in Section 4.5.13. The $\text{BDE}_g^{298\text{ K}}(\text{P-H})$ values were calculated using the column titled “ $\text{H}_{\text{sol, DLPNO}}$ ” and found to be 82.2, 75.8, and 82.1 kcal/mol, for $\text{HP}(\text{SiCl}_3)_2$, Ph_2PH , and PH_3 , respectively. The values of the unoccupied β -spin orbitals provided in the manuscript for the radical species below come from Method B (DLPNO-CCSD(T)/cc-pVTZ) described in Section 4.5.13.

Table 4.7 Calculated energies (Method A) for species relevant to minimum energy pathway calculations

Compound	ImF/cm ⁻¹	ω -B97X-D3/def2-TZVP/CPCM(hexane)			
		E _{h, DFT} ^a	H _{sol, DFT}	G _{sol, DFT}	G _{sol, DFT} ^{⊖ b}
H•	none	-0.502 19	-0.496 99	-0.510 01	-0.507 00
HP(SiCl ₃) ₂	none	-3682.593 29	-3682.556 27	-3682.612 19	-3682.609 17
•P(SiCl ₃) ₂	none	-3681.955 05	-3681.927 03	-3681.983 05	-3681.980 04
Ph ₂ PH	none	-805.282 85	-805.077 92	-805.126 08	-805.123 07
•PPh ₂	none	-804.654 01	-804.458 92	-804.507 43	-804.504 42
PH ₃	none	-343.150 07	-343.121 93	-343.146 81	-343.143 80
•PH ₂	none	-342.509 14	-342.491 68	-342.516 45	-342.513 44

^a All energies are in Hartrees

^b Corrected for the standard state by -1.89 kcal/mol; 1 hartree = 627.509 kcal/mol

Table 4.8 Calculated energies (Method B) for species relevant to minimum energy pathway calculations

Compound	DLPNO-CCSD(T)/cc-pVTZ/CPCM(hexane)			
	E _{h, DLPNO} ^a	H _{sol, DLPNO} ^c	G _{sol, DLPNO} ^d	G _{sol, DLPNO} ^{⊖ b, e}
H•	-0.500 00	-0.494 81	-0.507 82	-0.504 81
HP(SiCl ₃) ₂	-3678.367 61	-3678.330 60	-3678.386 52	-3678.383 50
•P(SiCl ₃) ₂	-3677.732 77	-3677.704 75	-3677.760 77	-3677.757 76
Ph ₂ PH	-803.920 26	-803.715 33	-803.763 49	-803.760 48
•PPh ₂	-803.294 78	-803.099 69	-803.148 20	-803.145 19
PH ₃	-342.693 12	-342.664 99	-342.689 87	-342.686 86
•PH ₂	-342.056 83	-342.039 37	-342.064 15	-342.061 13

^a All energies are in Hartrees

^b Corrected for the standard state by -1.89 kcal/mol; 1 hartree = 627.509 kcal/mol

^c (H_{sol, DFT}) - (E_{h, DFT}) + (E_{h, DLPNO})

^d (G_{sol, DFT}) - (E_{h, DFT}) + (E_{h, DLPNO})

^e (G_{sol, DFT}[⊖]) - (E_{h, DFT}) + (E_{h, DLPNO})

4.5.18 Spin density plots for $\cdot\text{P}(\text{SiCl}_3)_2$, $\cdot\text{PH}_2$, and $\cdot\text{PPh}_2$

The structures and wave-functions of $\cdot\text{P}(\text{SiCl}_3)_2$, $\cdot\text{PH}_2$, and $\cdot\text{PPh}_2$ were obtained from the DFT procedure outlined in Section 4.5.17. The spin densities were plotted (Figure 4.70) using MultiWFN.⁵⁶ The isosurfaces at the 0.01 level show that only $\cdot\text{PPh}_2$ has any appreciable spin density not located on the P atom.

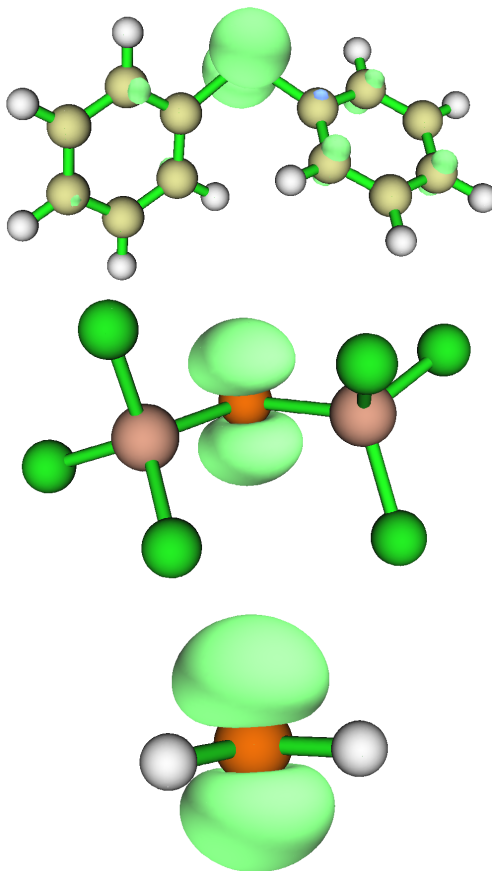


Figure 4.70 Plots of the spin density (0.01 isosurface) for $\cdot\text{PPh}_2$ (top), $\cdot\text{P}(\text{SiCl}_3)_2$ (middle), and $\cdot\text{PH}_2$ (bottom).

4.5.19 UV Irradiation of $\text{HP}(\text{SiCl}_3)_2$ in chlorobenzene

In the glovebox, $\text{HP}(\text{SiCl}_3)_2$ (10 mg, 0.033 mmol, 1 equiv) was weighed into the end of a pipette and washed into an NMR tube equipped with a J. Young valve using chlorobenzene (0.6 mL). The resulting solution was irradiated (254 nm) for 20 minutes in the RPR then analyzed by ^{31}P NMR spectroscopy. Irradiation for 1.5 hours led to full consumption of starting material. In addition to H_2PSiCl_3 , signals were assigned to PhPH_2 , $\text{PhP}(\text{SiCl}_3)\text{H}$, and $\text{PhP}(\text{SiCl}_3)_2$. $\text{PhP}(\text{SiCl}_3)_2$: $^{31}\text{P}\{^1\text{H}\}$ NMR (162 MHz, chlorobenzene, δ) -112.2 (s, $J_{\text{P-Si}} = 80.0$ Hz). ^{31}P NMR (162 MHz, chlorobenzene, δ) -112.2 (t, $J_{\text{P-H}} = 10.0$ Hz). $\text{PhP}(\text{SiCl}_3)\text{H}$: $^{31}\text{P}\{^1\text{H}\}$ NMR (162 MHz, chlorobenzene, δ) -103.8 (s). ^{31}P NMR (162 MHz, chlorobenzene, δ) -103.8 (dm, $J_{\text{P-H}} = 204$ Hz).

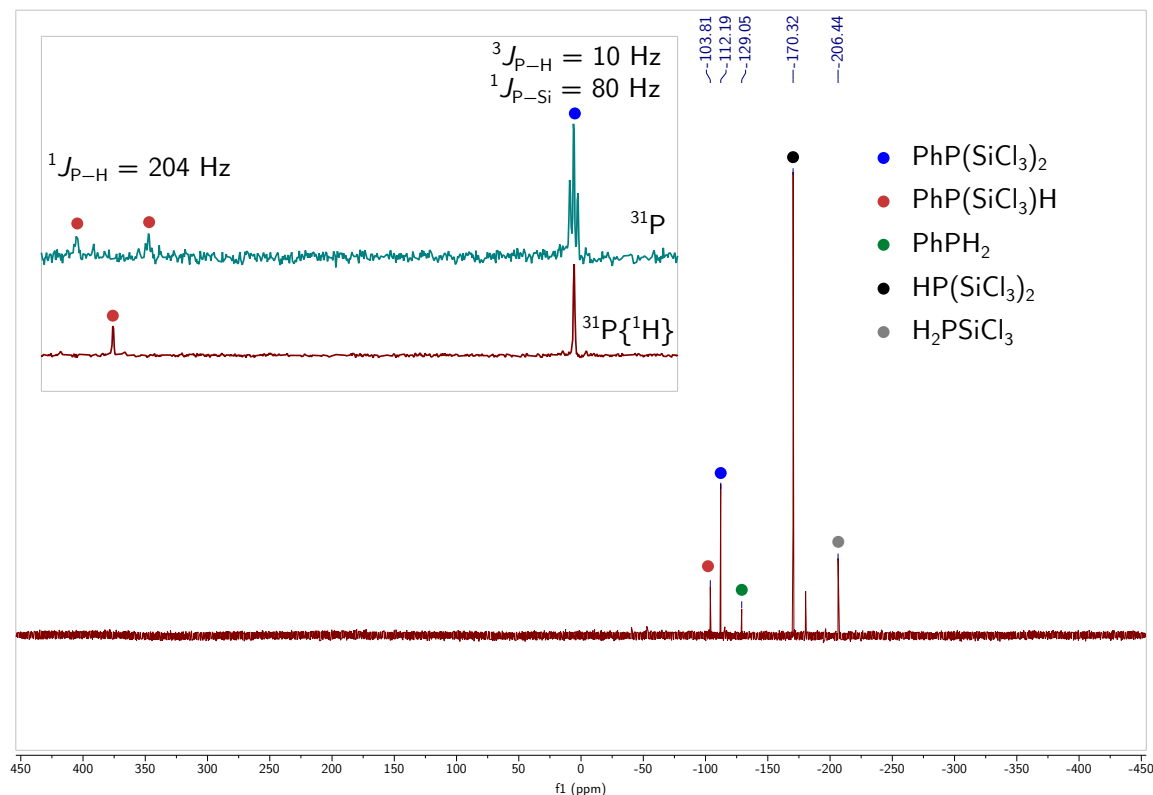


Figure 4.71 $^{31}\text{P}\{^1\text{H}\}$ NMR spectrum (inset: zoom of region of interest, top: $^{31}\text{P}\{^1\text{H}\}$; bottom: ^{31}P) of the reaction mixture prepared as described in Section 4.5.19 after UV irradiation (20 min), recorded at 162 MHz and 25 °C.

4.5.20 Oxidation of [TBA]1 with ferrocenium salts

In the glovebox, [TBA]1 (10 mg, 0.0185 mmol, 1 equiv) and [Fc][BArF₂₄] (19 mg, 0.0185 mmol, 1 equiv) were weighed into separate vials and dissolved in 1,2-difluorobenzene (0.3 mL each). The solutions were frozen in the glovebox coldwell until frozen. Upon thawing, the solutions were combined. The deep blue color of the ferrocenium salt immediately faded to give a pale orange solution. After approximately three minutes, yellow material began to precipitate from the reaction mixture. Analysis by NMR spectroscopy showed the presence of [TBA][BArF₂₄] and ferrocene in solution. No signal was observed by ³¹P NMR spectroscopy. The yellow precipitate was not subject to further investigations. In future work, the initially generated solution (prior to precipitation) should be analyzed by low-temperature EPR spectroscopy.

The hexafluorophosphate salt of ferrocenium was also investigated as the oxidant. The procedure above was performed using [TBA]1 (20 mg, 0.0369 mmol, 1 equiv) and [Fc][PF₆] (12 mg, 0.0369 mmol, 1 equiv) in DCM (0.6 mL total). Upon mixing of the two solutions, the immediate formation of a brown precipitate was observed. No species were observed by ³¹P NMR spectroscopy, indicating the possible decomposition of the hexafluorophosphate anion.

References

- [1] (a) Musina, E. I.; Balueva, A. S.; Karasik, A. A. *Organophosphorus Chemistry*; 2019; pp 1–63; (b) Svara, J.; Weferling, N.; Hofmann, T. In “*Phosphorus Compounds, Organic*” in *Ullmann’s Encyclopedia of Industrial Chemistry*; Wiley, Ed.; Wiley-VCH: Weinheim, Germany, 2006.
- [2] (a) Balázs, L. B.; Khalikuzzaman, J. B.; Li, Y.; Csókás, D.; Pullarkat, S. A.; Leung, P.-H. *Chem. Commun.* **2019**, *55*, 10936–10939; (b) Zhang, Y.; Tang, L.; Ding, Y.; Chua, J.-H.; Li, Y.; Yuan, M.; Leung, P.-H. *Tetrahedron Lett.* **2008**, *49*, 1762–1767; (c) Kamitani, M.; Itazaki, M.; Tamiya, C.; Nakazawa, H. *J. Am. Chem. Soc.* **2012**, *134*, 11932–11935; (d) J. Ackley, B.; K. Pagano, J.; Waterman, R. *Chem. Commun.* **2018**, *54*, 2774–2776; (e) Giuseppe, A. D.; Luca, R. D.; Castarlenas, R.; J. Pérez-Torrente, J.; Crucianelli, M.; A. Oro, L. *Chem. Commun.* **2016**, *52*, 5554–5557; (f) Yuan, J.; Zhu, L.; Zhang, J.; Li, J.; Cui, C. *Organometallics* **2017**, *36*, 455–459.
- [3] (a) Lu, Z.; Zhang, H.; Yang, Z.; Ding, N.; Meng, L.; Wang, J. *ACS Catal.* **2019**, *9*, 1457–1463; (b) Feng, J.-J.; Chen, X.-F.; Shi, M.; Duan, W.-L. *J. Am. Chem. Soc.* **2010**, *132*, 5562–5563; (c) Huang, Y.; A. Pullarkat, S.; Li, Y.; Leung, P.-H. *Chem. Commun.* **2010**, *46*, 6950–6952; (d) Sadow, A. D.; Haller, I.; Fadini, L.; Togni, A. *J. Am. Chem. Soc.* **2004**, *126*, 14704–14705; (e) Kovacic, I.; Wicht, D. K.; Grewal, N. S.; Glueck, D. S.; Incarvito, C. D.; Guzei, I. A.; Rheingold, A. L. *Organometallics* **2000**, *19*, 950–953.
- [4] (a) Lapshin, I. V.; Basalov, I. V.; Lyssenko, K. A.; Cherkasov, A. V.; Trifonov, A. A.

- Chem. Eur. J.* **2018**, *25*, 459–463; (b) Ghebreab, M. B.; Bange, C. A.; Waterman, R. *J. Am. Chem. Soc.* **2014**, *136*, 9240–9243; (c) Espinal-Viguri, M.; King, A. K.; Lowe, J. P.; Mahon, M. F.; Webster, R. L. *ACS Catal.* **2016**, *6*, 7892–7897; (d) Kawaoka, A. M.; Douglass, M. R.; Marks, T. J. *Organometallics* **2003**, *22*, 4630–4632.
- [5] (a) Bissessar, D.; Egly, J.; Achard, T.; Steffanut, P.; Bellemin-Laponnaz, S. *RSC Advances* **2019**, *9*, 27250–27256; (b) Moglie, Y.; José González-Soria, M.; Martín-García, I.; Radivoy, G.; Alonso, F. *Green Chem.* **2016**, *18*, 4896–4907.
- [6] Knights, A. W.; Chitnis, S. S.; Manners, I. *Chem. Sci.* **2019**, *10*, 7281–7289.
- [7] Bange, C. A.; Waterman, R. *Chem. - Eur. J.* **2016**, *22*, 12598–12605.
- [8] Gusarova, N. K.; Chernysheva, N. A.; Trofimov, B. A. *Synthesis* **2017**, *49*, 4783–4807.
- [9] Novas, B. T.; Bange, C. A.; Waterman, R. *Eur. J. Inorg. Chem.* **2019**, *2019*, 1640–1643.
- [10] Pringle, P. G.; Smith, M. B. *J. Chem. Soc., Chem. Commun.* **1990**, 1701–1702.
- [11] Geeson, M. B.; Cummins, C. C. *Science* **2018**, *359*, 1383–1385.
- [12] Geeson, M. B.; Ríos, P.; Transue, W. J.; Cummins, C. C. *J. Am. Chem. Soc.* **2019**, *141*, 6375–6384.
- [13] Swager, T. M.; Peeks, M. D. *Synfacts* **2018**, *14*, 592.
- [14] Slootweg, J. C. *Angew. Chem., Int. Ed.* **2018**, *57*, 6386–6388.
- [15] Slootweg, J. C. *Angew. Chem.* **2018**, *130*, 6494–6496.
- [16] Protasiewicz, J. D. *Science* **2018**, *359*, 1333–1333.
- [17] Delacroix, O.; Gaumont, A. *Curr. Org. Chem.* **2005**, *9*, 1851–1882.
- [18] Schubert, D. M.; Norman, A. D. *Inorg. Chem.* **1984**, *23*, 4130–4131.
- [19] (a) Schubert, D. M.; Brandt, P. F.; Norman, A. D. *Inorg. Chem.* **1996**, *35*, 6204–6209; (b) Schubert, D. M.; Hackney, M. L. J.; Brandt, P. F.; Norman, A. D. *Phosphorus, Sulfur Silicon Relat. Elem.* **1997**, *123*, 141–160; (c) Hackney, M. L. J.; Schubert, D. M.; Brandt, P. F.; Haltiwanger, R. C.; Norman, A. D. *Inorg. Chem.* **1997**, *36*, 1867–1872.
- [20] Martens, R.; Mont, W.-W. D. *Chem. Ber.* **1992**, *125*, 657–658.
- [21] Müller, L.-P.; Zanin, A.; Du Mont, W.-W.; Jeske, J.; Martens, R.; Jones, P. G. *Chem. Ber.* **1997**, *130*, 377–384.
- [22] Müller, L.-P.; Mont, W.-W. D.; Jeske, J.; Jones, P. G. *Chem. Ber.* **1995**, *128*, 615–619.
- [23] Müller, L.-P.; Zanin, A.; Jeske, J.; Jones, P. G.; du Mont, W.-W. In *Organosilicon Chemistry Set*; Auner, N., Weis, J., Eds.; Wiley-VCH Verlag GmbH: Weinheim, Germany, 2005; pp 286–290.
- [24] Anslyn, E. V.; Dougherty, D. A. *Modern Physical Organic Chemistry*; University Science: Sausalito, CA, 2006.
- [25] (a) Tian, F.; Dolbier, W. R. *Org. Lett.* **2000**, *2*, 835–837; (b) Tian, F.; Battiste, M. A.; Dolbier, W. R. *Org. Lett.* **1999**, *1*, 193–196.
- [26] (a) Chatgililoglu, C.; Ferreri, C.; Ballestri, M.; Mulazzani, Q. G.; Landi, L. *J. Am. Chem. Soc.* **2000**, *122*, 4593–4601; (b) Chatgililoglu, C.; Altieri, A.; Fischer, H. *J. Am. Chem. Soc.* **2002**, *124*, 12816–12823; (c) Chatgililoglu, C.; Samadi, A.;

- Guerra, M.; Fischer, H. *ChemPhysChem* **2005**, *6*, 286–291; (d) Biermann, U.; Butte, W.; Koch, R.; Fokou, P. A.; Türünc, O.; Meier, M. A. R.; Metzger, J. O. *Chem. - Eur. J.* **2012**, *18*, 8201–8207.
- [27] Fischer, H.; Radom, L. *Angew. Chem., Int. Ed.* **2001**, *40*, 1340–1371.
- [28] (a) Oddershede, J.; Geertsen, J.; Scuseria, G. E. *J. Phys. Chem.* **1988**, *92*, 3056–3059; (b) Chen, J. Y.-C.; Martí, A. A.; Turro, N. J.; Komatsu, K.; Murata, Y.; Lawler, R. G. *J. Phys. Chem. B* **2010**, *114*, 14689–14695.
- [29] Pryor, W. A.; Stanley, J. P. *J. Am. Chem. Soc.* **1971**, *93*, 1412–1418.
- [30] (a) Grimme, S.; Antony, J.; Ehrlich, S.; Krieg, H. *J. Chem. Phys.* **2010**, *132*, 154104; (b) Lin, Y.-S.; Li, G.-D.; Mao, S.-P.; Chai, J.-D. *J. Chem. Theory Comput.* **2013**, *9*, 263–272; (c) Weigend, F. *Phys. Chem. Chem. Phys.* **2006**, *8*, 1057–1065.
- [31] (a) Liakos, D. G.; Neese, F. *J. Chem. Theory Comput.* **2015**, *11*, 4054–4063; (b) Liakos, D. G.; Sparta, M.; Kesharwani, M. K.; Martin, J. M. L.; Neese, F. *J. Chem. Theory Comput.* **2015**, *11*, 1525–1539; (c) Guo, Y.; Riplinger, C.; Becker, U.; Liakos, D. G.; Minenkov, Y.; Cavallo, L.; Neese, F. *J. Chem. Phys.* **2018**, *148*, 011101; (d) Kendall, R. A.; Dunning, T. H.; Harrison, R. J. *J. Chem. Phys.* **1992**, *96*, 6796–6806.
- [32] Neese, F. *Wiley Interdiscip. Rev.: Comput. Mol. Sci.* **2018**, *8*, e1327.
- [33] Neese, F. *Wiley Interdisciplinary Reviews: Computational Molecular Science* **2012**, *2*, 73–78.
- [34] Daeffler, C. S.; Grubbs, R. H. *Org. Lett.* **2011**, *13*, 6429–6431.
- [35] Northrop, B. H.; Coffey, R. N. *J. Am. Chem. Soc.* **2012**, *134*, 13804–13817.
- [36] (a) Wicht, D. K.; Paisner, S. N.; Lew, B. M.; Glueck, D. S.; Yap, G. P. A.; Liable-Sands, L. M.; Rheingold, A. L.; Haar, C. M.; Nolan, S. P. *Organometallics* **1998**, *17*, 652–660; (b) Cheng, Y.-H.; Fang, Y.; Zhao, X.; Liu, L.; Guo, Q.-X. *Bull. Chem. Soc. Jpn.* **2002**, *75*, 1715–1722.
- [37] Berkowitz, J.; Curtiss, L. A.; Gibson, S. T.; Greene, J. P.; Hillhouse, G. L.; Pople, J. A. *J. Chem. Phys.* **1986**, *84*, 375–384.
- [38] Bordwell, F. G.; Cheng, J. P.; Harrelson, J. A. *J. Am. Chem. Soc.* **1988**, *110*, 1229–1231.
- [39] Warren, J. J.; Tronic, T. A.; Mayer, J. M. *Chem. Rev.* **2010**, *110*, 6961–7001.
- [40] Tavtorkin, A. N.; Toloraya, S. A.; Nifant'ev, E. E.; Nifant'ev, I. E. *Tetrahedron Lett.* **2011**, *52*, 824–825.
- [41] (a) Fox, R. B. *J. Am. Chem. Soc.* **1950**, *72*, 4147–4149; (b) Tebby, J. C.; Genov, D. G.; Wheeler, J. W. In “2.08 - Alkylphosphorus Compounds” in *Comprehensive Organic Functional Group Transformations*; Katritzky, A. R., Meth-Cohn, O., Rees, C. W., Eds.; Elsevier Science: Oxford, 1995; pp 425–477; (c) Wang, Z.; Pu, N.; Tian, Y.; Xu, C.; Wang, F.; Liu, Y.; Zhang, L.; Chen, J.; Ding, S. *Inorg. Chem.* **2019**, *58*, 5457–5467.
- [42] (a) Diemert, K.; Kottwitz, B.; Kuchen, W. *Phosphorus, Sulfur Silicon Relat. Elem.* **1986**, *26*, 307–320; (b) Diemert, K.; Kottwitz, B.; Kuchen, W. *J. Organomet. Chem.*

- 1986**, *307*, 291–305; (c) Cavaye, H.; Clegg, F.; Gould, P. J.; Ladyman, M. K.; Temple, T.; Dossi, E. *Macromolecules* **2017**, *50*, 9239–9248.
- [43] Wu, L.; Chitnis, S. S.; Jiao, H.; Annibale, V. T.; Manners, I. *J. Am. Chem. Soc.* **2017**, *139*, 16780–16790.
- [44] Pangborn, A. B.; Giardello, M. A.; Grubbs, R. H.; Rosen, R. K.; Timmers, F. J. *Organometallics* **1996**, *15*, 1518–1520.
- [45] Williams, D. B. G.; Lawton, M. *J. Org. Chem.* **2010**, *75*, 8351–8354.
- [46] Tofan, D.; Cummins, C. C. *Angew. Chem., Int. Ed.* **2010**, *49*, 7516–7518.
- [47] Levy, G. C.; Komoroski, R. A. *J. Am. Chem. Soc.* **1974**, *96*, 678–681.
- [48] Verstuyft, A. W.; Redfield, D. A.; Cary, L. W.; Nelson, J. H. *Inorg. Chem.* **1977**, *16*, 2776–2786.
- [49] Troupa, P.; Katsioulari, G.; Vassiliou, S. *Synlett* **2015**, *26*, 2714–2719.
- [50] Besse, V.; Le Pluart, L.; Cook, W. D.; Pham, T.-N.; Madec, P.-J. *J. Polym. Sci. A Polym. Chem.* **2013**, *51*, 149–157.
- [51] Thorshaug, K.; Swang, O.; Dahl, I. M.; Olafsen, A. *J. Phys. Chem. A* **2006**, *110*, 9801–9804.
- [52] Hanwell, M. D.; Curtis, D. E.; Lonie, D. C.; Vandermeersch, T.; Zurek, E.; Hutchison, G. R. *J. Cheminf.* **2012**, *4*, 17.
- [53] Cramer, C. J. *Essentials of Computational Chemistry*; John Wiley & Sons Ltd., 2004.
- [54] Glendening, E. D.; Landis, C. R.; Weinhold, F. *WIREs Comput Mol Sci* **2012**, *2*, 1–42.
- [55] Bader, R. F. W. *Chem. Rev.* **1991**, *91*, 893–928.
- [56] Lu, T.; Chen, F. *J. Comput. Chem.* **2012**, *33*, 580–592.
- [57] (a) Kütt, A.; Rodima, T.; Saame, J.; Raamat, E.; Mäemets, V.; Kaljurand, I.; Koppel, I. A.; Garlyauskayte, R. Y.; Yagupolskii, Y. L.; Yagupolskii, L. M.; Bernhardt, E.; Willner, H.; Leito, I. *J. Org. Chem.* **2011**, *76*, 391–395; (b) Tshepelevitsh, S.; Kütt, A.; Lõkov, M.; Kaljurand, I.; Saame, J.; Heering, A.; Plieger, P. G.; Vianello, R.; Leito, I. *Eur. J. Org. Chem.* **2019**, *2019*, 6735–6748.

Chapter 5

Organoiron- and Fluoride-Catalyzed Phosphinidene Transfer to Styrenic Olefins in a Stereoselective Synthesis of Unprotected Phosphiranes

Contents

5.1	Introduction	226
5.2	Results and Discussion	227
5.3	Conclusions	232
5.4	Future Work	233
5.5	Experimental methods	235
	References	279

Abstract

Catalytic phosphiranation has been achieved, allowing preparation of *trans*-1-R-2-phenylphosphiranes (R = *t*-Bu: **1-t**-Bu, *i*-Pr: **1-i**-Pr) from the corresponding dibenzo-7-(R)-7-phospha-norbornadiene (RPA, **A** = C₁₄H₁₀, anthracene) and styrene in 73% and 57%

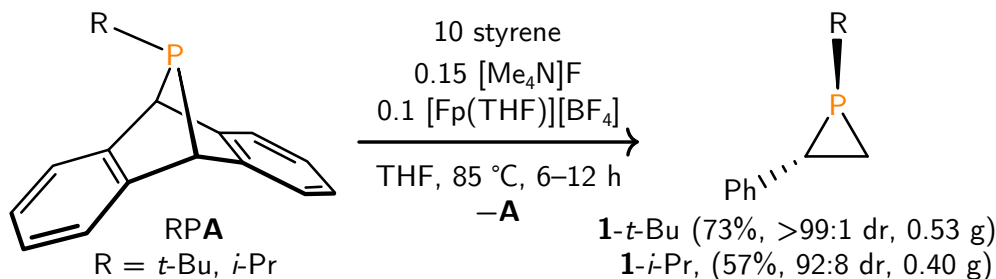
Reproduced in part with permission from: Geeson, M. B.; Transue, W. J.; Cummins, C. C. *J. Am. Chem. Soc.* **2019**, *141*, 13336–13340 (doi 10.1021/jacs.9b07069). Copyright © 2018 American Chemical Society.

isolated yields, respectively. The co-catalyst system requires tetramethylammonium fluoride (TMAF) and $[\text{Fp}(\text{THF})][\text{BF}_4]$ ($\text{Fp} = \text{Fe}(\eta^5\text{-C}_5\text{H}_5)(\text{CO})_2$). In the case of the *t*-Bu derivative, the reaction mechanism was probed using stoichiometric reaction studies, a Hammett analysis, and a deuterium labeling experiment. Together, these suggest the intermediacy of iron-phosphido $\text{FpP}(\text{F})(t\text{-Bu})$, generated independently from the stoichiometric reaction of $[\text{Fp}(t\text{-BuPA})][\text{BF}_4]$ with TMAF. Two other plausible reaction intermediates, $[\text{Fp}(t\text{-BuPA})][\text{BF}_4]$ and $[\text{Fp}(1-t\text{-Bu})][\text{BF}_4]$, were prepared independently and structurally characterized.

5.1 Introduction

Cyclopropanation, aziridination, and epoxidation reactions are widely used to construct strained three-membered rings desirable for further synthetic elaboration.¹ Transition-metal catalysts have been widely used to facilitate these transformations under mild reaction conditions with good stereoselective and enantioselective control.¹ In contrast, the phosphorus analog (“phosphirane”) remains in its infancy — this despite the documented utility of phosphiranes as catalyst ligands,² polymer precursors,³ and synthetic intermediates.⁴ Only a handful of transition metal-promoted phosphirane syntheses have been reported,^{5–8} and catalytic phosphirane transfer to give unprotected λ^3 -phosphiranes remains unknown despite decades of interest.^{6,7,9–11}

Perhaps one reason for the underdevelopment of catalytic phosphinidene transfer reactions stems from the lack of availability of appropriate precursors, a limitation recently articulated by de Bruin and Schneider.¹² Hallmarks of good substrates for group-transfer chemistry feature stable, neutral leaving groups, such as N_2 or iodobenzene.¹ In the case of phosphorus, only a limited number of catalytic group transfer reactions are known, generally involving activation of P–H bonds of primary phosphines in reactions disclosed by the groups of Waterman¹³ and Layfield.¹⁴



Scheme 5.1 Preparation of phosphiranes **1-*t*-Bu** and **1-*i*-Pr** from the corresponding **RPA** compounds.

We have developed dibenzo-7-phosphanorbornadiene compounds (**RPA**, **A** = anthracene, $\text{C}_{14}\text{H}_{10}$, Scheme 5.1), readily available from RPCl_2 and $\text{MgA}\cdot 3\text{THF}$,¹⁵ as useful synthetic equivalents for phosphinidenes.^{16–19} When R is a π -donating substituent, such as

Table 5.1 Control experiments.

Deviation from standard conditions ^a	Yield (%) ^b
None	90
No [Fp(THF)][BF ₄]	5
No TMAF	5
No [Fp(THF)][BF ₄] or TMAF	0
<i>t</i> -BuPH ₂ instead of <i>t</i> -BuPA	0
(<i>t</i> -BuP) ₃ instead of <i>t</i> -BuPA	0

^a 0.06 M *t*-BuPA in THF with reagent ratios shown in Scheme 5.1, 85 °C, 24 h

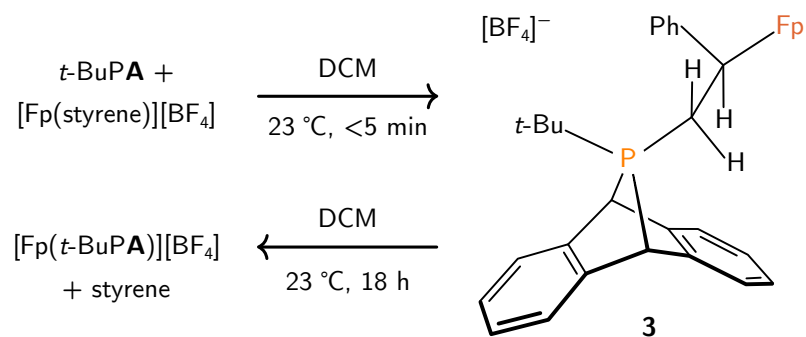
^b Yield of **1**-*t*-Bu determined by integration of the product relative to a standard by ³¹P{¹H} NMR spectroscopy

a dimethylamino group, the Me₂NPA species can undergo a thermal unimolecular fragmentation to give anthracene and a free singlet (amino)phosphinidene (Me₂NP) that can add to unsaturated substrates such as 1,3-cyclohexadiene to give a 7-phosphanorbornene.^{16,17} In contrast, when R is an alkyl substituent (for example, *t*-BuPA), the corresponding triplet phosphinidene is not transferred to unsaturated substrates, instead leading to recovery of starting material and formation of some (*t*-BuP)₃.^{16,17} Therefore, we sought to develop a process in which *t*-BuPA could be used as a reagent for catalytic *tert*-butyl phosphinidene transfer to alkenes, producing phosphirane products.

5.2 Results and Discussion

Following unproductive screening of a variety of catalysts (5.5.2) selected for their ability to effect cyclopropanation or aziridination, we scored a hit by using sources of the Fp⁺ cation in conjunction with fluoride. In analogy to known reactivity of [Fp(alkene)][BF₄] compounds with phosphines,^{20–22} we sought to promote P–C bond formation by treatment with *t*-BuPA. Treatment of a slurry of [Fp(styrene)][BF₄]²³ in dichloromethane with a stoichiometric amount of *t*-BuPA led to the rapid dissolution of all material. Analysis of this reaction mixture by electrospray ionization mass spectrometry (ESI-MS) and NMR spectroscopy (³¹P NMR: +141.8 ppm) was consistent with the addition of *t*-BuPA to the iron-coordinated styrene complex to produce an addition product (**2**) containing a phosphonium and iron-alkyl functionality within the same molecule (Scheme 5.2). Unfortunately, **2** could not be isolated in pure form. This was in part attributed to its relatively short lifetime in solution; after 24 h at 23 °C it had undergone complete conversion to [Fp(*t*-BuPA)][BF₄] and free styrene, suggesting that the formation of **2** is reversible (5.5.8).

Having observed C–P bond-formation, [Fp(styrene)][BF₄] and other sources of Fp⁺ were screened as catalysts for the phosphiranation reaction, leading to observation of the



Scheme 5.2 Reaction of *t*-BuPA with [Fp(styrene)][BF₄].

desired product by ³¹P NMR spectroscopy (−165.0 ppm). A complication was soon encountered as different sources of Fp⁺ gave wide ranges of yield. The best performing reactions employed [BF₄][−] as the counter anion, which was frequently observed to decompose at the reaction temperature (85 °C) as assayed by ¹⁹F NMR spectroscopy. This prompted an investigation of the possible catalytic role of fluoride, generated upon [BF₄][−] decomposition. Addition of the fluoride source tetramethylammonium fluoride (TMAF) in catalytic quantities (10 mol%) led to clean and reproducible formation of the desired phosphirane. The optimized reaction conditions comprise heating *t*-BuPA and styrene (10 equiv) with [Fp(THF)][BF₄] (10 mol%) and TMAF (15 mol%) in THF at 85 °C for 12 h (Scheme 5.1). Control experiments confirm the requirement of both catalysts for the formation of **1-t-Bu** (Table 5.1). Using other potential sources of *tert*-butyl phosphinidene in place of *t*-BuPA, *t*-BuPH₂ and (*t*-BuP)₃, did not lead to the formation of **1-t-Bu**.

The product was assigned exclusively as *trans*-1-*t*-Bu-2-phenylphosphirane (**1-t-Bu**) by comparison with previous literature reports^{24,25} as well as characterization by multinuclear NMR spectroscopy, high-resolution mass spectrometry (HRMS) and elemental analysis. Evidence for the relative stereochemistry of the *t*-Bu and phenyl substituents on the phosphirane ring is provided by ¹H NMR spectroscopy: the proton occupying the same face of the ring as the phosphorus lone pair is associated with a much larger ²J_{P-H} coupling constant (18.8 Hz) than are the two on the opposing face (2.6 and 2.2 Hz, respectively).²⁶ No evidence for the *cis* isomer was observed by NMR spectroscopy. Use of *i*-PrPA in place of *t*-BuPA led to the new compound **1-i-Pr** with only a small drop in diastereomeric ratio (Scheme 5.1).

Though previously observed by ³¹P NMR spectroscopy as one component of a mixture of several phosphorus-containing species, phosphirane **1-t-Bu** evidently has not previously been isolated as a pure substance.^{24,25} We found that **1-t-Bu** could be purified by simple distillation at reduced pressure as a colorless liquid (73%, 0.53 g) that froze at −35 °C, and could be stored for months at this temperature with no signs of decomposition. These observations are consistent with the properties reported for related phosphiranes.^{27,28}

The Fp⁺-coordinated phosphirane complex [Fp(**1-t-Bu**)] [BF₄][−] was prepared by inde-

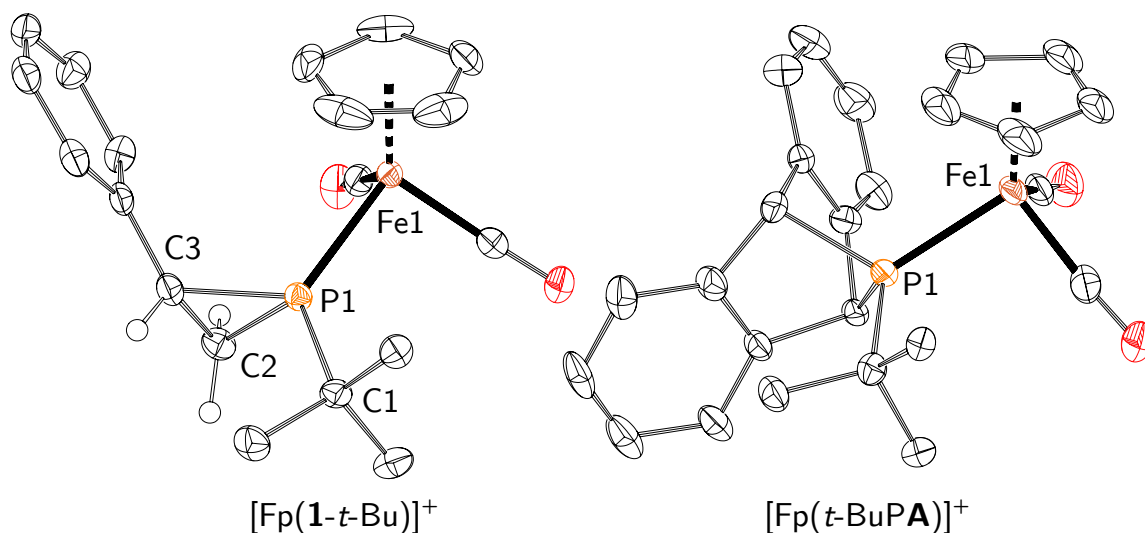


Figure 5.1 Molecular structures of $[\text{Fp}(\mathbf{1-t-Bu})][\text{BF}_4]$ and $[\text{Fp}(t\text{-BuPA})][\text{BF}_4]$ with thermal ellipsoids set at the 50% probability level. Selected hydrogen atoms and the tetrafluoroborate anions have been omitted for clarity. Selected bond distances and angles (\AA , $^\circ$) $[\text{Fp}(\mathbf{1-t-Bu})][\text{BF}_4]$: P1–Fe1: 2.2283(6); P1–C2: 1.811(2); P1–C3: 1.846(2); C2–C3: 1.524(3). $[\text{Fp}(t\text{-BuPA})][\text{BF}_4]$: Fe1–P1: 2.258(2).

pendent synthesis in order to determine its spectroscopic properties and possible role as an observable reaction intermediate. Treatment of $[\text{Fp}(\text{THF})][\text{BF}_4]$ with 1.1 equivalents of $\mathbf{1-t-Bu}$ in dichloromethane gave rise to $[\text{Fp}(\mathbf{1-t-Bu})][\text{BF}_4]$, isolated in 84% yield after precipitation by addition of pentane. Using the same synthetic procedure, $[\text{Fp}(t\text{-BuPA})][\text{BF}_4]$ could be prepared from $[\text{Fp}(\text{THF})][\text{BF}_4]$ and $t\text{-BuPA}$ in 98% yield. Both $[\text{Fp}(\mathbf{1-t-Bu})][\text{BF}_4]$ and $[\text{Fp}(t\text{-BuPA})][\text{BF}_4]$ were characterized by their ^{31}P NMR shifts (+220.7 and -76.2 ppm, respectively), in addition to structural characterization by X-ray crystallography (Fig. 5.1). The crystallographic study of $[\text{Fp}(\mathbf{1-t-Bu})][\text{BF}_4]$ confirms the spectroscopically assigned *trans* arrangement of the phenyl and *tert*-butyl substituents of the phosphirane ring of $\mathbf{1-t-Bu}$. The bond angles comprising this ring were found to be 49.26(9), 64.2(1) and 66.6(1) at P1, C3, and C2, respectively. With both Fp^+ -coordinated phosphines characterized, the reaction was monitored at 85 $^\circ\text{C}$ by ^{31}P NMR spectroscopy, confirming the presence of $[\text{Fp}(t\text{-BuPA})][\text{BF}_4]$ in the reaction mixture under conditions relevant to catalysis. $[\text{Fp}(\mathbf{1-t-Bu})][\text{BF}_4]$ was not observed under the same conditions, suggesting it either does not form or that $\mathbf{1-t-Bu}$ is rapidly displaced by a different ligand.

In order to shed light on a plausible mechanism by which phosphirane $\mathbf{1-t-Bu}$ forms under the reaction conditions the stoichiometric reaction of $[\text{Fp}(t\text{-BuPA})][\text{BF}_4]$ with TMAF was studied. Treatment of $[\text{Fp}(t\text{-BuPA})][\text{BF}_4]$ with equimolar TMAF (CH_2Cl_2 , 23 $^\circ\text{C}$) resulted in a rapid color change from bright yellow to bright orange. Analysis by NMR spectroscopy (^1H , ^{31}P , and ^{19}F) indicates formation of iron-phosphido $\text{FpP}(\text{F})(t\text{-Bu})$ (**3**) and

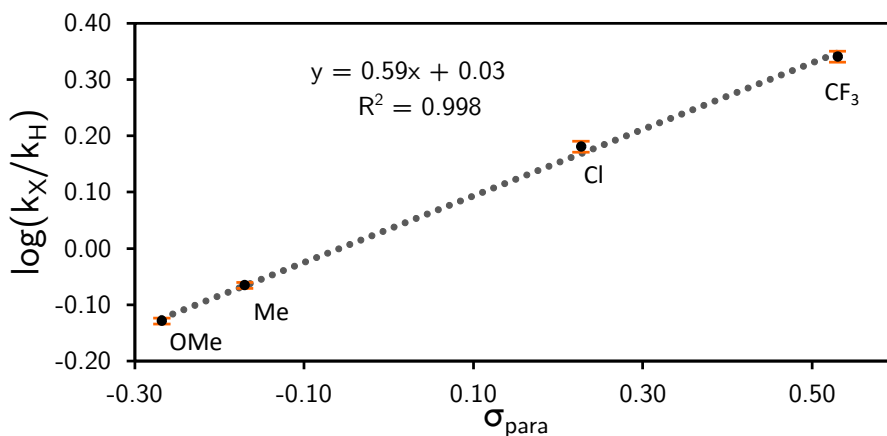


Figure 5.2 Hammett plot determined by competition experiments with *p*-substituted styrenes. Error bars correspond to the 95% confidence intervals.

anthracene, resulting from attack of fluoride at the phosphonium-like phosphorus center.¹⁹ Iron-phosphido **3** was characterized by the chemical shift of the ³¹P and ¹⁹F nuclei, found at +370.2 ppm (DFT calc. = +391.2 ppm) and -202.6 ppm (DFT calc. = -226.0 ppm), respectively, along with a ¹J_{P-F} value of 823.3 Hz. ¹H NMR data and HRMS were also consistent with the formulation of **3**. In terms of its relevance to catalysis, iron-phosphido **3**, which may be regarded as a phosphinidenoid,²⁹ was observed by NMR spectroscopy under the standard reaction conditions at 85 °C in THF-*d*₈, along with [Fp(*t*-BuPA)][BF₄], *t*-BuPA, and **1**-*t*-Bu. So far, attempts to isolate **3** have been unsuccessful, in part due to its high solubility in organic solvents. Interestingly, a closely related literature compound (Fp*P(Cl)(*t*-Bu), Fp* = Fe(η^5 -C₅Me₅)(CO)₂) is reported as being nucleophilic at phosphorus, reacting with the strong alkylating agent methyl iodide to give the phosphonium iodide [Fp*P(Cl)(*t*-Bu)(Me)][I].³⁰

A Hammett study was carried out to illuminate the nature of the rate determining step (RDS). Competition experiments were performed under the standard reaction conditions, using 5 equiv each of styrene and a *para*-substituted styrene as the substrates.³¹ The analysis showed that electron-poor styrenes react more rapidly than electron-rich styrenes, resulting in a Hammett parameter (ρ) of +0.59 (Fig. 5.2). This small positive value indicates build-up of negative charge in the RDS, consistent with attack of **3** toward styrene as the corresponding elementary step. A previous Hammett analysis of the addition of *para*-substituted styrenes to transient (CO)₅W-coordinated phosphinidenes gave a *negative* value for ρ of -0.60,³² highlighting the difference in mechanism between known reactions of electrophilic phosphinidene complexes with olefins versus our proposed pathway involving a nucleophilic iron-phosphido species.

Finally, *cis*- β -deuterostyrene was tested as a substrate under the standard reaction conditions, in order to differentiate between stepwise and concerted reaction mechanisms.

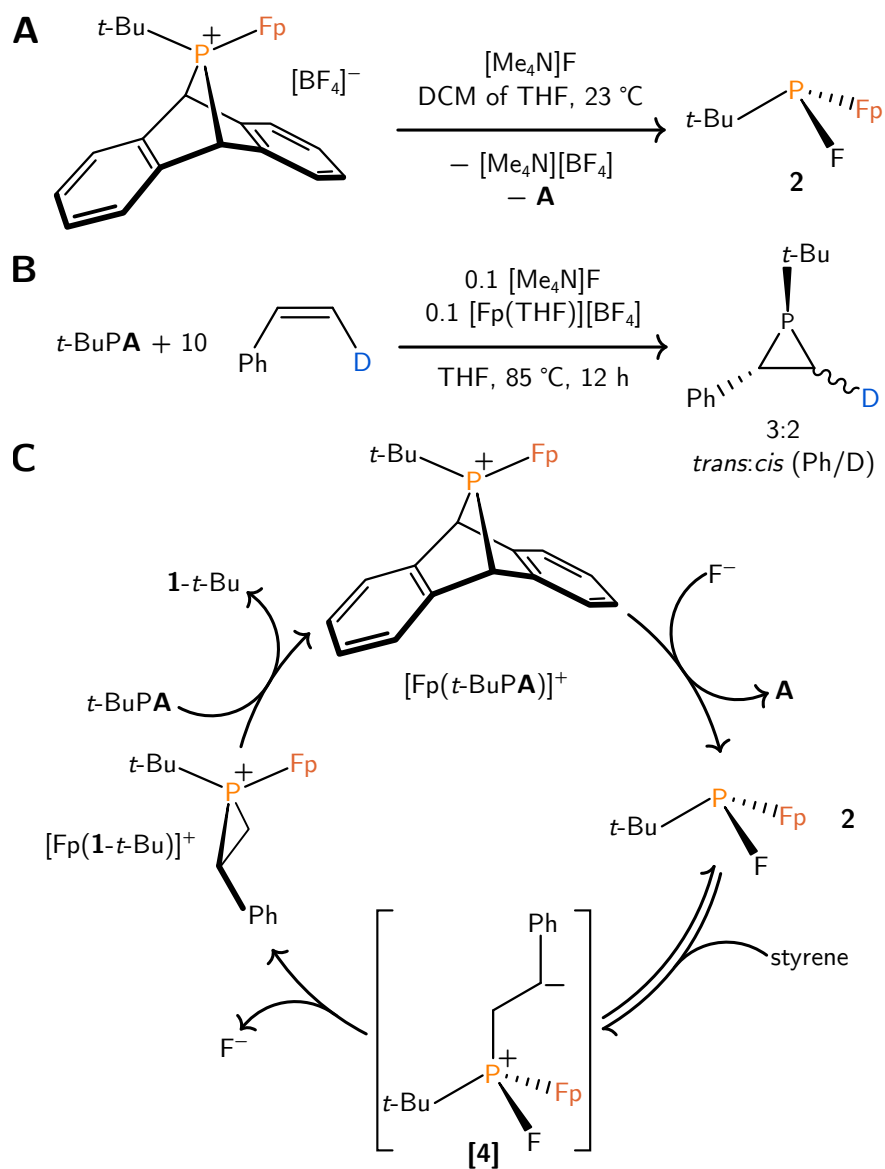


Figure 5.3 **A:** Stoichiometric reaction of $[\text{Fp}(t\text{-BuPA})][\text{BF}_4]$ with TMAF. **B:** Deuterium labeling study. **C:** Proposed catalytic cycle leading to the formation of **1-t-Bu**.

^2H NMR spectra confirmed the formation of two isomers of deuterated phosphirane product, in which the deuterium and phenyl substituents occupy *cis* and *trans* positions on the phosphirane ring, respectively (Fig. 5.3B). This observation indicates a stepwise pathway (ionic or radical) in which a reaction intermediate has a sufficient lifetime for C–C bond rotation to occur. Nucleophilic attack on styrene by phosphido **3** to give intermediate [4] (Fig. 5.3C), containing a C–C single bond, would fulfill this requirement. Under the reaction conditions, the bulk *cis*- β -deuterostyrene in solution was found to undergo scrambling to give a mixture of *cis*- and *trans*- β -deuterostyrene (3:1 ratio). However, this ratio is significantly less than that observed for the *cis*- and *trans* isomers (with respect to the Ph and D substituents) of the product phosphiranes (1:1.5 ratio), suggesting that the observation of both the *cis* and *trans* isomers (with respect to Ph and D) in the product phosphiranes is not an artifact of bulk styrene isomerization (5.5.13). Additionally, isomerization of the bulk styrene did not occur in a control experiment (standard conditions without *t*-BuPA), and is thus tentatively accounted for by *reversible* addition of iron-phosphido **3** to styrene. In this context, it is noteworthy that the related Fp-phosphido species Fp–P(Ph)₂ catalyzes the isomerization of excess dimethyl maleate to dimethyl fumarate.³³

In light of the forgoing mechanistic experiments, we put forward the working hypothesis shown in Fig. 5.3C. Initial ligand substitution of *t*-BuPA with [Fp(THF)]⁺ results in [Fp(*t*-BuPA)]⁺. The addition of a fluoride anion to [Fp(*t*-BuPA)][BF₄], resulting in compound **3**, is conceptually related to the ability of chloride to promote anthracene loss from a phosphonium derived from an RPA compound that we reported recently¹⁹ and was the subject of a more detailed computational study by Grimme and coworkers.³⁴ Next, addition of styrene to **3** furnishes intermediate [4] capable of rotation about the newly-formed C–C single bond, and which could plausibly go on to form [Fp(1-*t*-Bu)]⁺ with the ejection of fluoride. Closure of the phosphirane ring in this sequence presumably dictates the *trans* stereochemistry found in the product.

5.3 Conclusions

This work introduces a novel catalytic styrene phosphirane reaction. Phosphiranes are excellent target molecules for transition-metal catalyzed syntheses that do not suffer from product inhibition, as the phosphirane three-membered ring confers high *s* character on the included phosphorus lone pair with consequent diminished ligating ability and ease of dissociation relative to typical tertiary phosphines.³⁵ Importantly, the reaction allows for facile preparation of two phosphiranes in good yield, enabling their development as ligands for transition metals and as potential phosphorus-containing polymer precursors.^{3,36,37} The phosphiranes products are chiral and the potential future use of a chiral catalyst raises the possibility of preparing *P*-chiral phosphiranes from RPA compounds using readily accessible organoiron and fluoride catalysts.

5.4 Future Work

5.4.1 Experiments related to mechanism

A number of questions remain open on the topic of mechanism for this new phosphirane procedure. Answering these questions is expected to lead to an improved method for the synthesis of phosphiranes, including increased substrate scope, lower catalyst loadings, milder reaction conditions, and an enantioselective procedure that could lead to chiral phosphirane products.

The kinetics of the reaction mechanism could be studied by NMR spectroscopy, in order to determine the order of the reaction with respect to the reagents and catalysts. Eyring analysis could provide reaction barriers, which can be compared to values determined by DFT calculations. By quantifying the rates of styrene scrambling versus scrambling of the deuterium label on the product phosphirane when *cis*- β -deuterostyrene is used as the substrate, the proposed reversibility of styrene addition to the iron phosphido intermediate $\text{FpP}(\text{F})(t\text{-Bu})$ can be verified or alternative explanations provided.

Iron phosphido species **3** should be independently prepared and characterized. Initial efforts toward this goal, starting from readily available $\text{K}[\text{Fp}]$ and $t\text{-Bu-PCl}_2$, are described in Section A.4.12. With **3** in hand, it could be tested as a catalyst precursor that can reenter the catalytic cycle we proposed in our initial report. It could also be tested as a stoichiometric reagent for preparing **1**- $t\text{-Bu}$ by heating with styrene. Necessary for this stoichiometric reaction to occur could be the inclusion of $[\text{TBA}][\text{BF}_4]$, which would accurately represent the exact components of the reaction mixture generated in the catalytic procedure. An interesting experiment in this regard would be to use **3** (possibly in conjunction with $[\text{TMA}][\text{BF}_4]$) as the added catalyst for the synthesis of **1**- $i\text{-Pr}$ from $i\text{-PrPA}$ and styrene; if the presence of **1**- $t\text{-Bu}$ is detected, it will provide evidence for the transfer of a phosphinidene unit from **3** to styrene and support the proposed catalytic cycle.

Anions besides fluoride could be screened as co-catalysts for the reaction. Although fluoride was demonstrated to be necessary in the work described in this chapter, it could be that a species such as chloride, acetate, or benzoate might be superior as the co-catalyst. This might be anticipated on the basis of the strong P–F bond, which could be limiting the observed rate of catalysis. TMAF is also largely insoluble under the reaction conditions, and so THF-soluble fluoride source tris(dimethylamino)sulfonium difluorotrimethylsilicate (TASF) has shown initial promise as a competent co-catalyst (Section 5.5.15). Further work is required to compare the performance of fluoride sources.

5.4.2 Experiments related to developing an enantioselective procedure

Two routes can be envisioned for developing enantioselective variations on this phosphirane procedure: (i) use of a chiral Cp derivative or (ii) use of a chiral diphosphine ligand in place of the two CO ligands. The simplest class of catalyst that could be screened have the general formula $[(\text{drpn})(\text{Cp})\text{Fe}(\text{L})][\text{X}]$ (drpn = di-R-phosphino-n-ane, e.g. dppe, dcpe,

dppp etc.; L = L-type ligand e.g. CO, THF, MeCN *t*-BuPA; X = anion e.g. [BF₄]⁻, [BPh₄]⁻, [OTf]⁻) of which there number of known species in the literature. If these compounds are found to be successful, the chelating diphosphine ligand can be replaced with a chiral analog, such as BINAP. Another organoiron complex that is of interest as a potential catalyst is (dppp)(Cp*)(CO)₂FeF,³⁸ which could act as both the source of iron and fluoride that is required for reaction to turnover. Furthermore, this known complex features a chelating phosphine ligand which could in principal be substituted for a chiral analog.

Another possible way to impart chirality to the simple Fp-cation catalyst would be to use a chiral Cp ligand. In recent years, Cramer has developed a set of chiral Cp ligands that have been applied in asymmetric catalysis.³⁹⁻⁴¹ By incorporating one of these chiral Cp ligands into the simple Fp-cation, the enrichment of one enantiomer of the phosphirane products might be expected.

5.4.3 Phosphiranes as ligands

Chiral phosphiranes could themselves be used as ligands. Relevant to this topic is the preparation of (dba)Pd(**1-t**-Bu)₂ (dba = dibenzylideneacetone), which was prepared by treatment of Pd(dba)₂ with 2.5 equiv of **1-t**-Bu (Section A.4.11). In analogy to the classic homoleptic complexes of metals such as palladium and nickel with triphenylphosphine,⁴² the preparation of Pd(**1-R**)₄ (R = *t*-Bu, *i*-Pr) could be targeted.

Phosphiranes such as **1-t**-Bu could be benchmarked as ligands for reactions such as the Stille coupling. Ligands that are weak σ -donors (such as tri-2-furylphosphine or triphenylarsine) are often considered “privileged” in their ability to effect these reactions, and are superior because the rate determining step involves dissociation of a phosphine ligand from a palladium-derived oxidative addition complex.⁴³ Phosphiranes, already known as weak σ -donors by virtue of the small angles at phosphorus,³⁵ might therefore be expected to be good ligands for transition-metal-catalyzed reactions such as the Stille coupling.

5.4.4 Incorporation of phosphiranes into polymer materials

Polymers incorporating that incorporate lone-pair-containing phosphorus atoms are novel materials with several potential applications.^{36,37,44} With two new phosphiranes in hand, enabled by the methods described in this chapter, their polymerization could be explored to provide polyphosphiranes. Phosphirane polymerization has been explored, but has not been well-studied in more recent years.³ Conditions for polymerization reactions to be tested include thermal or microwave heating of neat material, or by using radical, anionic, or cationic initiators in solution.⁴⁵

5.5 Experimental methods

5.5.1 General methods

All manipulations were performed in a Vacuum Atmospheres model MO-40M glovebox under an inert atmosphere of purified N₂ or using standard Schlenk techniques. When reagents were removed from a stock bottle containing a Sure/Seal, the equivalent volume of dry nitrogen was injected into the bottle prior to removing the desired volume of solution with a syringe. All solvents were obtained anhydrous and oxygen-free by bubble degassing (argon) and purification by passing through columns of alumina and Q5.⁴⁶ Once collected, solvents were stored over activated 4 Å molecular sieves (20 wt%) inside the glovebox.⁴⁷ All glassware was oven-dried for at least 6 h prior to use, at temperatures greater than 150 °C.

MgA·THF₃ (A = C₁₄H₁₀, anthracene),^{16,17} *t*-BuPA,^{16,17} FpK⁴⁸ (Fp = (η⁵-C₅H₅)-(CO)₂Fe), FpI,⁴⁹ and [Fp(THF)][BF₄]⁵⁰ (crystallized according to Section 5.5.3) were prepared according to literature methods. Phenylacetylene (Alfa), 2.6 M *n*-butyllithium in hexane (MilliporeSigma), zirconocene chloride hydride (Strem) were used as received. Substituted styrene derivatives (Oakwood) were purified as described in Section 5.5.12. Tetramethylammonium fluoride (TMAF) (MilliporeSigma) was dried at 23 °C in vacuo for 12 hours prior to use. Dichloromethane-*d*₂, benzene-*d*₆, tetrahydrofuran-*d*₈, acetonitrile-*d*₃ and chloroform-*d* were purchased from Cambridge Isotope Labs and were degassed three times by the freeze-pump-thaw method and stored over activated 4 Å molecular sieves for 48 h in the glovebox prior to use. Diatomaceous earth (Celite 435, EM Science), 4 Å molecular sieves (Millipore-Sigma) and basic alumina (Millipore-Sigma) were dried by heating to 200 °C under dynamic vacuum for at least 48 h prior to use. The temperature of the aluminum shot used to heat reagents or reaction mixtures was measured using a Hanna Instruments K-type Thermocouple Thermometer (model HI935005).

NMR spectra were obtained on Varian Inova 300 and 500 instruments equipped with Oxford Instruments superconducting magnets, on a Jeol ECZ-500 instrument equipped with an Oxford Instruments superconducting magnet, or on a Bruker Avance 400 instrument equipped with a Magnex Scientific or with a SpectroSpin superconducting magnet. ¹H and ¹³C NMR spectra were referenced to residual CD₂Cl₂ (¹H = 5.32 ppm, ¹³C = 54.0 ppm), C₆D₆ (¹H = 7.16 ppm, ¹³C = 128.06 ppm), CD₃CN (¹H = 1.94 ppm, ¹³C = 118.26 ppm) or CDCl₃ (¹H = 7.26 ppm, ¹³C = 77.16 ppm). ³¹P NMR spectra were referenced externally to 85% H₃PO₄ (0 ppm).

Infrared spectra were collected using a Bruker ATR-IR Tensor 37. Samples were removed from the glovebox in sealed vials and briefly handled in air prior to data collection.

High resolution mass spectral (HRMS) data were collected using a Jeol AccuTOF 4G LC-Plus mass spectrometer equipped with an Ion-Sense DART source. Data were calibrated to a sample of PEG-600 and were collected in positive-ion mode. Samples were prepared in DCM (10 μM concentration) and were briefly exposed to air (<5 s) before

being placed in front of the DART source.

Electrospray ionization mass spectrometry (ESI-MS) was performed using a Micromass Q-TOF ESI spectrometer.

Elemental combustion analyses were performed by Midwest Micro Laboratories (Indianapolis, IN, USA).

5.5.2 Catalyst screening

A list of the species tested as catalysts for the preparation of **1-*t*-Bu** from *t*-BuPA and styrene is given in Table 5.2. A typical setup involved the addition of *t*-BuPA (10 mg, 0.0376 mmol, 1 equiv), styrene (39 mg, 0.376 mmol, 10 equiv), and the appropriate catalyst (0.00376 mmol, 0.1 equiv) together in THF in an NMR tube equipped with a J. Young valve. The reaction mixture was heated between 60–85 °C and analyzed by ³¹P NMR spectroscopy after 18–24 h for any formation of **1-*t*-Bu**. Fluoride FpF was considered as a possible replacement for the co-catalyst system, but despite the appearance of this compound in a handful of reports we were unable to uncover a detailed preparative procedure.^{8,51}

Table 5.2 Catalysts screened for catalytic phosphiranation ability

Compound	[R ₂ C] Transfer?	[RN] Transfer?	[RP] ^a Transfer?
Rh ₂ (OAc) ₄	yes ⁵²	yes ⁵³	no
Cu(OTf)	yes ⁵⁴	yes ⁵⁵	no
Co(TPP) ^b	yes ⁵⁶	yes ⁵⁷	no
Fe(TPP) ^b	yes ⁵⁸	(Fe ^{III}) ⁵⁹	no
Ru(CO)(TMP) ^b	yes ⁶⁰	yes ⁶¹	no
Ru(CO)(TPFPP) ^b	yes ⁶²	yes ⁶¹	no
RuCl ₂ (PPh ₃) ₃	yes ⁶³		no
OsCl ₂ (PPh ₃) ₃	yes ⁶⁴		no
B(C ₆ F ₅) ₃			no

^a No transfer under the conditions 0.1:1:10 catalyst–*t*-BuPA–styrene, 60–85 °C, 18–24 h, THF or benzene

^b Porphyrin abbreviations: ‘TPP’ tetraphenylporphyrin, ‘TMP’ tetramesitylporphyrin, ‘TPFPP’ tetrakis(perfluorophenyl)porphyrin.

5.5.3 Crystallization of [Fp(THF)][BF₄]

In the glovebox, [Fp(THF)][BF₄]⁵⁰ was crystallized by dissolving crude material (ca. 250 mg) in DCM (6 mL) to produce a dark red solution. The solution was filtered through microfiber filter paper in a Pasteur pipette. THF (14 mL) was carefully layered on top of the DCM solution and the resulting two-layer mixture placed in the glovebox freezer at –35 °C overnight, producing dark red needles. The crystals were collected on a frit (fine

porosity, 15 mL) then washed with THF (2×5 mL). The material was transferred to a vial and brought to constant mass under reduced pressure. The material was used without further characterization.

5.5.4 Preparation of [Fp(styrene)][BF₄]

5.5.4.1 From styrene oxide

[Fp(styrene)][BF₄] was prepared from styrene oxide along the lines of a literature procedure.²³ In the glovebox, FpK⁴⁸ (3.30 g, 15.27 mmol, 1 equiv) was added to a Schlenk flask (120 mL) equipped with a 24/40 opening and a stir bar. THF (20 mL) was added to the flask to give a slurry. Separately, a Schlenk flask (50 mL) containing THF (20 mL) was prepared. Both flasks were sealed and removed from the glovebox and connected to the Schlenk line in a fume hood. Styrene oxide (from the stock bottle) was weighed into a vial in the fume hood under an atmosphere of air, then added to the Schlenk flask containing THF against a counter flow of N₂. The Schlenk flask containing the slurry of FpK in THF was cooled to 0 °C using an ice bath and the Schlenk cap switched for a septum. The solution of styrene oxide in THF was added dropwise by cannula transfer to the vigorously stirring slurry of FpK over the course of five minutes. The flask was removed from the ice bath and stirred at 23 °C for 30 minutes. The flask was cooled to 0 °C and aqueous HBF₄ (50 % w:w, 7.44 g, 42.8 mmol, 2.8 equiv) was added from a syringe over the course of five minutes. The resulting mixture was stirred at 0 °C for 15 minutes, then diethyl ether (60 mL) was added by cannula transfer to give a yellow precipitate. The precipitate was allowed to settle then the supernatant decanted into a waste bottle in the fume hood by cannula transfer. The solids were washed with additional diethyl ether (4×35 mL). This was performed by transferring diethyl ether to the flask by cannula transfer, vigorous stirring of the slurry for 2 minutes, then removing the liquid by cannula filter. The cannula filter was prepared by securing a piece of filter paper around the end of a steel cannula using Teflon tape. The solid material was dried under a flow of nitrogen for one hour to give a yellow solid. The flask was sealed under N₂ and brought into the glovebox to give [Fp(styrene)][BF₄] as a yellow powder (1.88 g, 5.12 mmol, 33%).

5.5.4.2 From styrene

[Fp(styrene)][BF₄] was prepared from styrene and [Fp(THF)][BF₄] along the lines of a related literature procedure.⁵⁰ In the glovebox, crude [Fp(THF)][BF₄]⁵⁰ (200 mg, 0.59 mmol, 1 equiv) and styrene (309 mg, 2.97 mmol, 5 equiv) were weighed into a vial equipped with a stir bar (1 cm) and dissolved in DCM (5 mL). The resulting solution was stirred for 3 h, producing a yellow precipitate. The precipitate was collected on a frit (fine porosity, 15 mL) then washed with DCM (3×4 mL) then diethyl ether (4×4 mL). The solids were transferred to a pre-weighed vial and brought to constant mass under reduced pressure to give [Fp(styrene)][BF₄] as a yellow powder (140 mg, 0.381 mmol, 65%).

5.5.4.3 Crystallization procedure

Small quantities of recrystallized [Fp(styrene)][BF₄] from either of the preparative procedures above could be obtained by the following procedure. [Fp(styrene)][BF₄] (50 mg) was dissolved in DCM (15 mL). The resulting solution was filtered through microfibre filter paper in a Pasteur pipette into a fresh vial. The solution was placed in the glovebox freezer at -35 °C overnight to give small orange crystals of [Fp(styrene)][BF₄]. These were collected on a piece of filter paper in a Pasteur pipette, washed with DCM (3 × 2 mL) then transferred to a pre-weighed vial and brought to constant mass under reduced pressure.

5.5.5 Preparation of *trans*-1-*t*-Bu-2-phenylphosphirane (1-*t*-Bu)

In the glovebox, *t*-BuPA (1000 mg, 3.76 mmol, 1 equiv), styrene (3910 mg, 37.6 mmol, 10 equiv) and THF (21.0 g, 23.6 mL) were weighed into separate vials. [Fp(THF)][BF₄] (126 mg, 0.376 mmol, 0.1 equiv) and TMAF (52 mg, 0.564 mmol, 0.15 equiv) were weighed directly into a Schlenk flask (100 mL) equipped with a Teflon screw cap and a stir bar (2 cm). THF (ca. 10 mL) was used to dissolve *t*-BuPA and styrene and the resulting mixture was transferred to the Schlenk flask. The remaining THF was used to rinse the two vials and the resulting washings transferred to the Schlenk flask. The slurry was stirred at 23 °C for 30 min before being removed from the glovebox and placed in an oil bath that had been preheated to 85(±5) °C. The reaction mixture was heated with stirring for 12 hours then removed from the oil bath and allowed to cool to room temperature. The flask was brought into the glovebox and the solution concentrated to ca. 10 mL, resulting in the formation of a precipitate. The slurry was diluted with pentane (20 mL) then stirred for ten minutes. The reaction mixture was passed through a frit (30 mL, fine porosity) containing diatomaceous earth ($\frac{1}{2}$ full). The flask and diatomaceous earth were rinsed with pentane (3 × 5 mL). Volatile material was removed from the filtrate under reduced pressure to give a brown paste which was dried for an additional hour. The paste was dissolved in diethyl ether (100 mL) and the solution was filtered through a frit (30 mL, medium porosity) containing activated charcoal ($\frac{1}{2}$ full). Before passing the diethyl ether solution through the charcoal, fresh diethyl ether (10 mL) was passed through the charcoal in order to form a firmly packed bed. After filtering the reaction mixture, additional diethyl ether (100 mL) was passed over the charcoal to give a yellow filtrate. The combined filtrates were concentrated to ca. 6 mL then transferred to an H-cell apparatus for performing vacuum-transfer operations. The flask used to collect the filtrate was washed with additional diethyl ether (3 × 3 mL) and the washings transferred to the H-cell. The cell was removed from the glovebox and connected to a Schlenk line. Volatile material was removed under dynamic vacuum at 23 °C then the remaining material was distilled under static vacuum at 70 °C, using a cooling bath on the receiving side (-78 °C). The cell was brought into the glovebox and the distillate transferred to a pre-weighed vial using a pipette to give the desired product as a colorless oil (530 mg, 2.76 mmol, 73%). Anal. Calcd for C₁₂H₁₇P₁:

C, 74.97; H, 8.91; N, 0.00. Found: C, 74.63; H, 8.93; N, ≤ 0.02 . ^1H NMR (500 MHz, CDCl_3 , δ) 7.22 (t, $J = 7.6$ Hz, 2H), 7.11 (t, $J = 7.3$ Hz, 1H), 7.04 (d, $J = 7.6$ Hz, 2H), 2.45 (ddd, $J = 10.4, 7.7, 2.6$ Hz, 1H), 1.55 (ddd, $J = 10.3, 8.0, 2.2$ Hz, 1H), 1.25 (dt, $J = 18.8, 7.8$ Hz, 1H), 1.02 (d, $J = 12.2$ Hz, 9H). ^{13}C NMR (126 MHz, CDCl_3 , δ) 143.29 (d, $J = 8.4$ z), 128.44, 126.43 (d, $J = 5.4$ Hz), 125.45, 28.89 (d, $J = 15.5$ Hz), 26.43 (d, $J = 33.4$ Hz), 22.93 (d, $J = 41.0$ Hz), 13.56 (d, $J = 45.6$ Hz). $^{31}\text{P}\{^1\text{H}\}$ NMR (203 MHz, CDCl_3 , δ) -165.0 (s). ^{31}P NMR (203 MHz, CDCl_3 , δ) -165.0 (m). HRMS (m/z): $[\text{M} + \text{H}]^+$ calcd for $\text{C}_{12}\text{H}_{18}\text{P}_1$, 193.114614; found, 193.1135 (100%).

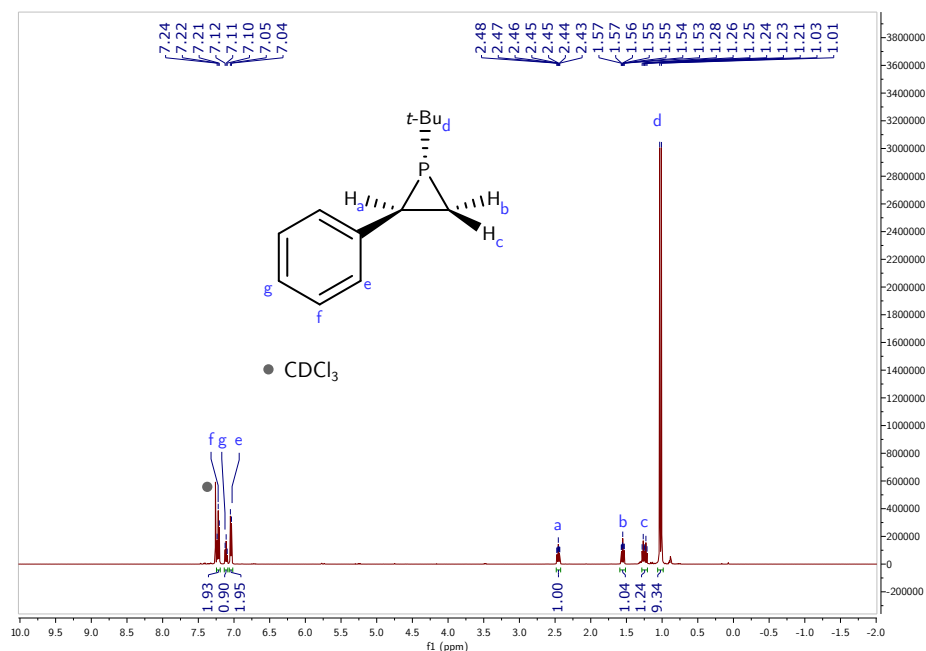


Figure 5.4 ^1H NMR spectrum of 1-*t*-Bu in CDCl_3 at 25 °C, recorded at 500 MHz.

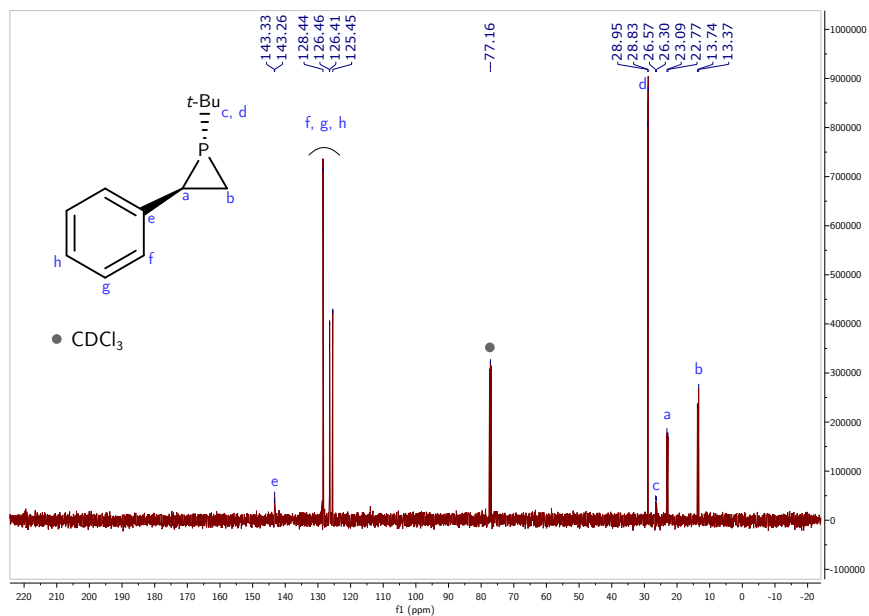


Figure 5.5 $^{13}\text{C}\{^1\text{H}\}$ NMR spectrum of **1-t-Bu** in CDCl_3 at $25\text{ }^\circ\text{C}$, recorded at 126 MHz.

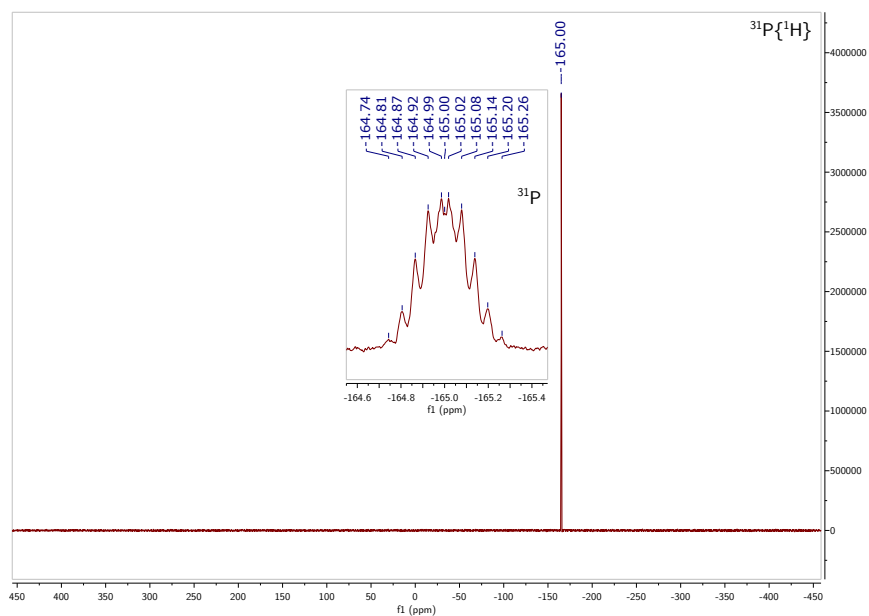


Figure 5.6 $^{31}\text{P}\{^1\text{H}\}$ NMR spectrum (inset: ^{31}P) of **1-t-Bu** in CDCl_3 at $25\text{ }^\circ\text{C}$, recorded at 203 MHz.

5.5.6 Preparation of *trans*-1-*i*-Pr-2-phenylphosphirane (1-*i*-Pr)

In the glovebox, *i*-PrPA (1000 mg, 3.96 mmol, 1 equiv), styrene (4118 mg, 39.6 mmol, 10 equiv) and THF (22.1 g, 24.8 mL) were weighed into separate vials. [Fp(THF)][BF₄] (133 mg, 0.396 mmol, 0.1 equiv) and TMAF (55 mg, 0.594 mmol, 0.15 equiv) were weighed directly into a Schlenk flask (100 mL) equipped with a Teflon screw cap and a stir bar (2 cm). THF (ca. 10 mL) was used to dissolve *i*-PrPA and styrene and the resulting mixture was transferred to the Schlenk flask. The remaining THF was used to rinse the two vials and the resulting washings transferred to the Schlenk flask. The slurry was stirred at 23 °C for 30 min before being removed from the glovebox and placed in an oil bath that had been preheated to 85(±5) °C. The reaction mixture was heated with stirring for 6 hours then removed from the oil bath and allowed to cool to room temperature. The flask was brought into the glovebox and the solution concentrated to ca. 10 mL, resulting in the formation of a precipitate. The slurry was diluted with pentane (20 mL) then stirred for ten minutes. The reaction mixture was passed through a frit (30 mL, fine porosity) containing diatomaceous earth ($\frac{1}{2}$ full). The flask and diatomaceous earth were rinsed with pentane (3 × 5 mL). Volatile material was removed from the filtrate under reduced pressure to give a brown paste which was dried for an additional hour. The paste was dissolved in diethyl ether (100 mL) and the solution was filtered through a frit (30 mL, medium porosity) containing activated charcoal ($\frac{1}{2}$ full). Before passing the diethyl ether solution through the charcoal, fresh diethyl ether (10 mL) was passed through the charcoal in order to form a firmly packed bed. After filtering the reaction mixture, additional diethyl ether (100 mL) was passed over the charcoal to give a yellow filtrate. The combined filtrates were concentrated to ca. 6 mL then transferred to an H-cell apparatus for performing vacuum-transfer operations. The flask used to collect the filtrate was washed with additional diethyl ether (3 × 3 mL) and the washings transferred to the H-cell. The cell was removed from the glovebox and connected to a Schlenk line. Volatile material was removed under dynamic vacuum at 23 °C then the remaining material was distilled under static vacuum at 70 °C, using a cooling bath on the receiving side (−78 °C). The cell was brought into the glovebox and the distillate transferred to a pre-weighed vial using a pipette to give the desired product as a colorless oil (401 mg, 2.24 mmol, 57%). **1-*i*-Pr-*trans*** (major isomer): ¹H NMR (500 MHz, CDCl₃, δ) 7.23 (t, *J* = 7.6 Hz, 2H), 7.12 (t, *J* = 7.3 Hz, 1H), 7.04 (d, *J* = 7.6 Hz, 2H), 2.43 (ddd, *J* = 10.1, 7.6, 2.6 Hz, 1H), 1.48 (ddd, *J* = 10.1, 7.6, 2.5 Hz, 1H), 1.32 (dt, *J* = 17.4, 7.5 Hz, 1H), 1.14 (dd, *J* = 14.8, 7.1 Hz, 3H), 1.09 (dd, *J* = 14.3, 7.1 Hz, 3H), 0.89 (ddq, *J* = 11.0, 7.0, 3.9, 3.5 Hz, 1H). ¹³C NMR (126 MHz, CDCl₃, δ) 143.17 (d, *J* = 8.0 Hz), 126.36 (d, *J* = 5.3 Hz), 30.51 (d, *J* = 28.2 Hz), 25.99 (d, *J* = 37.9 Hz), 21.53 (d, *J* = 17.9 Hz), 20.96 (d, *J* = 16.4 Hz), 16.19 (d, *J* = 42.5 Hz). ³¹P{¹H} NMR (203 MHz, CDCl₃, δ) −177.1 (s). ³¹P NMR (203 MHz, CDCl₃, δ) −177.1 (m). **1-*i*-Pr-*cis*** (minor isomer): ¹H NMR (500 MHz, CDCl₃, δ) 2.76 (dt, *J* = 13.6, 9.1 Hz, 1H). ³¹P{¹H} NMR (203 MHz, CDCl₃, δ) −181.0 (s). ³¹P NMR (203 MHz, CDCl₃, δ) −181.0 (m). *Note*: the two isomers were assigned on the basis of their ²*J*_{P-H} coupling constants for the benzylic

protons. The value of this constant was 2.6 Hz for the *trans* isomer and 13.6 Hz for the *cis* isomer. The coupling constants were determined by comparison of ^1H and $^1\text{H}\{^{31}\text{P}\}$ NMR spectra (Fig. 5.8). The diastereomeric ratio was determined from integration of the resonances corresponding to the benzylic protons (Fig. 5.8). HRMS (m/z): $[\text{M} + \text{H}]^+$ calcd for $\text{C}_{11}\text{H}_{16}\text{P}_1$, 179.098964; found, 179.098938 (79%).

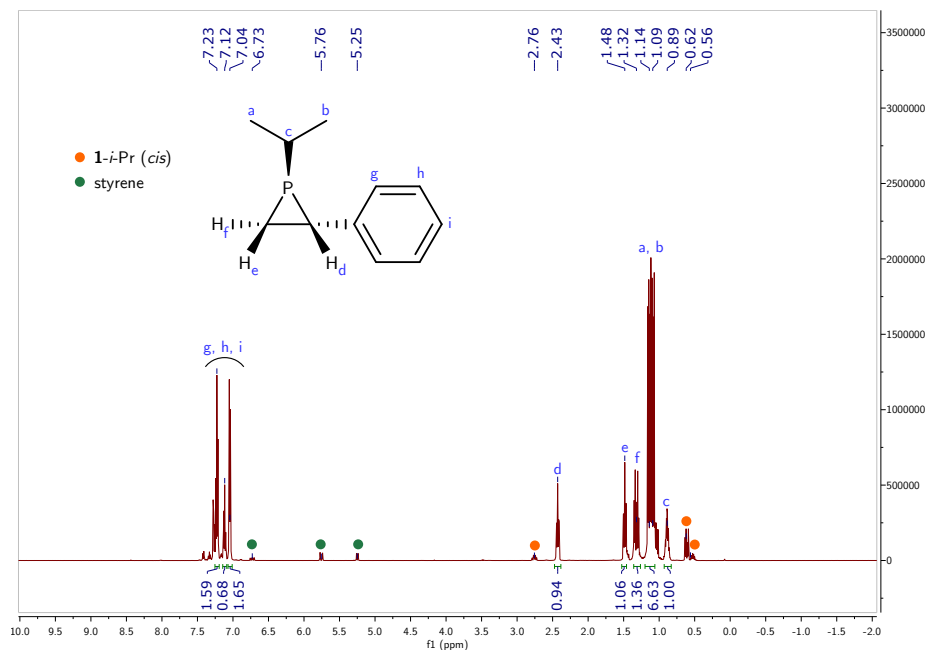


Figure 5.7 ^1H NMR spectrum of **1-*i*-Pr** in CDCl_3 at $25\text{ }^\circ\text{C}$, recorded at 500 MHz.

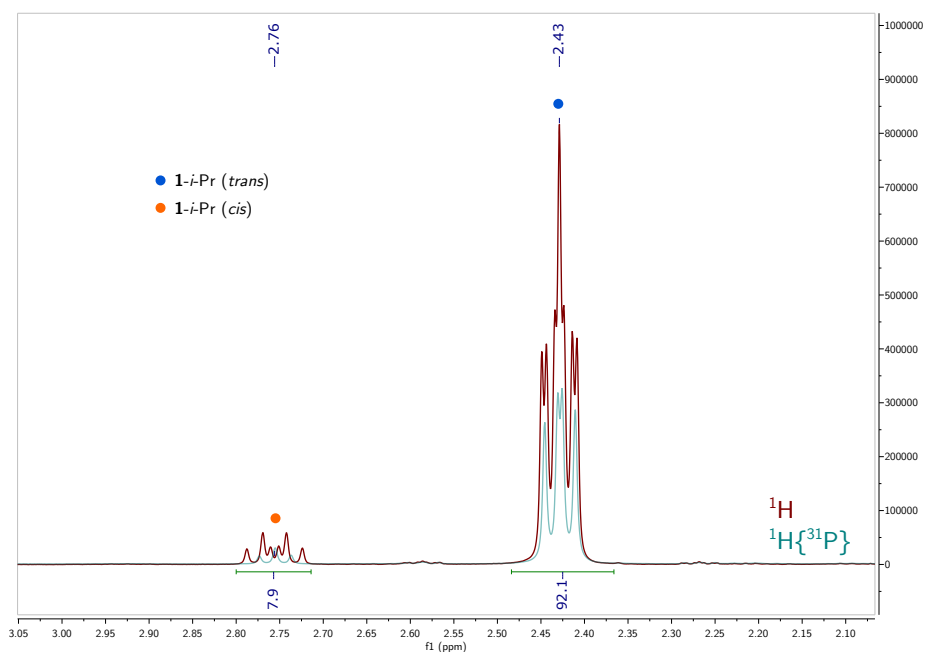


Figure 5.8 Zoom ^1H and $^1\text{H}\{^{31}\text{P}\}$ NMR spectra (benzylic region) of **1-*i*-Pr** in CDCl_3 at 25°C , recorded at 500 MHz. The two spectra were used to determine the $^2J_{\text{P-H}}$ coupling constants.

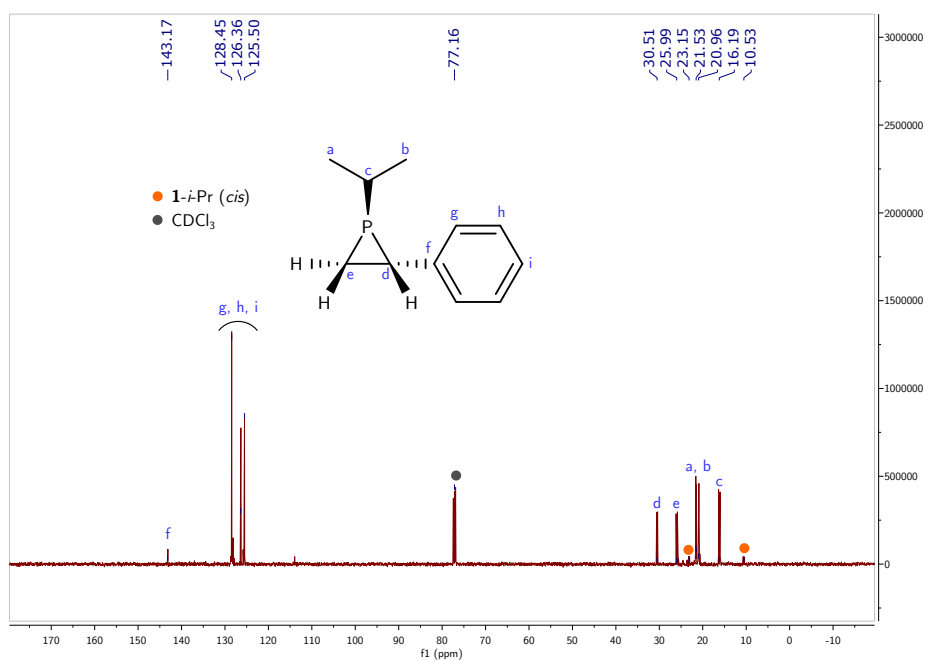


Figure 5.9 $^{13}\text{C}\{^1\text{H}\}$ NMR spectrum of **1-*i*-Pr** in CDCl_3 at 25°C , recorded at 126 MHz.

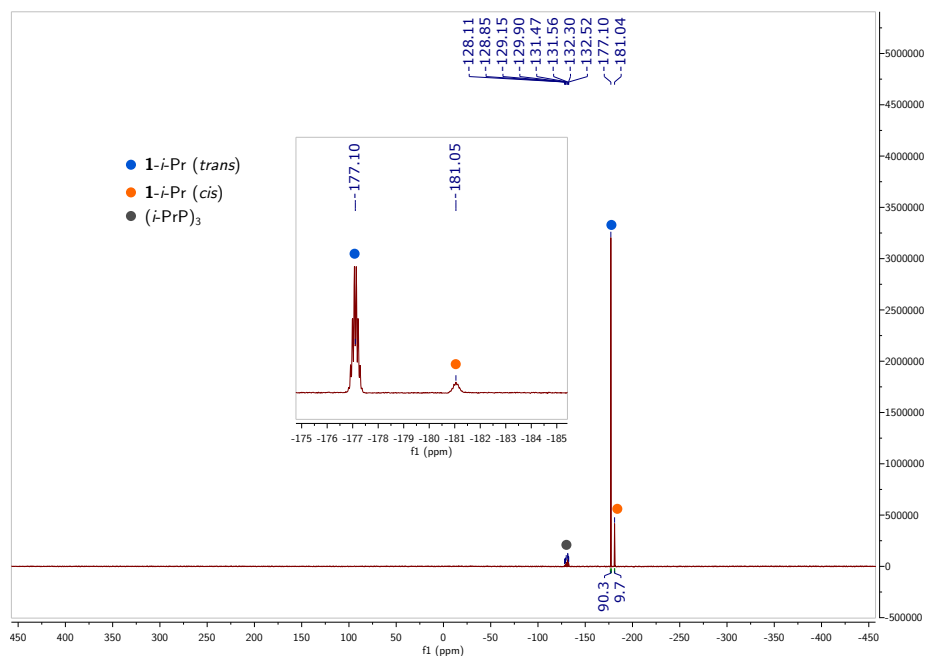


Figure 5.10 $^{31}\text{P}\{^1\text{H}\}$ NMR spectrum (inset: ^{31}P NMR spectrum) of **1-i-Pr** in CDCl_3 at 25°C , recorded at 203 MHz.

5.5.7 Generation and in situ characterization of $\text{FpP}(\text{F})(t\text{-Bu})$ (**3**)

In the glovebox, $[\text{Fp}(t\text{-BuPA})][\text{BF}_4]$ (11 mg, 0.021 mmol, 1 equiv) and TMAF (2 mg, 0.021 mg, 1 equiv) were weighed into the same vial and dissolved in CD_2Cl_2 (0.6 mL). While a solution of $[\text{Fp}(t\text{-BuPA})][\text{BF}_4]$ in DCM is bright yellow, this reaction mixture was bright orange. The solution was analyzed by ^1H , ^{31}P and ^{19}F NMR spectroscopy and HRMS. ^1H NMR (500 MHz, CD_2Cl_2 , δ) 4.97 (d, $J = 2.2$ Hz, 3H), 1.23 (dd, $J = 11.4, 1.6$ Hz, 9H). $^{31}\text{P}\{^1\text{H}\}$ NMR (203 MHz, CD_2Cl_2 , δ) +370.2 (d, $J = 823.3$ Hz). $^{19}\text{F}\{^1\text{H}\}$ NMR (471 MHz, CD_2Cl_2 , δ) -202.6 (d, $J = 823.3$ Hz). HRMS (m/z): $[\text{M} + \text{H}]^+$ calcd for $\text{C}_{11}\text{H}_{15}\text{O}_2\text{Fe}_1\text{F}_1\text{P}_1$, 285.014313; found, 285.014404 (29.7%); $[\text{M}(\text{F} \leftrightarrow \text{OH}) + \text{H}]^+$ calcd for $\text{C}_{11}\text{H}_{16}\text{O}_3\text{Fe}_1\text{P}_1$, 283.018650; found, 283.018921 (100%); $[\text{M} + \text{O} + \text{H}]^+$ calcd for $\text{C}_{11}\text{H}_{15}\text{O}_2\text{Fe}_1\text{F}_1\text{P}_1$, 301.009228; found, 301.009430 (17.3%). Another species displaying a $^1J_{\text{P-F}}$ coupling was also present in solution, although the identity of this species cannot be assigned at the present time. The NMR data for this unknown species are: $^{31}\text{P}\{^1\text{H}\}$ NMR (203 MHz, CD_2Cl_2 , δ) +378.8 (d, $J = 845.9$ Hz). $^{19}\text{F}\{^1\text{H}\}$ NMR (471 MHz, CD_2Cl_2 , δ) -131.6 (d, $J = 845.9$ Hz).

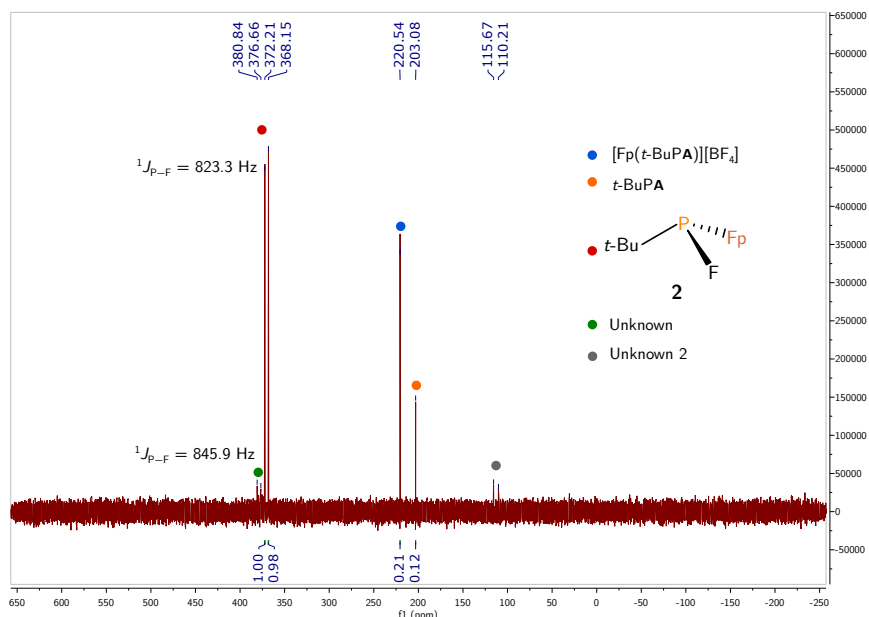


Figure 5.11 $^{31}\text{P}\{^1\text{H}\}$ NMR spectrum of **3** in CD_2Cl_2 at 25°C , recorded at 203 MHz. See section 5.5.7 for discussion of the unknown species.

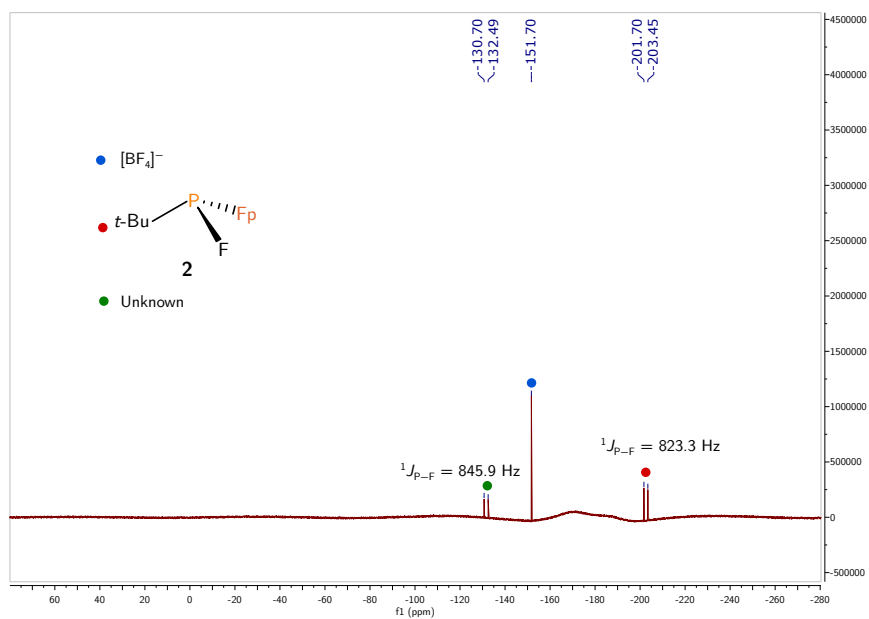


Figure 5.12 $^{19}\text{F}\{^1\text{H}\}$ NMR spectrum of **3** in CD_2Cl_2 at 25°C , recorded at 471 MHz. See section 5.5.7 for discussion of the unknown species.

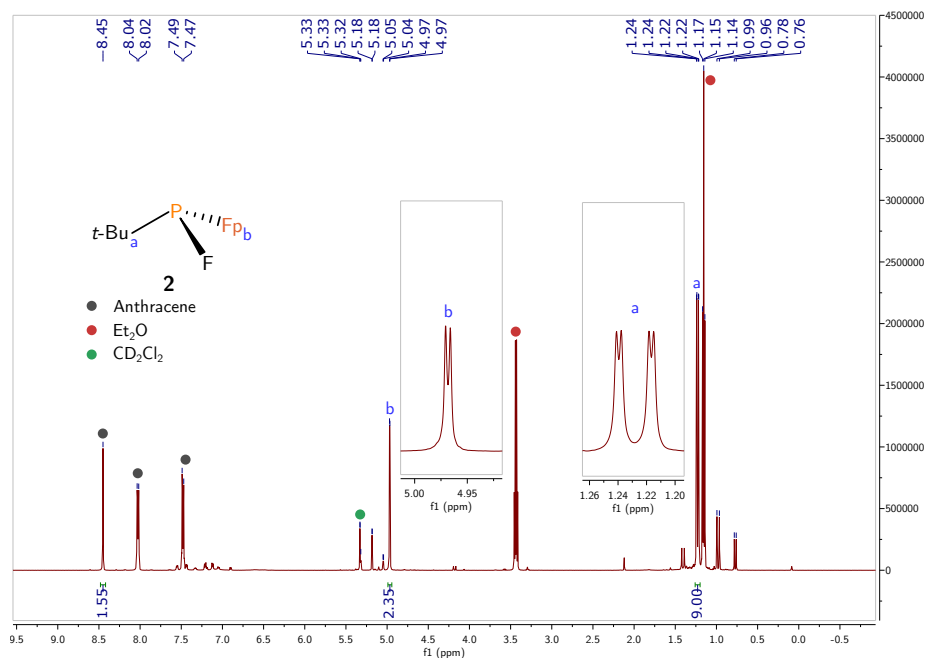


Figure 5.13 ^1H NMR spectrum of **3** in CD_2Cl_2 at $25\text{ }^\circ\text{C}$, recorded at 500 MHz.

5.5.8 Generation and in situ characterization of $[\text{Fp}-\text{CH}(\text{Ph})-\text{CH}_2-\text{P}(t\text{-Bu})\text{A}][\text{BF}_4]$ (**2**)

In the glovebox, *t*-BuPA (10 mg, 0.0375 mmol, 1 equiv) and $[\text{Fp}(\text{styrene})][\text{BF}_4]$ (14 mg, 0.0375 mmol, 1 equiv) were weighed into a scintillation vial and dissolved in CD_2Cl_2 (0.7 mL). The resulting solution was filtered through microfiber filter paper in a Pasteur pipette into an NMR tube. The sample was analyzed by a series of NMR experiments in order to determine the regioisomer of the product that formed. Most useful were the ^1H - ^{13}C HMBC (Fig. 5.18) and ^1H - ^1H NOE spectra (Fig. 5.17), which were used to correlate the protons a, b, and c (Scheme 5.3) on the former styrene molecule to the phenyl group and the anthracene framework. The reaction mixture was allowed to stand at $23\text{ }^\circ\text{C}$ for 18 h then it was analyzed by NMR spectroscopy showing the formation of $[\text{Fp}(t\text{-BuPA})][\text{BF}_4]$ and styrene. ^1H NMR (400 MHz, CD_2Cl_2 , δ) 7.71–7.58 (m, 2H), 7.46–7.35 (m, 4H), 7.31 (t, $J = 7.6$ Hz, 2H), 7.18 (dd, $J = 5.5, 3.1$ Hz, 2H), 7.14 (t, $J = 7.4$ Hz, 1H), 7.08 (d, $J = 7.2$ Hz, 2H), 4.91 (s, 1H), 4.76 (s, 1H), 4.57 (s, 5H), 3.20 (ddd, $J = 13.1, 6.8, 3.3$ Hz, 1H), 3.07 (ddd, $J = 15.6, 13.3, 4.3$ Hz, 1H), 2.94 (ddd, $J = 15.6, 9.7, 3.3$ Hz, 1H), 0.93 (d, $J = 15.5$ Hz, 9H). ^{13}C NMR (101 MHz, CD_2Cl_2 , δ) 217.38, 215.36 (d, $J = 1.9$ Hz), 153.00 (d, $J = 3.3$ Hz), 142.29 (d, $J = 6.4$ Hz), 141.90 (d, $J = 5.9$ Hz), 141.34 (d, $J = 7.0$ Hz), 140.57 (d, $J = 7.1$ Hz), 129.45, 129.05 (d, $J = 3.2$ Hz), 128.81 (d, $J = 6.8$ Hz), 128.01 (d, $J = 5.2$ Hz), 126.64 (d, $J = 6.9$ Hz), 126.20, 126.03–125.87 (m), 125.67, 125.39 (d, J

= 6.6 Hz), 125.11–124.84 (m), 124.66 (d, $J = 4.9$ Hz), 122.89 (d, $J = 11.5$ Hz), 86.87, 50.28 (d, $J = 37.3$ Hz), 49.18 (d, $J = 39.1$ Hz), 36.41 (d, $J = 12.0$ Hz), 33.90–33.31 (m), 28.04, 17.74 (d, $J = 19.0$ Hz). $^{31}\text{P}\{^1\text{H}\}$ NMR (203 MHz, CD_2Cl_2 , δ) +141.8 (s). ^{31}P NMR (203 MHz, CD_2Cl_2 , δ) +141.8 (m). ESI-MS(+): Fig 5.22.

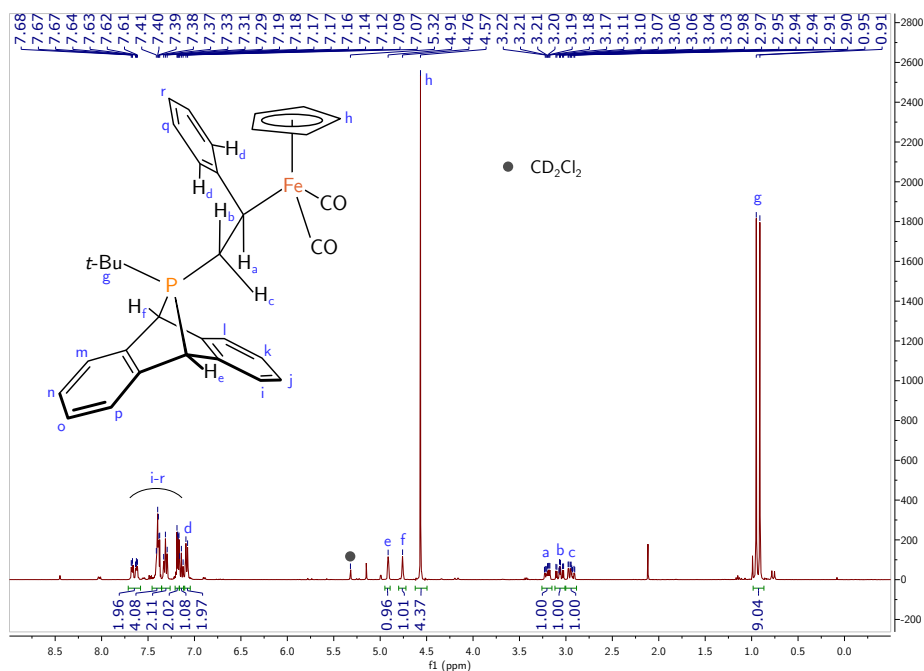


Figure 5.14 ^1H NMR spectrum of **2** in CD_2Cl_2 at 25 °C, recorded at 400 MHz.

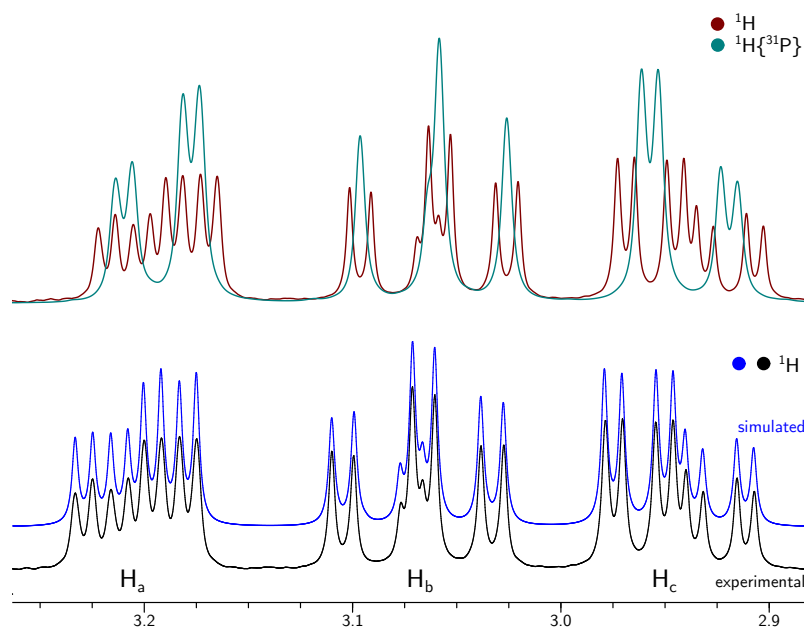


Figure 5.15 Top: experimental ^1H and $^1\text{H}\{^{31}\text{P}\}$ NMR spectra of **2**, zoomed on the region containing the methylene (CH_2) and methine (CH) bridge regions. This spectrum was recorded at 400 MHz in CD_2Cl_2 at 25 °C. **Bottom:** Experimental and simulated ^1H NMR spectrum of **2** in CD_2Cl_2 at 25 °C, recorded at 400 MHz. Hydrogen atom labeling is as indicated in Fig. 5.14.

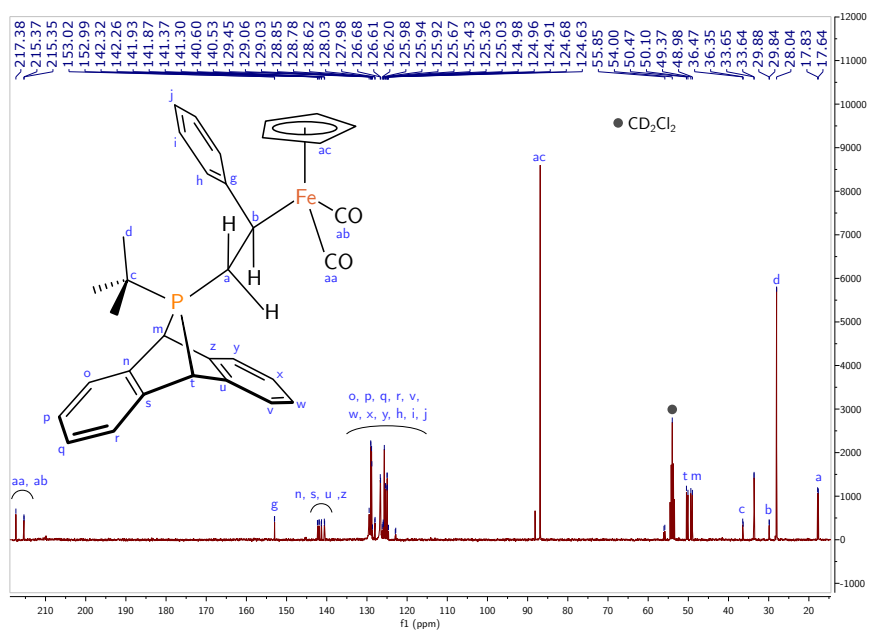


Figure 5.16 ^{13}C NMR spectrum of **2** in CD_2Cl_2 at 25 °C, recorded at 101 MHz.

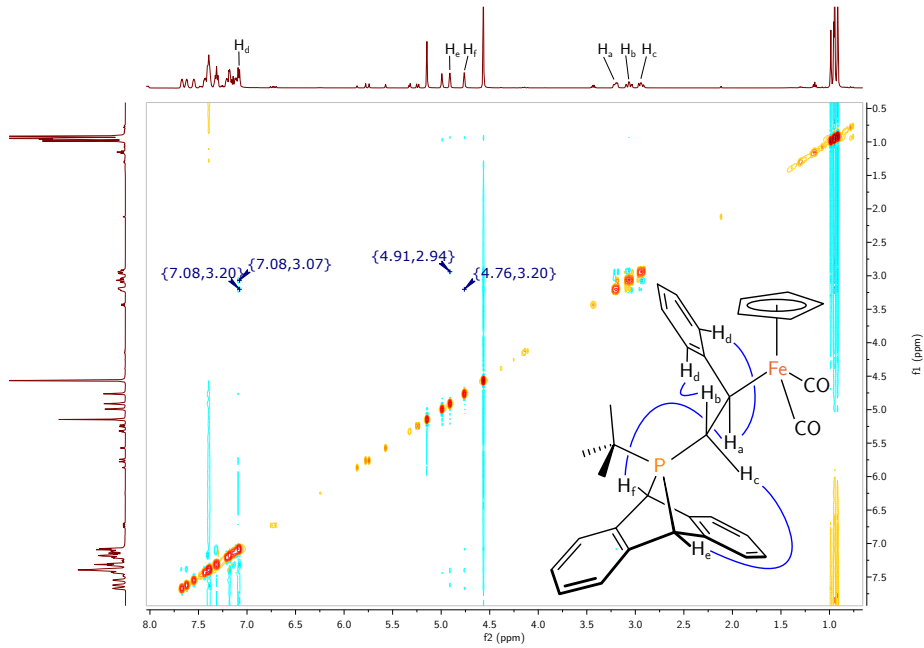


Figure 5.17 ^1H - ^1H NOE spectrum of **2** in CD_2Cl_2 at 25°C , recorded at 400 MHz.

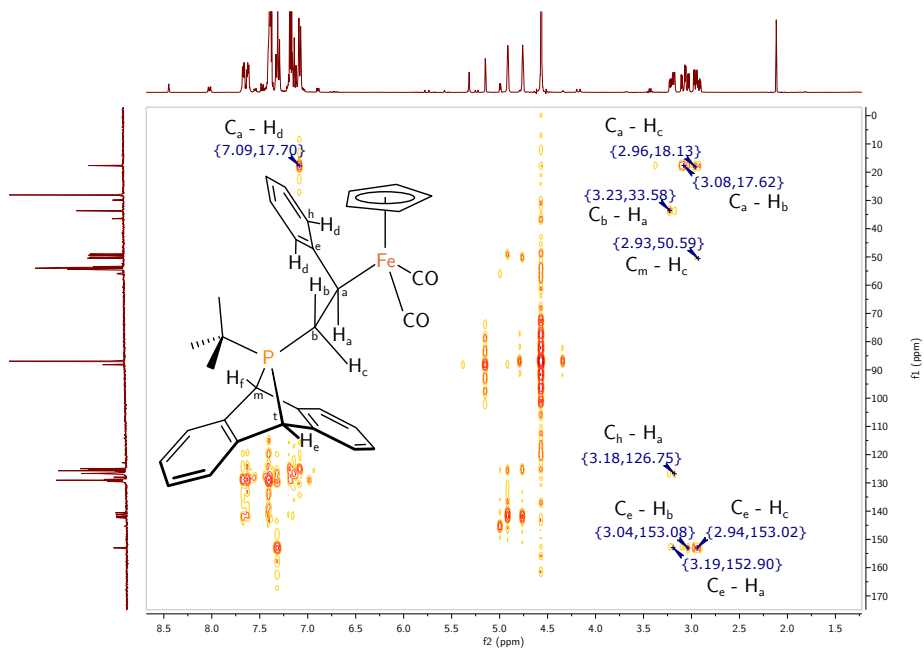
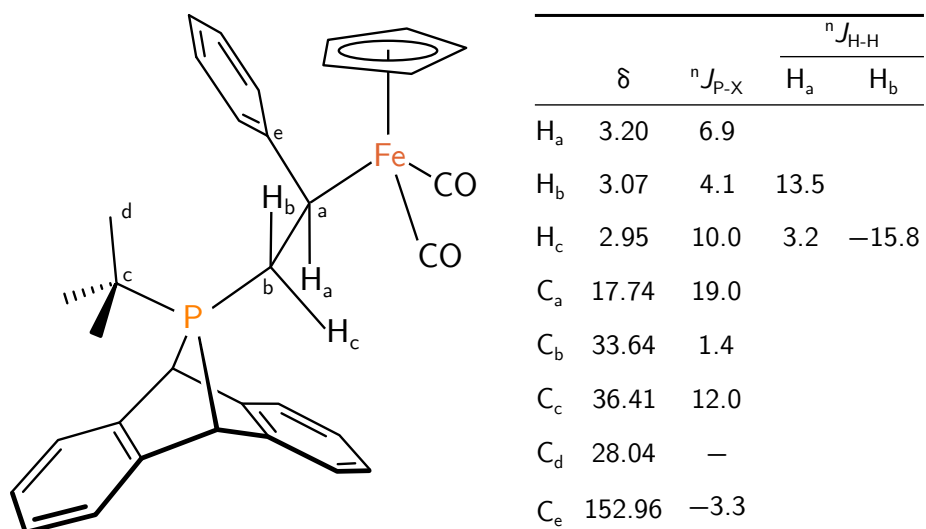


Figure 5.18 ^1H - ^{13}C HMBC spectrum of **2** in CD_2Cl_2 at 25°C , recorded at 400 MHz.



Scheme 5.3 Tabulated ${}^1\text{H}$, ${}^{13}\text{C}$, and ${}^{31}\text{P}$ NMR data for nuclei used to assign the regioisomer of the product. Coupling constants (P–H and H–H) were extracted from simulated spectra. P–C coupling constants were measured from the experimental spectra.

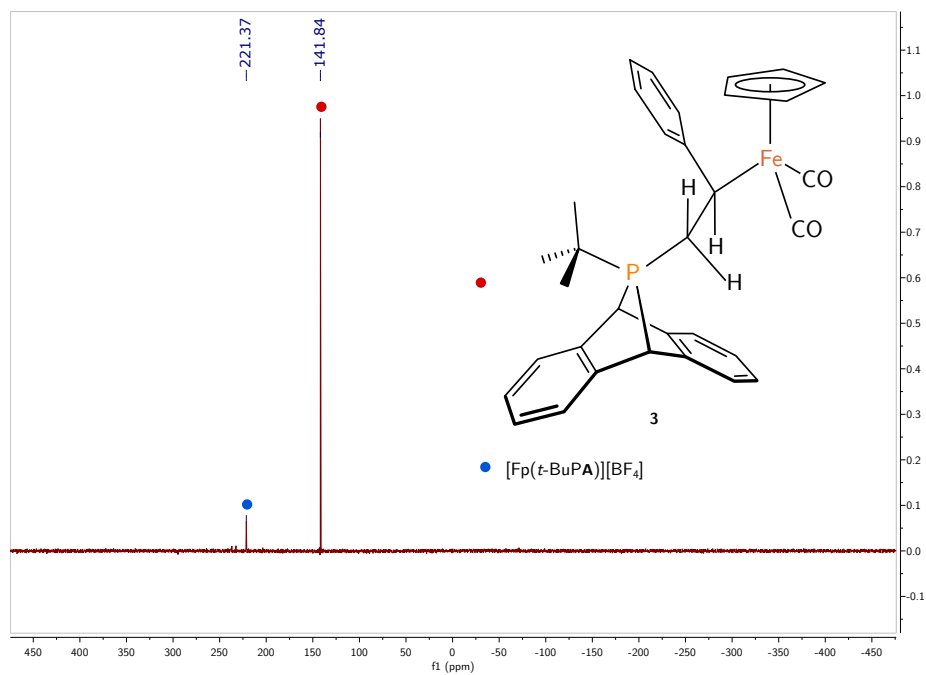


Figure 5.19 ${}^{31}\text{P}\{{}^1\text{H}\}$ NMR spectrum of **2** in CD_2Cl_2 at $25\text{ }^\circ\text{C}$, recorded at 203 MHz.

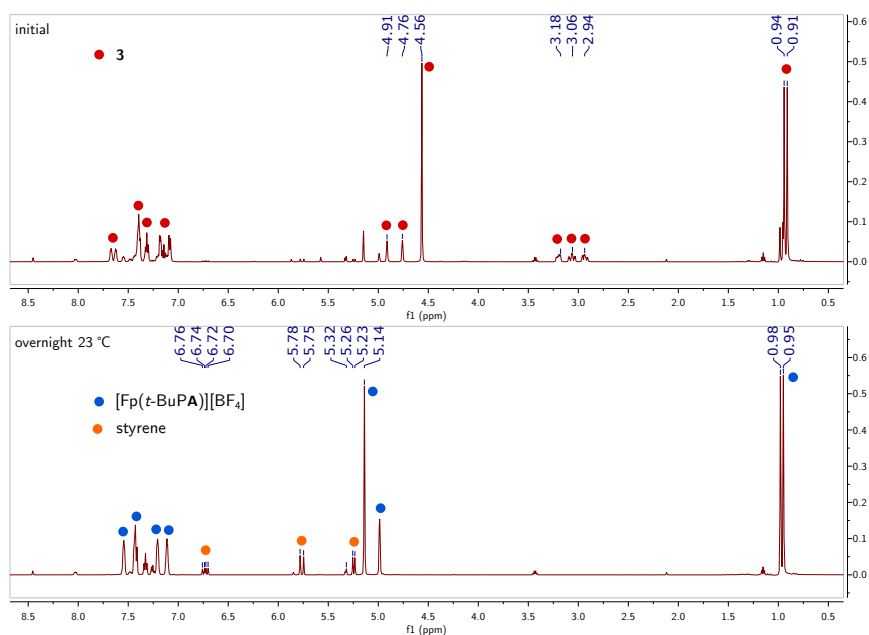


Figure 5.20 ^1H NMR spectra of **2** in CD_2Cl_2 at $25\text{ }^\circ\text{C}$, recorded at 500 MHz. **Top:** Initial NMR spectrum. **Bottom:** NMR spectrum after standing at $23\text{ }^\circ\text{C}$ for 24 h.

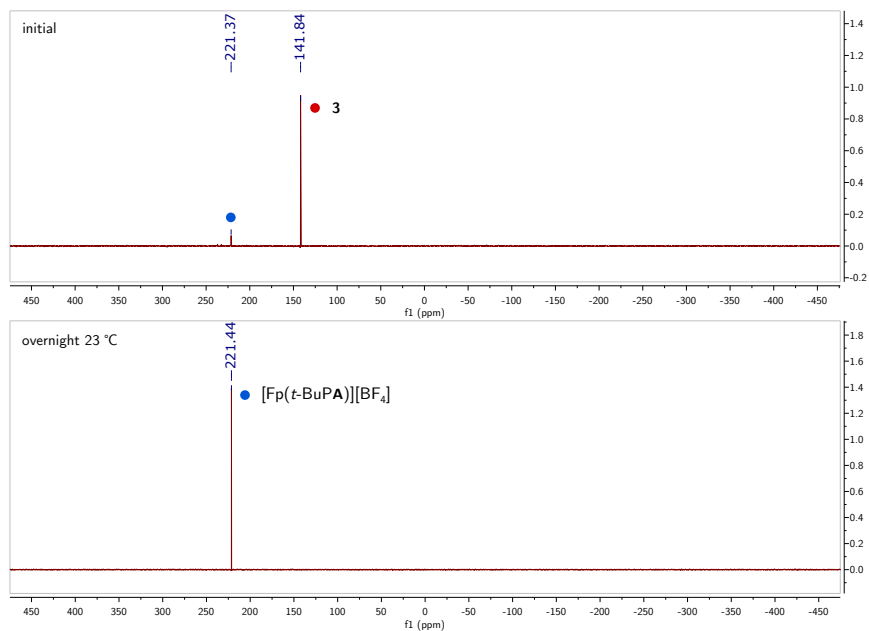


Figure 5.21 $^{31}\text{P}\{^1\text{H}\}$ NMR spectra of **2** in CD_2Cl_2 at $25\text{ }^\circ\text{C}$, recorded at 203 MHz. **Top:** Initial NMR spectrum. **Bottom:** NMR spectrum after standing at $23\text{ }^\circ\text{C}$ for 24 h.

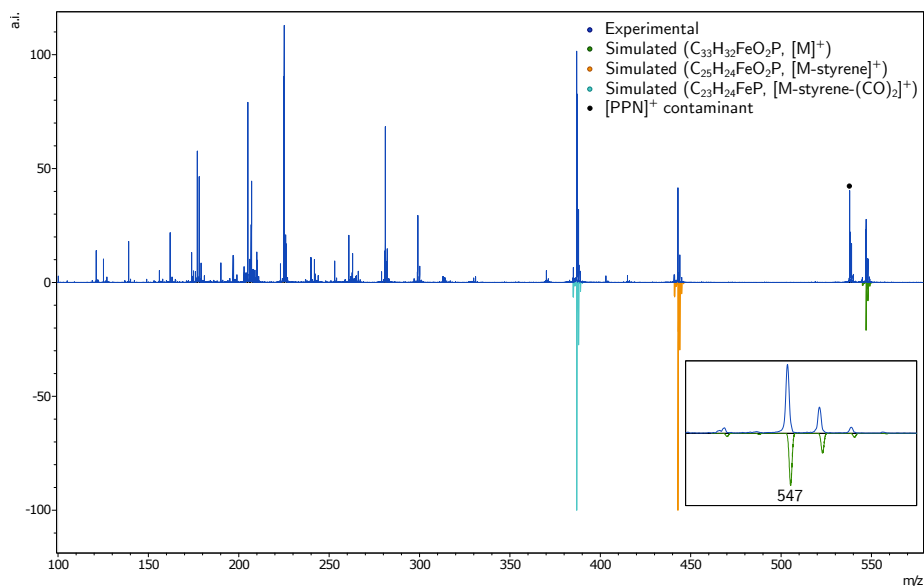


Figure 5.22 ESI mass spectrum (positive mode) of a DCM solution of **2**.

5.5.9 Preparation of $[\text{Fp}(t\text{-BuPA})][\text{BF}_4]$

In the glovebox, $[\text{Fp}(\text{THF})][\text{BF}_4]$ (108 mg, 0.321 mmol, 1 equiv) and *t*-BuPA (86 mg, 0.323 mmol, 1 equiv) were weighed into the same scintillation vial (20 mL) and dissolved in DCM (4 mL). The reaction mixture was stirred for 30 minutes then hexanes (10 mL) were added leading to the formation of a tan precipitate. The slurry was stirred vigorously for 30 minutes, then the solids were collected on a frit (fine porosity, 30 mL) and washed with hexanes (2×5 mL). The solid material was transferred to a vial and brought to constant mass in vacuo to give $[\text{Fp}(t\text{-BuPA})][\text{BF}_4]$ as a tan solid (166 mg, 0.313 mmol, 98%). Anal. Calcd for $\text{C}_{25}\text{H}_{24}\text{BF}_4\text{FeO}_2\text{P}$: C, 56.65; H, 4.56; N, 0.00. Found: C, 56.82; H, 4.73; N, ≤ 0.02 . ^1H NMR (500 MHz, CD_2Cl_2 , δ) 7.58–7.52 (m, 2H), 7.44 (dd, $J = 5.4, 3.2$ Hz, 2H), 7.21 (dd, $J = 5.5, 3.2$ Hz, 2H), 7.12 (dd, $J = 5.5, 3.2$ Hz, 2H), 5.15 (5H), 4.98 (d, $J = 3.2$ Hz, 2H), 0.97 (d, $J = 15.1$ Hz, 9H). ^{13}C NMR (126 MHz, CD_2Cl_2 , δ) 209.97 (d, $J = 17.1$ Hz), 145.47 (d, $J = 12.0$ Hz), 145.16 (d, $J = 3.6$ Hz), 128.05, 128.00, 125.95 (d, $J = 6.3$ Hz), 124.66 (d, $J = 5.2$ Hz), 55.97 (d, $J = 21.1$ Hz), 41.59, 29.86 (d, $J = 3.7$ Hz). $^{19}\text{F}\{^1\text{H}\}$ NMR (471 MHz, CD_2Cl_2 , δ) $-150.85, -150.91$. $^{31}\text{P}\{^1\text{H}\}$ NMR (203 MHz, CD_2Cl_2 , δ) 220.69 (s). ^{31}P NMR (203 MHz, CD_2Cl_2 , δ) 220.69 (dec., $J = 14.8$ Hz). ^{11}B NMR (161 MHz, CD_2Cl_2 , δ) -0.87 (s). ESI-MS(+): Fig 5.28. IR (cm^{-1}): 2008, 2036, 2053. *Note*: Three bands in the carbonyl region were observed instead of the anticipated two. The bands at 2053 and 2008 cm^{-1} are tentatively assigned as the symmetric and asymmetric CO stretching modes, respectively, based on comparison to other species of the type $[\text{Fp}(\text{PR}_3)][\text{BF}_4]$.⁶⁵

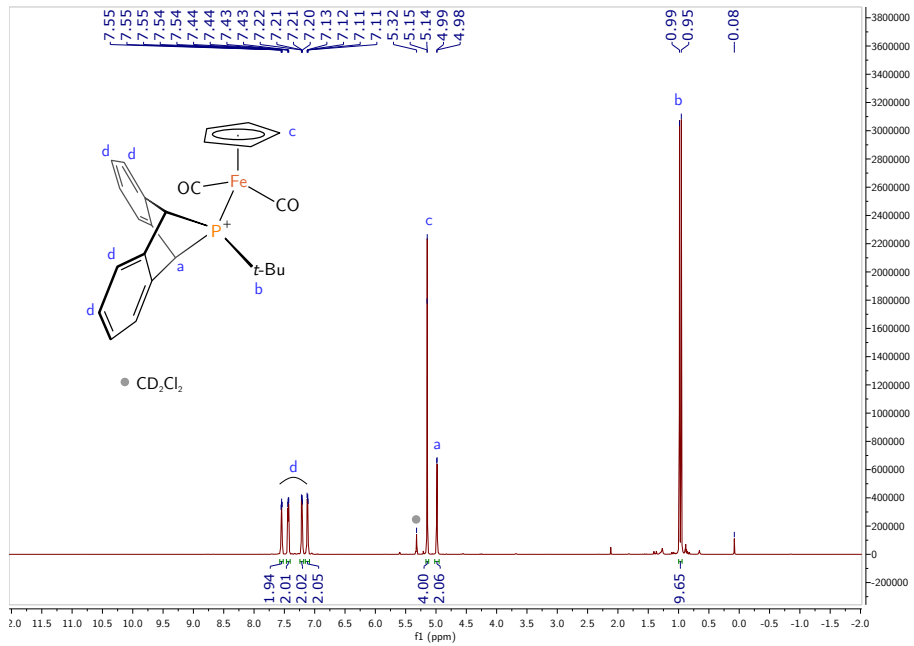


Figure 5.23 1H NMR spectrum of $[Fp(t-BuPA)][BF_4]$ in CD_2Cl_2 at 25 °C, recorded at 500 MHz.

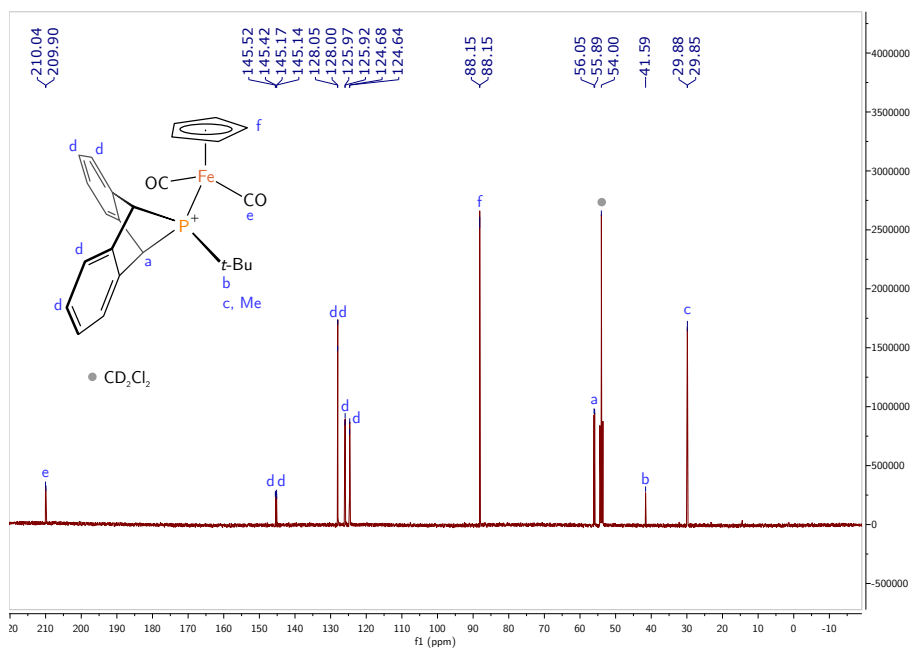


Figure 5.24 $^{13}C\{^1H\}$ NMR spectrum of $[Fp(t-BuPA)][BF_4]$ in CD_2Cl_2 at 25 °C, recorded at 126 MHz.

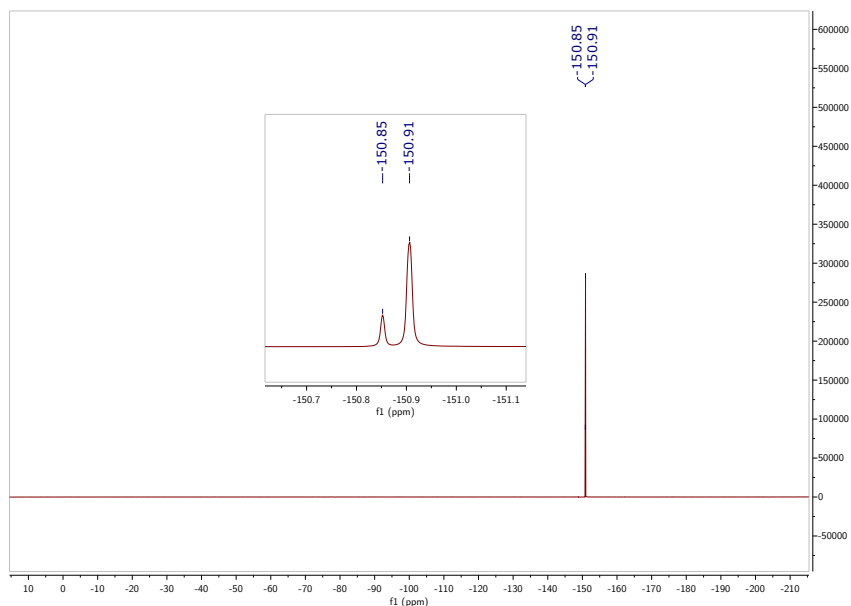


Figure 5.25 $^{19}\text{F}\{^1\text{H}\}$ NMR spectrum (inset: zoom of the tetrafluoroborate region) of $[\text{Fp}(t\text{-BuPA})][\text{BF}_4]$ in CD_2Cl_2 at $25\text{ }^\circ\text{C}$, recorded at 471 MHz. There are two resonances due to the ^{19}F nuclei showing an isotope shift from coupling to the ^{10}B and ^{11}B nuclei.

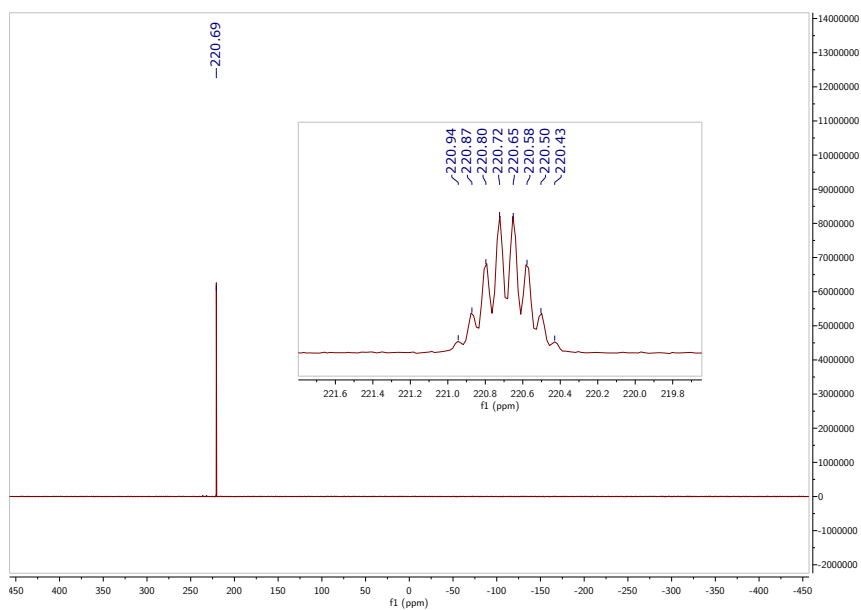


Figure 5.26 $^{31}\text{P}\{^1\text{H}\}$ NMR spectrum (inset: ^{31}P NMR spectrum) of $[\text{Fp}(t\text{-BuPA})][\text{BF}_4]$ in CD_2Cl_2 at $25\text{ }^\circ\text{C}$, recorded at 203 MHz.

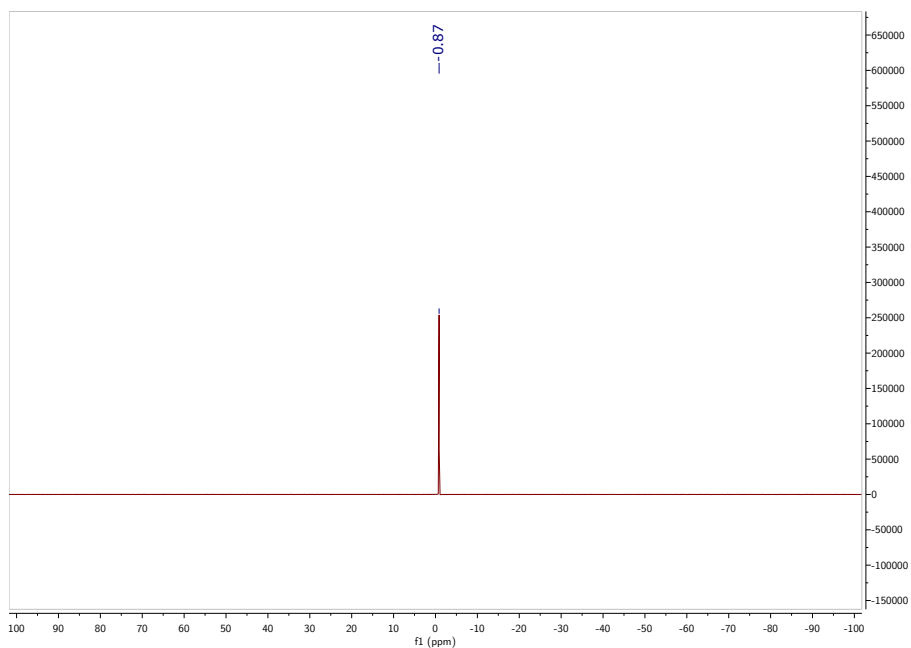


Figure 5.27 ^{11}B NMR spectrum of $[\text{Fp}(t\text{-BuPA})][\text{BF}_4]$ in CD_2Cl_2 at $25\text{ }^\circ\text{C}$, recorded at 161 MHz.

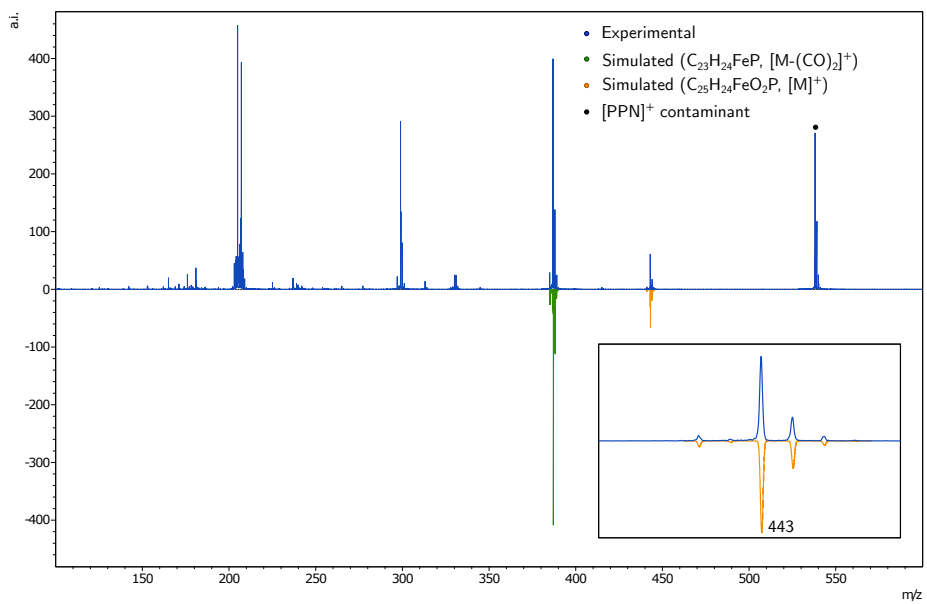


Figure 5.28 ESI mass spectrum (positive mode) of a DCM solution of $[\text{Fp}(t\text{-BuPA})][\text{BF}_4]$.

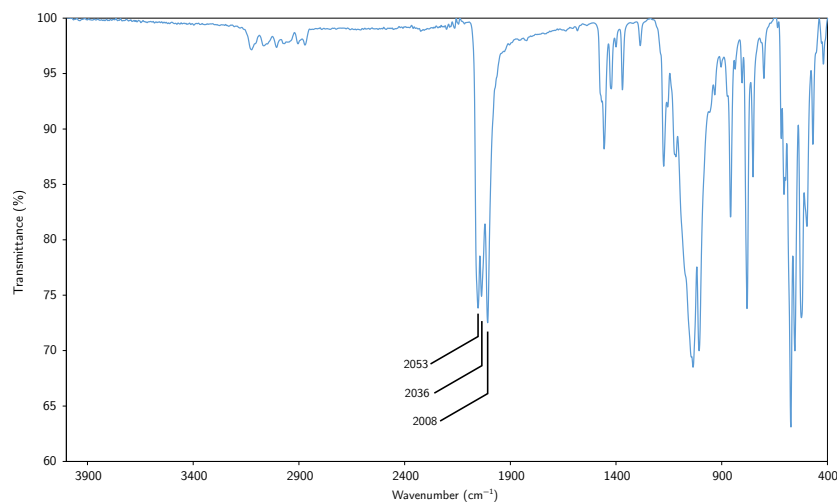


Figure 5.29 IR spectrum of $[\text{Fp}(t\text{-BuPA})][\text{BF}_4]$.

5.5.10 Preparation of $[\text{Fp}(1\text{-}t\text{-Bu})][\text{BF}_4]$

In the glovebox, 1-tert-butyl-2-phenylphosphirane (**1-*t*-Bu**, 106 mg, 0.55 mmol, 1.1 equiv) and $[\text{Fp}(\text{THF})][\text{BF}_4]$ (168 mg, 0.50 mmol, 1 equiv) were weighed into separate vials. $[\text{Fp}(\text{THF})][\text{BF}_4]$ was dissolved in DCM (2 mL) and **1-*t*-Bu** was dissolved in DCM (1 mL). The solution of phosphirane was added to the solution of $[\text{Fp}(\text{THF})][\text{BF}_4]$ with stirring. The vial used to weigh out **1-*t*-Bu** was rinsed with DCM (1 mL) and the washings were transferred to the reaction mixture. The solution was allowed to stir for 2 hours, then pentane (10 mL) was added resulting in the formation of an orange oil. Volatile material was removed under reduced pressure and the resulting oil was triturated with additional pentane (15 mL), each round using a spatula to break up any solids; this process resulted in formation of a yellow powder. A slurry of this yellow solid in pentane (15 mL) was stirred vigorously for 30 minutes, then the solids were collected on a frit (15 mL, fine porosity) and washed with additional pentane (3×4 mL). The material was transferred to a pre-weighed vial and brought to constant mass to give $[\text{Fp}(1\text{-}t\text{-Bu})][\text{BF}_4]$ as a yellow powder (197 mg, 0.42 mmol, 84% based on Fe). Anal. Calcd for $\text{C}_{19}\text{H}_{22}\text{BF}_4\text{FeO}_2\text{P}$: C, 50.05; H, 4.86; N, 0.00. Found: C, 50.69; H, 5.25; N, ≤ 0.02 . ^1H NMR (500 MHz, CD_2Cl_2 , δ) 7.50–7.25 (m, 5H), 4.95 (s, 5H), 3.54 (q, $J = 8.9, 8.0$ Hz, 1H), 2.11 (d, $J = 10.5$ Hz, 1H), 1.84 (t, $J = 9.0$ Hz, 1H), 1.28 (d, $J = 19.1$ Hz, 9H). ^{13}C NMR (126 MHz, CD_2Cl_2 , δ) 209.13 (d, $J = 22.5$ Hz), 208.82 (d, $J = 22.8$ Hz), 135.07 (d, $J = 4.1$ Hz), 129.90 (d, $J = 2.1$ Hz), 129.23 (d, $J = 4.5$ Hz), 128.76 (d, $J = 2.7$ Hz), 87.08, 36.55 (d, $J = 9.6$ Hz), 28.67 (d, $J = 4.5$ Hz), 26.66 (d, $J = 18.5$ Hz), 10.81 (d, $J = 12.9$ Hz). $^{19}\text{F}\{^1\text{H}\}$ NMR (471 MHz, CD_2Cl_2 , δ) -151.99 . $^{31}\text{P}\{^1\text{H}\}$ NMR (203 MHz, CD_2Cl_2 , δ) -76.23 (s). ^{31}P NMR (203 MHz, CD_2Cl_2 , δ) -76.23 (m). ^{11}B NMR (161 MHz, CD_2Cl_2 , δ) -1.11 (s). ESI-MS(+): Fig 5.35. IR (cm^{-1}): 2006 ($\nu_{\text{CO}(\text{assym})}$), 2047 ($\nu_{\text{CO}(\text{sym})}$).

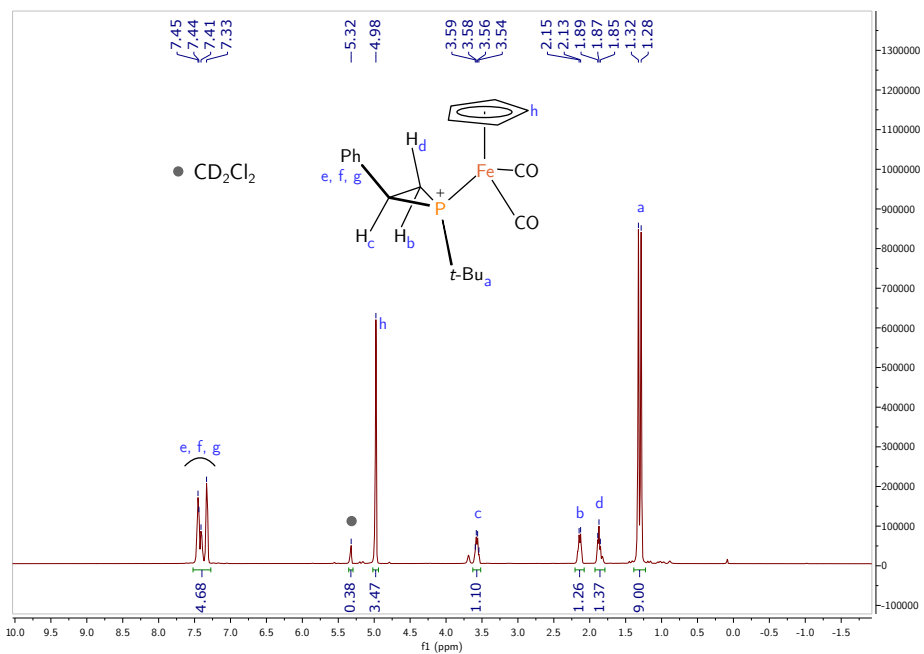


Figure 5.30 1H NMR spectrum of $[Fp(1-t-Bu)][BF_4]$ in CD_2Cl_2 at 25 °C, recorded at 500 MHz.

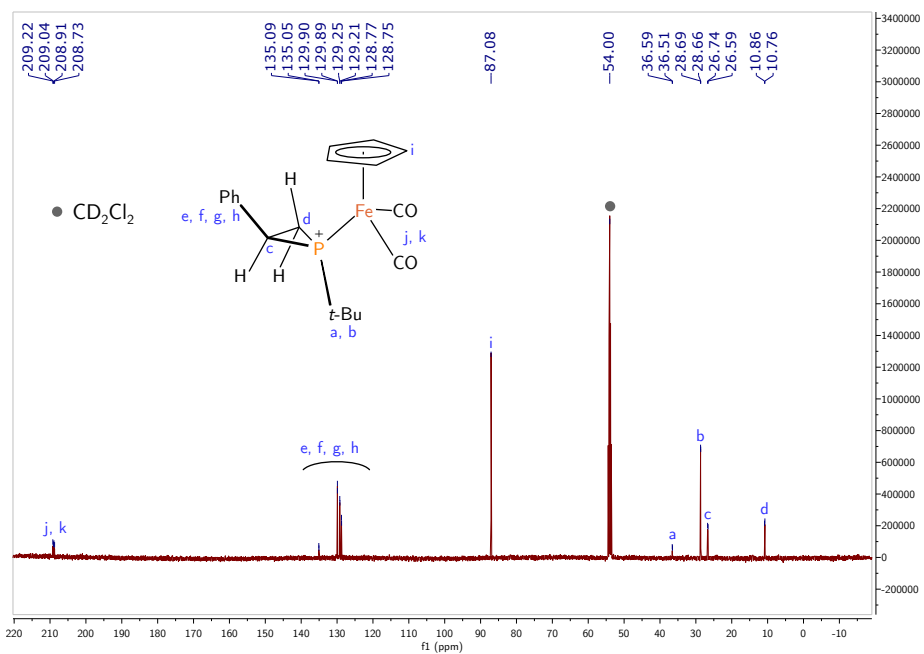


Figure 5.31 $^{13}C\{^1H\}$ NMR spectrum of $[Fp(1-t-Bu)][BF_4]$ in CD_2Cl_2 at 25 °C, recorded at 126 MHz.

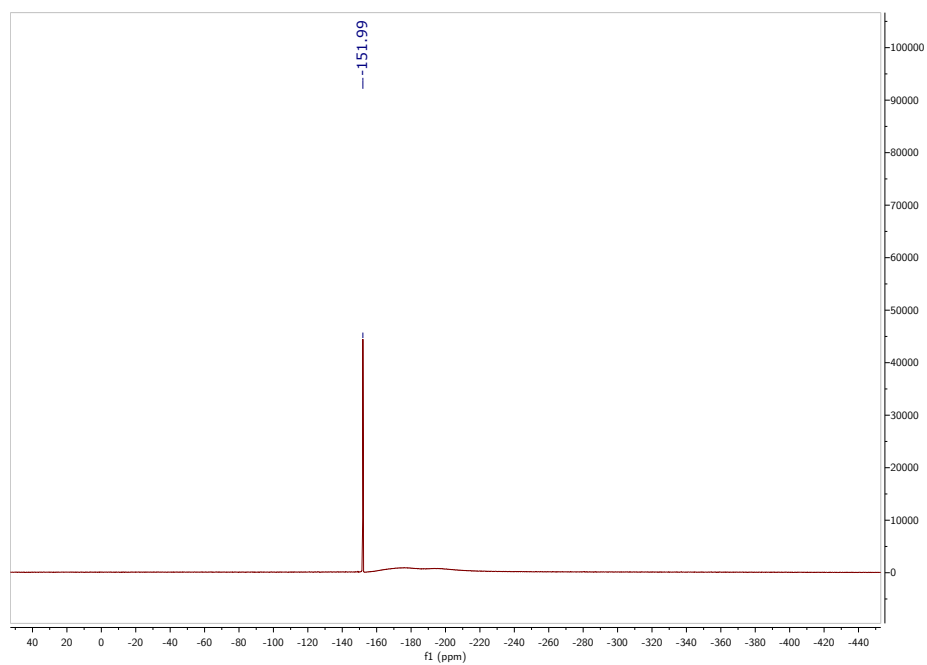


Figure 5.32 $^{19}\text{F}\{^1\text{H}\}$ NMR spectrum of $[\text{Fp}(1-t\text{-Bu})][\text{BF}_4]$ in CD_2Cl_2 at $25\text{ }^\circ\text{C}$, recorded at 471 MHz.

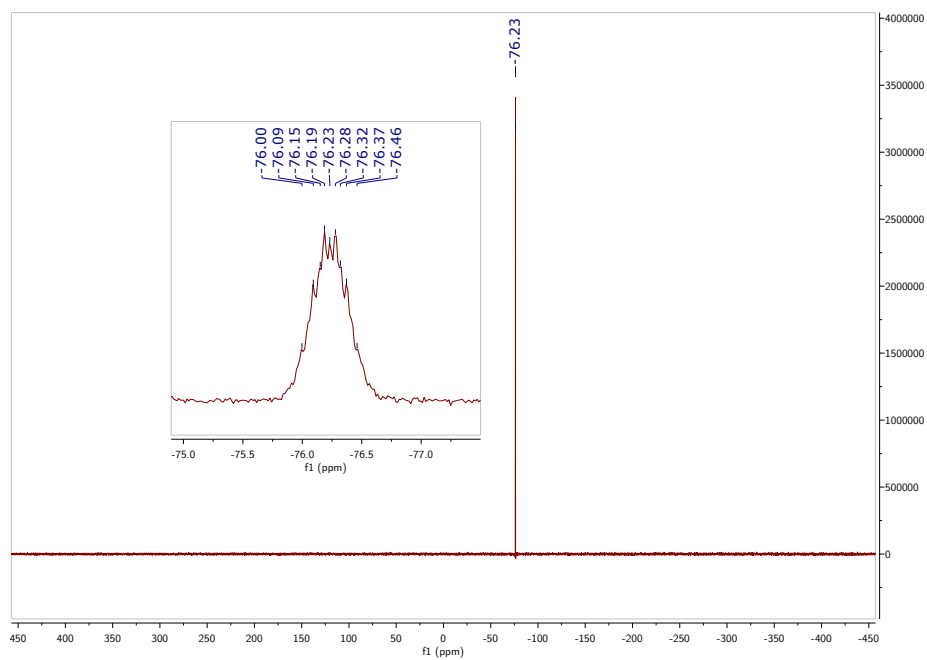


Figure 5.33 $^{31}\text{P}\{^1\text{H}\}$ NMR spectrum (inset: ^{31}P NMR spectrum) of $[\text{Fp}(1-t\text{-Bu})][\text{BF}_4]$ in CD_2Cl_2 at $25\text{ }^\circ\text{C}$, recorded at 203 MHz.

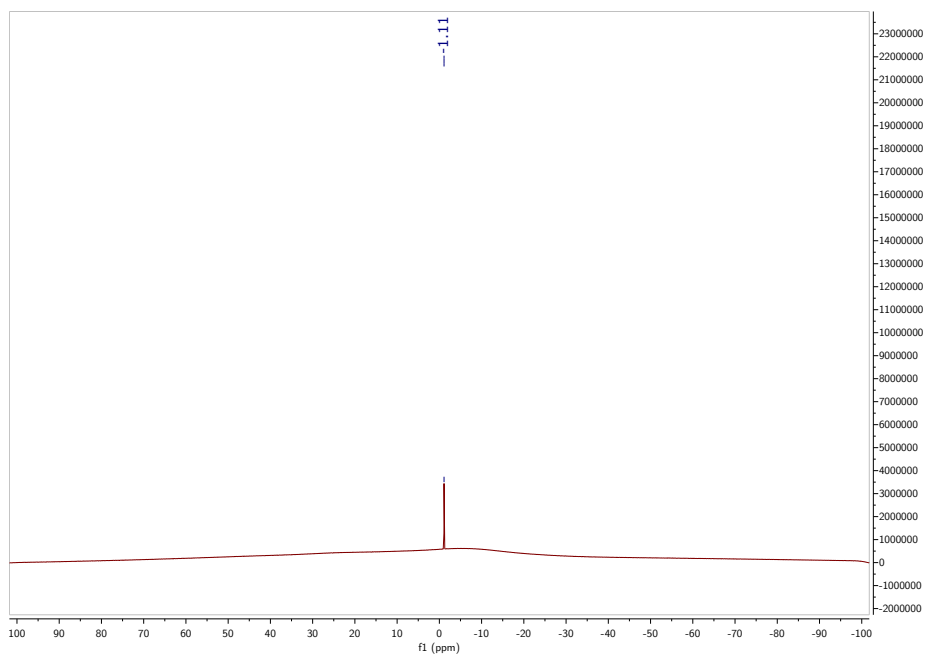


Figure 5.34 ^{11}B NMR spectrum of $[\text{Fp}(\mathbf{1-t-Bu})][\text{BF}_4]$ in CD_2Cl_2 at $25\text{ }^\circ\text{C}$, recorded at 161 MHz.

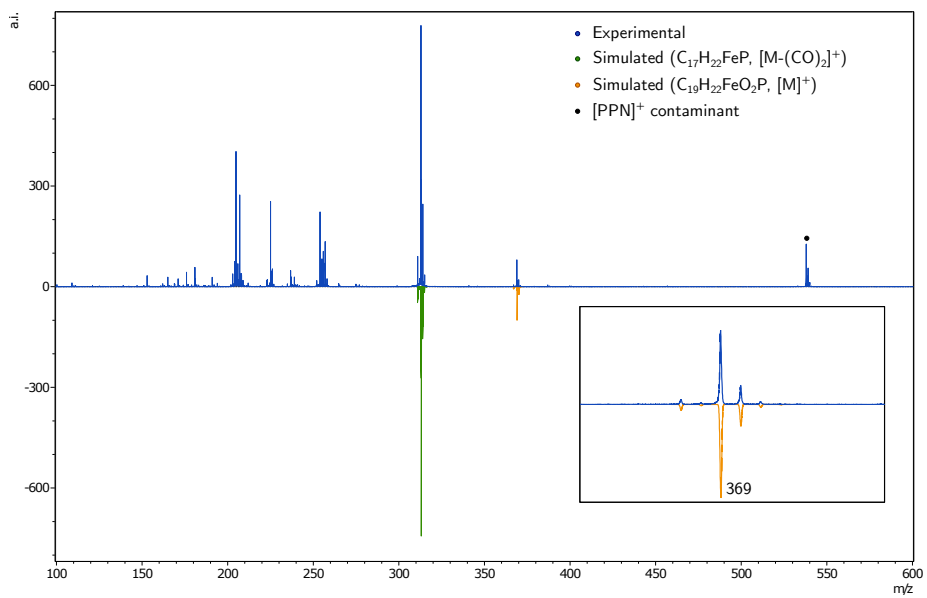


Figure 5.35 ESI mass spectrum (positive mode) of a DCM solution of $[\text{Fp}(\mathbf{1-t-Bu})][\text{BF}_4]$.

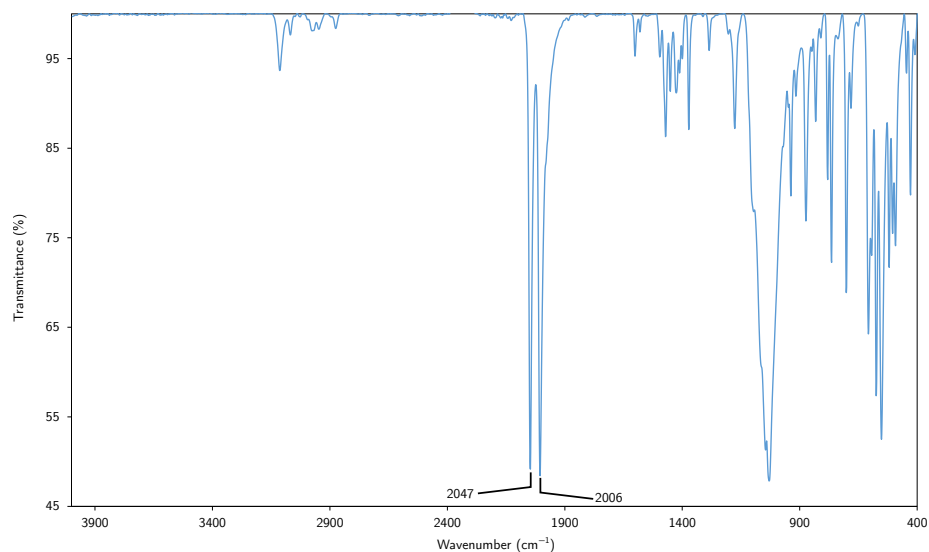


Figure 5.36 IR spectrum of $[\text{Fp}(\mathbf{1-t-Bu})][\text{BF}_4]$.

5.5.11 Synthesis of *i*-PrPA

A colorless and homogeneous solution of *i*-PrPCl₂ (1.0 g, 6.9 mmol, 1.00 equiv) in THF (75 mL) was prepared within a 200 mL round bottom flask equipped with a magnetic stir bar, and this was frozen in the glovebox cold well (liquid N₂). In two portions, orange solid MgA·3THF (2.9 g, 6.9 mmol, 1.00 equiv) was added to the thawing and rapidly stirring THF solution. After the first portion, the reaction mixture was allowed to stir until the orange color faded, and then it was frozen again. After the second portion, the mixture was stirred for 30 min as it warmed under foil to exclude light. The THF solvent was removed from the pale green and cloudy mixture under reduced pressure to give a pale yellow solid residue. Product was extracted from this residue using diethyl ether (3 × 20 mL), passing each extract through a 1" 1:2 Celite/charcoal plug (1.5" diameter). Volatile material was removed from the combined extracts under reduced pressure to give 0.86 g crude product as an off-white solid. The crude product was dissolved in minimal diethyl ether (*ca.* 12 mL) and stored at -35 °C overnight. Clear and colorless block-shaped crystals were collected on a frit (0.43 g, 1.7 mmol, 25%).

Anal. Calcd for C₁₇H₁₇P: C, 80.93; H, 6.79; N, 0.00. Found: C, 81.17; H, 6.79; N, ≤0.02. ¹H NMR (500 MHz, C₆D₆, δ) 7.21 (m, 2H), 7.01 (m, 2H), 6.95 (m, 2H), 6.77 (m, 2H), 3.80 (d, ²J_{P-H} = 14.1 Hz, 2H), 1.15 (hept, ³J_{H-H} = 7.1 Hz, 1H, *i*-Pr methine), 0.84 (dd, ³J_{P-H} = 14.2 Hz, ³J_{HH} = 7.1 Hz, 6H, *i*-Pr methyls). ¹³C NMR (126 MHz, C₆D₆, δ) 148.9, 146.5 (d, ²J_{P-C} = 16.9 Hz), 126.2, 124.8, 123.2 (d, ³J_{PC} = 3.1 Hz), 122.9, 52.3 (d, ¹J_{PC} = 15.7 Hz), 26.8 (d, ¹J_{PC} = 28.7 Hz, *i*-Pr methine), 18.4 (d, ²J_{PC} = 20.2 Hz, *i*-Pr methyls). ³¹P{¹H} NMR (203 MHz, C₆D₆, δ) 199 ppm.

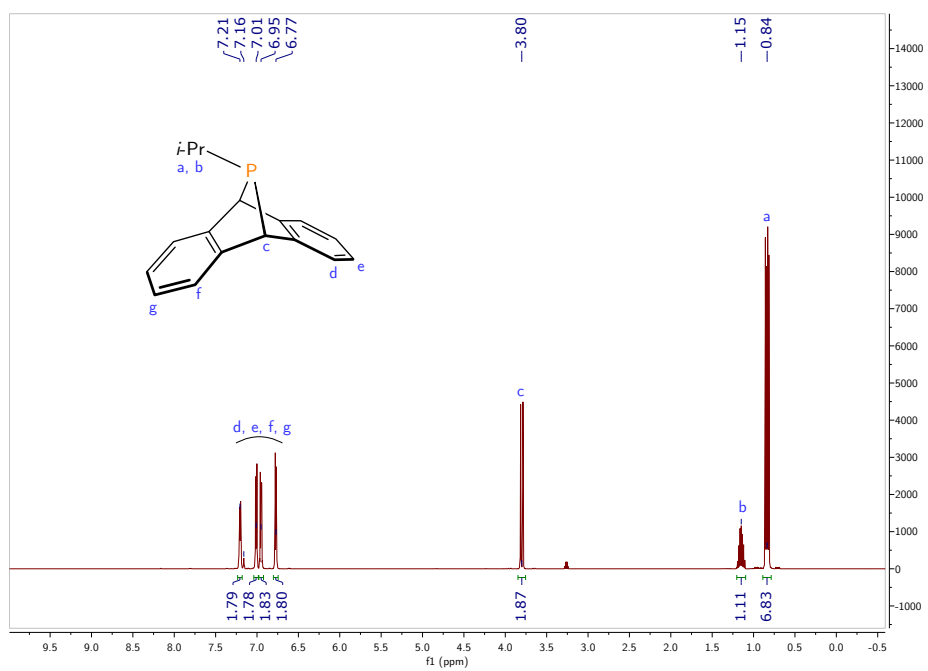


Figure 5.37 ^1H NMR spectrum of *i*-PrPA in C_6D_6 at $20\text{ }^\circ\text{C}$, recorded at 500 MHz.

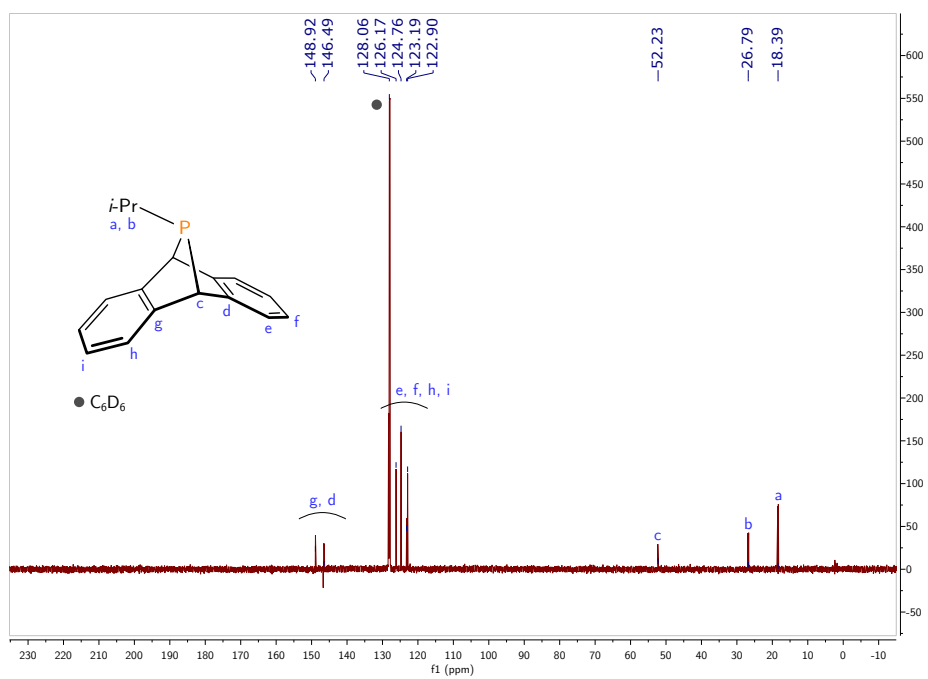


Figure 5.38 $^{13}\text{C}\{^1\text{H}\}$ NMR spectrum of *i*-PrPA in C_6D_6 at $20\text{ }^\circ\text{C}$, recorded at 126 MHz.

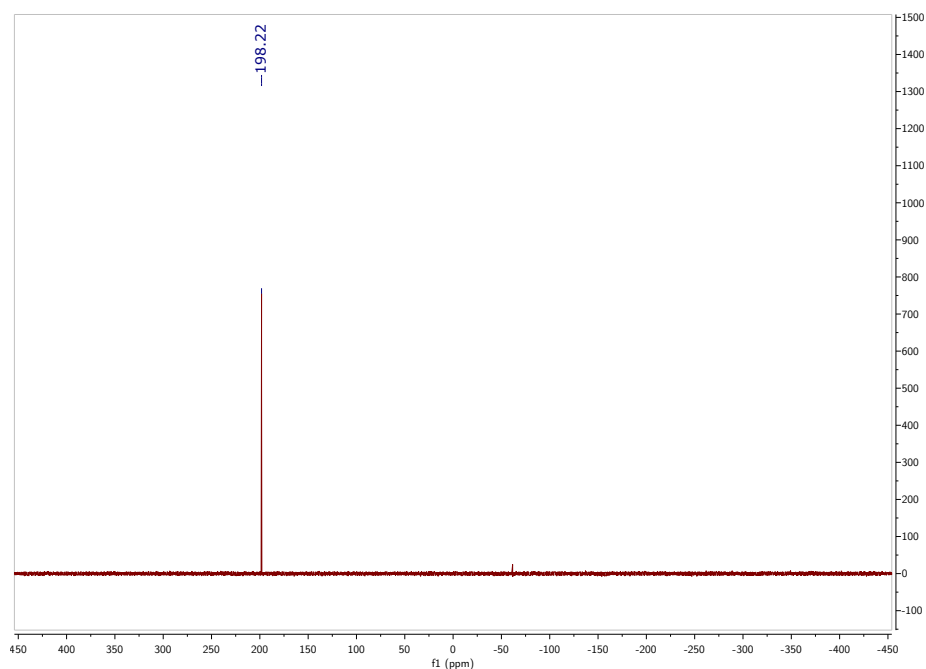


Figure 5.39 $^{31}\text{P}\{^1\text{H}\}$ NMR spectrum of *i*-PrPA in C_6D_6 at 20 °C, recorded at 203 MHz.

5.5.12 Hammett analysis using substituted styrenes

Preparation of styrene derivatives: In the fume hood, a styrene (ca. 1 mL) was passed through a plug of basic alumina (1.5 cm) in a Pasteur pipette containing microfiber filter paper, into an NMR tube equipped with a J. Young valve. The styrene was then degassed three times via the freeze-pump-thaw method. The NMR tube was back-filled with nitrogen and the sample brought into the glovebox. The styrene was passed through a second plug of activated basic alumina (1 cm) in a Pasteur pipette containing microfiber filter paper into a 2 dram vial. The styrene was used immediately to prepare the following stock solutions.

Preparation of styrene stock solutions: In the glovebox, the following stock solutions were prepared. These were stored in the glovebox freezer ($-35\text{ }^\circ\text{C}$) in between sample preparations. All experiments were performed within 36 h of preparing the stock solutions.

Solution A: *p*-trifluoromethyl styrene (272 mg, 1.58 mmol, 1 equiv), styrene (164 mg, 1.58 mmol, 1 equiv) and THF (1000 mg).

Solution B: *p*-chlorostyrene (218 mg, 1.58 mmol, 1 equiv), styrene (164 mg, 1.58 mmol, 1 equiv) and THF (1000 mg).

Solution C: *p*-methylstyrene (186 mg, 1.58 mmol, 1 equiv), styrene (164 mg, 1.58 mmol, 1 equiv) and THF (1000 mg).

Solution D: *p*-methoxystyrene (212 mg, 1.58 mmol, 1 equiv), styrene (164 mg, 1.58 mmol,

1 equiv) and THF (1000 mg).

Sample preparation: The following procedure was performed in triplicate. In the glovebox, four scintillation vials (2 dram) were each charged with TMAF (1.5 mg, 0.0157 mmol, 0.2 equiv), [Fp(THF)][BF₄] (2.7 mg, 0.00789 mmol, 0.1 equiv) and *t*-BuPA (21 mg, 0.0789 mmol, 1 equiv). To one of these vials was added either solution A (359 mg, containing *p*-(trifluoromethyl)styrene (68 mg, 0.395 mmol, 5 equiv), styrene (41 mg, 0.0395 mmol, 5 equiv) and THF (250 mg, 0.283 mL), solution B (347 mg, containing *p*-chlorostyrene (56 mg, 0.395 mmol, 5 equiv), styrene (41 mg, 0.0395 mmol, 5 equiv) and THF (250 mg, 0.283 mL), solution C (338 mg, containing *p*-methylstyrene (47 mg, 0.395 mmol, 5 equiv), styrene (41 mg, 0.0395 mmol, 5 equiv) and THF (250 mg, 0.283 mL) or solution D (344 mg, containing *p*-methoxystyrene (56 mg, 0.395 mmol, 5 equiv), styrene (41 mg, 0.0395 mmol, 5 equiv) and THF (250 mg, 0.283 mL). The four slurries were allowed to sit for 30 minutes, after which time most of the *t*-BuPA had dissolved. The four individual reaction mixtures were transferred to four individual NMR tubes equipped with J. Young valves, taking care to transfer any insoluble material. Each vial was washed with THF (280 mg, 0.317 mL) and the resulting solution was transferred to the appropriate NMR tube. The tube was then sealed and placed in the same preheated oil bath at 85(±5) °C for 17 h.

Sample analysis: The samples were analyzed by ³¹P{¹H} NMR spectroscopy (d₁ = 60 s, 8 transients, sweep width = 900 ppm, center frequency = 100 ppm). For the first set run in triplicate, a capillary containing PPh₃ in benzene-d₆ was included in the NMR tube as an external ³¹P NMR standard.

Data analysis: Spectra were opened in MestreNova and referenced to the triphenylphosphine external standard. Spectra were phased, the baselines were corrected, and the phosphirane signals were integrated. The integral of the parent phosphirane was defined as 1, and the ratio of the two styrene products was tabulated (Table 5.3).

Table 5.3 Experimental values determined from the Hammett analysis

X^a	σ^b	k_X/k_H			$\log(k_X/k_H)$			Mean	σ^c
		1	2	3	1	2	3		
CF ₃	0.53	2.14	1.74	2.24	0.33	0.24	0.35	0.34	0.01
Cl	0.23	1.46	1.51	1.58	0.16	0.18	0.20	0.18	0.02
Me	-0.17	0.87	0.87	0.84	-0.06	-0.06	-0.08	-0.07	0.01
OMe	-0.27	0.73	0.76	0.74	-0.14	-0.12	-0.13	-0.13	0.01

^a *para*-substituent on styrene

^b Hammett parameter

^c Standard deviation

^d Run 2 for the *para*-CF₃ substituted styrene was not included in the analysis. It was deemed an outlier based on the unreasonable numerical values obtained and the fact that multiple other species were observed by ³¹P NMR spectroscopy in the reaction mixture (possibly due to a leaky NMR tube).

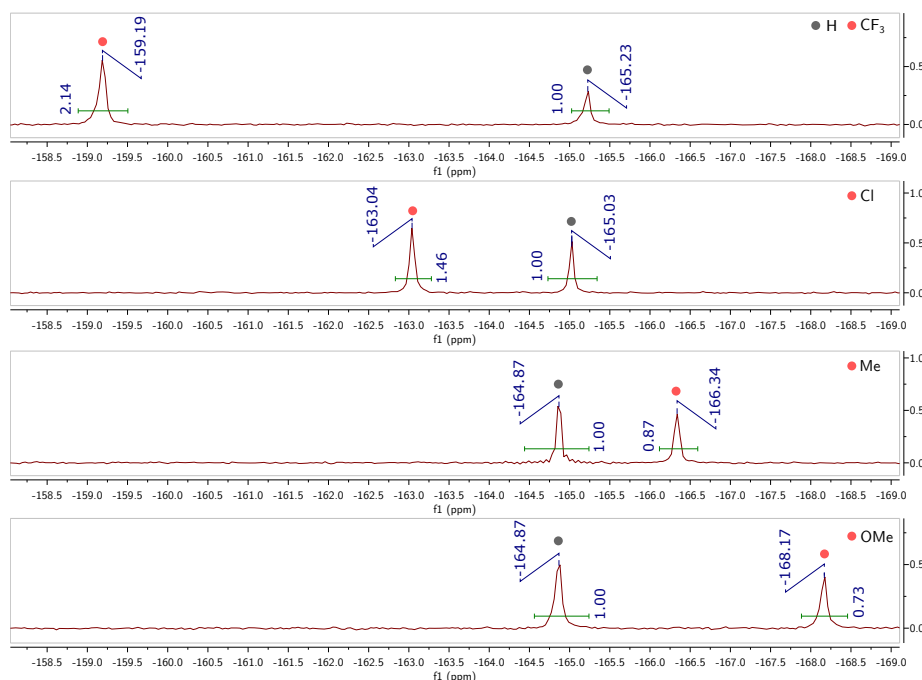


Figure 5.40 ³¹P{¹H} NMR spectra of the reaction mixtures obtained from the Hammett analysis (Run 1 of the study in triplicate) in THF at 25 °C, recorded at 203 MHz. The labeling scheme refers to the *para*-substituent on styrene.

5.5.13 Labeling studies

Cis- β -deuterostyrene was prepared along the lines of previous literature procedures.^{66,67}

5.5.13.1 Preparation of phenylacetylene-*d*

In the glovebox, THF (60 mL) was transferred to a Schlenk flask (100 mL). The flask was removed from the glovebox and connected to the Schlenk line. Phenylacetylene (4.185 g, 4.5 mL, 41 mmol, 1.0 equiv), directly from the stock bottle, was added against a positive flow of nitrogen. The resulting solution was cooled to -78 °C then a 2.5 M of *n*-butyllithium in hexane (17.2 mL, 43 mmol, 1.05 equiv) was added using a syringe over the course of five minutes. The mixture was stirred at -78 °C for 20 minutes, then allowed to warm to 23 °C and stirred for an additional 20 minutes at this temperature. The solution was cooled to -78 °C and D₂O (4 mL, 222 mmol, 5.4 equiv) was added using a syringe. The resulting mixture was allowed to warm to 23 °C and stirred for 20 minutes. The reaction mixture was quenched with 3.0 M HCl (20 mL), and the resulting mixture was extracted with diethyl ether (3×40 mL). The organic layer was dried with magnesium sulfate then concentrated to ca. 4 mL under reduced pressure. The crude product was purified by chromatography (pentane, $R_f = 0.5$) on silica (2×15 cm). The fractions containing the desired product were concentrated under vacuum to give phenylacetylene-*d* as a colorless oil (1.83 g, 17.8 mmol, 43%). The material was analyzed by NMR spectroscopy then used without further purification. The material was degassed three times via the freeze-pump-thaw method before being brought into the glovebox. ¹H NMR (500 MHz, CDCl₃, δ) 7.50 (dd, $J = 7.9, 1.6$ Hz, 2H), 7.39–7.30 (m, 3H). ¹³C NMR (126 MHz, C₆D₆, δ) 132.28, 128.92, 128.48, 128.45, 122.26, 83.36 (t, $^1J_{C-D} = 7.3$ Hz).

5.5.13.2 Preparation of *cis*- β -deuterostyrene

In the glovebox, zirconocene chloride hydride (Schwartz's reagent, 4.58 g, 17.7 mmol, 1 equiv) was transferred to a Schlenk flask and slurried in benzene (40 mL). Phenylacetylene-*d* was added using a pipette. The vial containing the phenylacetylene-*d* was rinsed with benzene (10 mL) and these washings were transferred to the Schlenk flask. The flask was removed from the glovebox, wrapped in foil, and stirred for 12 h. Volatile material was removed from the resulting orange solution on the Schlenk line and the resulting orange foam was triturated twice with hexanes. The resulting foam was dissolved in DCM (10 mL) and stirred for 10 minutes. H₂SO₄ (0.5 mL) and H₂O (0.5 mL) were combined in a vial and then added to the DCM solution over the course of a minute. The resulting mixture was stirred vigorously for 30 minutes. Pentane (40 mL) was added, inducing the formation of additional white precipitate. The mixture was filtered through a frit (medium porosity, 30 mL) containing diatomaceous earth ($\frac{2}{3}$ full), and the solids were washed with pentane (3×10 mL). The resulting solution was concentrated to ca. 3 mL on the Schlenk line. The resulting oil was purified by chromatography (pentane, $R_f = 0.5$) on silica ($2 \times$

15 cm). The fractions containing the desired product were combined and volatile material was removed to give a clear colorless oil (400 mg). Analysis of this oil by ^1H NMR showed a 1:1 molar ratio of the desired product to pentane. This ratio was deemed acceptable; prolonged drying of the product would lead to a lower yield because of the volatility of the product. ^1H NMR (500 MHz, CDCl_3 , δ) 7.42 (d, $J = 7.3$ Hz, 2H), 7.33 (t, $J = 7.6$ Hz, 2H), 7.27 (d, $J = 6.0$ Hz, 1H), 6.72 (dt, $J = 10.8, 2.4$ Hz, 1H), 5.24 (d, $J = 10.8$ Hz, 1H). ^{13}C NMR (126 MHz, C_6D_6 , δ) 137.56, 136.79, 128.51, 127.78, 126.20, 113.53 (t, $^1J_{\text{C-D}} = 23.8$ Hz). ^2H NMR (77 MHz, C_6D_6 , δ) 5.74 (d, $J = 2.4$ Hz).

5.5.13.3 GCMS analysis of as prepared *cis*- β -deuterostyrene

Commercial samples of styrene and ethylbenzene (MilliporeSigma) were used as received. *cis*- β -deuterostyrene was prepared as described in section 5.5.13.2. Samples were analyzed in DCM. The three traces and their corresponding mass spectra are shown in Fig. 5.41.

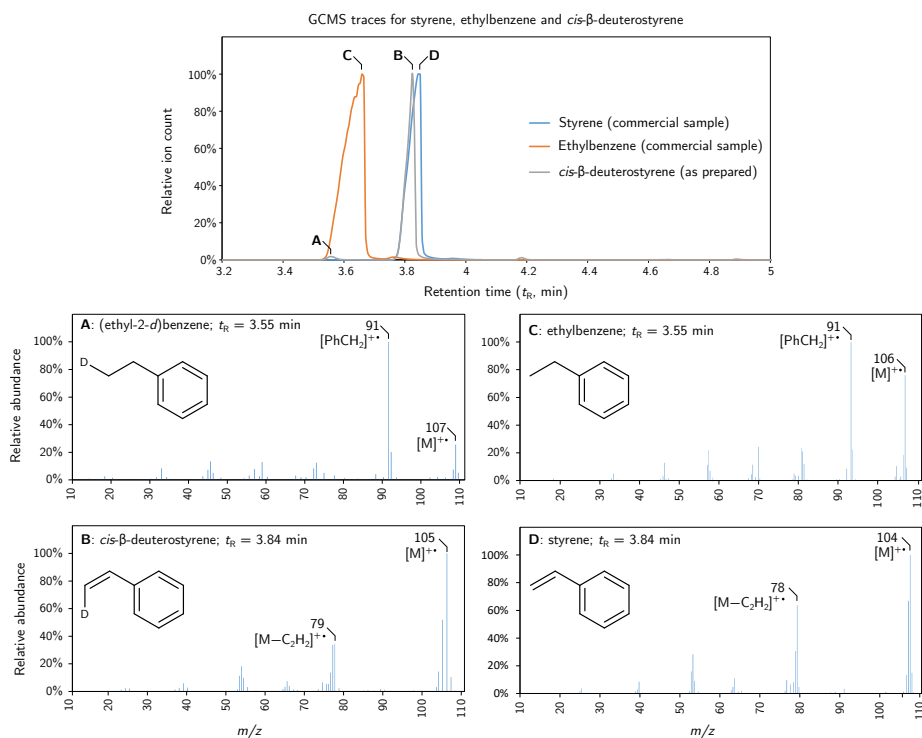


Figure 5.41 GCMS data (traces and mass spectra) for as prepared *cis*- β -deuterostyrene, ethylbenzene and styrene.

5.5.13.4 Use of *cis*- β -deuterostyrene as the substrate in catalysis

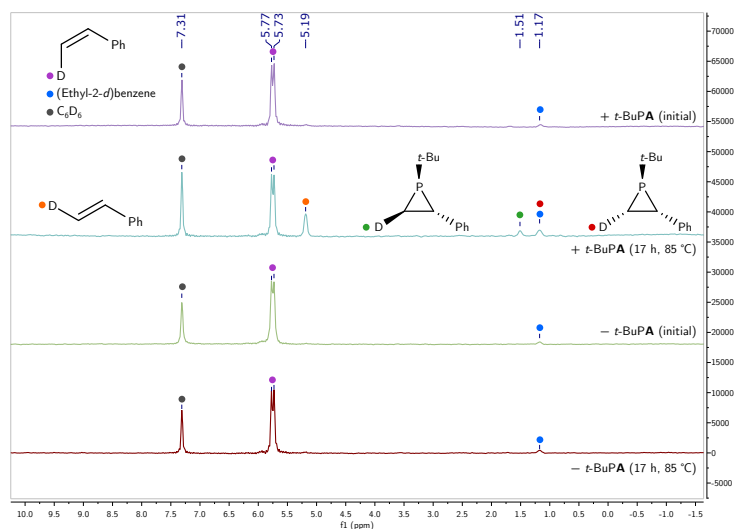


Figure 5.42 Stacked ^2H NMR spectra of the two reaction mixtures (control, $-t\text{-BuPA}$; standard conditions, $+t\text{-BuPA}$) after initial mixing and after 17 h at $85\text{ }^\circ\text{C}$. The spectra were acquired at 61 MHz at $25\text{ }^\circ\text{C}$.

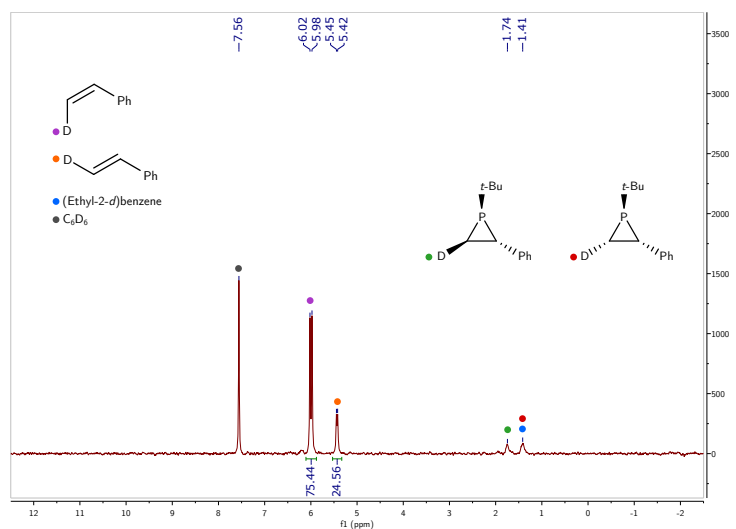


Figure 5.43 ^2H NMR spectrum of the experiment carried out under the standard reaction conditions using *cis*- β -deuterostyrene as the substrate after 17 h at $85\text{ }^\circ\text{C}$. The spectrum is shown in order to highlight the ratio of *cis* to *trans*- β -deuterostyrene in the bulk material that forms under the reaction conditions. The spectra were acquired at 61 MHz at $25\text{ }^\circ\text{C}$.

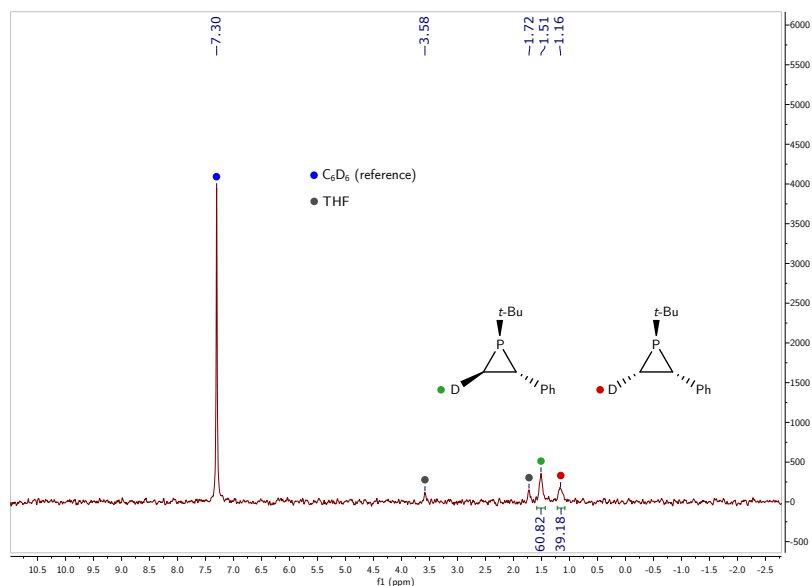


Figure 5.44 ^2H NMR spectrum of the experiment carried out under the standard reaction conditions using *cis*- β -deuterostyrene as the substrate and after removing volatile material (styrene, ethylbenzene) at 23 °C. The spectrum was acquired at 61 MHz at 25 °C.

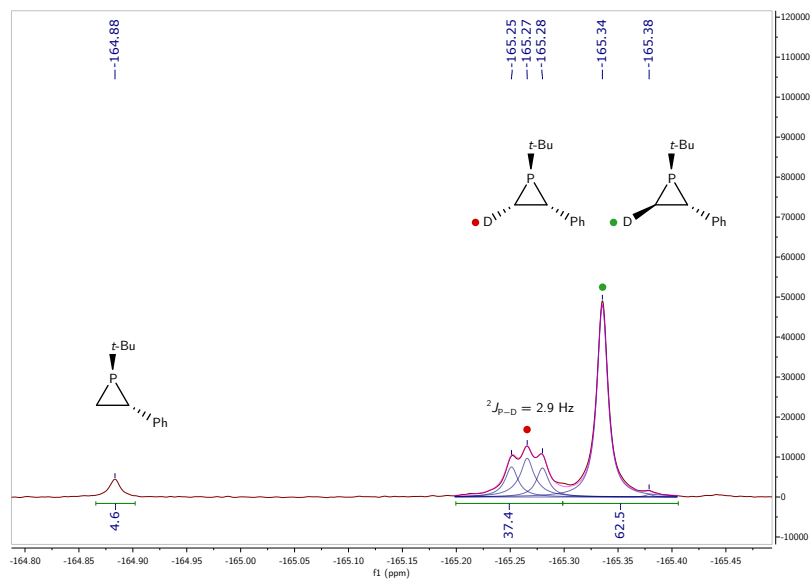


Figure 5.45 ^{31}P NMR spectrum of the experiment carried out under the standard reaction conditions using *cis*- β -deuterostyrene as the substrate and after removing volatile material (styrene, ethylbenzene) at 23 °C. The spectrum was acquired at 202 MHz at 25 °C.

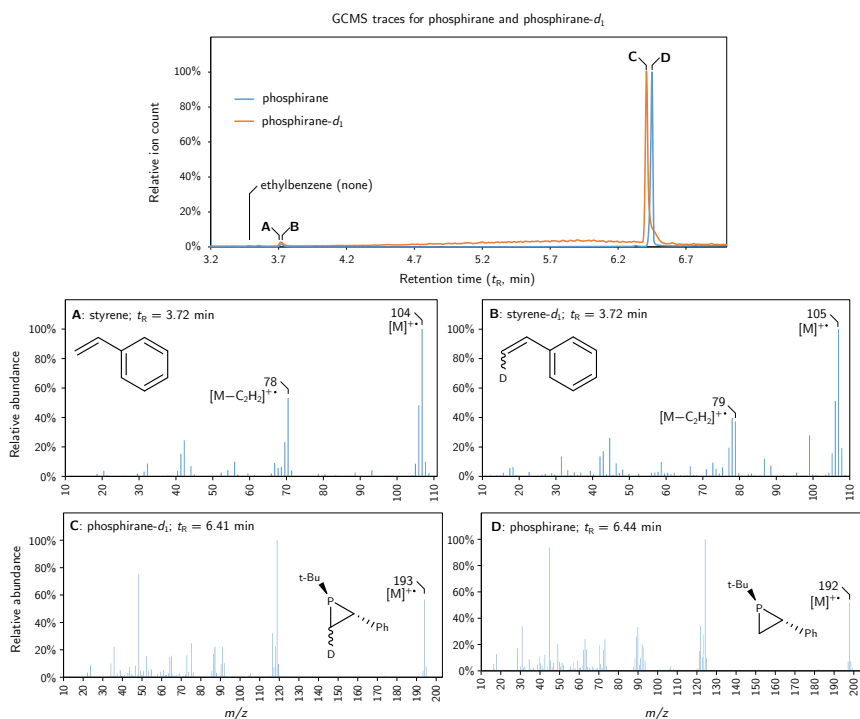


Figure 5.46 GCMS data (traces and mass spectra) for phosphirane and phosphirane-*d*₁.

5.5.14 NMR spectra of a reaction mixture used to prepare 1-*t*-Bu using the catalytic conditions, acquired at 85 °C

In the glovebox, *t*-BuPA (21 mg, 0.0789 mmol, 1 equiv), [Fp(THF)][BF₄] (2.7 mg, 0.00789 mmol, 0.1 equiv), TMAF (1.5 mg, 0.0158 mmol, 0.15 equiv), and styrene (85 mg, 0.789 mmol, 10 equiv) were weighed into a scintillation vial (20 mL) then slurried in THF-*d*₈ (0.3 mL). The resulting slurry was transferred to an NMR tube equipped with a J. Young valve. The vial was washed with additional THF-*d*₈ and the resulting mixture was added to the NMR tube. The sample was placed in the probe of a Bruker 500 MHz spectrometer which was heated from 25 °C to 85 °C over the course of an hour. The sample was removed and the temperature of the probe was measured using an ethylene glycol/DMSO standard (85 °C). The sample was then placed back in the probe and NMR spectra were acquired on the reaction mixture, which had undergone approximately 50% conversion to phosphirane 1-*t*-Bu. The ³¹P{¹H} NMR spectrum (Fig. 5.48) displayed the presence of *t*-BuPA and 1-*t*-Bu as the major species in solution, while [Fp(*t*-BuPA)][BF₄] and **3** were also observed along with at least one other P–F bond-containing species. ¹⁹F NMR (Fig. 5.49) confirmed the presence of **3**. ¹H NMR (Fig. 5.47) showed styrene, *t*-BuPA, 1-*t*-Bu, and anthracene as the major species in solution.

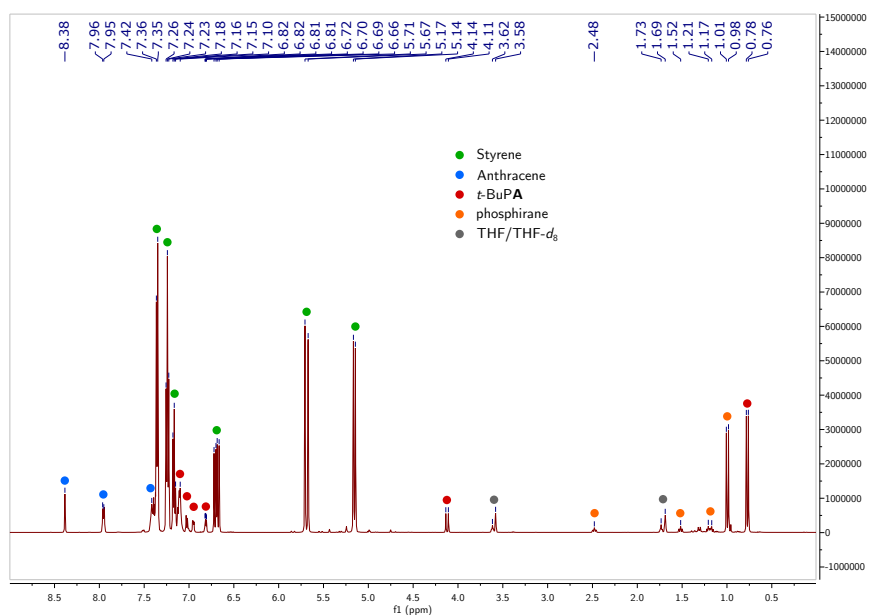


Figure 5.47 ^1H NMR spectrum of the reaction mixture described in Section 5.5.14 in $\text{THF-}d_8$, recorded at 500 MHz at 85 °C.

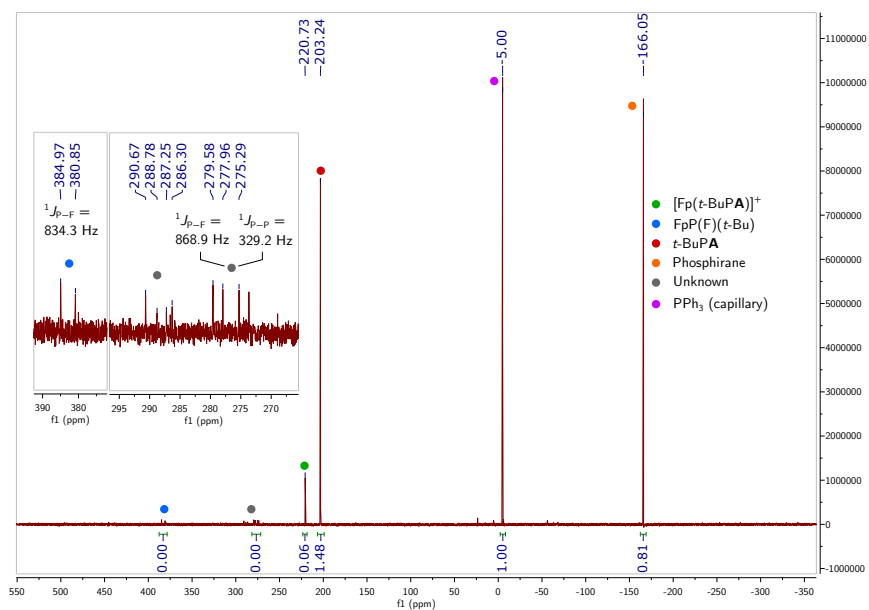


Figure 5.48 $^{31}\text{P}\{^1\text{H}\}$ NMR spectrum of the reaction mixture described in Section 5.5.14 in $\text{THF-}d_8$, recorded at 202 MHz at 85 °C.

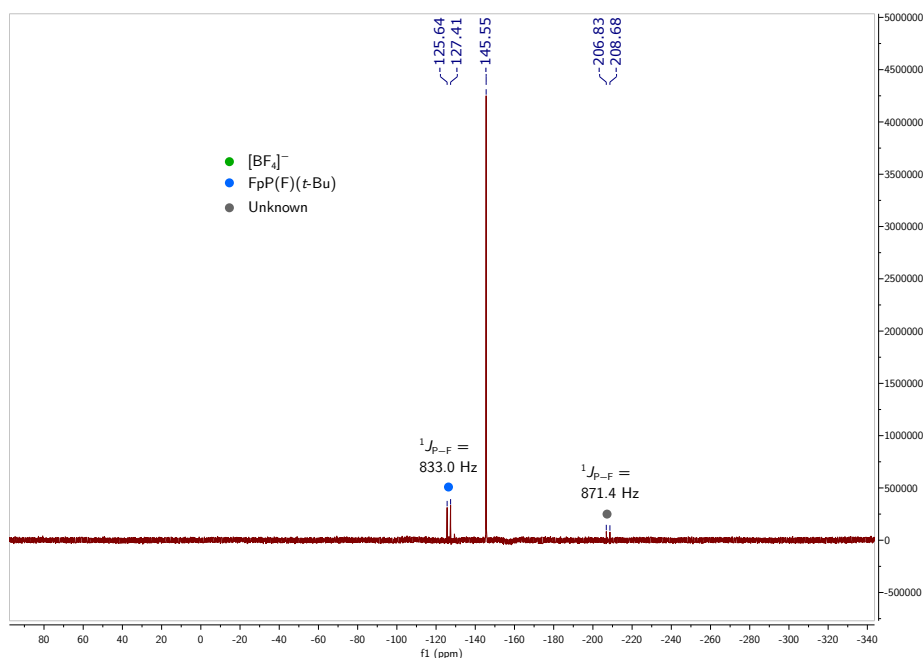


Figure 5.49 ^{19}F NMR spectrum of the reaction mixture described in Section 5.5.14 in $\text{THF-}d_8$, recorded at 471 MHz at 85 °C.

5.5.15 Investigation of cesium fluoride and tris(dimethylamino)sulfonium difluorotrimethylsilicate (TASF) as the sources of fluoride in catalysis

In the glovebox, *t*-BuPA (21 mg, 0.0789 mmol, 1 equiv), $[\text{Fp}(\text{THF})][\text{BF}_4]$ (2.7 mg, 0.00789 mmol, 0.1 equiv) and either cesium fluoride (1.8 mg, 0.012 mmol, 0.15 equiv) or TASF (3.3 mg, 0.012 mmol, 0.15 equiv) as the fluoride source were weighed into a vial (1 mL) and slurried in THF (0.3 mL). To an NMR tube equipped with a J. Young valve was weighed styrene (85 mg, 0.789 mmol, 10 equiv). The two different reaction mixtures were added to two different NMR tubes, each equipped with J. Young valves. The vials were each washed with THF (0.3 mL) and the washings were transferred to the appropriate NMR tube. To each NMR tube was added a capillary containing a C_6D_6 solution of PPh_3 . The samples were analyzed by ^{31}P NMR spectroscopy after 20 min at 23 °C and then after 24 h at 85 °C. Phosphirane **1**-*t*-Bu was observed in both cases, with spectroscopic yields of 72% and 44% for TASF and cesium fluoride, respectively, as determined by integration PPh_3 .

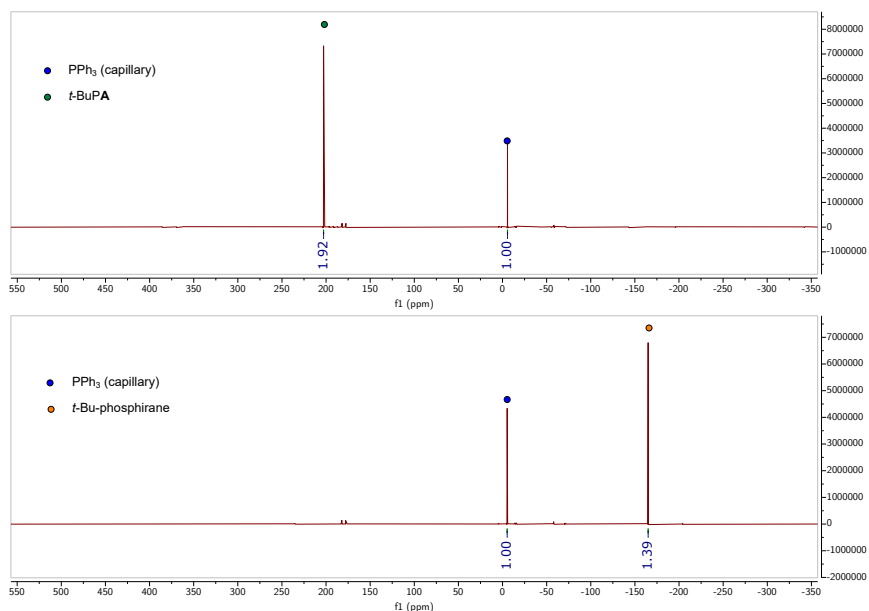


Figure 5.50 $^{31}\text{P}\{^1\text{H}\}$ NMR spectrum of the reaction mixture described in Section 5.5.15 using TASF as the source of fluoride in THF, recorded at 202 MHz at 25 °C.

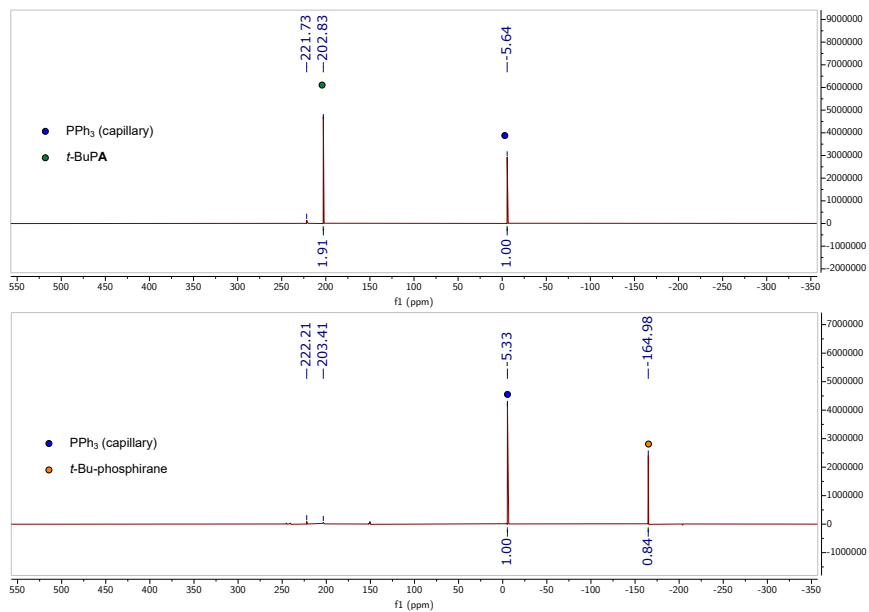


Figure 5.51 $^{31}\text{P}\{^1\text{H}\}$ NMR spectrum of the reaction mixture described in Section 5.5.15 using CsF as the source of fluoride in THF, recorded at 202 MHz at 25 °C.

5.5.16 X-ray crystallography

Single crystals suitable for X-ray diffraction were transferred from the glovebox under Paratone oil onto a microscope slide. A crystal was selected under a microscope and mounted in hydrocarbon oil on a nylon loop. Low-temperature (100 K) data were collected on a Bruker-AXS X8 Kappa Duo diffractometer coupled to a Smart Apex2 CCD detector with Mo $K\alpha$ radiation ($\lambda = 0.71073 \text{ \AA}$) with ϕ - and ω -scans. A semi-empirical absorption correction was applied to the diffraction data using SADABS^{68,69} unless otherwise stated. The structure was solved by direct methods using SHELXT^{70,71} and refined against F^2 on all data by full-matrix least squares with ShelXle.⁷² All non-hydrogen atoms were refined anisotropically. All hydrogen atoms were included in the model at geometrically calculated positions and refined using a riding model. The isotropic displacement parameters of all hydrogen atoms were fixed to 1.2 times the U_{eq} value of the atoms they are linked to (1.5 times for methyl groups).

5.5.16.1 X-ray structure of [Fp(*t*-BuPA)][BF₄]

[Fp(*t*-BuPA)][BF₄] was dissolved in DCM to give a yellow solution which was filtered through microfiber filter paper in a Pasteur pipette. The solution was carefully layered with THF and the mixture placed in the glovebox freezer at $-35 \text{ }^\circ\text{C}$ to yield orange needles. The crystal displayed non-merohedral twinning which was accounted for using methods in CELL_NOW⁷³ and TWINABS.⁷⁴ Refinement against the HKLF5 file gave a higher R_1 than the HKLF4 file, so the HKLF4 file was used for the final refinement. There were two molecules of THF in the asymmetric unit which were heavily disordered. Each was modeled as two separate THF molecules, using DFIX and SAME restraints where necessary. The DFIX commands could be removed at the end of the refinement to give a stable solution. The restraints SIMU and RIGU were applied to the entire structure. The high value of R_{int} (0.389), generating an A level alert in the checkCIF report, was attributed to the extremely poor data quality; non-merohedral twinning and severe solvent disorder. In general, the statistical data for this structure were poor (R_1 , wR_2 , largest diff. peak and hole).

CSD identification code	1936231
Reciprocal net code	P8_19032
Empirical formula	$C_{33}H_{40}BF_4FeO_4P$
Formula weight	674.28 g/mol
Color / morphology	orange / needle
Temperature	100(2) K
Wavelength	0.71073 Å
Crystal system	Triclinic
Space group	$P\bar{1}$
Unit cell dimensions	$a = 9.9636(10)$ Å $\alpha = 80.831(4)^\circ$ $b = 12.7003(13)$ Å $\beta = 69.746(4)^\circ$ $c = 13.9821(15)$ Å $\gamma = 70.594(3)^\circ$
Volume	1563.6(3) Å ³
Z	2
Density (calculated)	1.432 g/cm ³
Absorption coefficient	0.594 mm ⁻¹
$F(000)$	704
Crystal size	0.257 × 0.133 × 0.102 mm ³
Theta ranges for data collection	1.554 to 28.036°
Index ranges	-12 ≤ h ≤ 13, -16 ≤ k ≤ 16, 0 ≤ l ≤ 18
Reflections collected	7495
Independent reflections	7495 [$R_{int} = 0.3888$]
Completeness to $\theta = 25.242^\circ$	99.9%
Absorption correction	None
Max. and min. transmission	0.745619 and 0.387299
Refinement method	Full-matrix least-squares on F^2
Data / restraints / parameters	7495 / 1032 / 492
Goodness-of-fit on F^2	1.026
Final R indices [$I > 2\sigma(I)$]	$R_1 = 0.1411$, $wR_2 = 0.3506$
R indices (all data)	$R_1 = 0.1760$, $wR_2 = 0.3753$
Extinction coefficient	n/a
Largest diff. peak and hole	1.312 and -1.287 e·Å ⁻³

Table 5.4 X-ray crystallographic information for [Fp(*t*-BuPA)][BF₄].

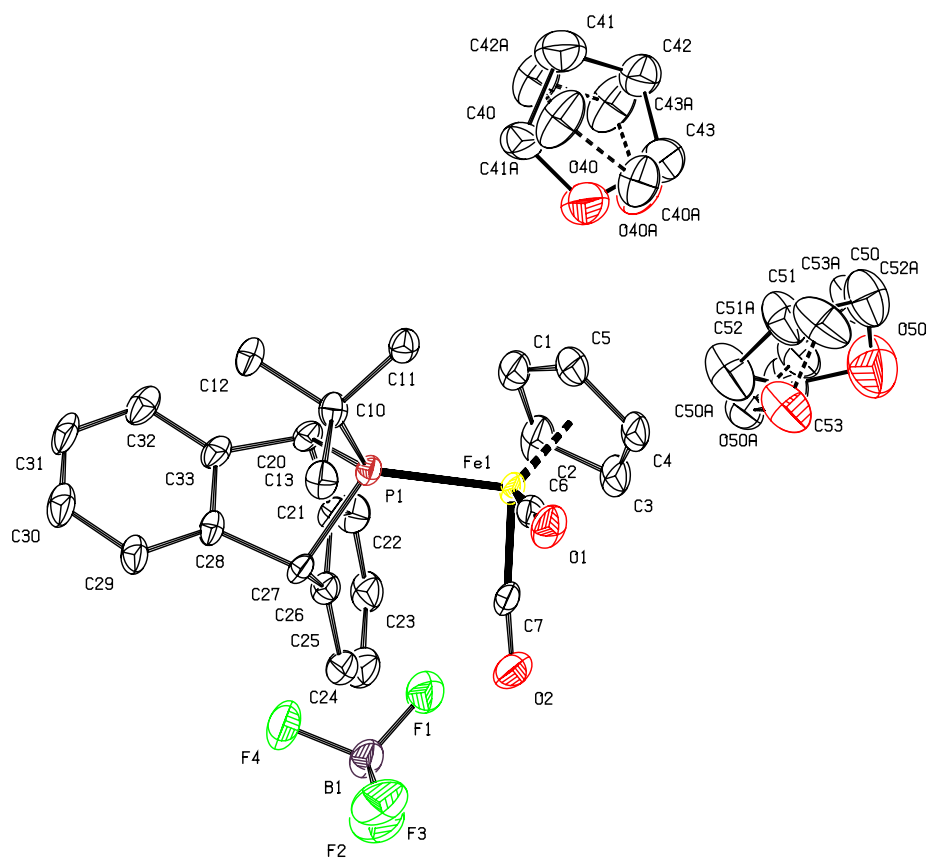


Figure 5.52 Molecular structure of $[\text{Fp}(t\text{-BuPA})][\text{BF}_4] \cdot 2\text{THF}$ with thermal ellipsoids shown at the 50% probability level and hydrogen atoms omitted for clarity.

5.5.16.2 X-ray structure of [Fp(1-*t*-Bu)][BF₄]

[Fp(1-*t*-Bu)][BF₄] was dissolved in DCM to give a yellow solution which was filtered through microfiber filter paper in a Pasteur pipette. The solution was carefully layered with THF and the mixture placed in the glovebox freezer at $-35\text{ }^{\circ}\text{C}$ to yield orange plates. The structure was first refined isotropically, then anisotropically. A twin law was determined using the TwinRotMap procedure in PLATON⁷⁵ and introduced using the TWIN command. Positions of hydrogen atoms were generated using the HFIX command. The weighting scheme was adjusted and the model considered complete. The high value of R_{int} (0.305), generating an A level alert in the checkCIF report, was attributed to the extremely high redundancy of the data (66.3). It has been shown that extremely high redundancy can lead to artificially high values of R_{int} and that in this case the value of $R\sigma$ is the preferred metric.⁷⁶ The value of $R\sigma$ was 0.0416, in line with the good to excellent remaining metrics (R_1 , wR_2).

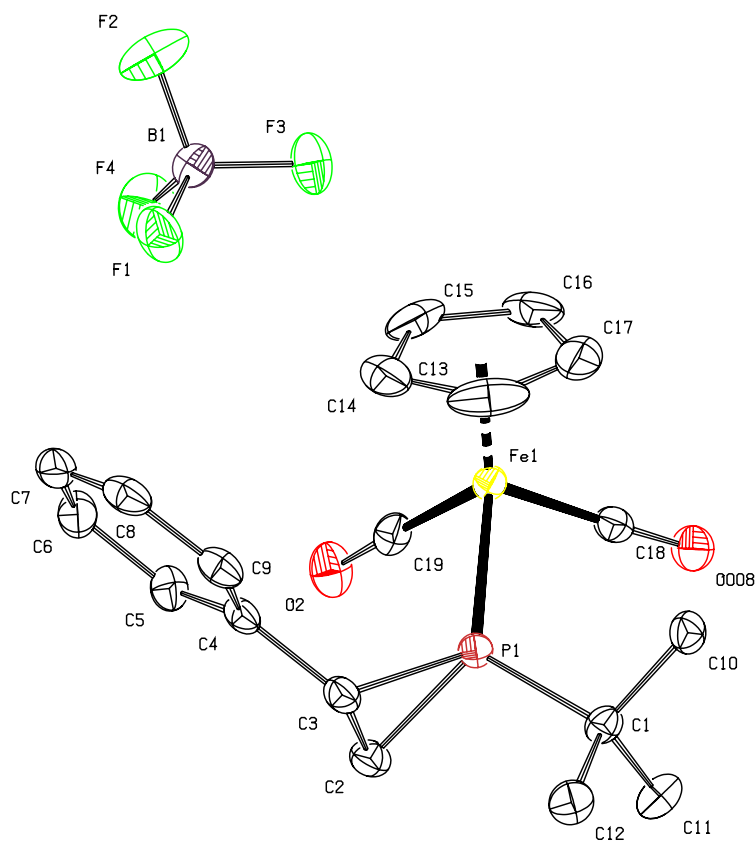


Figure 5.53 Molecular structure of [Fp(1-*t*-Bu)][BF₄] with thermal ellipsoids shown at the 50% probability level and hydrogen atoms omitted for clarity.

CSD identification code	1936232
Reciprocal net code	P8_19033
Empirical formula	C ₁₉ H ₂₂ BF ₄ FeO ₂ P
Formula weight	455.99 g/mol
Color / morphology	orange / plate
Temperature	100(2) K
Wavelength	0.71073 Å
Crystal system	Orthorhombic
Space group	<i>Pbca</i>
Unit cell dimensions	$a = 13.8260(9) \text{ \AA}$ $\alpha = 90^\circ$ $b = 16.6549(9) \text{ \AA}$ $\beta = 90^\circ$ $c = 17.2897(11) \text{ \AA}$ $\gamma = 90^\circ$
Volume	3981.3(4) Å ³
<i>Z</i>	8
Density (calculated)	1.522 g/cm ³
Absorption coefficient	0.886 mm ⁻¹
<i>F</i> (000)	1872
Crystal size	0.102 × 0.086 × 0.078 mm ³
Theta ranges for data collection	2.248 to 27.954°
Index ranges	-18 ≤ <i>h</i> ≤ 18, -21 ≤ <i>k</i> ≤ 21, -22 ≤ <i>l</i> ≤ 22
Reflections collected	316726
Independent reflections	4780 [<i>R</i> _{int} = 0.3049]
Completeness to $\theta = 25.242^\circ$	100.0%
Absorption correction	None
Max. and min. transmission	0.7407 and 0.6990
Refinement method	Full-matrix least-squares on <i>F</i> ²
Data / restraints / parameters	4780 / 0 / 256
Goodness-of-fit on <i>F</i> ²	1.066
Final <i>R</i> indices [<i>I</i> > 2σ(<i>I</i>)]	<i>R</i> ₁ = 0.0378, <i>wR</i> ₂ = 0.0966
<i>R</i> indices (all data)	<i>R</i> ₁ = 0.0511, <i>wR</i> ₂ = 0.1033
Extinction coefficient	n/a
Largest diff. peak and hole	0.486 and -0.495 e·Å ⁻³

Table 5.5 X-ray crystallographic information for [Fp(1-*t*-Bu)][BF₄].

5.5.17 NMR chemical shift calculations

DFT calculations were performed using ORCA 4.1.0. Geometry optimizations were performed at the ω -B97X-D3/def2-TZVP level of theory in conjunction with a CPCM solvation model. The input line is provided below and the coordinates of the optimized geometry of **3** are given in Table 5.7.

```
! wB97X-D3 RIJCOSX def2-TZVP def2/J TightSCF Grid4 GridX4 FinalGrid5
Opt NumFreq CPCM(THF)
```

NMR chemical shift calculations were performed using the PBE0 functional, the dispersion corrections of Grimme, and the pcSseg-3 basis set, optimized for NMR property predictions. The input file is provided below:

```
! PBE0 D3 RIJCOSX pcSseg-3 def2/J VeryTightSCF Grid7 NoFinalGrid GridX7
NoFinalGridX CPCM(THF)
!MoRead

%moinp "filename.gbwn"

*xyz 0 1
A   x y z
...
*

%eprnmr
Ori = GIAO
giao_2el=giao_2el_rijcosx
Nuclei = all P { shift }
end
```

Species	Nuclei	δ_{mol}	δ_{ref}	σ_{mol}	σ_{ref}
$[\text{BF}_4]^-$	^{19}F		-151.7		350.5
<i>t</i> -BuPA	^{31}P		+204.6		+98.4
3	^{19}F	-206.3		406.8	
3	^{31}P	+391.2		-88.2	

Table 5.6 Experimental, calculated, and predicted shieldings and chemical shifts of $[\text{BF}_4]^-$, *t*-BuPA, and **3**.

Table 5.7 Optimized coordinates of **3**

Atom	x	y	z
Fe	-0.293389164	6.186399807	5.069310859
C	0.389980044	5.01459132	6.194934213
C	-2.2274378	6.628024571	4.371195878
C	-1.055628219	8.034756989	5.751019902
C	-1.569909163	6.979346385	6.536283283
C	0.021651433	5.212579267	3.638440853
C	-2.303559399	6.103943115	5.680277019
C	-1.444495356	7.816040542	4.404500697
O	0.779408705	4.268846573	6.961959638
H	-2.667462101	6.188121761	3.488696634
H	-1.200205928	8.441419644	3.560316944
H	-2.815784145	5.202894707	5.978831003
H	-0.448113392	8.850566826	6.111063224
H	-1.433999308	6.858890265	7.600147364
O	0.14284123	4.54905046	2.718874989
C	3.165861821	6.281984256	4.314815899
P	1.713699096	7.272434571	4.963148422
C	4.425354268	7.020330315	4.794287296
C	3.109657229	6.375970041	2.784891209
C	3.25321313	4.824299137	4.762209872
H	2.423634982	4.221968905	4.38775445
H	3.270209091	4.745460706	5.850829313
H	4.176659164	4.37467748	4.383321794
H	4.400563733	8.077447213	4.51759744
H	5.309272302	6.571197385	4.331371516
H	4.540520146	6.954463651	5.876960277
H	3.079463055	7.416333058	2.451528673
H	2.247861533	5.861017771	2.360455404
H	4.005914265	5.914954094	2.35966862
F	2.145499749	7.283360184	6.562097314

Calculated chemical absolute shieldings were converted to predicted experimental shifts by calibration to reference compounds $[\text{BF}_4]^-$ and *t*-BuPA for ^{19}F and ^{31}P nuclei, respectively. The equation used to convert the calculated shieldings to predicted chemical shifts was:

$$\delta_{mol} = \sigma_{ref} + \delta_{ref} - \sigma_{mol} \quad (5.1)$$

The values of these variables, and the resulting predicted chemical shifts are provided in Table 5.6

References

- [1] (a) Lebel, H.; Marcoux, J.-F.; Molinaro, C.; Charette, A. B. *Chem. Rev.* **2003**, *103*, 977–1050; (b) Müller, P.; Fruit, C. *Chem. Rev.* **2003**, *103*, 2905–2920; (c) Lane, B. S.; Burgess, K. *Chem. Rev.* **2003**, *103*, 2457–2474.
- [2] (a) Kamer, P. C. J., van Leeuwen, P. W. N. M., Eds. “Highly Strained Organophosphorus Compound” in *Phosphorus(III) Ligands in Homogeneous Catalysis: Design and Synthesis*; John Wiley & Sons, Ltd: Chichester, UK, 2012; (b) Liedtke, J.; Loss, S.; Widauer, C.; Grützmacher, H. *Tetrahedron* **2000**, *56*, 143–156; (c) Grützmacher, H.; Liedtke, J.; Frasca, G.; Läng, F.; Pé, N. *Phosphorus, Sulfur Silicon Relat. Elem.* **2002**, *177*, 1771–1774; (d) Liedtke, J.; Rüegger, H.; Loss, S.; Grützmacher, H. *Angew. Chem., Int. Ed.* **2000**, *39*, 2478–2481.
- [3] (a) Kobayashi, S.; Kadokawa, J.-I. *Macromol. Rapid Commun.* **1994**, *15*, 567–571; (b) Kadokawa, J.-I.; Kobayashi, S. *Phosphorus, Sulfur Silicon Relat. Elem.* **2002**, *177*, 1387–1390.
- [4] Wit, J. B. M.; de Jong, G. B.; Schakel, M.; Lutz, M.; Ehlers, A. W.; Slotweg, J. C.; Lammertsma, K. *Organometallics* **2016**, *35*, 1170–1176.
- [5] Marinetti, A.; Mathey, F. *Organometallics* **1984**, *3*, 456–461.
- [6] Breen, T. L.; Stephan, D. W. *J. Am. Chem. Soc.* **1995**, *117*, 11914–11921.
- [7] Waterman, R.; Hillhouse, G. L. *J. Am. Chem. Soc.* **2003**, *125*, 13350–13351.
- [8] Vaheesar, K.; Kuntz, C. M.; Sterenberg, B. T. *J. Organomet. Chem.* **2013**, *745-746*, 347–355.
- [9] Goumans, T. P. M.; Ehlers, A. W.; Lammertsma, K. *J. Organomet. Chem.* **2005**, *690*, 5517–5524.
- [10] van Assema, S. G. A.; de Kanter, F. J. J.; Schakel, M.; Lammertsma, K. *Organometallics* **2006**, *25*, 5286–5291.
- [11] Amme, M. J.; Kazi, A. B.; Cundari, T. R. *Int. J. Quantum Chem.* **2010**, *110*, 1702–1711.
- [12] Abbenseth, J.; Delony, D.; Neben, M. C.; Würtele, C.; deBruin, B.; Schneider, S. *Angew. Chem., Int. Ed.* **2019**, *58*, 6338–6341.
- [13] Pagano, J. K.; Ackley, B. J.; Waterman, R. *Chem. - Eur. J.* **2018**, *24*, 2554–2557.
- [14] Pal, K.; Hemming, O. B.; Day, B. M.; Pugh, T.; Evans, D. J.; Layfield, R. A. *Angew. Chem., Int. Ed.* **2016**, *55*, 1690–1693.
- [15] Freeman, P. K.; Hutchinson, L. L. *J. Org. Chem.* **1983**, *48*, 879–881.
- [16] Velian, A.; Cummins, C. C. *J. Am. Chem. Soc.* **2012**, *134*, 13978–13981.
- [17] Transue, W. J.; Velian, A.; Nava, M.; García-Iriepa, C.; Temprado, M.; Cummins, C. C. *J. Am. Chem. Soc.* **2017**, *139*, 10822–10831.
- [18] Transue, W. J.; Yang, J.; Nava, M.; Sergeev, I. V.; Barnum, T. J.; McCarthy, M. C.; Cummins, C. C. *J. Am. Chem. Soc.* **2018**, *140*, 17985–17991.
- [19] Szkop, K. M.; Geeson, M. B.; Stephan, D. W.; Cummins, C. *Chem. Sci.* **2019**, *10*, 3627–3631.

- [20] Lennon, P.; Madhavarao, M.; Rosan, A.; Rosenblum, M. *J. Organomet. Chem.* **1976**, *108*, 93–109.
- [21] Knoth, W. H. *Inorg. Chem.* **1975**, *14*, 1566–1572.
- [22] Bai, W.; Chen, J.; Jia, G. “4.10 Reactions of Nucleophiles with Coordinated Alkynes, Alkenes, and Allenes” in *Comprehensive Organic Synthesis II*; Elsevier: Amsterdam, Netherlands, 2014; pp 580–647.
- [23] Giering, W. P.; Rosenblum, M.; Tancrede, J. *J. Am. Chem. Soc.* **1972**, *94*, 7170–7172.
- [24] Muldoon, J. A.; Varga, B. R.; Deegan, M. M.; Chapp, T. W.; Eördögh, A. M.; Hughes, R. P.; Glueck, D. S.; Moore, C. E.; Rheingold, A. L. *Angew. Chem., Int. Ed.* **2018**, *57*, 5047–5051.
- [25] Marinetti, A.; Mathey, F.; Ricard, L. *Organometallics* **1993**, *12*, 1207–1212.
- [26] Li, X.; Robinson, K. D.; Gaspar, P. P. *J. Org. Chem.* **1996**, *61*, 7702–7710.
- [27] Baudler, M.; Germeshausen, J. *Chem. Ber.* **1985**, *118*, 4285–4287.
- [28] Ficks, A.; Martinez-Botella, I.; Stewart, B.; Harrington, R. W.; Clegg, W.; Higham, L. J. *Chem. Commun.* **2011**, *47*, 8274.
- [29] (a) Nesterov, V.; Schnakenburg, G.; Espinosa, A.; Streubel, R. *Inorg. Chem.* **2012**, *51*, 12343–12349; (b) Nesterov, V.; Özbolat Schön, A.; Schnakenburg, G.; Shi, L.; Cangönül, A.; van Gastel, M.; Neese, F.; Streubel, R. *Chem. Asian J.* **2012**, *7*, 1708–1712; (c) Fassbender, J.; Schnakenburg, G.; Ferao, A. E.; Streubel, R. *Dalton Trans.* **2018**, *47*, 9347–9354; (d) Schmer, A.; Volk, N.; Espinosa Ferao, A.; Streubel, R. *Dalton Trans.* **2019**, *48*, 339–345.
- [30] Malish, W.; Angerer, W.; Cowley, A. H.; Norman, N. C. *J. Chem. Soc., Chem. Commun.* **1985**, *0*, 1811–1812.
- [31] Mullins, R. J.; Vedernikov, A.; Viswanathan, R. *J. Chem. Educ.* **2004**, *81*, 1357.
- [32] Hung, J. T.; Lammertsma, K. *Organometallics* **1992**, *11*, 4365–4366.
- [33] Ashby, M. T.; Enemark, J. H. *Organometallics* **1987**, *6*, 1323–1327.
- [34] Qu, Z.-W.; Zhu, H.; Grimme, S. *ChemistryOpen* **2019**, *8*, 807–810.
- [35] Mézailles, N.; Fanwick, P. E.; Kubiak, C. P. *Organometallics* **1997**, *16*, 1526–1530.
- [36] Dück, K.; Rawe, B. W.; Scott, M. R.; Gates, D. P. *Angew. Chem., Int. Ed.* **2017**, *56*, 9507–9511.
- [37] Priegert, A. M.; Rawe, B. W.; Serin, S. C.; Gates, D. P. *Chem. Soc. Rev.* **2016**, *45*, 922–953.
- [38] Tilstet, M.; Fjeldahl, I.; Hamon, J.-R.; Hamon, P.; Toupet, L.; Saillard, J.-Y.; Costuas, K.; Haynes, A. *J. Am. Chem. Soc.* **2001**, *123*, 9984–10000.
- [39] Ye, B.; Cramer, N. *Science* **2012**, *338*, 504–506.
- [40] Newton, C. G.; Kossler, D.; Cramer, N. *J. Am. Chem. Soc.* **2016**, *138*, 3935–3941.
- [41] Wang, S.-G.; Park, S. H.; Cramer, N. *Angew. Chem. Int. Ed.* **2018**, *57*, 5459–5462.
- [42] Angelici, R. J., Ed. *Inorganic Syntheses: Reagents for Transition Metal Complex and Organometallic Syntheses*; Inorganic Syntheses; John Wiley & Sons, Inc.: Hoboken, NJ, USA, 1990.
- [43] Farina, V.; Krishnan, B. *J. Am. Chem. Soc.* **1991**, *113*, 9585–9595.

- [44] Knights, A. W.; Chitnis, S. S.; Manners, I. *Chem. Sci.* **2019**, *10*, 7281–7289.
- [45] Vanderark, L. A.; Clark, T. J.; Rivard, E.; Manners, I.; Slootweg, J. C.; Lamertsmas, K. *Chem. Commun.* **2006**, 3332–3333.
- [46] Pangborn, A. B.; Giardello, M. A.; Grubbs, R. H.; Rosen, R. K.; Timmers, F. J. *Organometallics* **1996**, *15*, 1518–1520.
- [47] Williams, D. B. G.; Lawton, M. *J. Org. Chem.* **2010**, *75*, 8351–8354.
- [48] Plotkin, J. S.; Shore, S. G. *Inorg. Chem.* **1981**, *20*, 284–285.
- [49] King, R. B.; Stone, F. G. A.; Jolly, W. L.; Austin, G.; Covey, W.; Rabinovich, D.; Steinberg, H.; Tsugawa, R. In “*Cyclopentadienyl Metal Carbonyls and Some Derivatives*” in *Inorganic Syntheses*; Kleinberg, J., Ed.; John Wiley & Sons, Inc.: Hoboken, NJ, USA, 2007; pp 99–115.
- [50] Reger, D. L.; Coleman, C. *J. Organomet. Chem.* **1977**, *131*, 153–162.
- [51] (a) Kuhlmann, E. J.; Alexander, J. J. *Inorg. Chim. Acta* **1979**, *34*, 197–209; (b) Malisch, W.; Panster, P. *Chem. Ber.* **1975**, *108*, 2554–2573; (c) Malisch, W.; Panster, P. *J. Organomet. Chem.* **1974**, *64*, C5–C9; (d) Lappert, M. F.; Power, P. P. *J. Chem. Soc., Dalton Trans.* **1985**, 51–57, note: This report references “R. B. King, “Organometallic Synthesis,” eds. J. J. Eisch and R. B. King, Academic Press, New York, 1965, vol. 1, p. 175–176.” as having a preparative procedure for [Fp]F, although we were unable to locate it within this book.
- [52] Anciaux, A. J.; Hubert, A. J.; Noels, A. F.; Petinot, N.; Teyssie, P. *J. Org. Chem.* **1980**, *45*, 695–702.
- [53] Liang, J.-L.; Yuan, S.-X.; Chan, P. W. H.; Che, C.-M. *Org. Lett.* **2002**, *4*, 4507–4510.
- [54] Salomon, R. G.; Kochi, J. K. *J. Am. Chem. Soc.* **1973**, *95*, 3300–3310.
- [55] Evans, D. A.; Bilodeau, M. T.; Faul, M. M. *J. Am. Chem. Soc.* **1994**, *116*, 2742–2753.
- [56] Huang, L.; Chen, Y.; Gao, G.-Y.; Zhang, X. P. *J. Org. Chem.* **2003**, *68*, 8179–8184.
- [57] Gao, G.-Y.; Harden, J. D.; Zhang, X. P. *Org. Lett.* **2005**, *7*, 3191–3193.
- [58] Hamaker, C. G.; Mirafzal, G. A.; Woo, L. K. *Organometallics* **2001**, *20*, 5171–5176.
- [59] Vyas, R.; Gao, G.-Y.; Harden, J. D.; Zhang, X. P. *Org. Lett.* **2004**, *6*, 1907–1910.
- [60] Galardon, E.; Maux, P. L.; Simonneaux, G. *Chem. Commun.* **1997**, *0*, 927–928.
- [61] Leung, S. K.-Y.; Tsui, W.-M.; Huang, J.-S.; Che, C.-M.; Liang, J.-L.; Zhu, N. *J. Am. Chem. Soc.* **2005**, *127*, 16629–16640.
- [62] Zhang, J.-L.; Hong Chan, P. W.; Che, C.-M. *Tetrahedron Lett.* **2003**, *44*, 8733–8737.
- [63] Demonceau, A.; Dias, E. A.; Lemoine, C. A.; Stumpf, A. W.; Noels, A. F.; Pietraszuk, C.; Gulinski, J.; Marciniak, B. *Tetrahedron Lett.* **1995**, *36*, 3519–3522.
- [64] Demonceau, A.; Lemoine, C. A.; Noels, A. F.; Chizhevsky, I. T.; Sorokin, P. V. *Tetrahedron Lett.* **1995**, *36*, 8419–8422.
- [65] Dombek, B. D.; Angelici, R. J. *Inorg. Chim. Acta* **1973**, *7*, 345–347.
- [66] Peng, T. S.; Gladysz, J. A. *J. Am. Chem. Soc.* **1992**, *114*, 4174–4181.
- [67] Kohler, D. G.; Gockel, S. N.; Kennemur, J. L.; Waller, P. J.; Hull, K. L. *Nat. Chem.* **2018**, *10*, 333.
- [68] Bruker (2001). SADABS. Bruker AXS Inc., Madison, Wisconsin, USA.

- [69] Krause, L.; Herbst-Irmer, R.; Sheldrick, G. M.; Stalke, D. *J. Appl. Crystallogr.* **2015**, *48*, 3–10.
- [70] Sheldrick, G. M. *Acta Crystallogr., Sect. A: Found. Adv.* **2015**, *71*, 3–8.
- [71] Sheldrick, G. M. *Acta Crystallogr., Sect. A: Found. Crystallogr.* **2008**, *64*, 112–122.
- [72] Hübschle, C. B.; Sheldrick, G. M.; Dittrich, B. *J. Appl. Crystallogr.* **2011**, *44*, 1281–1284.
- [73] Bruker (2001). TWINABS. Bruker AXS Inc., Madison, Wisconsin, USA.
- [74] Sheldrick, G. M. (2008). CELL_NOW. Version 2008/4. Georg-August-Universität Göttingen, Göttingen, Germany.
- [75] Spek, A. L. (2009). *Acta Cryst.* D65, 148-155.
- [76] Diederichs, K.; Karplus, P. A. *Nat. Struct. Biol.* **1997**, *4*, 269.

Appendices

Appendix A

Coordination Chemistry of RPA Compounds

Contents

A.1 Introduction	287
A.2 Results and discussion	288
A.3 Conclusions and Future Directions	297
A.4 Experimental methods	298
Bibliography	321

A.1 Introduction

This appendix loosely follows the journey that culminated in the results presented in Chapter 5 on catalytic phosphinidene transfer for the synthesis of phosphiranes. The story is best told by a seemingly unrelated series of new compounds (Chart A.1) that feature bonds between elements of the d-block and phosphorus.

Prior to any interest in performing catalytic phosphinidene transfer, an initial goal of this project was to prepare a transition metal complex that contained phosphorus mononitride (PN) as a ligand. Phosphorus mononitride is isoelectronic with N_2 and P_2 , both of which have featured frequently as ligands in transition metal chemistry.^{1,2} Given the large number of heteronuclear diatomic molecules that have been stabilized within the coordination sphere of transition metals,³ it is surprising that no such complex yet exists for PN. A synthesis was planned that relies on elimination of trimethylsilyl chloride as a driving force and closely resembles the synthesis of P_2 complex (Scheme A.1).²

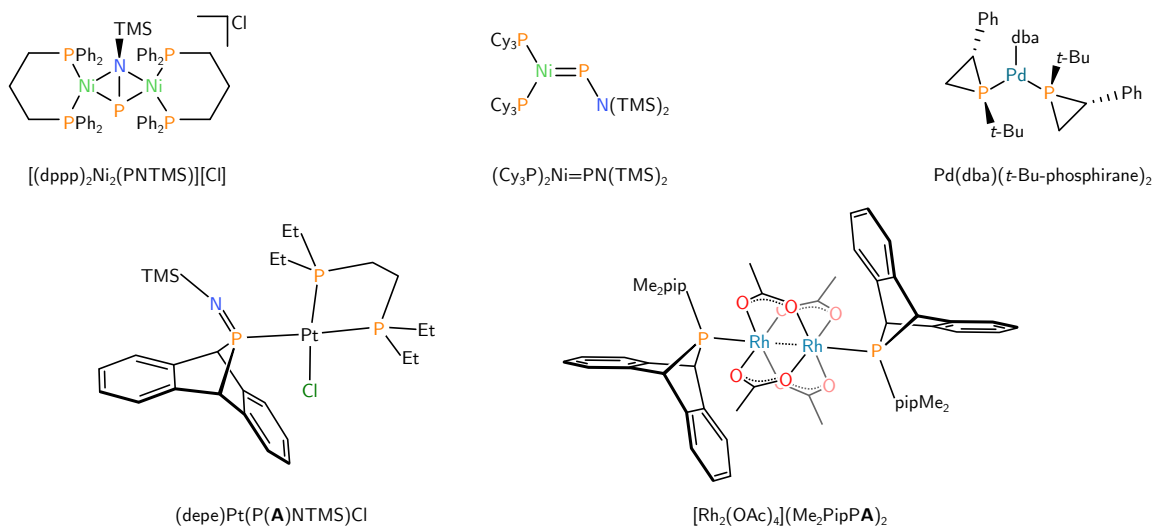


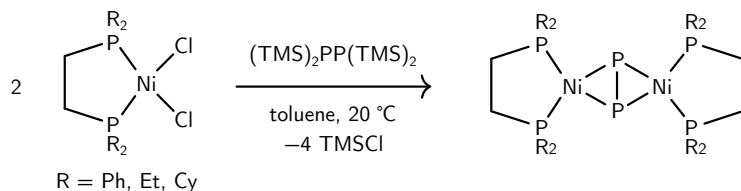
Chart A.1 Molecular structures of the compounds described in this Appendix.

A.2 Results and discussion

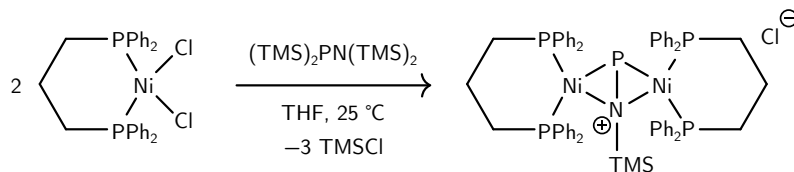
Treatment of a slurry of $(\text{dppp})\text{NiCl}_2$ ($\text{dppp} = 1,3\text{-bis}(\text{diphenylphosphino})\text{propane}$) in tetrahydrofuran (THF) with $(\text{TMS})_2\text{NP}(\text{TMS})_2$ gave rise to two new species, as assayed by ^{31}P spectroscopy (Fig A.1). One was identified as $(\text{dppp})_2\text{Ni}$, confirming the ability of phosphine $(\text{TMS})_2\text{NP}(\text{TMS})_2$ to reduce nickel(II) to nickel(0). The second species was observed by NMR spectroscopy as having two signals, one being a doublet resonance centered at 3.9 ppm ($J_{\text{P-P}} = 38.4$ Hz) arising from a nickel-coordinated dppp ligand. A second resonance was observed at the moderately downfield shift of 368.2 ppm as a binomial pentet with a $J_{\text{P-P}}$ constant matching the upfield resonance. Integration of the two signals provided a ratio of 4:1 (d:q), consistent with the observed NMR coupling pattern. Analysis by electrospray ionization mass spectrometry (ESI-MS, Fig A.7) showed a major species (ca. 50% relative abundance) with a mass to charge (m/z) ratio centered at 1058.20 and an isotope pattern matching the empirical formula corresponding to that of $[(\text{dppp})_2\text{Ni}_2\text{PNSiMe}_3]^+$. Together, these data indicate the formation of a species with the empirical formula $[(\text{dppp})_2\text{Ni}_2(\text{PNTMS})]\text{Cl}$.

Evidence for the formation of $[(\text{dppp})_2\text{Ni}_2(\text{PNTMS})]\text{Cl}$ is exciting because it can be considered an intermediate en route to the target compound, following simple elimination of trimethylsilyl chloride. Analysis by ^1H NMR spectroscopy confirmed the presence of the dppp ligand and a trimethylsilyl group in the molar ratio of 2:1, further supporting the assigned product. The reducing P–Si bonds are expected to display higher reactivity than the N–Si bonds, one of which presumably persists in $[(\text{dppp})_2\text{Ni}_2(\text{PNTMS})]\text{Cl}$. The ^{31}P nuclei of the dppp ligand are chemically equivalent on the NMR timescale at 25 °C,

Previous work: synthesis of a $[L_2Ni]_2(P_2)$ complexes via TMSCl elimination



This work: synthesis of $[L_2Ni]_2(PNTMS)(Cl)$ complex via *incomplete* TMSCl elimination



Scheme A.1 Top: Synthesis of $[L_2Ni]_2(P_2)$ complexes from L_2NiCl_2 and $(TMS)_2PP(TMS)_2$.² Bottom: Synthesis of $[(dppp)_2Ni_2(PNTMS)]Cl$ from $(dppp)NiCl_2$ and $(TMS)_2NP(TMS)_2$.

suggestive of fluxionality in solution that could be facilitated by a mobile chloride anion. Speculating on the structure $[(dppp)_2Ni_2(PNTMS)]Cl$, three plausible options are provided in Fig. A.2. If considered static on the NMR timescale, none of these would give rise to the observed A_4M coupling pattern in the experimental ^{31}P NMR spectrum of $[(dppp)_2Ni_2(PNTMS)]Cl$. However, fast interconversion of structures such as **A**, **B**, and **C** could lead to chemically equivalent phosphorus centers on the dppp ligand. The chemical shift of the bridging phosphorus hints at structure **C** being representative of the species in solution based on the chemical shift of a tangentially related amino(imino)phosphane ligand.⁴ The interconversion of **A** and **B** is reminiscent of the auto-ionization of a *cis*-macrocyclic diphosphine dichloride, previously reported by our group.⁵

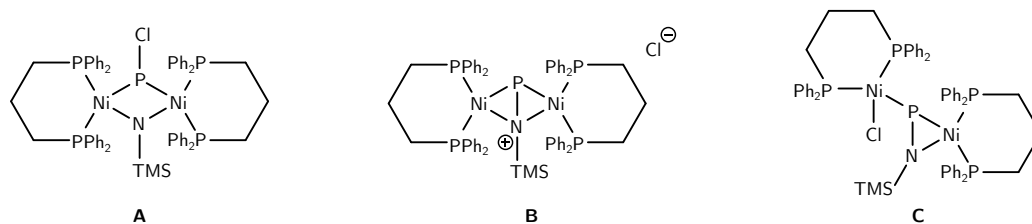


Chart A.2 Plausible molecular structures of $[(dppp)_2Ni_2(PNTMS)]Cl$.

To test the idea of a mobile chloride anion facilitating the fluxionality of $[(dppp)_2Ni_2(PNTMS)]Cl$ in solution, the complex was treated with reagents capable of chloride abstraction. The use of gallium(III) chloride (1 equiv) led to the formation of a new species with a A_2B_2M coupling pattern in the ^{31}P NMR spectrum (Fig. A.8). In the dppp region, two doublets were observed at 18.5 and 4.25 ppm, but with *different* values for

J_{P-P} of 22.2 and 23.6 Hz, respectively. A broad signal was observed at 120.5 ppm that displayed sufficient peak width at half height ($\Delta\nu_{1/2} = 149$ Hz,) to accommodate the expected triplet of triplets that would arise from coupling to the two sets of chemically inequivalent phosphorus nuclei in the dppp ligand. The chemical shift for the supposed bridging phosphorus nuclei undergoes a dramatic change in chemical shift of 247.7 ppm in the upfield direction as a result of chloride abstraction, suggestive of a large change in the average chemical environment of this nucleus. Given the two chemically inequivalent phosphorus centers in $[(dppp)_2Ni_2(PNTMS)]GaCl_4$, a structure with idealized C_{2v} symmetry is anticipated, i.e. **B** in Fig. A.2.

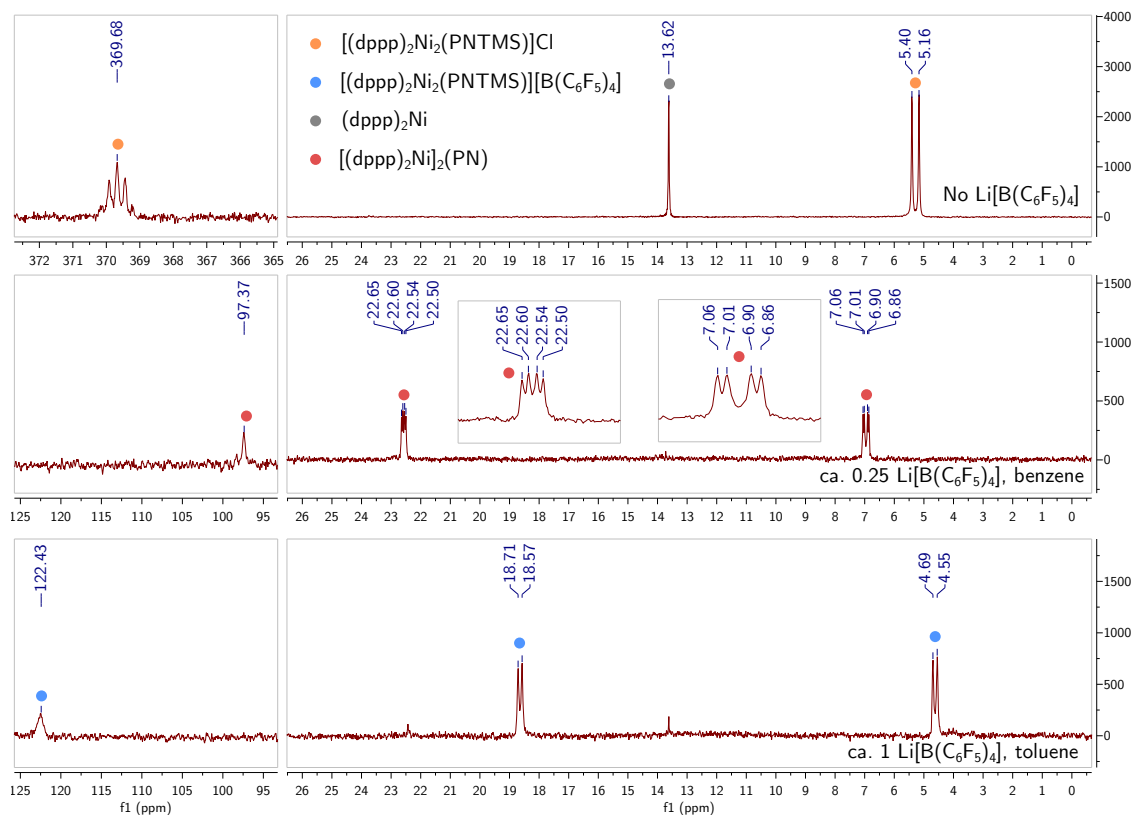
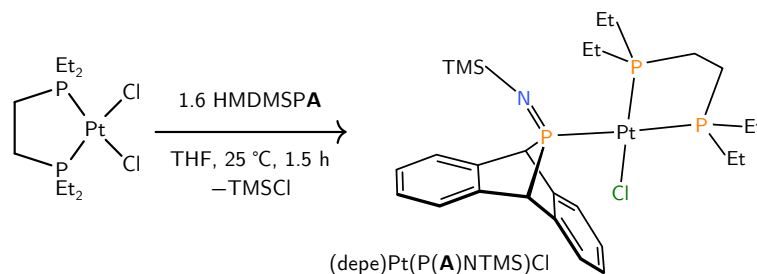


Figure A.1 Stack of $^{31}P\{^1H\}$ NMR spectra of the reaction mixture described in Section A.4.4. Top: solution of $[(dppp)_2Ni_2(PNTMS)]Cl$ before addition of $Li[B(C_5F_6)_4]$. Middle: reaction mixture after substoichiometric $Li[B(C_5F_6)_4]$. Bottom: Reaction mixture after a full equivalent of $Li[B(C_5F_6)_4]$.

In addition to gallium(III) chloride, $[(dppp)_2Ni_2(PNTMS)]Cl$ was treated with lithium tetrakis(pentafluoro)borate ($Li[B(C_5F_6)_4]$) in an attempt to abstract the chloride anion. Treatment of $[(dppp)_2Ni_2(PNTMS)]Cl$ with a full equivalent of $Li[B(C_5F_6)_4]$ in toluene

led to the formation of the same signals in the ^{31}P NMR spectrum as observed for GaCl_3 , indicating the formation of borate salt of $[(\text{dppp})_2\text{Ni}_2(\text{PNTMS})]^+$. Surprisingly, treatment of $[(\text{dppp})_2\text{Ni}_2(\text{PNTMS})]\text{Cl}$ with substoichiometric $\text{Li}[\text{B}(\text{C}_5\text{F}_6)_4]$ in benzene led to the formation of a different species, also displaying a $\text{A}_2\text{B}_2\text{M}$ splitting pattern in the ^{31}P NMR spectrum. The notable differences between the spectra of $[(\text{dppp})_2\text{Ni}_2(\text{PNTMS})]^+$ and this second species, tentatively assigned as $[(\text{dppp})\text{Ni}]_2(\text{PN})$, are the different chemical shifts for the bridging phosphorus nuclei of +122.4 and +97.4 ppm, respectively ($\Delta = 25$ ppm). Furthermore, the resonances attributed to $[(\text{dppp})\text{Ni}]_2(\text{PN})$ are observed as two chemically inequivalent dppp environments, featuring a $^2J_{\text{P-P}}$ value of 7.0 Hz and each showing an additional and larger coupling to the central phosphorus nuclei of 17.1 and 24.7 Hz, respectively (Fig. A.1). The seemingly small differences in reaction conditions that leads to these two different products are surprising, and further experiments are required in order to validate these preliminary experiments.

Despite these promising results, attention turned to the use of dibenzo-7-phospha-norbornadiene reagents (RPA, $\mathbf{A} = \text{C}_{14}\text{H}_{10}$, anthracene) to prepare a transition metal complex featuring a phosphorus mononitride ligand. While $(\text{TMS})_2\text{NP}(\text{TMS})_2$ can be regarded as a synthon for $[\text{PN}]^{4-}$ by treatment with four equivalents of chloride, HMDSPA can be considered a synthon for $[\text{PN}]^{2-}$ by reaction with two equivalents of chloride and elimination of anthracene. Thus, treatment of HMDSPA with one equivalent each of $\text{L}_n\text{M}^{\text{II}}\text{Cl}_2$ and $[\text{L}_n\text{M}^0]$ ($\text{L} = \text{L-type ligand}$, $\text{M} = \text{Ni, Pd, Pt}$) was envisaged as a plausible synthetic route to a PN bridging complex of the form $[\text{L}_2\text{M}]_2(\text{PN})$.



Scheme A.2 Synthesis of $[(\text{depePt}(\text{HMDSPA})\text{Cl})][\text{Cl}]$ from $(\text{depe})\text{PtCl}_2$ and HMDSPA.

These considerations led to exploration of the reaction between HMDSPA and $(\text{depe})\text{PtCl}_2$ ($\text{depe} = 1,2\text{-bis}(\text{diethylphosphino})\text{ethane}$). Treatment of the platinum(II) species with HMDSPA (1 equiv) led to the formation of $(\text{depe})\text{Pt}(\text{P}(\mathbf{A})\text{NTMS})\text{Cl}$ (Scheme A.2) over the course of 90 minutes with concomitant elimination of trimethylsilyl chloride. The $^{31}\text{P}\{^1\text{H}\}$ NMR spectrum of $(\text{depe})\text{Pt}(\text{P}(\mathbf{A})\text{NTMS})\text{Cl}$ displays an ABM splitting pattern, corresponding to inequivalent phosphorus nuclei on the depe ligand and a third environment arising from the $[\text{P}(\mathbf{A})\text{NTMS}]^-$ ligand, which can be considered the conjugate base of an iminophosphorane, i.e. an iminophosphoramide. Despite the formal negative charge

on a iminophosphoranide ligand (X-type) presumably residing on nitrogen, this ligand is coordinated via the phosphorus center. The presence of the anthracene fragment is unexpected, especially in light the tendency for cationic four-coordinate phosphonium salts of RPA compounds to undergo anthracene extrusion in the presence of halides to give P–X (X = Cl, F) bonds.^{6,7}

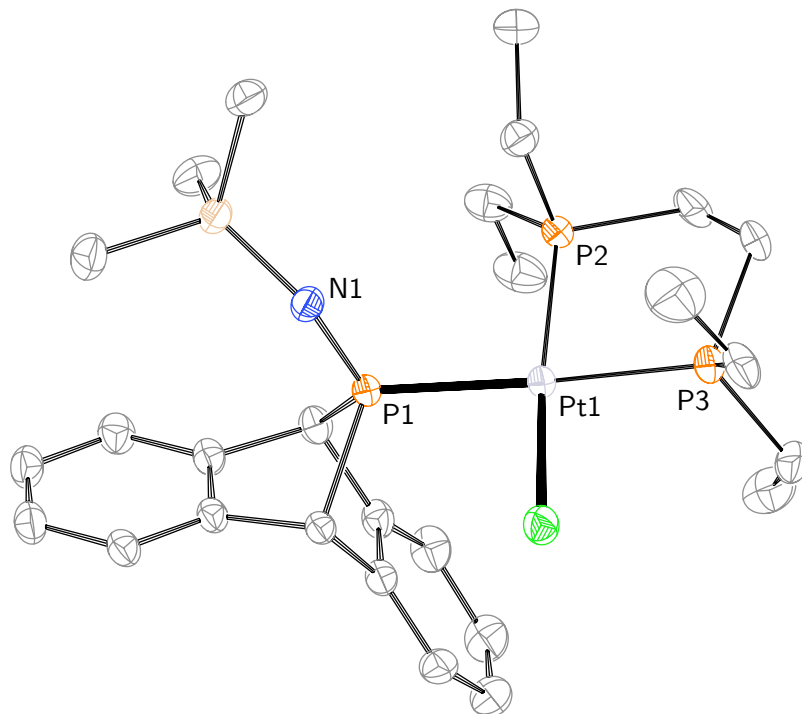


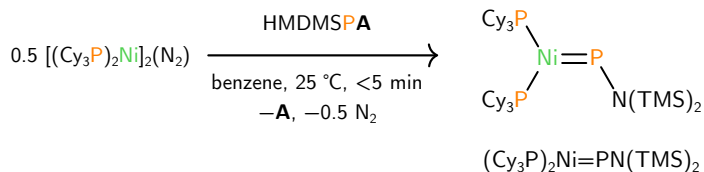
Figure A.2 Molecular structure of (depe)Pt(P(A)NTMS)Cl·THF with thermal ellipsoids shown at the 50% probability level. A solvent molecule of THF and hydrogen atoms omitted for clarity. Selected bond lengths (Å): P1–Pt1: 2.3317(6); P1–N1: 1.560(2); P2–Pt1: 2.182(6); P3–Pt1: 2.284(7).

Examination of the ³¹P and ¹H NMR spectra of a reaction mixture containing (depe)PtCl₂ and HMDSPA at early time points (ca. 10 min) indicated the formation a species with a similar ³¹P NMR spectrum to (depe)Pt(P(A)NTMS)Cl. At this early time point, the formation of trimethylsilyl chloride is negligible, and so this intermediate was assigned as [depePt(HMDSPA)Cl][Cl], the salt obtained from HMDSPA displacing a chloride ligand but prior to elimination of trimethylsilyl chloride. The rapid formation of this intermediate in comparison to the slower formation of (depe)Pt(P(A)NTMS)Cl suggests the second step could be rate limiting at 25 °C. The preference for chloride to form trimethylsilyl chloride as opposed to a P–Cl bond in this system presumably arises from the presence of the hexamethyldisilazide substituent on phosphorus; where P–Cl bond-formation has been observed the substituent on phosphorus of the RPA compound is an alkyl group such

as *t*-Bu.^{6,7} The hexamethyldisilazide substituent provides not only a silicon center which can compete for chloride by virtue of the strong Si–Cl bond, but also π -donation to the phosphonium center, tempering its electrophilicity and thus propensity to undergo attack by chloride.

Single crystals suitable for study by X-ray diffraction were grown by vapor diffusion of diethyl ether into a THF solution of (depe)Pt(P(**A**)NTMS)Cl at $-35\text{ }^{\circ}\text{C}$ (Fig A.2). The key structural parameter obtained from this study is the P–N bond length, which at $1.560(2)\text{ \AA}$ is markedly shorter than the sum of double bond covalent radii of 1.62 .⁸ The Pt–P(**A**)NTMS bond length ($2.3317(6)$) is slightly longer than the average Pt–P_{depe} bond length of $2.258(13)$.

Attention next turned to the reactivity of HMDSPA with sources of Ni⁰ to test whether the other “half” of the proposed synthesis of a [L₂M]₂(PN) species involving the redox-neutral elimination of anthracene. Treatment of the known⁹ Ni⁰ complex [Ni(PCy₃)₂]₂(N₂) with two equivalents of HMDSPA led to a major new species by ³¹P NMR spectroscopy that displayed signals at 1055.7 (t, ²J_{P–P} = 90.4 Hz) and 49.1 ppm (d, ²J_{P–P} = 90.4 Hz), while the ¹H NMR spectrum confirmed the formation of anthracene. Such a downfield chemical shift in the ³¹P NMR spectrum is diagnostic of the formation of the nickel phosphinidene species (Cy₃P)₂Ni=PN(TMS)₂, based on comparison of the spectroscopic data to (dtbpe)Ni=P(dmp) (dtbpe = bis(1,2-*tert*-butylphosphino)ethane), dmp = 2,6-dimethylphenyl, ³¹P (δ) 970 ppm) reported by Hillhouse and coworkers.¹⁰ Also observed in the ³¹P{¹H} NMR spectrum was diphosphene (TMS)₂NP=PN(TMS)₂,¹¹ which is not observed spectroscopically when HMDSPA is heated in solution.¹²



Scheme A.3 Synthesis of (Cy₃P)₂Ni=PN(TMS)₂ from [Ni(PCy₃)₂]₂(N₂) and HMDSPA.

Efforts to obtain structural characterization of (Cy₃P)₂Ni=PN(TMS)₂ were unsuccessful, and solutions of the compound were found to be metastable. Over time, significant amounts of free tricyclohexylphosphine formed with gradual loss of the phosphinidene signal in the ³¹P NMR spectrum. Nonetheless, the reactivity of a fresh solution (Cy₃P)₂Ni=PN(TMS)₂ with ethylene was probed to test whether phosphinidene transfer to provide a phosphirane was possible.¹³ Treatment of a degassed benzene solution of (Cy₃P)₂Ni=PN(TMS)₂ with a slight excess of ethylene led to rapid consumption of the phosphinidene resonance. In addition to free tricyclohexylphosphine, the formation of (Cy₃P)Ni(C₂H₄)₂ was observed by ³¹P spectroscopy.¹⁴ Two new signals were observed in the ³¹P spectrum at -144.3 and -95.0 ppm and these are tentatively assigned to the formation of free

and Ni-coordinated 1-hexamethyldisilaza-phosphirane, respectively. Though not previously reported, the assignment is based on the observation of the ^{31}P chemical shifts in the portion of the spectrum commonly occupied by phosphiranes and their corresponding complexes with transition metals.¹⁵ Further work and characterization data is required to confirm the identity of the species observed by ^{31}P NMR spectroscopy of this preliminary reaction.

These results prompted the start of a search for a suitable catalyst for the synthesis of phosphiranes from RPA (R = *t*-Bu, *i*-Pr) compounds and styrene, culminating in the organoiron- and fluoride-catalyzed system described in Chapter 5. Some of our earlier attempts explored the use of catalysts known for their ability to perform catalytic cyclopropanation or aziridination. One well-known catalyst for these classes of reactions is $\text{Rh}_2(\text{OAc})_4$, capable of generating rhodium-stabilized carbene or nitrene intermediates that lead to the respective three-membered rings in the presence of a suitable olefin. Given the analogy of these processes to phosphinidene-group transfer, the coordination chemistry of Me_2pipPA with $\text{Rh}_2(\text{OAc})_4$ was explored.

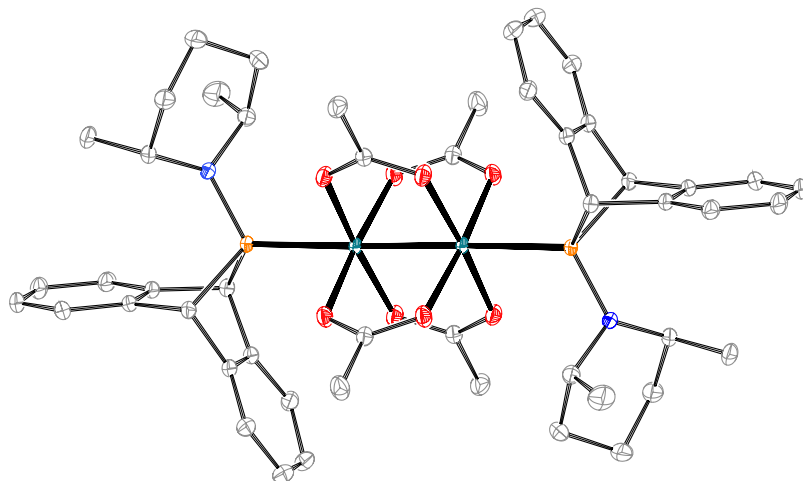
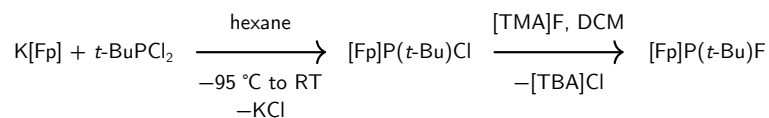


Figure A.3 Molecular structure of $\text{Rh}_2(\text{OAc})_4(\text{Me}_2\text{pipPA})_2 \cdot \text{CH}_2\text{Cl}_2$, with thermal ellipsoids at the 50% probability level. The solvent molecule and hydrogen atoms are omitted for clarity

Treatment of $\text{Rh}_2(\text{OAc})_4$ with HMDSPA (2 equiv) in dichloromethane led to the formation of a broad new resonance in the ^{31}P NMR spectrum centered at 169 ppm; the chemical shift of free Me_2pipPA is 189 ppm (benzene).¹⁶ The line width at half height ($\Delta\nu_{1/2}$) was found to be 1250 Hz at 25 °C, sharpening significantly to 125 Hz upon cooling the reaction mixture to -30 °C in the probe of the NMR spectrometer. The broad signal at room temperature points toward fluxionality at room temperature, possibly arising a rate of ligand exchange that is comparable to the NMR timescale. Single crystals of $\text{Rh}_2(\text{OAc})_4(\text{Me}_2\text{pipPA})_2$ were grown by vapor diffusion of diethyl ether into a concentrated

DCM solution of $\text{Rh}_2(\text{OAc})_4(\text{Me}_2\text{pipPA})_2$ at $-35\text{ }^\circ\text{C}$. The structure of $\text{Rh}_2(\text{OAc})_4(\text{Me}_2\text{pipPA})_2$ features approximate C_{2h} symmetry. The methyl groups on the 2 and 6 positions of the piperidine ring occupy the axial positions, as opposed to the expected equatorial positions that would ordinarily minimize 1,3-diaxial strain. Presumably, this is due to a competing steric interaction with the $\text{Rh}_2(\text{OAc})_4$ core.

The stability of a DCM solution of $\text{Rh}_2(\text{OAc})_4$ was monitored by NMR spectroscopy to determine whether elimination of anthracene occurred. After three days, the concentration of $\text{Rh}_2(\text{OAc})_4(\text{Me}_2\text{pipPA})_2$ had diminished by ca. 50%, with the concomitant formation of anthracene. Crudely analyzed using the Eyring equation for a unimolecular process, this single data point indicates an activation barrier for anthracene elimination of ca. 25 kcal/mol which is similar to the experimentally measured free-energy barrier for the unimolecular decomposition of Me_2pipPA at $85\text{ }^\circ\text{C}$ of ca. 27 kcal. Thus, the rhodium center does not seem to have a significant effect on the rate of anthracene elimination from Me_2pipPA at room temperature. No new species were observed in the ^{31}P NMR spectrum and so the fate of the aminophosphinidene fragment is unaccounted for at present.



Scheme A.4 Synthetic route to **3** starting from K[Fp] and $t\text{-BuPCl}_2$.

Following the publication of Chapter 5, some progress was made toward the isolation of proposed iron-fluorophosphido intermediate $\text{FpP}(t\text{-Bu})\text{F}$ (**3**). In order to obtain useful quantities of this compound, a preparation that involves salt metathesis between readily available K[Fp] and $t\text{-BuPCl}_2$ was explored. The formation of $\text{FpP}(t\text{-Bu})\text{Cl}$ from this first step was expected to undergo chloride to fluoride exchange using tetramethylammonium fluoride (TMAF). Initial experiments along these lines have provided spectroscopic identification for **3** but isolation of useful quantities of clean material has so far been elusive. Additional references from Malisch and co-workers, not cited in our original report, describe the reactivity of $(\text{Cp}/\text{Cp}^*)(\text{OC})_2\text{FePPh}_2$ with carbon-based electrophiles are of relevance to our proposed mechanism.^{17,18}

Finally, progress has been made to exploring the coordination chemistry of the phosphirane obtained from the catalytic procedure described in Chapter 5. The large number of structurally characterized compounds of the type $(\text{dba})\text{Pd}(\text{L})_2$ (dba = dibenzylideneacetone, L = L-type phosphine ligand) prompted us to prepare the 1-*tert*-butyl-2-phenylphosphirane analog to allow direct comparison with other phosphine ligands. Accordingly, $(\text{dba})\text{Pd}(\text{phosphirane})_2$ was prepared in 92% yield by treating a toluene solution of $\text{Pd}(\text{dba})_2$ with **1** (3 equiv) followed by precipitation with pentane. Single crystals suitable for study by X-ray diffraction were grown from a toluene solution of **1** layered with hexane at $-35\text{ }^\circ\text{C}$ (Fig. A.4).

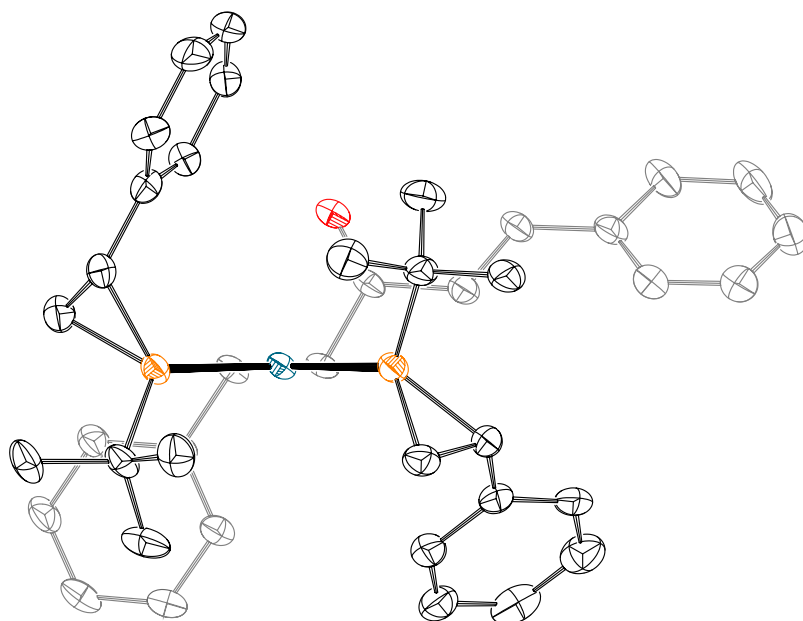


Figure A.4 Molecular structure of $(dba)Pd(\text{phosphirane})_2$ with thermal ellipsoids shown at the 50% probability level and hydrogen atoms omitted for clarity.

The bond metrical data for $(dba)Pd(\text{phosphirane})_2$, and a number of analogous species with different phosphine ligands, are provided in Table A.1. Bond lengths are provided to three significant figures to facilitate comparison of the data. The most notable feature of this analysis is the P–Pd bond length in $(dba)Pd(\text{phosphirane})_2$ of 2.25 Å, slightly shorter than other trialkyl/triaryl phosphines, and approaching the short P–Pd distance observed for triphenylphosphite. The short P–Pd bond length in $(dba)Pd(\text{phosphirane})_2$ can be attributed to the nature of the phosphirane lone pair, which is high in s orbital character.¹⁵ An s orbital has a smaller radial extension than the corresponding p orbital, resulting in the relatively short bond length. Another result of high s orbital character in the phosphorus lone pair is the associated low σ -donor ability when **1**-*t*-Bu acts as a ligand. Experimentally, this manifests itself in a short C=C double bond (1.35 Å) for the dba ligand in $(dba)Pd(\text{phosphirane})_2$ compared to the analogous C=C bond when strong σ donor ligands are present, such as PCy_3 (C=C: 1.45 Å.)

The relatively poor ability for σ donation when **1** acts as a ligand is of potential application in catalysis. For example, rates of Stille cross-coupling are accelerated by ligands that dissociate readily from the palladium center, such as triphenylarsine.²³ It will be of interest to benchmark **1** as a ligand in this reaction and compare it to the widely available data for a number of other L-type ligands.²³

L	Pd-P	Pd-C	C1-C2	P-Pd-P
P(OPh) ₃ ¹⁹	2.25	2.15	1.35	105.2
1	2.30	2.16	1.40	107.4
P(Bz) ₃ ²⁰	2.34	2.18	1.40	107.2
PPh ₃ ²¹	2.34	2.16	1.39	114.9
PCy ₃ ²¹	2.37	2.17	1.45	115.6
P(o-Tol) ₃ ²²	2.38	2.18	1.42	116.2

Table A.1 Bond metric data for a series of (dba)Pd(PR₃)₂ compounds. C1-C2 refers to the two carbons coordinated to the Pd center from the dba ligand.

A.3 Conclusions and Future Directions

The development of a method for forming TM-E (TM = group 10 transition metal element, E = P, N) bonds from TM-Cl and E-SiMe₃ bond-containing precursors has proven fruitful for the synthesis of both [(dppp)₂Ni₂(PNTMS)]Cl and (depe)Pt(P(**A**)NTMS)Cl. Both complexes are tantalizingly close to being developed as intermediates en route to the first transition metal complex featuring phosphorus mononitride as a ligand. [(dppp)₂Ni₂(PNTMS)]Cl is related to the target compound [(dppp)Ni]₂(PN) by the simple elimination of a trimethylsilyl group, and tentative ³¹P NMR data has been obtained for the product of this elimination upon treatment with Li[B(C₅F₆)₄] (0.25 equiv) in benzene. Other routes to explore for this interesting system include a more electron rich diphosphine ligand such as depe, which features in the corresponding synthesis of [(depe)Ni]₂(P₂) from (depe)NiCl₂ and P₂(TMS)₄. The use of a more electron rich ligand may provide the necessary driving force for chloride to remove the trimethylsilyl group. Other strategies for completing the synthesis of [(dppp)Ni]₂(PN) from [(dppp)₂Ni₂(PNTMS)]Cl could involve the use of TMAF; the strong Si-F bond and low solubility of [TMA]Cl would be expected to facilitate the formal elimination trimethylsilyl chloride.

Treatment of HMDSPA with [Ni(PCy₃)₂]₂(N₂) leads to the formation of a rare nickel-phosphinidene species. Although this compound has, to date, eluded isolation and full characterization it provides an example of RPA compounds acting as useful precursors for the preparation of transition-metal phosphinidene complexes. Initial reactivity studies of (Cy₃P)₂Ni=PN(TMS)₂ have hinted at the possibility of phosphinidene group transfer to ethylene, though further work is required to fully characterize the products of this reaction. Of interest will be to switch the two tricyclohexylphosphine ligands for one bidentate ligand in order to minimize dissociation by virtue of the chelate effect. The development of such a system, and its application to catalytic phosphinidene transfer may allow for increased scope in the catalytic phosphirane of olefins beyond styrene and its derivatives.

A.4 Experimental methods

A.4.1 General methods

All manipulations were performed in a Vacuum Atmospheres model MO-40M glovebox under an inert atmosphere of purified N₂ or using standard Schlenk techniques. When reagents were removed from a stock bottle containing a Sure/Seal, the equivalent volume of dry nitrogen was injected into the bottle prior to removing the desired volume of solution with a syringe. All solvents were obtained anhydrous and oxygen-free by bubble degassing (argon) and purification by passing through columns of alumina and Q5.²⁴ Once collected, solvents were stored over activated 4 Å molecular sieves (20 wt%) inside the glovebox.²⁵ All glassware was oven-dried for at least 6 h prior to use, at temperatures greater than 150 °C.

[Ni(PCy₃)₂]₂(N₂),⁹ (depe)PtCl₂,²⁶ HMDSPA,¹² Me₂pipPA¹⁶ were prepared according to literature methods. Rh₂(OAc)₄ (Alfa), GaCl₃ (Strem), Pd(dba)₂ (Strem) and (dppp)-NiCl₂ (Strem) were used as received. Deuterated solvents were purchased from Cambridge Isotope Labs and were degassed three times by the freeze-pump-thaw method and stored over activated 4 Å molecular sieves for 48 h in the glovebox prior to use. Diatomaceous earth (Celite 435, EM Science), 4 Å molecular sieves (Millipore-Sigma) and basic alumina (Millipore-Sigma) were dried by heating to 200 °C under dynamic vacuum for at least 48 h prior to use. The temperature of the aluminum shot used to heat reagents or reaction mixtures was measured using a Hanna Instruments K-type Thermocouple Thermometer (model HI935005).

NMR spectra were obtained on a Jeol ECZ-500 instrument equipped with an Oxford Instruments superconducting magnet, on a Bruker Avance 400 instrument equipped with a Magnex Scientific or with a SpectroSpin superconducting magnet, or on a Bruker Avance 500 instrument equipped with a Magnex Scientific or with a SpectroSpin superconducting magnet. ¹H and ¹³C NMR spectra were referenced to residual CD₂Cl₂ (¹H = 5.32 ppm, ¹³C = 54.0 ppm), C₆D₆ (¹H = 7.16 ppm, ¹³C = 128.06 ppm), CD₃CN (¹H = 1.94 ppm, ¹³C = 118.26 ppm) or CDCl₃ (¹H = 7.26 ppm, ¹³C = 77.16 ppm). ³¹P NMR spectra were referenced externally to 85% H₃PO₄ (0 ppm).

A.4.2 Synthesis of [(dppp)₂Ni₂(PNTMS)][Cl]

Inside a glovebox, a Schlenk flask (100 mL) was charged with (dppp)NiCl₂ (1.0 g, 1.85 mmol, 2 equiv) and a magnetic stir bar (2 cm). (TMS)₂NP(TMS)₂ (310 mg, 0.917 mmol, 1 equiv) was weighed into a vial and diluted in THF (20 mL). The resulting solution was transferred to the Schlenk flask and the resulting mixture was allowed to stir for one week. Volatile material was removed under reduced pressure to remove TMSCl. The solution was redissolved in THF (20 mL) and filtered through a frit (15 mL, fine porosity) to leave behind red crystals of (dppp)NiCl₂ (500 mg, 0.917 mmol, 50%). Volatile material was removed from the filtrate under reduced pressure and the sticky brown oil was triturated

with toluene (2×20 mL). The resulting oil was triturated with pentane (60 mL) to give dark brown solids which were collected on a frit (15 mL, fine porosity). The filtrate was concentrated under reduced pressure to a brown oil which was triturated with pentane (20 mL) to give brown solids which were collected on the same frit as the first batch of brown solids. The combined product was washed with pentane until the filtrate ran off colorless (ca. 20 mL). The product was transferred to a vial and brought to constant mass under reduced pressure (340 mg). Analysis of the product by $^{31}\text{P}\{^1\text{H}\}$ spectroscopy indicated a molar ratio of $[(\text{dppp})_2\text{Ni}_2(\text{PNTMS})]\text{Cl}$ to $(\text{dppp})\text{NiCl}_2$ of ca. 1:2.3. Adjusting for the $(\text{dppp})\text{NiCl}_2$ content, the yield of desired product is estimated as 255 mg, 0.230 mmol, 25%. $^{31}\text{P}\{^1\text{H}\}$ (162 MHz, C_6D_6 , δ) 368.2 (p, $^2J_{\text{P-P}} = 38.4$ Hz, 1P), 3.9 (d, $^2J_{\text{P-P}} = 38.4$ Hz, 4P). ^1H (400 MHz, C_6D_6 , δ) 7.95–7.29 (m, 16H), 7.04–6.90 (m, 24H), 2.44–1.98 (m, 8H), 1.87–1.37 (m, 4H), 0.19 (s, 6H). *Note:* The trimethylsilyl resonance integrates to 6H instead of the expected 9H because of the presence of $(\text{dppp})_2\text{Ni}$ contributing to the integration values of the dppp resonances (see $^{31}\text{P}\{^1\text{H}\}$ spectrum, Figure A.6).

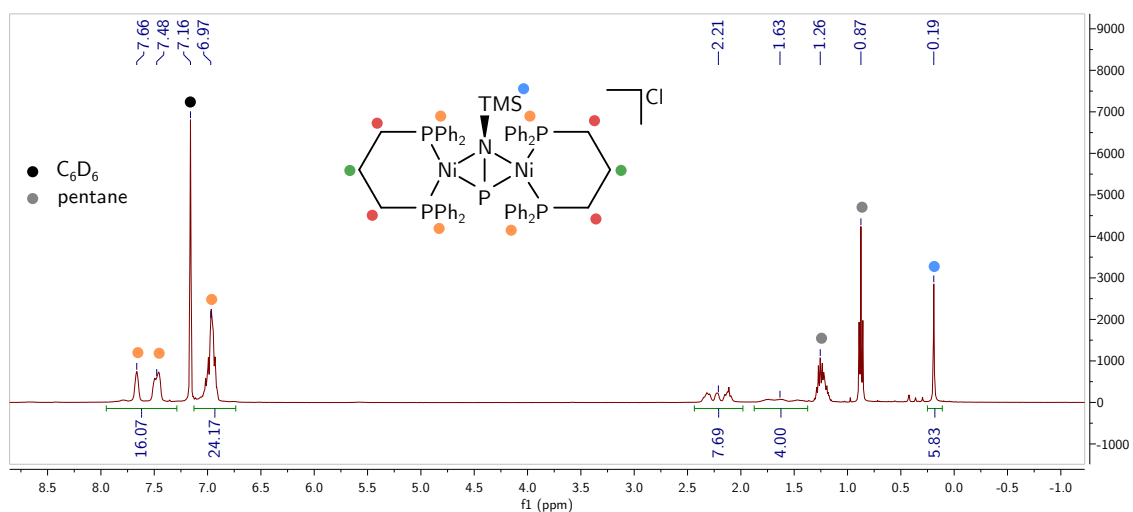


Figure A.5 ^1H NMR spectrum of $[(\text{dppp})_2\text{Ni}_2(\text{PNTMS})]\text{Cl}$ in C_6D_6 , recorded at 400 MHz and 25 °C.

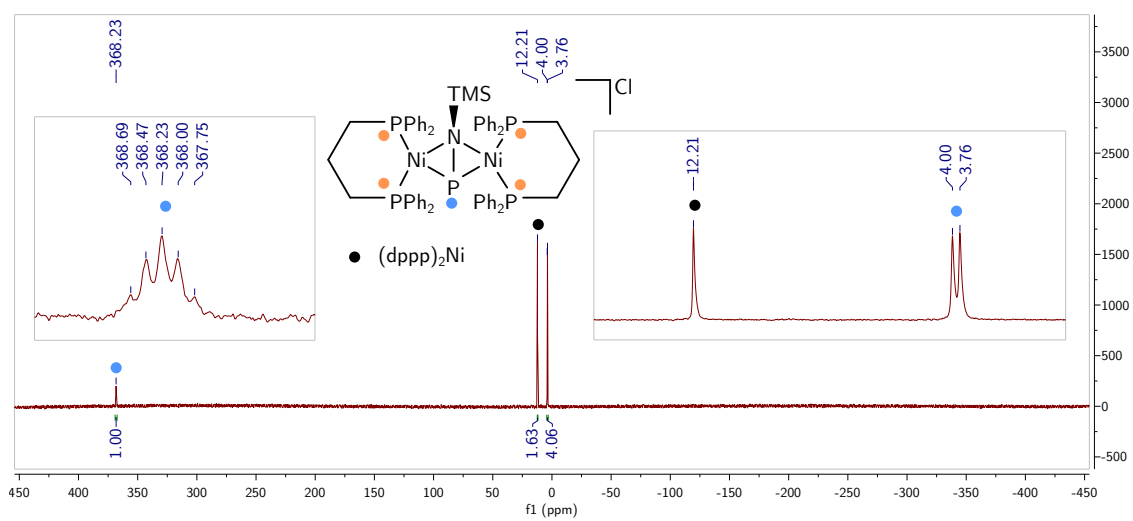


Figure A.6 $^{31}\text{P}\{^1\text{H}\}$ NMR spectrum of $[(\text{dppp})_2\text{Ni}_2(\text{PNTMS})]\text{Cl}$ in C_6D_6 , recorded at 162 MHz and 25 °C.

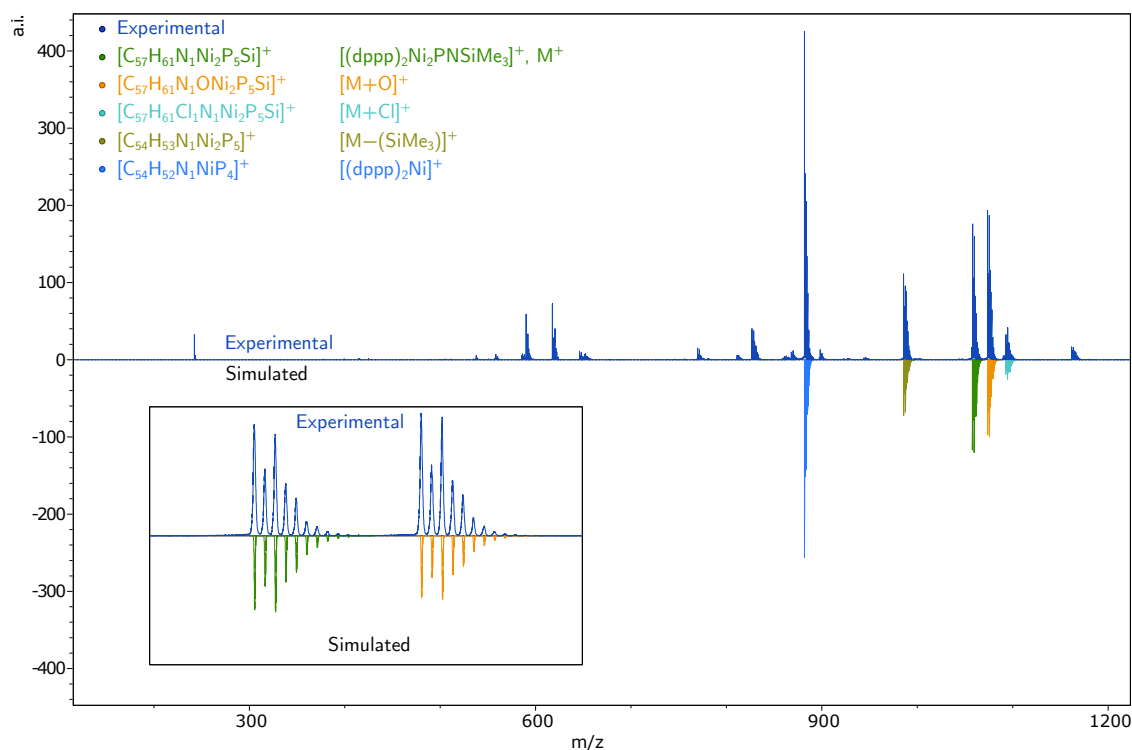


Figure A.7 ESI-MS(+) of $[(dppp)_2Ni_2(PNTMS)]Cl$.

A.4.3 Treatment of $[(dppp)_2Ni_2(PNTMS)]Cl$ with $GaCl_3$ to give $[(dppp)_2Ni_2(PNTMS)]GaCl_4$

$GaCl_3$ (12 mg, 0.068 mmol, 1 equiv) and $[(dppp)_2Ni_2(PNTMS)]Cl$ (75 mg, 0.068 mmol, 1 equiv) were weighed out into separate vials. Both were dissolved in toluene (2 and 4 mL, respectively) and the solution of $GaCl_3$ was transferred dropwise to the solution of $[(dppp)_2Ni_2(PNTMS)]Cl$. The solution was left to stir for 15 minutes then concentrated to 1 mL giving a brown oil and brown solution. The solution was passed through a piece of filter paper in a glass pipette. Toluene (1 mL, $-35\text{ }^\circ\text{C}$) was used to wash the residual brown oil in the vial, and this toluene wash passed through the same filter as the first. THF (2 mL) was used to combine the solid material on the filter paper and the brown oil. Volatile material was removed under reduced pressure and the resulting oil was triturated with toluene ($2 \times 1\text{ mL}$) then placed under vacuum for an additional 30 minutes. The brown oil was triturated with pentane (15 mL) until brown solids formed. The brown solids were collected on a fine glass frit and volatile material was removed under reduced pressure for 2 hours to give $[(dppp)_2Ni_2(PNTMS)]GaCl_4$ as a brown solid (87 mg, 0.068 mmol, 100%). *Note: this yield is artificially high due to the presence of $(dppp)_2Ni$ in the starting*

material. $^{31}\text{P}\{^1\text{H}\}$ (162 MHz, $\text{THF-}d_8$, δ) 120.5 (br, $\Delta\nu_{1/2} = 149$ Hz) 18.50 (d, $J = 22.2$ Hz), 4.25 (d, $J = 23.6$ Hz). ^1H (400 MHz, $\text{THF-}d_8$, δ) 7.66–6.98 (m, 40H), 2.52 (m, 8H), 1.9–1.75 (m, 4H), -0.23 (s, 9H).

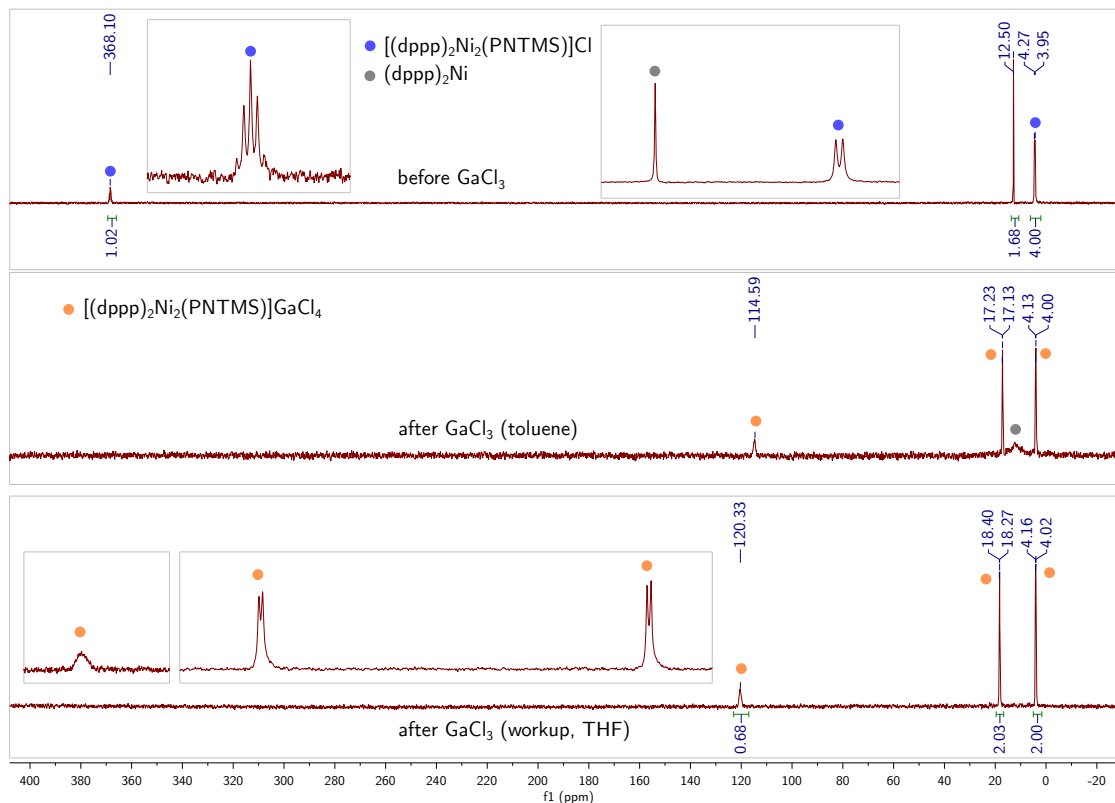


Figure A.8 Stack of $^{31}\text{P}\{^1\text{H}\}$ NMR spectra of the reaction mixture described in Section A.4.3. Top: solution of $[(\text{dppp})_2\text{Ni}_2(\text{PNTMS})]\text{Cl}$ before addition of GaCl_3 . Middle: crude reaction mixture after addition of GaCl_3 . Bottom: Obtained material dissolved in $\text{THF-}d_8$.

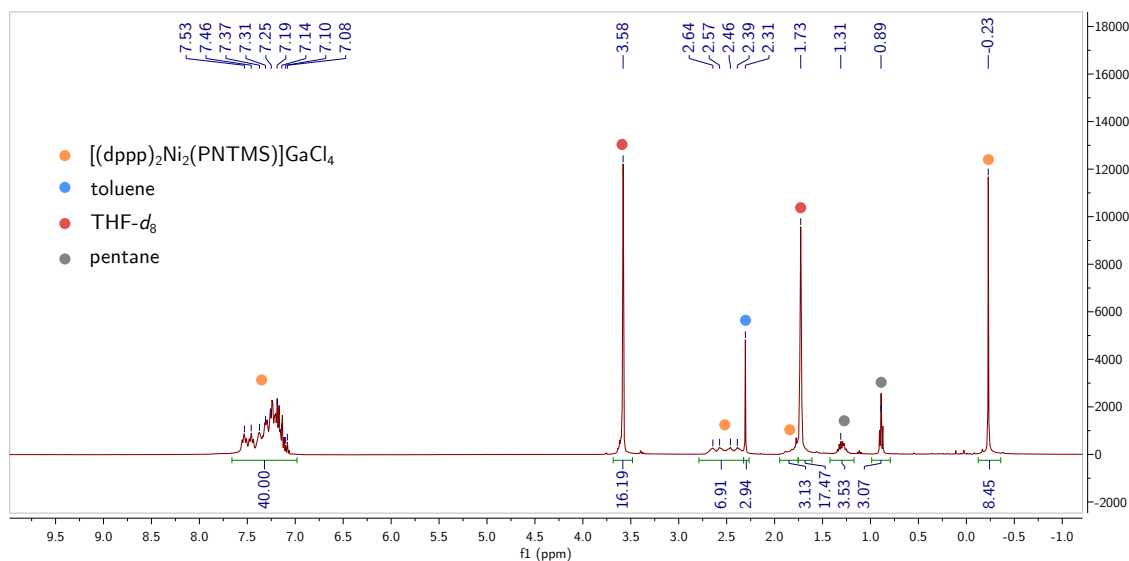


Figure A.9 ^1H NMR spectrum of $[(\text{dppp})_2\text{Ni}_2(\text{PNTMS})]\text{GaCl}_4$ in $\text{THF-}d_8$, recorded at 400 MHz and 25°C .

A.4.4 Treatment of $[(\text{dppp})_2\text{Ni}_2(\text{PNTMS})]\text{Cl}$ with $\text{Li}[\text{B}(\text{C}_5\text{F}_6)_4]$ (0.25 or 1.0 equiv)

Reaction 1 (1 equiv $\text{Li}[\text{B}(\text{C}_5\text{F}_6)_4]$, toluene): An NMR tube was charged with $[(\text{dppp})_2\text{Ni}_2(\text{PNTMS})]\text{Cl}$ (11 mg, 0.01 mmol, 1 equiv) and $\text{Li}[\text{B}(\text{C}_5\text{F}_6)_4]$ (8 mg, 0.01 mmol, 1 equiv) and the solids were dissolved in toluene. The reaction was monitored by $^{31}\text{P}\{^1\text{H}\}$ NMR spectroscopy and showed the formation of the same signals observed as was the case when $[(\text{dppp})_2\text{Ni}_2(\text{PNTMS})]\text{Cl}$ is treated with GaCl_3 , suggesting chloride abstraction. $^{31}\text{P}\{^1\text{H}\}$ (162 MHz, C_6D_6 , δ) 122.4 (br, $\Delta\nu_{1/2} = 141$ Hz), 18.6 (d, $^2J_{\text{P-P}} = 21.9$ Hz), 4.6 (d, $^2J_{\text{P-P}} = 23.4$ Hz).

Reaction 2 (0.25 equiv $\text{Li}[\text{B}(\text{C}_5\text{F}_6)_4]$, C_6D_6): An NMR tube was charged with $[(\text{dppp})_2\text{Ni}_2(\text{PNTMS})]\text{Cl}$ (11 mg, 0.01 mmol, 1 equiv) and $\text{Li}[\text{B}(\text{C}_5\text{F}_6)_4]$ (2 mg, 0.0025 mmol, 0.25 equiv) and the solids were dissolved in C_6D_6 . The reaction was monitored by $^{31}\text{P}\{^1\text{H}\}$ NMR spectroscopy and showed the formation of a new set of signals with an $\text{A}_2\text{B}_2\text{M}$ splitting pattern (the ‘M’ nucleus was observed as a broad signal). $^{31}\text{P}\{^1\text{H}\}$ (162 MHz, C_6D_6 , δ) 97.4 (br, $\Delta\nu_{1/2} = 74$ Hz), 22.6 (dd, $^2J_{\text{P-P}(\text{trans})} = 17.1$, $^2J_{\text{P-P}(\text{cis})} = 7.0$ Hz), 7.0 (dd, $^2J_{\text{P-P}(\text{trans})} = 24.7$ Hz, $^2J_{\text{P-P}(\text{cis})} = 7.0$ Hz).

The differences in product distribution based on these seemingly small minor changes in the reaction conditions is unknown at the present time. The presence of $(\text{dppp})_2\text{Ni}$ as an impurity could also be interacting with the lithium cation.

A.4.5 Synthesis of (depe)Pt(P(A)NTMS)Cl.

In the glovebox, a vial was charged with HMDSPA (135 mg, 0.36 mmol, 1.65 equiv) and dissolved in THF (2 mL). Another vial was charged with (depe)PtCl₂ (150 mg, 0.22 mmol, 1 equiv) to which the solution of HMDSPA was added. The vial that had contained HMDSPA was washed with THF (6 mL) and the washings were added to the reaction mixture. The solution was stirred for 1.5 h, after which time the volume was concentrated to approximately 1 mL. Addition of diethyl ether (10 mL) led to the formation of a precipitate which was collected atop a frit (fine porosity, 15 mL) and washed with diethyl ether (4 mL) to give spectroscopically pure (depe)Pt(P(A)NTMS)Cl as a beige powder (123 mg, 0.16 mmol, 72% yield). The product (70 mg) was recrystallized by dissolving in THF (0.5 mL) and filtering the resulting solution into a shell vial, followed by vapor diffusion of pre-cooled diethyl ether (4 mL, -35 °C) into the solution at -35 °C. In this way, single crystals suitable for study by X-ray diffraction were obtained. ¹H (400 MHz, CD₂Cl₂, δ) 7.32 (dd, *J* = 5.0, 3.4 Hz, 4H), 7.00 (tt, *J* = 5.6, 3.1 Hz, 4H), 4.70 (s, 1H), 2.35–0.65 (m, 24H), -0.34 (s, 9H). ³¹P{¹H} (162 MHz, C₆D₆, δ) see Table A.2.

Table A.2 NMR data for species relevant to the experiment described in Section A.4.6.

Species	δP_X ($^1J_{Pt-P}$)			$^2J_{P-P}$		
	P _N	P _{cis}	P _{trans}	N/cis	N/trans	cis/trans
(depe)PtCl ₂	-	57.5 (3547)	-	-	-	-
impurity in (depe)PtCl ₂	-	48.6 (2367)	-	-	-	-
HMDSPA	211.7	-	-	-	-	-
[depePt(HMDSPA)Cl][Cl]	166.7 (2514)	47.5 (3374)	69.8 (2246)	19	394	-
depePt(P(A)NTMS)Cl	148.5 (2543)	42.9 (3727)	60.9 (2268)	22	411	6

^a in CDCl₃

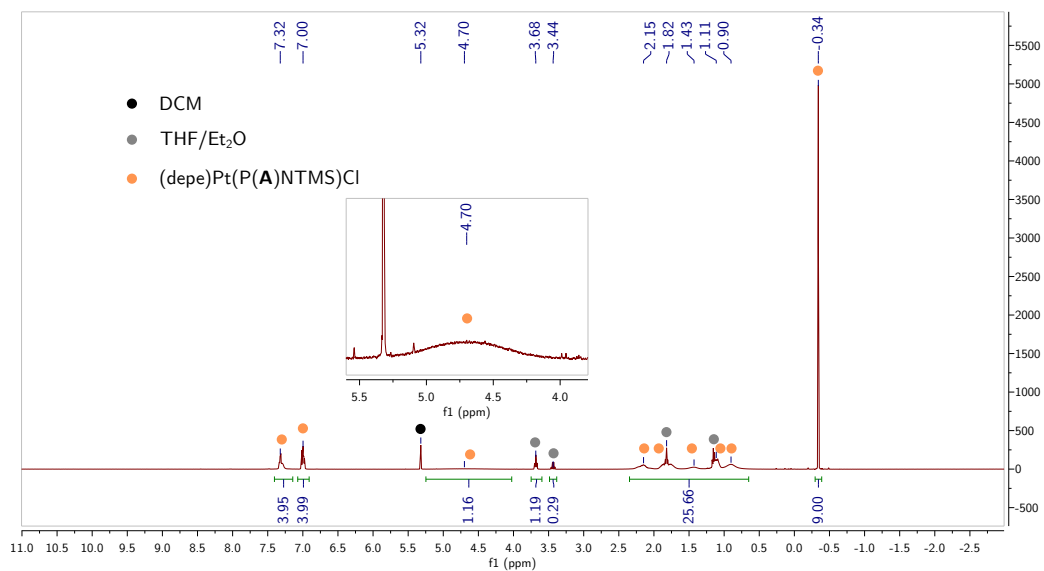


Figure A.10 ¹H NMR spectrum of (depe)Pt(P(A)NTMS)Cl in CD₂Cl₂, recorded at 400 MHz and 25 °C.

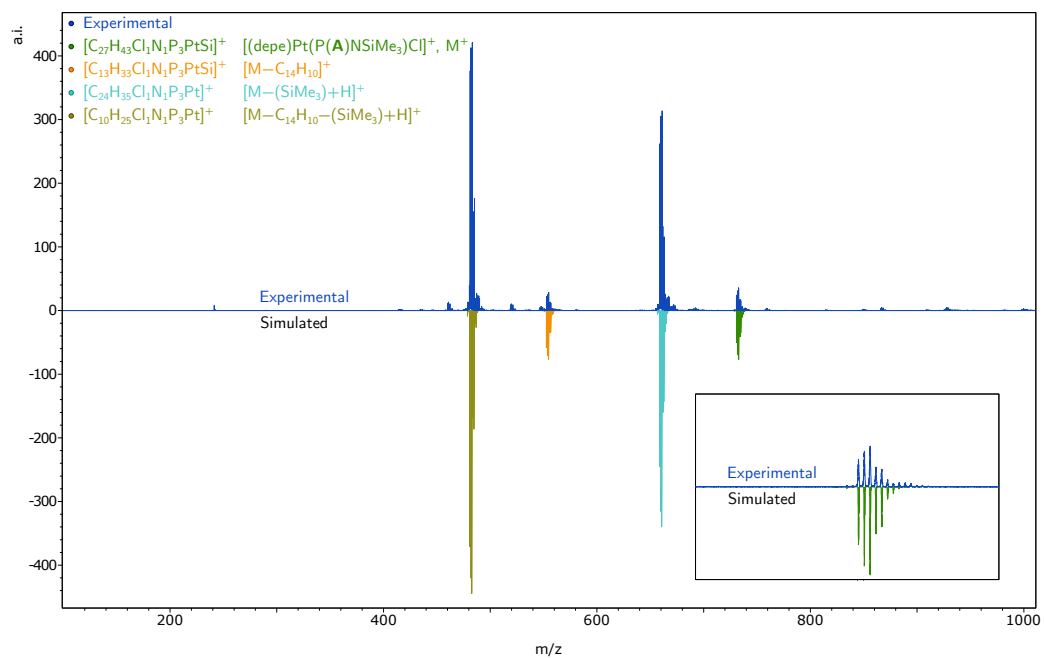


Figure A.11 ESI-MS(+) of (depe)Pt(P(A)NTMS)Cl.

A.4.6 Monitoring the reaction of HMDSPA with (depe)PtCl₂ by NMR spectroscopy.

In the glovebox, HMDSPA (20 mg, 0.054 mmol, 1 equiv) and (depe)PtCl₂ (26 mg, 0.054 mmol, 1 equiv) were weighed into a vial and dissolved in CD₂Cl₂ (0.7 mL). The resulting solution was transferred to an NMR tube and analyzed by NMR spectroscopy after ten minutes, 1 h, and 3 h, by which time the reaction had reached completion. An intermediate was assigned as [depePt(P(A))N(TMS)₂]Cl, i.e. prior to elimination of TMSCl. NMR data are tabulated in Table A.2.

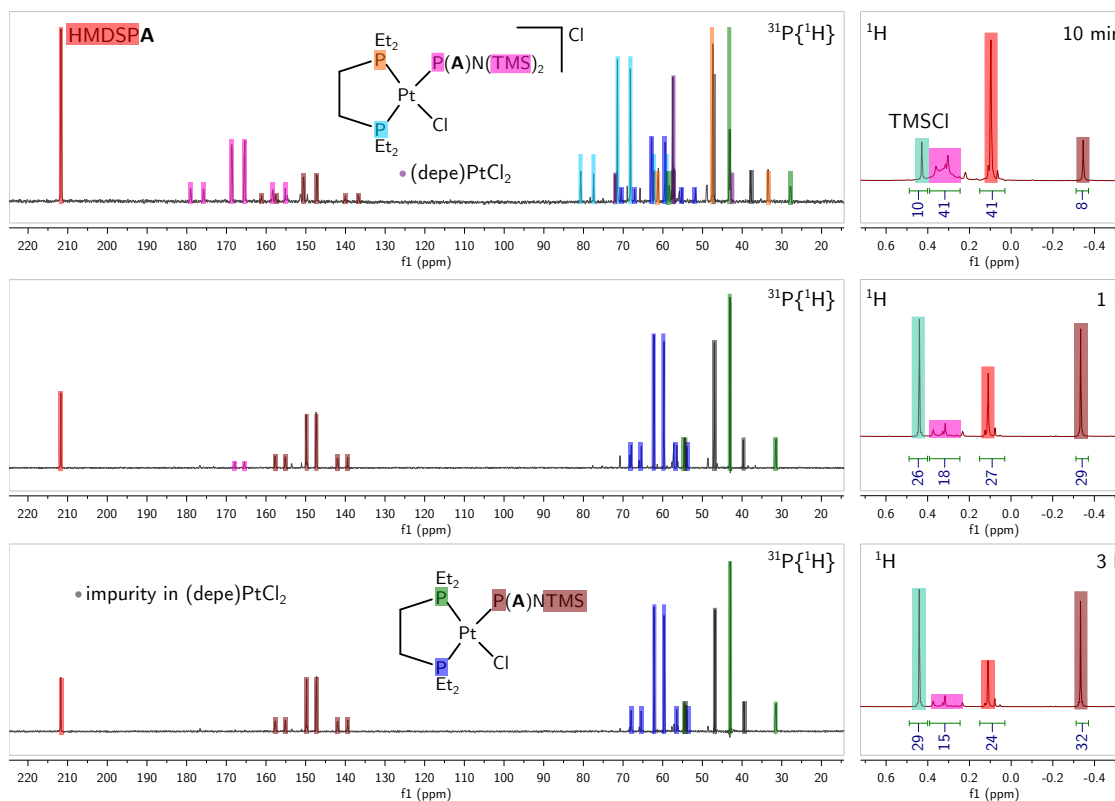


Figure A.12 Stack of ³¹P{¹H} (left) and ¹H (right) NMR spectra of the reaction mixture described in Section A.4.6 after, 10 min, 1 h, and 3 h. Resonances have been shaded to indicate the nuclei they correspond to. The integration values in the ¹H spectrum shows the temporal evolution of the TMS groups.

A.4.7 In situ generation of $(\text{Cy}_3\text{P})_2\text{Ni}=\text{PN}(\text{TMS})_2$

In the glovebox, $[\text{Ni}(\text{PCy}_3)_2]_2(\text{N}_2)$ (40 mg, 0.032 mmol, 1 equiv) was weighed into a vial and dissolved in C_6D_6 (0.4 mL). The resulting solution was transferred to an NMR tube and the sample was analyzed $^{31}\text{P}\{^1\text{H}\}$ NMR spectroscopy. HMDSPA (26 mg, 0.070 mmol, 2 equiv) was weighed into a vial and transferred to the NMR tube using C_6D_6 (0.3 mL) and the solution was analyzed by NMR spectroscopy. $^{31}\text{P}\{^1\text{H}\}$ (162 MHz, C_6D_6 , δ) +1055.7 (t, $^2J_{\text{P-P}} = 90.4$ Hz), 4+9.1 ppm (d, $^2J_{\text{P-P}} = 90.4$ Hz). ^1H (400 MHz, C_6D_6 , δ) 0.69 (s).

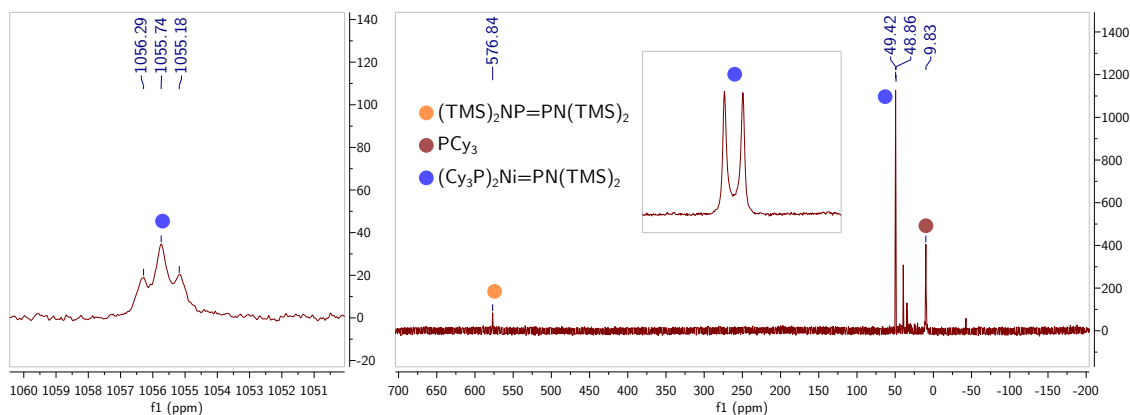


Figure A.13 $^{31}\text{P}\{^1\text{H}\}$ NMR spectrum of a reaction mixture in C_6D_6 prepared as described in Section A.4.7, recorded at 162 MHz and at 25 °C.

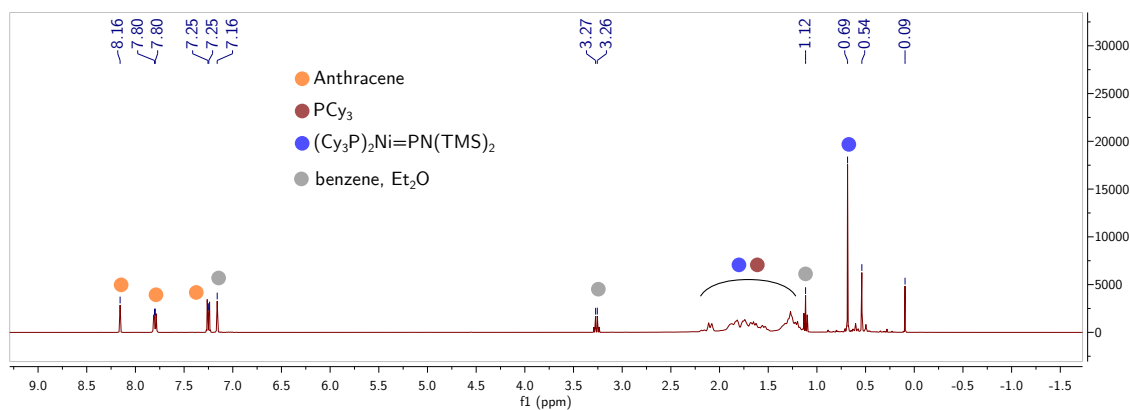


Figure A.14 ^1H NMR spectrum of a reaction mixture in C_6D_6 prepared as described in Section A.4.7, recorded at 400 MHz and at 25 °C.

A.4.8 Treatment of in situ generated $(\text{Cy}_3\text{P})_2\text{Ni}=\text{PN}(\text{TMS})_2$ with excess ethylene

In the glovebox, $[\text{Ni}(\text{PCy}_3)_2]_2(\text{N}_2)$ (20 mg, 0.016 mmol, 1 equiv) and HMDSPA (12 mg, 0.032 mmol, 2 equiv) were weighed into an NMR tube equipped with a J-Young valve and dissolved in C_6D_6 (0.6 mL). Analysis by $^{31}\text{P}\{^1\text{H}\}$ showed the formation of $(\text{Cy}_3\text{P})_2\text{Ni}=\text{PN}(\text{TMS})_2$. On the Schlenk line, the solution was degassed three times via the freeze-pump-thaw method then backfilled with ethylene (≥ 2 mL, ≥ 5 equiv). The tube was shaken and analyzed by NMR spectroscopy showing the presence of new signals in the $^{31}\text{P}\{^1\text{H}\}$ spectrum. One was assigned as $(\text{Cy}_3\text{P})\text{Ni}(\text{C}_2\text{H}_4)_2$ by comparison of the $^{31}\text{P}\{^1\text{H}\}$ chemical shift with prior literature reports.¹⁴ Two upfield resonances were observed at -144.3 and -95.0 that were tentatively assigned as HMDSP(C_2H_4) and Ni-coordinated HMDSP(C_2H_4), respectively, based on the chemical shifts of other free and metal-coordinated phosphiranes.

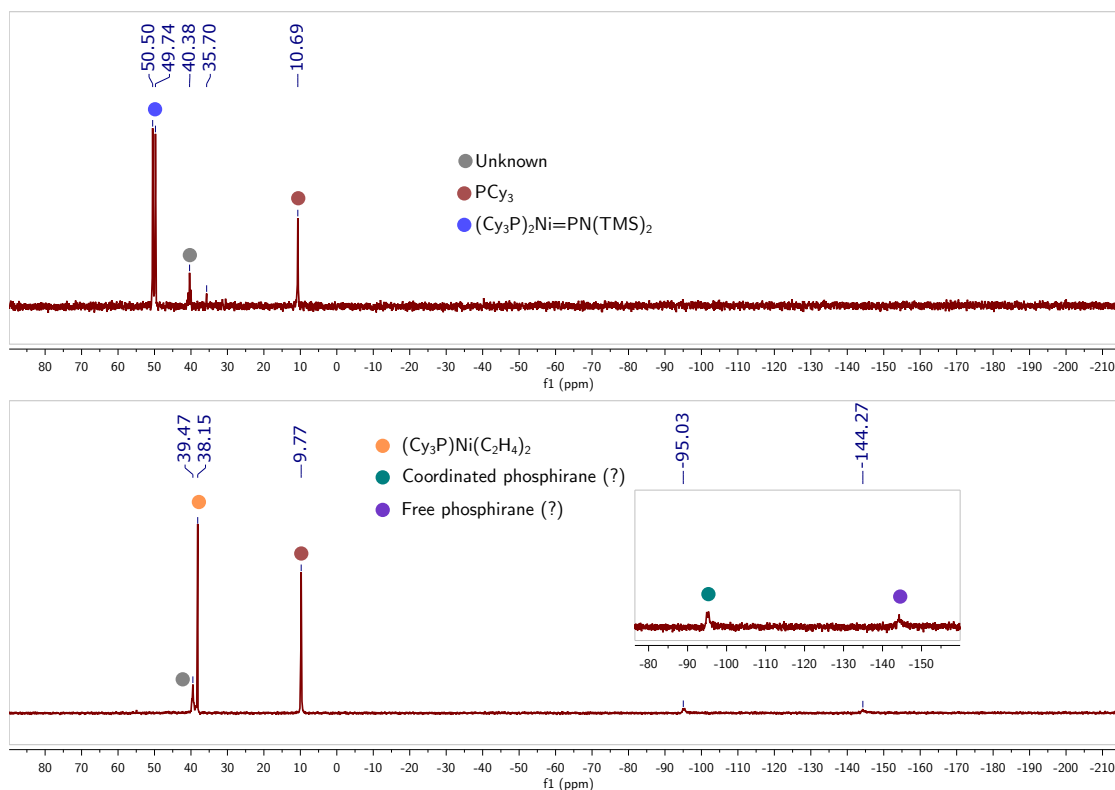


Figure A.15 $^{31}\text{P}\{^1\text{H}\}$ NMR spectrum of a reaction mixture in C_6D_6 prepared as described in Section A.4.7, recorded at 162 MHz and at 25 °C. Top: solution of $(\text{Cy}_3\text{P})_2\text{Ni}=\text{PN}(\text{TMS})_2$ before addition of ethylene. Bottom: solution after addition of ethylene.

A.4.9 Preparation of $\text{Rh}_2(\text{OAc})_4(\text{Me}_2\text{pipPA})_2$

In the glovebox, Me_2pipPA (15 mg, 0.045 mmol, 2 equiv) and $\text{Rh}_2(\text{OAc})_4$ (10 mg, 0.022 mmol, 1 equiv) were weighed into the same vial and dissolved in CD_2Cl_2 (0.7 mL) to give a dark red solution ($\text{Rh}_2(\text{OAc})_4$ is a green solid). Crystalline material was obtained by diffusion of diethyl ether into a concentrated DCM solution of $\text{Rh}_2(\text{OAc})_4(\text{Me}_2\text{pipPA})_2$ at $-35\text{ }^\circ\text{C}$. A yield was not obtained because the material was used in an X-ray diffraction study (Section A.4.13.1). ^1H (300 MHz, CD_2Cl_2 , δ) 7.41 (dd, $J = 5.3, 3.1$ Hz, 4H), 7.32 (dd, $J = 5.5, 3.2$ Hz, 4H), 7.04 (dd, $J = 5.3, 3.1$ Hz, 4H), 6.90 (dd, $J = 5.5, 3.2$ Hz, 4H), 4.80 (s, 4H), 3.80–3.60 (m, 4H), 1.61 (s, 12H), 1.55–1.11 (m, 12H), 0.88 (d, $J = 7.0$ Hz, 12H). $^{31}\text{P}\{^1\text{H}\}$ (203 MHz, CD_2Cl_2 , δ) 169.4 (s, $25\text{ }^\circ\text{C}$, $\Delta\nu_{1/2} = 1250$ Hz; $-30\text{ }^\circ\text{C}$, $\Delta\nu_{1/2} = 125$ Hz).

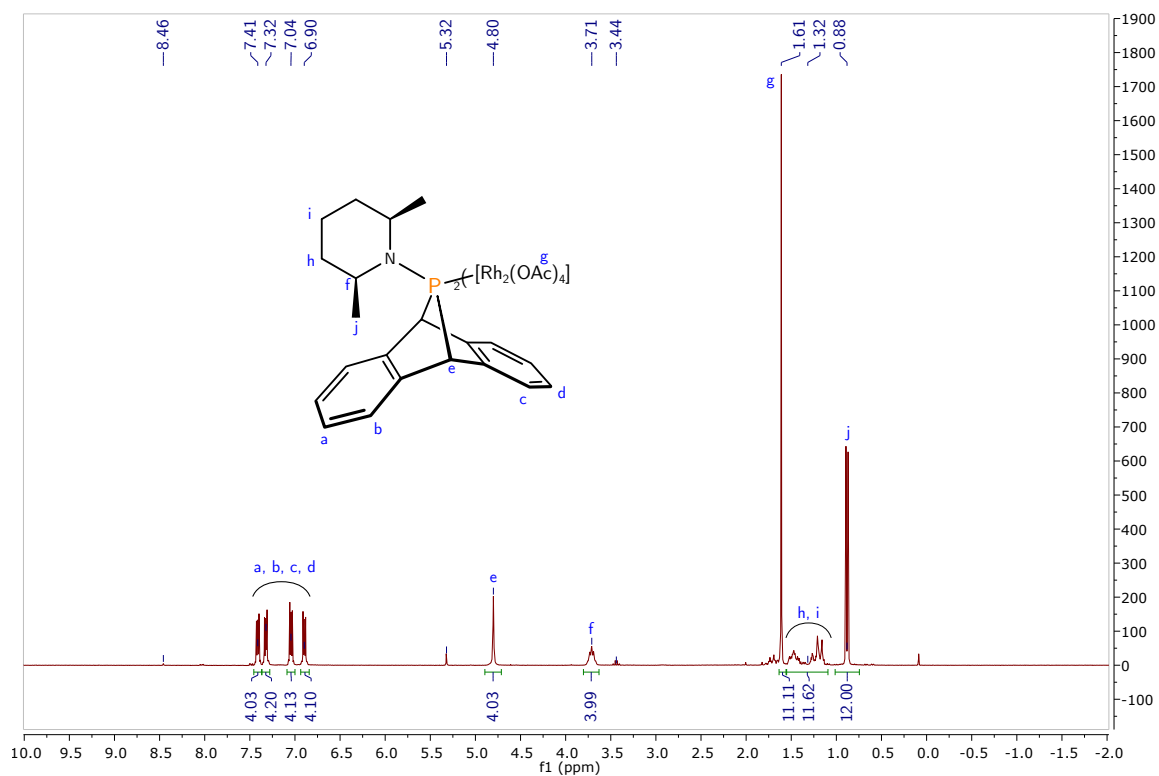


Figure A.16 ^1H NMR spectrum of $\text{Rh}_2(\text{OAc})_4(\text{Me}_2\text{pipPA})_2$ in CD_2Cl_2 at $25\text{ }^\circ\text{C}$, recorded at 300 MHz.

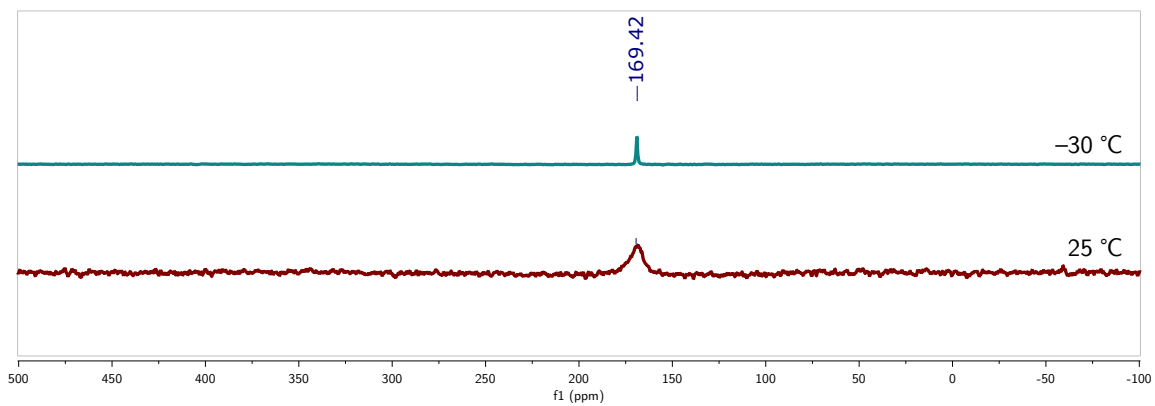


Figure A.17 $^{31}\text{P}\{^1\text{H}\}$ NMR spectrum of $\text{Rh}_2(\text{OAc})_4(\text{Me}_2\text{pipPA})_2$ in CD_2Cl_2 recorded at 203 MHz and at $-30\text{ }^\circ\text{C}$ (top) and $25\text{ }^\circ\text{C}$ (bottom), respectively.

A.4.10 Stability of $\text{Rh}_2(\text{OAc})_4(\text{Me}_2\text{pipPA})_2$ in solution at 25 °C.

$\text{Rh}_2(\text{OAc})_4(\text{Me}_2\text{pipPA})_2$ (14 mg, 0.012 mmol) was weighed into a vial, dissolved in CD_2Cl_2 and transferred to an NMR tube. The sample was analyzed by ^1H after 0, 24, and 36 h at ca. 23 °C showing an approximate ratio of 56:44 of anthracene to the bridgehead protons of $\text{Rh}_2(\text{OAc})_4(\text{Me}_2\text{pipPA})_2$ at the final time point. Analysis by $^{31}\text{P}\{^1\text{H}\}$ NMR spectroscopy after the first time point resulted in no observable signals, attributed to decreasing concentration of $\text{Rh}_2(\text{OAc})_4(\text{Me}_2\text{pipPA})_2$ and its broad line width (Section A.4.9).

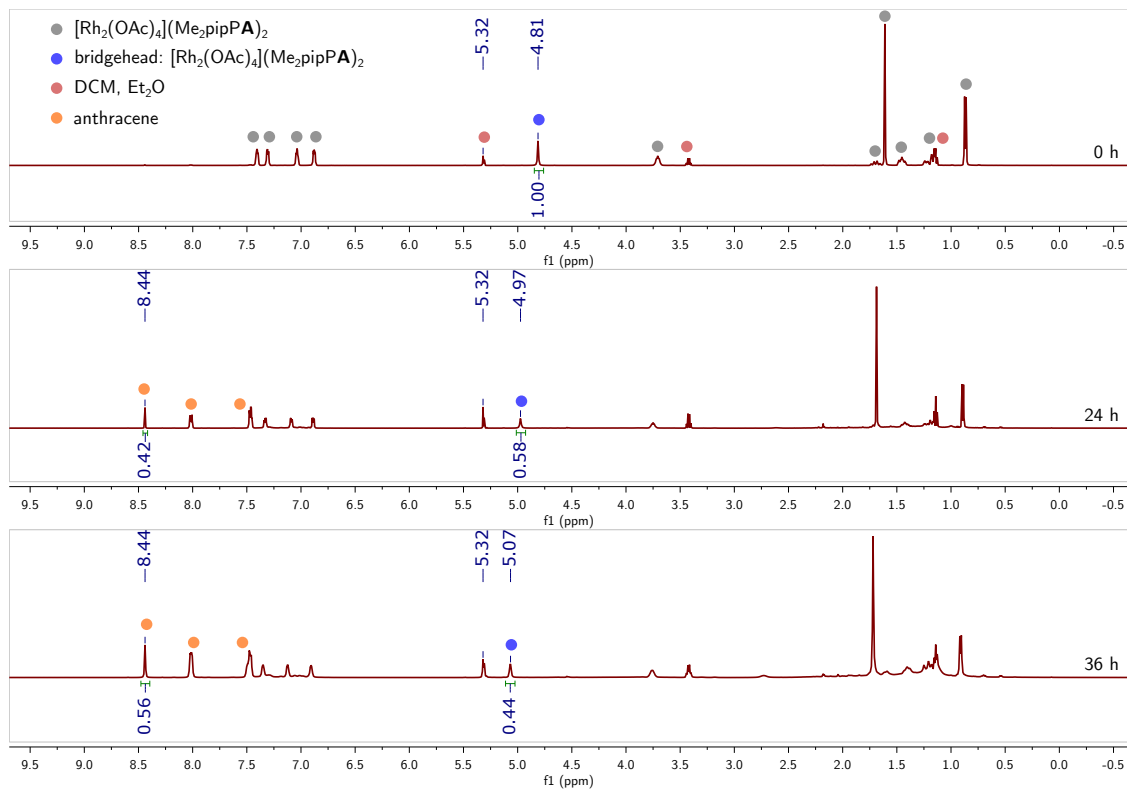


Figure A.18 Stack of $^{31}\text{P}\{^1\text{H}\}$ NMR spectra acquired of $\text{Rh}_2(\text{OAc})_4(\text{Me}_2\text{pipPA})_2$ at 0, 24, and 36 h at 23 °C in CD_2Cl_2 , recorded at 203 MHz and 25 °C.

A.4.11 Preparation of (dba)Pd(phosphirane)₂

In the glovebox, Pd(dba)₂ (249 mg, 0.43 mmol, 1 equiv) was weighed into a vial then toluene (3 mL) was added. Phosphirane **1** (250 mg, 1.3 mmol, 3 equiv) was added to the solution. The mixture was stirred for 3 h then concentrated to ca. 1 mL. Pentane (10 mL) was added, resulting in the formation of a yellow precipitate which was broken up with a spatula then stirred vigorously for 30 minutes. The solids were collected on a frit (fine porosity, 15 mL) and washed with pentane (4 × 5 mL). The material was collected in a pre-weighed vial and brought to constant mass under reduced pressure to give (dba)Pd(phosphirane)₂ as a yellow solid (288 mg, 0.397 mmol, 92% based on Pd(dba)₂). Anal. Calcd for C₄₁H₄₈OP₂Pd: C, 67.91; H, 6.67; N, 0.00. Found: C, 67.82; H, 6.96; N, ≤0.02. ¹H NMR (500 MHz, C₆D₆, δ) 8.0–7.73 (m, 1H), 7.55–6.46 (m, 17H), 5.73–4.62 (m, 4H), 2.35 (m, 2H), 1.68–1.07 (m, 4H), 1.03–0.01 (m, 15H). ¹³C NMR (126 MHz, C₆D₆, δ) 125.82, 125.66, 28.01, 27.58, 26.97. ³¹P{¹H} NMR (203 MHz, CD₂Cl₂, δ) –101.63, –102.24, –103.62, –104.14, –106.09, –107.05, –108.18, –112.38, –164.68. *Note:* The NMR spectra of (dba)Pd(phosphirane)₂ recorded in C₆D₆ at 25 °C display a broad signals, presumably a result of exchange between multiple species in solution. In general, the ¹H NMR spectrum contains resonances in the expected regions, totaling the anticipated integration values. The ³¹P{¹H} NMR spectrum shows a number of species around the –100 ppm region, assigned to Pd-coordinated phosphirane and some free phosphirane at –164.68. The ¹³C NMR spectrum displays extremely poor signal to noise, with only a handful observed resonances. Nonetheless, it has been included for completeness.

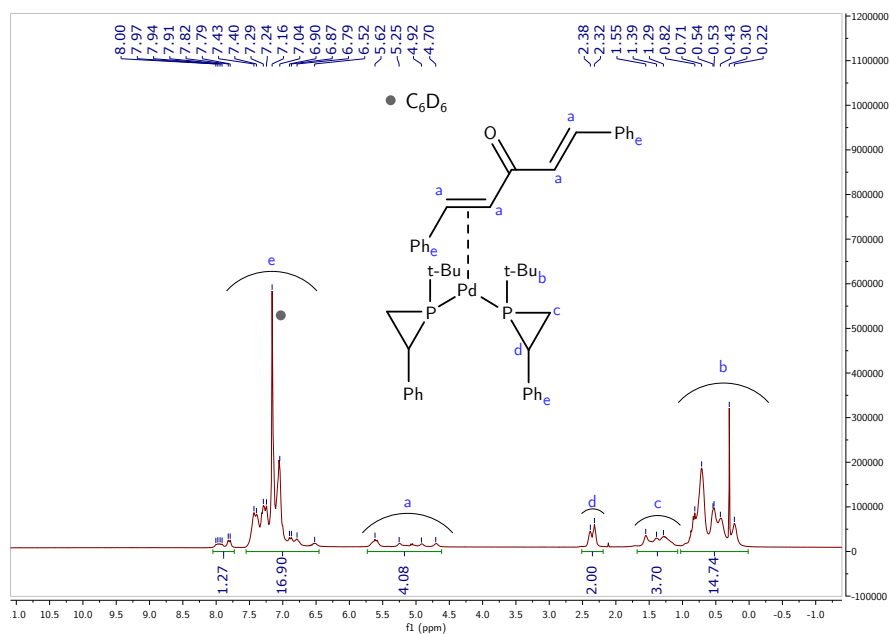


Figure A.19 ¹H NMR spectrum of (dba)Pd(phosphirane)₂ in C₆D₆ at 25 °C, recorded at 500 MHz.

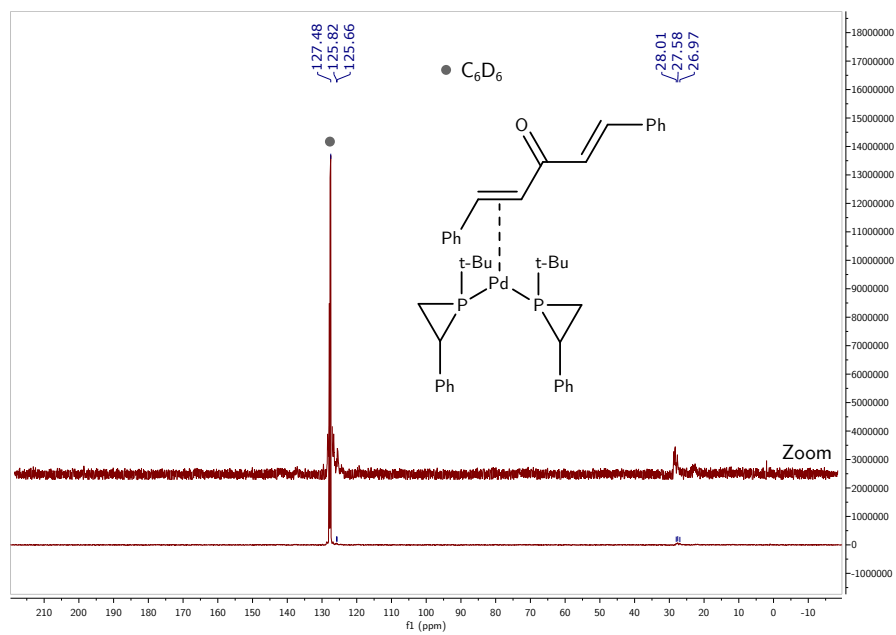


Figure A.20 ¹³C{¹H} NMR spectrum of (dba)Pd(phosphirane)₂ in C₆D₆ at 25 °C, recorded at 126 MHz.

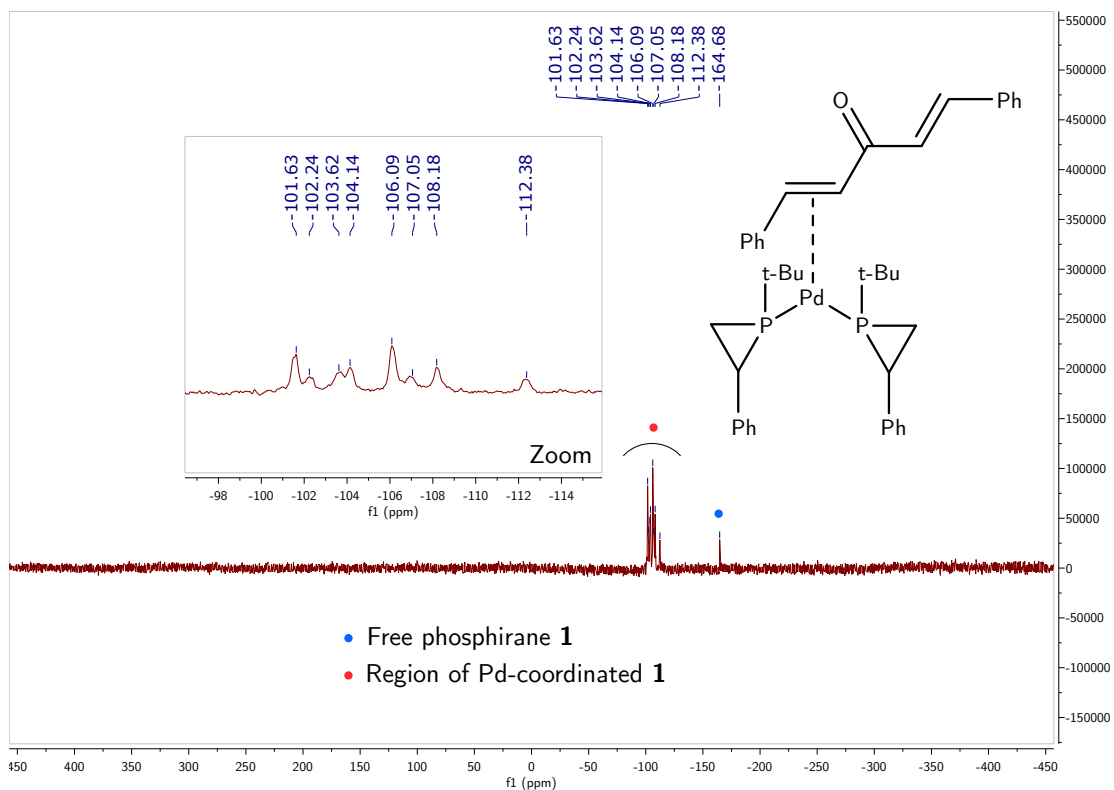


Figure A.21 $^{31}\text{P}\{^1\text{H}\}$ NMR spectrum (inset: ^{31}P NMR spectrum) of $(\text{dba})\text{Pd}(\text{phosphirane})_2$ in C_6D_6 at $25\text{ }^\circ\text{C}$, recorded at 203 MHz. See section A.4.11 for discussion on the poor signal to noise of this NMR spectrum.

A.4.12 Preliminary synthesis of **3** from K[Fp] and *t*-BuPCl₂.

In the glovebox, *t*-BuPCl₂ (159 mg, 1.0 mmol, 1 equiv) and K[Fp] (216 mg, 1.0 mmol, 1 equiv) were weighed into separate vials, to which hexanes (6 mL) was each added. The vials were placed in the glovebox freezer until the solvent had frozen. Upon thawing, the solution of *t*-BuPCl₂ was added to a thawing slurry of K[Fp] over the course of one minute. The solution was stirred for 3 h at room temperature then filtered through diatomaceous earth to give a deep red solution. Volatile material was removed from the filtrate under reduced pressure and the resulting oil was analyzed in DCM. The oil had a mass of 60 mg, which if pure product would give a yield of 21% (0.2 mmol). ³¹P{¹H} (202 MHz, DCM, δ) 269.3 (s).

The crude product was taken up in dichloromethane (ca. 5 mL) to give a deep red solution which was filtered through glass microfiber paper in a Pasteur pipette. A solution of TMAF (15 mg, 0.16 mmol, 0.8 equiv) in DCM (5 mL) was prepared. Both solutions were frozen in the glovebox coldwell. Upon thawing, the solution of TMAF was added to the solution of FpP(*t*-Bu)Cl to give a deep red homogeneous solution. Over the course of five minutes, a large amount of precipitate formed. The solution was filtered through glass microfiber filter paper in a Pasteur pipette and analyzed by ³¹P and ¹⁹F NMR spectroscopy. Attempts to crystallize the product from a concentrated pentane solution at -35 °C provided a brown oil. ³¹P{¹H} (202 MHz, DCM, δ) 370.1 (d, *J*_{P-F} = 823.9 Hz). ¹⁹F{¹H} (471 MHz, DCM, δ) -202.6 (d, *J*_{P-F} = 824.1 Hz).

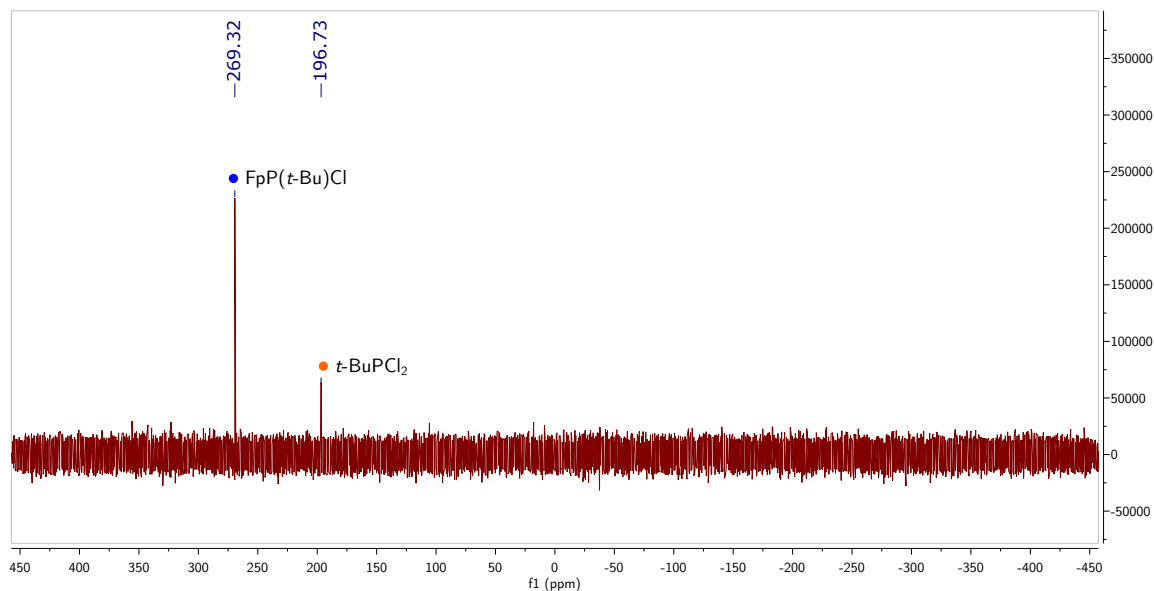


Figure A.22 ³¹P{¹H} NMR spectrum of FpP(*t*-Bu)Cl in DCM at 25 °C, recorded at 203 MHz.

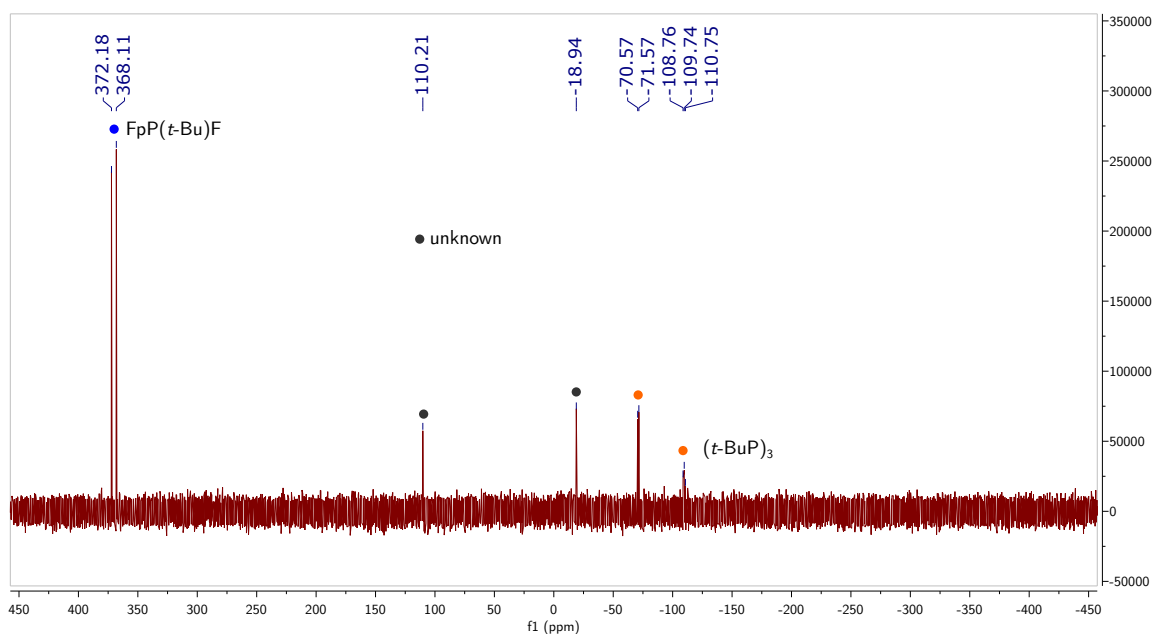


Figure A.23 $^{31}\text{P}\{^1\text{H}\}$ NMR spectrum of $\text{FpP}(t\text{-Bu})\text{F}$ in DCM at $25\text{ }^\circ\text{C}$, recorded at 203 MHz .

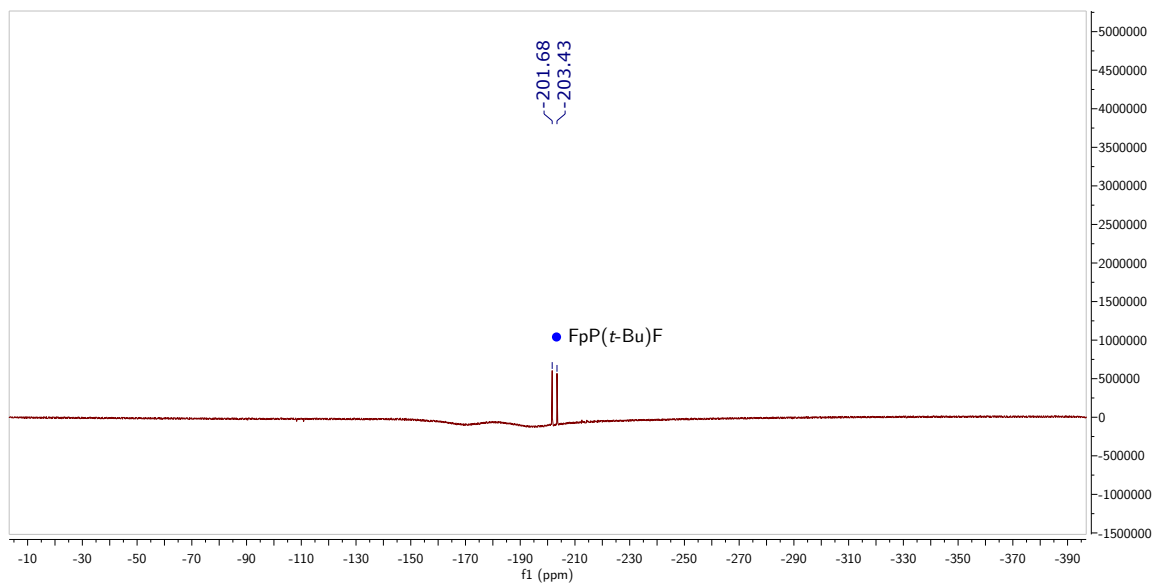


Figure A.24 $^{19}\text{F}\{^1\text{H}\}$ NMR spectrum of $\text{FpP}(t\text{-Bu})\text{F}$ in DCM at $25\text{ }^\circ\text{C}$, recorded at 471 MHz .

A.4.13 X-ray crystallography

Single crystals suitable for X-ray diffraction were transferred from the glovebox under Paratone oil onto a microscope slide. A crystal was selected under a microscope and mounted in hydrocarbon oil on a nylon loop. Low-temperature (100 K) data were collected on a Bruker-AXS X8 Kappa Duo diffractometer coupled to a Smart Apex2 CCD detector with Mo K α radiation ($\lambda = 0.71073 \text{ \AA}$) with ϕ - and ω -scans. A semi-empirical absorption correction was applied to the diffraction data using SADABS^{27,28} unless otherwise stated. The structure was solved by direct methods using SHELXT^{29,30} and refined against F^2 on all data by full-matrix least squares with ShelXle.³¹ All non-hydrogen atoms were refined anisotropically. All hydrogen atoms were included in the model at geometrically calculated positions and refined using a riding model. The isotropic displacement parameters of all hydrogen atoms were fixed to 1.2 times the U_{eq} value of the atoms they are linked to (1.5 times for methyl groups).

A.4.13.1 X-ray structure of $\text{Rh}_2(\text{OAc})_4(\text{Me}_2\text{pipPA})_2$

The refinement proceeded by first refining isotropically, then anisotropically. Hydrogen atoms were included using the relevant HFIX commands and the weighting scheme adjusted to give the final model.

A.4.13.2 X-ray structure of $(\text{depe})\text{Pt}(\text{P}(\text{A})\text{NTMS})\text{Cl}$

The model was first refined isotropically and the atoms comprising the HMDSPA fragment were refined anisotropically. Disorder in the $[\text{Pt}(\text{depe})]$ fragment (50:50) was modeled as a two part disorder. Chemically equivalent Pt–P, P–C, and C–C bond lengths were constrained to be the same as each other using the SADI command. Ellipsoid shapes were restrained on the entire structure using the SIMU and RIGU commands. The solvent THF molecule lies on a crystallographic inversion center and the disorder was thus treated in PART –1 and PART –2 with 50% occupancy each. Chemically equivalent C–O and C–C bonds were constrained (using DFIX) to 1.43 and 1.54 \AA , respectively. Chemically equivalent bond angles were restrained to be the same using the SADI command on distances of atoms two bonds apart. The model was refined anisotropically and the weighting scheme adjusted.

A.4.13.3 X-ray structure of $(\text{dba})\text{Pd}(\text{phosphirane})_2$

$(\text{dba})\text{Pd}(\text{phosphirane})_2$ was dissolved in toluene to give a yellow solution which was filtered through microfiber filter paper in a Pasteur pipette. The solution was carefully layered with hexanes and the mixture placed in the glovebox freezer at $-35 \text{ }^\circ\text{C}$ to yield yellow plates. The structure was first refined isotropically, then anisotropically. Positions of hydrogen atoms were generated using the HFIX command. The crystal suffered from merohedral

CSD identification code	N/A
Reciprocal net code	P8_19105
Empirical formula	$C_{52}H_{64}Cl_4N_2O_8P_2Rh_2$
Formula weight	1254.61 g/mol
Color / morphology	orange / block
Temperature	273(2) K
Wavelength	0.71073 Å
Crystal system	Triclinic
Space group	$P-1$
Unit cell dimensions	$a = 11.7985(10)$ Å $\alpha = 113.529(2)^\circ$ $b = 11.8924(11)$ Å $\beta = 99.441(2)^\circ$ $c = 12.3443(12)$ Å $\gamma = 111.717(2)^\circ$
Volume	1373.0(2) Å ³
Z	1
Density (calculated)	1.517 g/cm ³
Absorption coefficient	0.907 mm ⁻¹
$F(000)$	642
Crystal size	0.200 × 0.200 × 0.170 mm ³
Theta ranges for data collection	1.933 to 30.616°
Index ranges	$-16 \leq h \leq 16$, $-17 \leq k \leq 17$, $-17 \leq l \leq 17$
Reflections collected	81665
Independent reflections	8428 [$R_{\text{int}} = 0.0193$]
Completeness to $\theta = 25.242^\circ$	100.0%
Absorption correction	None
Max. and min. transmission	0.5191 and 0.5615
Refinement method	Full-matrix least-squares on F^2
Data / restraints / parameters	8428 / 0 / 320
Goodness-of-fit on F^2	1.039
Final R indices [$I > 2\sigma(I)$]	$R_1 = 0.0193$, $wR_2 = 0.0486$
R indices (all data)	$R_1 = 0.0208$, $wR_2 = 0.0496$
Extinction coefficient	n/a
Largest diff. peak and hole	0.623 and -0.559 e·Å ⁻³

Table A.3 X-ray crystallographic information for $Rh_2(OAc)_4(Me_2pipPA)_2$.

CSD identification code	N/A
Reciprocal net code	X8_16173
Empirical formula	C ₂₉ H ₄₇ Cl ₁ N ₁ O _{0.5} P ₃ Pt ₁ Si ₁
Formula weight	769.21 g/mol
Color / morphology	colorless / block
Temperature	100(2) K
Wavelength	0.71073 Å
Crystal system	Monoclinic
Space group	<i>P</i> 2 ₁ / <i>c</i>
Unit cell dimensions	<i>a</i> = 10.4307(9) Å α = 90° <i>b</i> = 21.129(2) Å β = 90.716(3)° <i>c</i> = 14.5912(13) Å γ = 90°
Volume	3215.6(5) Å ³
<i>Z</i>	4
Density (calculated)	1.589 g/cm ³
Absorption coefficient	4.654 mm ⁻¹
<i>F</i> (000)	1544
Crystal size	0.140 × 0.083 × 0.053 mm ³
Theta ranges for data collection	1.696 to 33.145°
Index ranges	-16 ≤ <i>h</i> ≤ 16, -32 ≤ <i>k</i> ≤ 32, -11 ≤ <i>l</i> ≤ 11
Reflections collected	94958
Independent reflections	12212 [<i>R</i> _{int} = 0.0494]
Completeness to $\theta = 25.242^\circ$	100.0%
Absorption correction	Semi-empirical from equivalents
Max. and min. transmission	0.6524 and 0.7465
Refinement method	Full-matrix least-squares on <i>F</i> ²
Data / restraints / parameters	12214 / 1162 / 510
Goodness-of-fit on <i>F</i> ²	1.038
Final <i>R</i> indices [<i>I</i> > 2σ(<i>I</i>)]	<i>R</i> ₁ = 0.0286, <i>wR</i> ₂ = 0.0600
<i>R</i> indices (all data)	<i>R</i> ₁ = 0.0426, <i>wR</i> ₂ = 0.0648
Extinction coefficient	n/a
Largest diff. peak and hole	2.640 and -1.074 e·Å ⁻³

Table A.4 X-ray crystallographic information for (depe)Pt(P(**A**)NTMS)Cl.

twinning, which was determined using TwinRotMat in PLATON.³² The weighting scheme was adjusted and the model considered complete.

CSD identification code	1936451
Reciprocal net code	X8_19033
Empirical formula	C ₄₁ H ₄₈ OP ₂ Pd
Formula weight	725.13 g/mol
Color / morphology	yellow / plate
Temperature	100(2) K
Wavelength	0.71073 Å
Crystal system	Tetragonal
Space group	<i>P</i> 4 ₃
Unit cell dimensions	$a = 9.3321(7)$ Å $\alpha = 90^\circ$ $b = 9.332$ Å $\beta = 90^\circ$ $c = 41.546(3)$ Å $\gamma = 90^\circ$
Volume	3618.1(6) Å ³
<i>Z</i>	4
Density (calculated)	1.331 g/cm ³
Absorption coefficient	0.632 mm ⁻¹
<i>F</i> (000)	1512
Crystal size	0.88 × 0.087 × 0.054 mm ³
Theta ranges for data collection	0.980 to 28.056°
Index ranges	-12 ≤ <i>h</i> ≤ 12, -12 ≤ <i>k</i> ≤ 12, -54 ≤ <i>l</i> ≤ 54
Reflections collected	200445
Independent reflections	8759 [<i>R</i> _{int} = 0.1060]
Completeness to $\theta = 25.242^\circ$	100.0%
Absorption correction	None
Max. and min. transmission	0.7456 and 0.6586
Refinement method	Full-matrix least-squares on <i>F</i> ²
Data / restraints / parameters	8759 / 1 / 413
Goodness-of-fit on <i>F</i> ²	1.075
Final <i>R</i> indices [<i>I</i> > 2σ(<i>I</i>)]	<i>R</i> ₁ = 0.0359, <i>wR</i> ₂ = 0.0790
<i>R</i> indices (all data)	<i>R</i> ₁ = 0.0388, <i>wR</i> ₂ = 0.0800
Absolute structure parameter	0.009(9)
Extinction coefficient	n/a
Largest diff. peak and hole	0.434 and -0.765 e·Å ⁻³

Table A.5 X-ray crystallographic information for (dba)Pd(phosphirane)₂.

References

- [1] Nishibayashi, Y., Ed. *Transition Metal-Dinitrogen Complexes: Preparation and Reactivity*; Wiley: Weinheim, Germany, 2019.
- [2] Schäfer, H.; Binder, D.; Fenske, D. *Angew. Chem., Int. Ed.* **1985**, *24*, 522–524.
- [3] Drance, M. J.; Sears, J. D.; Mrse, A. M.; Moore, C. E.; Rheingold, A. L.; Neidig, M. L.; Figueroa, J. S. *Science* **2019**, *363*, 1203–1205.
- [4] Scherer, O. J.; Walter, R.; Sheldrick, W. S. *Angew. Chem., Int. Ed.* **1985**, *24*, 525–526.
- [5] Knopf, I.; Tofan, D.; Beetstra, D.; Al-Nezari, A.; Al-Bahily, K.; Cummins, C. C. *Chem. Sci.* **2017**, *8*, 1463–1468.
- [6] Geeson, M. B.; Transue, W. J.; Cummins, C. C. *J. Am. Chem. Soc.* **2019**, *141*, 13336–13340.
- [7] Szkop, K. M.; Geeson, M. B.; Stephan, D. W.; Cummins, C. C. *Chem. Sci.* **2019**, *10*, 3627–3631.
- [8] Pyykkö, P.; Atsumi, M. *Chem. Eur. J.* **2009**, *15*, 12770–12779.
- [9] Darensbourg, M. Y.; Ludwig, M.; Riordan, C. G. *Inorg. Chem.* **1989**, *28*, 1630–1634.
- [10] Melenkivitz, R.; Mindiola, D. J.; Hillhouse, G. L. *J. Am. Chem. Soc.* **2002**, *124*, 3846–3847.
- [11] Niecke, E.; Rüger, R. *Angew. Chem., Int. Ed.* **1983**, *22*, 155–156.
- [12] Velian, A.; Cummins, C. C. *J. Am. Chem. Soc.* **2012**, *134*, 13978–13981.
- [13] Waterman, R.; Hillhouse, G. L. *Organometallics* **2003**, *22*, 5182–5184.
- [14] Moser, E.; Jeanneau, E.; Mézailles, N.; Olivier-Bourbigou, H.; Breuil, P.-A. R. *Dalton Trans.* **2019**, *48*, 4101–4104, Publisher: The Royal Society of Chemistry.
- [15] Mézailles, N.; Fanwick, P. E.; Kubiak, C. P. *Organometallics* **1997**, *16*, 1526–1530.
- [16] Transue, W. J.; Velian, A.; Nava, M.; García-Iriepa, C.; Temprado, M.; Cummins, C. C. *J. Am. Chem. Soc.* **2017**, *139*, 10822–10831.
- [17] Malisch, W.; Spörl, A.; Thirase, K.; Fey, O. *Z. Naturforsch., B: J. Chem. Sci.* **1998**, *53*, 1077–1083.
- [18] Malisch, W.; Klüpfel, B.; Schumacher, D.; Nieger, M. *Journal of Organometallic Chemistry* **2002**, *661*, 95–110.
- [19] Sawadjoon, S.; Orthaber, A.; Sjöberg, P. J. R.; Eriksson, L.; Samec, J. S. M. *Organometallics* **2014**, *33*, 249–253.
- [20] (a) Burrows, A. D.; Choi, N.; McPartlin, M.; Mingos, D. P.; Tarlton, S. V.; Vilar, R. *J. Organomet. Chem.* **1999**, *573*, 313–322; (b) Marsh, R. E. *Acta Crystallogr., Sect. B: Struct. Sci.* **2004**, *60*, 252–253.
- [21] Majchrzak, M.; Kostera, S.; Kubicki, M.; Kownacki, I. *Dalton Trans.* **2013**, *42*, 15535.
- [22] Harding, B. A.; Melvin, P. R.; Dougherty, W.; Kassel, S.; Goodson, F. E. *Organometallics* **2013**, *32*, 3570–3573.
- [23] Farina, V.; Krishnan, B. *J. Am. Chem. Soc.* **1991**, *113*, 9585–9595.
- [24] Pangborn, A. B.; Giardello, M. A.; Grubbs, R. H.; Rosen, R. K.; Timmers, F. J. *Organometallics* **1996**, *15*, 1518–1520.

- [25] Williams, D. B. G.; Lawton, M. *J. Org. Chem.* **2010**, *75*, 8351–8354.
- [26] Ferrer, M.; Mounir, M.; Rossell, O.; Ruiz, E.; Maestro, M. A. *Inorg. Chem.* **2003**, *42*, 5890–5899.
- [27] Bruker, SADABS. 2008.
- [28] Krause, L.; Herbst-Irmer, R.; Sheldrick, G. M.; Stalke, D. *J. Appl. Crystallogr.* **2015**, *48*, 3–10.
- [29] Sheldrick, G. M. *Acta Crystallogr., Sect. A: Found. Adv.* **2015**, *71*, 3–8.
- [30] Sheldrick, G. M. *Acta Crystallogr., Sect. A: Found. Crystallogr.* **2008**, *64*, 112–122.
- [31] Hübschle, C. B.; Sheldrick, G. M.; Dittrich, B. *J. Appl. Crystallogr.* **2011**, *44*, 1281–1284.
- [32] Spek, A. L. (2009). *Acta Cryst.* D65, 148-155.

Appendix B

Silicon-Chlorine Bond-Functionalization of the Bis(trichlorosilyl)phosphide and Trichlorosilylsulfide Anions

Contents

B.1	Introduction	324
B.2	Results and discussion	325
B.3	Conclusion	329
B.4	Future Work	329
B.5	Experimental methods	331
	Bibliography	345

Abstract

Functionalization reactions of the silicon-chlorine bonds in the anions $[\text{P}(\text{SiCl}_3)_2]^-$ and $[\text{SSiCl}_3]^-$ that leave the E-Si (E = P, S) bond intact are described. Treatment of these anions as their respective tetra-*n*-butylammonium (TBA) salts with the appropriate stoichiometry of tetramethylammonium fluoride (TMAF) results in the formation of $[\text{P}(\text{SiF}_3)_2]^-$ and $[\text{SSiF}_3]^-$. These species were characterized by multinuclear NMR spectroscopy and in the case of $[\text{P}(\text{SiF}_3)_2]^-$, structural analysis by X-ray diffraction reveals extremely short P-Si bonds (2.1123(11) Å) and appears to be the first structurally characterized phosphorus center featuring a trifluorosilyl group. Treatment of $[\text{TBA}][\text{P}(\text{SiCl}_3)_2]$

with methyllithium results in the known compound $\text{P}(\text{TMS})_3$, while treatment of $[\text{TBA}][\text{SSiCl}_3]$ with lithium dimethylamide (2 equiv) leads to the formation of $[(\text{Me}_2\text{N})_2\text{SiS}]_2$ which was characterized by multinuclear NMR and mass spectrometry. Finally, the ability of sulfur-containing $[\text{TBA}][\text{SSiCl}_3]$, $[\text{TBA}][\text{P}(\text{SiF}_3)_2]$, and $[(\text{Me}_2\text{N})_2\text{SiS}]_2$ for converting an amide to a thioamide are compared; in the case of $[\text{TBA}][\text{SSiCl}_3]$, 1-thioacetylpyrrolidine is obtained in 98% yield (as determined by ^1H spectroscopy).

B.1 Introduction

Compounds that feature bonds between the trichlorosilyl group ($-\text{SiCl}_3$) and main-group elements have experienced a recent surge in interest, principally resulting from the development of robust procedures for their preparation. Relatively simple compounds such as the homoleptic trichlorosilyl-substituted anions of P,^{1,2} Ge,³ C,⁴⁻⁷ and Si^{3,8,9} (Chart B.1) have been described in the past five years alone. Though previously known, compounds such as the trichlorosilylsulfide anion¹⁰ or bis(trichlorosilyl)ethylene¹¹⁻¹³ have been the subject of improved preparative procedures^{2,7} allowing access to synthetically useful quantities of these substances.

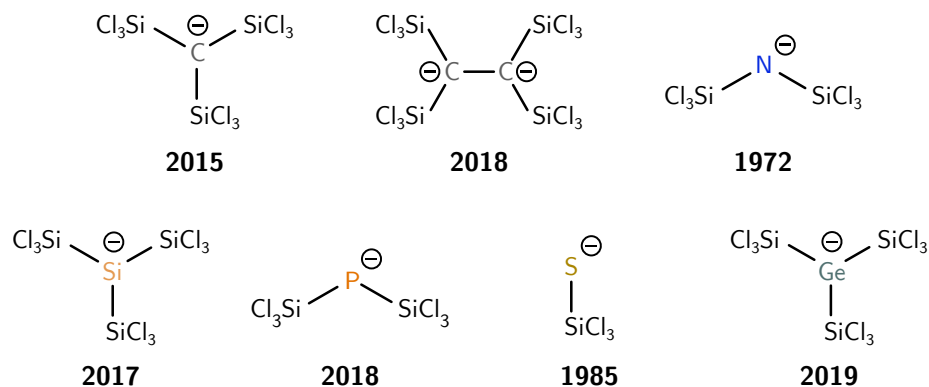


Chart B.1 Homoleptic trichlorosilyl-substituted main-group anions and the years of their discovery. Counter cations have been omitted for clarity.

The applications of trichlorosilyl-substituted main-group compounds in chemical synthesis are also growing in number. In the case of phosphorus, $[\text{TBA}][\text{P}(\text{SiCl}_3)_2]$ can be used to prepare organophosphorus compounds by reaction with an unactivated alkyl chloride. In the case of sulfur, $[\text{TBA}][\text{SSiCl}_3]$ can be used as a thionation reagent, for example in the preparation of benzyl mercaptan. Wagner and co-workers have prepared a set of exhaustively trichlorosilylated C_1 and C_2 compounds that can be used as building blocks for silicones and silsesquioxanes.⁷ The germanium and silicon analogues have been touted as potential chemical vapor deposition precursors³ or as weakly-coordinating anions,⁹ respectively.

In the majority of cases, the main-group element that bears trichlorosilyl substituents has been the focus of study, and typically represents the most Lewis-basic site and thus engages with Lewis-bases or electrophiles.^{1,2} Here, we turn our attention to the reactivity of the trichlorosilyl groups and explore functionalization of the heavily featured Si–Cl bonds in these compounds. Of relevance is the reported conversion of $\text{Ge}(\text{SiCl}_3)_4$ to $\text{Ge}(\text{SiH}_3)_4$ using $\text{Li}[\text{AlH}_4]$ by Wagner and co-workers³ and a related procedure for the preparation of Si_6H_{12} .¹⁴ Central to the present work are the trichlorosilyl-supported anions of phosphorus ($[\text{TBA}][\text{P}(\text{SiCl}_3)_2]$) and sulfur ($[\text{TBA}][\text{SSiCl}_3]$), prepared by trichlorosilane reduction of phosphate and sulfate, respectively.

B.2 Results and discussion

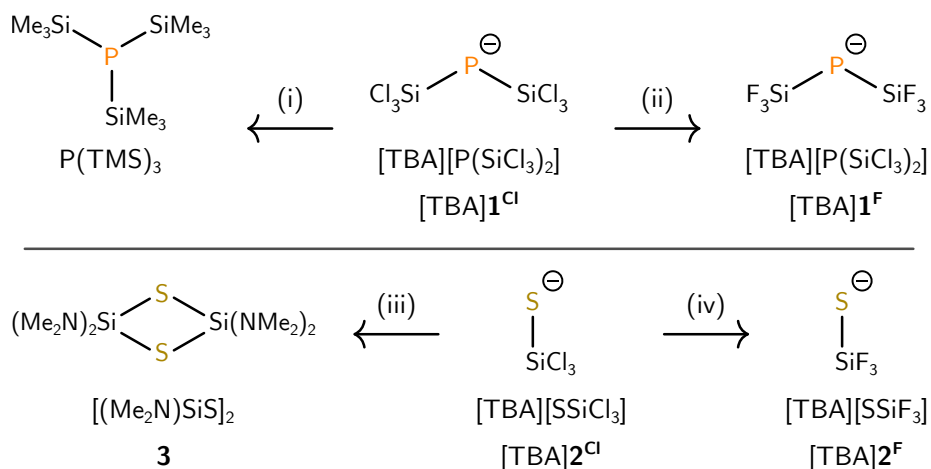


Figure B.1 Functionalization of $[\text{TBA}][\text{P}(\text{SiCl}_3)_2]$ and $[\text{TBA}][\text{SSiCl}_3]$ leading to the other compounds described in this work. Conditions: (i) MeLi (3.0 M in Et_2O , 7 equiv), THF; (ii) TMAF (6.5 equiv), DCM; (iii) LiNMe_2 (2 equiv), THF; (iv) TMAF (3 equiv), DCM.

Our studies began with exploring the substitution of chloride for fluoride at silicon. Treatment of $[\text{TBA}][\text{P}(\text{SiCl}_3)_2]$ with a single equivalent of tetramethylammonium fluoride (TMAF) led to the formation of a statistical mixture of bis(silyl)phosphide anions $[\text{P}(\text{SiF}_n\text{Cl}_{n-3})_2]$ ($n = 0-3$), with almost all of the possible permutations observable in the same ^{19}F NMR spectrum (Figure B.6). All of the fluoride resonances were observed as doublets, arising from coupling to the ^{31}P nuclei. Treatment of $[\text{TBA}][\text{P}(\text{SiCl}_3)_2]$ with a slight excess (6.5 equiv) of the required stoichiometry for complete exchange of chloride to fluoride groups resulted in the clean formation $[\text{TBA}][\text{P}(\text{SiF}_3)_2]$. The ^{31}P NMR spectrum features a binomial septet ($J_{\text{P-Si}} = 40.7$ Hz) centered with at the highly upfield chemical shift of -408.3 ppm. In the ^{19}F NMR spectrum, the corresponding doublet is observed along with ^{29}Si satellites ($J_{\text{Si-F}} = 325.3$ Hz). Turning to the sulfur analog, treatment

Table B.1 Selected calculated properties for the E–Si (E = P, S) bonds in $[\text{P}(\text{SiCl}_3)_2]^-$, $[\text{P}(\text{SiF}_3)_2]^-$, $[\text{SSiCl}_3]^-$, and $[\text{SSiF}_3]^-$.

species	\AA^a	NBO ^b	orbital character (%)				total (%)		NRT ^c (%)
			s _E	p _E	s _{Si}	p _{Si}	E	Si	
$[\text{P}(\text{SiCl}_3)_2]^-$	2.15	1.33	9	45	18	27	55	45	21
$[\text{P}(\text{SiF}_3)_2]^-$	2.14	1.41	9	50	17	22	60	40	10
$[\text{SSiCl}_3]^-$	1.99	1.46	16	47	14	22	64	36	45
$[\text{SSiF}_3]^-$	1.99	1.65	14	52	13	19	67	33	29

^a E–Si bond length, calculated at the $\omega\text{B97x-D3/def2-TZVPP/CPCM(DCM)}$ level of theory

^b Natural bond order of E–Si bond

^c Determined by Natural Resonance Theory analysis; “classic” Lewis structure with formal negative charge located on “E”

of $[\text{TBA}][\text{SSiCl}_3]$ with TMAF (3 equiv) in DCM led to the formation of one new species by ^{19}F NMR spectroscopy with a resonance at -121.9 ppm and displaying ^{29}Si satellites ($J_{\text{Si-F}} = 275.9$ Hz).

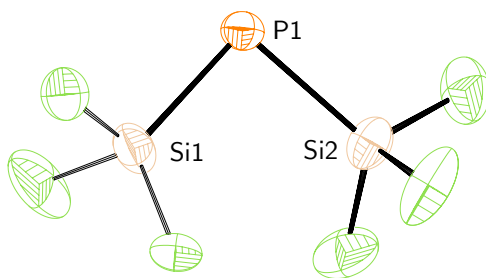


Figure B.2 Molecular structure of $[\text{TBA}][\text{P}(\text{SiF}_3)_2]$ with ellipsoids set at the 50% probability level. The TBA cation and rotational disorder around the P–Si1 bond are omitted for clarity. Selected bond metrics (\AA , $^\circ$): P1–Si1: 2.1149(8), P1–Si2: 2.1297(8), Si1–P1–Si2: 93.62(3).

Diffusion of diethyl ether into a concentrated DCM solution of $[\text{TBA}][\text{P}(\text{SiF}_3)_2]$ produced single crystals suitable for structural analysis by an X-ray diffraction study (Figure B.2). Compounds bearing P–SiF₃ groups are not common, with $\text{P}(\text{SiF}_3)_3$ ¹⁵ and $\text{H}_2\text{P}(\text{SiF}_3)$ ¹⁶ representing two well characterized examples, and as such, $[\text{TBA}][\text{P}(\text{SiF}_3)_2]$ appears to be the first structurally characterized compound bearing a P–SiF₃ group. The P–Si bonds are remarkably short with an average length of 2.1123(11) \AA : for reference the sum of the covalent radii is 2.27 \AA . The bond angle at phosphorus is 93.62(3) $^\circ$, indicating that phosphorus forms its bonds to silicon with a high degree of p orbital character.

This bonding picture is supported by analysis within the framework of Natural Bond orbital (NBO) theory^{17,18} which shows that the P–Si bonds in $[\text{P}(\text{SiF}_3)_2]^-$ are composed of 50% p orbital character, the highest for any of the anions studied using this procedure (Table B.1). Further analysis of $[\text{P}(\text{SiF}_3)_2]^-$ by Natural Resonance Theory within the NBO

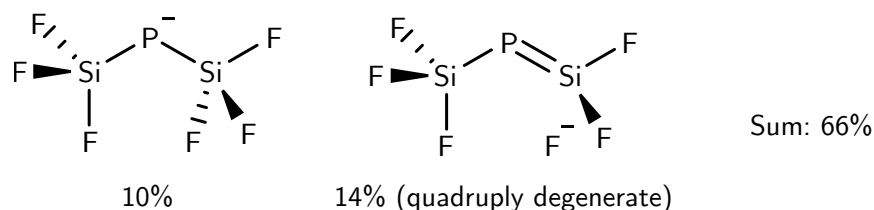


Figure B.3 Leading natural resonance structures for $[\text{P}(\text{SiF}_3)_2]^-$ as determined by the Natural Bond Orbital (NBO) method.

module shows the classical Lewis structure in which phosphorus carries the formal negative charge represents only a 10% contribution to the total. The lead structures (quadruply degenerate at 14% each) feature a $\text{P}=\text{Si}$ double bond and the formal negative charge localized on a fluoride that lies out of the plane defined by the $\text{Si}-\text{P}-\text{Si}$ angle. Overall, the $\text{P}-\text{Si}$ bond order is calculated to be 1.41, which is slightly higher than the case for $[\text{P}(\text{SiCl}_3)_2]^-$ at 1.33. Analyzed similarly, the natural bond order for $[\text{SSiF}_3]^-$ is 1.65, the highest for the anions studied, and features a reasonably ionic bond with S contributing two thirds of the shared electron density in the $\text{Si}-\text{S}$ bond. In general, the short $\text{E}-\text{Si}$ bond lengths can be attributed to the large amount of s character that Si uses to form these bonds, reserving much of its p character for $\text{Si}-\text{X}$ bonds ($\text{X} = \text{Cl}, \text{F}$), in accordance with Bent's rule.²

Methods for incorporating $-\text{SiCl}_3$ groups to form the anions presented in Chart B.1 generally require conditions that can, at least formally, generate the trichlorosilyl anion.^{8,19,20} This can be accomplished by either²¹ (i) the use of trichlorosilane with an appropriate base^{14,22-24} or (ii) treatment of Si_2Cl_6 with chloride to generate SiCl_4 and $[\text{SiCl}_3]^-$.²⁵ For the introduction of SiF_4 groups, exchange of SiCl_3 for SiF_3 using a fluoride source such as TMAF appears to be a good strategy because other methods require the use of SiF_4 which is a toxic gas. In addition to TMAF, AgBF_4 was shown to be capable at converting $-\text{SiCl}_3$ to $-\text{SiF}_3$ groups in a trichlorosilyl(nickel) species,²⁶ however, in our hands, this method was unsuitable for the preparation of $[\text{TBA}][\text{P}(\text{SiF}_3)_2]$ from $[\text{TBA}][\text{P}(\text{SiCl}_3)_2]$.

Following the replacement of chloride groups with fluoride groups, we sought to investigate the addition of electron rich substituents to the silicon center. Treatment of $[\text{TBA}][\text{P}(\text{SiCl}_3)_2]$ with a diethyl ether solution of methyl lithium led to the formation of $\text{P}(\text{TMS})_3$, assayed by its characteristic resonance at -251.9 ppm (DCM) that also displays ^{29}Si satellites with $J_{\text{P}-\text{Si}} = 26.5$ Hz. The addition of a third silicon center to phosphorus is presumably a result of the increasing nucleophilicity of the phosphide anions generated as the silicon substituents acquire more electron-donating substituents. The mass balance of the phosphorus that does not end up as $\text{P}(\text{TMS})_3$ is unaccounted for at present.

Transitioning to sulfur, treatment of $[\text{TBA}][\text{SSiCl}_3]$ with lithium dimethylamide (2 equiv) led to the formation of $[(\text{Me}_2\text{N})_2\text{SiS}]_2$ and $[\text{TBA}][\text{Cl}]$. Neutral $[(\text{Me}_2\text{N})_2\text{SiS}]_2$ was extracted from the ionic byproducts using hexane and after filtration and removal of volatile

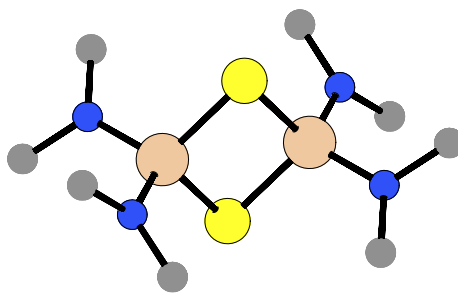


Figure B.4 DFT calculated structure of $[(\text{Me}_2\text{N})_2\text{SiS}]_2$ rendered using PLATON with hydrogen atoms omitted for clarity. Selected bond metrics (\AA , $^\circ$): S–Si: 2.15; N–Si: 1.71; Si–S–Si: 82.9; S–Si–S: 97.1. Grey: carbon; blue: nitrogen; beige: silicon; yellow: sulfur.

material it was isolated as a colorless oil, contaminated with ca. 25% tri-*n*-butylamine which presumably forms via E_2 elimination by deprotonation of the TBA cation by lithium dimethylamide. $[(\text{Me}_2\text{N})_2\text{SiS}]_2$ was characterized by ^1H and ^{29}Si NMR spectroscopy: both spectra display singlets at 2.62 and -26.7 ppm, respectively. The chemical shift of the ^{29}Si nuclei is in line with other species that can be considered the formal dimers of bis(amino)silanethiones²⁷ Further evidence for the formation of $[(\text{Me}_2\text{N})_2\text{SiS}]_2$ was provided by GC–MS analysis in which a peak for the molecular ion was observed at $m/z = 296.2$ (calcd: 296.1), and a series of peaks arising from fragmentation that correspond to loss of units corresponding to NMe_2 units. The geometry of $[(\text{Me}_2\text{N})_2\text{SiS}]_2$ was optimized using density functional theory ($\omega\text{B97X-D3/def2-TZVP/CPCM(Toluene)}$) and features a diamond-like S_2Si_2 (Figure B.4).

Next, we sought to understand how the substituent at silicon modulates reactivity of the Si–S bond by testing the ability of $[\text{TBA}][\text{SSiCl}_3]$, $[\text{TBA}][\text{SSiF}_3]$, and $[(\text{Me}_2\text{N})_2\text{SiS}]_2$ to convert an amide to a thioamide. Our interest in preparing thioamides using these reagents was piqued by a report in which a combination of elemental sulfur, trichlorosilane, and an organic base such as dimethylamino pyridine (DMAP) were able to effect this reaction at 110°C .²⁸ In this report, a form of reduced elemental sulfur ($[\text{S}]^{2-}$) was the proposed thionation agent, though the combination of these reagents hinted to us the formation of $[\text{P}(\text{SiCl}_3)_2]^-$. To test this hypothesis we set out to test $[\text{TBA}][\text{SSiCl}_3]$ as a substitute for the conditions in that report. Heating 1-acetylpyrrolidine with 3 equiv of $[\text{TBA}][\text{SSiCl}_3]$ in chlorobenzene at 110°C for 18 h gave rise to the formation of 1-acetylpyrrolidine, in 98% yield as assayed by ^1H NMR spectroscopy (Figure B.5). Comparison with $[\text{TBA}][\text{SSiF}_3]$ and $[(\text{Me}_2\text{N})_2\text{SiS}]_2$ as the thionation reagent suggests $[\text{TBA}][\text{SSiCl}_3]$ is the most active of the series, although further studies are required using spectroscopically pure $[(\text{Me}_2\text{N})_2\text{SiS}]_2$ and side-by-side analysis of the three potential reagents under the same reaction conditions (chlorobenzene, 110°C , 3 h).

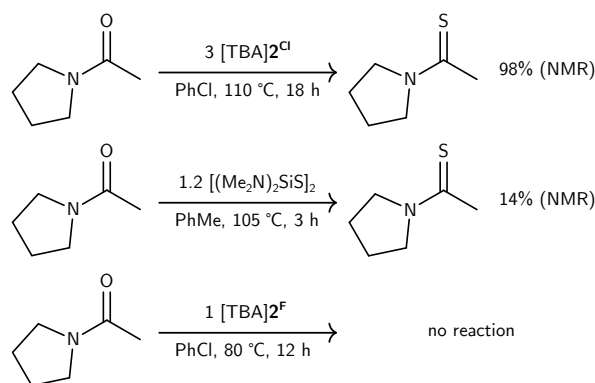


Figure B.5 Comparison of thionation ability of $[\text{TBA}][\text{P}(\text{SiCl}_3)_2]$, $[\text{TBA}][\text{P}(\text{SiF}_3)_2]$, and $[(\text{Me}_2\text{N})_2\text{SiS}]_2$ for converting 1-acetylpyrrolidine to 1-thioacetylpyrrolidine.

B.3 Conclusion

In conclusion, we demonstrate Si–Cl bonds are readily functionalized in at least two of the homoleptic trichlorosilyl-supported main-group anions. The E–Si bond remains intact, despite the use of reagents such as methyllithium, lithium dimethylamide, and the fluoride ion. These results expand the space of silyl-substituted main-group compounds, which are of interest to the fields of chemical vapor deposition and in the synthesis of silicones,⁷ organophosphorus,¹ and organosulfur² compounds.

B.4 Future Work

A number of experiments are still required in order for the work in the appendix to be published. Four of the key compounds in this regard are $[\text{TBA}][\text{P}(\text{SiF}_3)_2]$, $[\text{TBA}][\text{SSiF}_3]$, $[(\text{Me}_2\text{N})_2\text{SiS}]_2$, and $\text{P}(\text{TMS})_3$. The first three have not been described previously, and require preparative procedures to be developed, in addition to full characterization (NMR, elemental analysis). In the case of $[\text{TBA}][\text{SSiF}_3]$, structural determination by X-ray crystallography would provide bond metric data; the Si–S bond length would be of particular interest.

Although $\text{P}(\text{TMS})_3$ is a known compound, isolation and characterization are still required in order to obtain a yield for this procedure. A question arising from this reaction is related to stoichiometry; there are three silicon atoms per phosphorus in the product but only two in the starting material. A plausible explanation for this is that the phosphide center accumulates nucleophilic character as Si–Cl bonds are substituted for Si–Me bonds and that the formed phosphide is able to attack the Si–Cl bond to form the three P–Si bonds present in $\text{P}(\text{TMS})_3$. This hypothesis is related to the formation of an additional Si–S bond in $[(\text{Me}_2\text{N})_2\text{SiS}]_2$. In order to improve the synthesis of $\text{P}(\text{TMS})_3$, the addition

of trimethylsilyl chloride could be beneficial and provide the third equivalent of silicon. Control reactions to determine the rate of reaction of methyllithium with trimethylsilyl chloride would be necessary for developing such a procedure.

In terms of thionation, the three reagents [TBA][P(SiCl₃)₂], [TBA][P(SiF₃)₂], and [(Me₂N)₂SiS]₂ should be tested side-by-side for conversion of 1-acetylpyrrolidine to 1-thioacetylpyrrolidine. So far, the optimal conditions appear to be using chlorobenzene as the solvent with a reaction temperature of 110 °C and so these conditions should be used to make direct comparisons between between the three species. Functionalization of [TBA][SSiCl₃] with groups other dialkylamido groups could provide an improved reagent for thionation. The addition of nucleophiles such as DMAP could plausibly break up [(Me₂N)₂SiS]₂ into two equivalents of the DMAP-coordinated thiasilanone, on the basis of DFT calculations. The addition of TMAF, a source of fluoride, could conceivably lead to the formation of [TMA][FSi(S)(NMe₂)₂], which could also be tested as a thionation reagent.

B.5 Experimental methods

B.5.1 General methods

All manipulations were performed in a Vacuum Atmospheres model MO-40M glovebox under an inert atmosphere of purified N₂ or using standard Schlenk techniques. When reagents were removed from a stock bottle containing a Sure/Seal, the equivalent volume of dry nitrogen was injected into the bottle prior to removing the desired volume of solution with a syringe. All solvents were obtained anhydrous and oxygen-free by bubble degassing (argon) and purification by passing through columns of alumina and Q5.²⁹ Once collected, solvents were stored over activated 4 Å molecular sieves (20 wt%) inside the glovebox.³⁰ All glassware was oven-dried for at least 6 h prior to use, at temperatures greater than 150 °C.

[TBA]**1** and [TBA]**2** were prepared according to literature methods.² Tetramethylammonium fluoride (TMAF) (MilliporeSigma) was dried at 23 °C in vacuo for 12 hours prior to use. Lithium dimethylamide (MilliporeSigma) and methyllithium solution (3.0 M in Et₂O) were used as received (Millipore-Sigma). Deuterated solvents were purchased from Cambridge Isotope Labs and were degassed three times by the freeze-pump-thaw method and stored over activated 4 Å molecular sieves for 48 h in the glovebox prior to use. Diatomaceous earth (Celite 435, EM Science), 4 Å molecular sieves (Millipore-Sigma) and basic alumina (Millipore-Sigma) were dried by heating to 200 °C under dynamic vacuum for at least 48 h prior to use. The temperature of the aluminum shot used to heat reagents or reaction mixtures was measured using a Hanna Instruments K-type Thermocouple Thermometer (model HI935005).

NMR spectra were obtained on a Jeol ECZ-500 instrument equipped with an Oxford Instruments superconducting magnet, on a Bruker Avance 400 instrument equipped with a Magnex Scientific or with a SpectroSpin superconducting magnet, or on a Bruker Avance 500 instrument equipped with a Magnex Scientific or with a SpectroSpin superconducting magnet. ¹H and ¹³C NMR spectra were referenced to residual CD₂Cl₂ (¹H = 5.32 ppm, ¹³C = 54.0 ppm), C₆D₆ (¹H = 7.16 ppm, ¹³C = 128.06 ppm), CD₃CN (¹H = 1.94 ppm, ¹³C = 118.26 ppm) or CDCl₃ (¹H = 7.26 ppm, ¹³C = 77.16 ppm). ³¹P NMR spectra were referenced externally to 85% H₃PO₄ (0 ppm).

GC-MS data were collected using a nominal mass Agilent 5977B mass spectrometer detector (EI) attached to a 7890B gas chromatograph with autosampler.

B.5.2 Preparation of [TBA][P(SiF₃)₂] from **1**.

In the glovebox, [TBA]**1** (81 mg, 0.149 mmol, 1 equiv) and TMAF (90 mg, 93 mmol, 6.5 equiv) were weighed into separate vials and each dissolved in DCM (3 mL). The resulting solutions were frozen in the glovebox cold well. Upon thawing, the solution of TMAF was added to the solution of [TBA]**1** with stirring. The resulting solution was stirred for one hour then an aliquot (0.5 mL) was analyzed by ³¹P{¹H} showing formation of the desired

product. The solution was filtered to remove precipitated TMACl and volatile material was removed from the resulting filtrate to give a yellow oil. The oil was dissolved in DCM (1 mL) and passed through a piece of glass microfiber paper in a Pasteur pipette. The resulting solution was layered with diethyl ether (10 mL) and the mixture placed in the freezer overnight resulting in the formation of yellow solids and some oil. The mother liquor was removed by pipette and the solid residue was placed under dynamic vacuum for ten minutes. The material was dissolved in DCM (0.5 mL) and filtered into a shell vial (4 mL). The shell vial was placed in a scintillation vial that contained diethyl ether (10 mL). The setup was placed in the glovebox freezer resulting in the formation of crystals (colorless plates). A yield was not recorded because the obtained material was used for structural analysis by X-ray diffraction. ^1H NMR (500 MHz, DCM, δ) 3.28–3.17 (m, 8H), 1.61 (p, $J = 8.1$ Hz, 8H), 1.39 (h, $J = 7.3$ Hz, 8H), 0.98 (t, $J = 7.3$ Hz, 12H). ^{19}F NMR (471 MHz, DCM, δ) -109.3 (d, $J = 40.7$ Hz; $J_{\text{Si-F}} = 325.3$ Hz). $^{31}\text{P}\{^1\text{H}\}$ NMR (203 MHz, DCM, δ) -408.3 (sept, $J_{\text{P-F}} = 40.7$ Hz).

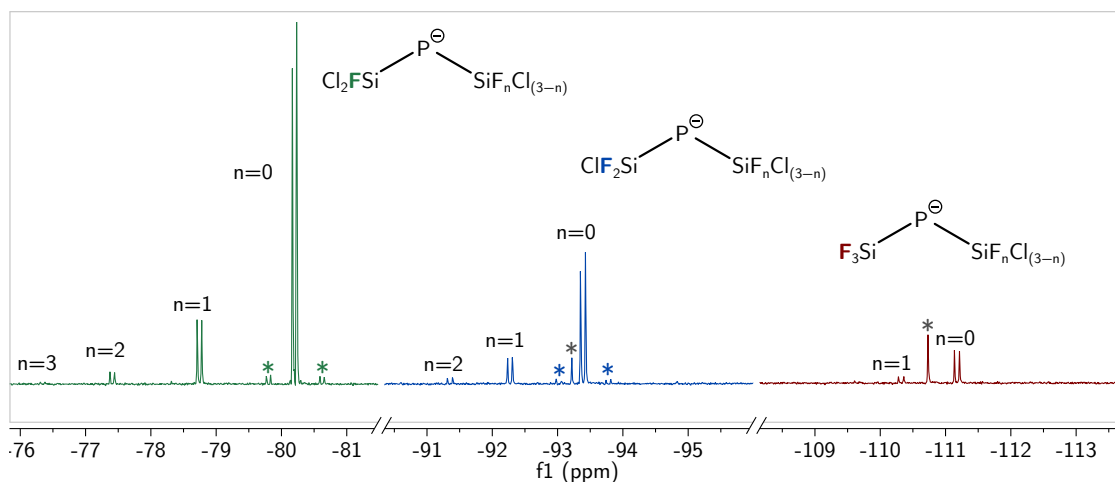


Figure B.6 ^{19}F NMR spectrum of a solution obtained when $[\text{TBA}][\text{P}(\text{SiCl}_3)_2]$ is treated with TMAF (1 equiv) in dichloromethane. Grey asterisk represents impurities, colored asterisks correspond to satellites arising from ^{29}Si nuclei (4.5% abundance, $l = 1/2$).

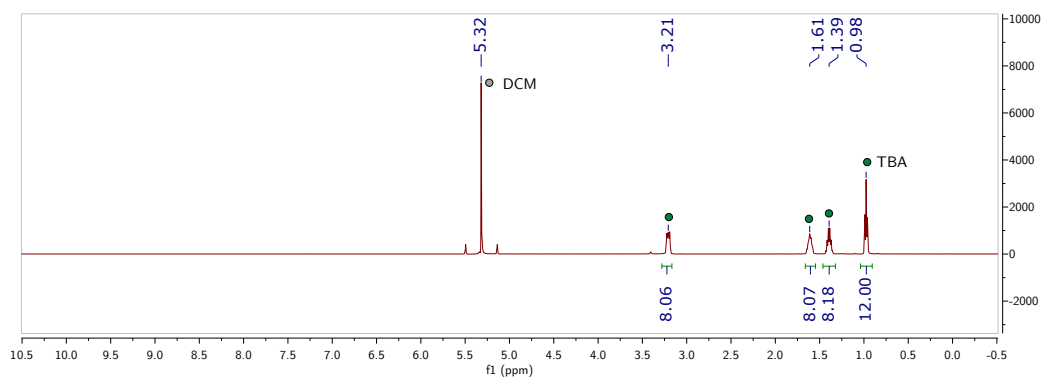


Figure B.7 ^1H NMR spectrum of $[\text{TBA}][\text{P}(\text{SiF}_3)_2]$ in DCM at $25\text{ }^\circ\text{C}$, recorded at 500 MHz .

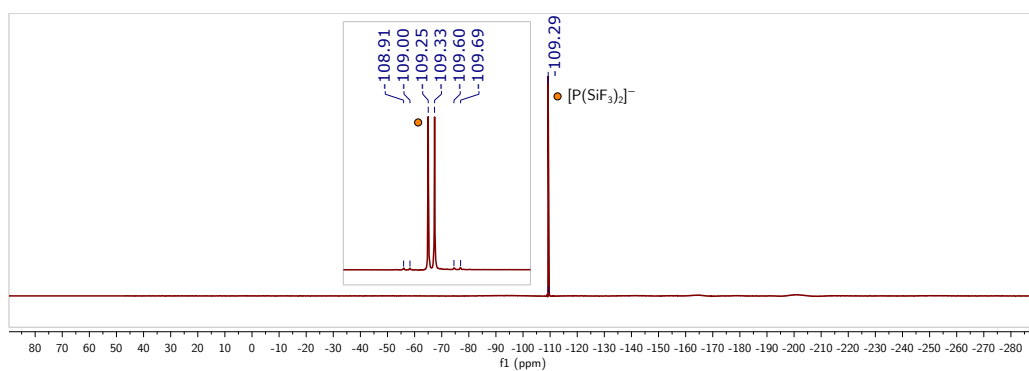


Figure B.8 ^{19}F NMR spectrum of $[\text{TBA}][\text{P}(\text{SiF}_3)_2]$ in DCM at $25\text{ }^\circ\text{C}$, recorded at 471 MHz .

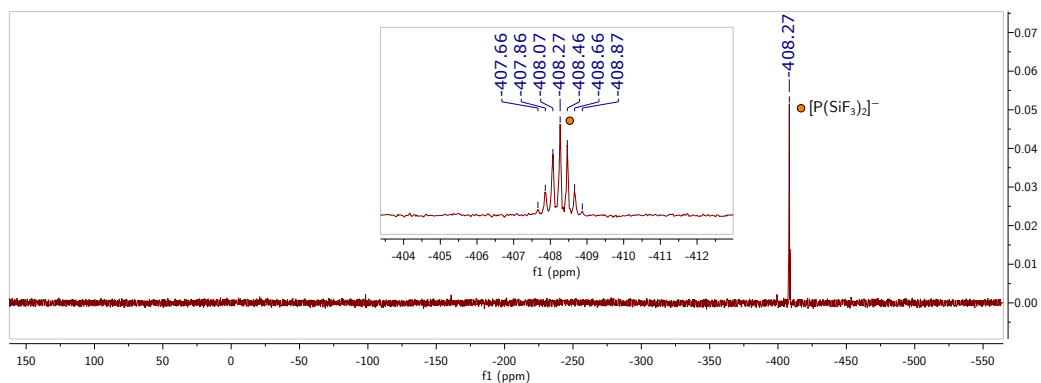


Figure B.9 $^{31}\text{P}\{^1\text{H}\}$ NMR spectrum of $[\text{TBA}][\text{P}(\text{SiF}_3)_2]$ in DCM at $25\text{ }^\circ\text{C}$, recorded at 203 MHz .

B.5.3 Observation of $\text{P}(\text{TMS})_3$ upon treatment of **1** with methyllithium.

In the glovebox, a solution of methyllithium in diethyl ether (3.0 M, 0.43 mL, 1.29 mmol, 7 equiv) was measured by syringe and transferred to a vial. [TBA]**1** was weighed into a vial and dissolved in THF (6 mL). The THF solution of [TBA]**1** was added dropwise to the solution of methyllithium. The solution took on a slight yellow color, which developed into an orange color after stirring for 24 h. After this time the solution was concentrated to ca. 1 mL and analyzed by ^{31}P NMR spectroscopy which displayed a major product at -251.9 ppm, consistent with the literature value for $\text{P}(\text{TMS})_3$ of -251 . The resonance in the recorded spectrum displays silicon satellites with a $J_{\text{P-Si}}$ value of 26.5 Hz which integrate to 15.9% of the resonance, consistent with the presence of three silicon atoms bonded to phosphorus (calcd: 14.6%). A yield or further characterization data was not obtained for $\text{P}(\text{TMS})_3$. $^{31}\text{P}\{^1\text{H}\}$ NMR (162 MHz, DCM, δ) -251.9 (s, $J_{\text{Si-F}} = 26.5$ Hz).

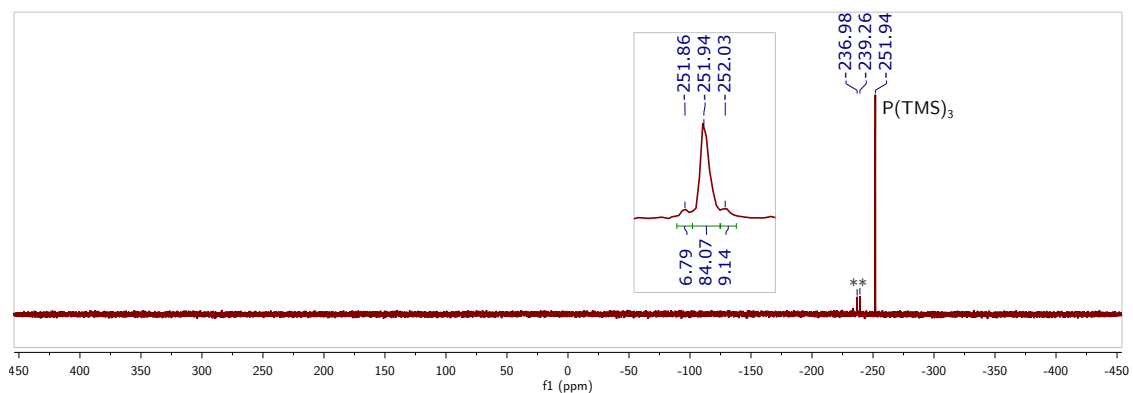


Figure B.10 $^{31}\text{P}\{^1\text{H}\}$ NMR spectrum of $\text{P}(\text{TMS})_3$ in THF at 25 °C, recorded at 162 MHz. Inset: Zoom of the resonance corresponding to $\text{P}(\text{TMS})_3$. Grey asterisks represents PH_3 .

B.5.4 Preparation of [TBA][SSiF₃] from **2**.

In the glovebox, [TBA]**2** (41 mg, 0.1 mmol, 1 equiv) and TMAF (28 mg, 0.3 mmol, 3 equiv) were weighed into separate vials and each dissolved in DCM (2 mL). The resulting solutions were frozen in the glovebox cold well. Upon thawing, the solutions were combined with stirring. The resulting reaction mixture was stirred for one hour then an aliquot (0.7 mL) was analyzed by NMR spectroscopy indicating formation of the desired product. The reaction mixture was filtered to remove tetramethylammonium chloride. Volatile material was removed from the filtrate to give a colorless oil. The oil was dissolved in DCM (1 mL) and passed through a piece of microfiber filter paper in a pipette. The resulting solution was layered with ether (10 mL) and the mixture placed in the freezer overnight. Crystals that formed were ultimately found to be unsuitable for structural analysis by X-ray diffraction. A yield for the product was not recorded because the material was used for an attempted

study by X-ray diffraction. ^1H NMR (500 MHz, DCM, δ) 3.30–3.21 (m, 8H), 1.65 (dt, $J = 16.0, 7.8$ Hz, 8H), 1.43 (h, $J = 7.4$ Hz, 8H), 1.01 (t, $J = 7.3$ Hz, 12H). ^{19}F NMR (471 MHz, DCM, δ) -121.9 ($J_{\text{Si-F}} = 275.9$ Hz).

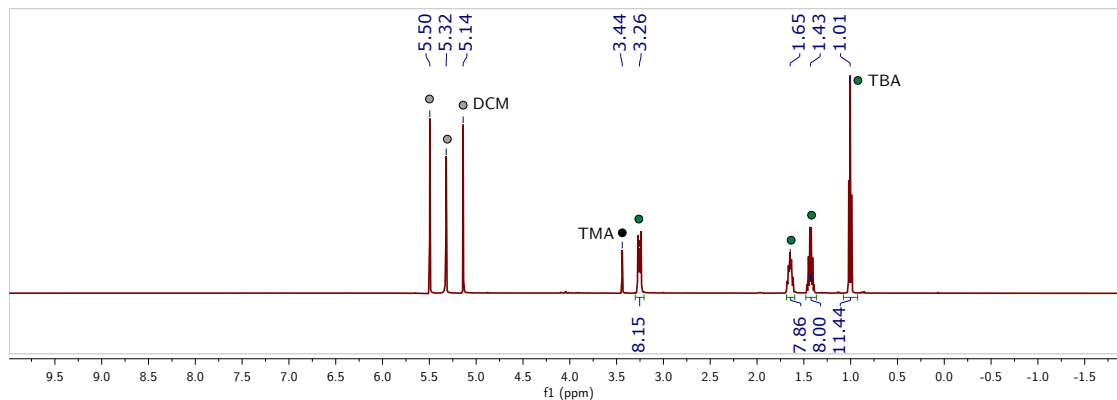


Figure B.11 ^1H NMR spectrum of $[\text{TBA}][\text{SSiF}_3]$ in DCM at 25 °C, recorded at 500 MHz. The large resonances either side of the central DCM resonance (suppressed) are ^{13}C satellites resulting from improper presaturation by the corresponding pulse sequence.

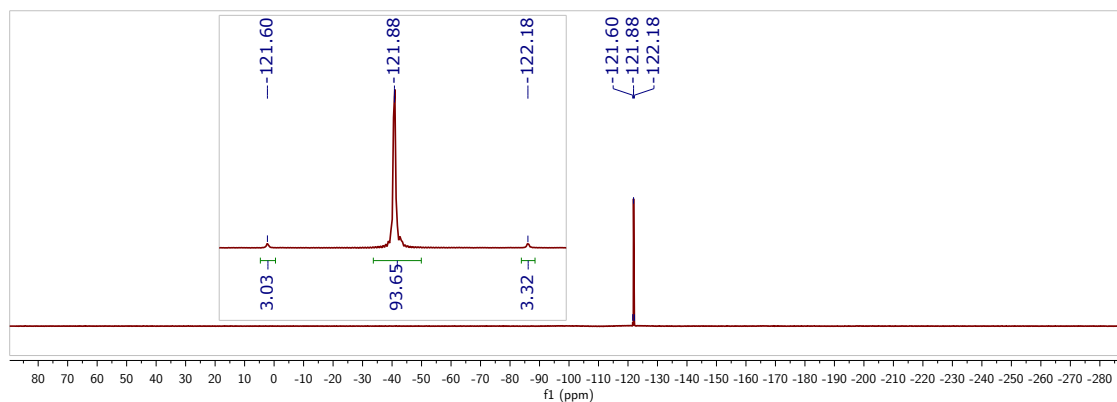


Figure B.12 ^{19}F NMR spectrum of $[\text{TBA}][\text{SSiF}_3]$ in DCM at 25 °C, recorded at 471 MHz. Inset: Zoom of the resonance corresponding to $[\text{TBA}][\text{SSiF}_3]$.

B.5.5 Preparation of $[(\text{Me}_2\text{N})_2\text{SiS}]_2$ from **2**.

In the glovebox, [TBA]**2** (200 mg, 489 μmol , 1 equiv) and LiNMe_2 (50 mg, 0.978 mmol, 2 equiv) were weighed into separate vials and each dissolved in THF (4 mL). The THF solution of lithium dimethylamide was added dropwise over the course of three minutes to the stirring solution [TBA]**2**. The resulting solution was stirred for 30 minutes then volatile material was removed under reduced pressure to give an off-white oil. The oil was triturated with hexane (2×8 mL) to give a white powder. The powder was extracted with hexane (8 mL, then 4 mL) and the extract was filtered through a piece of microfiber filter paper into a fresh vial. Volatile material was removed from the filtrate to give a colorless oil. The oil was analyzed in C_6D_6 . The solid material remaining from hexane extraction was analyzed in CDCl_3 . A sample was prepared from the C_6D_6 NMR sample for GCMS analysis in DCM. ^1H NMR (400 MHz, C_6D_6 , δ) 2.62 (s). Tri-*n*-butylamine was observed as an impurity in the ^1H NMR spectrum with multiplets centered at 2.38, 1.44, 1.35, 0.92. ^{29}Si NMR (99 MHz, THF, δ) -26.7 (s). GC-MS m/z (% relative intensity, ion): 44.1 (58, $\text{M}^+ - \text{S}_2\text{Si}_2(\text{NMe}_2)_3$), 166.0 (68, $\text{M}^+ - (\text{NMe}_2)_3 + 2\text{H}$), 208.1 (81, $\text{M}^+ - (\text{NMe}_2)_2$), 209.1 (73, $\text{M}^+ - (\text{NMe}_2)_2 + \text{H}$), 210.1 (78, $\text{M}^+ - (\text{NMe}_2)_2 + 2\text{H}$), 253.1 (76, $\text{M}^+ - \text{NMe}_2 + \text{H}$), 296.2 (100, M^+).

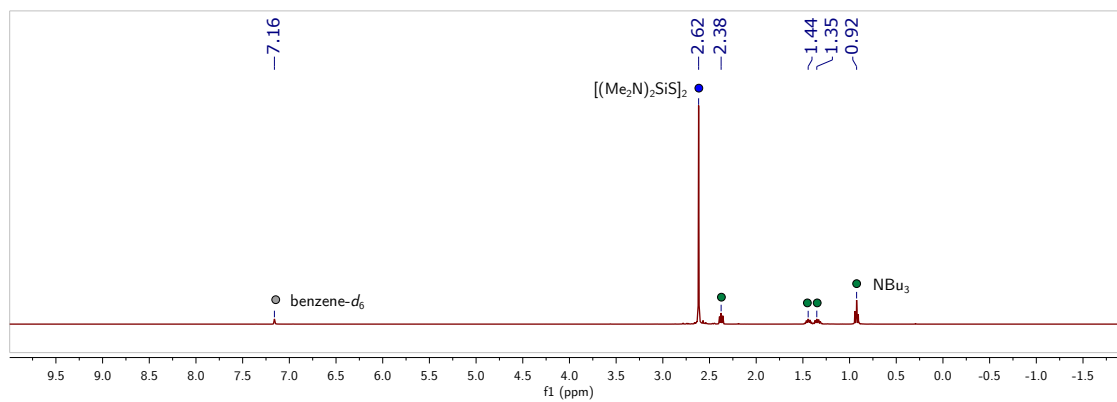


Figure B.13 ^1H NMR spectrum of $[(\text{Me}_2\text{N})_2\text{SiS}]_2$ in C_6D_6 at 25°C , recorded at 400 MHz.

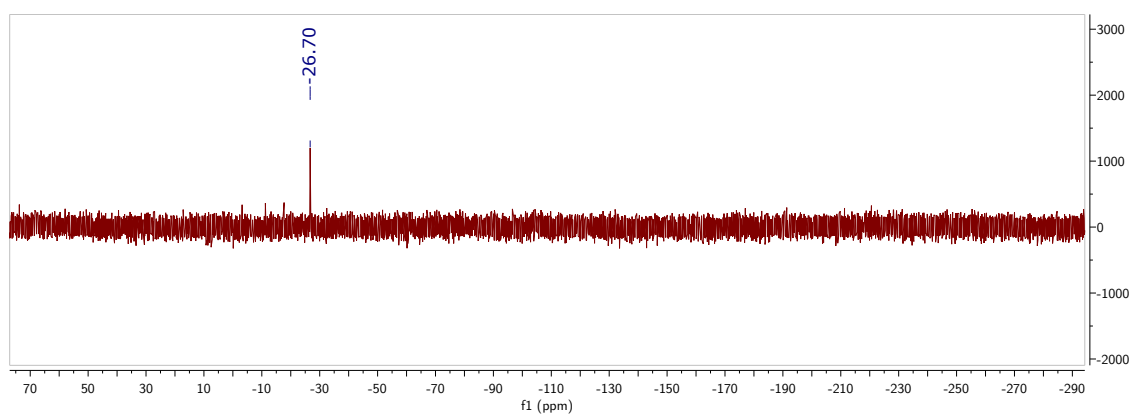


Figure B.14 ^{29}Si NMR spectrum of $[(\text{Me}_2\text{N})_2\text{SiS}]_2$ in C_6D_6 at 25°C , recorded at 99 MHz.

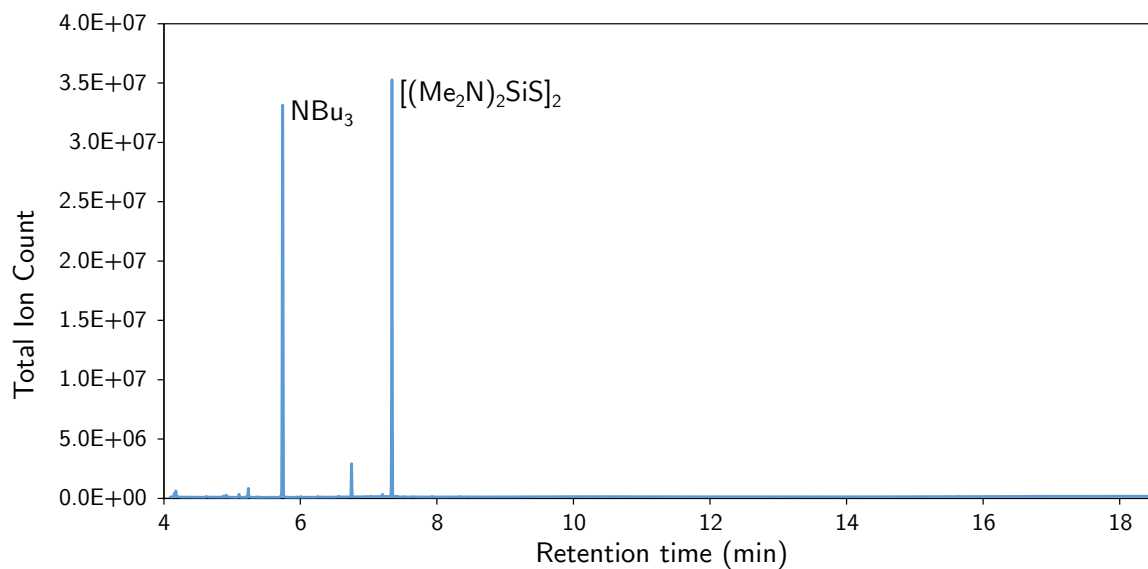


Figure B.15 GC-MS chromatogram of $[(\text{Me}_2\text{N})_2\text{SiS}]_2$, obtained as described in B.5.5.

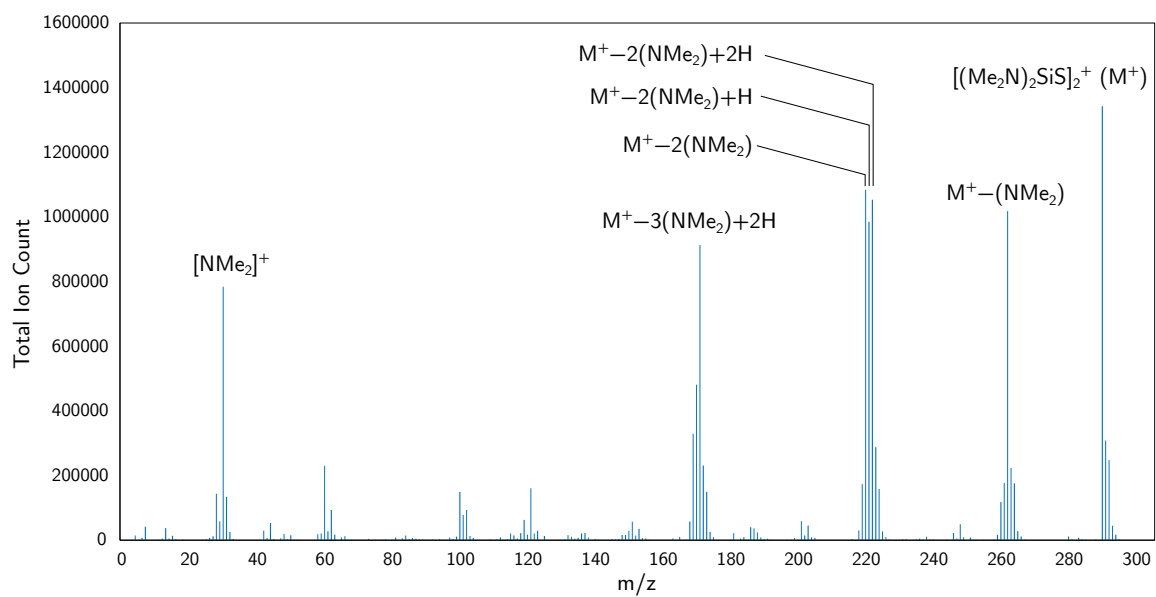


Figure B.16 ESI mass spectrum corresponding to the peak at $t_R = 7.35$ min in the GCMS trace of $[(\text{Me}_2\text{N})_2\text{SiS}]_2$.

B.5.6 Thionation of 1-acetylpyrrolidine with [TBA]2.

In the glovebox, a stock solution of 1-acetylpyrrolidine was prepared in toluene by diluting the amide (60 mg, 0.53 mmol) in toluene (6.600 g). To an NMR tube equipped with a J. Young valve was added [TBA]2 (54 mg, 0.133 mmol, 3 equiv). The stock solution of amide in chlorobenzene (560 mg, 0.044 mmol of amide) was added to the NMR tube which was sealed and analyzed by ^1H NMR spectroscopy. The samples were heated to 110 °C and analyzed by ^1H NMR spectroscopy after 1, 6, and 20 h showing yields of ca. 10%, 90%, 98% yield, respectively, as determined by integration of the methyl group resonances of the starting material and product in the ^1H NMR spectrum.

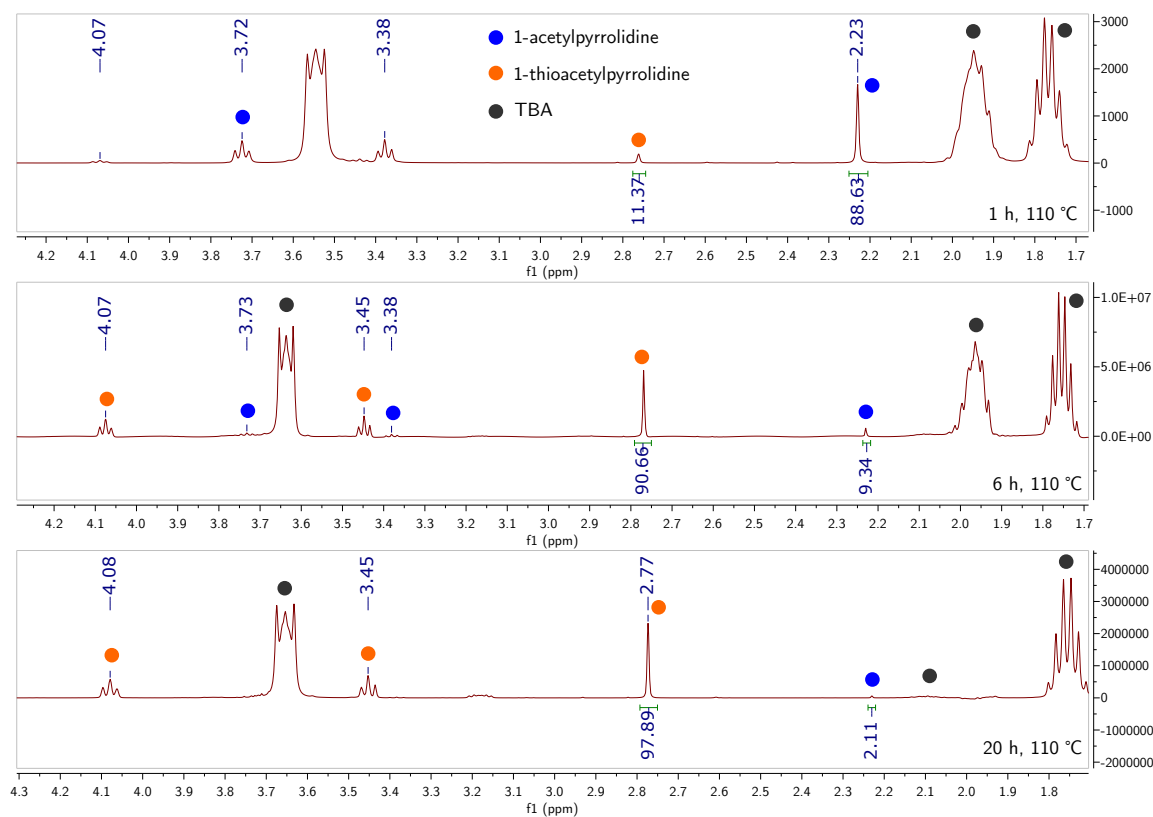


Figure B.17 Stack of ^1H NMR spectra corresponding to the reaction of 1-acetylpyrrolidine with [TBA]2, prepared as described in Section B.5.6, recorded at 400 MHz and 25 °C.

B.5.7 Attempted thionation of 1-acetylpyrrolidine with [TBA][SSiF₃].

In the glovebox, [TBA][P(SiF₃)₂] (30 mg, 0.0835 mmol, 2 equiv) was weighed into a NMR tube equipped with a J. Young Vale and dissolved in chlorobenzene. An initial set of NMR spectra were recorded (¹H, ¹⁹F), showing clean material. The tube was brought back into the box and 1-acetylpyrrolidine (5 mg, 0.044 mmol, 1 equiv) was added. The sample was heated at 80 °C and analyzed by NMR spectroscopy after 1 and 12 hours. Formation of the desired product was not observed by ¹H NMR spectroscopy while new, unidentified products were observed by ¹⁹F NMR spectroscopy (Figure B.19, -76.19, -96.29 ppm)

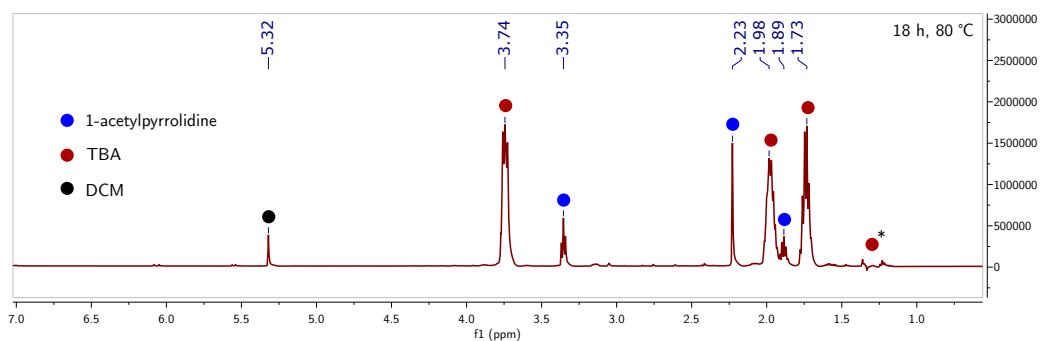


Figure B.18 ¹H NMR spectrum corresponding to the reaction of 1-acetylpyrrolidine with [TBA][SSiF₃], prepared as described in Section B.5.7, recorded at 500 MHz and 25 °C.

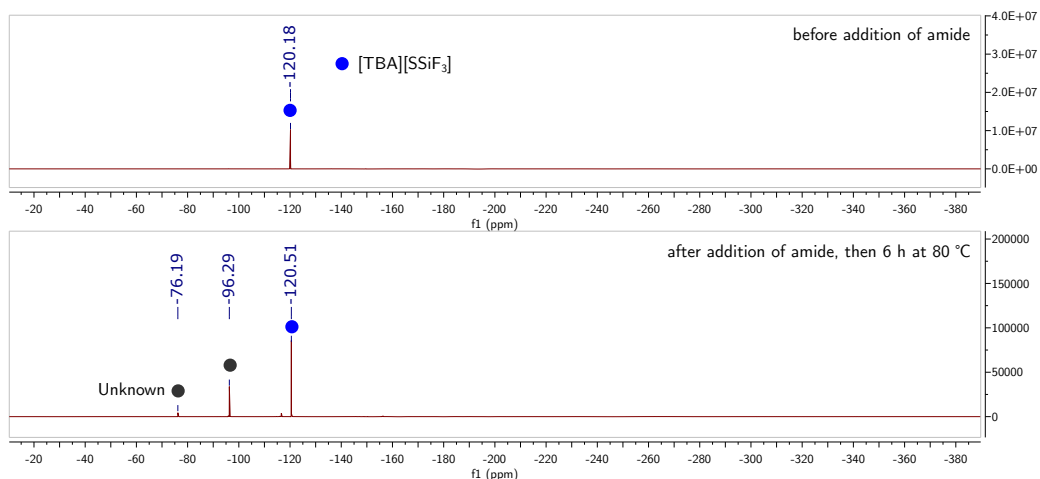


Figure B.19 ¹⁹F NMR spectrum corresponding to the reaction of 1-acetylpyrrolidine with [TBA][SSiF₃], prepared as described in Section B.5.7, recorded at 471 MHz and 25 °C.

B.5.8 Thionation of 1-acetylpyrrolidine with $[(\text{Me}_2\text{N})_2\text{SiS}]_2$.

*Note: This experiment requires repeating in chlorobenzene with 3 equiv of spectroscopically pure $[(\text{Me}_2\text{N})_2\text{SiS}]_2$, along the lines of the procedure described in Section B.5.6, to allow direct comparison of both thionation reagents. This material was contaminated with tri-*n*-butylamine.*

In the glovebox, 1-acetylpyrrolidine (15 mg, 0.133 mmol) was weighed into the end of a pipette and rinsed into a vial with toluene- d_8 (2 mL). The resulting solution (0.66 mL) was removed and added to an NMR tube to analyze the commercially available starting material. To the remaining solution (1.34 mL) containing 1-acetylpyrrolidine (10 mg, 0.088 mmol, 1 equiv) was added $[(\text{Me}_2\text{N})_2\text{SiS}]_2$ (40 mg, 0.101 mmol, 2.3 equiv of monomeric $[(\text{Me}_2\text{N})_2\text{SiS}]$, 75% w/w with NBu_3 , obtained from the experiment described in Section B.5.5). The solution was added in equal portions (0.67 mL) to two NMR tubes, one of which contained DMAP (2 mg, 0.016 mmol, 0.18 equiv). All three were analyzed by ^1H NMR spectroscopy then heated to 105 °C for 3 h. Partial conversion (ca. 13%) to 1-thioacetylpyrrolidine was observed in both cases after 3 h at 105 °C.

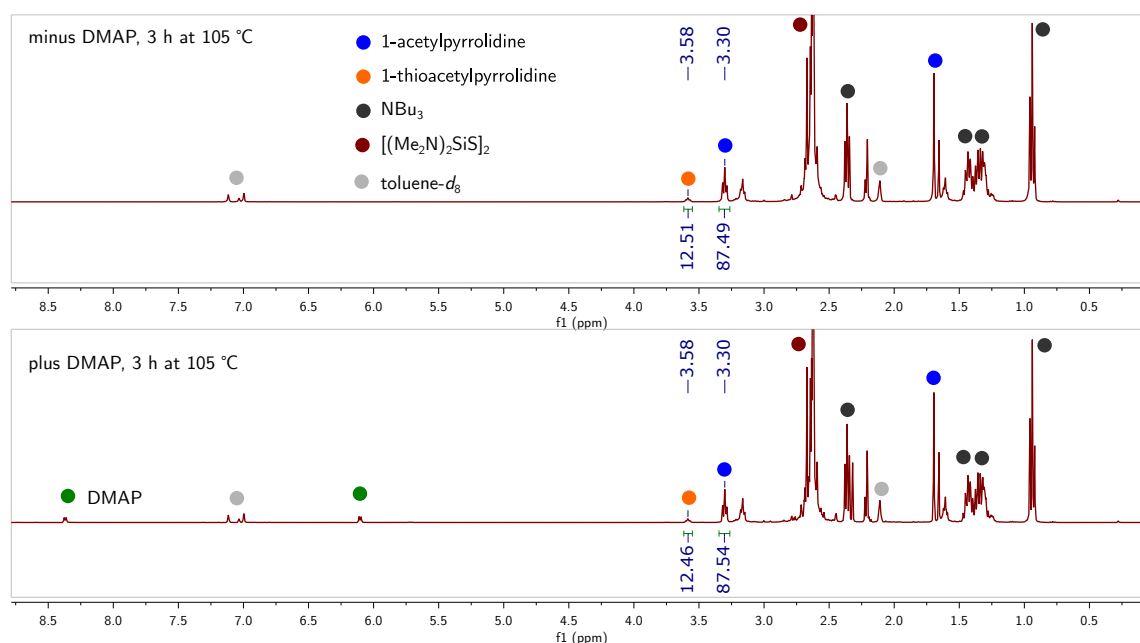


Figure B.20 ^1H NMR spectrum corresponding to the reaction of 1-acetylpyrrolidine with $[(\text{Me}_2\text{N})_2\text{SiS}]_2$, prepared as described in Section B.5.8, recorded at 400 MHz and 25 °C.

B.5.9 X-ray crystallography

Single crystals suitable for X-ray diffraction were transferred from the glovebox under Paratone oil onto a microscope slide. A crystal was selected under a microscope and mounted in hydrocarbon oil on a nylon loop. Low-temperature (100 K) data were collected on a Bruker-AXS X8 Kappa Duo diffractometer coupled to a Smart Apex2 CCD detector with Mo $K\alpha$ radiation ($\lambda = 0.71073 \text{ \AA}$) with ϕ - and ω -scans. A semi-empirical absorption correction was applied to the diffraction data using SADABS^{31,32} unless otherwise stated. The structure was solved by direct methods using SHELXT^{33,34} and refined against F^2 on all data by full-matrix least squares with ShelXle.³⁵ All non-hydrogen atoms were refined anisotropically. All hydrogen atoms were included in the model at geometrically calculated positions and refined using a riding model. The isotropic displacement parameters of all hydrogen atoms were fixed to 1.2 times the U_{eq} value of the atoms they are linked to (1.5 times for methyl groups).

The refinement proceeded by first restraining the TBA cation such that each butyl group had the same C–N and C–C bond lengths for chemically equivalent bonds, and equal N–C–C and C–C–C bond angles for chemically equivalent bond angles (using the SADI command). The cation was refined anisotropically and hydrogen atoms included using the relevant HFIX commands. Rotational disorder about the P–Si bond was observed, resulting in oblique thermal ellipsoids when the phosphide anion was refined; therefore SIMU and RIGU commands were applied to the entire structure. One half of the anion was modeled as having rotational disorder about the P–Si bond; all of the $-\text{SiF}_3$ groups were restrained to be equivalent (using the SADI command) through the Si–F, P–F, and F–F distances (i.e. Si–F bond lengths, and P–Si–F, F–Si–F bond angles). The model was refined anisotropically and the weighting scheme adjusted to give the final model.

CSD identification code	N/A
Reciprocal net code	P8_19105
Empirical formula	C ₁₆ H ₃₆ F ₆ N ₁ P ₁ Si ₂
Formula weight	443.61 g/mol
Color / morphology	colorless / plate
Temperature	100(2) K
Wavelength	0.71073 Å
Crystal system	Orthorhombic
Space group	<i>Pbca</i>
Unit cell dimensions	$a = 16.1739(10) \text{ Å}$ $\alpha = 90^\circ$ $b = 14.8214(8) \text{ Å}$ $\beta = 90^\circ$ $c = 19.6930(13) \text{ Å}$ $\gamma = 90^\circ$
Volume	4720.8(5) Å ³
<i>Z</i>	8
Density (calculated)	1.248 g/cm ³
Absorption coefficient	0.265 mm ⁻¹
<i>F</i> (000)	1888
Crystal size	0.512 × 0.256 × 0.162 mm ³
Theta ranges for data collection	2.068 to 24.437°
Index ranges	-18 ≤ h ≤ 18, -17 ≤ k ≤ 17, -22 ≤ l ≤ 22
Reflections collected	88445
Independent reflections	3905 [<i>R</i> _{int} = 0.0429]
Completeness to $\theta = 25.242^\circ$	99.9%
Absorption correction	None
Max. and min. transmission	0.5191 and 0.5615
Refinement method	Full-matrix least-squares on <i>F</i> ²
Data / restraints / parameters	3905 / 462 / 267
Goodness-of-fit on <i>F</i> ²	1.024
Final <i>R</i> indices [<i>I</i> > 2σ(<i>I</i>)]	<i>R</i> ₁ = 0.0366, <i>wR</i> ₂ = 0.0949
<i>R</i> indices (all data)	<i>R</i> ₁ = 0.0409, <i>wR</i> ₂ = 0.0978
Extinction coefficient	n/a
Largest diff. peak and hole	0.508 and -0.585 e·Å ⁻³

Table B.2 X-ray crystallographic information for [TBA][P(SiF₃)₂].

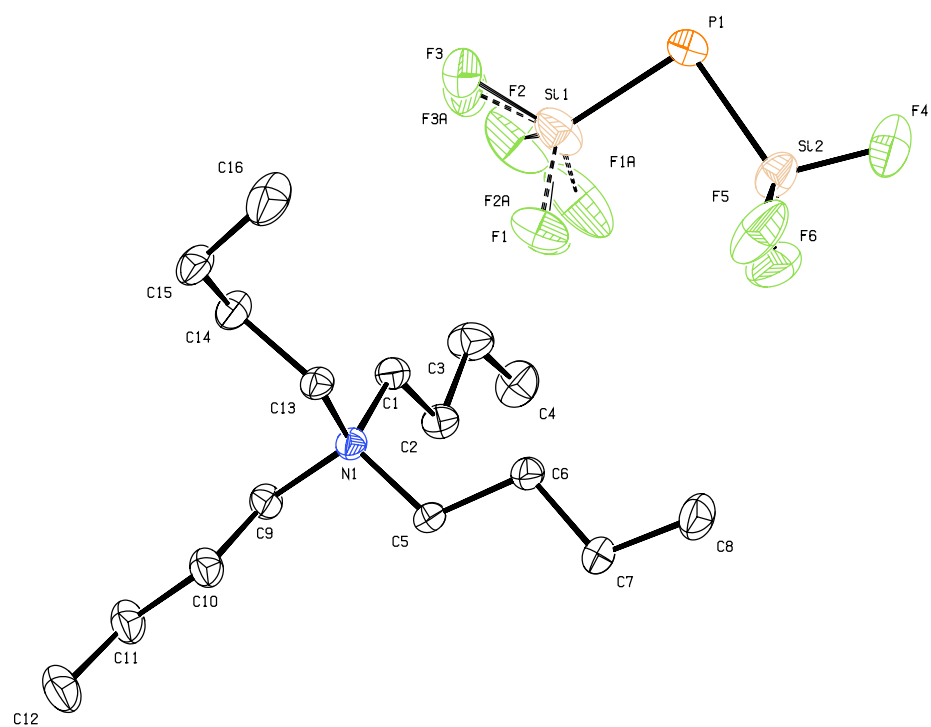


Figure B.21 Molecular structure of [TBA][P(SiF₃)₂] with ellipsoids set at the 50% probability level and hydrogen atoms omitted for clarity.

References

- [1] Geeson, M. B.; Cummins, C. C. *Science* **2018**, *359*, 1383–1385.
- [2] Geeson, M. B.; Ríos, P.; Transue, W. J.; Cummins, C. C. *J. Am. Chem. Soc.* **2019**, *141*, 6375–6384.
- [3] Teichmann, J.; Kunkel, C.; Georg, I.; Moxter, M.; Santowski, T.; Bolte, M.; Lerner, H.-W.; Bade, S.; Wagner, M. *Chem. - Eur. J.* **2019**, *25*, 2740–2744.
- [4] J. Tillmann, *Chlorid-induzierter Aufbau perchlorierter Oligosilane ausgehend von Si_2Cl_6 oder $HSiCl_3$* , PhD thesis, Frankfurt/Main, **2015**.
- [5] F. Gründler, *Synthese von perchlorierten Cyclohexasilanen durch chloridgesteuerte Disproportionierung von Hexachlordisilan: Eigenschaften und Reaktionsparameter*, Bachelor thesis, Freiberg, **2015**.
- [6] Böhme, U.; Gerwig, M.; Gründler, F.; Brendler, E.; Kroke, E. *Eur. J. Inorg. Chem.* **2016**, *2016*, 5028–5035.
- [7] Georg, I.; Teichmann, J.; Bursch, M.; Tillmann, J.; Endeward, B.; Bolte, M.; Lerner, H.-W.; Grimme, S.; Wagner, M. *J. Am. Chem. Soc.* **2018**, *140*, 9696–9708.
- [8] Teichmann, J.; Bursch, M.; Köstler, B.; Bolte, M.; Lerner, H.-W.; Grimme, S.; Wagner, M. *Inorg. Chem.* **2017**, *56*, 8683–8688.
- [9] Olaru, M.; Hesse, M. F.; Rychagova, E.; Ketkov, S.; Mebs, S.; Beckmann, J. *Angew. Chem., Int. Ed.* **2017**, *56*, 16490–16494.
- [10] Müller, U.; Krug, V. *Z. Naturforsch., B: J. Chem. Sci.* **1985**, *40*.
- [11] Müller, R.; Beyer, H. *Chem. Ber.* **1959**, *92*, 1018–1027.
- [12] Fritz, G.; Beetz, A. G.; Matern, E.; Peters, K.; Peters, E.-M.; Schnering, H. G. v. *Z. Anorg. Allg. Chem.* **1994**, *620*, 136–144.
- [13] Rüdinger, C.; Beruda, H.; Schmidbaur, H. *Z. Naturforsch., B: J. Chem. Sci.* **1994**, *49*, 1348–1360.
- [14] Choi, S.-B.; Kim, B.-K.; Boudjouk, P.; Grier, D. G. *J. Am. Chem. Soc.* **2001**, *123*, 8117–8118.
- [15] Sharp, K. G. *J. Chem. Soc., Chem. Commun.* **1977**, 564.
- [16] Langford, G. R.; Moody, D. C.; Odom, J. D. *Inorg. Chem.* **1975**, *14*, 134–136.
- [17] Weinhold, F.; Landis, C. R. *Valency and bonding: a natural bond orbital donor-acceptor perspective*; Cambridge University Press: Cambridge, UK ; New York, 2005.
- [18] Glendening, E. D.; Badenhop, J. K.; Reed, A. E.; Carpenter, J. E.; Bohmann, J. A.; Morales, C. M.; Landis, C. R.; Weinhold, F. NBO 6.0. 2013.
- [19] Benkeser, R. A.; Voley, K. M.; Grutzner, J. B.; Smith, W. E. *J. Am. Chem. Soc.* **1970**, *92*, 697–698.
- [20] Oehme, H.; Weiss, H. *J. Organomet. Chem.* **1987**, *319*, C16–C18.
- [21] Teichmann, J.; Wagner, M. *Chem. Commun.* **2018**, *54*, 1397–1412.
- [22] Müller, L.-P.; Zanin, A.; Du Mont, W.-W.; Jeske, J.; Martens, R.; Jones, P. G. *Chem. Ber.* **1997**, *130*, 377–384.
- [23] Müller, L.-P.; Mont, W.-W. D.; Jeske, J.; Jones, P. G. *Chem. Ber.* **1995**, *128*, 615–619.

- [24] Müller, L.-P.; Zanin, A.; Jeske, J.; Jones, P. G.; du Mont, W.-W. In “Trichlorosilane/Triethylamine-An Alternative to Hexachlorodisilane in Reductive Trichlorosilylation Reactions?” in *Organosilicon Chemistry Set*; Auner, N., Weis, J., Eds.; Wiley-VCH Verlag GmbH: Weinheim, Germany, 2005; pp 286–290.
- [25] Tillmann, J.; Meyer, L.; Schweizer, J. I.; Bolte, M.; Lerner, H.-W.; Wagner, M.; Holthausen, M. C. *Chem. - Eur. J.* **2014**, *20*, 9234–9239.
- [26] Choe, S.-B.; Schneider, J. J.; Klabunde, K. J.; Radonovich, L. J.; Ballintine, T. A. *J. Organomet. Chem.* **1989**, *376*, 419–439.
- [27] (a) Haaf, M.; Schmiedl, A.; Schmedake, T. A.; Powell, D. R.; Millevolte, A. J.; Denk, M.; West, R. *J. Am. Chem. Soc.* **1998**, *120*, 12714–12719; (b) Zark, P.; Schäfer, A.; Mitra, A.; Haase, D.; Saak, W.; West, R.; Müller, T. *J. Organomet. Chem.* **2010**, *695*, 398–408; (c) Zhang, S.-H.; Yeong, H.-X.; So, C.-W. *Chem. - Eur. J.* **2011**, *17*, 3490–3499.
- [28] Shibahara, F.; Sugiura, R.; Murai, T. *Org. Lett.* **2009**, *11*, 3064–3067.
- [29] Pangborn, A. B.; Giardello, M. A.; Grubbs, R. H.; Rosen, R. K.; Timmers, F. J. *Organometallics* **1996**, *15*, 1518–1520.
- [30] Williams, D. B. G.; Lawton, M. *J. Org. Chem.* **2010**, *75*, 8351–8354.
- [31] Bruker, SADABS. 2008.
- [32] Krause, L.; Herbst-Irmer, R.; Sheldrick, G. M.; Stalke, D. *J. Appl. Crystallogr.* **2015**, *48*, 3–10.
- [33] Sheldrick, G. M. *Acta Crystallogr., Sect. A: Found. Adv.* **2015**, *71*, 3–8.
- [34] Sheldrick, G. M. *Acta Crystallogr., Sect. A: Found. Crystallogr.* **2008**, *64*, 112–122.
- [35] Hübschle, C. B.; Sheldrick, G. M.; Dittrich, B. *J. Appl. Crystallogr.* **2011**, *44*, 1281–1284.

Appendix C

Redox-Neutral Reactions of Phosphoric Acid

Contents

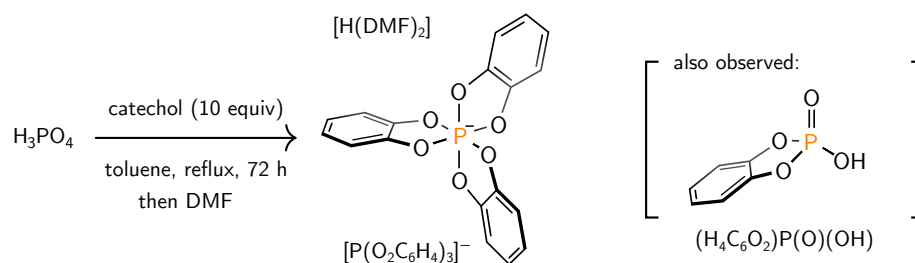
C.1 Introduction	347
C.2 Results and discussion	348
C.3 Conclusions and Future Directions	351
C.4 Experimental methods	352
Bibliography	367

C.1 Introduction

A number of experiments have been performed with the goal of preparing phosphorus chemicals in the +5 oxidation state directly from phosphoric acid and its salts. Specifically, this appendix focuses on redox-neutral procedures where phosphorus *remains* in the +5 state throughout the course of the reaction. The motivations for such processes are laid out in Chapter 1. These efforts have resulted in the synthesis of trimethyl phosphate (OP(OMe)₃) and the tris-(*o*-phenylenedioxy)phosphate anion, [P(O₂C₆H₄)]⁻, directly from crystalline phosphoric acid. The isolation of [TBA][Li][HPO₄], a dibasic phosphate that appears to have good stability in anhydrous acetonitrile, reacts with CO₂ to generate pyrophosphate via an unknown intermediate, tentatively assigned as carboxyphosphate. The isolation or spectroscopic characterization of carboxyphosphate, a postulated intermediate in organisms, is of potential interest to biologists and as a phosphorylation reagent by loss of bicarbonate.

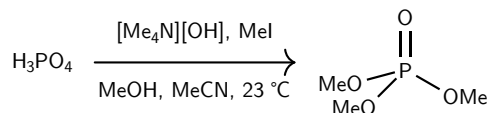
C.2 Results and discussion

The reported chlorine-free protocol for processing germanium¹ inspired an attempt to prepare the known tris-(*o*-phenylenedioxy)phosphate anion ($[\text{P}(\text{O}_2\text{C}_6\text{H}_4)]^-$)²⁻⁴ directly from phosphoric acid and catechol. The conjugate acid of this anion is capable of protonating DMF to form $[\text{P}(1,2\text{-O}_2\text{C}_6\text{H}_4)][\text{H}(\text{DMF})_2]$.⁵ Preparation of this species was attempted in refluxing toluene using a Dean-Stark apparatus to remove water from the reaction mixture. This dehydrative procedure was somewhat hampered by the low boiling point of catechol, which collected in the Dean-Stark trap and formed a toluene/water emulsion. Similarly, the use of molecular sieves in a Soxhlet extractor to remove water from the distillate led to discoloration of the sieves. Nonetheless, the characteristic signal for the hexacoordinate phosphate anion was observed at -82.6 ppm in the ³¹P NMR spectrum, demonstrating the feasibility of this dehydrative route to access the desired anion.



Scheme C.1 Reaction of phosphoric acid with catechol to provide $[\text{P}(1,2\text{-O}_2\text{C}_6\text{H}_4)][\text{H}(\text{DMF})_2]$. Phosphoester $(\text{H}_4\text{C}_6\text{O}_2)\text{P}(\text{O})(\text{OH})$ was also observed by ³¹P NMR spectroscopy.

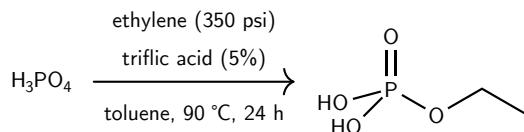
The species $(\text{H}_4\text{C}_6\text{O}_2)\text{P}(\text{O})(\text{OH})$ containing a five-membered ring was also observed by ³¹P NMR spectroscopy, and is a plausible intermediate en route to the product. This species is of interest because it has been identified to undergo rapid ring-opening,⁶ and could be an intermediate in the catechol-catalyzed phosphorylation of alcohols.⁷ To the best of our knowledge, neither of these species has been prepared directly from phosphoric acid.



Scheme C.2 Exhaustive alkylation of phosphoric acid with tetramethylammonium hydroxide/methyl iodide to give trimethyl phosphate.

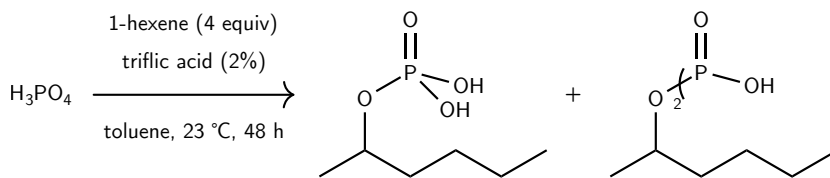
Next, attention was turned to direct alkylation of phosphoric acid and phosphates using methyl iodide. In reactions performed by undergraduate student Miller Tan, repeated cation exchange to the tetramethylammonium salt of orthophosphate followed by treatment with methyl iodide led to the formation of trimethyl phosphate, identified by a binomial

decet ($J_{\text{P-H}} = 11 \text{ Hz}$) in the ^{31}P NMR spectrum. The product was extracted using diethyl ether and isolated in 8% yield after removing volatile material. Despite the low yield, this initial procedure could hold promise for connecting the dots directly from wet process phosphoric acid to trialkyl phosphates, which are prime candidates for selective reduction to P(III) compounds such as trialkyl phosphites. Trialkyl phosphates can also undergo reactions with carbon-based nucleophiles such as Grignard reagents to give phosphorus-carbon bond-containing phosphonates,⁸ and such a method would provide phosphorus-carbon bonds without phosphorus leaving the +5 oxidation state.



Scheme C.3 Reaction of phosphoric acid with ethylene to provide ethyl phosphate.

In addition to the salt metathesis route to organophosphates described above, we wondered whether it might be possible to form the phosphoester linkage by addition of a phosphoric acid O–H bond to an olefin. Such a process would bear a strong resemblance to the report synthesis of carbon esters by addition of carboxylic acids to olefins in the presence of triflic acid.⁹ We treated phosphoric acid with ethylene at a pressure of 350 psi at 90 °C for 24 h and identified the formation of ethyl phosphate by NMR spectroscopy (Scheme C.3). A literature report from 1935 detailed the polymerization of ethylene and propene by phosphoric acid,¹⁰ and this competing reactivity could account for the low spectroscopic yield of ethyl phosphate (ca. 6%).



Scheme C.4 Reaction of phosphoric acid with 1-hexene to provide a mixture of alkyl phosphates.

The observation of ethyl phosphate hinted that the use of other olefins might also lead to phosphoester formation. This hypothesis was tested by treating phosphoric acid with 1-hexene in toluene, with 5 mol % of triflic acid added as a catalyst (Scheme C.4). After 48 h at 23 °C, analysis of the reaction mixture by NMR spectroscopy provided evidence for phosphoester formation. At least three different compounds with phosphoester linkages were observed to form by NMR spectroscopy (characterized by a ^1H – ^{31}P HMBC experiment), suggesting that either multiple isomers of hexyl phosphate form or that multiple additions of 1-hexene to phosphoric acid can occur (Scheme C.4).

A final investigation into the chemistry of phosphate involved attempts prepare a salt of

phosphorylation reagent for the phosphate present in solution, leading to pyrophosphate.

C.3 Conclusions and Future Directions

Initial efforts toward using phosphoric acid and its salts for the synthesis of chemicals has been made, with special attention being paid to avoiding changes in the oxidation state at phosphorus. This has resulted in the formation of phosphorus esters such as trimethyl phosphate, ethyl phosphate, and hexyl phosphates. The formation of six-coordinate $[\text{P}(\text{O}_2\text{C}_6\text{H}_4)]^-$ is of interest, particularly with regard to its reaction with carbon-based nucleophiles such as Grignard reagents. It may even act as phosphorylation reagent for alcohols, amines, or nucleosides.

The alkylation of phosphoric acid and orthophosphate with synthons for the methyl cation is of interest to obtain a good preparative procedure for trimethyl phosphate. Of particular interest would be the study of trisodium phosphate with chloromethane, using high temperatures and pressures. This reaction would be attractive because the sole byproduct would be sodium chloride.

The formation of a phosphoester from the reaction of phosphoric acid with alkenes is a promising and atom-efficient method to prepare these compounds, which are of industrial importance.¹⁶ It will be of interest to study the reaction at higher temperature. The use of a catalyst may offer selectivity for the anti-Markovnikov product over the Markovnikov addition products that have been observed under the acidic conditions used herein.

Is carboxyphosphate forming, and if so can it be trapped? A simple experiment to determine whether it forms will be to perform the reaction with $^{13}\text{CO}_2$ and study the initial products that form by ^{13}C NMR spectroscopy. This experiment would also provide evidence for the formation of bicarbonate which is the expected byproduct of pyrophosphate formation, if it is indeed forming. If carboxyphosphate forms, clearly it does not survive for long in solution. One strategy would be to chemically trap it, perhaps by alkylation with a reagent such as methyl iodide or by silylation with trimethylsilyl chloride. Alternatively, it may be intercepted by a nucleophile such as an amine to provide an amide and phosphate.

C.4 Experimental methods

C.4.1 General methods

All manipulations were performed in a Vacuum Atmospheres model MO-40M glovebox under an inert atmosphere of purified N₂ or using standard Schlenk techniques. When reagents were removed from a stock bottle containing a Sure/Seal, the equivalent volume of dry nitrogen was injected into the bottle prior to removing the desired volume of solution with a syringe. All solvents were obtained anhydrous and oxygen-free by bubble degassing (argon) and purification by passing through columns of alumina and Q5.¹⁷ Once collected, solvents were stored over activated 4 Å molecular sieves (20 wt%) inside the glovebox.¹⁸ All glassware was oven-dried for at least 6 h prior to use, at temperatures greater than 150 °C.

Crystalline phosphoric acid (Millipore-Sigma), lithium hexamethyldisilazide (LiH-MDS, Millipore-Sigma) and methyl iodide (Strem) were used as received. Catechol (Alfa) was recrystallized thrice from hot toluene. CO₂ was purchased from Airgas and used as received. Deuterated solvents were purchased from Cambridge Isotope Labs and were degassed three times by the freeze-pump-thaw method and stored over activated 4 Å molecular sieves for 48 h in the glovebox prior to use. Diatomaceous earth (Celite 435, EM Science), 4 Å molecular sieves (Millipore-Sigma) and basic alumina (Millipore-Sigma) were dried by heating to 200 °C under dynamic vacuum for at least 48 h prior to use. The temperature of the aluminum shot used to heat reagents or reaction mixtures was measured using a Hanna Instruments K-type Thermocouple Thermometer (model HI935005).

NMR spectra were obtained on a Jeol ECZ-500 instrument equipped with an Oxford Instruments superconducting magnet, on a Bruker Avance 400 instrument equipped with a Magnex Scientific or with a SpectroSpin superconducting magnet, or on a Bruker Avance 500 instrument equipped with a Magnex Scientific or with a SpectroSpin superconducting magnet. ¹H and ¹³C NMR spectra were referenced to residual CD₂Cl₂ (¹H = 5.32 ppm, ¹³C = 54.0 ppm), C₆D₆ (¹H = 7.16 ppm, ¹³C = 128.06 ppm), CD₃CN (¹H = 1.94 ppm, ¹³C = 118.26 ppm) or CDCl₃ (¹H = 7.26 ppm, ¹³C = 77.16 ppm). ³¹P NMR spectra were referenced externally to 85% H₃PO₄ (0 ppm).

C.4.2 Reaction of crystalline phosphoric acid with catechol

In the fumehood, phosphoric acid (5.53 g, 56 mmol, 1 equiv) was quickly weighed and transferred to a Schlenk flask (500 mL) containing anhydrous toluene (90 mL). Catechol (53 g, 481 mmol, 8.6 equiv) was added to the flask. A Dean-Stark trap was connected to the top of the flask, followed by a reflux condenser. The setup was placed under an atmosphere of nitrogen, and heated to reflux for 72 h. An amount of water collected in the Dean-Stark trap; the upper toluene layer was quite cloudy indicating an emulsion of toluene, water, and catechol. Upon prolonged reaction times, this resulted in water not dropping to the bottom of the trap as intended, but instead collecting above the toluene. An aliquot of the reaction mixture was dissolved in DMSO and analyzed by ^{31}P NMR spectroscopy.

The round bottom flask was removed from the Dean-Stark apparatus and connected instead to a Soxhlet extractor that had been filled with molecular sieves. The solution was heated to reflux for 48 h, after which time the sieves had turned dark brown, indicating their decomposition. A small amount of the material was analyzed by ^{31}P NMR spectroscopy in DMF, showing the presence of $[\text{P}(\text{O}_2\text{C}_6\text{H}_4)]^{-5}$ and $(\text{H}_4\text{C}_6\text{O}_2)\text{P}(\text{O})(\text{OH})^7$ $[\text{P}(1,2\text{-O}_2\text{C}_6\text{H}_4)][\text{H}(\text{DMF})_2]$: $^{31}\text{P}\{^1\text{H}\}$ NMR (203 MHz, DMF, δ) -82.6 (s). $(\text{H}_4\text{C}_6\text{O}_2)\text{P}(\text{O})(\text{OH})$: $^{31}\text{P}\{^1\text{H}\}$ NMR (203 MHz, DMF, δ) $+11.99$ (s).

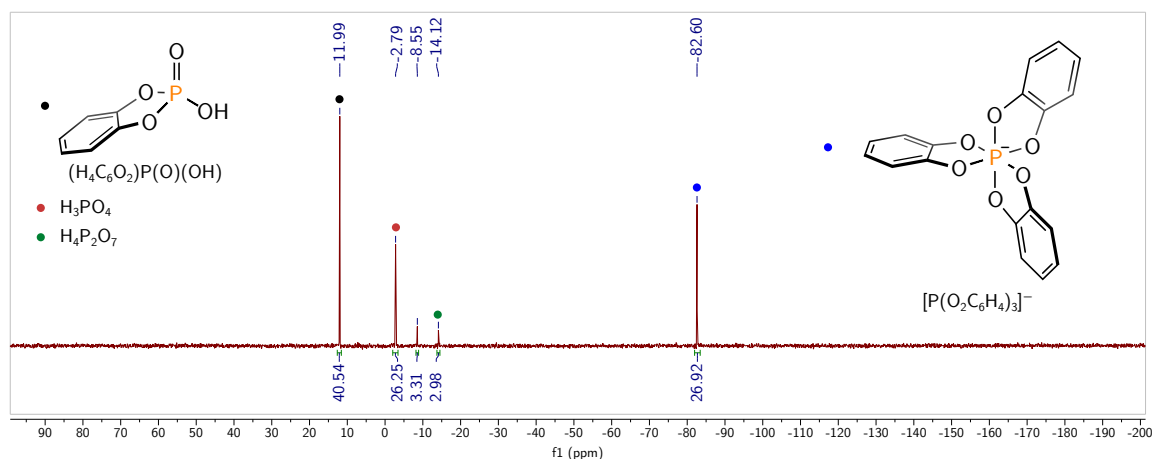


Figure C.1 $^{31}\text{P}\{^1\text{H}\}$ NMR spectrum of the reaction mixture described in Section C.4.2 in DMF, recorded at 203 MHz at 25 °C.

C.4.3 Preparation of trimethyl phosphate from phosphoric acid and methyl iodide

Note: This experiment was performed by Miller Tan under the supervision of the author. H_3PO_4 (0.994 g, 10.14 mmol, 1 equiv) was dissolved in a methanol solution of tetramethylammonium hydroxide (25%, 8.540 mL, 20.28 mmol, 2 equiv) and diluted with additional methanol (6 mL). Methyl iodide (1.900 mL, 30.64 mmol, 3 equiv) was added to the solution. The reaction was stirred at 40 °C for 16 h, after which time an aliquot was analyzed by NMR spectroscopy. A second addition tetramethylammonium hydroxide solution in methanol (25%, 8.540 mL, 20.28 mmol, 2 equiv) followed by methyl iodide (1.900 mL, 30.64 mmol, 3 equiv) were added and the resulting mixture was left to stir for 72 h. Volatile material was removed under reduced pressure and the material was redissolved in acetonitrile (10 mL) and an additional portion of tetramethylammonium hydroxide solution in methanol (25%, 0.680 mL, 1.615 mmol, 1 equiv) was added. The resulting mixture was stirred for 30 min then methyl iodide (1.900 mL, 30.64 mmol, 3 equiv) was added dropwise to solution and the resulting mixture was left to stir for 16 h. Volatile material was removed under reduced pressure and the residue was extracted with diethyl ether (3×10 mL). The extract was filtered through glass microfiber filter paper and volatile material was removed from the filtrate under reduced pressure to give trimethyl phosphate (110.5 mg, 0.788 mmol, 8%). ^1H NMR (500 MHz, C_6D_6 , δ) 3.33 (d, $J = 11.0$ Hz, 9H). ^{13}C NMR (126 MHz, C_6D_6 , δ) 53.70 (d, $J = 5.5$ Hz). $^{31}\text{P}\{^1\text{H}\}$ NMR (203 MHz, C_6D_6 , δ) 3.08 (s). ^{31}P NMR (203 MHz, C_6D_6 , δ) 3.08 (d, $J_{\text{P-H}} = 11.0$ Hz).

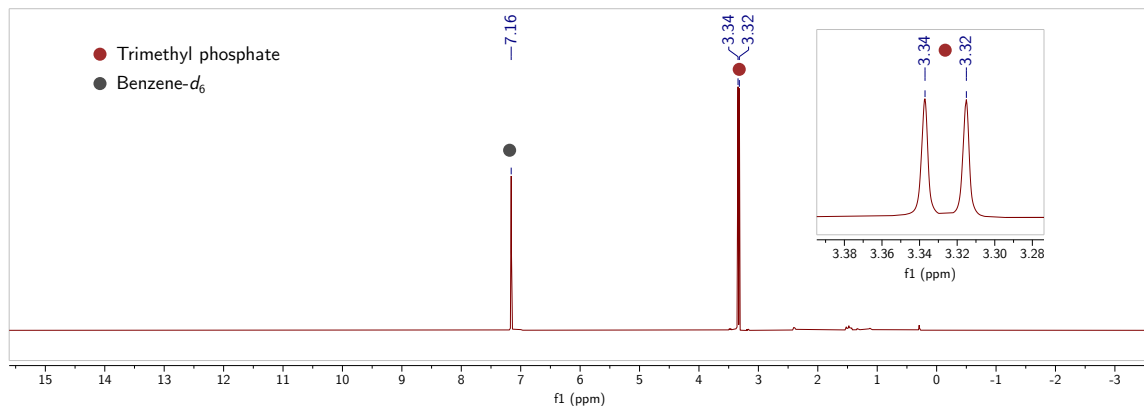


Figure C.2 ^1H NMR spectrum of trimethyl phosphate in C_6D_6 , recorded at 500 MHz at 25 °C.

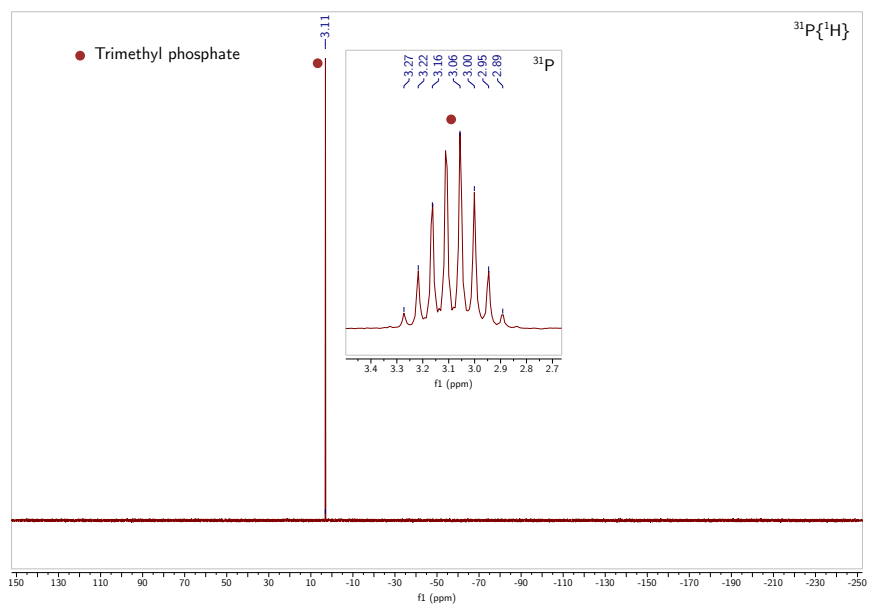


Figure C.3 $^{31}\text{P}\{^1\text{H}\}$ NMR spectrum of trimethyl phosphate in C_6D_6 , recorded at 203 MHz at 25 °C.

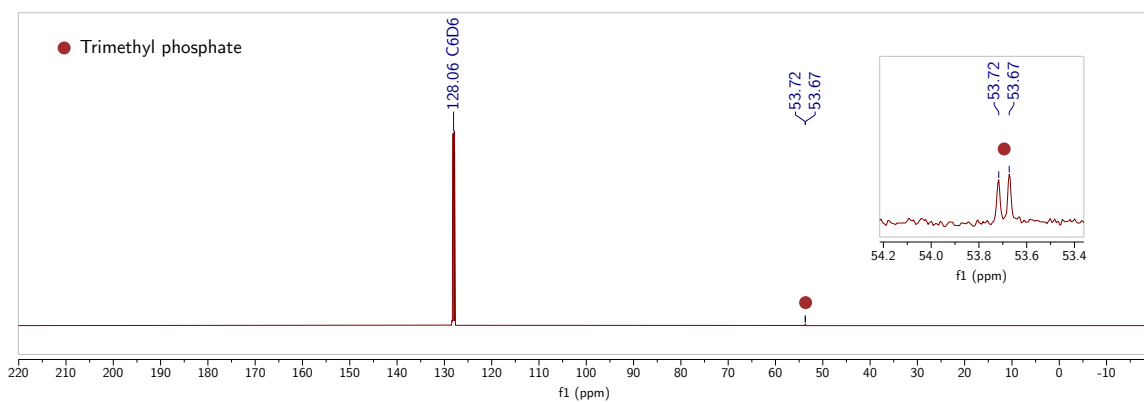


Figure C.4 $^{13}\text{C}\{^1\text{H}\}$ NMR spectrum of trimethyl phosphate in C_6D_6 , recorded at 126 MHz at 25 °C.

C.4.4 Reaction of crystalline phosphoric acid with ethylene

In the glovebox, phosphoric acid (980 mg, 10 mmol, 1 equiv) and triflic acid (75 mg, 0.5 mmol, 0.05 equiv) were weighed into a glass liner (300 mL) containing a stir bar (5 cm). The liner was removed from the box in a sealed container, then quickly transferred in the fume hood to a 300 mL Parr bomb. The bomb was sealed and a low (ca. 20 psi) pressure of ethylene was flowed through the bomb for around 2 minutes in order to purge the system. The bomb was then pressurized with ethylene to 350 psi and heated to 90 °C. The mixture was stirred for 24 h then carefully vented. The liner contained a clear colorless liquid and a small amount of pale red oil. The colorless liquid contained no phosphorus-containing species, as determined by ^{31}P NMR spectroscopy. The pale red oil was diluted in $\text{DMSO-}d_6$ and analyzed by NMR spectroscopy, showing the presence of some ethyl phosphate.

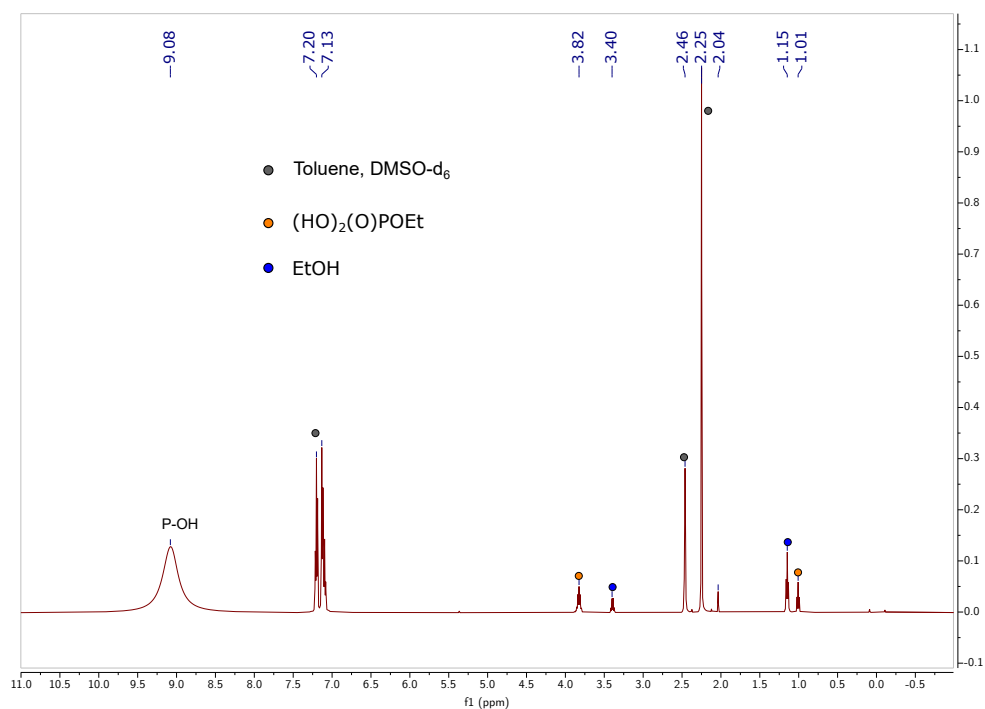


Figure C.5 ^1H NMR spectrum of the reaction mixture generated according to Section C.4.4 in $\text{DMSO-}d_6$, recorded at 500 MHz at 25 °C.

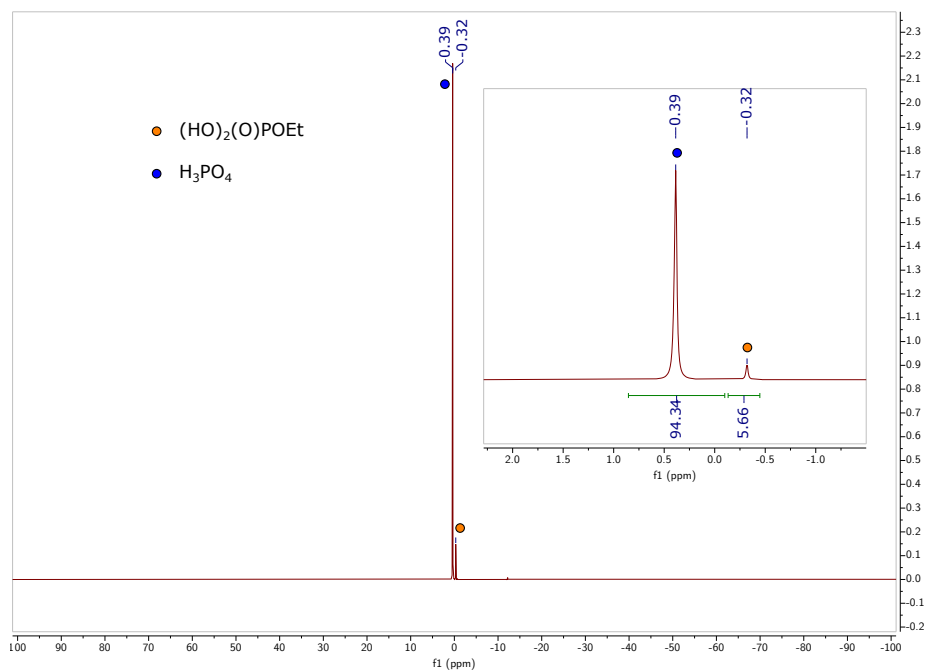


Figure C.6 $^{31}\text{P}\{^1\text{H}\}$ NMR spectrum of the reaction mixture generated according to Section C.4.4 in $\text{DMSO-}d_6$, recorded at 203 MHz at 25 °C.

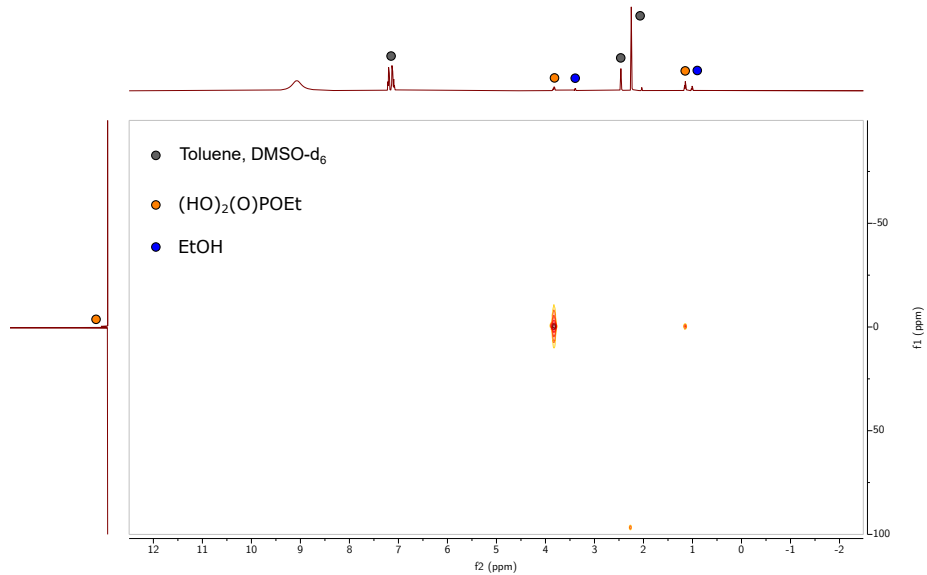


Figure C.7 $^1\text{H-}^{31}\text{P}$ HMBC NMR spectrum of the reaction mixture generated according to Section C.4.4 in $\text{DMSO-}d_6$, recorded at 500 MHz at 25 °C.

C.4.5 Reaction of crystalline phosphoric acid with 1-hexene

In the glovebox, phosphoric acid (98 mg, 1.0 mmol, 1 equiv) was weighed into a Schlenk flask. Triflic acid (3 mg, 0.02 mmol, 0.02 equiv) was weighed into a vial and transferred to the flask using toluene (2×1 mL). The flask was sealed and removed from the glovebox. 1-hexene (0.5 mL, 4.0 mmol, 4 equiv) was added against a flow of nitrogen and the solution was stirred for 48 h at 23 °C. The reaction mixture was diluted with ethanol (20 mL) and an aliquot was removed (1 mL). Volatile material was removed from the aliquot and the residue redissolved in DMSO- d_6 . The sample was analyzed by NMR spectroscopy showing the formation of a mixture of alkyl phosphates, identified by the observation of J_{P-H} couplings in the NMR spectra.

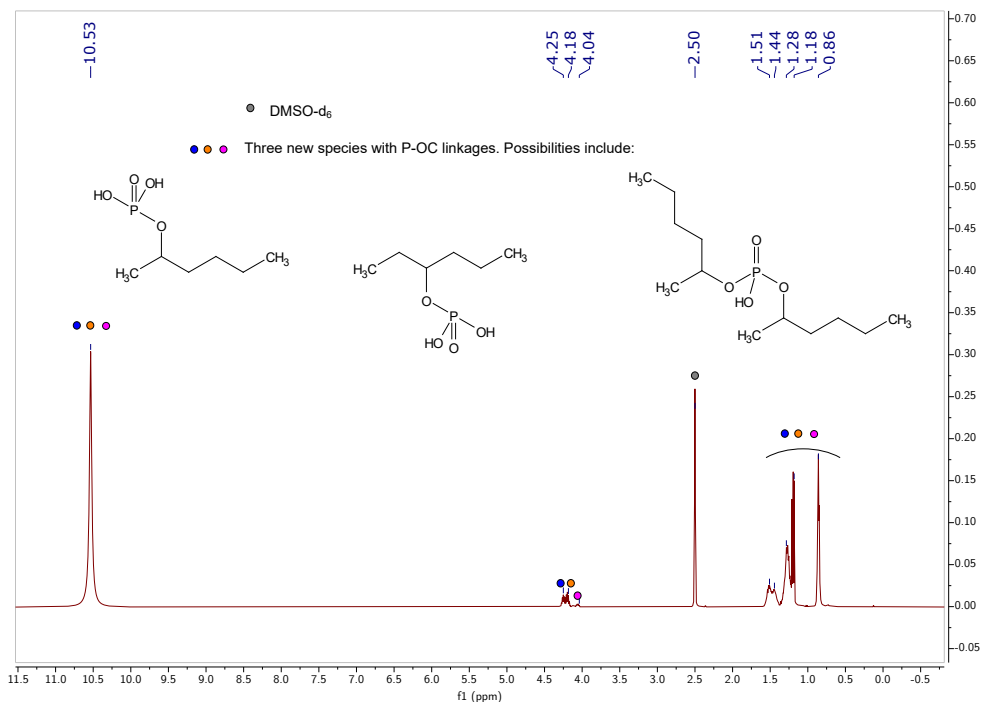


Figure C.8 ^1H NMR spectrum of the reaction mixture generated according to Section C.4.5 in DMSO- d_6 , recorded at 500 MHz at 25 °C.

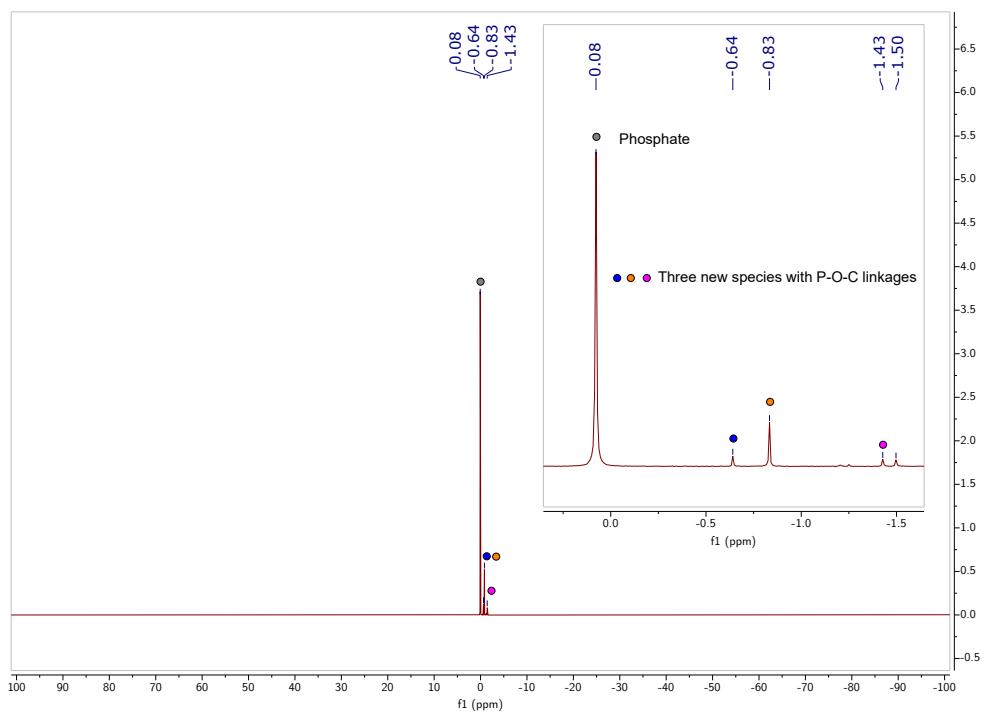


Figure C.9 $^{31}\text{P}\{^1\text{H}\}$ NMR spectrum of the reaction mixture generated according to Section C.4.5 in $\text{DMSO-}d_6$, recorded at 203 MHz at 25 °C.

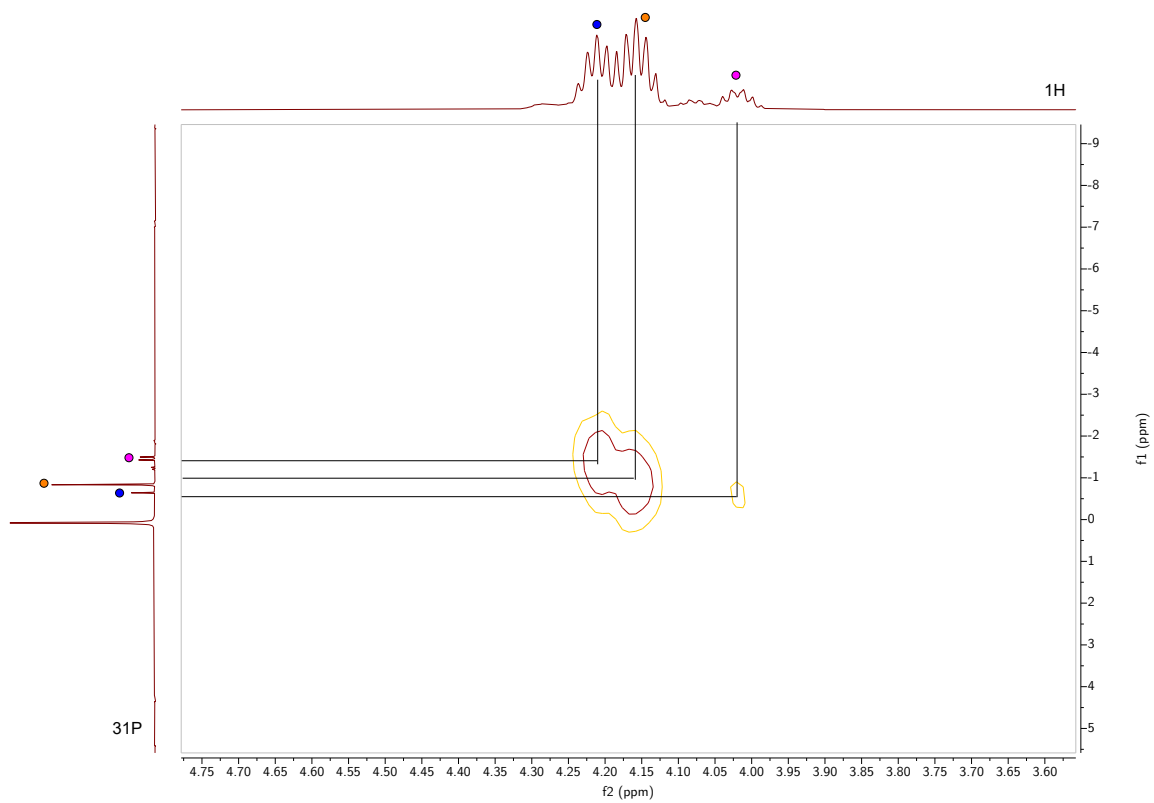


Figure C.10 ^1H - ^{31}P HMBC NMR spectrum of the reaction mixture generated according to Section C.4.5 in $\text{DMSO-}d_6$, recorded at 500 MHz at 25 °C.

C.4.6 Testing the stability of [TBA][M][HPO₄] (M = Li, K) in THF and MeCN

Four reactions were set up, using either the Li or K salt of [M]HMDS and using either THF or MeCN as the solvent. In the glovebox, [TBA][H₂PO₄] (25 mg, 0.0735 mmol, 1 equiv) was either dissolved (MeCN) or slurried (THF) in the appropriate solvent (0.6 mL). The solid [M]HMDS (M = K, Li, 0.0735 mmol, 1 equiv) was added and the resulting solutions were analyzed by ³¹P{¹H} and ¹H (pre-saturation experiment) NMR spectroscopy. Only the combination of [Li]HMDS and acetonitrile as the solvent led to a soluble product that did not show the presence of tri-*n*-butylamine (the presence of which indicates TBA decomposition).

C.4.7 Preparation of [TBA][Li][HPO₄]

In the glovebox, [TBA][H₂PO₄] (200 mg, 0.588 mmol, 1 equiv) and LiHMDS (98 mg, 0.588 mmol, 1 equiv) were weighed into separate vials. The phosphate salt was dissolved in MeCN (4 mL), and solid LiHMDS was added to the solution. The reaction mixture was stirred for 20 min then filtered (microfiber paper, pipette) into a vial (20 mL). The resulting solution was layered with diethyl ether (10 mL) and placed in the freezer. After three days no precipitate was observed. Additional ether (6 mL) was added and after two days white crystals had formed. The solution was decanted away and the wet crystals analyzed in MeCN which showed the presence of tetra-*n*-butylammonium. A yield was not recorded for this procedure. ¹H NMR (500 MHz, acetonitrile, δ) 8.72 (s, 1H), 3.92 (td, J = 8.4, 3.6 Hz, 8H), 2.38 (m, 8H), 2.15 (p, J = 7.8 Hz, 8H), 1.75 (dd, J = 7.1, 2.4 Hz, 12H). ³¹P{¹H} NMR (203 MHz, C₆D₆, δ) 6.37 (s), 8.83 (s, br).

C.4.8 Treatment of [TBA][Li][HPO₄] with CO₂

In the glovebox, [TBA][H₂PO₄] (25 mg, 0.0735 mmol, 1 equiv) was dissolved in CD₃CN (0.6 mL) and was analyzed NMR spectroscopy, showing clean material. LiHMDS (12 mg, 0.0735 mmol, 1 equiv) was weighed into a vial, and the solution of [TBA][H₂PO₄] was poured onto the solid material. The LiHMDS dissolved over 30 s to give a slightly yellow solution. The sample was analyzed by NMR spectroscopy, showing loss of the acidic phosphate protons in the ¹H NMR spectrum; they are expected to have exchanged with deuterium atoms present in the solvent. The tube was degassed twice via the freeze-pump-thaw method and the tube back filled with CO₂. The sample was left under a CO₂ atmosphere for 20 min then analyzed by NMR spectroscopy. Two new signals were observed in the ³¹P{¹H} NMR spectrum, which after 20 min had converged to one new signal. The chemical shifts of the intermediates were -5.91 and -5.50 ppm, respectively. The experiment should be repeated with ¹³CO₂ to look for phosphorus-carbon coupling.

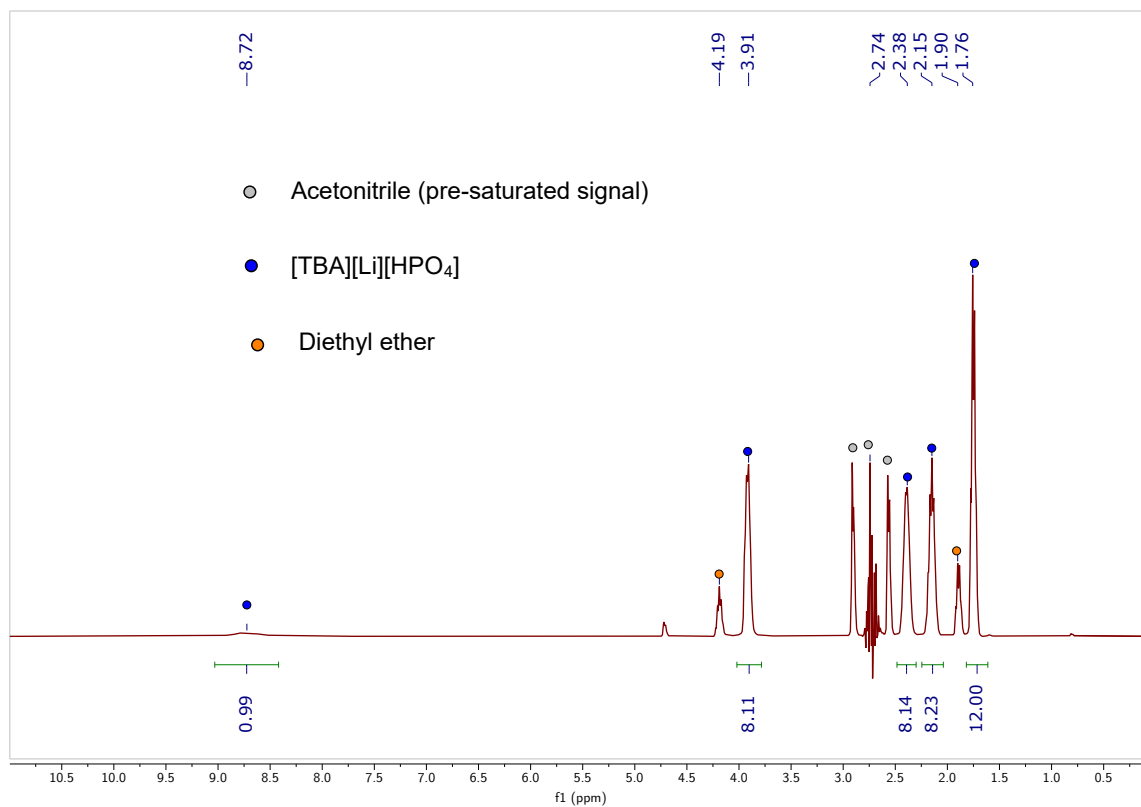


Figure C.11 ^1H NMR spectrum (pre-saturation sequence) of $[\text{TBA}][\text{Li}][\text{HPO}_4]$ in acetonitrile, recorded at 400 MHz at 25 °C.

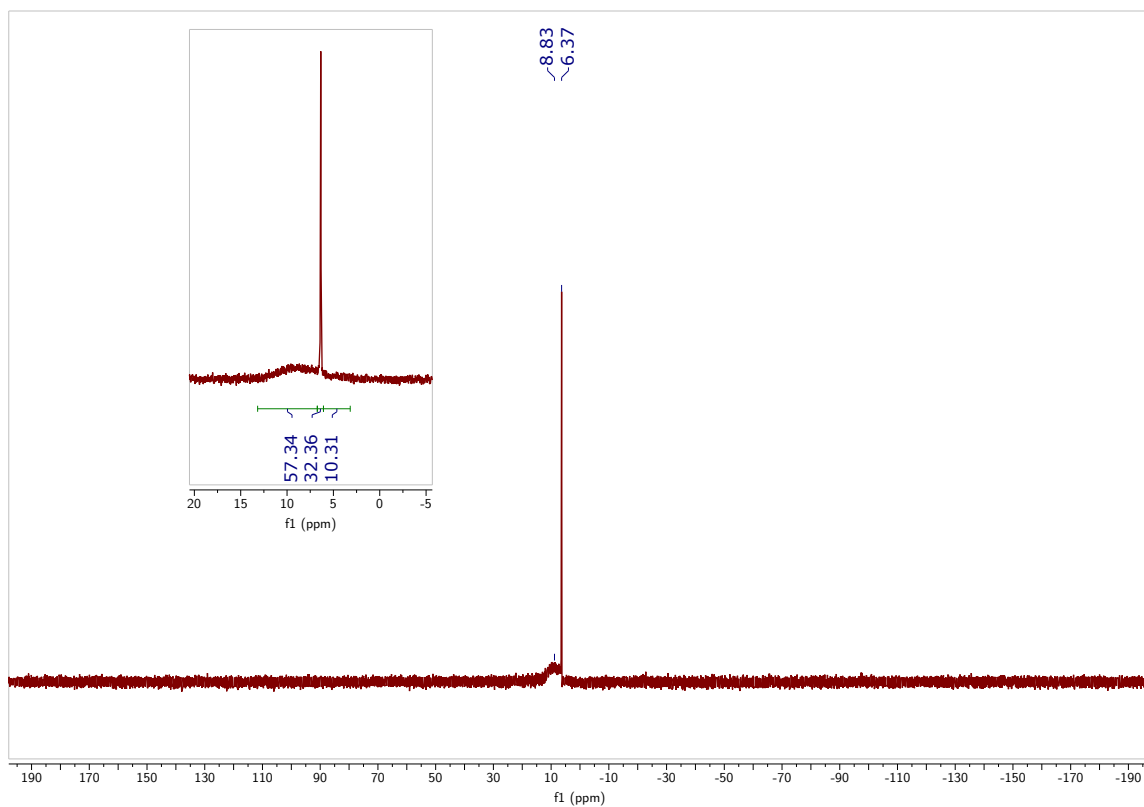


Figure C.12 $^{31}\text{P}\{^1\text{H}\}$ NMR spectrum of $[\text{TBA}][\text{Li}][\text{HPO}_4]$ in acetonitrile, recorded at 162 MHz at 25 °C.

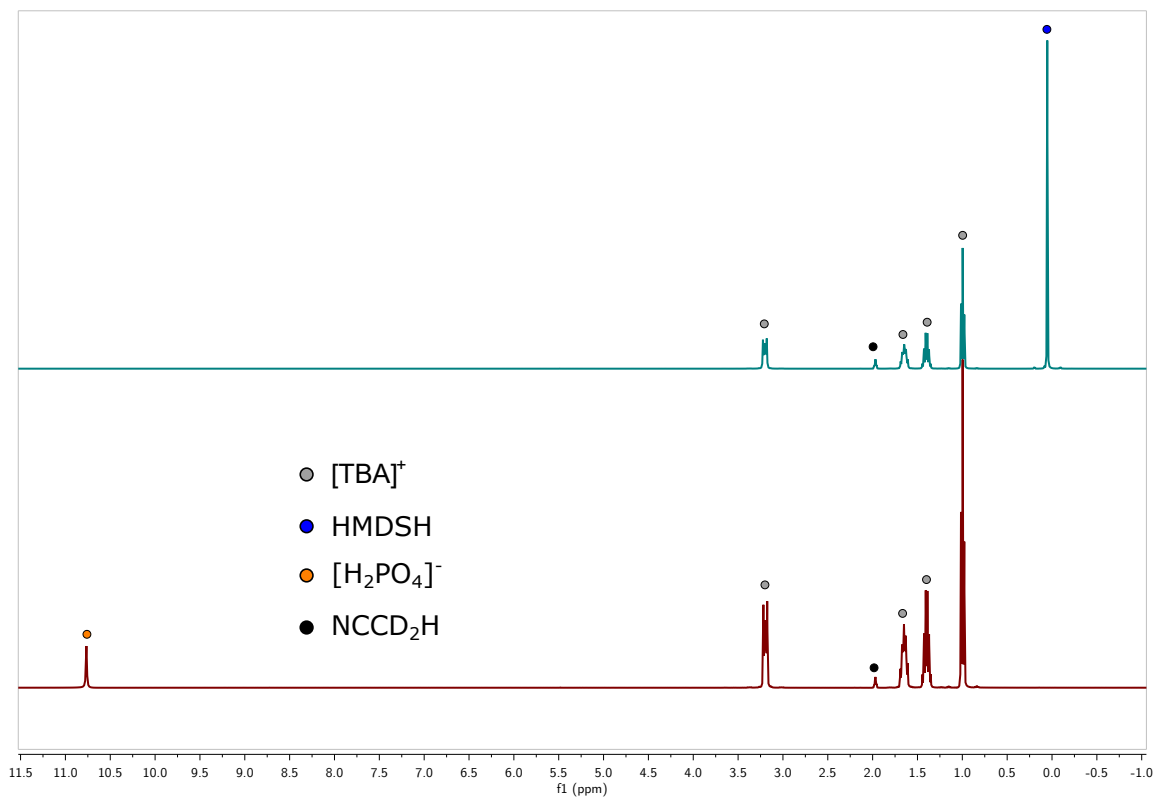


Figure C.13 ¹H NMR spectrum of the reaction mixture before (bottom) and after (top) addition of LiHMDS to [TBA][H₂PO₄] in CD₃CN, recorded at 400 MHz at 25 °C.

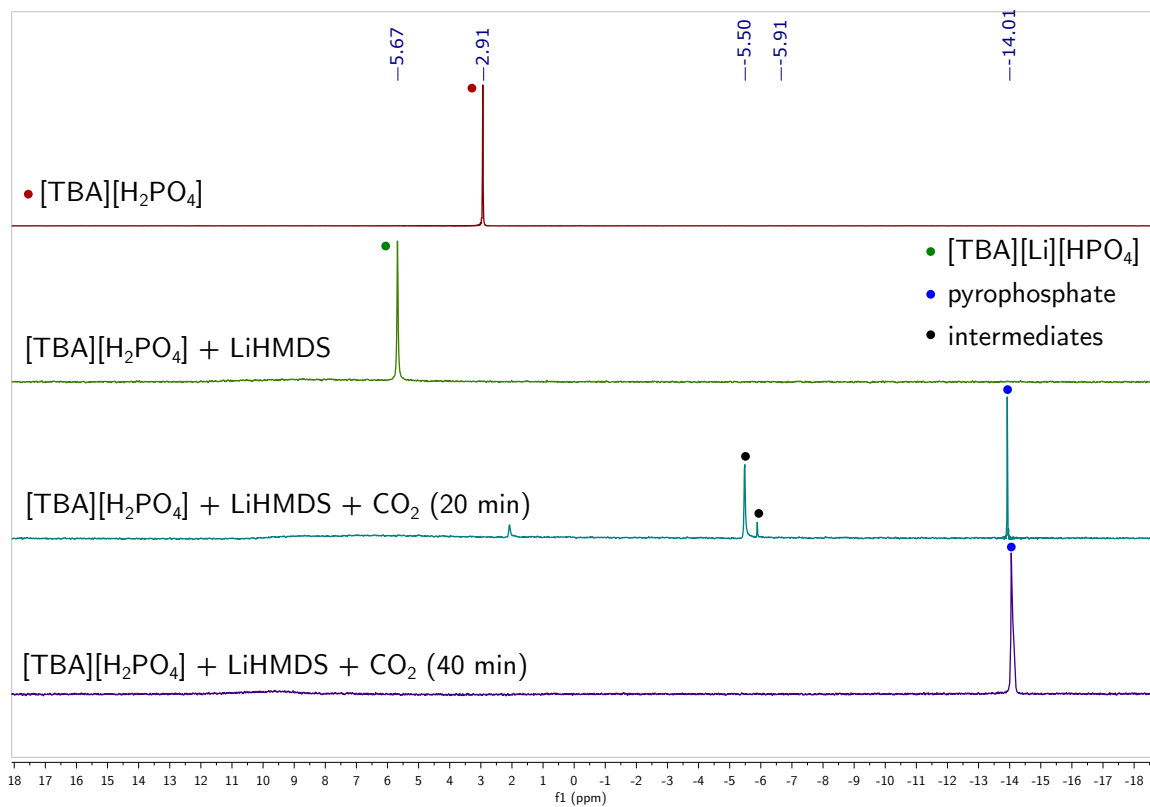
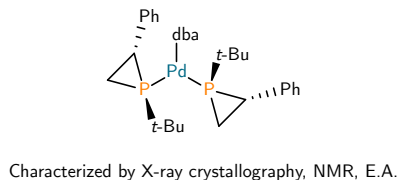
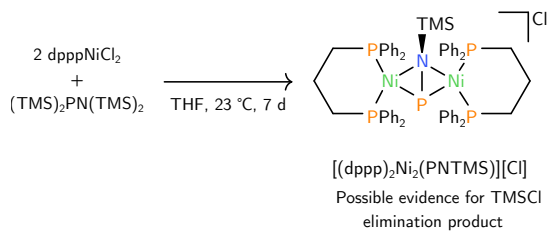


Figure C.14 $^{31}\text{P}\{^1\text{H}\}$ NMR spectrum of the reaction mixture at the different stages described in Section C.4.8, in CD_3CN and recorded at 162 MHz at 25 °C.

References

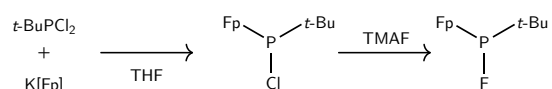
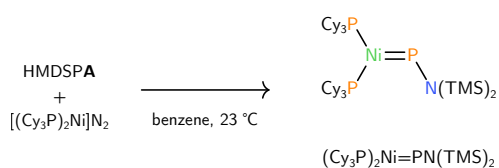
- [1] Glavinović, M.; Krause, M.; Yang, L.; McLeod, J. A.; Liu, L.; Baines, K. M.; Friščič, T.; Lumb, J.-P. *Sci. Adv.* **2017**, *3*, e1700149.
- [2] Allcock, H. R.; Bissell, E. C. *J. Am. Chem. Soc.* **1973**, *95*, 3154–3157.
- [3] Allcock, H. R.; Bissell, E. C. *J. Chem. Soc., Chem. Commun.* **1972**, 676.
- [4] Allcock, H. R. *J. Am. Chem. Soc.* **1963**, *85*, 4050–4051.
- [5] Siu, P. W.; Gates, D. P. *Organometallics* **2009**, *28*, 4491–4499.
- [6] Kaiser, E. T.; Kudo, K. *J. Am. Chem. Soc.* **1967**, *89*, 6725–6728.
- [7] Ishihara, K.; Sakakura, A.; Sakuma, M.; Katsukawa, M. *Heterocycles* **2008**, *76*, 657.
- [8] Eymery, F.; Iorga, B.; Savignac, P. *Tetrahedron* **1999**, *55*, 13109–13150.
- [9] Li, Z.; Zhang, J.; Brouwer, C.; Yang, C.-G.; Reich, N. W.; He, C. *Org. Lett.* **2006**, *8*, 4175–4178.
- [10] Ipatieff, V. N.; Pines, H. *Ind. Eng. Chem.* **1935**, *27*, 1364–1369.
- [11] Knopf, I.; Ono, T.; Temprado, M.; Tofan, D.; Cummins, C. C. *Chem. Sci.* **2014**, *5*, 1772.
- [12] Miles, B. W.; Raushel, F. M. *Biochemistry* **2000**, *39*, 5051–5056.
- [13] Anderson, P. M.; Meister, A. *Biochemistry* **1965**, *4*, 2803–2809.
- [14] Sauers, C. K.; Jencks, W. P.; Groh, S. *J. Am. Chem. Soc.* **1975**, *97*, 5546–5553.
- [15] Broussard, T. C.; Pakhomova, S.; Neau, D. B.; Bonnot, R.; Waldrop, G. L. *Biochemistry* **2015**, *54*, 3860–3870.
- [16] Svara, J.; Weferling, N.; Hofmann, T. “Phosphorus Compounds, Organic”, *Ullmann’s Encyclopedia of Industrial Chemistry*; Wiley: Weinheim, Germany, 2006.
- [17] Pangborn, A. B.; Giardello, M. A.; Grubbs, R. H.; Rosen, R. K.; Timmers, F. J. *Organometallics* **1996**, *15*, 1518–1520.
- [18] Williams, D. B. G.; Lawton, M. *J. Org. Chem.* **2010**, *75*, 8351–8354.

Index of Unpublished Compounds and Reactions



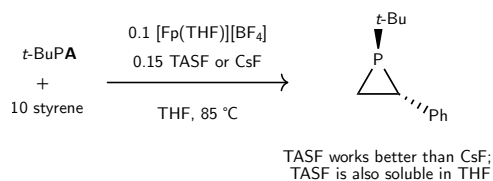
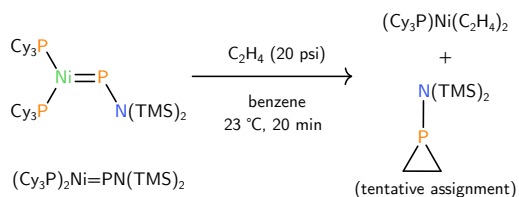
Discussion: Section A.2; Exp: Section A.4.2

Discussion: Section A.2; Exp: Section A.4.11



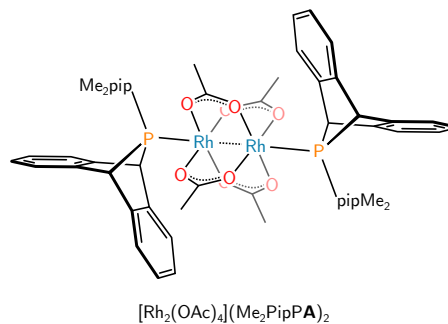
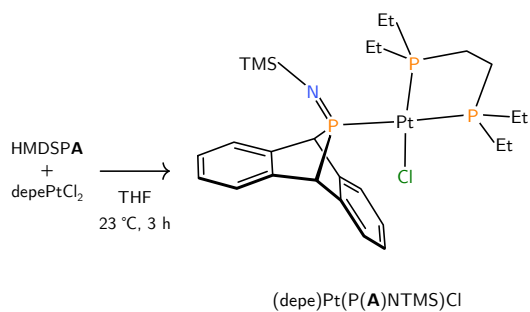
Discussion: Section A.2; Exp: Section A.4.7

Discussion: Section A.2; Exp: Section A.4.12



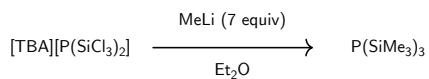
Discussion: Section A.2; Exp: Section A.4.8

Discussion: Section 5.4.1; Exp: Section 5.5.15.

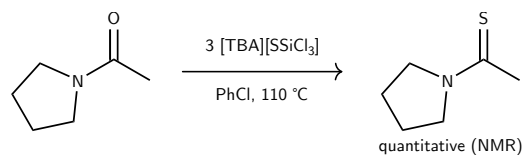


Discussion: Section A.2; Exp: Section A.4.5.

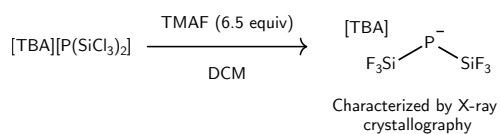
Discussion: Section A.2; Exp: Section A.4.9.



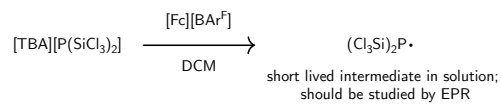
Discussion: Section B.2; Exp: Section B.5.3



Discussion: Section B.2; Exp: Section B.5.6



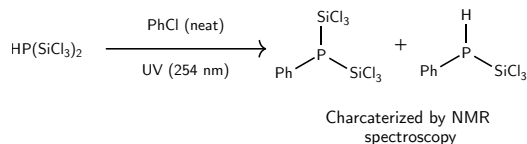
Discussion: Section B.2; Exp: Section B.5.2



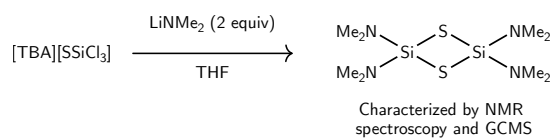
Discussion: Section 4.4; Exp: Section 4.5.20



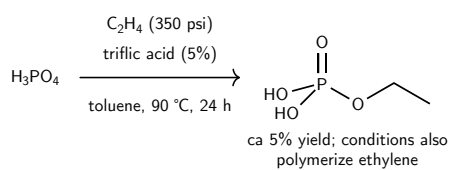
Discussion: Section B.2; Exp: Section B.5.4



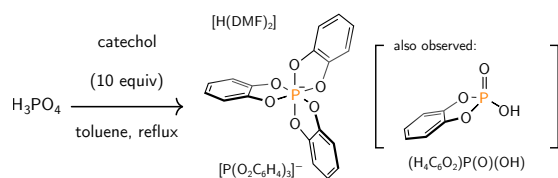
Discussion: Section 4.4; Exp: Section 4.5.19



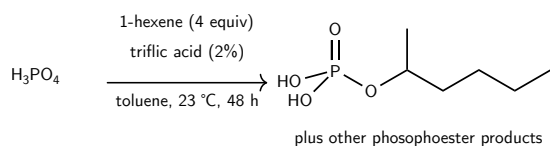
Discussion: Section B.2; Exp: Section B.5.5



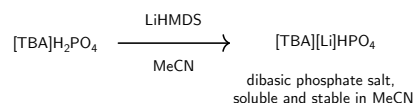
Discussion: Section C.2; Exp: Section C.4.4



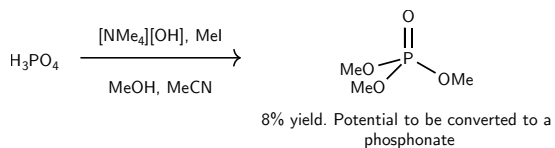
Discussion: Section C.2; Exp: Section C.4.2



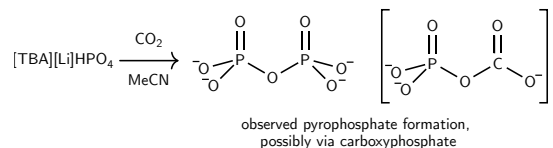
Discussion: Section C.2; Exp: Section C.4.5



Discussion: Section C.2; Exp: Section C.4.7



Discussion: Section C.2; Exp Section C.4.3



Discussion: Section C.2; Exp: Section C.4.8

